Systematic characterization of a large number of Microtubule-Associated Proteins using purification-free TIRF-reconstitution assays

Jijumon A.S.

Thèse de doctorat

NNT : 2021UPASL007

université PARIS-SACLAY

Systematic characterization of a large number of Microtubule-Associated Proteins using purification-free TIRF-reconstitution assays

Thèse de doctorat de l'université Paris-Saclay

École doctorale n° 577 : Structure et Dynamique des systèmes Vivants (SDSV)
Spécialité de doctorat : Sciences de la vie et de la santé
Unité de recherche : Université Paris-Saclay, CNRS, Intégrité du Génome, ARN et Cancer, 75248, Paris 05, France.
Référent : Faculté des sciences d'Orsay

Thèse présentée et soutenue à Paris-Saclay, le 16 février 2021, par

Jijumon A. S.

Composition du Jury

Christian POÜS Professeur, Innovation Thérapeutique : du Fondamental à l'appliqué, Université Paris-Saclay	Président
Thomas SURREY Professeur, Centre for Genomic Regulation (CRG), Barcelona	Rapporteur & Examinateur
Isabelle ARNAL Directrice de recherche, Grenoble-Institut des Neurosciences	Rapporteure & Examinatrice
Laurent BLANCHOIN Directeur de recherche, Institut de Biosciences et Biotechnologies de Grenoble, CEA	Examinateur

Direction de la thèse

Carsten JANKE Directeur de recherche, Institut Curie - Orsay	Directeur de thèse

Acknowledgements

First of all, I would like to express my sincere gratitude to my supervisor Dr. Carsten Janke for giving an opportunity to work in his lab, for his mentorship and guidance. I really appreciate his support and advisements from the bottom of my heart for all the interesting, unique and challenging projects. His remarks, help and engagement throughout the learning process of this PhD thesis have improved my scientific understandings, my soft skills and helped me in taking my steps further closer towards an independent researcher.

I would like to express my sincere gratitude to Magda, Satish and Mariya for their help and support at all stages of the project. Also, I would like to thank Sudi, Puja, Fatlinda and Veronique for willingly extending their help whenever I needed it. I am so glad that I got a wonderful research environment and supportive colleagues. I will really miss our lunchtimes, gatherings, good moments in bars, and lab trips we made together for conferences and retreats.

I am grateful to the Curie central facility and department of genome integrity, RNA and cancer (UMR 3348) for sharing their precious resources and support in the course of the project. I also want to thank Laetitia Besse, Claire Lovo and Marie-Noëlle Soler from the PICT-Orsay, microscope facility for the access to TIRF microscope and common facilities. I am also thankful to Cederic who helped for some of the image analysis and quantifications.

I would also like to sincerely thank Dr. Phong Tran (Institut Curie, Paris) and Dr. Thomas Müller-Reichert (Technische Universität Dresden) for their valuable time for evaluating my project progress and for their instructive comments and suggestions during all TAC (Thesis Advisory Committee) meetings.

I also would like to thank Minhaj Sirajuddin and his student Mamta Bangera from Instem, Bangalore, India for the cryo-EM studies they have done for my project and training I got for microtubule *in vitro* reconstitution. I really enjoyed those 1-week lab visits in 2017 and 2018.
I am thankful to European Union's Horizon 2020 research and innovation programme under Marie Skłodowska-Curie grant agreement (no. 675737) for funding my three years of PhD, and FRM (grant number: FDT201904008210.) for funding my final year. Special thanks to FRM for giving two months of additional funding due to COVID-19 pandemic. I would like to thank

University of Paris-Saclay/ Paris-Sud, and SDSV (Structure et dynamique des systèmes) for conducting this doctoral programme and allowing me to pursue my PhD thesis project. I am also very thankful to all members of divide MSCA-ITN. I really enjoyed all the healthy-intellectual discussions and our journey together as a family. I will really miss that gang and wonderful moments we had together in different countries in Europe.

My fiancé (Dr. Rugsana Gulistan), my mother (Sabira M.) and my sister (Dr. Jijimol A. S.) have been a great support throughout the process as always. I am extremely thankful to my fiancé for her boundless love and for always offering to help. Finally, I would like to thank all those who have supported me throughout the process by keeping me harmonious, from people at the reception to the technicians who I saw in the corridor for putting a smile on their face. I will be grateful to all of you forever for your love, help and support.

Index

Summary in English

Microtubules (MTs) are dynamic filaments involved in a plethora of functions such as cell division, cell shape, ciliary beating, neuronal differentiation. Strict regulation of MT functions is therefore of high importance for the cellular homeostasis, and any perturbations could potentially lead to diseases like cancer, ciliopathies and neurodegeneration. At the protein level, there are accumulating studies showing that MT properties can be controlled via interaction with a large variety of MT-associated proteins (MAPs). Our knowledge of MAPs has been enriched over time, but up to this date no systematic studies exist that aim to describe and categorize these proteins according to their binding mechanisms and structural effects on MTs. In my PhD project, I have developed an assay for rapid and systematic analysis of MAPs using cleared lysates of cultured human cells in which I overexpress a variety of different MAPs. The dynamic behaviour of growing MTs in the presence of those MAPs were imaged using TIRF microscopy. This allows me to study the behaviour of around 50 MAP candidates in a situation close to their natural environment, but eliminating complexity coming from different organelles and crammed cytoskeleton filaments inside the confined intracellular space. Indeed, most MAPs were nicely soluble in the extract approach, while purification attempts of several of them led to protein precipitation, thus making classical in-vitro reconstitution approaches impossible.

This novel approach allowed me to compare many MAPs under similar experimental conditions, and helped to define several novel proteins as bona-fide MAPs. I demonstrate that previously uncharacterized MAPs have strikingly different effects on MT polymerization and MT structure, thus creating a variety of distinct MT arrays. I further extended this cell-free pipeline to study structures of MAPs bound to MTs by cryo-electron microscopy, or to study the MT interactions of MAPs carrying patient mutations. Finally, I demonstrated that my approach can be used to test the sensitivity of MAPs to tubulin PTMs, as well as to study the role of MAPs in actin-MT crosstalk. In the future, this novel approach will allow for a better mechanistic understanding of how MAPs and MTs together control cytoskeleton functions.

Summary in French

Le cytosquelette des microtubules (MTs) est constitué de filaments dynamiques impliqués dans une multitude de fonctions telles que la division cellulaire, le maintien de forme des cellules, les battements ciliaires ou encore la différenciation neuronale. Une régulation stricte des fonctions des MTs est donc d'une grande importance pour l'homéostasie cellulaire, et toute perturbation pourrait potentiellement conduire à des maladies comme le cancer, les ciliopathies ou la neurodégénérescence.

Dans un contexte cellulaire, les propriétés des MTs peuvent être contrôlées par leurs interactions avec une grande variété de protéines associées (MT-associated proteins ; MAPs). Notre connaissance de ces interacteurs s'est continuellement enrichie au cours des dernières décennies, mais il n'existe à ce jour aucune étude systématique visant à décrire et à classer ces protéines en fonction de leurs mécanismes de liaison et de leurs effets structuraux sur les MTs. Dans mon projet de thèse, j'ai mis au point un essai permettant une analyse rapide et systématique à la base des lysats clarifiés de cellules humaines surexprimant une multitude des différents MAPs. Le comportement dynamique des MT en présence d'environ 50 MAPs différentes a été imagé à l'aide de la microscopie TIRF. Cela nous permet d'étudier le comportement des MAP dans une situation proche de leur environnement naturel, mais en éliminant la complexité de l'espace intracellulaire, telle que l'encombrement par des organelles et des filaments du cytosquelette à l'intérieur de l'espace intracellulaire confiné. En effet, la plupart des MAPs étaient bien solubles dans notre approche d'extraction, tandis que les approches de purification pour plusieurs d'entre elles ont conduit à leur précipitation, rendent les expériences de reconstitution in vitro classique impossible.

Mon nouveau approche m'a permis de définir plusieurs nouvelles protéines comme de véritables MAP. J'ai montré que des MAPs non-caractérisées auparavant ont des effets étonnamment différents sur la polymérisation et la structure des MTs, créant ainsi une variété de réseaux de MT distincts. J'ai également démontré que mon approche permet d'étudier les structures des MAPs associées aux MTs par cryo-microscopie électronique, ou d'étudier le dynamique des MTs porteuses de mutations trouvées dans les pathologies humaines. J'ai également démontré que mon approche permet à tester la sensibilité des MAPs aux modifications posttraductionnelles de la tubuline, ou d'étudier le rôle des MAPs dans les interactions entre l'actine et les MTs. Mon approche expérimentale permet donc de mieux comprendre comment les MAP et les MT contrôlent ensemble le fonctionnement du cytosquelette.

List of Abbreviations

ATP	**Adenosine triphosphate**
b. p.	**base pair**
BRB80	**Britton–Robinson buffer 80**
BSA	**bovine serum albumin**
CCPs	**Cytosolic carboxypeptidases**
Cryo-EM	**Cryo-Electron Microscopy**
DMEM	**Dulbecco's modified Eagle's medium**
E. *coli*	***Escherichia coli***
EDTA	**Ethylenediaminetetraacetate**
EGFP	**Enhanced Green Fluorescent Protein**
EGTA	**ethylene glycol-bis (β-aminoethylether) N, N, N',N' tetraacetic acid**
FBS	**fetal bovine serum**
GMPCPP	**guanylyl 5′-α, β-methylene diphosphonate**
GTP	**Guanosine-5'-triphosphate**
HEK	**Human Embryonic Kidney**
IPTG	**isopropyl beta-D-1-thiogalactopyranoside**
k Da	**kilo Dalton**
MAPs	**Microtubule Associated Proteins**
MTs	**Microtubules**
PBS	**phosphate-buffered saline**
PCR	**polymerase chain reaction**
Pen/strep	**penicillin/ streptomycin**
PIC	**Protease Inhibitor Cocktail**
PIPES	**piperazine-N,N′-bis(2-ethanesulfonic acid)**
PMSF	**phenylmethylsulfonyl fluoride**
PTMs	**Posttranslational modifications**
SDS-PAGE	**sodium dodecyl sulphate-polyacrylamide gel electrophoresis**
SILAC	**Stable isotope labelling by amino acids in cell culture**
SLIC	**Sequence and Ligation Independent Cloning**
TEMED	**N,N,N',N'-tetramethylethylenediamine**

TIRF-M	**Total Internal Reflection Fluorescence Microscopy**
Tris	**tris(hydroxymethyl)aminomethane**
TTLLs	**Tubulin Tyrosine Ligase Like**

List of MAPs abbreviations

ATF5	**Activating transcription factor 5**
ATIP3	**Angiotensin II type 2 (AT(2)) receptor-interacting protein 3**
CFAP 20	**Cilia Flagella Associated Proteins**
CGN	**Cingulin**
CLIP-170	**Cytoplasmic Linker Protein of 170 kDa**
Crmp2	**Collapsin response mediator protein 2**
Crmp4	**Collapsin response mediator protein 4**
CSAP	**Centriole, cilia and spindle-associated protein**
DCLK1	**Doublecortin like kinase 1**
DCX	**Doublecortin**
EF-1 alpha	**elongation factor 1 alpha**
EMAP (1-6)	**Echinoderm Microtubule-associated protein (1-6)**
Jpl1	**Jupiter-like 1**
Jpl2	**Jupiter-like 2**
MACF1	**Microtubule actin cross-linking factor 1**
MACF2	**Microtubule actin cross-linking factor 2**
MAP1A	**Microtubule-associated protein 1A**
MAP2	**Microtubule-associated protein 2**
MAP4	**Microtubule-associated protein 4**
MAP6	**Microtubule-associated protein 6**
MAP7	**Microtubule-associated protein 7**
MAP7D1	**Microtubule-associated protein 7D1**
MAP7D2	**Microtubule-associated protein 7D2**
MAP7D3	**Microtubule-associated protein 7D3**
MAP8	**Microtubule-associated protein 8 (also known as MAP1S)**
MAP9	**Microtubule-associated protein 9**
MAP10	**Microtubule-associated protein 10**
MAP11	**Microtubule-associated protein 11**
NRD1	**Nardilysin**
Parkin	**Parkin**

POC1	**Proteome of centrioles 1**
POC2	**Proteome of centrioles 2**
PRC1	**Protein regulator of cytokinesis 1**
Protein 4.1R	**Protein 4.1R**
SAXO1	**Stabilizer of Axonemal Microtubules 1**
SAXO2	**Stabilizer of Axonemal Microtubules 2**
SNPH	**Syntaphilin**
Tau 3R	**Tau with 3 MT-binding tandem repeats**
Tau 4R	**Tau with 4 MT-binding tandem repeats**
TOG	**Tumour-Overexpressed Gene**
TPX2	**Targeting protein for Xklp2**
TRAK1	**Trafficking kinesin-binding protein 1**
TRAK2	**Trafficking kinesin-binding protein 2**

1. Introduction

In this thesis, first I would like to introduce to the reader relevant concepts related to my project such as cytoskeleton, microtubules, and the regulatory mechanism of microtubule properties (this includes microtubule-associated proteins (MAP)s and the tubulin code). Since my PhD project is primarily focused on a large number of structural MAPs, I also added a published review (where I am a co-author) about structural MAPs in the annex section 6.1. In addition, I also wrote short descriptions about each structural MAP I used in the project, which is included in the annex section 6.2.

In the result section, I added two chapters describing my major results, along with some related side projects that are so far not part of a manuscript.

Chapter-1 in the result section is my central project. I developed a method to characterize large numbers of MAPs using a cell-free lysate approach. This part is formatted as a publication manuscript, which we will finalise and send for publication soon. As a manuscript, it has an introduction, result section, conclusions, figures, methods and its own reference list. I discuss this work in detail in the main discussion section of the thesis. Chapter-1 also contains an additional result, which is not there in the main manuscript.

Chapter-2 focuses on the development of methods to study the role of tubulin PTMs in MAP-MT interactions. This chapter contains a published protocol (on which I am a co-first author), and side projects in which I explored different approaches to measure the impact of tubulin PTMs on microtubule-MAP interactions. In connection to the protocol in chapter 2, I also added another published protocol on which I am co-author in the annex section 6.3.

The ensuing discussion and conclusion considers all the major findings from my Ph.D. thesis, and puts them in a larger context.

1.1 Cytoskeleton

The cytoskeleton or "skeleton of the cell" is a network of protein filaments within a cell's cytoplasm, which is involved in many cellular functions such as cell shaping, cell movement as a whole and motility of organelles within the cell. The cytoskeleton of eukaryotes has four major components: actin filaments or microfilaments (4 nm diameter), microtubules (MTs, 25 nm diameter), intermediate filaments (10 nm diameter) and septin filaments (8.25 nm diameter) (Bodakuntla et al. 2019; Sheffield et al. 2003).

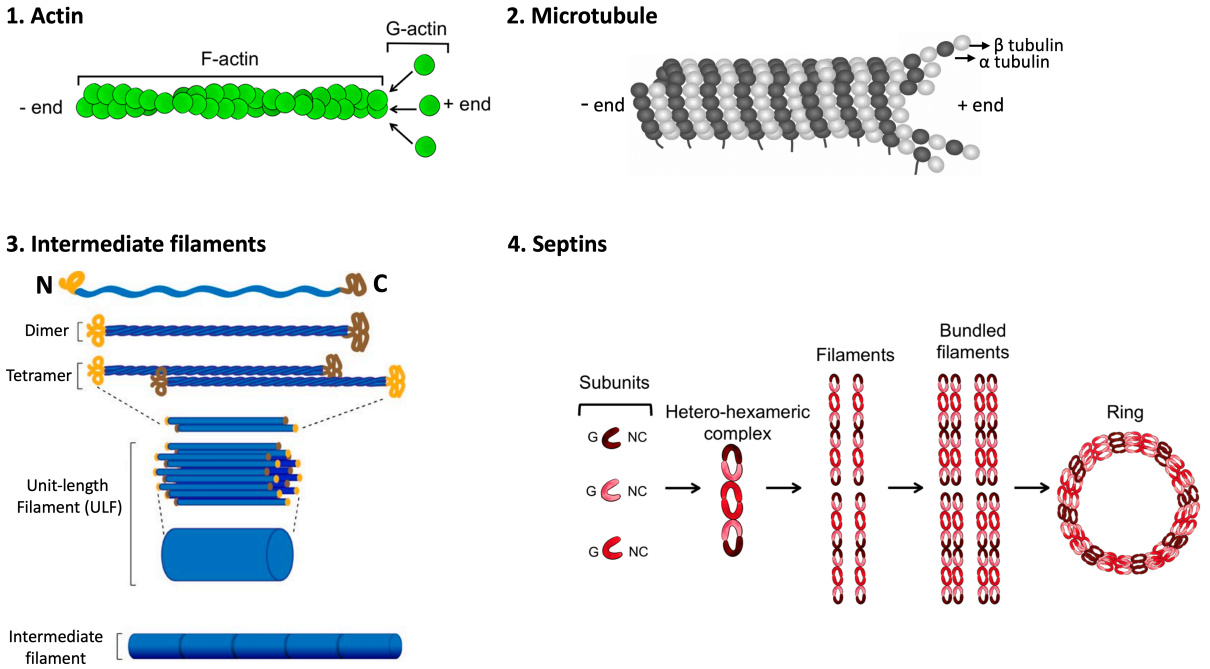

Figure 1: The eukaryotic cytoskeleton is composed of four major cytoskeletal polymers. Cytoskeleton filaments include actin or microfilaments, microtubules, intermediate filaments and septin filaments (adapted from (Mostowy 2014) and from https://www.mechanobio.info/cytoskeleton-dynamics/).

Actin was discovered by Brúnó F. Straub in 1942 at the University of Szeged, Hungary. Actin is a ~42-kDa protein, which is ubiquitous and highly conserved in all eukaryotes (Straub and Feuer 1989). It is present both in the cytoplasm and inside the nucleus. The functional form of actin is a helical polymer called F-actin (F for filamentous), assembled from monomeric subunits of G-actin (G for globular). The transition between these two states is under the control of ATP hydrolysis and a large number of actin-binding proteins (Mostowy 2014). In F-actin, one end, called the barbed end or plus end, favours actin polymerization. The other end, called

pointed or minus end, favours actin depolymerization. Actin is involved in a wide range of cellular functions such as cytokinesis, myosin mediated intracellular transport of organelles and vesicles, muscle contraction, cell shape, cell movement and polarity (Fletcher 2010).

Intermediate filaments (IFs), are major structural elements found in the cytoplasm and nucleus of every vertebrate cell. IFs are nonpolar structures which do not require nucleotide hydrolysis for assembly(Herrmann and Aebi 2004). IF proteins commonly assemble to form polar dimers, and dimers assemble antiparallelly forming nonpolar tetramers. Eight tetrameric units further assemble to form a unit length filament or ULF. Subsequently annealing of individual ULFs end to end forms intermediate filaments (shown in Fig. 1) (Eriksson et al. 2009; Mostowy 2014). Intermediate filaments are mostly known for its structural and mechanical roles in maintaining cell shape and cytoskeletal integrity, and have also been reported to be involved in signal transduction (Klymkowsky, Bachant, and Domingo 1989). Vimentin, desmin, nuclear laminins, neurofilaments and glial fibrillary acid protein (GFAP) are some of the examples of intermediate filaments (Hol and Capetanaki 2017).

Septins, the latest member of the cytoskeleton family, is involved in a variety of cellular functions such as cytokinesis, cell morphogenesis, motility and ciliogenesis. Septins are GTP-binding proteins that can associate with actin filaments, MTs, and cellular membranes. Septin units form intermediate complexes by interacting with each other through their GTP binding domain or G interface, and through their N- and C-terminal regions called the NC interface (shown in Fig. 1). End-to-end attachment of these complexes forms septin filaments, which further form bundles by lateral interactions and ring-like higher-order structures (Hartwell 1971; Kinoshita 2003; Mostowy 2014).

Among all four cytoskeletal elements, the primary focus of my project are MTs, which are described in detail in the next section (1.2). Along with MTs, I also studied some aspects of actin filaments in the context of actin-MT crosstalk.

1.2 Microtubules

1.2.1 Discovery, structure and MT properties

Tubulin is a ~50 kDa protein, discovered as the main constituent of MTs by Gary Borisy (Borisy and Taylor 1967), and named "tubulin" in 1968 (Mohri 1968). In eukaryotic cells, tubulin forms constitutive heterodimers of α- and β-tubulins, which spontaneously associate longitudinally end-to-end into linear protofilaments. These protofilaments join laterally to form a hollow, cylindrical, tube-like structure called MT. The number of protofilaments in the MTs ranges from 10 to 15 and vary between species and cell types. In many species, the predominant forms are 13-protofilament MTs, which have a 25-nm outer, and a 14-nm inner diameter (Gittes et al. 1993b) (Fig. 2).

Both, α- and β-tubulins have identical atomic structures, and both tubulin monomers, form a core of two interacting β-sheets surrounded by α-helices (Nogales, Wolf, and Downing 1998). The compacted monomer structure can be divided into three functional domains: the N-terminal domain containing the nucleotide-binding region, an intermediate domain where MT-stabilizing-drug Taxol binds, and a C-terminal domain where many tubulin posttranslational modifications are found, and that probably attracts different MT interacting proteins (Nogales, Wolf, and Downing 1998; Steinmetz and Prota 2018).

MTs are polar filaments having a fast-growing plus (+) end exposing β-tubulin subunits, and a slow-growing minus (-) end exposing α-tubulin. MTs mostly grow and shrink at the + end by the addition of αβ-tubulin heterodimers, a process regulated by GTP (Fig. 2B). Each tubulin dimer can bind to two GTP molecules. Binding of GTP happens at the N-site (non-exchangeable) of α-tubulin and regulatory E-site (exchangeable) of β-tubulin. GTP bound to α-tubulin is stable and has a structural function, while GTP bound to β-tubulin slowly hydrolyses after MT assembly. Tubulin dimers are in the GTP-bound state during MT assembly, while the GDP-tubulin lattice is more prone to promote MT disassembly (Weisenberg 1972a; Mitchison and Kirschner 1984a; Lowe et al. 2001; Akhmanova and Steinmetz 2015). Tubulin heterodimers interact with each other through reversible non-covalent interactions. The strength of these interactions is important for the dynamic properties of MTs, and thus for their biological functions (Nogales 2000; Abdrabou, Brandwein, and Wang 2020).

MTs undergo constant growth (addition of new tubulin heterodimers) and shrinkage (MT disassembly) cycles in cells - a behaviour commonly known as dynamic instability (Fig. 2) (Mitchison and Kirschner 1984a). As tubulin heterodimers added to the growing MT plus ends are in GTP-bound state, initial assembly generates a cap of GTP-bound tubulin that protects the plus end from depolymerization. When MT stops growing, hydrolyses of GTP reaches the MT plus end, where it induces a rapid MT depolymerization (Drechsel and Kirschner 1994; Desai and Mitchison 1997). The spontaneous disassembly of a MT is called catastrophe. MT disassembly can be spontaneously halted and growth can be re-initiated by addition of GTP-tubulin in an event known as rescue (Mitchison and Kirschner 1984a; Desai and Mitchison 1997; Akhmanova and Steinmetz 2015) (Fig. 2B).

Depending on the number of protofilaments, MTs have a lattice seam (Fig. 2B). The most common type of MTs with 13 protofilaments have an opposite lateral contact at the seam, where an α-tubulin subunit from one protofilament contacts a β-tubulin of the adjacent filament. This discontinuity in the helical lattice also contribute to the dynamic properties of MTs (Nogales et al. 1999; Akhmanova and Steinmetz 2015).

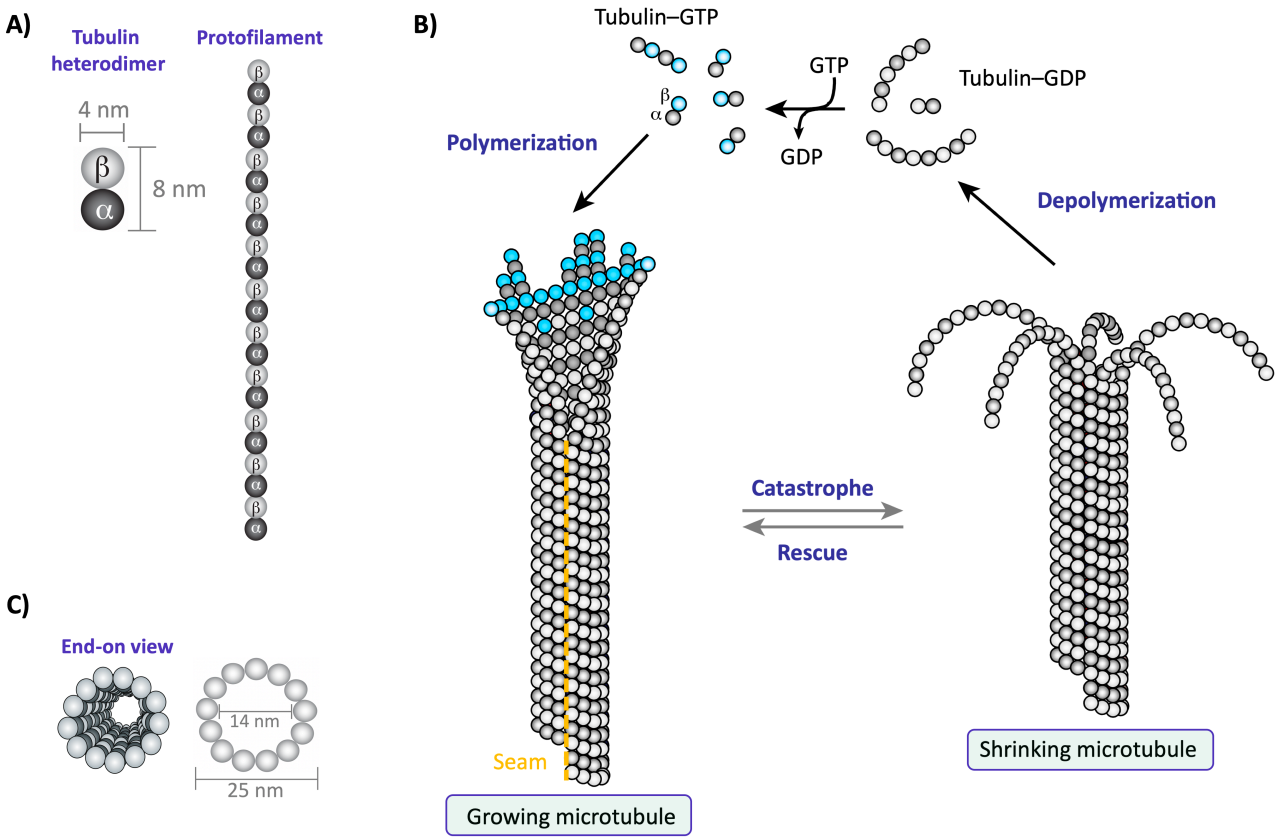

Figure 2: Structure and dynamic instability of MTs. A) Globular α/β-tubulin heterodimers associated end-to-end to form linear protofilaments. Lateral association of protofilaments leads to the formation of wall of MTs. **B)** MTs undergo polymerization-depolymerization cycles. Addition of GTP-tubulin at the plus ends leads to the MT growth. The hydrolysis of GTP to GDP induces MT depolymerisation from the plus end. At the MT lattice seam, α-tubulin subunits from one protofilament contact β-tubulin subunits of the neighbouring protofilament. **C)** MTs are hollow cylindrical structures typically composed of 13 protofilaments in eukaryotes, with an inner diameter of 14 nm and outer diameter of 25 nm. Panel B is adapted from (Steinmetz and Prota 2018).

Over a period of many years, the molecular properties of tubulin and MTs were extensively studied in in vitro and also using cellular studies. Following are some of the MT metrics. Tubulin constitutes ~3% of total soluble protein in extracts from cell lines (Hiller and Weber 1978). In most cells, the average MT growth rate is 0.2-0.4 μm/s (Zwetsloot, Tut, and Straube 2018), and 0.6-3 μm/min in in vitro conditions (Mitchison and Kirschner 1984b; Walker et al. 1988). The shrinkage rate of MTs in in-vitro conditions is 20-30 μm/min, and with an association rate constant of ~2-10 $\mu M^{-1}s^{-1}$(Mitchison and Kirschner 1984b; Walker et al. 1988; Desai and Mitchison 1997).

Along with α- and β-tubulin, there are four other members in the tubulin superfamily: gamma-, delta-, epsilon- and zeta-tubulin, but none of them is incorporated into the MT lattice (Findeisen et al. 2014). Gamma-tubulin acts as a template for MT nucleation by forming the gamma-tubulin ring complex (Moritz et al. 2000). Delta- and epsilon-tubulin are associated with centrioles, and zeta-tubulin is associated with centriolar basal feet in multiciliated cells (Turk et al. 2015). Unlike α-, β- and gamma-tubulin, other tubulin family members are not well conserved across eukaryotic cells and are thus less studied (Findeisen et al. 2014).

1.2.2. Cellular functions of microtubules

MTs are involved in many essential cellular functions such as cell division, cell differentiation and motility, and intracellular transport. Although MTs are hollow cylindrical tubes, they are mechanically rigid (Gittes et al. 1993a), and thus can assemble into subcellular structures that have to exert forces. MTs form a variety of intracellular structures: mitotic and meiotic spindles, which ensure the successful segregation of chromosomes; individual or bundled MT tracks in neurons that are used as rails for intracellular transport, as well as the axonemes of cilia and flagella (Fig. 3) (Gadadhar et al. 2017). In neurons, MTs play an important role in maintaining neuronal morphology and establishing neuronal polarity. In cilia and flagella, MTs are the structural components of the axoneme, which generates the ciliary and flagellar beat. Moreover, axonemal MTs play a crucial role in the transport of organelles and protein complexes, a process known as intraflagellar-transport (IFT). Other MT-based subcellular structures are the marginal bands in blood platelets, the midbody during cytokinesis, the centrioles of centrosomes (also known as MT-organizing centres, MTOC) and basal bodies of flagella and cilia (Goodson and Jonasson 2018).

MT-based structures are also involved in host-pathogen interactions. For example, the conoid of *Toxoplasma gondii* and ventral disc/suction plate of *Giardia lamblia* are both MT-based structures, used for the organism's viability and pathogenicity (Hu, Roos, and Murray 2002; Brown et al. 2016).

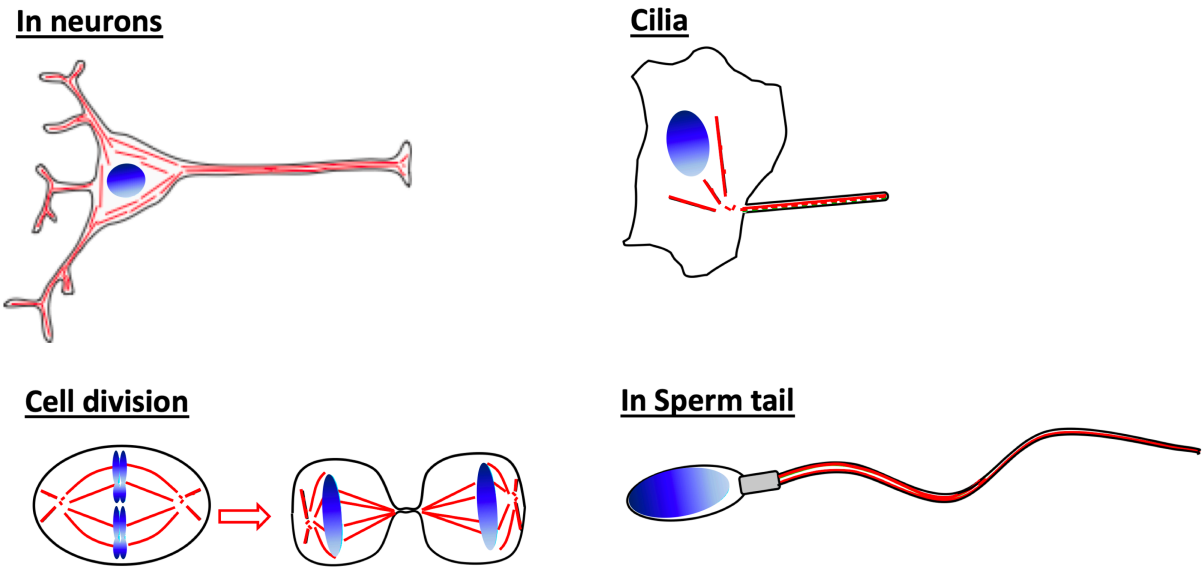

Figure 3: Functional diversity of microtubules. The MT cytoskeleton is adapted to many cellular functions such as in the axonal transport in neurons, mitotic and meiotic spindle for the successful segregation of chromosomes during cell division, and axoneme structures in cilia and flagella. MTs are represented in red (adapted from (Magiera, Singh, et al. 2018)).

This wide functional diversity of the MTs raises one of the key biological question of what regulates MT specificity, and how it is achieved. Currently there are two major mechanisms aiming to explain selective MT control: **1) MTs are modulated via interactions with a wide variety of MT-associated proteins (MAPs); 2) Different subtypes of MTs are generated by the incorporation of α- and β-tubulin isotypes, and posttranslational modifications (PTMs) of tubulins, a concept known as the tubulin code.**

There are growing evidences showing that the combinatorial expression of different MAPs in different cell types could modulate the dynamic, structural and functional properties of MTs (Monroy et al. 2020; Ramkumar, Jong, and Ori-McKenney 2018; Bodakuntla et al. 2019), a concept which is elaborately described later in this introduction section.
On the other hand, the tubulin code hypothesis states that along with the expression of different tubulin isotypes, the tubulin heterodimer undergoes many PTMs, which could alter the dynamic

properties of MTs, and tune interactions with MAPs, thus destining MTs to specific cellular functions (Janke and Magiera 2020). In the recent years, evidences are accumulating in support of the tubulin code hypothesis (Janke and Magiera 2020; Gadadhar et al. 2017).

1.2.3. Tubulin code: tubulin isotypes and post translational modifications of tubulin

MTs display very little structural variations, however, structurally conserved MTs can be diversified by two means. One at the genomic level by the expression of diverse α- and β-tubulin genes, which encode tubulin isotypes that can assemble into distinct MTs (Ludueña and Banerjee 2008a, 2008b). Second, at the protein level, tubulins are subject to a variety of PTMs, which can be added to assembled MTs, thus directly controlling their properties and functions (Janke and Magiera 2020; Gadadhar et al. 2017).

1.2.3.1. Tubulin isotypes

The amino acid sequences of α- and β-tubulins are highly conserved across all eukaryotes. However, many species express several tubulin isotypes, that are encoded by different tubulin genes. In human, nine α- and nine β-tubulin isotypes have been identified. Many isotypes are expressed in specific tissues and/or cell types (Ludueña and Banerjee 2008a, 2008b; Fukushima et al. 2009). For most of the tubulin isotypes, variations between amino acid sequences are very low, especially in the tubulin body - the core structure of α- and β-tubulins. A bit more sequence divergence is found in the carboxy-terminal (C-terminal) tails of tubulins, which are unstructured and project to the outer surface of MTs (Fig. 4).

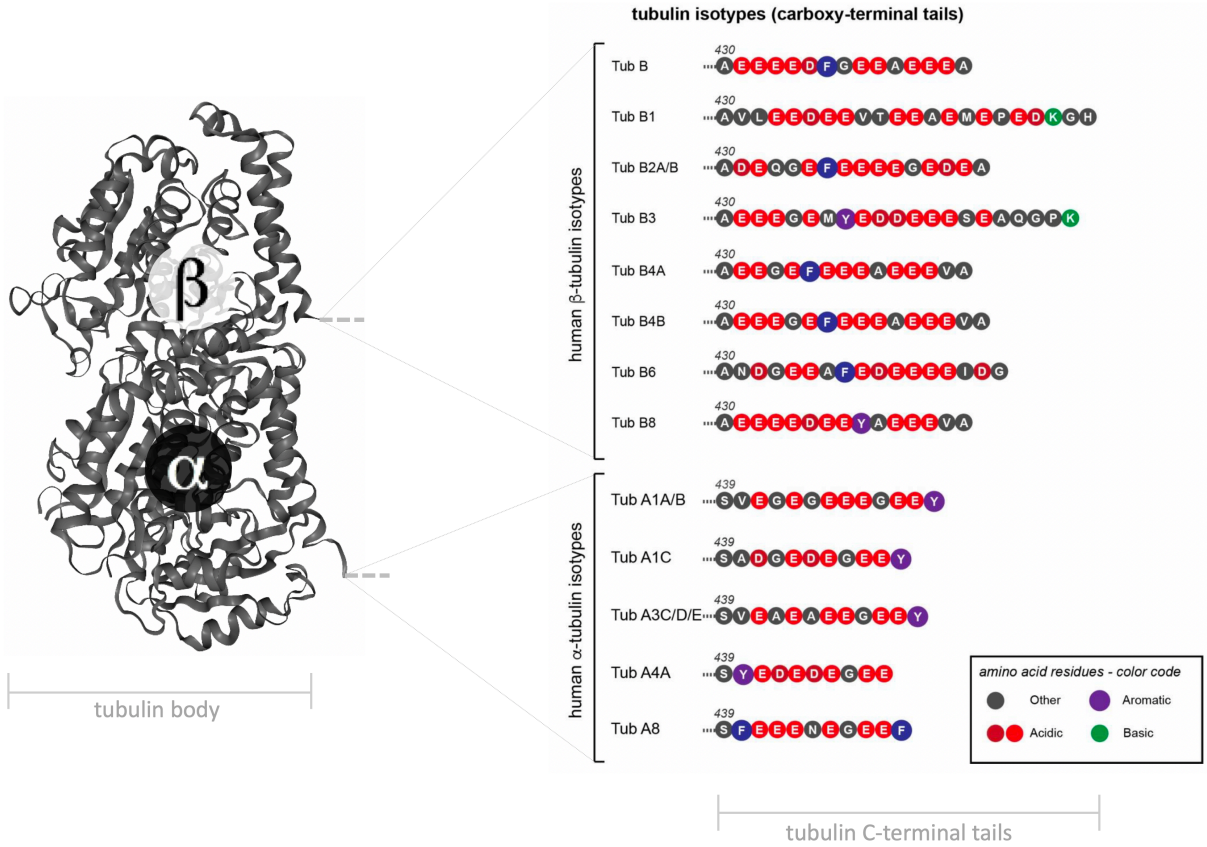

Figure 4. Heterogeneity in the amino acid sequence of both α- and β-tubulin carboxy-terminal tails. Single-letter codes of amino acids starting at the last amino acid of the folded tubulin bodies. Amino acids in the unstructured C-terminal tails are colour-coded according to their biochemical properties. The C-terminal tails of both α- and β-tubulin are highly acidic due to a large number of glutamate residues. Adapted from (Janke 2014).

Molecular cloning of tubulin genes in the late 1970s led to the discovery of different tubulin isotypes (Cleveland, Kirschner, and Cowan 1978; Cleveland et al. 1980). Initially these isotypes were expected to form individual MTs, however it was later found that tubulin isotypes can freely intermingle and thus assemble into mosaic MTs (Lewis, Gu, and Cowan 1987). In addition, it has been demonstrated that the expression of different tubulin isotypes is cell-specific and regulated in a developmental manner. For instance, β-tubulin isotype TUBB3 (βIII-tubulin) is known to be a marker for neuronal MTs, while TUBB1 (βVI-tubulin) is expressed specifically in blood platelets and megakaryocytes (Leandro-Garcia et al. 2010; Wang et al. 1986). A recent study about the isotype pool of platelet MTs has shown that TUBA4A (α4A-tubulin) is enriched during the late phases of megakaryocyte differentiation (Strassel et al. 2019). In mice, embryonic suppression of βIII-tubulin expression in the neurons led to migration defects of neurons, and these defects could not be rescued by expression of other β-tubulin isotypes (Saillour et al. 2014). In Drosophila melanogaster, β3-tubulin is expressed primarily in tissues of mesodermal origin in pupae and embryos during development (Kimble, Incardona, and Raff 1989). Furthermore, it has been reported that the α-tubulin isotypes TUBA1A and TUBA8 have distinct functions in organizing neuronal MTs (Belvindrah et al. 2017; Kawauchi 2017). Thus, it is established that different cell types could have a distinct expression of tubulin isotypes, and these isotypes can perform unique functions in maintaining cellular homeostasis.

The discovery of a growing number of mutations in tubulin genes in a variety of human diseases have provided further insights into the functional importance of tubulin isotypes. Tubulin mutations are famously associated with a wide spectrum of neurological disorders (reviewed in (Chakraborti et al. 2016)). Strikingly, different mutations in the same tubulin gene can leads to distinct disease phenotypes, suggesting the position of mutation on the tubulin also plays a role in altering the molecular properties of tubulin, and thus, in the disease phenotype.

The molecular mechanism of how specific tubulin isotypes regulate MT functions are not yet completely clear. The major challenge in studying molecular mechanism of tubulin isotypes is the difficulty to purify specific isotype for in vitro studies. A first study using chimeric yeast tubulin suggested that tubulin isotypes could affect the interaction of MTs with its interacting partner proteins, in particular those containing unique amino acids in their C-terminal tails, such as mammalian β3-tubulin (Sirajuddin, Rice, and Vale 2014a). The recent development of new methods to purify recombinant tubulin (Minoura et al. 2013a; Vemu et al. 2016) or tubulin from

different sources (Widlund et al. 2012a; Souphron et al. 2019) will allow for the development of novel approaches to understand the molecular functions of tubulin isotypes, thus helping to understand their roles in cellular homeostasis and diseases.

1.2.3.2. Tubulin post-translational modifications

Tubulin PTMs are the second component of the tubulin code. PTMs are a general mechanism of regulating the functions of a protein. PTMs are generated by the addition of molecules to defined amino acids (modification sites) of target proteins, catalysed by modifying enzymes. Most PTMs are also reversible, and this step is catalysed by demodifying enzymes.
Tubulin undergoes a wide range of PTMs. Generally, PTMs that target the structured tubulin body might affect intrinsic properties of MTs, such as stability and dynamics, while PTMs on tubulin C-terminal tails are expected to predominantly regulate MT-MAP interactions.
Some tubulin PTMs are mono-modification, such as acetylation and phosphorylation, which add only one molecule to the tubulin target site. Other PTMs such as polyglycylation and polyglutamylation are polymodifications, which generate chains of amino acids of varying length on a given modification site. Mono-modifications are generally considered as binary signals (on and off modes), and polymodifications on the other hand could act as progressive regulators, and might be responsible for the fine-tuning of protein interactions with MTs (van Dijk et al. 2007) (Valenstein and Roll-Mecak 2016).

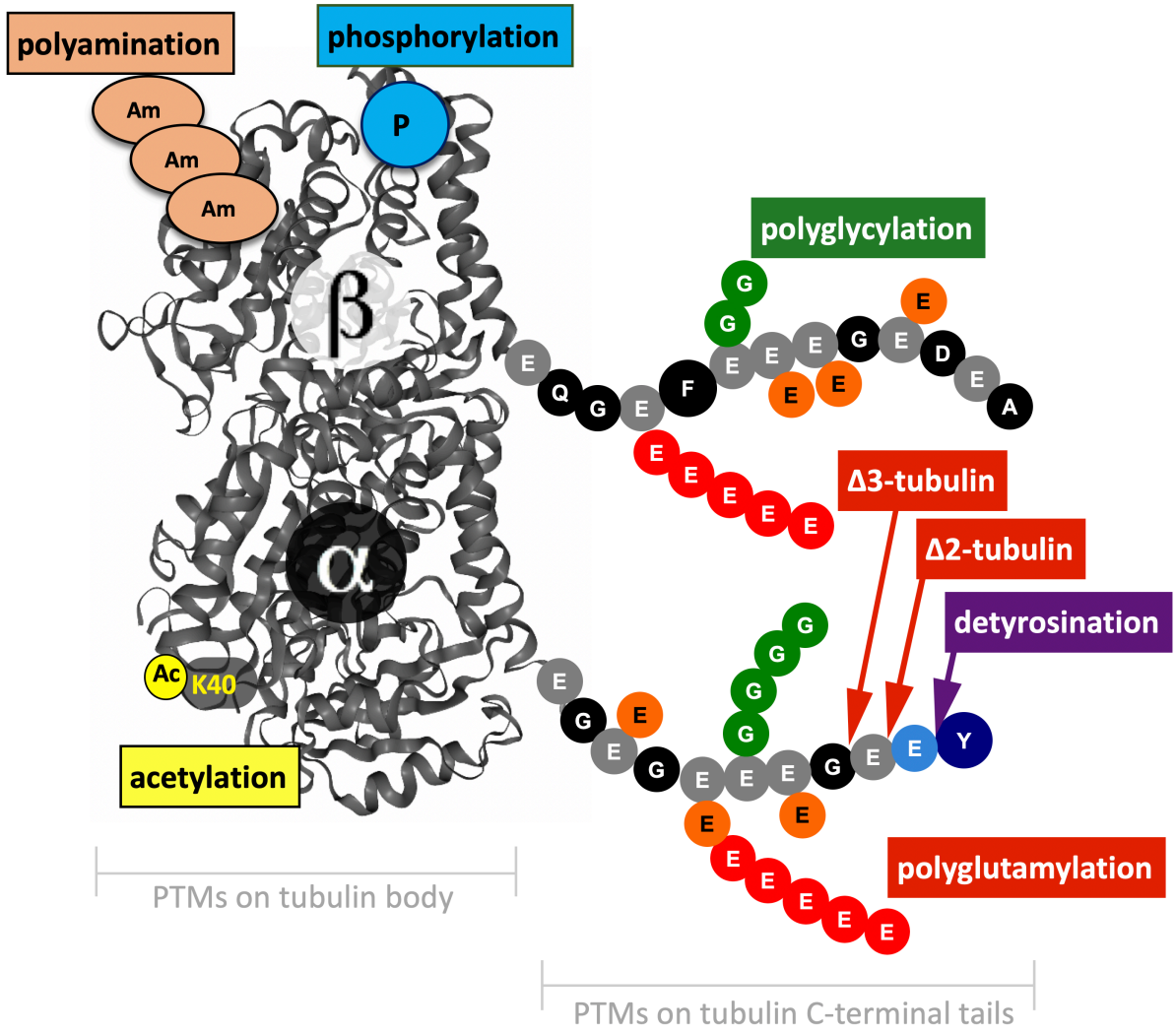

Figure 5. Major posttranslational modifications of tubulin.
Polyamination (Am), phosphorylation (P) and Acetylation (Ac) are the major tubulin PTMs on the folded globular tubulin core, while polyglycylation, polyglutamylation, detyrosination, and C-terminal Δ2- and Δ3-tubulin modifications occur on the unstructured C-terminal tubulin tails that project away from the MT lattice. Adapted from (Magiera and Janke 2014).

Several tubulin PTMs were shown to occur on both α- and β-tubulin, such as phosphorylation (Caudron et al. 2010; Sgro et al. 2016), polyamination (Song et al. 2013), ubiquitylation (Huang, Diener, and Rosenbaum 2009; Ren, Zhao, and Feng 2003b), arginylation (Wong et al. 2007), glycosylation (Hino et al. 2003), sumoylation (Panse et al. 2004; Rosas-Acosta et al. 2005), palmitoylation (Caron 1997; Caron et al. 2001; Wolff 2009), methylation (Park et al. 2016; Xiao et al. 2010), acetylation (L'Hernault and Rosenbaum 1985), detyrosination (Arce et al. 1975), polyglutamylation (Edde et al. 1990), polyglycylation (Redeker et al. 1994), and Δ2-tubulin modifications (Hallak et al. 1977; Johnson 1998). A number of these PTMs are common to other proteins as well, and many of them are not well characterized for tubulins. The best characterized tubulin PTMs are detyrosination/tyrosination, polyglutamylation, polyglycylation and acetylation. The detyrosination/tyrosination cycle is specific to tubulin. Polymodifications such as polyglutamylation and polyglycylation have been initially discovered on tubulin, but have also other substrates that are so far barely characterized (van Dijk et al. 2008b; Sun et al. 2016). Most of the well-studied PTMs occurs at the tubulin C-terminal tails, except tubulin acetylation which occurs at the tubulin body (Fig. 5). As these hot spots of tubulin PTMs are unstructured and projected outside the MT lattice, it is highly likely to play as a key regulator of interactions with MAPs. Therefore, it is crucial to strictly control the tubulin modifications to maintain functions of MT cytoskeleton for cellular homeostasis.

Tubulin undergoes many different PTMs on both tubulin body and C-terminal tails. Here I discuss only the best-characterized tubulin PTMs in detail. This includes detyrosination/ tyrosination, Δ2- and Δ3-tubulin modification, polyglutamylation, polyglycylation and acetylation.

Detyrosination/ tyrosination

Almost all the α-tubulin genes encode a C-terminal tyrosine residue (Fig. 4) that can be removed (detyrosinated) and added back (retyrosinated). Thus, tubulin C-terminal tyrosine undergoes cycles of detyrosination and retyrosination events. The enzymatic addition of tyrosine to tubulin was the first reported tubulin modification (Arce et al. 1975), and later it was shown that the modification is reversible (Hallak et al. 1977). Tyrosination of tubulin is catalysed by an enzyme called Tubulin Tyrosine Ligase (TTL) (Raybin and Flavin 1975) (Fig. 6A) and removal of tyrosine is catalysed by tubulin carboxypeptidases (TCPs) composed of vasohibins (VASH1 and VASH2), together with the small vasohibin binding protein (SVBP)

(Aillaud et al. 2017; Nieuwenhuis et al. 2017) (Fig. 6A). TTL prefers soluble tubulin heterodimers as substrate over MTs (Prota et al. 2013; Raybin and Flavin 1975), whereas TCP detyrosinates tubulin on the assembled MTs (Kumar and Flavin 1981). Recent studies revealed the structural basis of the activity of vasohibin-SVBP complex showing the key residues responsible for the recognition and removal of tyrosine (Adamopoulos et al. 2019; Li, Hu, et al. 2019; Liao et al. 2019; Wang, Bosc, et al. 2019). Due to the exposure of penultimate glutamate at the C-terminal tail, detyrosinated tubulin was initially referred to as Glu-tubulin (Gundersen, Kalnoski, and Bulinski 1984). With the discovery of polyglutamylation modification (Edde et al. 1990), it has since been changed to detyr-tubulin to avoid confusion.

Most of the cell types have both tyrosinated and detyrosinated tubulin. However, detyrosinated MTs have been linked mostly on long-lived MTs in the cells such as neurons. Studies show that detyrosination makes the MTs less vulnerable to depolymerization by mitotic centromere-associated kinesin (MCAK) and the neuronal kinesin family member 2A (KIF2A) (Peris et al. 2006). In agreement with these results, an overgrowth of MTs was observed in mice lacking TTL in which detyr-tubulin is strongly accumulated (Erck et al. 2005). Besides, a variety of motor proteins was shown to be regulated by detyrosination, which includes kinesin-1 (Dunn et al. 2008; Kaul, Soppina, and Verhey 2014; Konishi and Setou 2009; Kreitzer, Liao, and Gundersen 1999; Liao and Gundersen 1998), kinesin-2 (Sirajuddin, Rice, and Vale 2014a), and the mitotic kinesin motor centrosome-associated protein E (CENP-E) (Barisic et al. 2015). Interestingly, dynein in complex with dynactin and BicD2 showed a strong preference to tyrosinated MTs (McKenney et al. 2016). Furthermore, tubulin tyrosination has also been demonstrated to regulate the interaction of cytoplasmic linker protein 170 (CLIP-170), a plus-end MT binding protein (Bieling et al. 2008a; Nirschl et al. 2016; Peris et al. 2006).

Δ2- and Δ3-tubulin

The Δ2-tubulin modification is characterised by the absence of two penultimate amino acid residues (-Glu-Tyr), and Δ3-tubulin by the absence of three amino acids (-Glu-Glu-Tyr) from the C-terminal tubulin tails. Following the removal of tyrosine from the tubulin C-terminus, detyrosinated tubulin can be further converted into Δ2-tubulin by the removal of a penultimate glutamate residue (Fig. 6B). Δ2-tubulin is an irreversible modification generated by enzymes from cytosolic carboxypeptidase (CCPs) family (Fig. 6B). CCP enzymes are also responsible for the generation of Δ3-tubulin (Aillaud et al. 2016; Berezniuk et al. 2012). Neither Δ2- nor Δ3-tubulin can be tyrosinated, as the presence of two consecutive glutamates at the C-terminus

of α-tubulin are required for the activity of TTL (Rudiger, Wehland, and Weber 1994; Prota et al. 2013). To date, there have been no reports showing any specific roles of Δ2-tubulin and Δ3-tubulin in any cellular functions. However, it is assumed that the inability of retyrosinating Δ2-tubulin leads to a detyrosinated-locked state, which is one of the reasons for the stabilization and specialized MT functions in neurons and axonemes (Konno, Setou, and Ikegami 2012). More studies need to be conducted for the understanding of the molecular functions of Δ2- and Δ3-tubulin modifications in the regulation of MT functions.

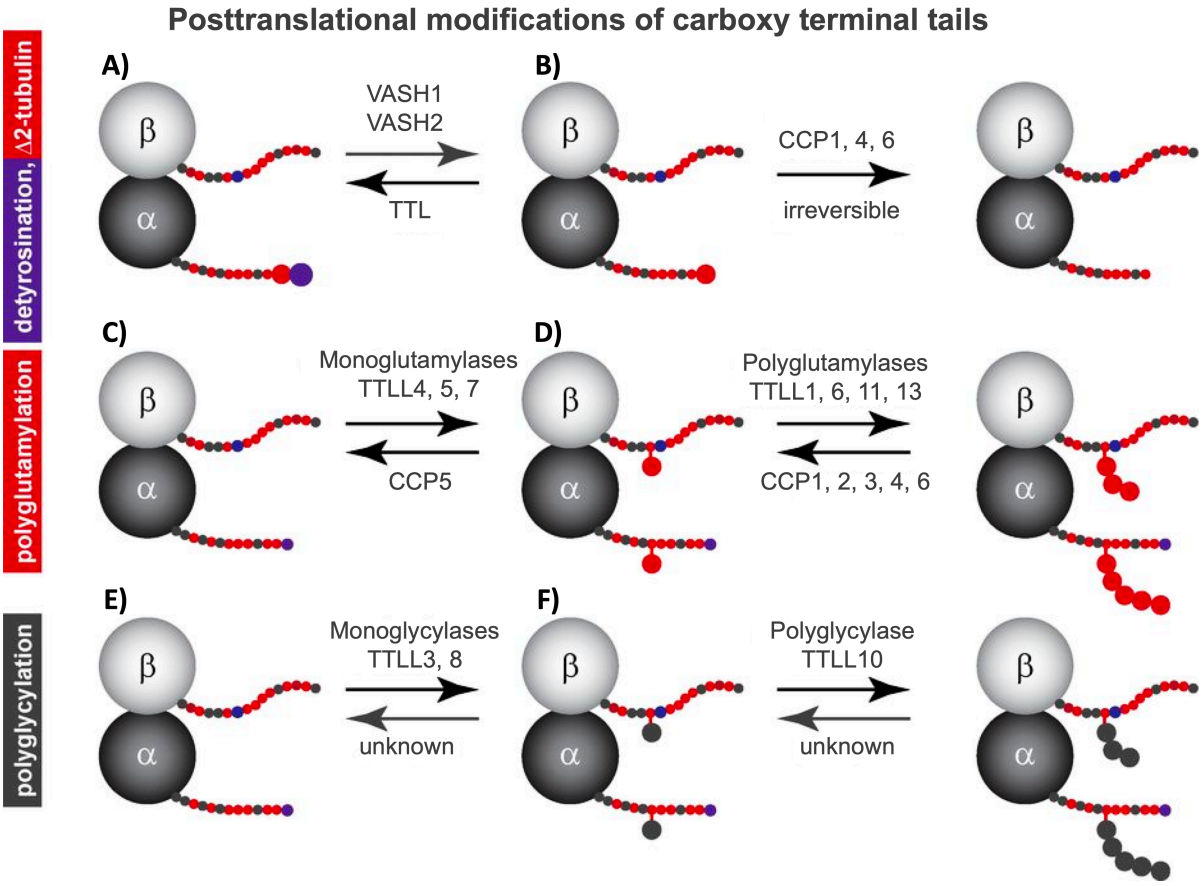

Figure 6: Enzymes responsible for the modification of tubulin C-terminal tails.
A) Detyrosination of α-tubulin is catalysed by VASH1 and VASH 2 enzymes, and tyrosination is catalysed by Tubulin Tyrosine Ligase (TTL). **B)** CCP1, 4 and 6 generate Δ2-tubulin by removing the penultimate C-terminal glutamate residue of the detyrosinated α-tubulin. **C)** Monoglutamylases TTLL4, 5 and 7 initiate catalytic addition of glutamate at the branchpoint of both α- and β-tubulin C-terminal tails, and CCP5 can remove the branchpoint glutamate. **D)** Polyglutamylases TTLL1, 6, 11 and 13 elongate the glutamate side chain, and CCP1, 2, 3, 4 and 6 can shorten the elongated glutamate chains. **E)** Monoglycylases TTLL3 and 8 initiate the catalytic addition of glycine at the branchpoint of both α- and β-tubulin C-terminal tails, polyglycylase TTLL10 elongates the glycine side chain. The enzymes responsible for the removal of the glycine side chain is still unknown. Adapted from (Janke and Magiera 2020).

Tubulin glutamylation

Tubulin polyglutamylation is the catalytic addition of a variable number of glutamate residues onto the γ-carboxyl group of a glutamate acceptor residue in the tubulin C-terminal tail. Tubulin glutamylation was first reported on α-tubulin from brain tissue in 1990 (Edde et al. 1990), and later found on two different β-tubulin isotype (Rüdiger et al. 1992; Alexander et al. 1991).

Using biochemical and immunological methods, the first multiprotein complex having glutamylase activity was purified from mouse brains (Regnard et al. 2003), and demonstrated to contain the catalytic TTL-like1 (TTLL1) subunit (Janke et al. 2005). Strikingly, TTLL1 alone does not have any enzymatic activity; it works as a multiprotein complex (Janke et al. 2005). TTLLs have homology with the TTL enzyme that catalyses tubulin tyrosination (Ersfeld et al. 1993). The discovery of TTLL1 bolstered in the identification of other enzymes in the TTLL family. In mammals, there are seven well-characterized glutamylases in TTLL family: TTLL1, 4, 5, 6, 7, 11 and 13. Among those, TTLL1, 5, 6, 11 and 13 preferentially modify the α-tubulin, whereas the TTLL4 and 7 are specific for β-tubulin (van Dijk et al. 2007) (Fig. 6). In addition, TTLL4, 5 and 7 preferentially catalyse the initiation reaction by adding the first glutamate residues of the side chain, whereas TTLL1, 6, 11 and 13 preferentially elongate these chains (van Dijk et al. 2007).
Deglutamylating enzymes belong to the Cytosolic Carboxypeptidase (CCP) family (Kimura et al. 2010; Rogowski et al. 2010). Similar to glutamylases, deglutamylases also have preferences, such as shortening long side chains versus removing the branched residues. In addition, CCPs also deglutamylate other protein substrates with gene-encoded C-terminal glutamate residues (Rogowski et al. 2010).

Early immunostaining studies with GT335, a glutamylation-specific monoclonal antibody (Wolff et al. 1992), showed that glutamylation gradually enriches on MTs during neuronal differentiation (Audebert et al. 1993; Audebert et al. 1994), as well as on ciliary and flagellar axonemes (Fouquet et al. 1994). Besides, studies have shown that glutamylation can also occur on other proteins (van Dijk et al. 2008a).

There is growing evidence showing the role of tubulin polyglutamylation in the regulation of MT functions by interacting with several MAPs and motor proteins. For example, it has been demonstrated that polyglutamylation could regulate the activity of MT severing enzymes

spastin and katanin (Lacroix et al. 2010; Valenstein and Roll-Mecak 2016; Shin et al. 2019). In case of spastin, when the TTLL6, a polyglutamylase adding long glutamate chains was expressed in cells, the number of MTs was reduced dramatically, in contrary this was not the case when the TTLL4, an enzyme that generates short glutamate chains, was expressed in cells. These results demonstrate the importance of strict regulation of glutamate side-chain length (Lacroix et al. 2010). Similar to spastin, a recent study with katanin showed that TTLL7, a polyglutamylase that modifies mostly β-tubulin could induce MT severing, but not for spastin (Shin et al. 2019). This suggests differential polyglutamylation on α- or β-tubulin also might affect the severing activity. In addition, it has been shown that tubulin polyglutamylation activates spastin-mediated MT severing in a non-linear, biphasic manner. That is, MT severing occurs in a window of polyglutamylation levels determined by the number of glutamate residues on the side chain (Valenstein and Roll-Mecak 2016).

Earlier studies with neuronal MAPs such as tau, MAP1 and MAP2 show that polyglutamylation might influence their binding behaviour to MTs (Boucher et al. 1994; Bonnet et al. 2001).
A recent observation has shown that glutamylation can influence the behaviour of MT motor proteins. In vitro experiments with MT reconstitution and TIRF microscopy using chemically mimicked polyglutamylation on tubulin chimeras strongly suggested that polyglutamylation could regulate the velocity and processivity of motor proteins (Sirajuddin, Rice, and Vale 2014b). A recent in vitro study suggests that the pausing and motility of kinesin-3 family member, KIF1A was affected by tubulin polyglutamylation (Lessard et al. 2019). Tubulin polyglutamylation was also suggested to selectively influence the intracellular transport driven by different MT motor proteins. Neurons cultured from mice lacking TTLL1 showed an altered localization of KIF1A, but not KIF3A and KIF5 motor proteins. Perturbed KIF1A motility was linked to synaptic transmission defects, as KIF1A is involved in carrying synaptic cargoes (Ikegami et al. 2007). Indeed, very recent studies demonstrated that tubulin polyglutamylation has a direct role in the regulation of axonal transport (Gilmore-Hall et al. 2019; Magiera, Bodakuntla, et al. 2018; Bodakuntla et al. 2020).

Tubulin glycylation

Polyglycylation is the second type of polymodifications, initially discovered on axonemal α- and β-tubulin of Paramecium (Redeker et al. 1994). Polyglycylation is the catalytic addition of one or more glycine residues on a glutamate acceptor cite within the C-terminal tails of tubulin.

Similar to glutamylases, glycylases also belongs to the TTLL family. There are three glycylases known in mammals: TTLL3, 8 and 10 (Fig. 6) (Rogowski et al. 2009). All three TTLLs modifies both α- and β-tubulin, nonetheless TTLL8 and 10 show a preference for α-tubulin (Rogowski et al. 2009). TTLL3 and 8 are monoglycylases that catalyse the initial transfer of a glycine residue onto a receptor glutamate residue in the C-terminal tail, whereas TTLL10 is the only known polyglycylase which elongates the glycine side chains (Fig. 6). In human sperm, the flagellum is found to have only monoglycylation and not polyglycylation (Bre et al. 1996). Later it was shown that TTLL10 is not active in humans due to two mutations in its catalytic domain, suggesting elongation of glycine side chain might not be essential for this modification (Rogowski et al. 2009). To date, there are no deglycylases reported.

In comparison to glutamylation, glycylation is less broadly represented PTM. Initial studies using AXO49 and TAP952 antibodies for glycylation detected only axonemes of cilia and flagella, but no other MT species (Bre et al. 1996; Bressac et al. 1995; Levilliers, Fleury, and Hill 1995) has so far been only observed on the axonemes of cilia and flagella.
An observation in mouse ependymal multicilia reveals that monoglycylation is found early during cilia maturation, and polyglycylation is detectable only in the matured multi-cilia. In addition, inactivation of TTLL8 and TTLL3 in mouse provokes loss of multicilia in the brain ependymal cells (Bosch Grau et al. 2013).

Inactivation of TTLL3A in Tetrahymena leads to defects in ciliary axoneme such as shortened axonemes, rotated peripheral doublets and lack of MT central pairs. Silencing of TTLL3 in zebrafish led to right-left axis defects in embryos (Wloga et al. 2009). Strikingly, the level of tubulin glutamylation in cilia increases upon the suppression of glycylation in several ciliated tissues, suggesting that glycylation and glutamylation levels are inversely correlated (Wloga et al. 2009). In drosophila, depletion of the glycylase TTLL3B led to the disassembly of sperm axonemes during sperm maturation (Rogowski et al. 2009). In mouse ependymal cells, shRNA-mediated depletion of TTLL8 in a TTLL3-knockout mouse also led to the loss of motile cilia (Bosch Grau et al. 2013). These complementary data suggested that glycylation has a role in the maintenance of axonemes. In total, these studies confirm glycylation is crucial for the normal function and structure of axonemes.

Tubulin acetylation

Tubulin acetylation was the second tubulin modification to be discovered. It was identified in flagellar α-tubulin of Chlamydomonas reinhardtii (L'Hernault and Rosenbaum 1985). Unlike other tubulin PTMs, acetylation was found at the inner lumen of polymerized MTs at the Lysine 40 (K40) residue of α-tubulin (Maruta, Greer, and Rosenbaum 1986). The K40-acetylation of tubulin is catalysed by the tubulin acetyltransferase α-TAT1 (Mec17 in C. elegans) (Akella et al. 2010; Shida et al. 2010), and the acetylation is removed by histone deacetylase 6 (HDAC6), or sirtuin 2 (SIRT2 (North et al. 2003)). α-TAT1 is known to be specific for the α-tubulin (Kalebic et al. 2013), whereas HDAC6 and SIRT2 can also deacetylate substrates other than tubulin. Another study showed that acetylation also occurs at Lysine 252 (K252) of β-tubulin, and is catalysed by acetyltransferase SAN (Chu et al. 2011). This acetylation is located at the contact side in between tubulin heterodimers, and shown to cause difficulties for the incorporation of dimers into MT lattice. It might therefore have an effect on MT dynamics (Chu et al. 2011).

Like most tubulin PTMs, acetylation of K40 is enriched in cilia and sperm axonemes, and neurons. Acetylation levels of cytosolic MTs also increase in cultured cells treated with taxol (Schulze et al. 1987). Since tubulin K40 acetylation appears after the assembly of MTs and labelled mostly long-lived MTs, it was considered a marker for the age and stability of MTs (Piperno, LeDizet, and Chang 1987). For a long time, there was a lack of evidence showing the direct role of tubulin acetylation and MT stability. A recent study showed that tubulin acetylation protects long-living MTs against mechanical stress by facilitating the self-repair of MTs (Portran et al. 2017; Schaedel et al. 2015). Strikingly, tubulin acetylation has also been suggested to activate MT-severing enzymes, which might confuse the link between acetylation and MT stability. Nevertheless, another recent study showed that MT severing could help MT to self-repair (Vemu et al. 2018) and increase rather than diminish the MT mass in cells (Kuo et al. 2019).

It remains unexplored how a PTM in the MT lumen could regulate the interaction of MTs with different interacting proteins on the outer surface. Recent studies show that MT inner proteins (MIPs), such as MAP6/ STOP (Cuveillier et al. 2020), bind in the lumen of MTs. Further studies need to be performed to understand the role of acetylation in the binding characteristics of MIPs and also other MAPs.

1.3. Microtubule Associated Proteins (MAPs)

MAPs are a group of proteins which can directly interact with MTs, and control the dynamic properties, structure of MTs, as well as their interactions with membranes, organelles and other protein complexes. MAPs have been initially identified as proteins co-pelleting along with MTs in the biochemical process of tubulin purification from porcine, bovine or ovine brains. These early experiments led to the discovery of the first MAPs such as MAP1 and MAP2, but with the invention of new techniques such as GFP-screening strategy (Manabe et al. 2002a), immunostaining (for MT-MAP colocalization) and sequencing, we now know more than 100 proteins in the MAP family in mammals (for the history and timeline of MAP discoveries, see our review (Bodakuntla et al. 2019), annex 6.1). Interestingly, new MAPs have been discovered and reported not only by researchers working on MTs, but also by those working in other domains. Because of these parallel discoveries, the nomenclature of this group of proteins is complicated, sometimes confusing, and many MAPs have more than one name. Later on, based on their specific MT localization and functions, MAPs are classified into different subgroups.

In general, MAPs can be subdivided into four major categories: molecular motors, MT-severing proteins, plus- and minus-tip-binding proteins (+TIPs or -TIPs), and structural MAPs (often referred to simply as MAPs). Each of these MAP categories is briefly described in the following chapters. However, my project focuses mainly on the members of the structural MAPs subgroup.

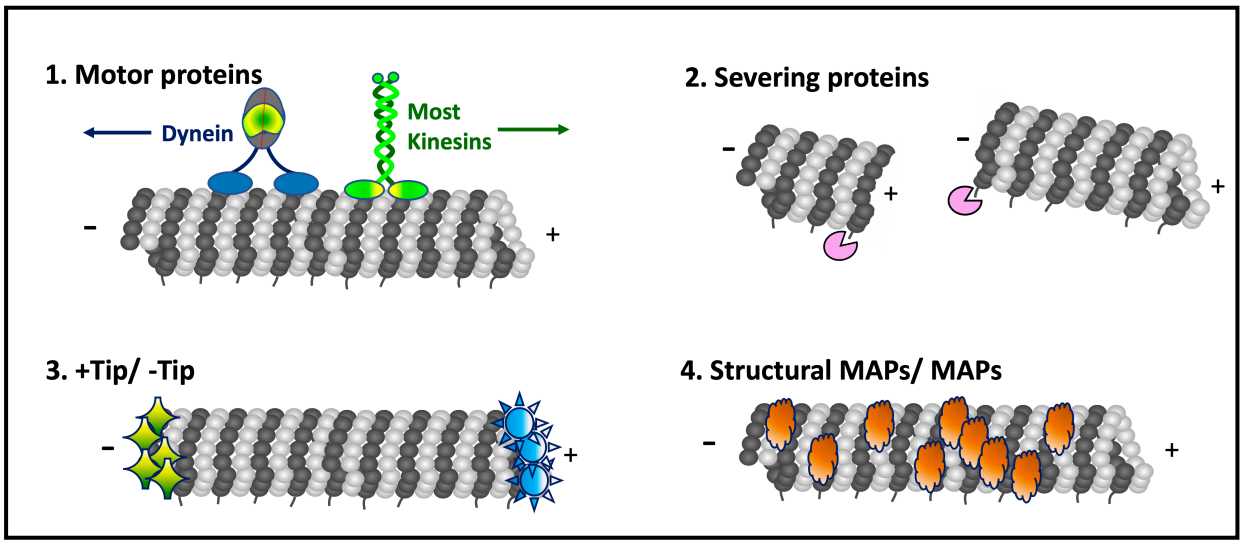

Figure 7: Classification of Microtubule-Associated Proteins (MAPs). There are four major categories of MAPs, which includes MT motor proteins, comprising kinesins (most kinesin walk towards MT plus end) and dyneins (walking towards the minus end of MTs), MT severing enzymes, TIPs which accumulate on either plus ends (+TIPs) or minus ends (-TIPs) of the MTs, and structural MAPs that decorate the whole MT lattice without any general preference in localization.

1.3.1. Molecular motor (Kinesin and Dynein)

MT-based molecular motors include kinesins and cytoplasmic dyneins. Both groups of molecular motors are ATP-driven proteins. In the kinesin superfamily (KIF) proteins, most kinesins walk towards the MT plus end, while all dynein motors walk towards the minus end (Hirokawa et al. 2009).

Kinesins

There are 45 kinesin superfamily genes in the mouse, which are further classified into 15 families (Hirokawa et al. 2009). The first kinesin molecule was reported in 1985 (Vale, Reese, and Sheetz 1985). Kinesin-1 is a heterotetramer protein comprising two heavy chains and two light chains, and can be further subdivided into three regions: head, stalk/ neck and tail. The motor function is performed by the globular head region that has a MT binding site and an ATPase site (Goldstein 1995). The stalk or neck region forms a continuous coiled coil structure, which could act as a rigid lever. The C-terminal tail domain is a fan-shaped structure and is thought to be having a role in cargo binding and directionality (Hirokawa et al. 1989; Woehlke and Schliwa 2000; Duselder et al. 2015). The kinesin light chains (KLCs) associate with the heavy chains by interacting through the stalk and tail domains. Additionally, there are different light chain isoforms, and they are proposed to play a regulatory role in controlling the specificity of cargo types (Burkhardt 1998). For some kinesins, adaptor or scaffold proteins are required to link the motor to the vesicles or other cargoes such as TRAK1 (Hirokawa et al. 2009; Brickley and Stephenson 2011).

The general mechanism and regulation of some of the kinesin-mediated transport types are explored with the technological advancement in microscopy and structural biology. Different PTMs of the kinesin proteins and/or complex formations by differential interactions with the adaptor proteins might determine the kinesin–cargo combinations. Further details are reviewed in (Hirokawa et al. 2009; Verhey and Rapoport 2001).

The cellular functions of kinesins include transport of vesicles and organelles. Kinesins also takes part in mitosis and meiosis, such as in attaching chromosomes to the spindle, in spindle assembly and separation of chromosomes. Also, kinesins have a crucial role in the dynamic properties of MTs. For instance, kinesin-13 or MCAK (Mitotic centromere-associated kinesin) has a depolymerizing activity on MTs (Endow, Kull, and Liu 2010). Interestingly, some of the

kinesins act as therapeutic targets for diseases like cancer (Wacker and Kapoor 2010). Further details are reviewed in (Endow, Kull, and Liu 2010).

Kinesin-associated diseases are inked to faulty transport of cell cargoes, transport of pathogens or pathogenic components and defective motor functions. Based on the type of cargoes, we can categorize the disease types: one, in which the physiological cargoes are not transported normally (e.g. perturbations and clogging of cargoes in axonal transport), and another is when non-physiological cargoes (viral particles or other pathogen invasions) take control over normal kinesin transport. Further details can be found in (Mandelkow and Mandelkow 2002; Goldstein 2001).

Dyneins

In contrast to kinesins, dynein motors require adaptor proteins to bind to MTs. Dyneins are involved in wide range of cellular functions such as in ciliary trafficking, in cell division and in transport of organelles and vesicles. Based on function and structural criteria, the dynein family of proteins can be split into two categories: axonemal dynein, responsible for the beating of cilia and flagella, and cytoplasmic dyneins involved in mitosis, intracellular transport, cell movement and cell polarization (Gibbons and Rowe 1965) (Paschal, Shpetner, and Vallee 1987) (Paschal and Vallee 1987; Hook and Vallee 2006; Olenick and Holzbaur 2019; Reck-Peterson et al. 2018).

Dyneins are multi-subunit proteins, each comprised of 1-3 heavy chains containing the motor domains, accessory subunits (light intermediate chains, intermediate chains, light chains) and a stalk with a globular structure to interact with the MTs. In the heavy chain, there are two prominent structures: a small N-terminal domain, which forms the base of the molecule and interacts with accessory subunits, and a big motor domain, which has AAA ATPase units. The energy released upon ATP hydrolysis by the AAA units is carried to the MT-binding stalk in the base of the molecule, where it generates the force inducing the displacement of the protein (Gee, Heuser, and Vallee 1997). The stalk of the dynein is an anti-parallel coiled-coil structure with a globular part that associates with MTs. The presence or absence of accessory subunits varies based on their function as axonemal or cytoplasmic dyneins (Hook and Vallee 2006). Recent studies show that dynein requires many activators and adaptor proteins for its function, which is reviewed in (Olenick and Holzbaur 2019; Reck-Peterson et al. 2018).

The cellular functions of cytoplasmic dyneins include transport of a wide range of cargoes, such as membrane cargoes (endoplasmic reticulum, Golgi apparatus, melanosomes, autophagosomes, mitochondria, peroxisomes), RNA cargoes (transport of mRNA), protein cargoes (aggresomes and misfolded proteins), transcription factors, transport of intermediate filaments and microtubules, centrosomal components and viruses. Among these some cargoes are transported actively along MTs by dynein, while for others dynein helps to position them. Further details are reviewed in (Reck-Peterson et al. 2018).

Dynein is also an integral part of the MT-based structure at the centre of flagella and cilia, called axonemes. Coordinated binding and unbinding of axonemal dyneins slides MTs and causes the axoneme structures to bend, thus generating the characteristic flagellar and ciliary beat. Most of the axonemal dyneins are anchored on axonemes except for two - dynein 1B and dynein 2, responsible for intraflagellar transport (IFT) (Kardon and Vale 2009).

Cytoplasmic dynein is regulated through allosteric mechanisms that lead to the active and inactive dynein conformations. Also, dynein motor functions can be altered by the association with other molecules such as LIS1, NudE, NdEL, Bicaudal D and spindly (Vallee, McKenney, and Ori-McKenney 2012; Chen et al. 2014). Recent studies show that deletion of the tubulin C-terminal tails reduces the processivity of yeast cytoplasmic dynein *in vitro* (Grotjahn and Lander 2019). There is also evidence suggesting that dynein is associated with neurodevelopmental disorders (Chen et al. 2014; Eschbach and Dupuis 2011). Mutations in dynein 2 (DYNC2H1), which is involved in IFT, cause short rib polydactyly syndrome (SRP) type III and Jeune asphyxiating thoracic dystrophy (JATD). Both diseases lead to shortened tubular bones and ribs (Hou and Witman 2015).

1.3.2. MT-depolymerising MAPs

MT severing was first observed in Xenopus egg extracts in 1991 (Vale 1991). Two years later, the first severing enzyme katanin was purified from sea urchin eggs (McNally and Vale 1993). Later, two other enzymes were added in to this family of proteins: spastin and fidgetin (Hazan et al. 1999; Frickey and Lupas 2004). All severing enzymes are grouped in the AAA protein superfamily, and require chemical energy from ATP hydrolysis. Severing enzymes are involved in many cellular functions such as in morphogenesis, mitosis and meiosis, cilia biogenesis, axon guidance and cell migration. More information about the discovery, cellular localization, mechanism of action and structural aspects of each severing enzyme are reviewed in (Sharp and Ross 2012; Roll-Mecak and McNally 2010).

In addition to these three major severing enzymes, vertebrates also contain paralogues: katanin-like1, katanin-like2; fidgetin-like 1 (FIGNL1) and fidgetin-like 2 (FIGNL2). Among these, FIGNL1 was shown to bind MTs *in vitro* (Fassier et al. 2018), but the functions of other paralogues are relatively less studied.

Similar to the severing enzymes, there are also MT depolymerizers or destabilizers, which induce MT disassembly, however their mode of action on the MT is different. Some examples of MT depolymerizers are MCAK in kinesin-13 family of proteins (Desai et al. 1999), ELP70 (EMAP-like protein-70) or EML2 (Echinoderm MAP like Protein-2) (Eichenmuller et al. 2002), and FOR 20 (FOP-related protein of 20 kDa) (Feng et al. 2017).

1.3.3. Plus- and Minus-TIPs (+TIPs and -TIPs)

A group of proteins associated with dynamic MT ends are called TIPs. The +TIP group of MAPs binds prominently to the growing or plus tip of the MT, and the -TIP group of proteins binds prominently at the minus end. End binding proteins (EB1, EB2 and EB3), XMAP215, some kinesins and dynein are the examples of +TIPs. Patronin in invertebrates and CAMSAP (calmodulin-regulated spectrin-associated proteins) in mammals are examples of -TIPs. The tip-specific binding affinity of this group of proteins is concentration dependent, and outside the physiological range, most of them decorate the entire MT lattice, however with a weaker affinity than the tips (Akhmanova and Steinmetz 2015).

Plus TIPs / +TIPs

MT plus-end tracking proteins or +TIPs typically accumulate at growing MT plus ends. +TIPs like EB1 and CLIP-170 end-track only growing MT ends, and disassociate upon MT shrinkage. On the contrary, the yeast proteins Dam1p and Kar9p can end track both growing and shrinking MTs (Akhmanova and Steinmetz 2010). The first reported +TIP was CLIP-170 (cytoplasmic linker protein of 170 kDa) in 1999 (Diamantopoulos et al. 1999). One signature element of the amino acid sequences of +TIPs in general are the linear sequence motifs such as CH (calponin homology) domain, EBH (EB homology) domain, CAP-Gly domain, and SxIP (Ser-x-Ile-Pro and x can be any amino acids) and EEY/F motifs. These sequences help +TIPs to dynamically interact with each other and with MTs in low concentration ranges. The cellular functions and binding mechanisms of +TIPs are detailed in (Akhmanova and Steinmetz 2010).

Minus TIPs / -TIPs

Minus-TIPs / -TIPs bind prominently to the minus end of MTs. Compared to the +TIPs, -TIPs got less attention in the beginning, possibly because of the less dynamic properties of the MT minus ends. Members of the -TIPs family are calmodulin-regulated spectrin-associated proteins (CAMSAP1, 2 and 3) in mammals and patronin in invertebrates; SPIRAL2 (in plants), as well as ASPM/Asp, and the KANSL complex (Akhmanova and Steinmetz 2019). In addition to this, the major protein complex associated with the MT minus end is the γ-tubulin ring complex (γ-TURC). It has been shown that γ-TURC can act as a template for MT nucleation, and also binds and caps the minus ends of already formed MTs. With the help of an anchoring protein, ninein, the γ-TURC can attach to centrosomes, but also to other cellular structures, such as the apical sides of epithelial cells, or desmosomes, from where it could nucleate non-centrosomal MTs (Akhmanova and Steinmetz 2015). Unlike the plus-end localizing sequence motifs found in +TIPs, there is not much known about any conserved sequences in -TIPs, however a conserved C-terminal CKK domain (CAMSAP, KIAA1078 and KIAA1543 domain) found in all CAMSAPs is important for their minus-end binding property. What has been known so far about the cellular functions and binding mechanisms of -TIPs is reviewed in (Akhmanova and Steinmetz 2019; Akhmanova and Hoogenraad 2015).

1.3.4. Structural MAPs/ MAPs

Structural MAPs or just "MAPs" are a heterogenous group of proteins that bind directly to, and decorate the entire MT lattice irrespective of MT polarity, and are mostly thought to stabilize MTs. The overexpression of most of these MAPs inside cells leads to swift MT bundling and/or protein clumping artefacts due to their unstructured molecular architecture. This might be one of the reasons why many structural MAPs are little explored as compared to the other categories of MT-interacting proteins. There are more than a 100 eukaryotic MAPs reported so far, but among them only very few are biochemically characterized.

1.3.5. Defining a structural MAP

The early definition of a MAP was that any protein that can co-assemble with MTs which polymerize from purified tubulin in vitro, or any protein which co-label with immunostained MTs in cells and detach upon colchicine treatment were called as a MAP (Huber, Alaimo-Beuret, and Matus 1985). This definition is still well-grounded and followed in the MT field. Over the years, 100s of MAPs are reported, and currently, we have four major categories of MAPs: motor proteins, severing enzymes, TIPs and structural MAPs (Bodakuntla et al. 2019). A popular definition of a structural MAP is that if a protein can decorate the entire MT lattice and can stabilize MTs against disassembly, then it is called as a structural MAP. This was demonstrated for several MAPs such as tau, MAP2, MAP7, which were reported earlier using biochemical and molecular studies (Bre and Karsenti 1990; Lewis et al. 1989; Bulinski and Bossler 1994). Strikingly, along with stabilization properties, some of these proteins also showed nucleating and bundling abilities (Borisy et al. 1975; Bechstedt and Brouhard 2012; Bulinski and Borisy 1979; Bulinski and Bossler 1994; Chen et al. 1992; Moores et al. 2006). In addition, recent advancement in microscopic techniques deciphered more molecular functions of structural MAPs such as MAPs as MT depolymerizers, polymerisers, elongators, cytoskeleton crosslinkers, and membrane anchors (Scott et al. 1992; Mollinari et al. 2002b; Bernier et al. 1996; Sawamura et al. 1990b; Bowne-Anderson, Hibbel, and Howard 2015).

In a different perspective, any protein found to interact with MTs is first called a MAP. Upon its biochemical characterisation, its molecular functions might reveal that this new MAP belongs to one of the well-defined MAP categories, such as molecular motor, severing enzymes, or TIPs. Only if the protein does not fit in any of these categories, it remains known

as a structural MAP. For example, a tubulin-modifying enzyme that can decorates MTs might have been considered as a structural MAP until the discovery of its enzymatic activity. Because of this, there are currently more proteins of unknown functions within the group of structural MAPs as compared to other MAP categories. Therefore, development of new high throughput methods to study these poorly studied proteins are important, and their mechanistic characterization might help in our understanding of their possible links to different physiological processes and diseases.

I am a co-author of a review detailing our knowledge about structural MAPs which has been published recently by our lab (Bodakuntla et al. 2019). Please see the **annex section 6.1** for the published article.

1.3.6. Emerging functions of proteins that are previously known as structural MAPs

As discussed above, the term "structural MAP" is used for a heterogenous group of proteins that bind and prevent MTs from disassembly. Growing evidence currently suggests that proteins from the structural MAP category can show distinct functions (Fig. 8). For example, a group of proteins called as MT-inner proteins (MIPs) have recently come into focus as they decorate the luminal side of the MTs (Ichikawa and Bui 2018), and have novel properties in the regulation of MT structure and dynamics (Schmidt-Cernohorska et al. 2019). Some of the examples for MIPs are MAP6/ STOP and FAP 20 (Yu and Galjart 2020; Dymek et al. 2019; Cuveillier et al. 2020).

Two other major functions of structural MAPs known for decades are MT bundling and crosslinking of different cytoskeletal filaments. Upon overexpression in mammalian cells, all bona fide MAPs decorate MTs, and some of them, such as tau, induce bundling of MTs (Barlow et al. 1994; Kanai et al. 1989). Besides, it was shown that a minimal MT-binding domain of tau was sufficed to induce MT bundling in vitro (Scott et al. 1992). Other examples of MT bundlers are PRC1 (Mollinari et al. 2002b), CLASP (Ebina, Ji, and Sato 2019), Spef1 (Zheng et al. 2019), Cep169 (Mori et al. 2015), Cep55 (Zhao, Seki, and Fang 2006), and Xnf7 (Maresca et al. 2005). Strikingly, it has been reported that some MAPs could sense the orientation of MT polarity, such as parallel (e.g. TRIM46 (van Beuningen et al. 2015)) or antiparallel (e.g. PRC1 (Bieling, Telley, and Surrey 2010; Subramanian et al. 2010)) MT arrays. Based on structural data, a

mechanism by which a MAP could promote MT bundling was proposed recently. Upon binding, the negative charge of tubulin C-terminal tail can be neutralized by the positive charge patches on MAPs, thus MAPs could reduce the electrostatic repulsion and can induce MT bundling (Wang et al. 2014). Further studies need to be conducted to test this for all the MT bundlers.

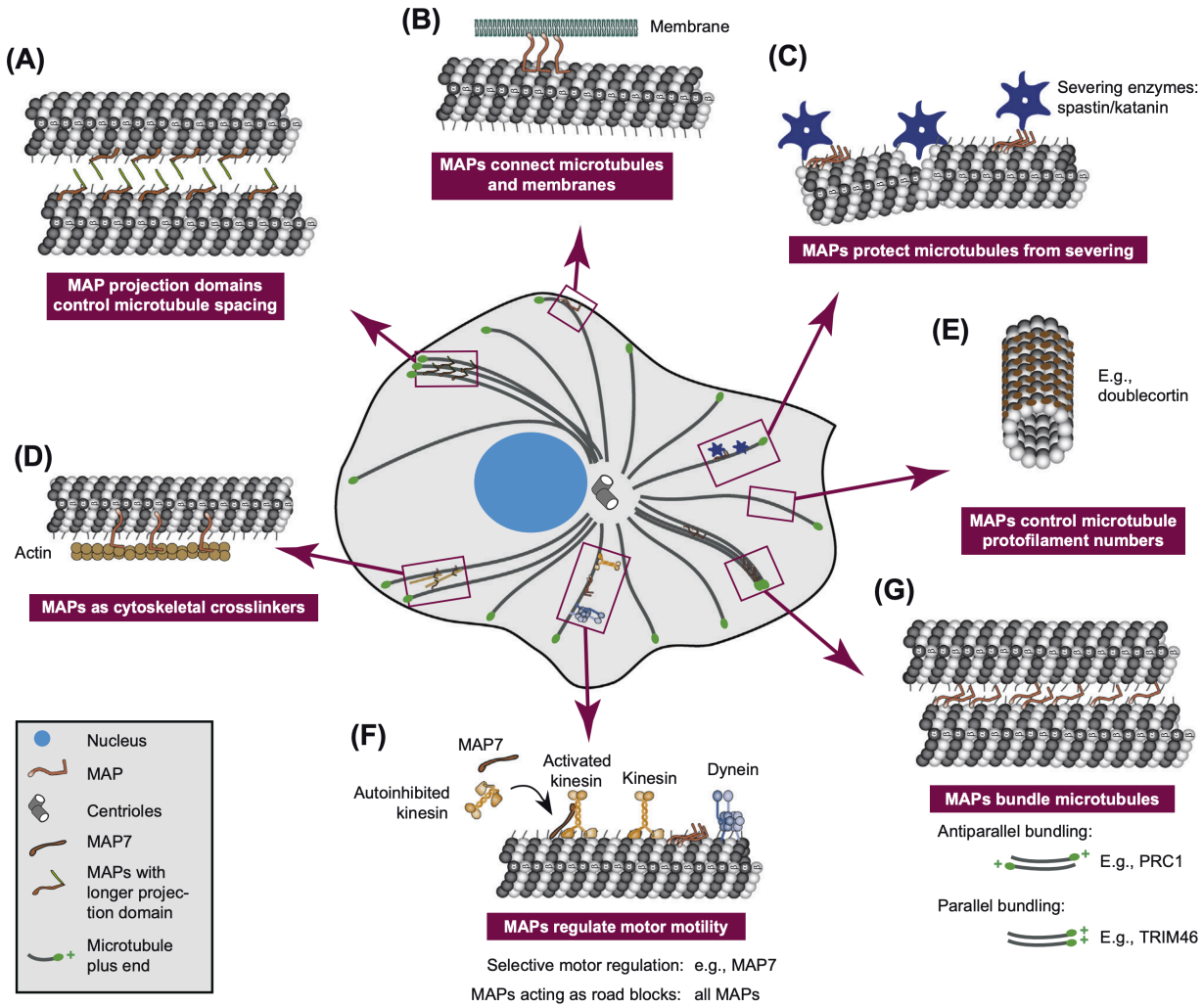

Figure 8: Schematic representation showing emerging functions of proteins that are previously known as structural MAPs. A) MAP binding could influence the spacing between parallel or antiparallel MTs **B)** MAPs could act as linker between MT network and cell membranes **C)** MAPs could protect MTs from severing and thereby prevents from MT disassembly **D)** MAPs could crosslink MTs with other cytoskeletal components such as actin and intermediate filaments **E)** Some MAPs could alter the structural properties of MTs by altering the protofilament number **F)** MAPs could modulate the binding and motility of MT motor proteins, either altering the motility parameters by interacting with them, or by occupying their path at the MT surface **G)** MAPs could promote the parallel or antiparallel MT bundling (adapted from (Bodakuntla et al. 2019)).

Several MAPs showed their potential as a cytoskeletal crosslinker (Fig. 8), which includes MACFs (Bernier et al. 1996) (Sawamura et al. 1990b), MAP2 (Sattilaro 1986), MAP4 (Matsushima et al. 2012), tau (Correas, Padilla, and Avila 1990; Elie et al. 2015), drebrin (Ketschek et al. 2016a), DAAM (Szikora et al. 2017a) and Navigator-1 (Sanchez-Huertas et al. 2020). Among these, MACF1 and MACF2 are the best characterised cytoskeleton crosslinkers. Both proteins interact with all three cytoskeletal components, actin, MTs and intermediate filaments. By contrast, many other MAPs were assumed to be cytoskeletal crosslinkers because they were reported to interact with actin filaments in individual actin-binding experiments, while only few MAPs were tested in the presence of both actin and MT in vitro. It can therefore not be excluded that binding with one cytoskeletal polymer might affect the ability of a MAP to bind the other, which would exclude crosslinking activity. Therefore, many of the MAPs today considered as cytoskeletal crosslinkers still need to be confirmed as such.

MACF1 was first discovered as actin crosslinking factor 7 (ACF7) (Bernier et al. 1996) and MACF2 as bullous pemphigoid antigen 1 (BPAG1) (Sawamura et al. 1990b), or dystonin (Bernier et al. 1995). Both MAPs are first reported to crosslink actin and MTs (Leung et al. 1999; Karakesisoglou, Yang, and Fuchs 2000b), later demonstrated that they also interact with intermediate filaments (Yang et al. 1996; Leung, Sun, and Liem 1999b). Further details of the MACFs and similar crosslinkers are explained in the annex section 6.2.

Another striking function of MAPs is that they can impact on the molecular architecture of MTs. For instance, it has been reported that DCX or doublecortin determines the number of protofilaments in a polymerizing MTs (Fourniol et al. 2010) (Fig. 8). This might explain why we have MTs with more diverse protofilament number in the in vitro assembled MTs than in cells (Chretien et al. 1992).

MT lattice repair could be one previously neglected molecular function of MAPs. Proteins such as CLASP mediates MT repair by limiting MT lattice damage, and can regulate the incorporation of tubulin dimers (Aher et al. 2020; Aher et al. 2018). A recent observation showed that walking of motor proteins also could damage MT lattice and MAPs could help for the lattice repair (Schaedel et al. 2015; Dumont, Do, and Hess 2015; Aumeier et al. 2016). Many MAPs might have such repairing properties depending on their local concentrations, and this need to be tested.

A recent observation showed that MAPs such as SSNA1 and TPX2 are involved in the branching of MTs, and SSNA1-mediated MT branching was implicated in neuronal development (Basnet et al. 2018; Alfaro-Aco, Thawani, and Petry 2017). Interestingly, it has been shown that tau and TPX2 forms phase-separated condensates with soluble tubulin and can induce new MT nucleation events (Hernandez-Vega et al. 2017; King and Petry 2020). Tau also showed a property of binding the MT lattice in patches called tau islands, which where demonstrated to influence the progressive motility of kinesin motor proteins (Siahaan et al. 2019; Tan et al. 2019).

MAPs can also function as co-factors for other MT-based functions. For example, in vitro reconstitution and TIRF microscopy assays demonstrated that MAPs such as MAP7, tau, MAP2, DCX, DCLK1 and MAP9 are involved in controlling the interactions and processivity of MT motors proteins (Monroy et al. 2018; Monroy et al. 2020), which brings the concept of MAP code.

1.3.7. MAP code

Inside cell, motor proteins and MAPs bind simultaneously on the MTs. How the binding properties of different non-motor MAPs affect the distribution and functions of motor protein is still not clear. The concept of the MAP code states that combinatorial action of different non-motor MAPs differentially controls the motility of motor proteins, and therefore MAP code might control the polarized transport in cells (Monroy et al. 2020; Monroy et al. 2018). In other words, MAP code is all about motor proteins and structural MAPs, and their coordination and cross regulations. To date, we know more than 100 MAPs, and within a cell the MT cytoskeleton is the motor path decorated by a large number of MAPs. How MAPs collectively and individually contribute to sort specific motor protein on MT lattice is a key biological question, especially in highly polarized cells such as neurons. In addition, there is growing evidence showing the functional importance of different structural MAPs and motor proteins in many cellular processes and human diseases, understanding their cross-regulation could bolster the idea of MAP code.

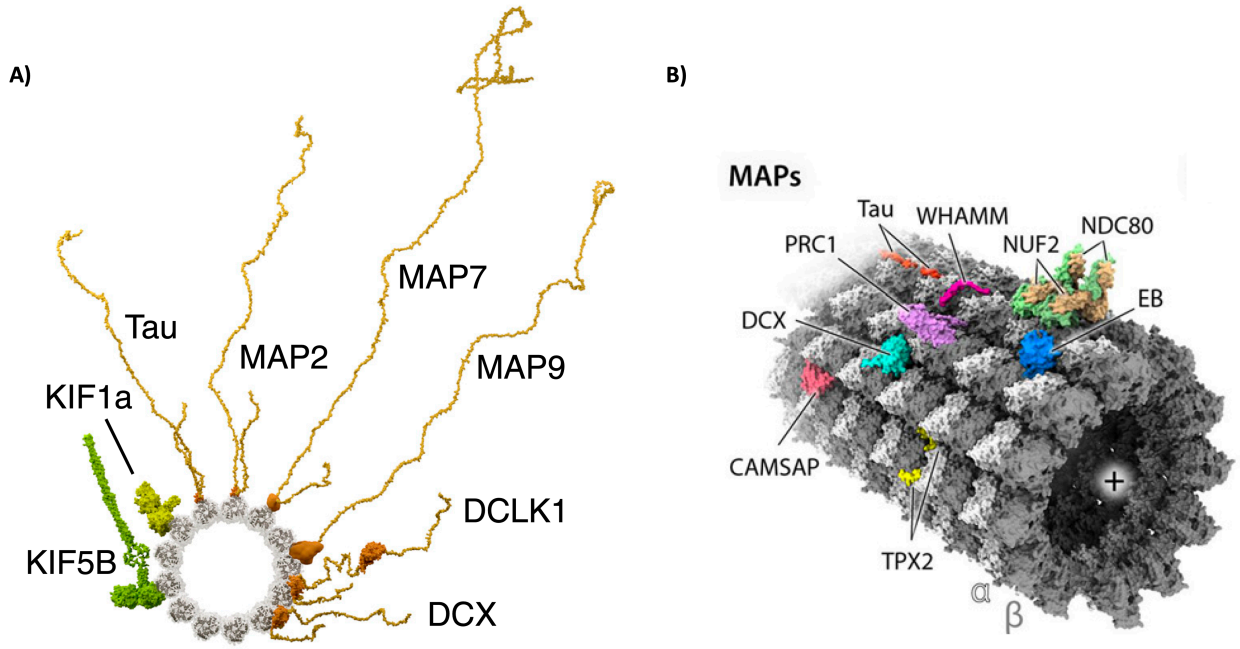

Figure 9. Structural MAPs differentially control distinct classes of MT motor proteins. **A)** MAP code: combinations of non-motor proteins could affect the motility of motor proteins. Model of minus-end view of MT bound to different structural MAPs and kinesin motors. Pseudo-models of full-length unfolded MAPs are shown with projection domains and domain linkers (adapted from (Monroy et al. 2020)) **B)** Atomic models of MAP-MT binding regions, showing different MAPs placed on the surface of MT lattice from single-particle cryo-EM. The representative images are generated with ChimeraX (Goddard et al. 2018) (adapted from (Manka and Moores 2018)).

There is accumulating evidence showing the role of MAPs in the regulation of motor proteins. For instance, the neuronal MAP tau could inhibit processivity of kinesin-1 and kinesin-3 motors (Chaudhary et al. 2018; Dixit et al. 2008; Monroy et al. 2018; McVicker, Chrin, and Berger 2011; Vershinin et al. 2007), but in contrast does not influence active dynein-dynactin complexes (Tan et al. 2019). The reason for this difference was found to be mainly steric hindrance for kinesin, and not for dynein due to its smaller MT-binding domain (Kellogg et al. 2018; Shigematsu et al. 2018; Tan et al. 2019).

Another example of the structural-MAP mediated motor-MAP regulation is the MAP2. In neurons, MAP2 is predominantly localized in dendrites and the axonal initial segment, and has been shown to inhibit kinesin-1 in vivo (Gumy et al. 2017). Similarly, MAP7 has been shown to have important role for a range of kinesin-1 functions such as enhancing the kinesin-1 affinity for MTs in vivo (Barlan, Lu, and Gelfand 2013; Metivier et al. 2019; Metzger et al. 2012; Sung

et al. 2008; Tymanskyj et al. 2018). Moreover, MAP7 has recently been shown to facilitate the recruitment of kinesin-1 to the MT lattice in vitro (Hooikaas et al. 2019; Monroy et al. 2018). Another recent observation showed that doublecortin (DCX) and its paralog, doublecortin-like kinase-1 (DCLK1) interacts with the motor domain of kinesin-3 thus influencing kinesin-3-mediated cargo transport to dendrites (Lipka et al. 2016; Liu et al. 2012). The MT crosslinker PRC1 (protein regulator of cytokinesis 1; aka Ase1p in yeast) has been reported to be important in the recruitment of the kinesin-5 motor Cin8p from budding yeast (Khmelinskii et al. 2009), the kinesin-6 motor Klp9p from fission yeast (Fu et al. 2009), and the kinesin-4 family member Xklp1 from Xenopus laevis (Bieling, Telley, and Surrey 2010). In addition, The MAP TPX2 has been demonstrated to be crucial for the recruitment of the kinesin-5, Eg5, to spindle MTs, which involves in the spindle assembly (Ma et al. 2011; Balchand et al. 2015).

Many of these studies were performed in two-protein systems, for instance characterizing the functions of one structural MAP against one motor proteins, or vice versa. A very recent study introduced the idea of using multiple MAPs and motor proteins on the same MT lattice to explore the concept of MAP code (Monroy et al. 2020; Monroy et al. 2018). In these multi-protein experiments, it has been shown that MAP2c and tau act as inhibitors of kinesin-1 and kinesin-3 by preventing their landing of motors at the MT lattice. On the other hand, MAPs such as DCX, DCLK1, and MAP9 selectively inhibited kinesin-1, but not kinesin-3. Furthermore, MAP9 (aka ASAP) inhibits the processivity of dynein-dynactin-BicD (DDB) complex (Monroy et al. 2020; Monroy et al. 2018). It is expected that the combinatorial activity of MAPs that control motor-mediated transport in cells is strictly controlled. Experimentally testing how multiple structural MAPs control motor protein behaviour in cells is cumbersome and challenging because of lack of appropriate tools. For instance, to characterize the functions of multiple MAPs in vitro, there is a need of purifying individual proteins in a functional form, followed by the need to find compatible buffer conditions in which all the proteins to be combined are soluble and functional. Thus, we need new methods and strategies to explore the combinatorial action of a large variety of MAPs to expand research on MAP code and its physiological implications.

1.3.8. Why we need to study structural MAPs? What are the biological questions that need to be answered?

MTs are involved in a plethora of specialized cellular functions and any perturbation in these cellular processes could affect the normal cellular homeostasis and potentially leads to different diseases. One of the key biological question is how structurally conserved MTs are able to perform diverse functions in different cell types. Although there are several proposed mechanisms explaining how MTs perform such varieties of functions, the molecular mechanisms are not yet clear. Nonetheless, many new MAPs are reporting, but the biochemical characterization of these proteins are not progressing sufficiently comparing their pace of discoveries. To date, more than 100 structural MAPs are reported, but only a few of them are well characterized. Given their potential importance in a variety of human diseases, there is a fundamental need of understanding the molecular functions of these poorly studied proteins in relation with MT cytoskeleton.

Structural MAPs are associated with several human diseases (details of MAPs and their links to diseases are described in annex 6.2). For instance, pathological aggregation of neuronal MAP tau is a hallmark of Alzheimer's disease and other tauopathies (Goedert, Eisenberg, and Crowther 2017). MAP4 is implicated in many types of cancers (Xia et al. 2018) (Murphy and Stearns 1996). MAPs such as PRC1, CLASPs and EML1-4 are studied in great detail in context to cell division and cancer (Forth et al. 2014; Pereira et al. 2006) (Maiato, Sampaio, and Sunkel 2004) (Bieling et al. 2010) (Lansky et al. 2015) (Fry et al. 2016). Aneuploidy is linked to dysfunctions of the mitotic spindle, a MT-based structure. Compounds that disrupt MT dynamics are widely used as chemotherapeutic agents for different types of cancers (Jordan and Wilson 2004). The strong side effects of these compounds show that they also affect the normal cellular functions. Thus, it would be beneficial to target only MT subpopulations instead of the entire cellular MT cytoskeleton. The mechanistic understanding of MAP-MT interactions might allow to explore MAPs as a novel therapeutic target for drug development, especially for targeting specific MT subpopulations.

Apart from MTs, many structural MAPs have multiple other binding partners, such as other cytoskeletal elements (actin, intermediate filaments, septins), key proteins from signalling pathways, or enzymes and membrane-bound proteins (Bernier et al. 1996; Sawamura et al. 1990b; Corti et al. 2003; Adib et al. 2019). To get a comprehensive picture of the functional

network of whole proteins and their complex organisation inside a cell, it is fundamental to study the MT-cytoskeleton-related functions of these proteins.

Some MAPs are highly abundant in specific cell types and tissues, based on which they were classified as for instance neuronal MAPs, or and cell-division MAPs. However, there are still many MAPs for which such a clear functional classification is lacking. Despite low expression levels or so-far not clearly identified functions, these MAPs could play important and highly specific roles in the assembly of specific MT arrays. The first step to explore their potential physiological functions is to determine how they affect the structural, functional and dynamic properties of MTs.

Altogether, there is a clear need of the molecular characterisation of the large variety of structural MAPs in order to understand their role in the regulation of structural and functional properties of MT cytoskeleton, and how this is involved in different cellular processes and human diseases.

So far, there are more than 100 proteins reported as MAPs, and more than 50 MAP candidates were tested in my PhD project.

The following information of each MAP candidates used in this study is detailed in the annex 6.2 of the thesis.

- **Alternative names of MAPs**
- **Background information (e.g. discovery, domain organization)**
- **MAP and MTs (what is known about the roles of MAPs in relation to MT cytoskeleton)**
- **Physiological functions (known physiological functions of the MAP in general)**
- **Links to diseases (both direct and indirect evidences)**
- **Major interacting partners other than MTs**
- **Chemical drugs targeting a MAP (if there is any)**

2. Aims of the study

MTs are involved in a plethora of cellular functions such as cell division, cell shaping, neuronal differentiation and ciliary beating. Thus, strict regulation of MT functions is important, and perturbations are often linked to several diseases. At the molecular level, MT properties can be controlled by two major mechanisms: **1) via the interaction of MTs with a large variety of MT-associated proteins (MAPs), 2) by the expression of alternative tubulin genes and PTMs of tubulin, together referred to as the tubulin code.**

Objective 1:

To develop a method to study interactions of MTs with a large number of MAPs in similar conditions using *in vitro* reconstitution approach and TIRF microscopy.

One of the key molecular players in regulating MT structure and functions are MAPs, and growing studies showed that MAPs could also act as MT depolymerizers, polymerisers, bundlers, elongators, nucleators, crosslinkers, and membrane anchors (Bowne-Anderson, Hibbel, and Howard 2015). Our knowledge of MAPs has been enriched over time, but only a few MAPs are well characterized. There are more than 100 of those proteins reported so far, and up to date no systematic studies exist that characterizes and categorizes MAPs according to their binding mechanisms and structural effects on individual MTs. Thus, one of the major goals of my PhD project was to develop a method allowing to study a large number of MAPs on dynamic MTs.

The specific aims of the objective 1 were the following:

Specific aim 1: To establish MT *in vitro* reconstitution and TIRF microscopy techniques in the lab, and develop a novel pipeline to study a large number of MAPs under similar conditions.

Specific aim 2: To screen ~50 mammalian MAPs and determine how different MAPs act on dynamic MTs. The MAPs include (i) well-characterized MAPs, (ii) known MAPs that have so

far not been characterized by in vitro reconstitution experiments, and (iii) 'suspected MAPs'; proteins that had been claimed to be MAPs without convincing experimental evidence.

Specific aim 3: To characterise MAPs that showed novel properties on dynamic MTs in more detail using techniques such as cryo-electron microscopy.

Specific aim 4: To study the role of MAPs in actin-MT crosstalk, and to test the MT binding behaviour of MAPs carrying patient mutations.

Associated side project in context to **objective 1:**

1) Investigating how CLIP-170 co-condensates with tubulin as periodic droplets on MT lattice and facilitate the nucleation of new MTs from it.

Objective 2:

To develop a method for the purification of tubulin with controlled post-translational modifications (PTMs) by polymerization-depolymerization cycles from mammalian cell lines.

In addition to the MAPs, the tubulin code is a molecular mechanism that directly regulates the building blocks of MTs, the tubulins, by alternative gene expression and a variety of PTMs. The tubulin code is expected to control a wide variety of MT properties, functions and interaction with MAPs. So far, only few examples for this regulation have been revealed. A powerful tool to test the role of the tubulin code is therefore needed.

To date, most of the in vitro experiments for the molecular characterization of MTs have used tubulin purified from bovine or porcine brain, which is a mixture of different tubulin isotypes enriched with several tubulin PTMs. This heterogeneity of tubulin made it difficult to study the role of tubulin code. It was thus necessary to develop methods allowing for the generation of assembly-competent tubulin with controlled tubulin PTMs and isotype composition. I thus participated in the development of a method to purify tubulin with controlled PTMs.

Associated side projects in context to **objective 2:**

1) Studying the role of tubulin PTMs in MAP-MT interactions.

- **1a)** To study the role of tubulin PTMs on MAP-MT binding affinity by co-sedimentation assays using purified proteins.
- **1b)** To establish and perform tricolour-TIRF microscopy for *in vitro* reconstitution of competitive MAP-MT interactions in presence of different tubulin PTMs.

2) Establishing an *in vitro* setup to study the effect of temperature on the stability and the dynamic properties of tubulin isotypes with disease-related mutations.

Novel techniques established

Alongside with my main project, I also established **new techniques** useful for other projects in the lab.

1) MT *in vitro* reconstitution and TIRF microscopy technique using both purified proteins and cell lysates, including a method for glass surface treatment of microscopy slides and coverslips.

2) A setup to study the role of temperature in reconstituted dynamic MTs using Cherry temperature controller and cell lysates.

3. Results

Results: chapter 1

3.1 Systematic characterization of a large number of Microtubule-Associated Proteins using purification-free TIRF-reconstitution assays

Context, major results and author contributions:

MT-interacting proteins were first discovered in the 1970s, co-pelleted with polymerized MTs during the tubulin purification from bovine or porcine brains (Weingarten et al. 1975b; Murphy and Borisy 1975a; Sloboda, Dentler, and Rosenbaum 1976). Currently, there are more than 100 MAPs reported in mammals, but only a few major MAPs are classified based on their functions on dynamic or stable MTs. This includes motor proteins, severing MAPs, MT nucleators, +/-TIPs, and structural MAPs.

The early definition of a MAP was that any protein able to copolymerize with purified tubulin in vitro, or any protein which co-localises with cellular MTs and loses this localisation upon MT depolymerisation in the cells was called a MAP (Huber, Alaimo-Beuret, and Matus 1985). This definition is still valid and followed in the MT cytoskeleton field, however, it might require some refinement. For example, in cellular studies, overexpression of several MAPs lead to non-physiological MT bundling or the formation of MAP aggregates, which makes it difficult to determine their physiological functions. Also, antibodies are not easily available for all known MAPs, which makes it difficult to study the endogenous proteins and their localizations. On the other hand, testing a MAP candidate in in vitro typically requires its purification, which often is difficult due to protein precipitation issues, thus work-intense optimisation procedures, such as testing many buffer conditions are needed to obtain soluble and functional proteins. This slowed down the advancement of molecular characterization of MAPs, and restricted the in-depth characterisation of MAPs to a handful of selected proteins. Therefore, a faster and simpler method is required to study a large number of MAPs at individual-MT resolution. In addition to the role of MAPs in different cellular processes such as cell division, there are growing evidence showing MAPs are involved in a wide range of human diseases.

More and more structural MAPs are linked to diseases (see the annex 6.2 section showing disease links of each MAP used in this project in the description of respective MAPs). Thus,

the molecular characterization of structural MAPs is very important, and the mechanistic understanding of how MAPs regulate MT functions in different diseases and cellular processes might help in the development of drugs targeting MAPs and MTs.

The central project of my PhD thesis was to develop a purification-free TIRF-microscopy-based assay to directly compare a large number of MAPs and potential MAPs and their effect on dynamic and structural properties of MTs. The approach I developed allowed me to characterise more than 50 proteins, and compare their binding behaviour on growing MTs at individual-MT resolution. Using my purification-free pipeline, I identified novel MT properties induced by previously known MAPs, which had not been reported before. For instance, a truncated version of MACF1 (MT-Actin Crosslinking Factor-1) induced the formation of hooked ends at the growing ends of MTs, which arrested MT elongation. MAP2 also led to the generation of curved structures, but in contrast to MACF1 protofilaments were peeling off the lattice, and subsequently decorated with MAP2 aggregates or droplets. Another MAP, CSAP (Cilia Spindle Associated Protein) induces the formation of MT coils. I further observed MAP7 generated MT asters, and MAP8 induced fragmentation of long MTs after initially decorating them. EML1 (Echinoderm MAP-like protein 1) showed a preferred binding affinity to the growing ends of MTs, which was distinct from the known +TIP binders such as EB proteins.

Apart from the observation of novel MT properties, my approach allowed me to test the role of MAPs in actin-MT crosstalk. Some MAPs appeared to induce actin-MT co-alignment in the extracts, while other MAPs appeared to prevent it.

The recent rise of cryo-electron microscopy in structural biology could allow the characterisation of many MAPs bound to MTs. However, the bottleneck of protein purification has also restricted the number of proteins that could be studied by structural approaches until now. I therefore tested the feasibility of my purification-free lysate approach in cryo-electron microscopy studies. Focussing on EML1, we found that we could reconstitute its structure at 15 Å resolution, which was sufficient to demonstrate that it decorates MTs along single protofilaments.

Finally, I used the lysate-based approach to study the impact of disease-related mutations on MAP behaviour. For this, I compared the binding affinity of mutated EML1 (EML1^{T243A}) with

the wild type EML1 on dynamic MTs, and found that EML1^{T243A} has a lower binding affinity to MTs as compared to wildtype EML1.

In total, purification-free lysate approach is a method which helps to study a large number of MAPs on dynamic MTs at higher resolution with a multitude of applications, which could help to understand the mechanistic roles of MAPs in the cellular processes involving MT cytoskeleton.

Author contributions:

My contributions:

I established the MT reconstitution and cell lysate method in the lab. I performed MT reconstitution assays and TIRF microscopy for 58 MAP candidates used in this study, and I conducted the assays in the presence and absence of actin for all bona fide MAPs. I performed western blots and BCA assays for the quantification of proteins in lysates. I contributed to the molecular cloning of some of the MAP constructs used in this study, and helped to prepare samples for cryo-EM experiments. I did the image processing of all TIRF-M images and its analysis. I purified tubulin from HeLa suspension culture and used it for the assays. I also participated in the tubulin purification from the pig brain, which was used for the preparation of MT seeds. I also purified proteins such as dead kinesin, MACF1, Nrd1 and Crmp2a. I analysed and prepared all the figures from the TIRF assays, and wrote the first draft of results, conclusion, and method details of the manuscript. I contributed to the refinement of texts and figures in all sections of the manuscript.

Contribution of co-authors:

C. Janke, S. Bodakuntla, F. Maksut, M. Genova contributed to the cloning of MAP constructs. S. Bodakuntla and F. Maksut performed the cell studies (immunostaining and imaging of MAP constructs). M. Genova purified the MACF1 protein construct used in this study. M. Bangera performed the cryo-EM experiments with the supervision of M. Sirajuddin. L. Besse provided tools for image processing and analysis. M. M. Magiera supervised the purification of tubulin. C. Janke supervised the development of this method and wrote the first draft of the introduction and results section. S. Bodakuntla prepared immuno-fluorescence images of cells expressing MAPs. C. Janke, S. Bodakuntla, M. Genova contributed for the refinement and corrections of texts of all the sections of the manuscript.

Here I added my main PhD project in an “article manuscript format”, including introduction, results, conclusion, methods, figures (main and supplementary), and references. The results are discussed elaborately in the main discussion (4) section. The manuscript is latter referred to as “Jijumon et al. manuscript” in the main discussion (4) and conclusion (5) sections.

Systematic characterization of a large number of Microtubule-Associated Proteins using purification-free TIRF-reconstitution assays

Jijumon A.S.[1,2], Satish Bodakuntla[1,2], Mariya Genova[1,2], Mamta Bangera[3], Laetitia Besse[4], Fatlinda Maksut[1,2], Maria M. Magiera[1,2], Minhaj Sirajuddin[3] and Carsten Janke[1,2]

[1]Institut Curie, PSL Research University, CNRS UMR3348, F-91405 Orsay, France
[2]Institut Curie, Université Paris-Saclay, CNRS UMR3348, F-91405 Orsay, France
[3]Institute for Stem Cell Science and Regenerative Medicine (inStem), Bangalore, India
[4]Institut Curie, Université Paris-Saclay, Centre d'Imagerie Multimodale INSERM US43, CNRS UMS2016, F-91405 Orsay, France

Keywords: Microtubules, Microtubule Associated Proteins, Purification-free TIRF assays, microtubule reconstitution, medium-throughput

Abstract

The microtubule (MT) cytoskeleton is a complex and dynamic system of filaments involved in a plethora of functions such as cell division, maintenance of cell shape, ciliary beating or neuronal differentiation. Strict regulation of MT functions is therefore of high importance for the cellular homeostasis, and any perturbations could potentially lead to diseases like cancer, ciliopathies and neurodegeneration.

In a cellular context, MT properties can be controlled via the interaction of MTs with a large variety of microtubule-associated proteins (MAPs). Our knowledge of such interactors has been continuously enriched over the past decades, but up to this date no systematic studies exist that aim to describe and categorize these proteins according to their binding mechanisms and structural effects on MTs.

In the present work, we have developed an assay for a rapid and systematic analysis using cleared lysates of cultured human cells overexpressing the MAPs of interest. The dynamic behaviour of growing MTs in presence of around 50 different MAPs was imaged using TIRF microscopy. This allows us to study the behaviour of MAPs in a situation close to their natural environment, but eliminating the complexity of the intracellular space, such as crowding of different organelles and cytoskeleton filaments inside the confined intracellular space. Indeed, most MAPs were soluble in our extract approach, while purification approaches for many of them led to protein precipitation.

Our novel approach allowed us to define several novel proteins as bona-fide MAPs. We show that previously uncharacterized MAPs have strikingly different effects on MT polymerization and MT structure, thus creating a variety of distinct MT arrays. Our cell-free approach further allowed us to study MAP-MT interactions by cryo-electron microscopy and to study role of MAPs in actin-MT crosstalk. Our experimental pipeline thus allows for a better mechanistic understanding of how MAPs and MTs together control cytoskeleton functions.

Introduction

The microtubule (MT) cytoskeleton is a key structural and mechanical component of every eukaryotic cell. Microtubules form a wide variety of dynamic arrays and structures that are implicated in many different cellular functions, such as cell division, cell motility, cell shape and intracellular transport. It has been known for decades that building these structures requires distinct sets of microtubule-associated proteins (MAPs). Any protein that is able to interact with MTs could be technically classified as a MAP, however the term has been mostly adapted to describe non-motile and non-enzymatic proteins that bind MT network, and that are often referred to as "structural MAPs" (Olmsted 1986; Mandelkow and Mandelkow 1995; Bodakuntla et al. 2019).

Compared to the significant advances that have been made in understanding the function of MT-based molecular motors (Hirokawa et al. 2009; Veigel and Schmidt 2011; Roberts et al. 2013), severing enzymes (McNally and Roll-Mecak 2018), or proteins that regulate MT plus or minus ends (Akhmanova and Steinmetz 2015), only few members of the structural MAP family have been extensively biochemically and functionally characterized (Bodakuntla et al. 2019). These few well-characterised MAPs are often linked to pathologies, such as the neuronal MAP tau, which is the principal component of the pathological paired helical filaments - a hallmark of Alzheimer's disease and other tauopathies (Goedert, Eisenberg, and Crowther 2017). Likewise, MAP4, a MAP implicated in different forms of cancer (Xia et al. 2018; Murphy, Hinman, and Levine 1996), or MAPs important for cell division such as PRC1 and CLASPs (Forth et al. 2014; Pereira et al. 2006; Maiato, Sampaio, and Sunkel 2004; Bieling, Telley, and Surrey 2010; Lansky et al. 2015) have been studied in greater detail.

Recent work demonstrates that MT functions as we know them may result from an interplay between different MAPs on the same MT (Monroy et al. 2020). Moreover, advances in mutation mapping revealed many novel links between a variety of MAPs and a broad spectrum of human diseases (Suppl. Table 1 and citations within). It thus appears that the current focus on some selected, well-characterised MAPs impedes advances towards a holistic understanding of MT architecture and functions. This provides a major stumbling stone in advancing the general understanding of MT regulation in cells, and also impedes the exciting possibility to exploit the newly discovered links between MAPs and human diseases (Suppl. Table 1) for therapeutic

means. However, studying MAPs on a broader scale was so far not possible due to experimental limitations. Cell-based approaches, which could easily be upscaled to study a large number of proteins, are limited by the fact that the overexpression of MAPs leads to a variety of artefacts, such as excessive MT bundling, which often results in perturbations of normal cellular functions and cell death. On the other hand, to determine the molecular functions of novel MAPs, in-depth biochemical and biophysical characterisation is needed, which classically employs *in vitro* reconstitution assays that require purification of the MAP in a functional form. Recent studies succeeded in purifying and studying the role of multiple MAPs, such as MAP7, tau, MAP2, DCX, DCLK1 and MAP9 (Monroy et al. 2020), or the role of the four members of the MAP7 family in controlling kinesin-1 (Hooikaas et al. 2019). However, given that protein purification is a tedious process in which many conditions need to be tested, and some proteins even entirely resist biochemical purification, this approach will remain impracticable for medium- or large-scale analyses.

To overcome these limitations, we here established an *ex-vivo* pipeline that allows studying a wide variety of MAPs at a single-MT resolution in cell-free, TIRF microscopy-based assays without prior protein purification. Our pipeline is universal, requires a small number of components, and can be expanded to virtually any MAP of interest. Using this approach allowed us to characterize the MT interactions of more than 50 proteins, including well-known MAPs, as well as proteins that were merely suspected to be MAPs based on colocalization studies in cells or bioinformatic analyses (Suppl. Table 1). All tested proteins were invariably soluble in our *ex-vivo* approach, thus allowing us to unambiguously determine their MT-binding activities. We discovered a variety of striking, and so-far unknown activities of MAPs on MTs, thus opening an entirely novel angle of research on MT structures. Our assay further allows us to directly determine the implication of MAPs in co-aligning F-actin and MTs. Finally, we demonstrate that MT-MAP assemblies can be directly used to obtain high-resolution structures by cryo-electron microscopy, which will significantly increase the feasibility and throughput of structural studies of the MT cytoskeleton. Our pipeline is thus a unique, powerful tool to analyse both novel and previously known MAPs at medium throughput, and to discover a wide variety of unveiled properties that could be overlooked with other approaches.

Results

1) Setting up an ex-vivo pipeline for medium-throughput characterisation of MAPs

Overview of the ex-vivo pipeline:

To be able to carry out analyses of any MAP candidate in our *ex-vivo* pipeline (Fig. 1A), one precondition was to be entirely independent of external resources for the MAP constructs. Therefore, we started the pipeline by cloning the genes of interest using the fast and simple SLIC method (Fig. 1A, step 1). The expression of fluorescently-tagged proteins was then tested in U-2 OS cells, allowing to roughly verify the intracellular localisation of the proteins (Fig. 1A, step 2). For *ex-vivo* analyses, the verified expression vectors were transfected into HEK-293 cells, from which soluble cytosolic lysates containing the overexpressed, fluorescently-tagged proteins were generated (Fig. 1A, step 3). These lysates were directly introduced into a flow chamber containing immobilized GMPCPP MT seeds (Gell et al. 2010), and MT polymerisation was recorded by TIRF microscopy (Fig. 1A, step 4). The key advantage of our *ex-vivo* approach is that all components needed for MT polymerization, i.e. free tubulin and GTP, come directly from the cell lysates, which makes the assay highly reproducible and independent from additional factors, such as the availability of purified tubulin of reproducible quality.

Initially, all MAP-containing extracts were tested under similar assay conditions, which could subsequently be further refined depending on the initial observations. We estimated the protein concentration of all cell lysates using the bicinchoninic acid (BCA) protein assay, and adjusted total protein concentrations to a defined value for all samples (Fig. 1A, step 5). A first round of assays was performed with the fixed lysate concentration, irrespective of the expression levels of the GFP-tagged MAPs. To further determine the dependency of the observed MAP behaviour on their concentration in the lysates, we estimated the concentration of the GFP-MAPs in the extracts by immuno blot analyses, and subsequently performed dilution series for those MAPs. We further performed ultrastructural studies using cryo-electron microscopy, or competition experiments between MAPs on the same MTs. Our *ex-vivo* approach further allowed us to systematically study impact of each tested MAP on MT-actin crosstalk.

Step 1: Molecular cloning

For the molecular cloning, we first established a set of versatile expression vectors based on the pTRIP backbone (Gentili et al. 2015). Our vectors contain a CAG promoter, a GFP or mCherry tag, and allow to tag proteins on the C- or N-terminus. Tags were positioned according to what was described in the literature for MAPs that had previously been studied, or by default on the C-terminal end of the MAP if no information was available. Cloning of the MAP candidates was performed using SLIC (Sequence- and ligation-independent cloning) method (Jeong et al. 2012) (Fig. S1). The SLIC procedure is straight-forward, time-saving, and requires only a minimal set of molecular biology reagents. PCR Primers for SLIC cloning are designed with homologous overhangs of ≥15 bp. (Fig. S1).

To determine the correct open reading frames (ORFs) for the proteins of interest, we searched public databases such as NCBI or EMBL-EBI for different ORF variants, and compared murine and human variants with the goal to identify the most complete ORF for each MAP, which was particularly important for proteins that were so far little characterised. As the expression profiles for many MAPs were not well known, we amplified the ORF of interest from a panel of cDNAs from brain, testes and immortalised cell lines. Using this approach, we succeeded amplifying most ORFs of interest, and strikingly in some cases our approach allowed us to identify several splice isoforms (out of the 60 MAP candidates we cloned, we found multiple isoforms in 8 cases). For MAPs that are particularly big (the MT-actin crosslinking factors MACF1 and MACF2; MAP4) we cloned fragments containing the predicted or known MT-binding domains. Details such as accession numbers, ORF size, position of the fluorescent tag, and primers used for the amplification of the ORF are listed in Suppl. Table 1.

After the SLIC cloning, single clones were isolated tested by restriction digestion and DNA sequencing. In case the obtained sequences were different from those annotated in the database, multiple clones were sequenced to determine whether those differences are subject to PCR-induced mutations, or polymorphisms. The finally selected clones (mutation-free and if possible different splice isoforms of the same protein) were directly tested by expression in U-2 OS cells.

Step 2: Intracellular localisation and impact on MT organisation by MAPs

All fluorescently-tagged MAPs were first expressed in U-2 OS cells to determine their MT localisation in cells (Fig. 1B and Fig. S2-S4). The expression plasmids were transfected into U-2 OS cells, and visually inspected after 24 h. MAPs with strong expression levels, as judged from fluorescence intensity, were fixed for immunostaining, while weakly expressed MAPs were fixed after 48 h. Cells were labelled with an anti-tubulin antibody to visualize the MT cytoskeleton, and co-localisation of the fluorescently tagged MAPs was determined by microscopy (Fig. 1B and Fig. S2-S4).

All the expressed proteins in our study showed three principal cellular behaviours: (i) binding and bundling of MTs (i.e., Tau, MAP2 and MAP7) (ii) diffuse localisation throughout the cytoplasm (i.e., Parkin and MAP11) and (iii) specific intracellular localisation such as perinuclear or near centrosome (i.e., EMAP6 and POC) (Fig. 1B and Fig. S2-S4). Within the group of (i) proteins that co-localise with MTs, we found two characteristic behaviours: either the MAP generated thick bundles of MTs (e.g. Tau, MAP2), or we observed the formation of wavy, smaller MT bundles (e.g. GLFND1, MAP7D3). Strikingly, even cells expressing higher levels of the latter MAPs did not convert the MTs into thick bundles as seen for MAPs of the former category.

While these observations allowed us to roughly determine which of the tested proteins behave like MAPs, overexpressed MAPs in cells do not inform about the behaviour of these proteins on individually growing MTs, as they all lead to non-physiological MT bundling.

Step 3: Generating lysates for ex-vivo experiments

All expression vectors that have successfully been tested in cells (step 2) were transfected into HEK 293 cells (Fig. 2A). Following our observations in step 2, MAPs were expressed for either 24 h, or 48 h for MAPs with low expression levels. For the preparation of lysates, cells were collected in warm DMEM medium, and spun down at 450 g, 4°C for 10 min. Subsequently, the cell pellets were lysed in lysis buffer, and were clarified by ultracentrifugation (see method section for details). Supernatants were collected, their protein concentrations were estimated with BCA protein assay, and adjusted to 8 mg/ml. Considering that the tubulin concentrations in cells are strictly regulated (Cleveland 1989; Lin, Gasic, et al. 2020), controlling the total

protein concentrations also assures similar concentrations of tubulin in all lysates. This guarantees that the follow-up experiments with different lysates are carried out under comparable conditions, with the only variable factor being the overexpressed MAPs.

All steps starting from the low-speed centrifugation step (Fig. 2A) were performed at cold (4°C) or on ice to assure MT depolymerization and efficient detachment of MAPs from MTs. Concentration-adjusted cell lysates were snap-frozen in liquid nitrogen, and stored at -80°C for one month. The MAP lysates are then directly used for TIRF assays, as well as other follow-up experiments such as cryo-electron microscopy (Fig. 2A).

Step 4: Ex-vivo assay for medium-throughput characterisation of MAPs in cell lysates

Our ex-vivo assays use Total Internal Reflection Fluorescence (TIRF) microscopy (Gell et al. 2010) to observe the dynamic assembly of MTs from cell lysates and the impact of fluorescently labelled MAPs on the assembly behaviour. All assays are initially performed at a total protein concentration of 8 mg/ml (see step 3), thus assuring similar conditions for MT polymerisation. Imaging chambers were prepared using glass slides and coverslips, sandwiched with stripes of double-sided sticky tape (Fig. 2B). First, fluorescently labelled GMPCPP-MT were flushed into the chamber (Fig. 2B) and let it to immobilise with inactive kinesin-1. Excess and unattached seeds were washed out with warm BRB80 buffer, and the density of the GMPCPP MT seeds in each chamber was checked by TIRF microscopy before flushing in the lysates (all wash steps are performed with one chamber volume of warm BRB80 buffer). Next, freshly thawed cell lysate was flushed into the imaging chamber, and the slide was immediately mounted under the TIRF microscope, manually focussed with the help of the fluorescent MT seeds, and videos were acquired for up to 11 min (see method section for details).

During the duration of the acquisition, fluorescently-tagged MAPs were used as a proxy to visualize MTs in the assay, which precluded the need of any additional MT labelling that could interfere with MT assembly and/or MAP binding. At the end of time-lapse imaging, the chamber was washed with warm BRB80 buffer to stop MT polymerisation and remove excess proteins (i.e., the remaining unbound MAP, tubulin, and other proteins from lysates). We then captured still images of GMPCPP seeds and MAPs decorating MTs, which is advantageous to visualise weaker-binding MAPs on MTs by reducing the background signal.

Strikingly, along with MT polymerisation, we also observed actin polymerisation in our TIRF assays by consuming soluble actin and ATP from the cell lysates. MTs and actin filaments were visualised by staining with the tubulin antibody YL1/2, and with the fluorescent actin-binding drug SiR-Actin. We first flushed YL1/2 into the chamber and incubated for 5 min. After a wash with BRB80, anti-rat Alexa 565 antibody was flushed in and incubated for another 5 min. The chamber was washed again, and 500 nM SiR-actin was incubated for another 5 min. After a final wash, the chambers are returned to the TIRF microscope, and still images were acquired. SiR-actin-stained actin filaments were captured at 647 nm, YL1/2-labelled MTs at 565 nm, and GFP-tagged MAPs at 488 nm.

To determine the impact of the actin polymerisation on the MT polymerisation in the presence of the different MAPs, we repeated the same set of experiments in the presence of 11 μM of Latrunculin A to prevent actin polymerisation (Spector et al. 1983; Coue et al. 1987).

In order to validate our assay, first we tested two well-characterized MT-interacting proteins: the MT-severing enzyme spastin and end-binding protein 3 (EB3) which is a well-characterised MT +TIP protein. Purified spastin is known to efficiently sever MTs, and EB3 reliably tracks the growing plus ends of MTs. Both proteins show these characteristic activities in vitro with purified components, as well as in cells after overexpression (Roll-Mecak and Vale 2008) (Akhmanova and Steinmetz 2008). In our TIRF assays with cell lysates, spastin efficiently severed taxol-stabilised MTs (Fig. 2C), and GFP-tagged EB3 was tracking the plus ends of the growing MT (Fig. 2C). For spastin severing assays, we used pre-polymerised MTs stabilised with taxol, while EB3 experiments were performed with cell lysates on immobilized GMPCPP seeds, similar to all other assays performed below. These two observations validated our ex-vivo approach as a tool to study MT-MAP interactions.

We thus performed assays with 58 cell lysates containing overexpressed GFP-tagged MAP candidates. Out of the 58 tested proteins, 30 clearly co-localised with dynamic MTs (Fig. 3 and Fig. S5-S11).

To assure the reproducibility of our observations, we performed at least three independent TIRF assays with at least three independently prepared cell lysates for each MAP. To test the impact of actin polymerisation on the observed MAP behaviour, we performed at least one assay in the presence of 11 μM of Latrunculin A to avoid actin polymerisation for all MAP candidates.

Absence of actin did not impede any of the MAPs we tested here to associate with MTs, nor did it change the appearance of the MT networks (Fig. S5, S7 and S9). This suggests that co-polymerisation or the co-alignment of actin fibres by some of the tested MAPs has no dominant effect on the MT arrays induced by these MAPs. Surprisingly, several MAPs appeared to co-align actin fibres with MTs (e.g. GLFND1), some appeared to prevent the alignment (e.g. MAP 10) and some shows a mixed alignment (e.g. EML3) (Fig. S12A and S12B).

Our assays revealed that apart from affecting the polymerisation dynamics of MTs, different MAPs induced a variety of unique MT structures and behaviours. The most striking novel MAP activities were for MAP2, MACF1, MAP7, MAP8, and CSAP (Fig. 3A, B, C, and S5).

2) Discovery of novel activities of MAPs in the formation of MT arrays

Following the systematic characterisation of 58 MAP candidates in our pipeline, in this chapter we highlight some of the novel properties exhibited by known MAPs that we discovered using our ex vivo method. All figures showing novel MT phenotypes induced by MAPs in Fig. 3 and 5S are representative images from more than three independent TIRF assays from at least three independent cell lysate preparations.

<u>MAP2 induces protofilament peeling and protein clustering</u>

MAP2 is highly expressed in neurons (Matus 1988), and found in a range of different splicing isoforms. MAP2A and MAP2B are high-molecular weight (≈280 kDa) variants (Kindler et al. 1990), while and MAP2C (≈51 kDa) and MAP2D (≈54 kDa) are lower molecular weight isoforms that have retained the MT binding regions (Ludin et al. 1996; Murphy and Borisy 1975). MAP2 is considered as a structural protein crucial for neurite outgrowth, MT architecture in dendrites (Lewis et al. 1989), and in neuronal plasticity processes (Fanara et al. 2010; Harada et al. 2002).

In our ex-vivo approach, we found that 2C and 2D isoforms of MAP2 induce MT protofilament peeling, and subsequently decorates the curled protofilament as spherical protein clumps (Fig. 3 and S5). MAP2 clumps on protofilament curling events are observed both on MT lattices and also at growing MT plus ends (Fig. 3C).

MAP7 induces formations of aster-like MT arrays

MAP7 was identified and characterized as EMAP115 (Epithelial MT-associated protein of 115 kDa) from HeLa cells in 1993 (Masson and Kreis 1993). MAP7 has an N-terminal MT binding domain and a C-terminal kinesin-1 binding domain, which allows it to recruit kinesin-1 motors to MTs (Sung et al. 2008). MAP7 is important for a range of cellular functions, such as nuclear positioning in muscles (Metzger et al. 2012), axon branching in dorsal root ganglion (DRG) neurons (Tymanskyj et al. 2017), oocyte polarity (Sung et al. 2008), regulation of mitotic spindle length in neural stem cells (Gallaud et al. 2014), or for organelle transport (Barlan, Lu, and Gelfand 2013).

In our ex-vivo experiments, MAP7 induces the formation of aster-like MT arrays. What distinguishes these arrays from those generated by other MAPs is that multiple MT branches can originate from a single position (Fig. 3 and S5). These MT-nucleating positions were mostly found on one end of the GMPCCP-MT seeds, but we also observed spontaneously polymerising MTs.

In mammals, the MAP7 family comprises four different proteins: MAP7, MAP7D1, MAP7D2 and MAP7D3 (Bulinski and Bossler 1994; Metzger et al. 2012; Yadav, Verma, and Panda 2014). We thus tested the other members of the MAP7 family, and found that neither MAP7D1, MAP7D2, or MAP7D3 form aster-like MT arrays under similar conditions (Fig. S10 and S11). Therefore, the observed activity appears to be unique for MAP7.

MACF1 generates hooks at growing MT plus ends

MACF1 was first reported in 1996 as actin crosslinking factor 7 (ACF7) (Bernier et al. 1996). MACF1 is a protein of ~600 kDa known to crosslink MTs with actin and intermediate filaments (Leung et al. 1999; Yang et al. 1996). The F-actin-binding domain of MACF1 is localised within the N-terminal portion of the protein, while the MT-binding is assured by the C-terminal domain. Strikingly, both domains are separated by long stretches of spectrin repeats, suggesting that MACF1 functions as a linker and spacer of the two cytoskeletal networks (Sun, Leung, and Liem 2001). MACF1 is involved in cell migration (Wu, Kodama, and Fuchs 2008), wound

healing (Wu et al. 2011), brain development (Goryunov et al. 2010), axon outgrowth, and dendritic arborization (Sanchez-Soriano et al. 2009; Ka and Kim 2016).
Because of the large size of MACF1, and our focus on MAPs, we cloned a truncated version encoding 1020 amino acids of the C-terminus (amino acid 4305-end). This shorter version starts after the spectrin repeats and contains the MT-binding domain of MACF1. This construct, called MACF1-C1020, decorates the lattice of growing MTs. Strikingly, MTs grown in the presence of MACF1-C1020 spontaneously form hooked ends that prevent their further elongation (Fig. 3 and 5S). The hooks formed through MACF1-C1020 are either single hooks (MTs curled into one coil), or double hooks (MTs curled into two coils) (Fig. 6A and B). To determine the diameters of these hooks, we using Hough circle transformation plugin in ImageJ. Using this, we found that single hooks have a diameter of ≈1.1 μm and double hooks have a diameter of ≈0.8 μm (Fig. 6A and B).

MAPs from the EML family show a spectrum of distinct behaviours on dynamic MTs

EMAPs (Echinoderm MT-Associated Proteins) are a family of MAPs discovered in echinoderms. The first member of the family was the 77-kDa EMAP1 discovered in sea urchin eggs (Suprenant et al. 1993). EMAP orthologues in other organisms and are referred to as EMLs or ELPs (both for EMAP-like proteins) in mammals, where six members have been identified. EMLs can show typical behaviours of MAPs: Purified mouse EML1 directly binds MTs in vitro and co- localises with MTs in both interphase and mitosis in neuronal progenitor cells (Kielar et al. 2014). Loss of EML1 resulted in slower MT plus-end growth, an altered shape, and an increased spindle length in neuronal progenitor cells in the developing cerebral cortex (Bizzotto et al. 2017). Some of the EMLs forms oncogenic fusion proteins with kinases and are involved in in different human cancer (Fry et al. 2016).

We tested EML1, 2, 3 and 4 in our ex-vivo assays. Strikingly, all four proteins behaved very different. EML1, 3 and 4 associated by growing MTs while MT polymerisation was not induced by EML2, nor did EML2 decorate MTs (Fig. S6 and S7). This observation confirms the previous study that demonstrated a MT depolymerising activity for EML2 (Eichenmuller et al. 2002). EML1 decorated growing MTs and, while decorating the entire length of the MT lattice, accumulated toward the growing ends of MT (Fig. 3 and 5S). EML3 and EML4, by contrast, did not show such plus-end preferences. Both proteins decorated the MT lattice, however, in a distinct manner: EML3 slowly accumulates at already polymerised MTs, while EML4 strongly

associates with growing MTs (Fig. S6 and S7). The comparison of four different MAPs of the same family revealed that similar proteins can have highly divergent modes of interaction with MTs.

MAP8/ MAP1S induces length-dependent MT fragmentation on dynamic MTs

MAP8, also known as MAP1S, is expressed in various tissues, most evidently in neurons, but at low levels compared to other MAPs (Orban-Nemeth et al. 2005). It has been shown that MAP8 can bridge autophagosomes and mitochondria to MTs (Xie et al. 2011) and is linked to aggregation of mitochondria and genome destruction (Liu et al. 2005). High levels of MAP8 induce MT stabilization, thereby disrupting the axonal transport and eventually leading to the death of neurons (Ding et al. 2006). *In vitro* studies using purified proteins have shown that the MAP8 light chain can bind, bundle and stabilize MTs (Orban-Nemeth et al. 2005; Liu et al. 2005).

In our lysate experiments, we found that MAP8 decorates growing MTs and leads to their fragmentation into short MTs over time (Fig. 3 and 5S). This was further confirmed with the MT staining after the TIRF time-lapse assay. Latrunculin experiments showed that the fragmentation property of MAP8 is independent of actin filament formations (Fig. 5S).

CSAP induces the formation of MT coils

Cilia and Spindle-Associated Protein (CSAP) was first reported in 2012 as a MAP that specifically colocalises with polyglutamylated MTs on centrioles, mitotic spindles, and cilia in cultured human cells (Backer et al. 2012). It was later shown that CSAP acts as a regulator of the tubulin polyglutamylation on cellular MTs by helping the recruitment of polyglutamylating enzymes from the TTLL family to MTs (Bompard et al. 2018).

In our ex-vivo approach, we found that CSAP induces the growth of MTs into helices with an average helix width of ~700 nm (Fig. 3 and S1). In order to visualise these MT coils, we used an off-TIRF imaging mode, which ensures a higher penetration depth. CSAP induced spontaneous formation of coiled MT, however we also observed MTs coils forming from GMPCPP seeds.

3) Refinement of the ex-vivo pipeline for in-depth characterisation of MAPs

Determining the impact of MAP concentrations in ex-vivo experiments

The capacity of MAPs to control MT assembly and dynamics, and their ability to induce the formation of specific MT arrays are known to be concentration-dependent processes (Bowne-Anderson, Hibbel, and Howard 2015; Roger et al. 2004; Sandoval and Vandekerckhove 1981; Monroy et al. 2018; Siahaan et al. 2019). While in vitro reconstitution experiments from purified components allow a strict control of protein concentrations, this is more difficult in our ex-vivo approach that uses the cell lysates. Our observations of intriguing novel activities of a number of MAPs (Fig. 3) raised the obvious question whether these activities are concentration-dependent.

To test how the MAP concentrations in our lysate approach affect a specific MT behaviour they induce, we decided to dilute the GFP-MAP in our lysates by fixing the lysate concentration at 8 mg/ml, and therefore the tubulin concentration in our assays constant. This can be done by diluting lysates from GFP-MAP expressing cells with a lysate from non-transfected cells. At the same time, we estimated the concentration of the GFP-tagged MAPs in the lysates by quantitative immunoblots using a GFP antibody.

We tested this approach for two MAPs that showed specific novel behaviours on dynamic MTs: MACF1 and EML1. To estimate the concentrations of EML and MACF1 in the cell lysates, we loaded dilution series of the lysates together with a dilution series of purified GFP (50, 25, 12.5, 6.25 and 3.125 ng/lane) (Fig. 4A). We quantified the signals of the anti-GFP antibody by chemiluminescence (Fig. 4A), and plotted them to determine the linear range of the detection within the GFP standard curve. We then verified if the GFP-MAP signals were within this linear range, and calculated the concentrations of the overexpressed MAPs based on the intensity of the purified GFP signals (Fig. 4C). Fig. 4D shows the Coomassie-stained gel of purified GFP protein used for the quantification of GFP-MAPs in the lysates. Having estimated the concentration of GFP-MAPs in the lysates, we performed dilution experiments for both MACF1-C1020 and EML1 by fixing total protein concentration in the lysates at 8 mg/ml (by BCA protein assay) and tested four different dilutions for each MAP.

The prominent phenotype induced by MACF1-C1020 is the formation of hooks at the growing ends of MTs (Fig. 3). Starting from an initial maximum concentration of ~140 nM MACF1-C1020-GFP (Fig. 4), we performed experiments with extracts in which MACF1-C1020-GFP was adjusted to 140, 70, 35 and 17.5 nM. After live imaging, we quantified the number of MTs that form hooks at the growing MT plus ends from still images taken after 11 min (Fig. 5A). We observed that the MACF1-mediated hook formation is prominent in a certain range of concentration, and the penetration of the phenotype is low below and above this concentration range (Fig. 5E).

For EML1 we had observed an enrichment of EML1-GFP toward the growing plus end of MTs. This, however, was not comparable to the +TIP tracking of proteins like EB3, which form a distinct peak at the +TIPs. EML1 rather forms a gradient over a longer stretch of the growing MT with a maximum of decoration near the growing end (Fig. 5D). After quantification of EML1-GFP in lysates, we found that a concentration of ~400 nM (Fig. 4), which however is too high to see the formation of EML1-GFP gradients at growing MTs. We thus performed assays with a dilution series of 200, 100, 50 and 25 nM (Fig. 5B), and visualised the intensity of EML1-GFP along the entire length of MTs, as visualised in the false-coloured heat maps of EML1-GFP along one MT (Fig. 5C). In addition, we found that the plus end binding affinity of EML1 reduced by lowering the EML1 concentrations in the lysates (Fig. 5F).

The two representative examples in which we tested the concentration-dependency of the MT behaviours observed in our ex vivo settings showed that it is possible to obtain quantitative insights into phenomena observed by this type of assay. We demonstrated that the observed MT phenotypes induced by MACF1-C1020 and EML1 are concentration-dependent, and that the optimal concentrations for them to occur can be estimated by our approach.

From ex-vivo to in vitro

One of the key questions in our lysate-based approach is to determine the impact of other, so far unknown factors present in the cell lysates on the observed MT behaviour. As our initial goal in establishing the ex-vivo approach was to circumvent the necessity of protein purification, which is often the limiting step for in vitro reconstitution experiments, purification of all of the MAPs we have analysed so far is not a valid option to answer this question. However, as all tested MAPs were soluble in our cell lysates, we aimed at purifying some

selected MAPs directly from those lysates and test their activities as purified components. To do so we first added a Strep II tag to the GFP-tagged constructs, expressed the fusion protein in HEK293 cells, and then purified them directly from the cell lysates using Strep-affinity purification (Hua and Jiang 2020). Using this approach, we purified MACF1-C1020-GFP-Strep II in a soluble form (Fig. 7A).

We then tested whether the very peculiar MT phenotype of MACF1-C1020, the formation of hooks on growing MT ends, could be reproduced with purified components in a minimal system. We combined tubulin purified from Hela cells (Souphron et al. 2019) with purified MACF1-C1020-GFP (Fig. 7A) and observed MT growth by TIRF microscopy (Fig. 7). Strikingly, within a range of MACF1-C1020-GFP concentrations tested (413 nM -1.652 µM), no MT growth and decoration by MACF1-C1020-GFP was observed. At a concentration of ~820 nM, we observed rare events of formation of MACF1-C1020-GFP- rings (Fig. 7A, first panel, shown with arrows in magenta), which could not be identified as MTs.

To test if this was due to loss of activity of the purified MACF1-C1020-GFP, we re-added ~820 nM of purified MACF1-C1020-GFP to a lysate of untransfected cells and repeated the experiment. In cell extracts, purified MACF1-C1020-GFP decorated polymerising MTs and induced the formation of hooks as previously observed in the lysates (Fig. 7A, second panel, hooks are shown with arrows in magenta). This demonstrates that among the MT behaviours we observed in our ex-vivo approach, certain might not be induced by the activity of a MAP alone in in vitro assays with the purified components. This again underpins the strength of our ex-vivo approach in overcoming the purification bottleneck that in most cases makes the in vitro reconstitution of MT-MAP assemblies a cumbersome and time-consuming endeavour. Fig. 7B shows the Coomassie-stained SDS PAGE gel of purified MACF1-GFP and HeLa tubulin used for the experiments.

Ultrastructural studies of MAP-MT interactions using cell lysates

One of the greatest challenges to understand the functions of MAPs at the molecular level is that many of them are intrinsically unstructured proteins. Recent advances in cryo-electron microscopy have allowed to solve high-resolution structures of MAPs bound to MTs. Strikingly, these studies demonstrated that MAPs can adapt defined structures upon their binding to the MT surface, and delivered detailed insight into their mode of binding (Kellogg

et al. 2018; Adib et al. 2019; Manka and Moores 2018; Zhang, Roostalu, et al. 2017). Similar to in-vitro reconstitution experiments, these structural studies require purified, functional MAPs, thus encountering the known limitations of protein purification. Having demonstrated that most MAPs we have tested here were functional in cell lysates, we aimed at testing the possibility to use these lysates to obtain high-resolution structures directly of MAPs decorating MTs. To test this possibility, we aimed at solving the structures of EML1, EML4 and MACF1-C1020 bound to MTs. The crystal structure of the EML1 TAPE domain (~70 kDa) has been solved with 2.6-Å resolution (Richards et al. 2015), but the binding architecture of full length EML1-MT is still unknown.

Prepolymerised GMPCPP MT seeds were seeded in warm BRB80 on a cryo-EM grid mounted in the Vitrobot (Fig. 8A). The seeds were incubated for 10-20 s for adsorption to the grid before 3 µl of freshly thawed cell lysate containing overexpressed GFP-MAP was applied. After 20-30 s incubation grids were plunge-frozen in liquid ethane, and imaged with Titan Krios (FEI) G3 transmission electron microscope. Electron micrographs of all three MAPs show a clear decoration of the MTs in the micrographs (Fig. 8B). EML1 and EML4 generate straight MTs, whereas MACF1 shows MTs ending with splayed ends, as well as structures resembling protofilament rings (Fig. 8B). Fig. 8C shows the top (14-protofilaments) and lateral view of MTs decorated by full-length EML1(details of image processing and 3D reconstruction are in the method section). The helical reconstructed image shows full-length EML1 binds MTs along the MT protofilament with a resolution of 3.7 Å. Fig. 8D shows EML1 density with fitted models for α- and β-tubulin might interact with flexible tubulin C-terminal tails.

Visualising direct competition between different MAPs using cell lysates

A currently emerging question is how do different MAPs interact on, and compete for the same MTs. Recent studies have provided direct evidence that MAPs compete for binding on MTs. Given that those MAPs also affect the activity of MT-based motor proteins, it is likely that the balance between different MAPs on MTs could determine their specific functions in cells. For instance, MAP7 and Tau compete for MT binding and influence the motor motility of kinesin-1 and kinesin-3 in vitro. MAP9 competes with DCX and DCLK1 for binding on MT lattice and influences the motility of kinesin-3 (Monroy et al. 2018; Monroy et al. 2020). Those studies are again limited by several obstacles, such as the possibility to obtain soluble and functional purified MAPs, or the compatibility of buffers in which the different components of the assay

(MAPs, motor proteins, MTs) are functional. Given that many MAPs are functional in cell lysates, we tested the possibility to perform competition experiments using our ex vivo approach.

As an example, we chose to directly visualise how a mutation of EML1 affects the MT-binding of this MAP. EML1^{Thr243Ala} is a mutation found in patients with subcortical heterotopia, a neurodevelopmental disorder leading to brain malformation (Kielar et al. 2014; Uzquiano et al. 2019). We first tested whether both, wildtype and mutated form of EML1 interact with dynamic MTs in our TIRF assay (Fig. 9A). While wildtype EML1 tagged with GFP efficiently formed and decorated long MTs, EML1^{Thr243Ala}-GFP induced the formation of shorter MTs (Fig. 9C), which however were still decorated with EML1^{Thr243Ala}-GFP (Fig. 9A).

To determine whether this EML1^{Thr243Ala}-GFP fails to efficiently polymerise MTs due to a loss or gain of function, we combined two lysates expressing EML1-mCherry and EML1^{Thr243Ala}-GFP and imaged in both colours over 5 min. While EML1^{Thr243Ala}-GFP alone was able to bind to MTs (Fig. 9A), we observed no MT binding of EML1^{Thr243Ala}-mCherry in the presence of wildtype EML1-GFP. This indicates that EML1^{Thr243Ala} has a lower affinity to MTs than wildtype EML1, and is therefore efficiently outcompeted by the wildtype version of EML1. To exclude a potential bias by different fluorescent tags, experiments were repeated with swapped fluorescent tags (Fig. S13). To determine the relative binding of the two EML1 variants, total MT length decorated by GFP and mCherry versions of EML1 were measured using ImageJ at definite time points (Fig. 9D and S13B).This clearly demonstrates that the Thr243Ala mutation in EML1 directly affects the MT-binding affinity of this MAP, which might in turn affect the overall dynamics and architecture of the MT cytoskeleton in patients carrying this mutation (Kielar et al. 2014; Uzquiano et al. 2019).

Conclusion

Structural MAPs have for decades been considered as stabilisers of MTs. So far, there are hundreds of proteins reported as MAPs, but only a few of them are well characterized. Moreover, even the well-characterised MAPs have been analysed in independent studies. To date, there are no systematic studies that compare a set of different MAPs under similar experimental conditions, which has impeded the emergence of a more general picture of the

role of MAPs in controlling MT functions. MAPs are intimately linked to many functions of living cells, such as cell division, assembly and functioning of cilia, neuronal functions. At the same time, MAPs are also linked to several human diseases, most famously to neurodevelopmental and neurodegenerative disorders.

Given the broad physiological importance of MAPs, and the growing number of barely characterised MAPs, there is a clear need for a method capable allowing to study the impact of MAPs on the behaviour of dynamic MTs at a medium-throughput scale.

Here we set up a method to characterise a large number of MAPs in parallel, thus allowing for the first time the direct comparison of their different effects on the assembly dynamics of MTs. In our studies, we chose a representative set of MAP candidates independent of their cellular roles; some of them were known as neuronal MAPs, others are cell division MAPs, and some of the MAPs analysed here are abundant in cilia and flagella.

To make our pipeline independent from the outside sources, we based it on de-novo molecular cloning of each candidate MAP. All proteins were tested for MT localisation in cells, where most of the bona-fide MAPs either bundle, or partially decorate MTs. This rather uniform behaviour of MAPs overexpressed in cells is one of the reasons all ‘structural MAPs’ are commonly considered as MT bundlers, however, it should be noted that all these overexpression experiments induce non-physiological conditions due to an over-abundance of the MAPs. This inspired the development of our method which is based on cell-lysates, thus circumventing the known difficulties of protein purification and the related optimisation steps, but still allowing the cell-free reconstitution of MT arrays using TIRF microscopy. The simplicity of the cell extracts coupled with virtually all advantages of the in vitro system allowed us to characterise a large number of MAPs (>50), which could easily be expanded in the future. This in turn allows for studying not only MAPs, but also mutated forms of these proteins, which are more and more identified in a large variety of human diseases. Moreover, we demonstrated that our approach can be used to obtain high-resolution structures of MAPs bound to MTs by cryo-electron microscopy. Given that most of the MAPs we analysed were soluble and functional, this provides the possibility to perform such studies with a much higher throughput than previously possible methods.

The most surprising, and thus striking result of our study is that we discovered a plethora of behaviours of MTs induced by MAPs that had not been described so far. For instance, MACF1 forms hooked MT ends, CSAP induces helicoid MTs, MAP7 generates MT asters, MAP2 induces MT protofilament peeling, MAP8 leads to MT fragmentation, and EML1 forms gradients along the MT lattice. In addition, our approach provided a straight-forward tool to

study the role of MAPs in actin-MT crosstalk. We further tested the feasibility of our assay to perform MAP competition experiments. Competition between MAPs is emerging as a key regulator of MT functions and specialisation in cells, and a MAP-code hypothesis has been proposed in analogy to the tubulin-code.

We thus demonstrated using fluorescently labelled proteins in cell extracts directly for ex-vivo reconstitution of cytoskeletal assemblies using TIRF microscopy is a fast, simple and medium-throughput approach to potentially characterize any proteins associated with MTs. Our success in obtaining a wide range of soluble, functional proteins in this assay impressively illustrates the power of this method. By demonstrating the possibility to expand the assay to ultrastructural analyses, to study cytoskeletal crosstalk and inter-MAP competition, and to characterise disease-related mutations we illustrate the potential of the ex-vivo pipeline to advance our mechanistic understanding of the MT cytoskeleton and its associated proteins involved in a wide variety of cellular functions and human diseases.

Method details

MAP cloning using Sequence and Ligation Independent Cloning (SLIC) method

The open reading frames for proteins of interest were cloned from cDNA libraries from different mouse organs (brain and testis) or immortalised cell lines into pTRIP (Gentili et al. 2015) vector under the CMV-enhanced chicken beta-actin (CAG) promoter (Alexopoulou, Couchman, and Whiteford 2008) using SLIC method (Jeong et al. 2012) as described previously (Bodakuntla, Janke, and Magiera 2020) (Suppl. Fig. S1). Briefly, pTRIP vector was linearized with restriction enzymes NheI or BsrGI/BamHI and gel-purified. pTRIP vector was opened at NheI site to tag the GFP C-terminally to the MAP (MAP-GFP) and was opened at BsrGI and BamHI to tag the GFP N-terminally to the MAP (GFP-MAP). MAP candidates were amplified from cDNA libraries using respective primers (Suppl. Table 1) that contain at least 15 bp homology to the ends of the target vector and gel-purified. Linearized vector (2 vol) was mixed with the insert (7 vol) on ice. 0.3 vol of T4 DNA polymerase was added to the mix for 2.5 minutes at room temperature to generate 5' overhangs. The reaction was stopped on ice, and E. coli competent cells were added to the mix, transformed, and plasmids were selected on ampicillin containing LB-agar plates. Plasmid DNA from about six clones per cloning reaction was purified and confirmed by enzymatic digestion. This was followed by complete sequencing of 2-3 positive clones to ensure the sequence identity of the proteins.

Cell fixation, immunostaining and imaging

U2OS cells plated on coverslips were transfected with pTRIP vector encoding different proteins of interest for 24 or 48 hours and were fixed following earlier described protocols (Magiera and Janke 2013). Briefly, the cells were incubated with Hank's Balanced Salt solution (HBSS) buffer and microtubule-stabilizing buffer (MTSB) containing homo-bifunctional cross-linker Dithio-bis (succinimidyl propionate; DSP; #22585 Thermo Fisher Scientific) for 10 mins each. This was followed by fixing the cells with 4% paraformaldehyde (diluted in MTSB) for 15 mins. The cells were then permeabilized with 0.5% Triton X-100 in MTSB for 5 mins and followed by blocking in 5% bovine serum albumin (BSA) prepared in PBS containing 0.1% Triton X-100 (PBST) (blocking solution). Cells were incubated with primary antibody (Anti-α-tubulin antibody 12G10, 1/1,000, developed by J. Frankel and M. Nelson, obtained from the Developmental Studies Hybridoma Bank, developed under the auspices of the NICHD, and

maintained by the University of Iowa)) diluted in blocking solution for 1 h at room temperature (RT). Cells were then incubated with secondary antibody (goat anti-mouse Alexa Fluor 568, 1:1,000; Thermo Fisher Scientific #A11019) diluted in blocking solution for 1 h at RT. Coverslips were mounted onto glass slides using ProLong Gold anti-fade medium (#P36930, Thermo Fisher Scientific). Images were acquired using Optigrid (Leica systems) microscope equipped with a 63x (numerical aperture 1.40) oil immersion objective and the ORCA-Flash4.0 camera (Hamamatsu) set at binning 1 X 1. The microscope was operated through Leica MM AF imaging software. Images were processed using Fiji (Schneider, Rasband, and Eliceiri 2012) and adobe photoshop. Final figures were prepared using Adobe illustrator.

Cell culture and transfection for lysate preparation

1.0×10^6 HEK 293 cells (Human embryonic kidney cells) were seeded on 22-cm^2 petri dishes. For getting a sufficient quantity of lysates for multiple experiments, six Petri dishes were used for each MAP construct. Cells were grown up to ~80% cell confluency in DMEM medium supplemented with 10% (vol/vol) FBS, 2 mM L-Glutamine, and 1× Penicillin-Streptomycin (Pen Strep). Subsequently, cells were transfected using jet PEI (5 µg of DNA and 10 µl of jetPEI per dish in a serum-free DMEM, supplemented with 2 mM L-Glutamine, and 1× Pen Strep) according to the manufacturer's guidelines. Transfected cells were cultured at 37 °C with 5% (vol/vol) CO2, for 24 - 48 hours based on the GFP expression. Before lysate preparation, all dishes were strictly checked under a simple fluorescence microscope for homogenous GFP expression levels. Dishes with low transfection efficiency or cell lethality due to random errors were discarded and repeated with a new set of cells in order to maintain nearly constant tubulin-MAP ratios.

Cell lysate preparation for TIRF microscopy and cryo-EM

Lysate preparation was done based on a modified version from Soppina et al., 2014 (Soppina et al. 2014) for COS-7 lysates and Bergman et al., 2018 for yeast cell lysates. The first part of the process is the removal of the media from the transfected cells, then gently washed the cells with warm PBS (1.5 ml 1X PBS per dish), detached with trypsin (500 µl of trypsin-EDTA per dish, without any incubation), and collected in 2 ml of warm DMEM media having FBS. Media containing detached cells were transferred to a 15- or 50-ml falcon tube based on the number

of Petri dishes used, followed by cold centrifugation (453 g, 4°C, 10 min) (Fig. 2A). Subsequently, the media was removed, and cell pellets were resuspended in the lysis buffer (1× BRB80 with 0.05% Triton-X100 and 1× protease inhibitor cocktail). 150-300 µl of buffer volume was used in order to keep the lysate concentrated, and the whole lysate was transferred from a falcon tube to a 1.5 ml Beckman ultracentrifuge tube. For efficient lysis, cells were pipetted up down on the ice for another 5-8 minutes with short incubations on ice. Then, samples were sonicated with three short pulses (probe details: 6.5 mm probe diameter (Branson #101-148-070), set at "Output control" 1, "Duty cycle" 10%). After the lysis, samples were ultra-centrifuged (Beckman TLA 55; 33,800 g, 4°C, 25 min) with a Beckman Coulter optima MAX-XP benchtop ultracentrifuge. Subsequently, the supernatant was collected and made aliquots of 5-10 µl and snap-frozen immediately. MAP lysate samples can be stored at -80 °C for one month and can be used for TIRF assays and Cryo-EM studies. All steps after the collection of cells should be strictly on ice, which ensures MT depolymerization and detachment of bound MAPs (Fig. 2A).

Protein quantification and western blotting

For controlling the concentrations of tubulin and MAP in lysate experiments, and to make it more reproducible and interpretable, we mainly measured three parameters: 1) total protein concentration in the lysates (by BCA protein assay), 2) tubulin in the lysates (by immunoblots with tubulin antibody) and 3) GFP tagged MAPs (by immunoblots with GFP antibody).
Total protein concentration informs the approximate amount of tubulin in the cell lysate (~3% of the total protein is tubulin (Hiller and Weber 1978)). For this, MAP lysates were thawed and diluted in 1× PBS and used for total protein estimation by Bicinchoninic acid (BCA) protein assay in a 96 well plate. Each MAP samples were made as multiplicates for 2-3 dilutions. By following the manufacturer's catalog, freshly prepared BCA reagent was used for each experiment with a sample to reagent ratio of 1:8. The mix was incubated at 37°C for 30 minutes, and absorbance was measured at 570 nm with a microplate reader (TriStar² LB 942 Multimode Microplate Reader with a MikroWin 2010 software). The absorbance values of the BSA standard dilution series were plotted and fitted to a linear equation and obtained the total protein concentration using the linear equation (Brady et al., Anal Biochem. 2015).

The approximate amount of MAP and tubulin concentration in the lysates was quantified using immunoblot. All of the MAP constructs used in this study have an N- or C-terminus GFP tag. As a first step, the concentration of purified GFP protein and (Fig. 4D) was estimated using a Coomassie-stained SDS PAGE gel by comparing it with different known BSA concentrations. As a second step, cell lysates were diluted to 3 different concentrations and performed western blots (Fig. 4A) within a linear range of antibody detection for both GFP tagged MAP and tubulin separately. The GFP antibody Torrey pines biolabs(Cat: TP401) (1:2500) was used against GFP tagged MAPs. By comparing the band intensity of the known concentration of brain tubulin and purified GFP protein, the unknown concentration of tubulin and MAPs were estimated using ImageJ(https://openwetware.org/wiki/Protein_Quantification_Using_ImageJ).

Cleaning of glass slides and assembly of flow chambers

TIRF flow chambers were prepared according to a modified protocol as Gell et al. 2010. For the preparation of TIRF chambers, glass slides (76 × 26 mm; Thermo scientific) and coverslips (22 × 22 mm; thickness no. 1.5, VWR) were sonicated in acetone, ethanol, and water separately. For this, two clean bottles were taken, filled with 100% acetone, and added the glass slide and coverslips. In the glass slide, each slide was wiped with kimtech paper before putting it into the acetone and added one by one (to make sure that they are not stuck together). Subsequently, bottles were sonicated in a water bath for 15 minutes at room temperature. After sonication, acetone was discarded and rinsed with water (adequate amount to immerse glass slides/ coverslips). The bottles were then refilled with fresh ultra-pure water and sonicated as before, followed by a final sonication in 100% ethanol. Cleaned glass slides and coverslips can be stored in fresh 100% ethanol for up to one month.

TIRF flow chambers (Fig. 2B) were assembled by following Li et al. 2012 and Gell et al. 2010. Glass slides stored in 100% ethanol were dried using a flame and placed on a clean surface. Four long strips of double-sided adhesive tape were pasted to get three chambers on a single glass slide (Fig. 2B). Subsequently, double-sided tape on the glass slide was pressed with the backside of the forceps to stick it firmly and peeled off the other side with forceps. Afterwards, a new coverslip stored in 100% ethanol was dried using a flame and placed on top of sticky tape and hit gently with the rear side of the forceps. The typical volume of a single chamber is around 7-10 µl. Prepared chambers can be stored at room temperature for a few weeks.

For TIRF reconstitution assays with purified proteins, the glass slides and chambers were prepared as detailed in Bieling et al. 2010. Coverslips (22 × 22 mm; thickness no. 1.5, VWR) were cleaned first by sonicating in 3 M NaOH, followed by sonicating in the Piranha solution. Cleaned coverslips were silanized with (3-Glycidyloxypropyl) trimethoxysilane or GOPTS (Sigma), and were coupled with polyethylene glycol (PEG), by adding a mixture of hydroxyl-PEG-3000-amine (Rapp Polymere, 103000–20) and biotin-PEG-3000-amine (Rapp Polymere, 133000-25-20) (Bieling et al., 2010). Finally, glass slides were passivated with poly(L-lysine)-PEG (SuSoS) just before the assembly of flow chambers (Bieling et al., 2010).

Preparation of GMPCPP seeds

GMPCPP seeds were prepared with a 20-µM total tubulin concentration, which contains 10-15% rhodamine-labelled brain tubulin (Cytoskeleton Inc.), and unlabelled pig brain tubulin (purified as described in Castoldi & Popov, 2003) in 1X BRB80 buffer (80 mM K-Pipes pH 6.8, 1 mM EGTA and 1 mM $MgCl_2$). The mix was then centrifuged (98,400 g, 4°C, 30 min) at cold in order to get rid of tubulin precipitates and polymerized MTs. Subsequently, the supernatant containing soluble tubulin was transferred to a fresh tube, added 0.5 mM of GMPCPP (Jena Biosciences), and incubated on ice for 5 min. Afterwards, the tube was moved to 37°C and incubated for 1 h. Subsequently, the mix was centrifuged (19,949 g, 10 min) at 37°C and washed the pellet with warm BRB80 buffer (19,949 g, 3 min, 37°C). The final MT pellet was resuspended in warm BRB80 buffer, having 10% glycerol, snap-frozen in small aliquots, and stored at -80°C. For longer storage at -80°C, double cycled GMPCPP seeds were prepared as described in Gell et al. 2010.

MT reconstitution and TIRF microscopy

For attaching MTs, KIF5B with a walker mutation (C275A; Nakata and Hirokawa, 1995) was purified from E. coli and used as described in Lacroix et al., J Cell Biol., 2010. Flow chambers were first blocked by flushing in 50 µg/ml of ß-Casein in BRB80 and incubated for 5 minutes. Subsequently, 0.75 µM of dead kinesin was flushed in, absorbed with a filter paper from the other end, and incubated for 5 minutes. After a wash with warm BRB80 buffer, diluted GMPCPP seeds in warm BRB80 was flushed into the chamber and waited for 5 minutes for immobilizing the seeds. Excess and unattached seeds were washed out using warm BRB80 buffer and loaded under the TIRF microscope to confirm similar GMPCPP seed density for all

MAP experiments. After that, a fresh tube of lysate from -80°C was thawed, adjusted to 8 mg/ml total protein concentration (concentrated lysates were diluted with 1X BRB80 buffer), flushed into the chamber and immediately started the image acquisition. All the image data for this study were acquired using a Nikon TIRF inverted microscope (100X oil objective), imaging area: 68.1 X 68.1 µm, 1.49 numerical aperture (NA), and images were captured by evolve CCD camera using a Metamorph software with a Modular interface for TIRF. TIRF plane was illuminated with 488 nm for GFP tagged MAP and 561 nm for GMPCPP seeds (rhodamine-labeled brain tubulin (Cytoskeleton Inc.)) for 11.612 min total duration with a frame interval of 1.98 (≈ 0.5 frames/ second or 1 frame per 2 seconds). This was strictly followed for all the 50 MAP assays.

Once the time-lapse imaging was finished, the chamber was washed with warm BRB80 buffer to get rid of excess unbound MAPs and soluble tubulin. Visualization of MTs was accomplished using antibody staining. For this YL1/2 antibody (MCA77G, AbD Serotec) in 1:100 dilution, it was flushed first to the chamber and incubated for 5 min. Afterward, the chamber was washed with warm BRB80 buffer, subsequently flushed in Alexa 565 rat secondary antibody, and incubated for another 5 minutes. Excess secondary Ab was washed off with warm BRB80 buffer and flushed in 500 nM of SiR-Actin to visualize actin filaments. After 5 minutes of incubation with SiR-Actin, the chamber was washed and loaded for TIRF microscopy.
For the experiments to check the role of MAPs in actin-MT crosstalk or the role of actin in MT phenotypes, lysates for each MAPs were split into two sets and performed TIRF assays. One set with actin monomer sequestering drug Latrunculin A (11 µM) and the second without the drug. Subsequently, the formation of filamentous actin was visualized with SiR-Actin (at 647 nm) for both cases, and images were captured and analyzed separately. MT dynamic assays with purified proteins, were performed as described in Bieling et al., 2010 and Roostalu et al., Elife. 2020.

Image and data Analysis for TIRF assays

All the TIRF images for 50 MAPs, both with actin (3-color TIRF) and without actin (2-color TIRF), were analyzed using Fiji software. Raw images and videos underwent shading correction with a homemade macro. The free plugins such as Hough circle transform (https://imagej.net/Hough_Circle_Transform) were used for the automatic detection and measurement of the diameter of MT hooks induced by MACF1. The width (Suppl. Fig. 14) of

CSAP induced MT coils was measured manually by drawing line and measured the length in Fiji software. The length of MTs decorated by wild type and mutant EML1 in competition experiments were estimated using the FeatureJ plugin in ImageJ. All the graphs in this study were plotted using Prism-GraphPad software.

Sample preparation for cryo-electron microscopy

Quantifoil gold holey carbon grids R 1.2/1.3 were glow discharged in a GloQube Glow Discharge (Quorum Technologies) system for 90 seconds. Sample application and vitrification were carried out in a Vitrobot (ThermoFisher Scientific) set to 25°C and 100% humidity using a Whatman No. 1 filter paper for blotting.

The cellular lysate containing overexpressed MAPs (EML1, MACF1-C1020, and EML4) stored at -80°C was thawed and warmed only before application on the grids. 1 µl of the GMPCPP MT seeds (prepared as above for the TIRF MT reconstitution assays) in warm BRB80 was applied on the grid mounted in the Vitrobot. After a brief incubation of 10-20 s to allow for adsorption of the seeds onto the grid, 3 µl of pre-warmed lysate was applied to the same grid. The grids were then blotted after an incubation time of 20 s with a blot force of 0 and blot time of 3 s before plunging into liquid ethane.

Electron microscopy

The frozen grids were transferred to an Autoloader under liquid nitrogen conditions and mounted into a Cs corrected Titan Krios (FEI) G3 transmission electron microscope operating at 300keV and attached to the Falcon III detector. Data collection was carried out using the automated pipeline of the EPU software system. 30 frames were collected per movie in the linear mode at a dose rate of 1.35 electrons/pixel/sec and a total dose of 44.17 electrons/Å2. Images were collected at a magnification of 59,000x, resulting in a pixel size of 1.38Å and a defocus range between -1.8 to -3.0 µm.

Image processing and 3D reconstruction

Images were manually inspected for the presence of ice contaminants and filament quality, and unwanted micrographs were discarded. Motion correction of the movie frames was done using

the inbuilt feature of MotionCorr2 (He and Sjors, 2017) in RELION 3.0. CTF estimation was done by GCTF (Zhang K., 2016) on dose weighted and motion-corrected summed images. Particles were manually boxed using the helical picking option of RELION 3.0 using a box size of 600 Å and overlapping inter-box distance of 82 Å. Processing was carried out using RELION 3.0 and customized scripts to reconstruct MTs with a seam (pseudo-helical symmetry) (Cook A., 2020). 2x binned particles were used during the initial stages of processing. The particles were segregated into classes based on protofilament numbers by one round of 3D classification using low passed synthetic references of MTs made up of different protofilament numbers including 11, 12, 13, 14, 15 and 16. The class containing 14 protofilament MTs which formed the dominant class was selected for further processing. A few cycles of refinement were used to improve the alignment of all the particles. A 14 protofilament MT with pixels doubled for loop regions of S9-S10 and H1-S2 (different in α and β tubulin), and low passed to 6 Å was used as the reference in these stages (Adib R, 2019). Phi angle was determined for the particles, and the modal value was assigned to all particles in a single MT. This was further checked by 3D classification using low passed references of 14 protofilament MT (with enhanced pixels for S9-S10 and H1-S2 loop regions) rotated and shifted (by one monomer repeat of 4 nm) to accommodate all possible 28 positions for a 14 protofilament MT with seam. The segments were flipped to the modal positions and corresponding phi angles were assigned to all segments in a given MT. Finally, refinement was carried out on unbinned aligned particles using a low passed 14 protofilament MT reference without applying helical symmetry.

Acknowledgements

This work was supported by the ANR-10-IDEX-0001-02, the LabEx Cell'n'Scale ANR-11-LBX-0038 and the Institut de convergence Q-life ANR-17-CONV-0005. CJ is supported by the Institut Curie, the French National Research Agency (ANR) awards ANR-12-BSV2-0007 and ANR-17-CE13-0021, the Institut National du Cancer (INCA) grant 2014-PL BIO-11-ICR-1, and the Fondation pour la Recherche Medicale (FRM) grant DEQ20170336756. JAS was supported by the European Union's Horizon 2020 research and innovation programme under the Marie Skłodowska-Curie grant agreement No 675737, and the FRM grant FDT201904008210. SB was supported by the FRM grant FDT201805005465.
MMM is supported by the Fondation Vaincre Alzheimer grant FR-16055p.
We thank Thomas Surrey's lab (Francis Crick Institute, London) for the surface treatment trainings (in vitro MT reconstitution experiments). We also thank Clara Nahmias (Gustave

Roussy Cancer Center) for providing the ATIP3 constructs. We are grateful to Cedric Messaoudi, M.-N. Soler and C. Lovo from the Multimodal Imaging Center (MIC) CNRS UMR2016 / Inserm US43) for the imaging facility.

Declaration of interests

The authors declare no competing interests.

Figure Legends:

Figure 1: Schematic overview of the pipeline used to study more than 50 MAPs, and overexpression studies of selected MAPs in cells.

A) Overview of the strategy used to study around 50 MAP candidates 1) Molecular cloning of more than 50 MAPs using SLIC (Sequence and Ligation Independent Cloning) method, 2) MAP overexpression studies in U2-OS cells to observe the cellular localization of MAP candidates, 3) Preparation of cell lysates from HEK cells having overexpressed MAPs for the ex-vivo screen using TIRF microscopy, 4) Use of cell lysates for the ex-vivo screen of all the MAP candidates using MT reconstitution and TIRF microscopy, and cryo- electron microscopy of selected MAPs, and 5) Refinement of the ex-vivo observation in more controlled conditions.

B) U2-OS cells were transfected with Syntaphilin C, MACF1-C1020, Tau 4R, MAP11 and MAP7D3 tagged with GFP for 24 hours and were stained for MTs. Representative images of a cell with a particular MAP expression and its binding to MTs has been shown in the figure. MACF1-C1020, MAP7D3 induced a wavy network of MT bundles whereas Tau induced rather thick bundles of MTs. MAP11 showed diffused localization throughout cellular cytoplasm. Syntaphilin C showed weak binding to MTs. Scale bar 20 μm.

Figure 2) Flow diagram of different steps of the ex-vivo method used to study MAPs using TIRF microscopy and cryo-electron microscopy, and its validation with two well-characterized MAPs- spastin and EB3.

A) Ex-vivo pipeline showing different steps of lysate preparation from HEK 293 (Human Embryonic Kidney 293) cells and subsequent use of the lysate for TIRF microscopy, and cryo-electron microscopy. HEK 293 cells transfected with MAPs of interest tagged with a GFP were collected by short speed centrifugation at 4 °C, followed by lysis in BRB80 buffer on ice. Lysed cells were centrifuged at high speed and the supernatant fraction (which contains soluble MAPs of interest) was collected, snap-frozen, and stored at -80 °C. Lysates for all the MAPs were further used for MT reconstitution experiments by TIRF microscopy. Besides, for selected MAPs, the lysates were used for cryo-EM studies to see the MAP-MT binding architecture.
B) Assay chamber used for the MT reconstitution experiment and TIRF microscopy using cell lysates.

C) Ex-vivo cell lysate approach was first validated with two well-characterized proteins associated with MTs- Spastin and EB3. The first row is the time-lapse TIRF images of spastin mediated severing (arrows in magenta) of taxol-stabilized MTs (in green). The overexpressed spastin in HEK 293 cells was used for this assay. The second row is the time-lapse of EB3 comets (blue arrows) on growing MTs. GMPCPP MT seeds are shown in green, –and EB3

tagged with GFP are shown in white. Here the tubulin polymerizing from GMPCPP seeds are the endogenous HEK 293 tubulin. n ≥ 5 technical repeats from n ≥ 3 independent set of lysates. Scale bars = 5 μm. Time-lapse (minutes: seconds).

Figure 3) Time montage of different MAPs showing their novel properties, and staining of reconstituted microtubules and actin filaments from cell lysates.

A) Time-lapse (minutes: seconds) images of MAPs showing unique MT phenotypes. 2C and 2D isoform of MAP2 induces protofilament peeling from growing MT lattice, and decorates curled protofilaments as MAP2 clumps. MAP7 induced MT-aster formations, MACF1-C1020 induced the formation of MT hooked ends at the growing end, and MAP8 induced MT fragmentation. EML1 shows a higher binding affinity on growing MT ends than the MT lattice. CSAP induced MT coil formations. n = 5-10 independent TIRF assays from 3-6 independent sets of lysates. In the time-lapse images, GMPCPP MT seeds are in green, and MAPs tagged with GFP is in white. Scale bars = 5 μm.

B) Immunostained MTs with YL1/2 antibody and actin filaments stained with Sir-actin. MTs are shown in green, actin filaments are shown in red, and MAP decorating MTs are shown in white.

C) Zoomed-in view of the individual MT phenotype induced by different MAPs, and schematic representation of the corresponding phenotypes (MT GMPCPP seeds are shown in green, and MAP decorating MTs are shown in grey).

Figure 4) Quantification of unknown concentrations of MAPs and tubulin from lysates using known concentrations of purified GFP and tubulin.

A) Unknown concentrations of MAPs tagged with GFP in lysates were analyzed and compared with the known concentration of purified GFP by Western blot using GFP antibodies. The first five lanes have 3.125, 6.25, 12.5, 25, and 50 ng of purified GFP; the remaining lanes have three unknown concentrations of MACF1-C1020 and EML1 lysates, and the highest concentration of lysates for the control (wild type).

B) The titration curve obtained from a scatter plot (known concentration of purified GFP versus band intensities from western blot) was used to estimate the unknown concentration of total GFP tagged MAPs in the cell lysate.

C) Coomassie blue-stained SDS PAGE gel images of purified GFP (from HEK cells) used for the quantifications.

Figure 5) Hook formations by MACF1-C1020, and plus-end affinity of EML1 are a concentration-dependent process.

A) MT reconstitution and TIRF microscopy of four different concentrations of MACF1-C1020 using lysates. The MACF1-C1020 concentration is determined using the western blots as shown in Fig. 4, and the TIRF experiments were performed at 17.5 nM, 35 nM, 70 nM, and 140 nM of MACF1-C1020 concentrations.

B) MT reconstitution and TIRF microscopy of four different concentrations of EML1 using lysates. The EML1 concentration is determined using the western blots as shown in Fig. 4, and the experiments were performed at 200 nM, 100 nM, 50 nM, and 25 nM of EML1 concentrations.

C) Heat map of EML1 intensity showing EML1 has a higher binding affinity at the growing end of the MTs comparing the negative end.

D) Representative lattice intensity profile of EML1 decorating growing MT.

E) Quantifications of MACF1-C1020 hook phenotype for four different MAP concentrations.

F) Quantifications of EML1 plus end affinity for four different EML1 concentrations.

Figure 6) Quantification of MACF1-C1020 mediated hook formations.

A) MACF1-MT reconstitution experiments used for the automated detection of MT hooks and measurement of their diameter. Top panel shows the time-lapse images used for the detection of hooks before pre-processing, the skeletonized hooks used for the detection of circles/ hooks (middle panel), bottom panel shows the detected circles in orange, and MTs are shown in green. Scale bars = 10 μm.

B) Single hook and double hook formations were the two prominent MT phenotypes observed for MACF1-C1020. Using Hough Circle Transform, the measured hook diameters are 1.1 um (for single hooks) and 0.8 um (for double hooks).

Figure 7) TIRF reconstitution assay with purified MACF1-C1020 and HeLa tubulin.

A) Coomassie blue-stained SDS PAGE gel images of purified MACF1-C1020-GFP (from HEK 293 cells) and tubulin (from HeLa cells) used for in vitro MT reconstitution and TIRF assays.

B) Time-lapse images of MT reconstitution assays with MACF1-C1020 purified from HEK 293 cells. Top panel shows the MT reconstitution experiments of purified MACF1-C1020 mixed with wild type cell lysates showing MT hook formations. Bottom panel shows the MT reconstitution experiments with only purified proteins: MACF1-C1020 (826 nM) and HeLa tubulin (12 µM). GMPCPP MT seeds are shown in green, and GFP tagged MACF1-C1020 are shown in white. Scale bars = 5 µm.

Figure 8) Ex-vivo lysate approach for studying MAP-MT binding architecture using cryo-electron microscopy provides important insights into MAP binding.

A) Flow diagram showing the pipeline of cryo-electron microscopy approach using MAP lysates.

B) Cryo-electron micrographs showing MTs in the absence and presence of MAP (EML1, MACF1-C1020 and EML4) lysates. Scale bar = 100nm.

C) Top and lateral views of a symmetrized helical reconstruction (resolution, 3.7 Å) lowpassed to 15 Å of 14 protofilament MTs, shown in grey with extra density, most likely corresponding to EML1-GFP (shown in green). EML1 binds along the protofilament of a MT.

D) Density for a single protofilament from the symmetrized reconstruction lowpassed to 15 Å, shown as a mesh. The fitted models for alpha and beta-tubulin are shown in light and dark grey, respectively. The associated extra densities corresponding to EML1-GFP are shown in green, and might be interacting with the flexible C-terminal tails, whose position has been indicated in the figure.

Figure 9) Ex-vivo approach for MAP competition experiments: EML1 T243A mutant binds less and promotes less microtubule elongation comparing wild type EML1.

A) TIRF-microscopy still images of wild type EML1-GFP (top panel), and EML1 T243A-GFP (bottom panel). MTs are shown in green, and GFP tagged EML1 is shown in white. Scale bar = 5 µm.

B) Time-lapse of competition experiments: EML1 T243A-mCherry mutant and EML1-GFP wild type compete for binding on MT lattice. GMPCPP MT seeds and EML1 T243 mutant tagged with mCherry are shown in Cyan, and wildtype EML1 tagged with GFP is shown in Magenta. Top row is the time-lapse for EML1-GFP wild type, middle row is the EML1-mCherry mutant and bottom row is the merge of both channels. Scale bar = 5 µm.

C) Quantification of MT length for individual experiments with EML1 T243A mutant and EML1 wild type, both tagged with GFP (from Fig. 9A).

D) Quantification of MT length decorated by wild type EML1-GFP (Magenta) and mutant EML1-mCherry (Cyan) for different time points from the above competition experiment (Fig. 9B).

Supplementary figure 1: Overview of molecular cloning of MAP candidates using the SLIC method.

A) Vector map of the pTRIP-CAG-EGFP-2A lentiviral plasmid. MAPs were cloned into the lentiviral vector by opening at NheI site to generate a C-terminally GFP-tagged fusion protein, or with BsrGI and BamHI to generate a N-terminally GFP-tagged fusion protein.

B) Flow diagram of the different steps in the sequence- and ligation-independent cloning (SLIC) method. The gel-purified linearized pTRIP vector (2 vol) and the amplified PCR product (7 vol) were mixed on ice. The mix was then treated with T4 DNA polymerase to generate 3'overhangs and was transferred to the ice. E. coli competent cells were added, bacterial transformation was performed and plated on LB agar plates having ampicillin antibiotic according to standard protocols. Plasmids were amplified, isolated, and confirmed by both restriction digestion and DNA sequencing (adapted from (Jeong et al. 2012)).

Supplementary figure 2: Organisation of microtubule cytoskeleton in cells with overexpressed MAPs-part 1.

U2-OS cells were transfected with MAPs (MACF1, Cingulin, Nardilysin, MAP2D, CLIP-170, CRMP4, Syntaphilin A, GLFND1, TRAK1, POC, Syntaphilin C, MAP7D3, MAP7D1, EMAP6, TRAK1, Parkin, MAP10 and GLFND2) tagged with GFP for 24 hours and were stained for MTs. Representative images of a cell with a MAP expression and its binding to MTs has been shown in the figure. MTs are shown in Magenta and GFP tagged MAPs are shown in green. Scale bar = 20 µm.

Supplementary figure 3: Organisation of microtubule cytoskeleton in cells with overexpressed MAPs-part 2.

U2OS cells were transfected with MAPs (MAP7, EMAP3, Tau 3R, Tau 4R, MAP2C, MAP4, EMAP2, EMAP4, CSAP, MAP9, Doublecortin big, DCLK_4, DCLK_5, Jpl2, Spef1, EMAP1, MAP11 and CCDC66) tagged with GFP for 24 hours and were stained for MTs. Representative images of a cell with a particular MAP expression and its binding to MTs has been shown in the figure. MTs are shown in Magenta and GFP tagged MAPs are shown in green. Scale bar = 20 µm.

Supplementary figure 4: Organisation of microtubule cytoskeleton in cells with overexpressed MAPs-part 3.

U2OS cells were transfected with MAPs (ATIP3_domain1, ATIP3_domain 2, MAP6, CKAP4, Protein 4.1, CKAP2, Jpl1, Hice1 and C11ORF49) tagged with GFP for 24 hours and were stained for MTs. Representative images of a cell with a particular MAP expression and its binding to MTs has been shown in the figure. MTs are shown in Magenta and GFP tagged MAPs are shown in green. Scale bar = 20 µm.

Supplementary figure 5: Time montage of different MAPs showing their novel properties in the absence of actin filaments.

A) Time-lapse (minutes: seconds) images of MAPs showing unique MT phenotypes. 2C and 2D isoform of MAP2 induces protofilament peeling from growing MT lattice, and decorates curled protofilaments as MAP2 clumps. MAP7 induced MT-aster formations, MAP8 induce MT fragmentation, and EML1 shows a higher binding affinity on growing MT ends than the MT lattice. n = 5-10 independent TIRF assays from 3-6 independent sets of lysates. In the time-lapse images, GMPCPP MT seeds are shown in green, and MAPs tagged with GFP is shown in white. Scale bars = 5 µm.

B) Immunostained MTs with YL1/2 antibody and actin filaments stained with Sir-actin. MTs are shown in green, actin filaments are shown in red, and MAP decorating MTs are shown in white.

Supplementary figure 6: TIRF reconstitution assays to study MAP-MT interactions using ex-vivo approach in presence of actin -part 1.

A) Time lapse images (in rows) of TIRF-M assays for control (untransfected/ wild type lysate), MAP 10, EML3, GLFND1, EML2, Syntaphilin B, Syntaphilin C, and EML4 lysates. The GFP tagged MAPs are decorating MTs polymerized using tubulin from cell lysates. In the time montages, GMPCPP MT seeds are shown in green and GFP tagged MAPs are shown in white. Scale bar = 5 µm.

B) Still images of reconstituted MTs and actin filaments in presence of different MAPs using cell lysates. Immunostained MTs with YL1/2 antibody are shown in green, MAPs tagged with GFP are shown in white, and actin filaments (stained with SiR-actin) are shown in red. Scale bar = 5 µm.

Supplementary figure 7: TIRF reconstitution assays to study MAP-MT interactions using ex-vivo approach without actin- part 1.

A) Time lapse images (in rows) of TIRF-M assays in presence of Latrunculin A (F-actin inhibitor drug) for control (untransfected/ wild type lysate), MAP 10, EML3, GLFND1, EML2, Syntaphilin B, Syntaphilin C, and EML4 lysates. The GFP tagged MAPs are decorating MTs polymerized using tubulin from cell lysates. In the time montages, GMPCPP MT seeds are shown in green and GFP tagged MAPs are shown in white. Scale bar = 5 µm.

B) Still images of reconstituted MTs and actin filaments in presence of different MAPs using cell lysates. Immunostained MTs with YL1/2 antibody are in green, MAPs tagged with GFP are shown in white, and actin filaments stained with SiR-actin are shown in red. Scale bar = 5 µm.

Supplementary figure 8: TIRF reconstitution assays to study MAP-MT interactions using ex-vivo approach in presence of actin- part 2.

A) Time lapse images (in rows) of TIRF-M assays for TRAK1, TRAK2, DCX big, DCX small, DCLK1, MACF2, Parkin and PRC1 lysates. The GFP tagged MAPs are decorating MTs polymerized using tubulin from cell lysates. In the time montages, GMPCPP MT seeds are shown in green and GFP tagged MAPs are shown in white. Scale bar = 5 µm.

B) Still images of reconstituted MTs and actin filaments in presence of different MAPs using cell lysates. Immunostained MTs with YL1/2 antibody are shown in green, MAPs tagged with GFP are shown in white, and actin filaments stained with SiR-actin are shown in red. Scale bar = 5 µm.

Supplementary figure 9: TIRF reconstitution assays to study MAP-MT interactions using ex-vivo approach without actin- part 2.

A) Time lapse images (in rows) of TIRF-M assays in presence of Latrunculin A (F-actin inhibitor drug) for TRAK1, TRAK2, DCX big, DCX small, DCLK1, MACF2, Parkin and PRC1 lysates. The GFP tagged MAPs are decorating MTs polymerized using tubulin from cell lysates. In the time montages, GMPCPP MT seeds are shown in green and GFP tagged MAPs are shown in white. Scale bar = 5 µm.

B) Still images of reconstituted MTs and actin filaments in presence of different MAPs using cell lysates. Immunostained MTs with YL1/2 antibody are shown in green, MAPs tagged with GFP are shown in white, and actin filaments stained with SiR-actin are shown in red. Scale bar = 5 µm.

Supplementary figure 10: TIRF reconstitution assays to study MAP-MT interactions using ex-vivo approach in presence of actin- part 3.

A) Time lapse images (in rows) of TIRF-M assays for ATIP3, CFAP, MAP7D1, MAP7D2, CKAP2, Cingulin, POC and GLFND2 lysates. The GFP tagged MAPs are decorating MTs polymerized using tubulin from cell lysates. In the time montages, GMPCPP MT seeds are shown in green and GFP tagged MAPs are shown in white. Scale bar = 5 μm.

B) Still images of reconstituted MTs and actin filaments in presence of different MAPs using cell lysates. Immunostained MTs with YL1/2 antibody are shown in green, MAPs tagged with GFP are shown in white, and actin filaments are shown in red. Scale bar = 5 μm.

Supplementary figure 11: TIRF reconstitution assays to study MAP-MT interactions using ex-vivo approach without actin- part 3.

A) Time lapse images (in rows) of TIRF-M assays in presence of Latrunculin A (F-actin inhibitor drug) for ATIP3, CFAP, MAP7D1, MAP7D2, CKAP2, Cingulin, POC and GLFND2 lysates. The GFP tagged MAPs are decorating MTs polymerized using tubulin from cell lysates. In the time montages, GMPCPP MT seeds are shown in green and GFP tagged MAPs are shown in white. Scale bar = 5 μm.

B) Still images of reconstituted MTs and actin filaments in presence of different MAPs using cell lysates. Immunostained MTs with YL1/2 antibody are shown in green, MAPs tagged with GFP are shown in white, and actin filaments are shown in red. Scale bar = 5 μm.

Supplementary figure 12: Reconstituted microtubules and actin-filaments from cell lysates to study the influence of MAPs in actin-MT crosstalk.

A) Schematic diagram summarizing three categories of the observation in the actin-MT crosstalk from all MAP studies. For some MAPs, there is an actin-MT co-alignment; for some, there is no alignment, and a third category with mixed phenotype with both co-aligned and non-aligned actin and MT filaments.

B) Still images of MTs (red) and actin filaments (green) reconstituted using cell lysates. The first panel shows the MAP channel shown in grey, the second panel is for the MT channel shown in red, the third panel is for actin filaments shown in green, and the fourth panel is the merge of actin and MTs. Each column represents an example of the observed phenotypes. In the case of GLFND1, there is strong co-alignment between F-actin and MTs; for MAP 10, there is no co-alignment between F-actin and MTs, and EML3 showed a mixed phenotype. Scale bar = 10 μm.

Supplementary figure 13: Ex-vivo approach for MAP competition experiments: T243A EML1-GFP mutant binds less to wild-type EML1-mCherry.

A) Time-lapse of EML1 competition experiments: EML1 T243A-GFP mutant and EML1-mCherry wild type compete for binding on MT lattice. GMPCPP MT seeds and EML1 wild type tagged with mCherry are shown in Cyan, and EML1 T243 mutant tagged with GFP is shown in Magenta. First panel is the channel with wild type EML1-mCherry, second panel is the channel with EML1-GFP mutant, and third panel is the merge of both channels. Scale bar = 5 µm.

B) Quantification of MT length decorated by wild type EML1-mCherry (Magenta) and mutant EML1-GFP (Cyan) for different time points from the above competition experiment (supplementary figure 13 A).

Supplementary figure 14: Quantification of helix width of MT coils induced by CSAP.

A) Manual quantification of the helix width of MT coils by CSAP shows an average helix width of 0.71 µm.

Jijumon et al., Figure 1

Schematic overview of the pipeline used to study more than 50 MAPs, and overexpression studies of selected MAPs in cells.

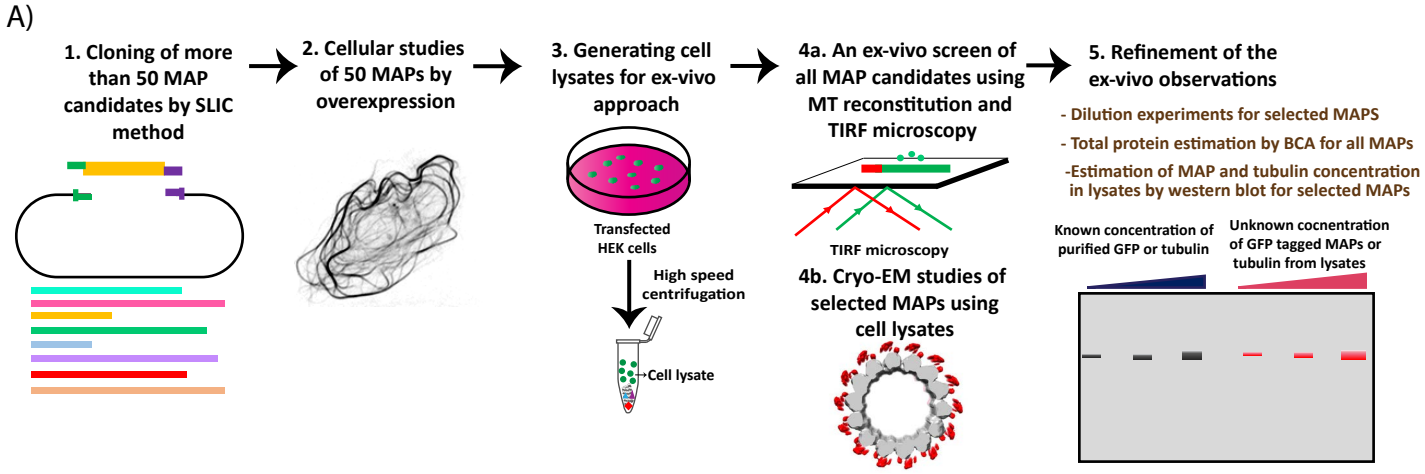

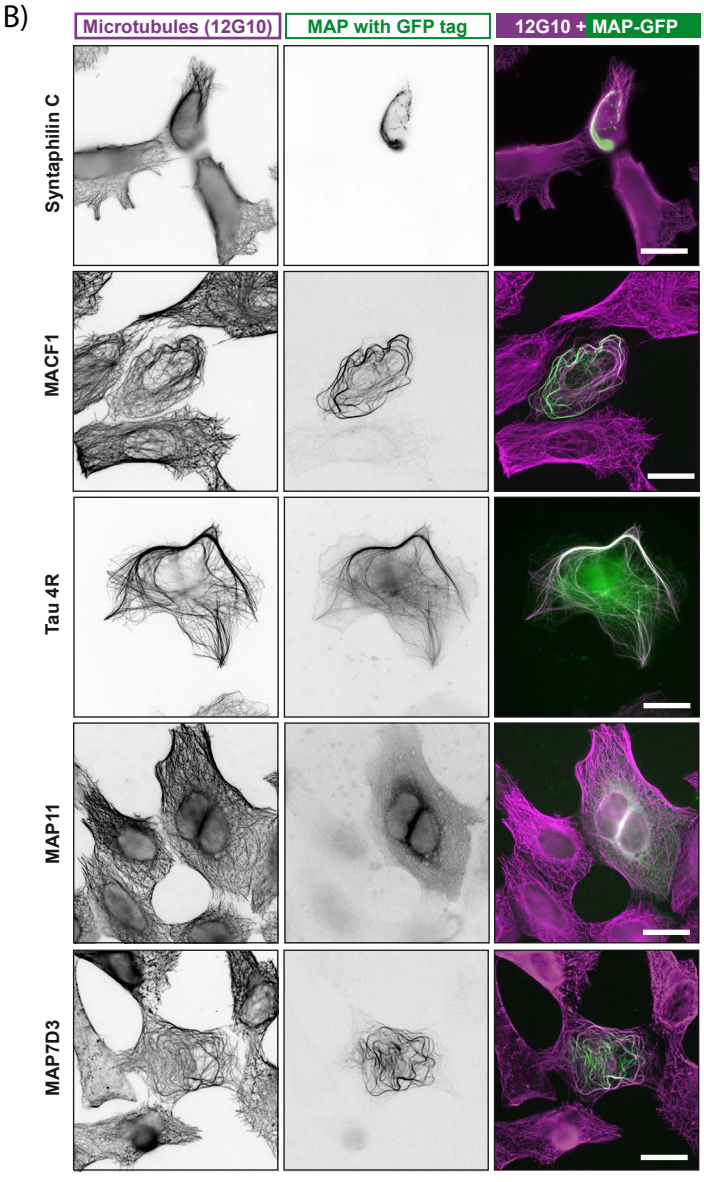

Jijumon et al., Figure 2

Flow diagram of different steps of the ex-vivo method to study MAPs using TIRF microscopy and cryo-electron microscopy, and validation of ex-vivo method with two well-characterized MAPs- spastin and EB3.

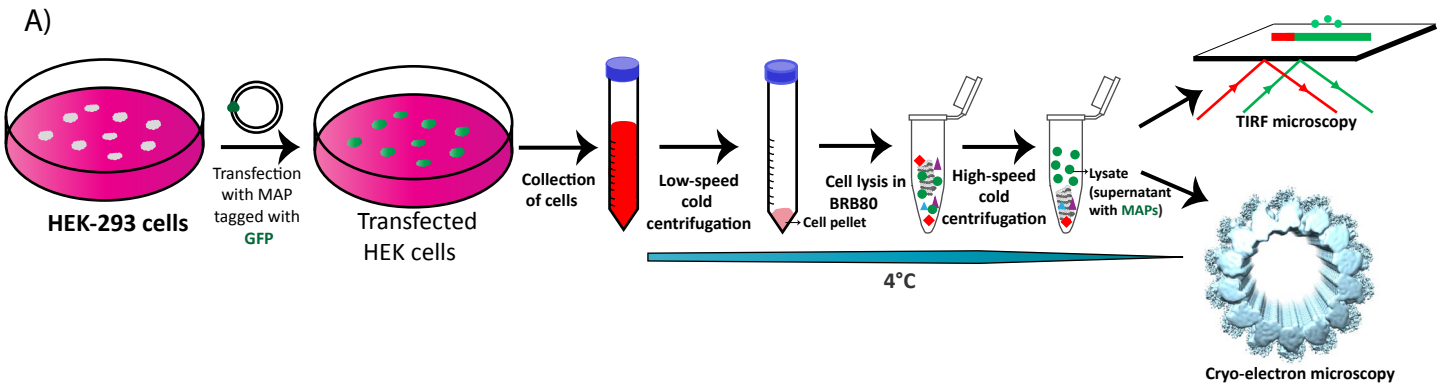

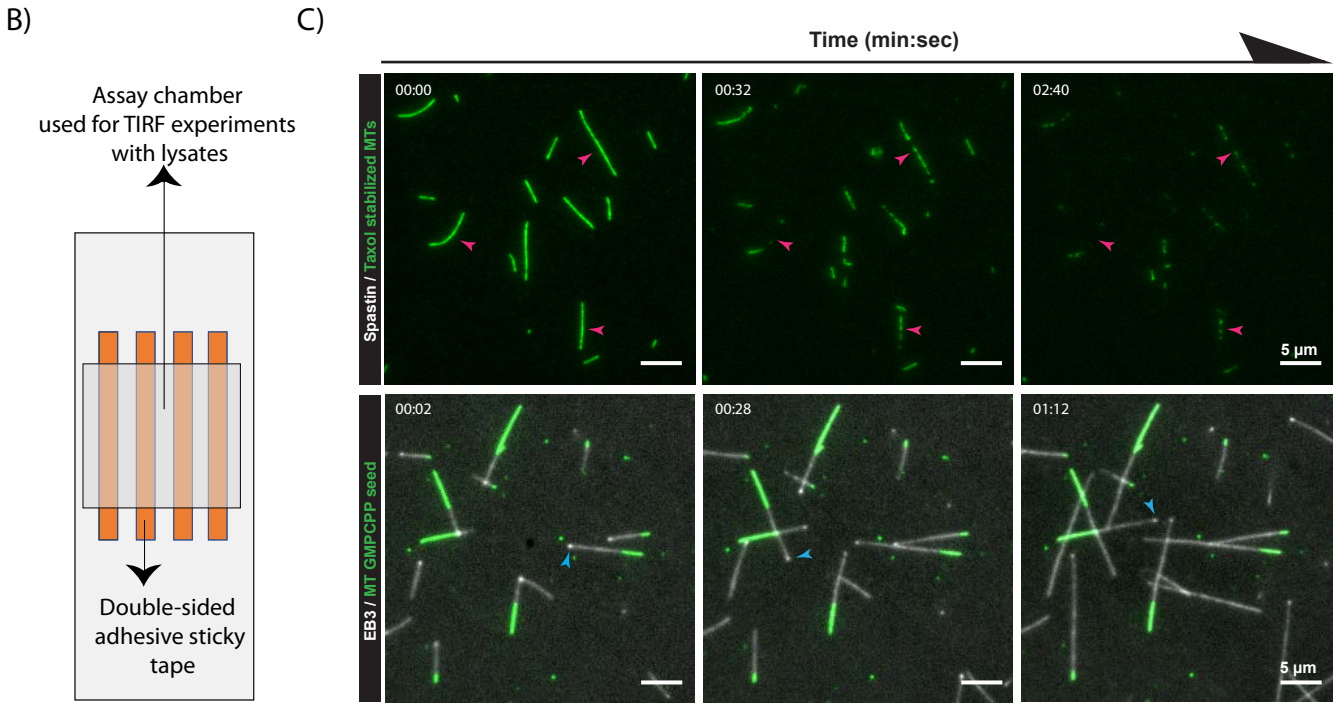

Jijumon et al., Figure 3

Time montage of different MAPs showing their novel properties, and staining of reconstituted microtubules and actin filaments from cell lysates.

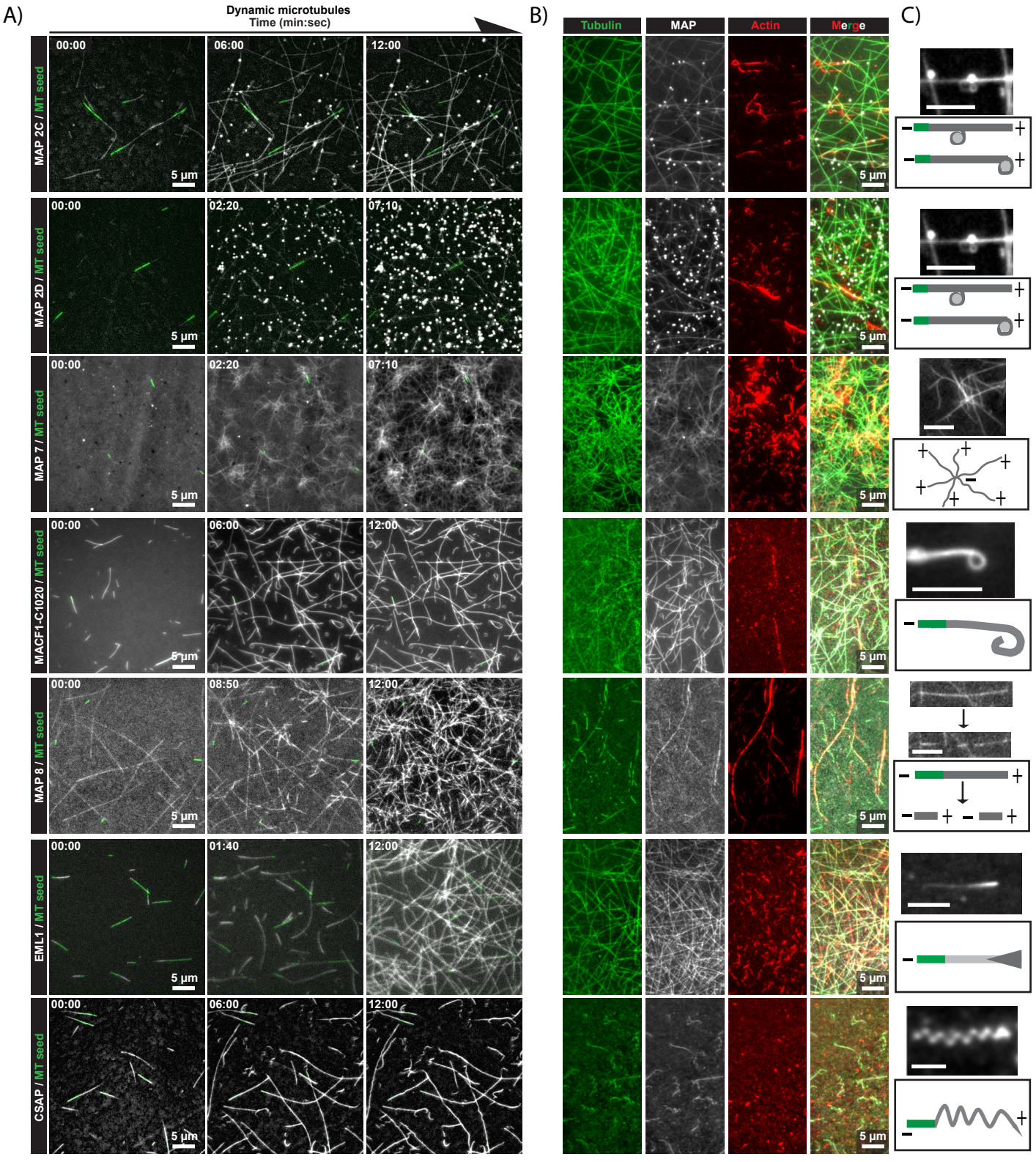

Jijumon et al., Figure 4

Quantification of unknown concentrations of MAPs and tubulin from lysates using known concentrations of purified GFP and tubulin..

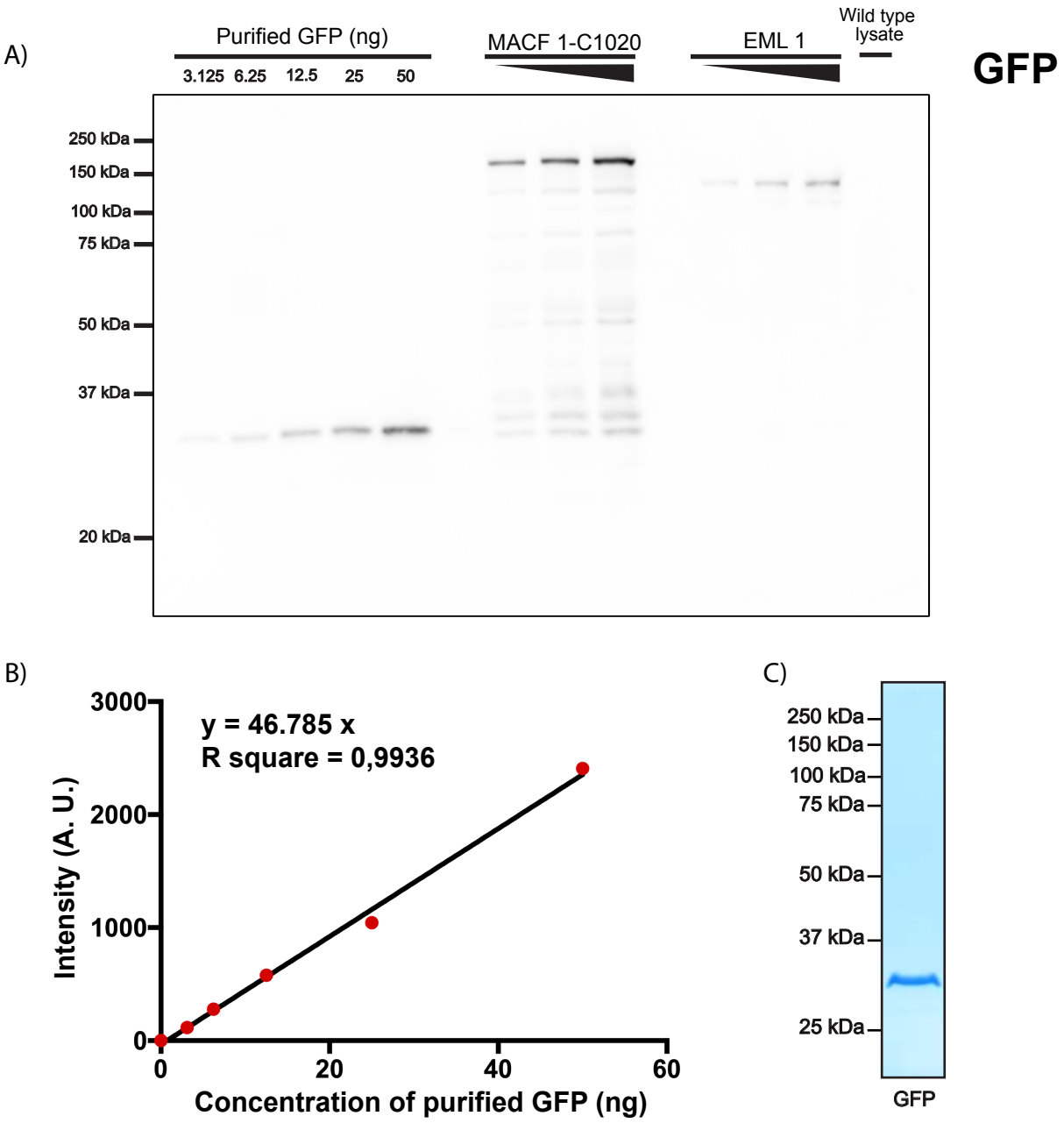

Approximate MAP concentrations in lysates:

MACF1-C1020-GFP: 19 ng/µl (140 nM)

EML1-GFP : 47 ng/µl (400 nM)

Jijumon et al., Figure 5

Hook formations by MACF1 and plus end affinity of EML1 is a concentration dependent process.

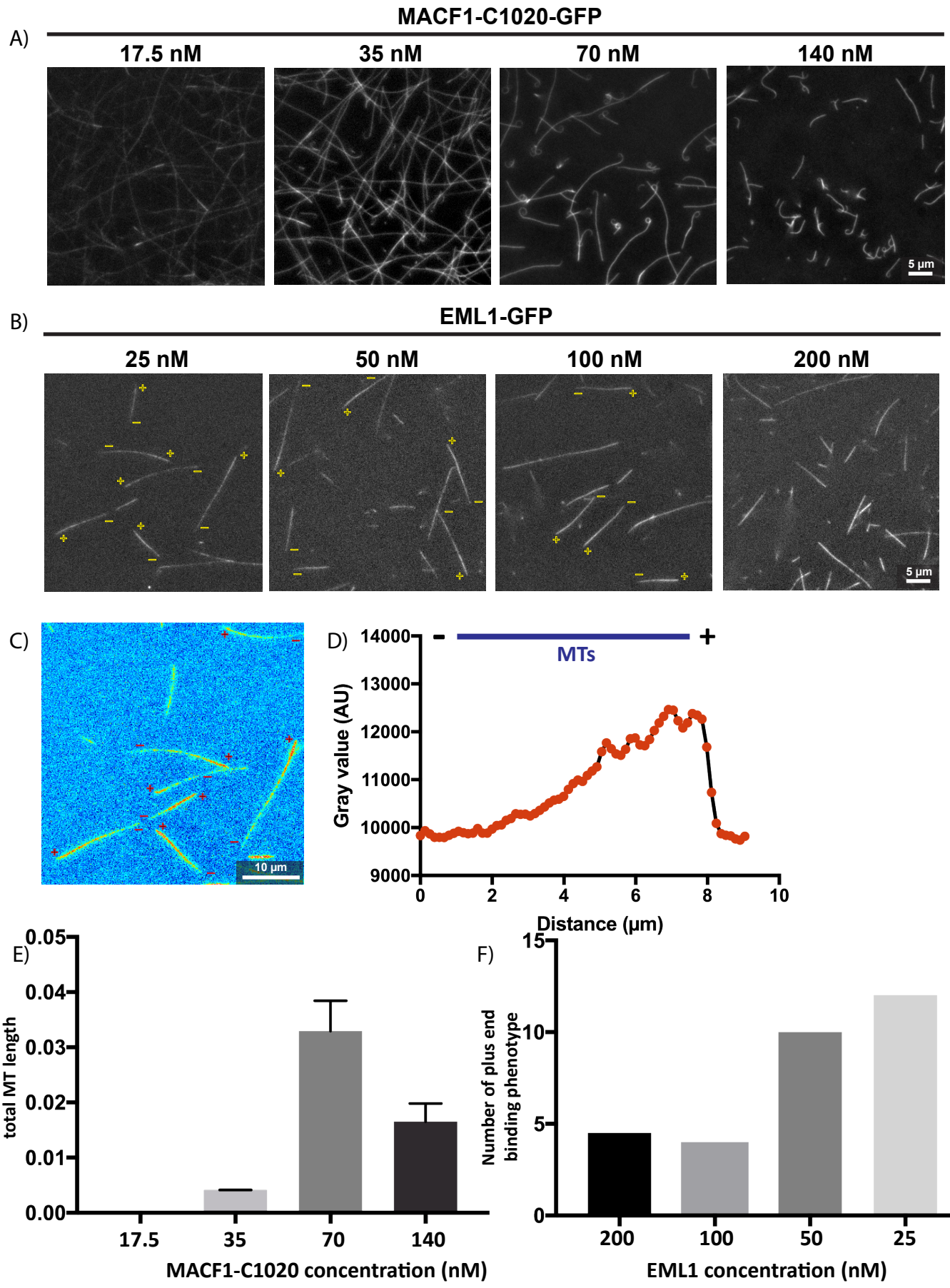

Jijumon et al., Figure 6

Figure 06: Quantification of MACF1-C1020 mediated hook formations

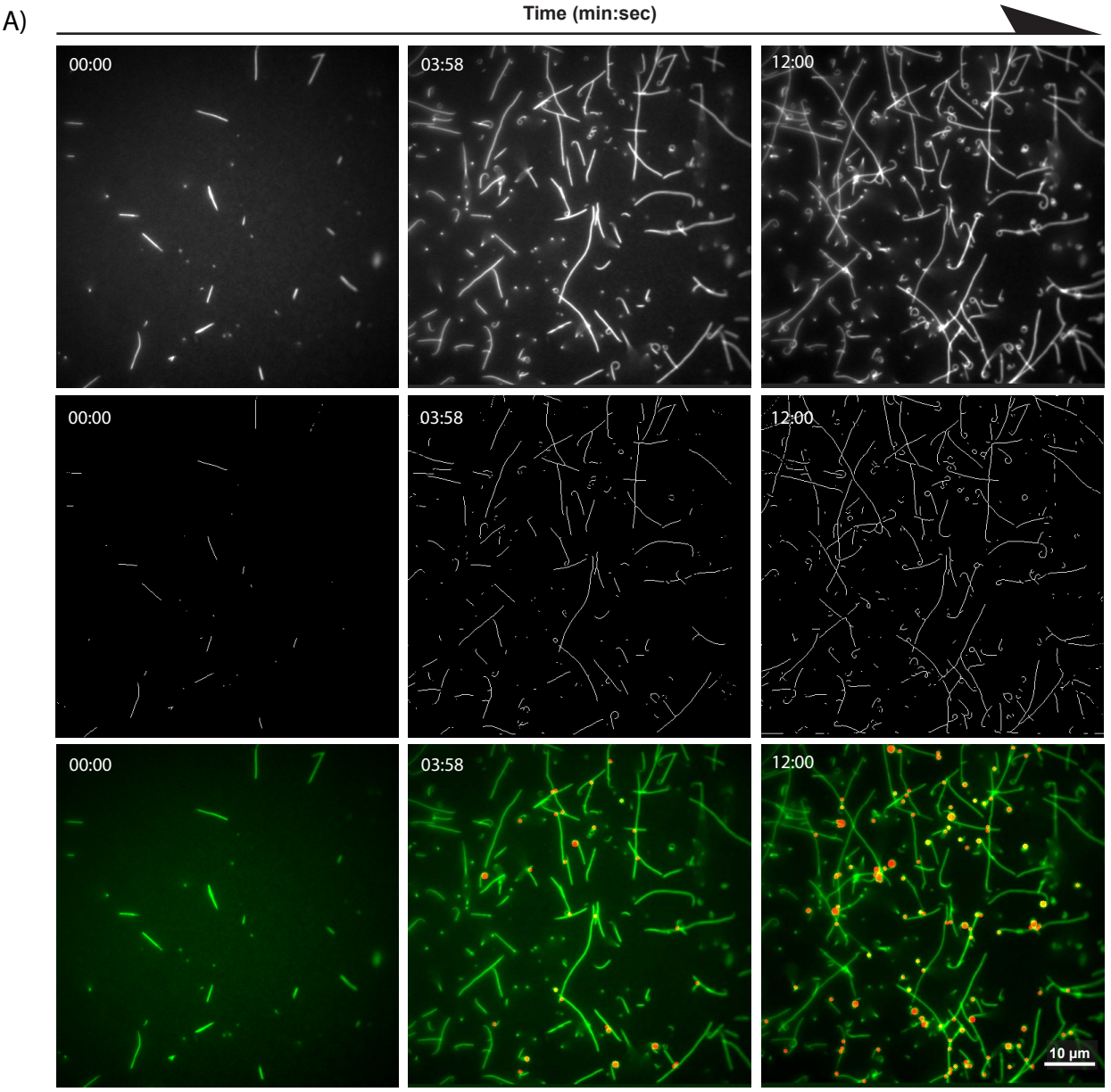

Jijumon et al., Figure 7

TIRF reconstitution assay with purified MACF1-C1020-GFP and HeLa tubulin

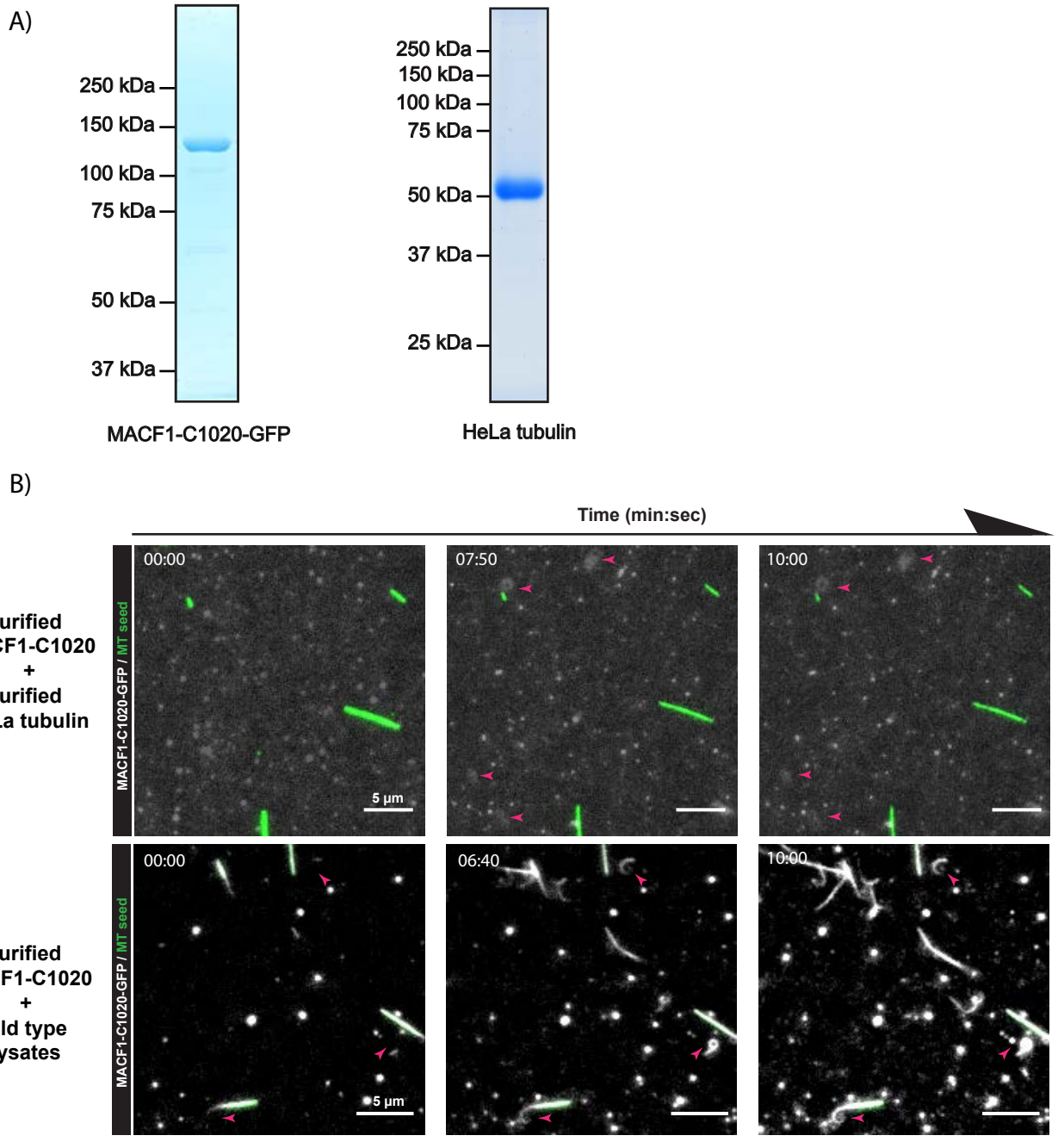

Jijumon et al., Figure 8

Ex-vivo lysate approach for studying MAP-MT binding architecture using cryo-electron microscopy provides important insights into MAP binding.

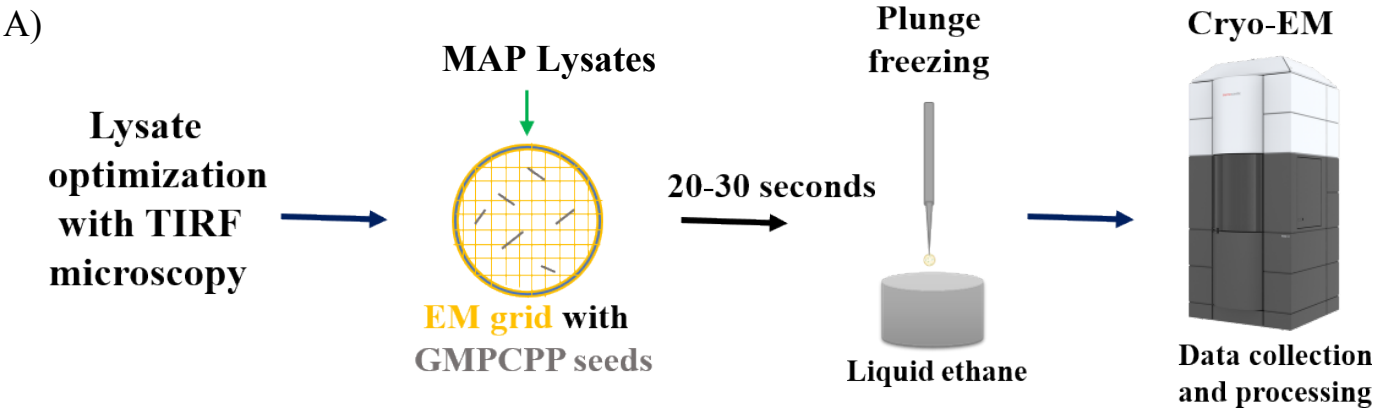

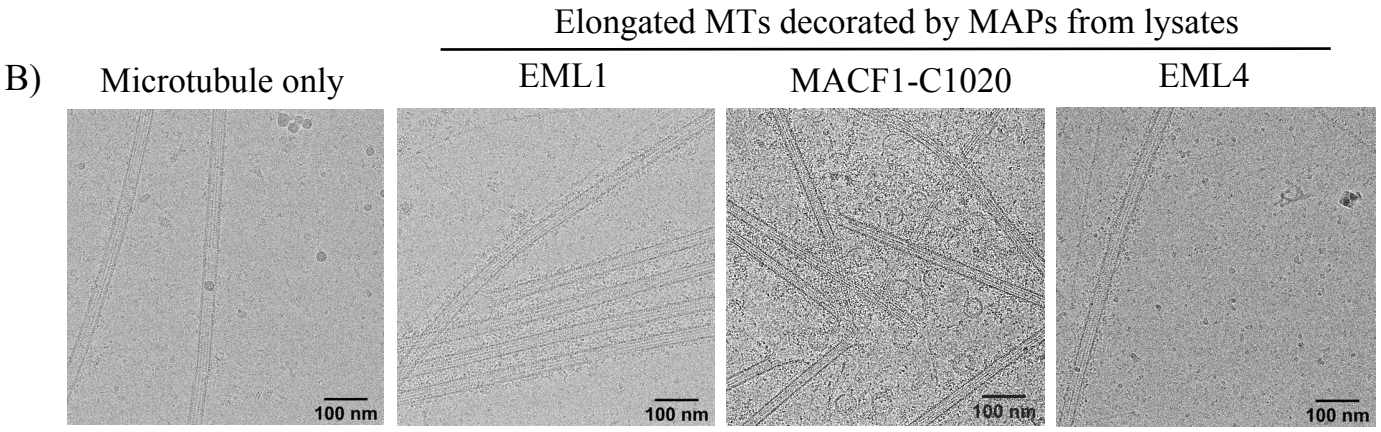

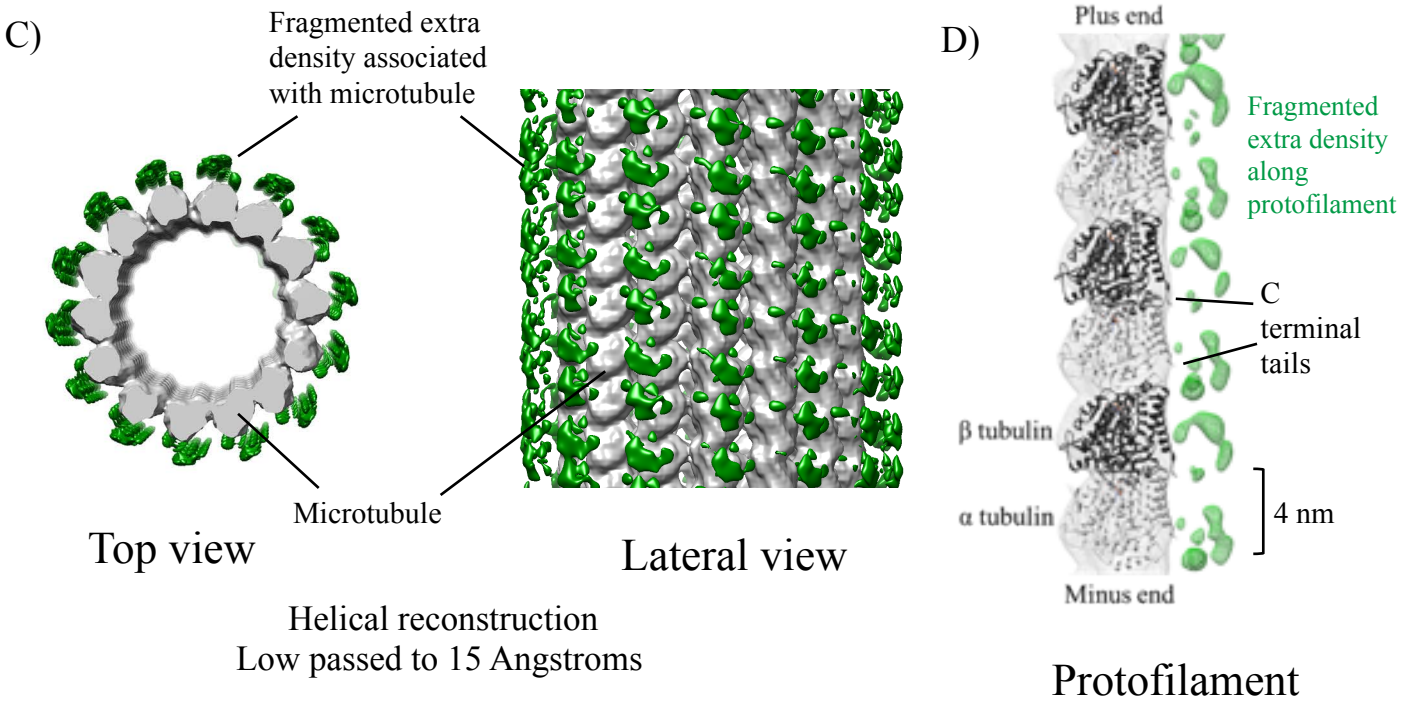

Jijumon et al., Figure 9

T243A EML1 mutant binds less and promotes less microtubule elongation comparing wild type EML1

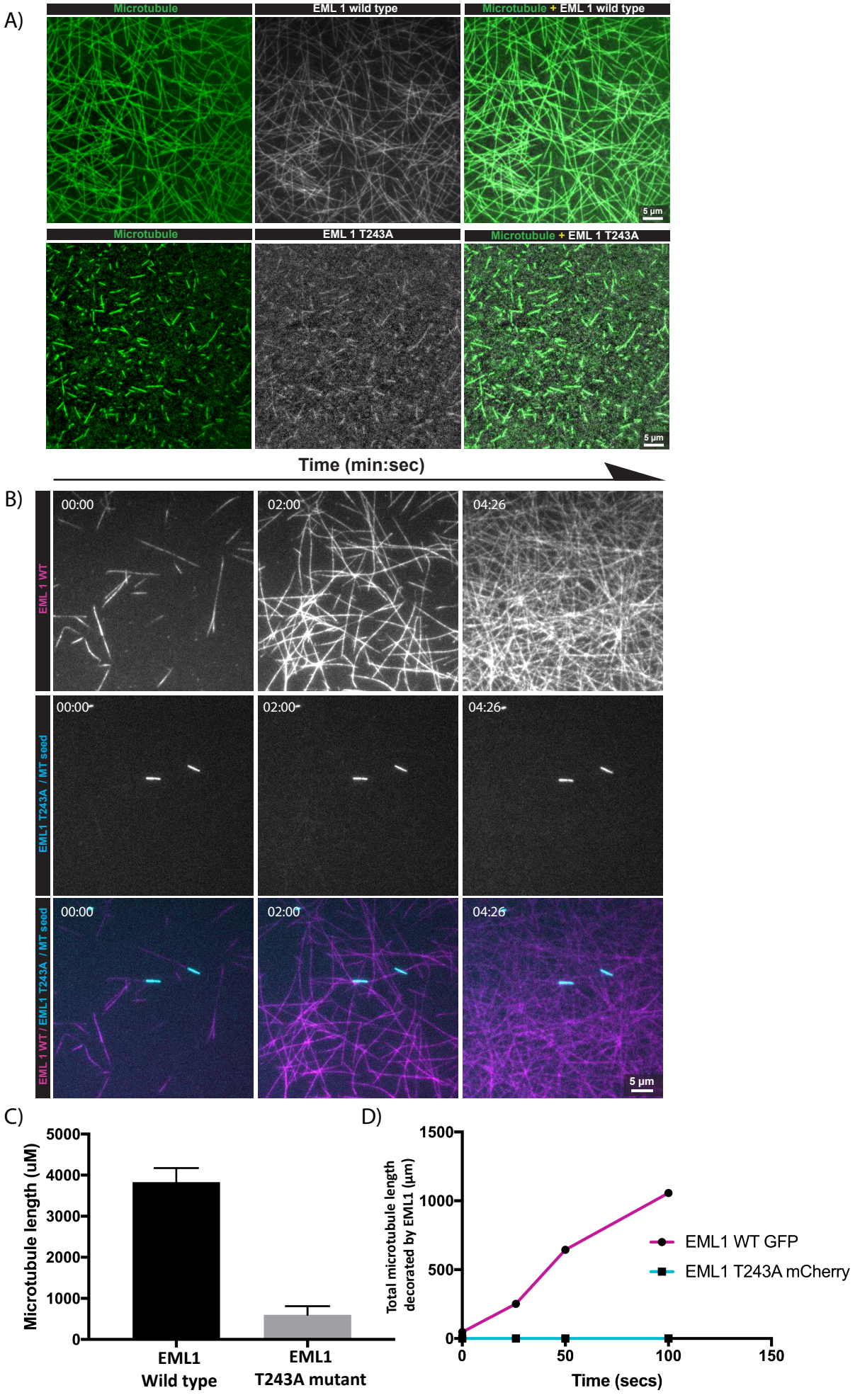

Jijumon et al., Supplementary figure 1

Overview of molecular cloning of more than 50 MAPs using SLIC method.

A)

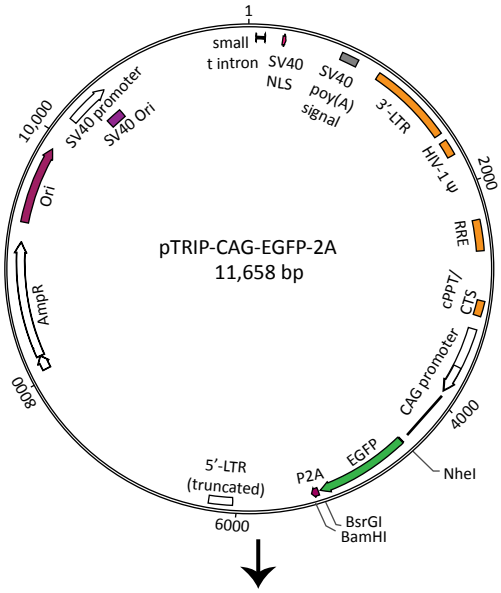

B)

Amplification of MAP inserts by PCR (with homologous overhangs of ≥15 bp) using mouse testicles or brain cDNAs as templates

Linearized lentiviral vector with restriction enzymes (for C-terminal tagging, pTRIP vector was digested with NheI, and for N-terminal tagging with BsrGI and BamHI).

pTRIP vector

SLIC reaction mix on ice (10 µl):

7 µl gel purified PCR product,
2 µl gel purified vector (restriction-digested and linearized),
1 µl buffer
0.2 µl T4 DNA polymerase enzyme (to generate 3' overhangs)

Incubation at room temperature:
2.5- 3 minutes including time for a short spin

Immediate transfer of mix to ice, and addition of 100 µl E. coli competent cells

20 minutes incubation on ice

pTRIP vector

MAP insert

E. coli competent cells

Bacterial transformation

Antibiotic selection, plasmid amplification, and confirmation by restriction digestion and sequencing

Jijumon et al., Supplementary figure 2

Organisation of microtubule cytoskeleton in cells with overexpressed MAPs

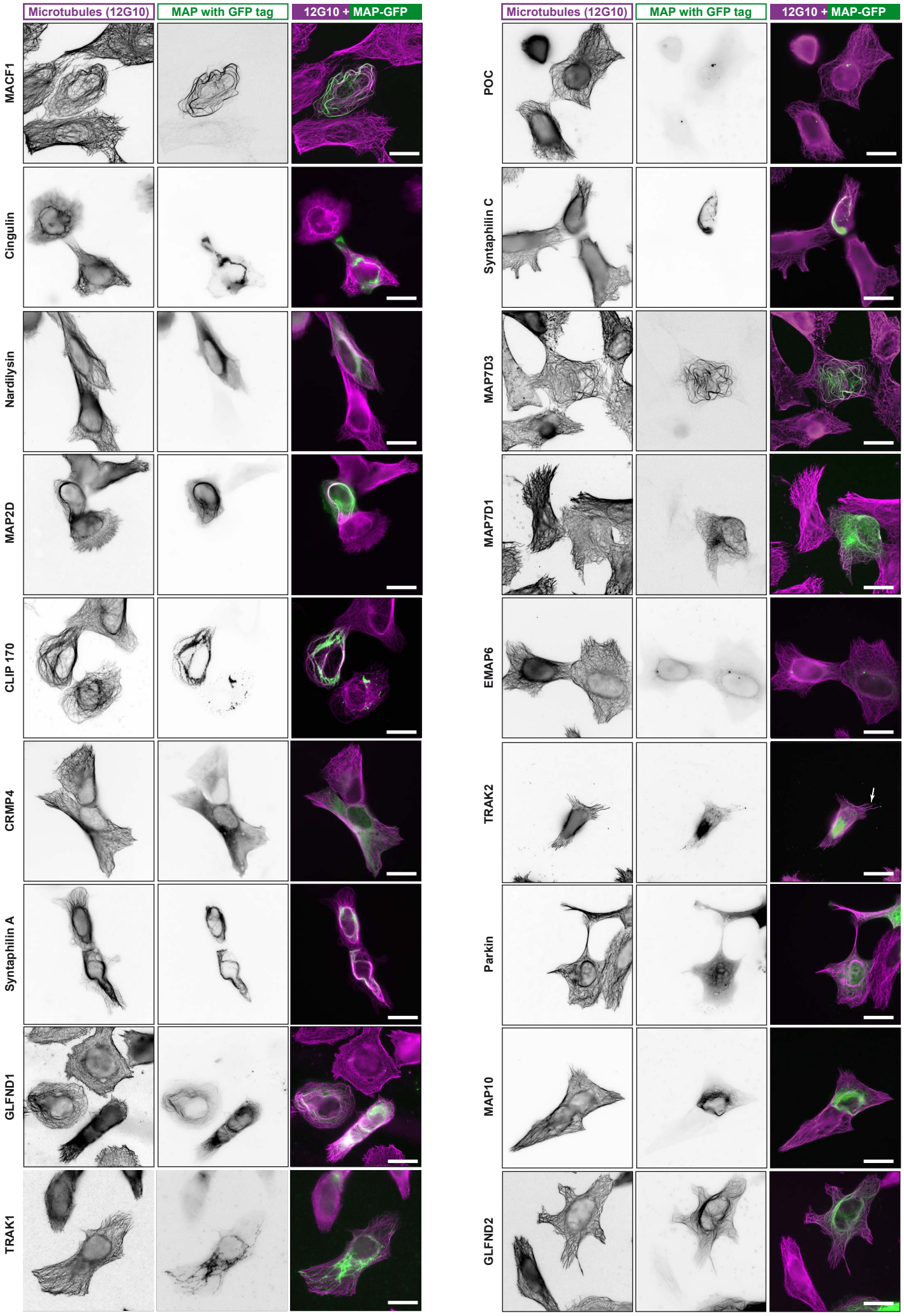

Jijumon et al., Supplementary figure 3

Organisation of microtubule cytoskeleton in cells with overexpressed MAPs

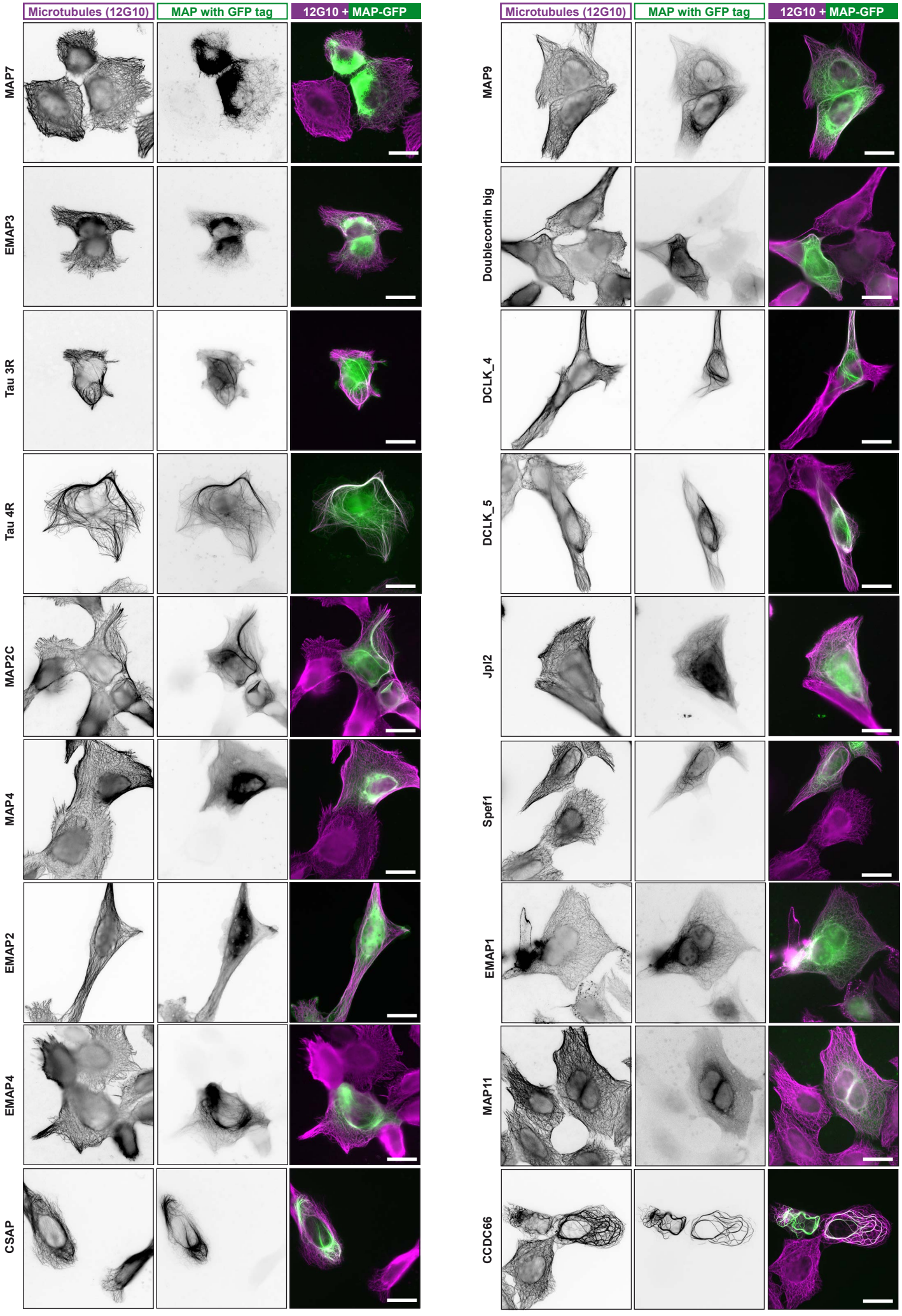

Jijumon et al., Supplementary figure 4

Organisation of microtubule cytoskeleton in cells with overexpressed MAPs

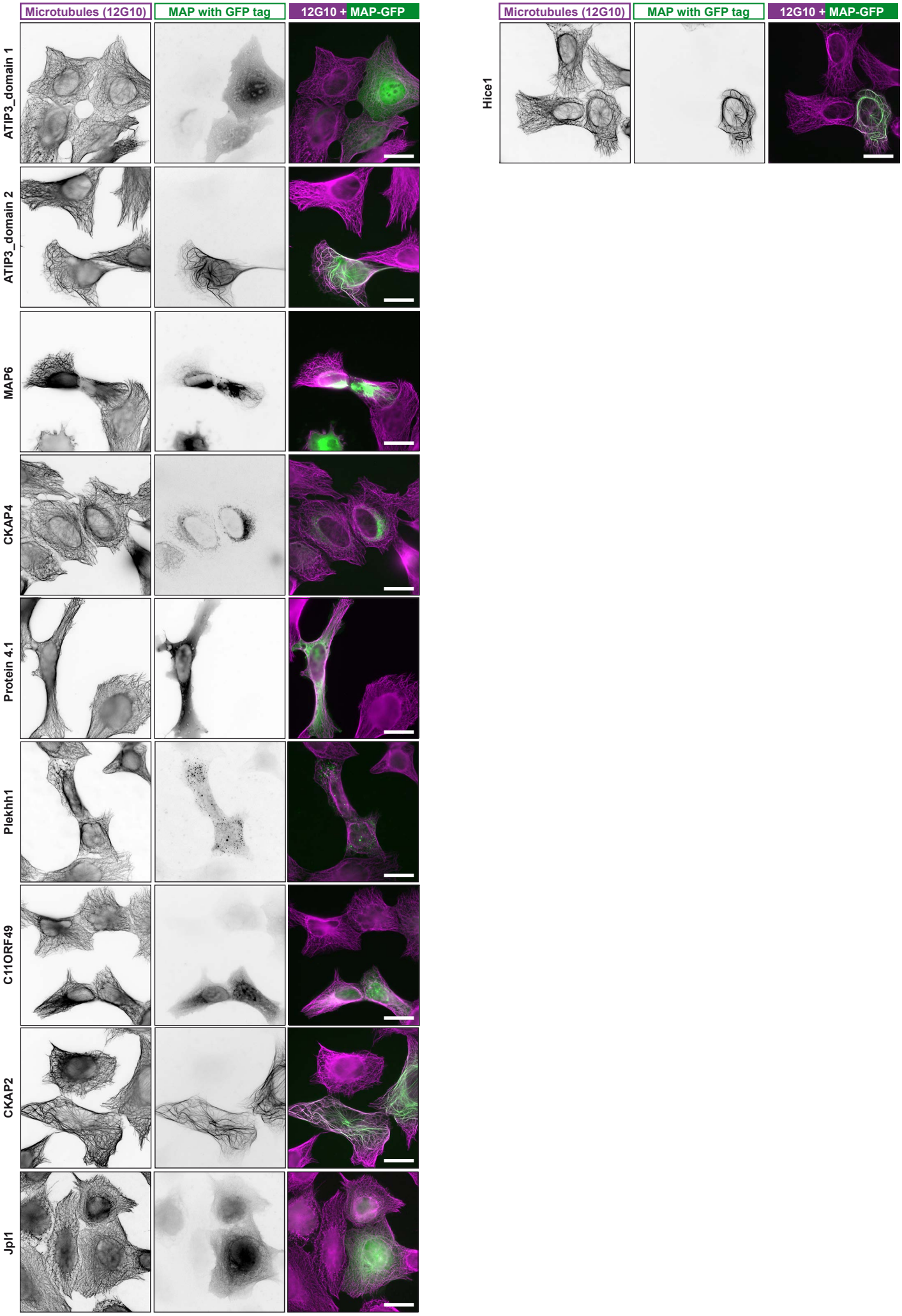

Jijumon et al., Supplementary figure 5

Time montage of different MAPs showing their novel properties(in the absence of actin), and staining of reconstituted microtubules and actin filaments from cell lysates.

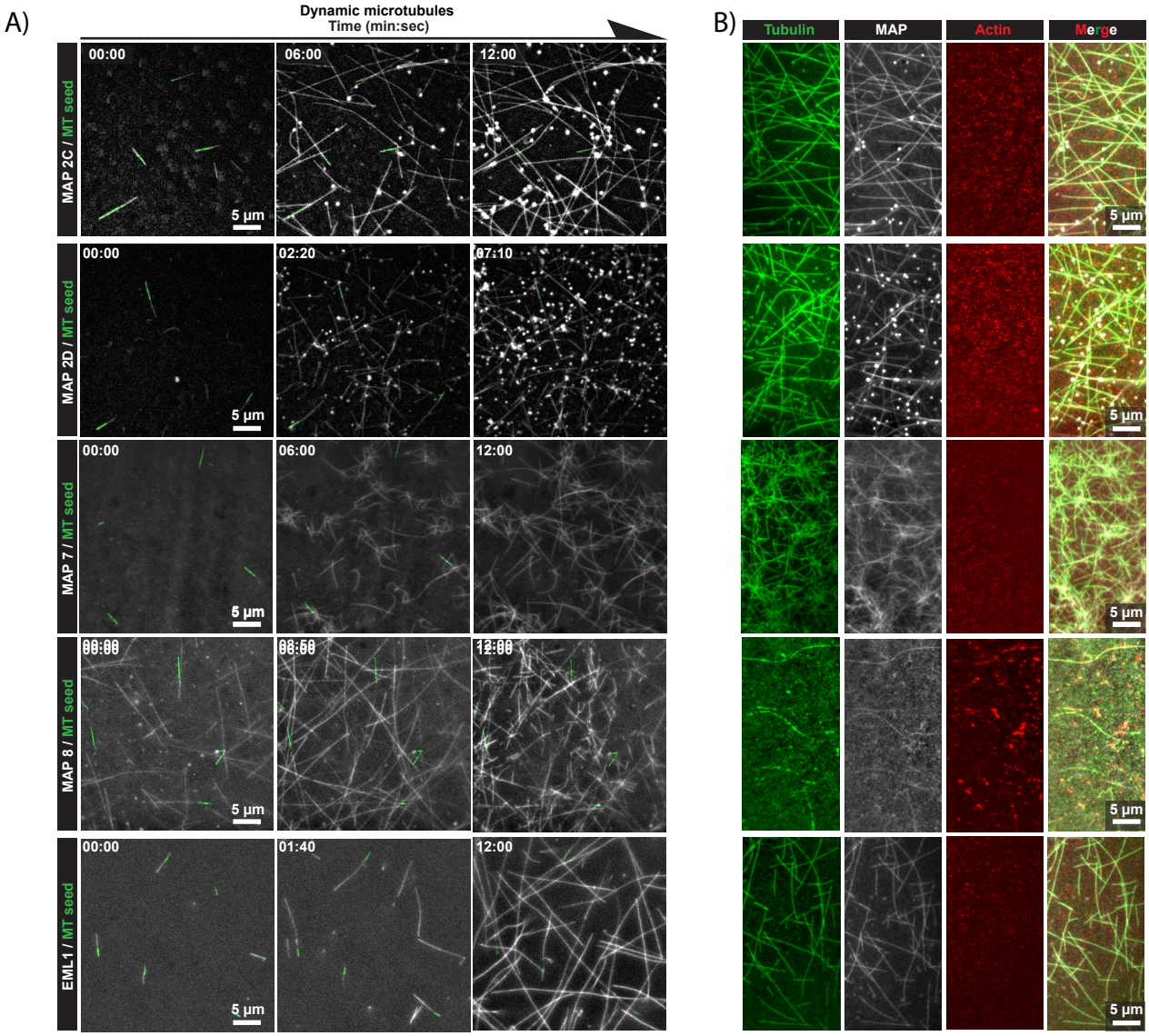

Jijumon et al., Supplementary figure 6

TIRF reconstitution assays to study MAP-MT interactions using ex-vivo approach in the presence of actin

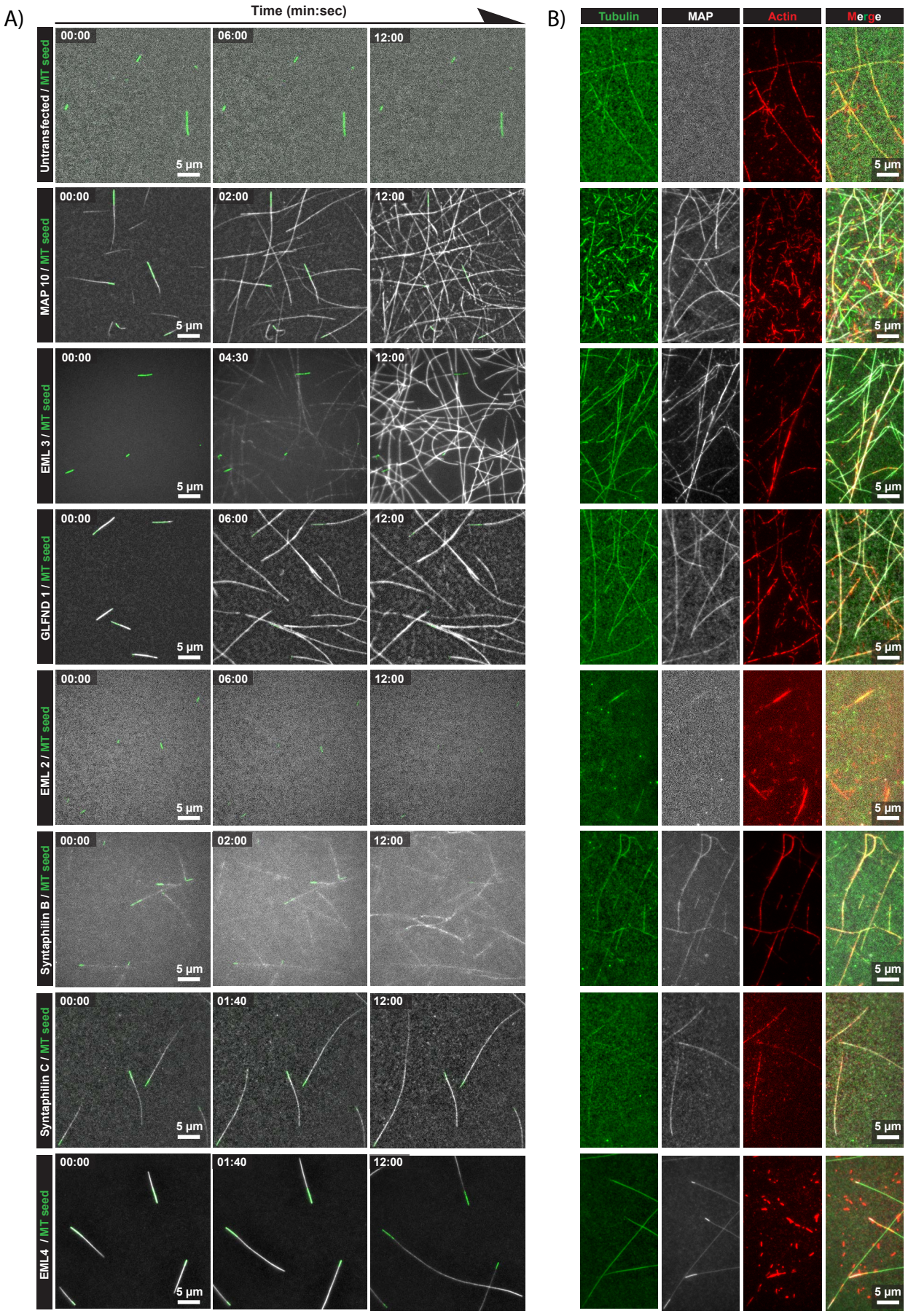

Jijumon et al., Supplementary figure 7

TIRF reconstitution assays to study MAP-MT interactions using ex-vivo approach in the absence of actin

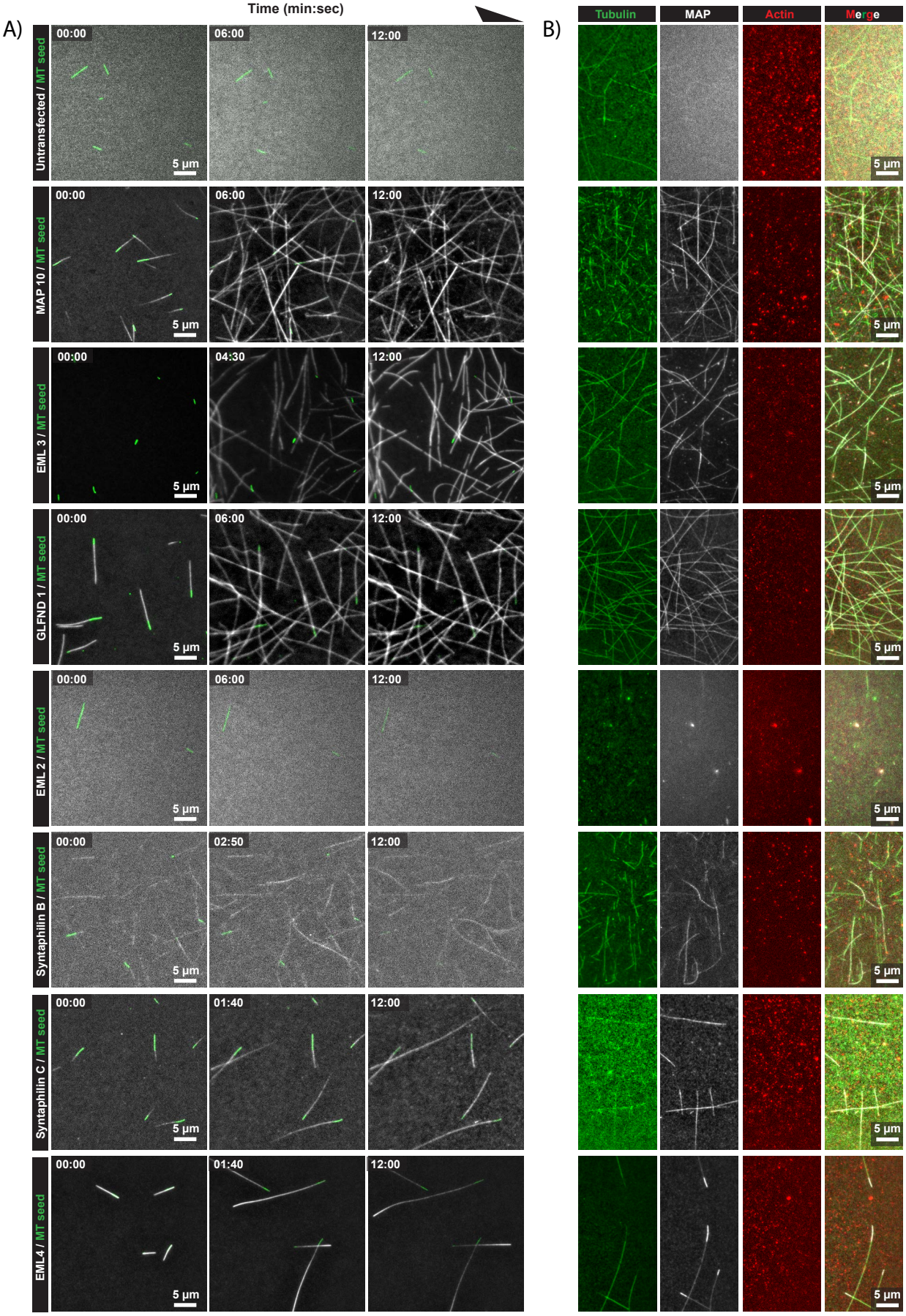

Jijumon et al., Supplementary figure 8

TIRF reconstitution assays to study MAP-MT interactions using ex-vivo approach in presence of actin

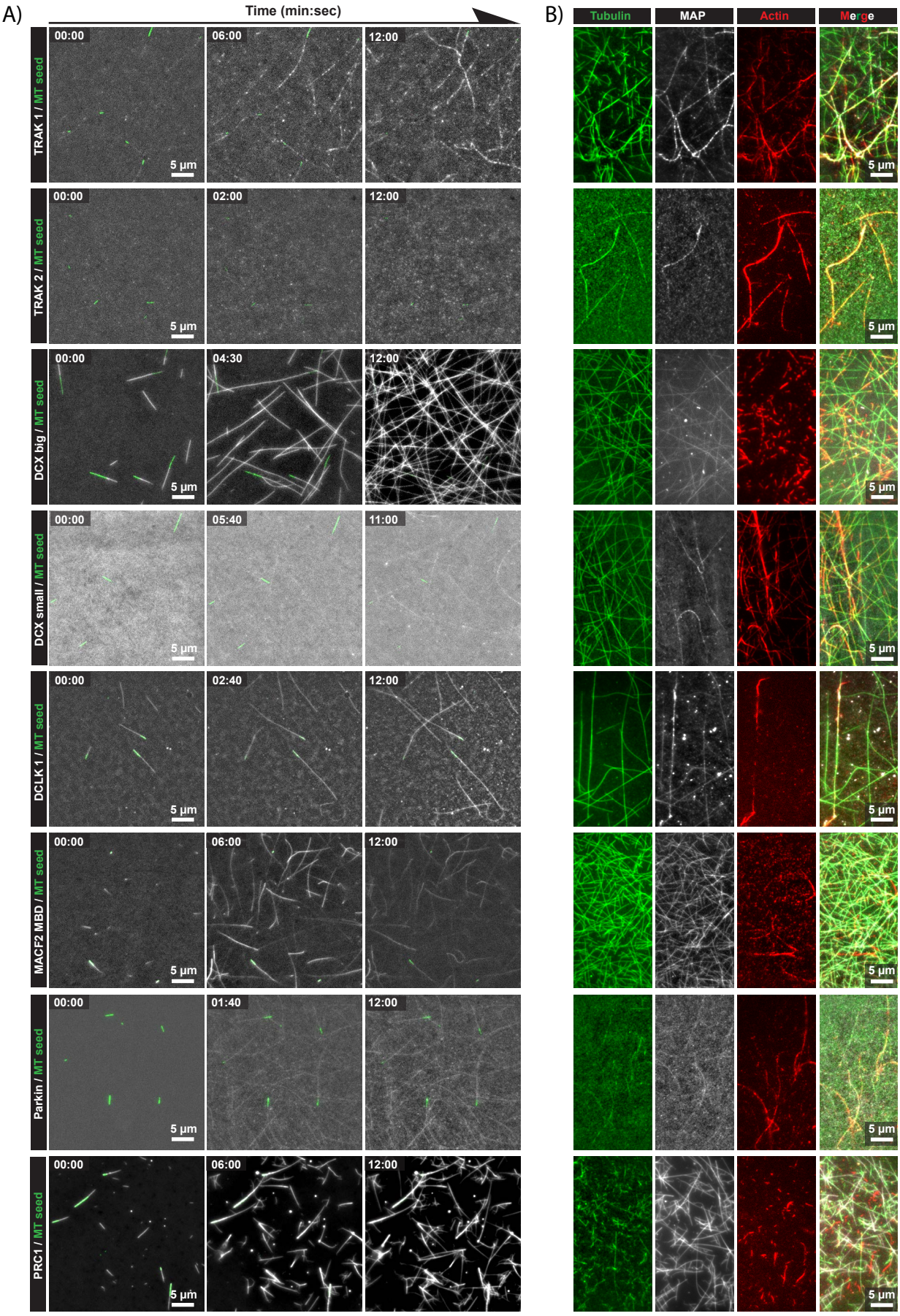

Jijumon et al., Supplementary figure 9

TIRF reconstitution assays to study MAP-MT interactions using ex-vivo approach in the absence of actin

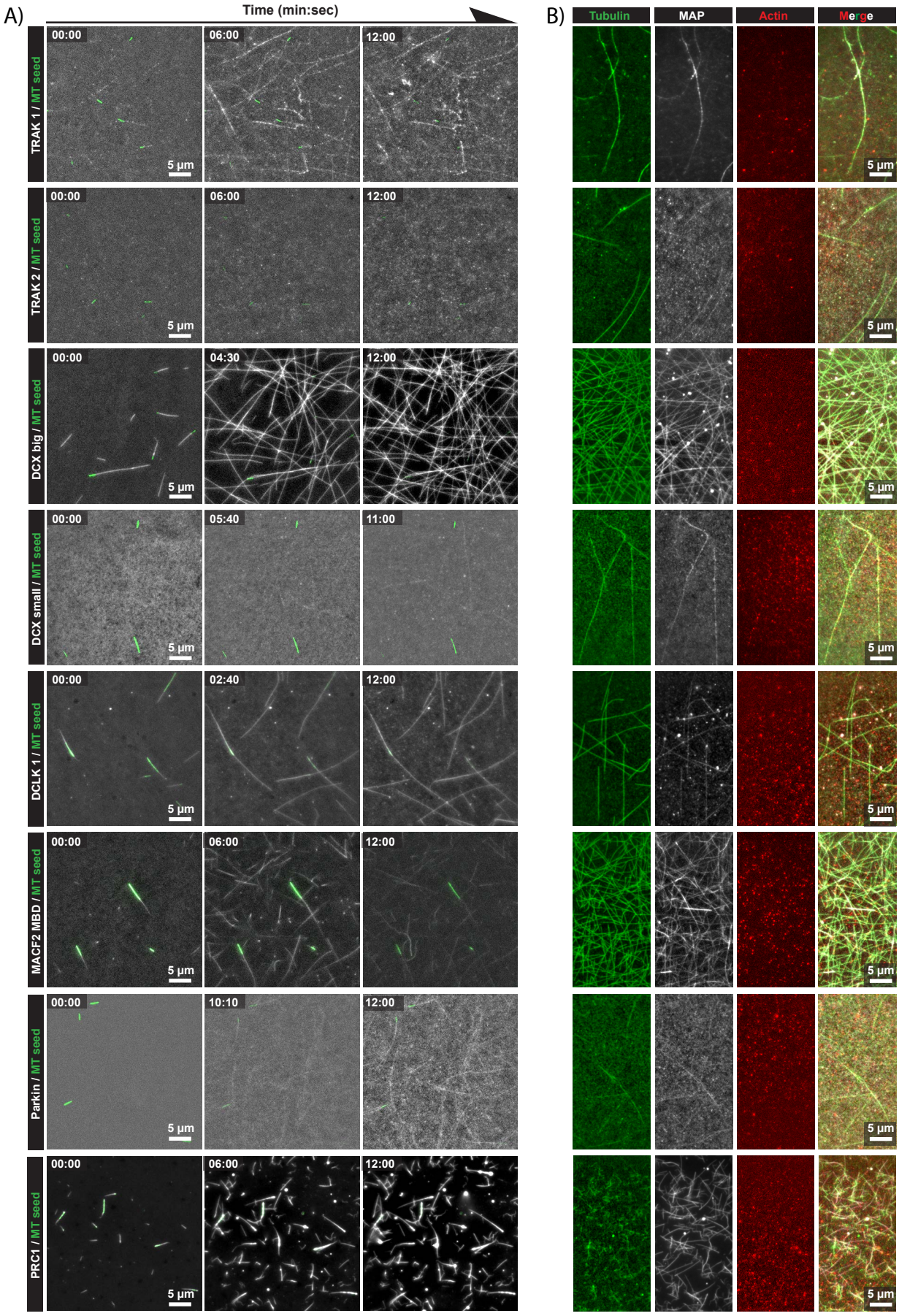

Jijumon et al., Supplementary figure 10

TIRF reconstitution assays to study MAP-MT interactions using ex-vivo approach in presence of actin

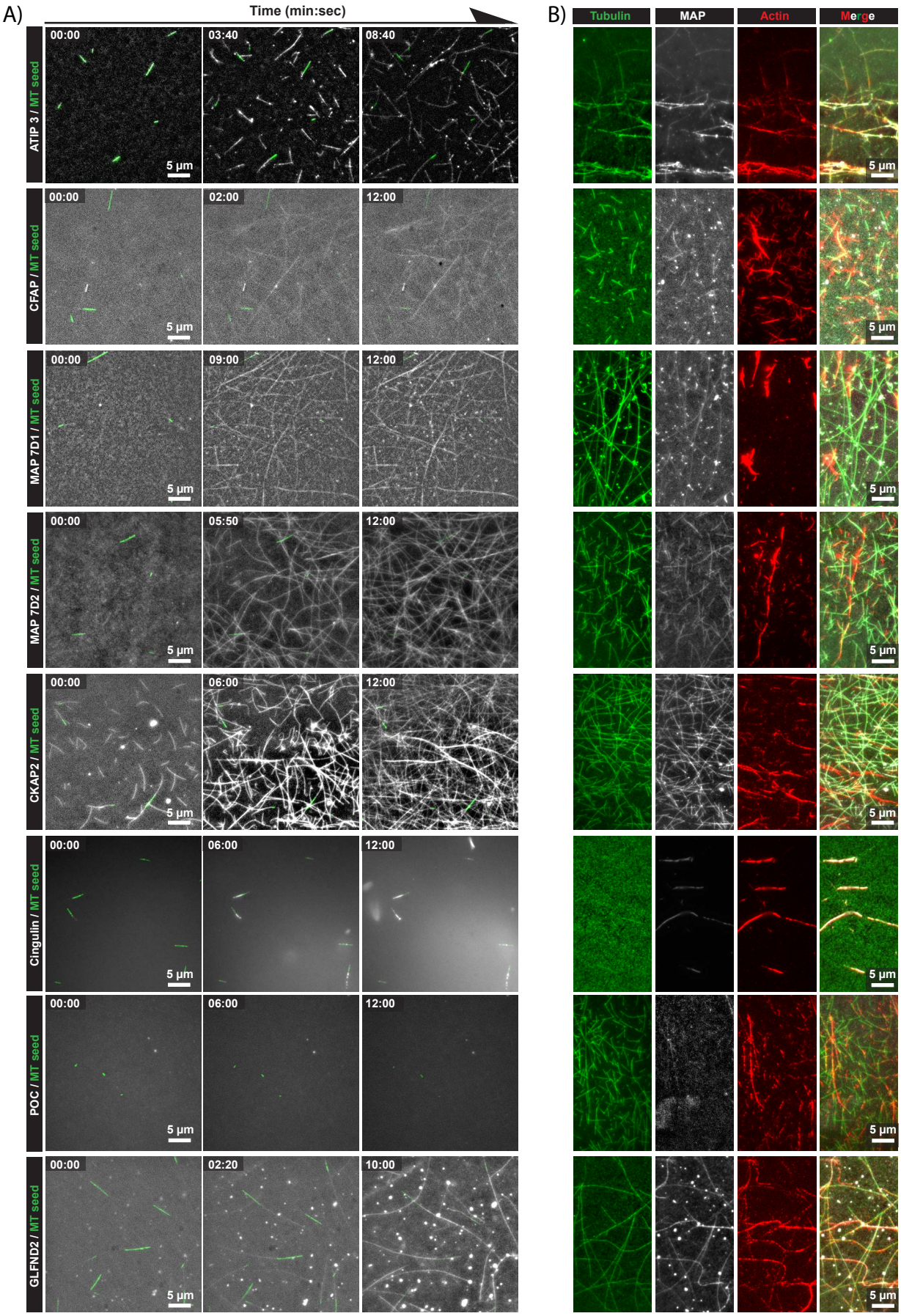

Jijumon et al., Supplementary figure 11

TIRF reconstitution assays to study MAP-MT interactions using ex-vivo approach in the absence of actin

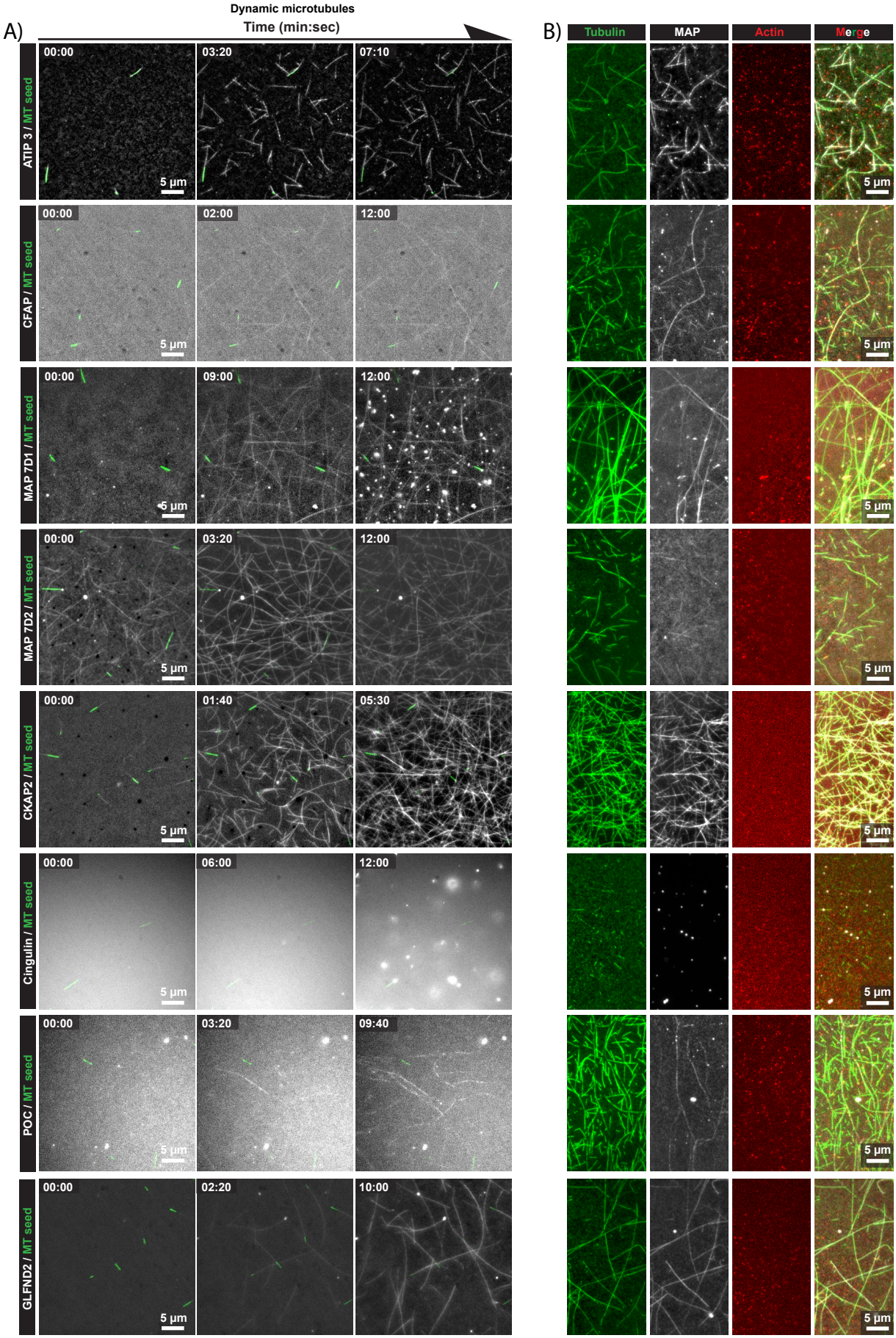

Jijumon et al., Supplementary figure 12

Reconstituted microtubules and actin-filaments from cell lysates to study the influence of MAPs in actin-MT crosstalk

A)

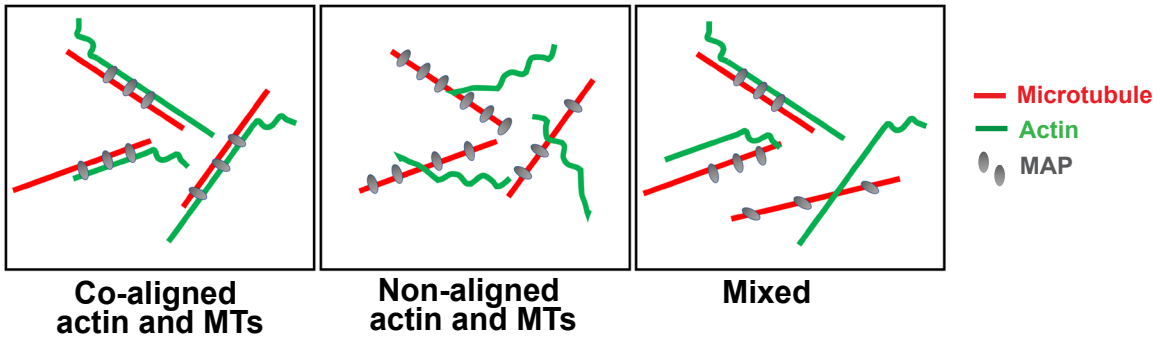

B)

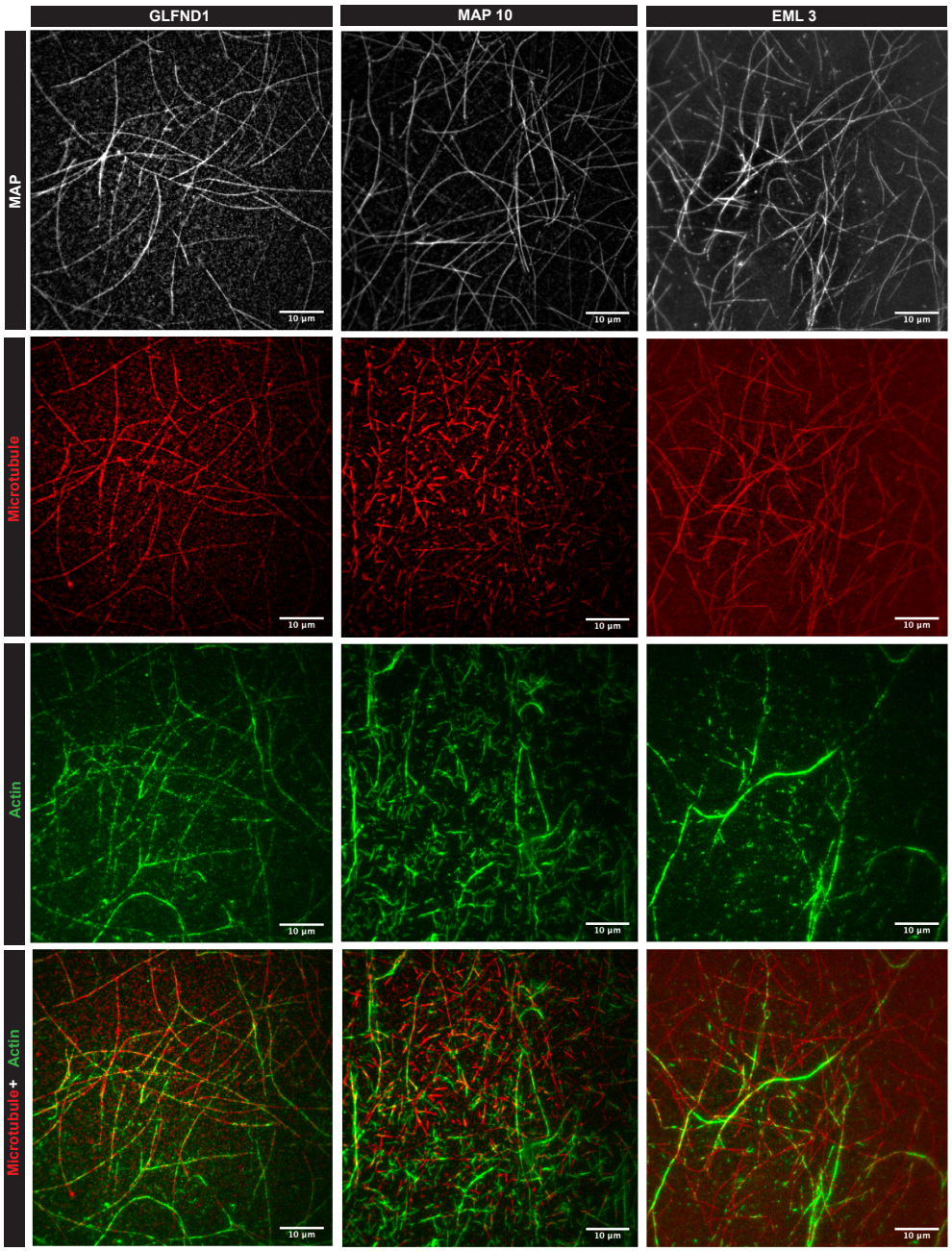

Jijumon et al., Supplementary figure 13

Supplementary figure 9: Ex-vivo approach for MAP competition experiments: T243A EML1-GFP mutant binds less comparing wild type EML1-mCherry.

A)

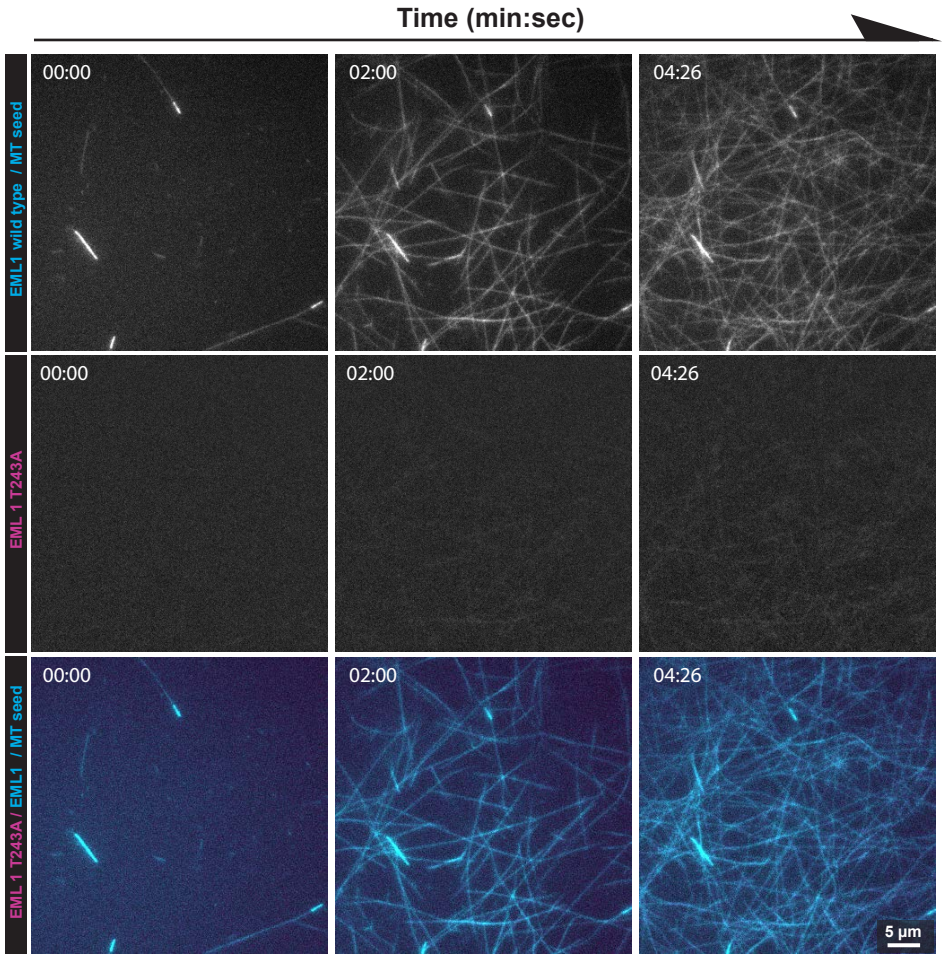

B)

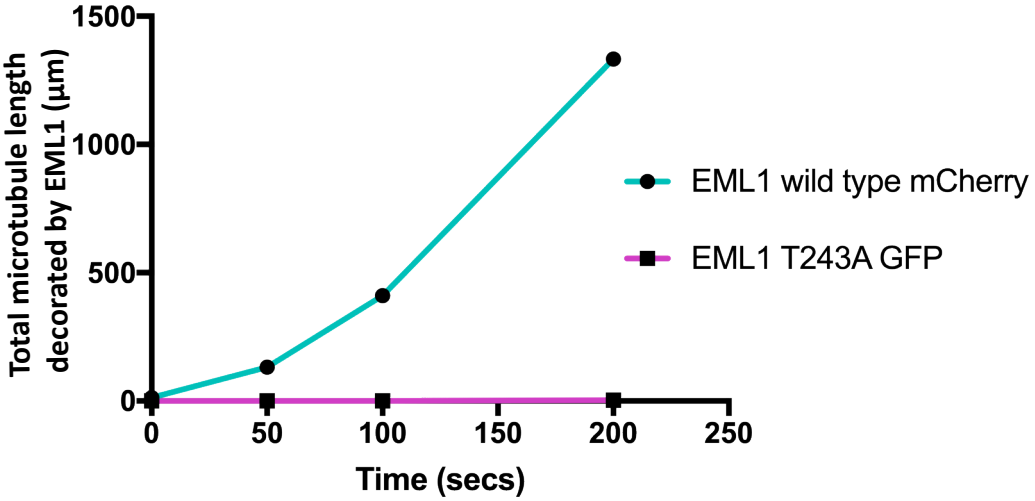

Jijumon et al., Supplementary figure 14

Quantification of helix width of MT coils induced by CSAP.

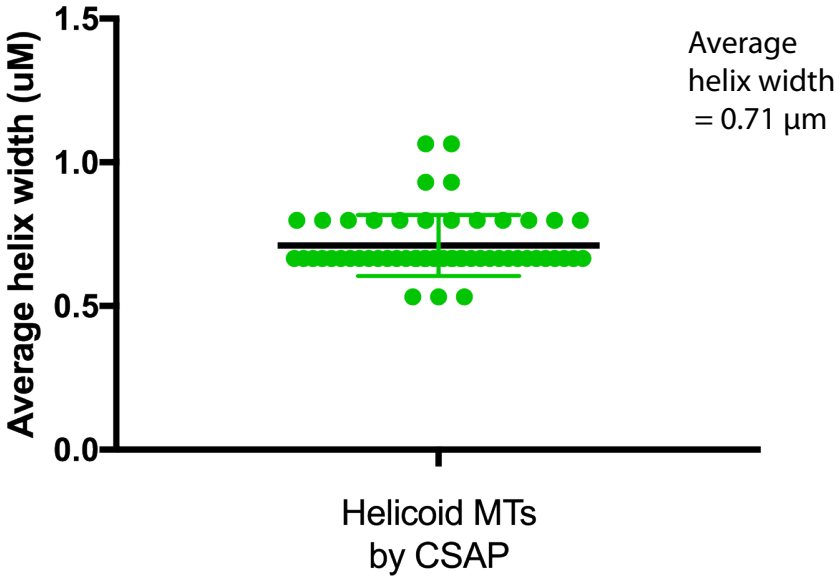

Supplementary table 1: Microtubule-associated proteins used in this the study and their relevant information:

Serial No.	Protein name	Accession number	Size (AA)	Position of GFP tag (N- or C-term)	Primer sequence (forward and reverse, 5' – 3')	References that suggested/ shown as MAPs	Direct or indirect links to diseases	References
1.	Tau 3R	XM_006532409.2	370	N	Forward - cggcatggacgagctgtacaagGGAAGCGGAGCT ATGGCTGACCCTCGCCAGGAG Reverse - ggtcgacactagtggatcc TtACAAACCCTGCTTGGCCAAGG	(Weingarten, Lockwood et al. 1975, Cleveland, Hwo et al. 1977, Cleveland, Hwo et al. 1977)	Alzheimer's disease, Parkinson's disease, Pick's disease, progressive supranuclear palsy, parkinsonism-dementia complex of Guam	(Joachim, Morris et al. 1987, Goedert, Wischik et al. 1988, Murayama, Mori et al. 1990) (Matsumoto, Hirano et al. 1990, Arif, Kazim et al. 2014)
2.	Tau 4R	NM_005910.5	441	N	Forward - cggcatggacgagctgtacaagGGAAGCGGAGCT ATGGCTGACCCTCGCCAGGAG Reverse - ggtcgacactagtggatcc TtACAAACCCTGCTTGGCCAAGG	(Weingarten, Lockwood et al. 1975, Cleveland, Hwo et al. 1977, Cleveland, Hwo et al. 1977)	Same as above	(Goedert, Wischik et al. 1988)
3.	MAP2C	BC051410.1	467	N	Forward - cggcatggacgagctgtacaagGGAAGCGGAGCT ATGGCCGACGAGCGGAAAGATG Reverse - ggtcgacactagtggatcc TtACAAGCCCTGCTTAGCAAGCG	(Dentler, Granett et al. 1975, Murphy and Borisy 1975)	Schizophrenia, epilepsy, Alzheimer's disease, myotonic dystrophy, Prion disease, stress, spinal cord injury	(Neve, Harris et al. 1986, Rosoklija, Keilp et al. 2005, Jalava, Lopez-Picon et al. 2007, Yan, Sun et al. 2010, Velazquez-Bernardino, Garcia-Sierra et al. 2012, Zhang and Dong 2012, Abdanipour, Schluesener et al. 2015)
4.	MAP2D	NM_001039934.1	498	N	Forward - cggcatggacgagctgtacaagGGAAGCGGAGCT ATGGCCGACGAGCGGAAAGATG Reverse - ggtcgacactagtggatcc TtACAAGCCCTGCTTAGCAAGCG	(Dentler, Granett et al. 1975, Murphy and Borisy 1975)	--	--

5.	MAP4	BC050893.1	1086	N	Forward - cggcatggacgagctgtacaagGGAAGCGGAGCT ATGGCCGACCTCAGTCTTGTGG Reverse - ggtcgacactagtggatcc TtAATTTGTCTCCTGGATCTGGCTG	(Bulinski and Borisy 1979)	Alzheimer's disease, cardiac hypertrophy, breast cancer, ovarian cancer	(Bash-Babula, Toppmeyer et al. 2002, Kumarapeli and Wang 2004, Ray, Ruan et al. 2008, Yang, Xu et al. 2018)
6.	MAP4B	BC050893.1	1055	N	Forward - cggcatggacgagctgtacaagGGAAGCGGAGCT ATGGCCGACCTCAGTCTTGTGG Reverse - ggtcgacactagtggatcc TtAATTTGTCTCCTGGATCTGGCTG	(Bulinski and Borisy 1979)	--	--
7.	MAP6/ STOP	NM_010837.3	906	C	Forward - agaattattccgctagcATGGCGTGGCCGTGCATC ACAAG Reverse - accatGGTGGCgctagcAGGGGATCCCTCAAT ATATTCCGTATGG	(Webb and Wilson 1980)	Parkinson's disease, autism, oral leukoplakia, schizophrenia, amyotrophic lateral sclerosis	(Letournel, Bocquet et al. 2003, Shimizu, Iwayama et al. 2006, Abe, Yamashita et al. 2016, Wei, Sun et al. 2016, Ma, Song et al. 2019)
8.	MAP7	NM_001358787.1	752	C	Forward - agaattattccgctagcATGCCTGGGTCAGCTACA GCGATCCG Reverse - accatGGTGGCgctagcTATAACTTCTGCGGTC TGTTGTGTCTGC	(Bulinski and Borisy 1980, Masson and Kreis 1993)	Human cervical cancer, multiple sclerosis, thymic epithelial tumor, myeloid leukemia, hepatocellular carcinoma, stage II colon cancer, Barrett's carcinoma, sacral dysgenesis	(Langer, Specht et al. 2004, Sood, Bader et al. 2004, Blum, Graham et al. 2008, Geng, Ng et al. 2011, Fu, Fu et al. 2016, Zhao, Wu et al. 2018, Navarro-Barriuso, Mansilla et al. 2019, Zhang, Liu et al. 2020)
9.	MAP7D1	NM_144941.3	846	C	Forward - agaattattccgctagcATGGAGAGTGGCCCGCGT GTGGAG Reverse - accatGGTGGCgctagcAAGAACTTCTGTGACC TGTGGAGGCTG	(Bulinski and Borisy 1980, Metzger, Gache et al. 2012) (Niida and Yachie 2011)	No reports	--
10.	MAP7D2	NM_001313751.1	748	C	Forward - agaattattccgctagc ATGGAGCGCAGCGGTGGGAACG Reverse - accatGGTGGCgctagc ACAGAAGGTATTCAGGGTAGTTTC	(Bulinski and Borisy 1980, Metzger, Gache et al. 2012) (Niida and Yachie 2011)	Gastric cancer	(Liu, Wu et al. 2018)
11.	MAP7D3	NM_177293.3	876	C	Forward - agaattattccgctagcATGGCGGACCCCACTTTT GCTGCTAC	(Bulinski and Borisy 1980, Metzger,	Pediatric Wilms tumor, muscle hypertrophy, breast cancer	(Tala, Xie et al. 2014, Willis, Wood et al. 2016, Lin, Wu et al. 2020)

					Reverse - accatGGTGGCgctagcCACATCACTCTCTTCTGCCTCTTTTCC	Gache et al. 2012) (Niida and Yachie 2011) (Yadav, Verma et al. 2014)		
12.	MAP 8/ MAP1s	NM_173013.3	973	C	Forward - agaattattccgctagc ATGGCGGCGCCGGAGGCTGTGGAG Reverse - accatGGTGGCgctagc GAACTCCACCTTGCAGGCGGGGAAG	(Wong, Tse et al. 2004)	Colorectal cancer, Liver Fibrosis and Hepatocellular Carcinoma, Crohn's disease, renal fibrosis, adenocarcinomas	(Song, Hu et al. 2015, Xu, Yue et al. 2016, Bai, Bai et al. 2017, Yue, Li et al. 2017, Wang, Zhang et al. 2019)
13.	MAP 9/ ASAP	NM_001081230.1	646	C	Forward - agaattattccgctagc ATGTCCGATGAAATCTTCAGCACAAC Reverse - accatGGTGGCgctagc AAATACTTTTGAGGGCGCAGTTCTGC	(Saffin, Venoux et al. 2005)	Colorectal and breast cancers, gastric carcinoma, ovarian cancer, hepatocellular carcinoma	(Rouquier, Pillaire et al. 2014, Yamada, Yasui et al. 2016, Liu, Xiao et al. 2018, Schiewek, Schumacher et al. 2018)
14.	MAP 10	NM_028908.3	891	C	Forward - agaattattccgctagc ATGGCGACCACGGCGGCCGGGCGG Reverse - accatGGTGGCgctagcCACTGTGTATCCTGGAAGTTTATTTATTACTAACTCG	(Fong, Leung et al. 2013)	No reports	--
15.	MAP 11/C7orf43	NM_153161.3	580	C	Forward - agaattattccgctagc ATGGAGTCCCAATGCGACTACTCG Reverse - accatGGTGGCgctagc CTTGACGGGCTCCACCACCAGGAC	(Perez, Bar-Yaacov et al. 2019)	Microcephaly, hepatocellular carcinoma	(Amisaki, Tsuchiya et al. 2019, Perez, Bar-Yaacov et al. 2019)
16.	EMAP1	BC053094.1	800	C	Forward - agaattattccgctagc ATGGAGGACGGCTTCTCCAGC Reverse - accatGGTGGCgctagc AATGACTCGCCACTGCATGATGC	(Keller and Rebhun 1982, Vallee and Bloom 1983)	Usher syndrome, neuronal heterotopia, breast, colorectal and lung cancers, T-cell acute lymphoblastic leukemia, Joubert and Meckel ciliopathy syndromes	(Eudy, Ma-Edmonds et al. 1997, De Keersmaecker, Graux et al. 2005, Lin, Li et al. 2009, Kielar, Tuy et al. 2014, Wiegering, Ruther et al. 2018)
17.	EMAP2	NM_028153.1	668	C	Forward - agaattattccgctagc ATGAGTAGTTTTGGAATTGGGAAAACC Reverse - accatGGTGGCgctagc GGCCACCCGCCACTGCAGCAC	(Keller and Rebhun 1982, Vallee and Bloom 1983)	No reports	--
18.	EMAP3	BC023878.1	897	C	Forward - agaattattccgctagc ATGGACGGGGCTGCGGGGCCCGG	(Keller and Rebhun 1982, Vallee	No reports	--

					Reverse - accatGGTGGCgctagc CACGTCCAGGGAGGAGGCAGGGG	and Bloom 1983)		
19.	EMAP4	NM_001114362.1	919	C	Forward - agaattattccgctagc ATGGACGGTTTCGCCGGCAGCC Reverse - accatGGTGGCgctagc GCACAGGGGTGTTATGCCTCGC	(Keller and Rebhun 1982, Vallee and Bloom 1983)	Colorectal, breast and non-small cell lung cancer (NSCLC), POEMS syndrome	(Lin, Li et al. 2009, Nagao, Mimura et al. 2019).
20.	NrD1	BC036128.1	1161	C	Forward - agaattattccgctagc ATGCTGAGGAGAGTCGCGGTTGCTG Reverse - accatGGTGGCgctagc TTTGACTATTTTATGGTAGGGGAAGAGGC	(Ohno, Hiraoka et al. 2009)	Alzheimer's disease, schizophrenia, down syndrome and cancer	Bernstein, 2013 #9573}
21.	Crmp2A	NM_001378767.1	673	C	Forward - agaattattccgctagc ATGGCCGAGAGAAAGCAATCTGGAAAG Reverse - accatGGTGGCgctagc GCCCAGGCTGGTGATGTTGGC	(Fukata, Itoh et al. 2002, Tan, Cha et al. 2015)}	Crmp2 in prion diseases, schizophrenia, Alzheimer's disease (AD), Parkinson's disease, multiple sclerosis **no direct evidences for 2A and 2B	(Gu and Ihara 2000, Shinkai-Ouchi, Yamakawa et al. 2010, Petratos, Ozturk et al. 2012, Togashi, Hasegawa et al. 2019, Toyoshima, Jiang et al. 2019)
22.	Crmp2B	NM_009955.3	572			(Fukata, Itoh et al. 2002, Tan, Cha et al. 2015)	**no direct evidences for 2A and 2B	--
23.	Crmp4	NM_009468.4	570		Forward - GACTCAGATctcgagACC ATGTCCTACCAGGGCAAGAAGAACATTC Reverse - TCTATCTTTggatcc ACTCAGGGATGTGATGTTAGAACGGC	(Fukata, Itoh et al. 2002, Tan, Cha et al. 2015)	Colorectal cancer, prostate cancer	(Gao, Pang et al. 2010, Chen, Cai et al. 2016)
24.	MACF1	AF150755.1	1019		Forward - GACTCAGATctcgagACC ATGGAACTACATTCCCAGCTGAGAGCC Reverse - TCTATCTTTggatcc TCGCTTGGGACCTGGAGTCCTGGG	(Bernier, Mathieu et al. 1996)	Lissencephaly, Parkinson's Disease, Spectraplakinopathy type 1, glioblastoma	(Jorgensen, Mosbech et al. 2014, Afghani, Mehta et al. 2017, Wang, Li et al. 2017, Dobyns, Aldinger et al. 2018)
25.	MACF2/ dystonin	NM_001276764.1	1042		Forward - GACTCAGATctcgagACC ATGGAAGTCTGCACCGCCTTTGCC Reverse - TCTATCTTTggatcc TCTCTTCGAAGACTTGTCTAATTTGCTGGC	(Sawamura, Nomura et al. 1990) (Bernier, Brown et al. 1995)	Dystonia, multiple sclerosis, Alzheimer's Disease	(Brown, Bernier et al. 1995, Laffitte, Burkhard et al. 2005, Kokkonen, Herukka et al. 2017)
26.	CSAP	NM_028536.1	252	C	Forward - agaattattccgctagc ATGTCCCCGGGCAGCGGGGTG Reverse - accatGGTGGCgctagc CGCCCTCGCTGAGTAGCACCG	(Backer, Gutzman et al. 2012)	Retinal degeneration, neurodegeneration and male infertility	(Bompard, van Dijk et al. 2018)

27.	Cingulin			C	Dog cinglulin full-length plasmid form Sandra Citi (Paschoud et al Mol. Membr. Biol 2008) and Rytis Prekeris.	(Yano, Torisawa et al. 2018)	Mesothelioma	(Oliveto, Alfieri et al. 2018)
28.	Syntaphilin C	NM_001291077.1	459		Forward - agaattattccgctagc ATGGCCATGTCCCTGCAGGGAAGTAG Reverse - accatGGTGGCgctagc GAGCTGAGAGCCACCGGCTGTGCTG	(Kang, Tian et al. 2008)	Prostate cancer, multiple sclerosis	(Mahad, Ziabreva et al. 2009, Hwang, Bryant et al. 2019)
29.	Syntaphilin A	NM_198214.3	528		Forward - agaattattccgctagc ATGGCCATGTCCCTGCAGGGAAGTAG Reverse - accatGGTGGCgctagc GAGCTGAGAGCCACCGGCTGTGCTG	(Kang, Tian et al. 2008)	--	--
30.	GLFND1	NM_183178.2	496	N	Forward - cggcatggacgagctgtacaagGGAAGCGGAGCTA TGGAAGACCAGAGGGAGGCGCTAAG Reverse - ggtcgacactagtggatcc tTAGGTGAGGCTGGTATTGGAACTGC	(Manabe, Whitmore et al. 2002)	No reports	--
31.	GLFND2	NM_001195284.1	497	N	Forward - cggcatggacgagctgtacaagGGAAGCGGAGCTA TGGACTCGCAGAAAGAAGCTCTAC Reverse - ggtcgacactagtggatccTTACTGAGTGACATTGT TCAGGCTGC	(Manabe, Whitmore et al. 2002)	No reports	--
32.	SAXO1	NM_001081096.1	476	C	Forward: cggactcgagACC ATGGGGAAGAGGACTTGCATCTGCAAC Reverse: ccgcggatcc GGCTGACACTTCTAGTTCCTTCTGACC	(Dacheux, Roger et al. 2015)	No reports	--
33.	SAXO2	XM_006507956.1	389	C	Forward: cggactcgagACC ATGAGGAACTGGTGTCTGTGCCAG Reverse: ccgcggatcc AAAGGCCTTCACTGCAGGAATAATCTTGC	(Dacheux, Roger et al. 2015)	No reports	--
34.	CLIP 170	AK220172.1	1315	N	Forward - cggcatggacgagctgtacaagGGAAGCGGAGCT ATGAGTATGCTAAAACCCAGCGG Reverse - ggtcgacactagtggatcc TtAGAAGGTCTCGTCGTCATTGCAG	(Rickard and Kreis 1990)	Hodgkin's disease, CDKL5 deficiency disorder, Anaplastic large cell lymphoma (ALCL), pancreatic cancer, distal hereditary motor neuropathy type II (distal HMN II)	(Bilbe, Delabie et al. 1992, Delabie, Shipman et al. 1992, Irobi, Nelis et al. 2001, Li, Sun et al. 2013, Barbiero, Peroni et al. 2020)
35.	CFAP 20	NM_008187.2	193	C	Forward - agaattattccgctagc ATGTTCAAGAACACGTTCCAGAGTG Reverse - accatGGTGGCgctagc TTGTTTGGCCTTGTTCTGAACTGG	(Mendes Maia, Gogendeau et al. 2014)	No reports	

36.	TRAK1	NM_175114.3	939	N	Forward - cggcatggacgagctgtacaagGGAAGCGGAGCTATGGCATTGGCAATTCAGCTCAGGC Reverse - ggtcgacactagtggatcc TtACCGCAAGCTAGTCTGTTTGGGG	(Henrichs, Grycova et al. 2020)	Encephalopathy, hyperekplexia	(Barel, Malicdan et al. 2017, Sagie, Lerman-Sagie et al. 2018)
37.	TRAK 2	NM_172406.3	913	N	Forward - cggcatggacgagctgtacaagGGAAGCGGAGCTATGAGTCAATCCCAGAATGCCATTTTCAAATC Reverse - ggtcgacactagtggatcc TtAATCTTCCTTCAGGATACCCATTTTGGG	(Henrichs, Grycova et al. 2020)	Atherosclerosis	(Lake, Taylor et al. 2017)
38.	Parkin	AB019558.1	465	C	Forward - agaattattccgctagc ATGATAGTGTTTGTCAGGTTCAACTCC Reverse - accatGGTGGCgctagc CACGTCAAACCAGTGATCTCCCATG	(Ren, Zhao et al. 2003)	Parkinson's disease, MERRF syndrome, atherogenesis, Juvenile Huntington's Disease, lung cancer, hepatocellular carcinoma, retinal degeneration, chronic obstructive pulmonary disease (COPD)	(Kitada, Asakawa et al. 1998, Leermakers, Schols et al. 2018, Aladdin, Kiraly et al. 2019, Li, Wang et al. 2019, Zhang, Lin et al. 2019, Zhu, Aredo et al. 2019, Tyrrell, Blin et al. 2020, Villanueva-Paz, Povea-Cabello et al. 2020)
39.	DCX s, DCX	AY560329.1	360	C	Forward - agaattattccgctagc ATGGAACTTGATTTTGGACATTTTGACGAAC Reverse - accatGGTGGCgctagc CATGGAATCGCCAAGTGAATCAGAGTC	(Francis, Koulakoff et al. 1999)	Epilepsy, neuroblastoma, autism, double-cortex syndrome, subcortical laminar heterotopia (SCLH).	(des Portes, Francis et al. 1998, Aigner, Fluegel et al. 2000, Vourc'h, Petit et al. 2002, Oltra, Martinez et al. 2005, D'Alessio, Konopka et al. 2010, Zhang, Shi et al. 2017)
40.	DCX b		510	C	Forward - agaattattccgctagc ATTGTATTGAGATGCAAAGGCTGCTTCC Reverse - accatGGTGGCgctagc CATGGAATCGCCAAGTGAATCAGAGTC	(Francis, Koulakoff et al. 1999)	--	--
41.	DCLK1_4	NM_001111053.2	363	C	Forward - agaattattccgctagc ATGTCGTTCGGCAGAGATATGGAGTTG Reverse - accatGGTGGCgctagc CACTGAGTCTCCTACTGAGTCCAAATC	(Lipka, Kapitein et al. 2016)	DCLK1: Non-small cell lung cancer (NSCLC), head and neck squamous cell carcinoma (HNSCC), ovarian clear cell carcinoma (OCCC), breast cancer, gastric cancer	(Meng, Yu et al. 2013, Liu, Tsang et al. 2016, Kadletz, Thurnher et al. 2017, Tao, Tanaka et al. 2017, Wu, Ruan et al. 2017)
42.	DCLK1_5	NM_001195538.2	740	C	Forward - agaattattccgctagc ATGTCGTTCGGCAGAGATATGGAGTTG Reverse - accatGGTGGCgctagc AAAGGGCGAATTGGGGGAGCGAACAG	(Lipka, Kapitein et al. 2016)		

43.	PRC1	NM_145150.3	606		Forward - agaattattccgctagc ATGAGGAGAAGTGAGGTGCTAGCAG Reverse - accatGGTGGCgctagc GGACTGGATGTTGGTTGAATTGAGGATTC	(Pellman, Bagget et al. 1995, Mollinari, Kleman et al. 2002, Bieling, Telley et al. 2010)	gastric carcinoma, breast carcinoma, hepatocellular carcinoma	(Brynychova, Ehrlichova et al. 2016, Chen, Rajasekaran et al. 2016, Zhang, Shi et al. 2017)
44.	ATIP3	NP_001001924	440		Form Clara Nahmias	(Molina, Velot et al. 2013)	hepatocellular carcinoma, breast carcinoma, prostate cancer	(Di Benedetto, Pineau et al. 2006, Rodrigues-Ferreira, Di Tommaso et al. 2009, Louis, Chow et al. 2011)
45.	ATIP3 D1	NP_001001924			Form Clara Nahmias	(Molina, Velot et al. 2013)		
46.	ATIP3 D2	NP_001001924			Form Clara Nahmias	(Molina, Velot et al. 2013)		
47.	ATIP3 D3	NP_001001924	1260		Form Clara Nahmias	(Molina, Velot et al. 2013)		
48.	MAP11b	NM_153161.3	490	C	Forward - agaattattccgctagc ATGGAGTCCCAATGCGACTACTCG Reverse - accatGGTGGCgctagc CTTGACGGGCTCCACCACCAGGAC	(Perez, Bar-Yaacov et al. 2019)	MAP 11: Microcephaly, hepatocellular carcinoma	(Amisaki, Tsuchiya et al. 2019, Perez, Bar-Yaacov et al. 2019).
49.	Jupiter homologue mJpl1	NM_008258.2	154	N	Forward - cggcatggacgagctgtacaagGGAAGCGGAGCTA TGACCACTACCACTACCTTTAAGGG Reverse - ggtcgacactagtggatcc tTAACCCAAGACCAGGCTGGACTTG	(Karpova, Bobinnec et al. 2006)	No reports	--
50.	Jupiter homologue mJpl2	NM_198937.2	190	N	Forward - cggcatggacgagctgtacaagGGAAGCGGAGCTA TGTTCCAGGGCGCGGACAGCCAAG Reverse - ggtcgacactagtggatcc TtAATAGAAGGAGAGGCTGGATTTGCC		No reports	--
51.	Protein 4.1	NM_183428	868	C	Forward - agaattattccgctagc ATGATGACAACGGCTACTTCTGGGAAC Reverse - accatGGTGGCgctagc CTCCTCAGAGATCTCTGTCTCCTG	(Huang, Jagadeeswaran et al. 2004)	Heart failure, encephalomyelitis, myeloid malignancies,neuroacanthocytosis	(Orlacchio, Calabresi et al. 2007, Alanio-Brechot, Schischmanoff et al. 2008, Liu, Zhou et al. 2014, Wei, Yang et al. 2016)

54.	CKAP2	BC145666.1	664	C	Forward - agaattattccgctagc ATGGCAGAGTCCAGGAAACGCTTC Reverse - accatGGTGGCgctagcTTCCTCTTCCGCTACG TCGGTCTC	(Watanabe, Shimizu et al. 1996, Jin, Murakumo et al. 2004)	Glioma, breast cancer, cervical carcinoma.	(Guo, Song et al. 2017, Sim, Bae et al. 2017, Wang, Huang et al. 2018)
59.	Nrd1	BC036128.1	1161	C	Forward - agaattattccgctagc ATGCTGAGGAGAGTCGCGGTTGCTG Reverse - accatGGTGGCgctagcTTTGACTATTTTATGG TAGGGGAAGAGGC	(Chesneau, Prat et al. 1996) (Hospital, Chesneau et al. 2000)	Alzheimer's disease, schizophrenia, down syndrome and cancer	(Bernstein, Stricker et al. 2013)
60.	TRAK1	NM_175114	939	N	Forward - cggcatggacgagctgtacaagGGAAGCGGAGCTA TGGCATTGGCAATTCAGCTCAGGC Reverse - ggtcgacactagtggatcc TtACCGCAAGCTAGTCTGTTTGGGG	(Henrichs, Grycova et al. 2020)	Encephalopathy, hyperekplexia	(Barel, Malicdan et al. 2017, Sagie, Lerman-Sagie et al. 2018)
62.	TRAK2	NM_172406.3	913	N	Forward - cggcatggacgagctgtacaagGGAAGCGGAGCTA TGAGTCAATCCCAGAATGCCATTTTCAAAT C Reverse - ggtcgacactagtggatccTtAATCTTCCTTCAGGAT ACCCATTTTGGG	(Henrichs, Grycova et al. 2020)	Atherosclerosis	(Lake, Taylor et al. 2017)
63.	CFAP20	NM_008187.2	193	C	Forward - agaattattccgctagc ATGTTCAAGAACACGTTCCAGAGTG Reverse - accatGGTGGCgctagc TTGTTTGGCCTTGTTCTGAACTGG	(Mendes Maia, Gogendeau et al. 2014)	No reports	--
64.	Parkin	AB019558.1	464	C	Forward - agaattattccgctagc ATGATAGTGTTTGTCAGGTTCAACTCC Reverse - accatGGTGGCgctagc CACGTCAAACCAGTGATCTCCCATG	(Ren, Zhao et al. 2003)	Parkinson's disease, MERRF syndrome, atherogenesis, Juvenile Huntington's Disease, lung cancer, Hepatocellular carcinoma, retinal degeneration, chronic obstructive pulmonary disease (COPD)	(Kitada, Asakawa et al. 1998, Leermakers, Schols et al. 2018, Aladdin, Kiraly et al. 2019, Li, Wang et al. 2019, Zhang, Lin et al. 2019, Zhu, Aredo et al. 2019, Tyrrell, Blin et al. 2020, Villanueva-Paz, Povea-Cabello et al. 2020)
65.	EMAP3	BC023878.1	897	C	Forward - agaattattccgctagc ATGGACGGGGCTGCGGGGCCCGG Reverse - accatGGTGGCgctagc CACGTCCAGGGAGGAGGCAGGGG	(Tegha-Dunghu, Neumann et al. 2008)	No reports	--

References

Abdanipour, Alireza, Hermann J Schluesener, Taki Tiraihi, and Ali Noori-Zadeh. 2015. 'Systemic administration of valproic acid stimulates overexpression of microtubule-associated protein 2 in the spinal cord injury model to promote neurite outgrowth', *Neurol Res*, 37: 223-8.

Abe, Masanobu, Satoshi Yamashita, Yoshiyuki Mori, Takahiro Abe, Hideto Saijo, Kazuto Hoshi, Toshikazu Ushijima, and Tsuyoshi Takato. 2016. 'High-risk oral leukoplakia is associated with aberrant promoter methylation of multiple genes', *BMC Cancer*, 16: 350.

Adib, Rozita, Jessica M Montgomery, Joseph Atherton, Laura O'Regan, Mark W Richards, Kees R Straatman, Daniel Roth, Anne Straube, Richard Bayliss, Carolyn A Moores, and Andrew M Fry. 2019. 'Mitotic phosphorylation by NEK6 and NEK7 reduces the microtubule affinity of EML4 to promote chromosome congression', *Sci Signal*, 12: 10.1126/scisignal.aaw2939.

Afghani, Najlaa, Toral Mehta, Jialiang Wang, Nan Tang, Omar Skalli, and Quincy A Quick. 2017. 'Microtubule actin cross-linking factor 1, a novel target in glioblastoma', *Int J Oncol*, 50: 310-16.

Aigner, L, D Fluegel, J Dietrich, S Ploetz, and J Winkler. 2000. 'Isolated lissencephaly sequence and double-cortex syndrome in a German family with a novel doublecortin mutation', *Neuropediatrics*, 31: 195-8.

Akhmanova, Anna, and Michel O Steinmetz. 2015. 'Control of microtubule organization and dynamics: two ends in the limelight', *Nat Rev Mol Cell Biol*, 16: 711-26.

Akhmanova, Anna, and Michel O. Steinmetz. 2008. 'Tracking the ends: a dynamic protein network controls the fate of microtubule tips', *Nat Rev Mol Cell Biol*, 9: 309-22.

Aladdin, Azzam, Robert Kiraly, Pal Boto, Zsolt Regdon, and Krisztina Tar. 2019. 'Juvenile Huntington's Disease Skin Fibroblasts Respond with Elevated Parkin Level and Increased Proteasome Activity as a Potential Mechanism to Counterbalance the Pathological Consequences of Mutant Huntingtin Protein', *Int J Mol Sci*, 20.

Alanio-Brechot, Cecile, Pierre-Olivier Schischmanoff, Madeleine Feneant-Thibault, Therese Cynober, Gil Tchernia, Jean Delaunay, and Loic Garcon. 2008. 'Association between myeloid malignancies and acquired deficit in protein 4.1R: a retrospective analysis of six patients', *Am J Hematol*, 83: 275-8.

Alexopoulou, Annika N, John R Couchman, and James R Whiteford. 2008. 'The CMV early enhancer/chicken beta actin (CAG) promoter can be used to drive transgene expression during the differentiation of murine embryonic stem cells into vascular progenitors', *BMC Cell Biol*, 9: 2.

Amisaki, Masataka, Hiroyuki Tsuchiya, Tomohiko Sakabe, Yoshiyuki Fujiwara, and Goshi Shiota. 2019. 'Identification of genes involved in the regulation of TERT in hepatocellular carcinoma', *Cancer Sci*, 110: 550-60.

Arif, Mohammad, Syed Faraz Kazim, Inge Grundke-Iqbal, Ralph M Garruto, and Khalid Iqbal. 2014. 'Tau pathology involves protein phosphatase 2A in parkinsonism-dementia of Guam', *Proc Natl Acad Sci U S A*, 111: 1144-9.

Backer, Chelsea B, Jennifer H Gutzman, Chad G Pearson, and Iain M Cheeseman. 2012. 'CSAP localizes to polyglutamylated microtubules and promotes proper cilia function and zebrafish development', *Mol Biol Cell*, 23: 2122-30.

Bai, Wenxia, Jian'an Bai, Yanhai Li, Delong Tian, and Ruihua Shi. 2017. 'Microtubule-associated protein 1S-related autophagy inhibits apoptosis of intestinal epithelial cells via Wnt/beta-catenin signaling in Crohn's disease', *Biochem Biophys Res Commun*, 485: 635-42.

Barbiero, I, D Peroni, P Siniscalchi, L Rusconi, M Tramarin, R De Rosa, P Motta, M Bianchi, and C Kilstrup-Nielsen. 2020. 'Pregnenolone and pregnenolone-methyl-ether rescue neuronal defects caused by dysfunctional CLIP170 in a neuronal model of CDKL5 Deficiency Disorder', *Neuropharmacology*, 164: 107897.

Barel, Ortal, May Christine V Malicdan, Bruria Ben-Zeev, Judith Kandel, Hadass Pri-Chen, Joshi Stephen, Ines G Castro, Jeremy Metz, Osama Atawa, Sharon Moshkovitz, Esther Ganelin, Iris Barshack, Sylvie Polak-Charcon, Dvora Nass, Dina Marek-Yagel, Ninette Amariglio, Nechama Shalva, Thierry Vilboux, Carlos Ferreira, Ben Pode-Shakked, Gali Heimer, Chen Hoffmann, Tal Yardeni, Andreea Nissenkorn, Camila Avivi, Eran Eyal, Nitzan Kol, Efrat Glick Saar, Douglas C Wallace, William A Gahl, Gideon Rechavi, Michael Schrader, David M Eckmann, and Yair Anikster. 2017. 'Deleterious variants in TRAK1 disrupt mitochondrial movement and cause fatal encephalopathy', *Brain*, 140: 568-81.

Barlan, Kari, Wen Lu, and Vladimir I Gelfand. 2013. 'The microtubule-binding protein ensconsin is an essential cofactor of kinesin-1', *Curr Biol*, 23: 317-22.

Bash-Babula, Judy, Deborah Toppmeyer, Marie Labassi, Janice Reidy, Michelle Orlick, Rachelle Senzon, Elizabeth Alli, Thomas Kearney, David August, Weichung Shih, Jin-Ming Yang, and William N Hait. 2002. 'A Phase I/pilot study of sequential doxorubicin/vinorelbine: effects on p53 and microtubule-associated protein 4', *Clin Cancer Res*, 8: 1057-64.

Bernier, G, A Brown, G Dalpe, Y De Repentigny, M Mathieu, and R Kothary. 1995. 'Dystonin expression in the developing nervous system predominates in the neurons that degenerate in dystonia musculorum mutant mice', *Mol Cell Neurosci*, 6: 509-20.

Bernier, G, M Mathieu, Y De Repentigny, S M Vidal, and R Kothary. 1996. 'Cloning and characterization of mouse ACF7, a novel member of the dystonin subfamily of actin binding proteins', *Genomics*, 38: 19-29.

Bernstein, H-G, R Stricker, H Dobrowolny, J Steiner, B Bogerts, K Trubner, and G Reiser. 2013. 'Nardilysin in human brain diseases: both friend and foe', *Amino Acids*, 45: 269-78.

Bieling, Peter, Ivo A Telley, and Thomas Surrey. 2010. 'A minimal midzone protein module controls formation and length of antiparallel microtubule overlaps', *Cell*, 142: 420-32.

Bilbe, G, J Delabie, J Bruggen, H Richener, F A Asselbergs, N Cerletti, C Sorg, K Odink, L Tarcsay, and W Wiesendanger. 1992. 'Restin: a novel intermediate filament-associated protein highly expressed in the Reed-Sternberg cells of Hodgkin's disease', *EMBO J*, 11: 2103-13.

Bizzotto, Sara, Ana Uzquiano, Florent Dingli, Dmitry Ershov, Anne Houllier, Guillaume Arras, Mark Richards, Damarys Loew, Nicolas Minc, Alexandre Croquelois, Anne Houdusse, and Fiona Francis. 2017. 'Eml1 loss impairs apical progenitor spindle length and soma shape in the developing cerebral cortex', *Sci Rep*, 7: 17308.

Blum, Craig, Amanda Graham, Matt Yousefzadeh, Jessica Shrout, Katie Benjamin, Murli Krishna, Raza Hoda, Rana Hoda, David J Cole, Elizabeth Garrett-Mayer, Carolyn Reed, Michael Wallace, and Michael Mitas. 2008. 'The expression ratio of Map7/B2M is prognostic for survival in patients with stage II colon cancer', *Int J Oncol*, 33: 579-84.

Bodakuntla, Satish, Carsten Janke, and Maria M Magiera. 2020. 'Knocking Out Multiple Genes in Cultured Primary Neurons to Study Tubulin Posttranslational Modifications', *Methods Mol Biol*, 2101: 327-51.

Bodakuntla, Satish, A S Jijumon, Cristopher Villablanca, Christian Gonzalez-Billault, and Carsten Janke. 2019. 'Microtubule-Associated Proteins: Structuring the Cytoskeleton', *Trends Cell Biol*, 29: 804-19.

Bompard, Guillaume, Juliette van Dijk, Julien Cau, Yoann Lannay, Guillaume Marcellin, Aleksandra Lawera, Siem van der Laan, and Krzysztof Rogowski. 2018. 'CSAP Acts as a Regulator of TTLL-Mediated Microtubule Glutamylation', *Cell Rep*, 25: 2866-77 e5.

Bowne-Anderson, Hugo, Anneke Hibbel, and Jonathon Howard. 2015. 'Regulation of Microtubule Growth and Catastrophe: Unifying Theory and Experiment', *Trends Cell Biol*.

Brown, A, G Bernier, M Mathieu, J Rossant, and R Kothary. 1995. 'The mouse dystonia musculorum gene is a neural isoform of bullous pemphigoid antigen 1', *Nat Genet*, 10: 301-6.

Brynychova, Veronika, Marie Ehrlichova, Viktor Hlavac, Vlasta Nemcova-Furstova, Vaclav Pecha, Jelena Leva, Marketa Trnkova, Marcela Mrhalova, Roman Kodet, David Vrana, Jan Kovar, Radka Vaclavikova, Ivan Gut, and Pavel Soucek. 2016. 'Genetic and functional analyses do not explain the association of high PRC1 expression with poor survival of breast carcinoma patients', *Biomed Pharmacother*, 83: 857-64.

Bulinski, J C, and G G Borisy. 1979. 'Self-assembly of microtubules in extracts of cultured HeLa cells and the identification of HeLa microtubule-associated proteins', *Proc Natl Acad Sci U S A*, 76: 293-7.

———. 1980. 'Microtubule-associated proteins from cultured HeLa cells. Analysis of molecular properties and effects on microtubule polymerization', *J Biol Chem*, 255: 11570-6.

Bulinski, J C, and A Bossler. 1994. 'Purification and characterization of ensconsin, a novel microtubule stabilizing protein', *J Cell Sci*, 107 (Pt 10): 2839-49.

Chen, Jianxiang, Muthukumar Rajasekaran, Hongping Xia, Xiaoqian Zhang, Shik Nie Kong, Karthik Sekar, Veerabrahma Pratap Seshachalam, Amudha Deivasigamani, Brian Kim Poh Goh, London Lucien Ooi, Wanjin Hong, and Kam M Hui. 2016. 'The microtubule-associated protein PRC1 promotes early recurrence of hepatocellular carcinoma in association with the Wnt/beta-catenin signalling pathway', *Gut*, 65: 1522-34.

Chen, Si-Le, Shi-Rong Cai, Xin-Hua Zhang, Wen-Feng Li, Er-Tao Zhai, Jian-Jun Peng, Hui Wu, Chuang-Qi Chen, Jin-Ping Ma, Zhao Wang, and Yu-Long He. 2016. 'Targeting CRMP-4 by lentivirus-mediated RNA interference inhibits SW480 cell proliferation and colorectal cancer growth', *Exp Ther Med*, 12: 2003-08.

Chesneau, Valerie, Annik Prat, Dominique Segretain, Veronique Hospital, Alain Dupaix, Thierry Foulon, Bernard Jegou, and Paul Cohen. 1996. 'NRD convertase: a putative processing endoprotease associated with the axoneme and the manchette in late spermatids', *J Cell Sci*, 109 (Pt 11): 2737-45.

Cleveland, D W. 1989. 'Autoregulated control of tubulin synthesis in animal cells', *Curr Opin Cell Biol*, 1: 10-4.

Cleveland, D. W., S. Y. Hwo, and M. W. Kirschner. 1977a. 'Physical and chemical properties of purified tau factor and the role of tau in microtubule assembly', *J Mol Biol*, 116: 227-47.

———. 1977b. 'Purification of tau, a microtubule-associated protein that induces assembly of microtubules from purified tubulin', *J Mol Biol*, 116: 207-25.

Coue, M, S L Brenner, I Spector, and E D Korn. 1987. 'Inhibition of actin polymerization by latrunculin A', *FEBS Lett*, 213: 316-8.

D'Alessio, Luciana, Hector Konopka, Ester Maria Lopez, Eduardo Seoane, Damian Consalvo, Silvia Oddo, Silvia Kochen, and Juan Jose Lopez-Costa. 2010. 'Doublecortin (DCX) immunoreactivity in hippocampus of chronic refractory temporal lobe epilepsy patients with hippocampal sclerosis', *Seizure*, 19: 567-72.

Dacheux, Denis, Benoit Roger, Christophe Bosc, Nicolas Landrein, Emmanuel Roche, Lucie Chansel, Thomas Trian, Annie Andrieux, Aline Papaxanthos-Roche, Roger Marthan,

Derrick R Robinson, and Melanie Bonhivers. 2015. 'Human FAM154A (SAXO1) is a microtubule-stabilizing protein specific to cilia and related structures', *J Cell Sci*, 128: 1294-307.

De Keersmaecker, Kim, Carlos Graux, Maria D Odero, Nicole Mentens, Riet Somers, Johan Maertens, Iwona Wlodarska, Peter Vandenberghe, Anne Hagemeijer, Peter Marynen, and Jan Cools. 2005. 'Fusion of EML1 to ABL1 in T-cell acute lymphoblastic leukemia with cryptic t(9;14)(q34;q32)', *Blood*, 105: 4849-52.

Delabie, J, R Shipman, J Bruggen, B De Strooper, F van Leuven, L Tarcsay, N Cerletti, K Odink, V Diehl, and G Bilbe. 1992. 'Expression of the novel intermediate filament-associated protein restin in Hodgkin's disease and anaplastic large-cell lymphoma', *Blood*, 80: 2891-6.

Dentler, W L, S Granett, and J L Rosenbaum. 1975. 'Ultrastructural localization of the high molecular weight proteins associated with in vitro-assembled brain microtubules', *J Cell Biol*, 65: 237-41.

des Portes, V, F Francis, J M Pinard, I Desguerre, M L Moutard, I Snoeck, L C Meiners, F Capron, R Cusmai, S Ricci, J Motte, B Echenne, G Ponsot, O Dulac, J Chelly, and C Beldjord. 1998. 'doublecortin is the major gene causing X-linked subcortical laminar heterotopia (SCLH)', *Hum Mol Genet*, 7: 1063-70.

Di Benedetto, M, P Pineau, S Nouet, S Berhouet, I Seitz, S Louis, A Dejean, P O Couraud, A D Strosberg, D Stoppa-Lyonnet, and C Nahmias. 2006. 'Mutation analysis of the 8p22 candidate tumor suppressor gene ATIP/MTUS1 in hepatocellular carcinoma', *Mol Cell Endocrinol*, 252: 207-15.

Ding, Jianqing, Elizabeth Allen, Wei Wang, Angela Valle, Chengbiao Wu, Timothy Nardine, Bianxiao Cui, Jing Yi, Anne Taylor, Noo Li Jeon, Steven Chu, Yuen So, Hannes Vogel, Ravi Tolwani, William Mobley, and Yanmin Yang. 2006. 'Gene targeting of GAN in mouse causes a toxic accumulation of microtubule-associated protein 8 and impaired retrograde axonal transport', *Hum Mol Genet*, 15: 1451-63.

Dobyns, William B, Kimberly A Aldinger, Gisele E Ishak, Ghayda M Mirzaa, Andrew E Timms, Megan E Grout, Marjolein H G Dremmen, Rachel Schot, Laura Vandervore, Marjon A van Slegtenhorst, Martina Wilke, Esmee Kasteleijn, Arthur S Lee, Brenda J Barry, Katherine R Chao, Krzysztof Szczaluba, Joyce Kobori, Andrea Hanson-Kahn, Jonathan A Bernstein, Lucinda Carr, Felice D'Arco, Kaori Miyana, Tetsuya Okazaki, Yoshiaki Saito, Masayuki Sasaki, Soma Das, Marsha M Wheeler, Michael J Bamshad, Deborah A Nickerson, Elizabeth C Engle, Frans W Verheijen, Dan Doherty, and Grazia M S Mancini. 2018. 'MACF1 Mutations Encoding Highly Conserved Zinc-Binding Residues of the GAR Domain Cause Defects in Neuronal Migration and Axon Guidance', *Am J Hum Genet*, 103: 1009-21.

Eichenmuller, Bernd, Patrick Everley, Jean Palange, Denise Lepley, and Kathy A Suprenant. 2002. 'The human EMAP-like protein-70 (ELP70) is a microtubule destabilizer that localizes to the mitotic apparatus', *J Biol Chem*, 277: 1301-9.

Eudy, J D, M Ma-Edmonds, S F Yao, C B Talmadge, P M Kelley, M D Weston, W J Kimberling, and J Sumegi. 1997. 'Isolation of a novel human homologue of the gene coding for echinoderm microtubule-associated protein (EMAP) from the Usher syndrome type 1a locus at 14q32', *Genomics*, 43: 104-6.

Fanara, P, K H Husted, K Selle, P-Y A Wong, J Banerjee, R Brandt, and M K Hellerstein. 2010. 'Changes in microtubule turnover accompany synaptic plasticity and memory formation in response to contextual fear conditioning in mice', *Neuroscience*, 168: 167-78.

Fong, Ka-Wing, Justin Wai-Chung Leung, Yujing Li, Wenqi Wang, Lin Feng, Wenbin Ma, Dan Liu, Zhou Songyang, and Junjie Chen. 2013. 'MTR120/KIAA1383, a novel

microtubule-associated protein, promotes microtubule stability and ensures cytokinesis', *J Cell Sci*, 126: 825-37.

Forth, Scott, Kuo-Chiang Hsia, Yuta Shimamoto, and Tarun M Kapoor. 2014. 'Asymmetric friction of nonmotor MAPs can lead to their directional motion in active microtubule networks', *Cell*, 157: 420-32.

Francis, F., A. Koulakoff, D. Boucher, P. Chafey, B. Schaar, M. C. Vinet, G. Friocourt, N. McDonnell, O. Reiner, A. Kahn, S. K. McConnell, Y. Berwald-Netter, P. Denoulet, and J. Chelly. 1999. 'Doublecortin is a developmentally regulated, microtubule-associated protein expressed in migrating and differentiating neurons', *Neuron*, 23: 247-56.

Fry, Andrew M, Laura O'Regan, Jessica Montgomery, Rozita Adib, and Richard Bayliss. 2016. 'EML proteins in microtubule regulation and human disease', *Biochem Soc Trans*, 44: 1281-88.

Fu, Lin, Huaping Fu, Lei Zhou, Keman Xu, Yifan Pang, Kai Hu, Jing Wang, Lei Tian, Yuanyuan Liu, Jijun Wang, Hongmei Jing, Wenrong Huang, Xiaoyan Ke, and Jinlong Shi. 2016. 'High expression of MAP7 predicts adverse prognosis in young patients with cytogenetically normal acute myeloid leukemia', *Sci Rep*, 6: 34546.

Fukata, Yuko, Tomohiko J. Itoh, Toshihide Kimura, Celine Menager, Takashi Nishimura, Takashi Shiromizu, Hiroyasu Watanabe, Naoyuki Inagaki, Akihiro Iwamatsu, Hirokazu Hotani, and Kozo Kaibuchi. 2002. 'CRMP-2 binds to tubulin heterodimers to promote microtubule assembly', *Nat Cell Biol*, 4: 583-91.

Gallaud, Emmanuel, Renaud Caous, Aude Pascal, Franck Bazile, Jean-Philippe Gagne, Sebastien Huet, Guy G Poirier, Denis Chretien, Laurent Richard-Parpaillon, and Regis Giet. 2014. 'Ensconsin/Map7 promotes microtubule growth and centrosome separation in Drosophila neural stem cells', *J Cell Biol*, 204: 1111-21.

Gao, X, J Pang, L-Y Li, W-P Liu, J-M Di, Q-P Sun, Y-Q Fang, X-P Liu, X-Y Pu, D He, M-T Li, Z-L Su, and B-Y Li. 2010. 'Expression profiling identifies new function of collapsin response mediator protein 4 as a metastasis-suppressor in prostate cancer', *Oncogene*, 29: 4555-66.

Gell, Christopher, Volker Bormuth, Gary J Brouhard, Daniel N Cohen, Stefan Diez, Claire T Friel, Jonne Helenius, Bert Nitzsche, Heike Petzold, Jan Ribbe, Erik Schaffer, Jeffrey H Stear, Anastasiya Trushko, Vladimir Varga, Per O Widlund, Marija Zanic, and Jonathon Howard. 2010. 'Microtubule dynamics reconstituted in vitro and imaged by single-molecule fluorescence microscopy', *Methods Cell Biol*, 95: 221-45.

Geng, Wei, Kevin T P Ng, Chris K W Sun, Wing Lung Yau, Xiao Bing Liu, Qiao Cheng, Ronnie T P Poon, Chung Mau Lo, Kwan Man, and Sheung Tat Fan. 2011. 'The role of proline rich tyrosine kinase 2 (Pyk2) on cisplatin resistance in hepatocellular carcinoma', *PLoS ONE*, 6: e27362.

Gentili, Matteo, Joanna Kowal, Mercedes Tkach, Takeshi Satoh, Xavier Lahaye, Cecile Conrad, Marilyn Boyron, Berangere Lombard, Sylvere Durand, Guido Kroemer, Damarys Loew, Marc Dalod, Clotilde Thery, and Nicolas Manel. 2015. 'Transmission of innate immune signaling by packaging of cGAMP in viral particles', *Science*, 349: 1232-6.

Goedert, M., C. M. Wischik, R. A. Crowther, J. E. Walker, and A. Klug. 1988. 'Cloning and sequencing of the cDNA encoding a core protein of the paired helical filament of Alzheimer disease: identification as the microtubule-associated protein tau', *Proc Natl Acad Sci U S A*, 85: 4051-5.

Goedert, Michel, David S Eisenberg, and R Anthony Crowther. 2017. 'Propagation of Tau Aggregates and Neurodegeneration', *Annu Rev Neurosci*, 40: 189-210.

Goryunov, Dmitry, Cui-Zhen He, Chyuan-Sheng Lin, Conrad L Leung, and Ronald K H Liem. 2010. 'Nervous-tissue-specific elimination of microtubule-actin crosslinking factor 1a

results in multiple developmental defects in the mouse brain', *Mol Cell Neurosci*, 44: 1-14.

Gu, Y., and Y. Ihara. 2000. 'Evidence that collapsin response mediator protein-2 is involved in the dynamics of microtubules', *J Biol Chem*, 275: 17917-20.

Guo, Qi-Sang, Yu Song, Ke-Qin Hua, and Shu-Jun Gao. 2017. 'Involvement of FAK-ERK2 signaling pathway in CKAP2-induced proliferation and motility in cervical carcinoma cell lines', *Sci Rep*, 7: 2117.

Harada, Akihiro, Junlin Teng, Yosuke Takei, Keiko Oguchi, and Nobutaka Hirokawa. 2002. 'MAP2 is required for dendrite elongation, PKA anchoring in dendrites, and proper PKA signal transduction', *J Cell Biol*, 158: 541-9.

Henrichs, Verena, Lenka Grycova, Cyril Barinka, Zuzana Nahacka, Jiri Neuzil, Stefan Diez, Jakub Rohlena, Marcus Braun, and Zdenek Lansky. 2020. 'Mitochondria-adaptor TRAK1 promotes kinesin-1 driven transport in crowded environments', *Nat Commun*, 11: 3123.

Hiller, G, and K Weber. 1978. 'Radioimmunoassay for tubulin: a quantitative comparison of the tubulin content of different established tissue culture cells and tissues', *Cell*, 14: 795-804.

Hirokawa, Nobutaka, Yasuko Noda, Yosuke Tanaka, and Shinsuke Niwa. 2009. 'Kinesin superfamily motor proteins and intracellular transport', *Nat Rev Mol Cell Biol*, 10: 682-96.

Hooikaas, Peter Jan, Maud Martin, Tobias Muhlethaler, Gert-Jan Kuijntjes, Cathelijn A E Peeters, Eugene A Katrukha, Luca Ferrari, Riccardo Stucchi, Daan G F Verhagen, Wilhelmina E van Riel, Ilya Grigoriev, A F Maarten Altelaar, Casper C Hoogenraad, Stefan G D Rudiger, Michel O Steinmetz, Lukas C Kapitein, and Anna Akhmanova. 2019. 'MAP7 family proteins regulate kinesin-1 recruitment and activation', *J Cell Biol*, 218: 1298-318.

Hospital, Veronique, Valerie Chesneau, Agnes Balogh, Catherine Joulie, Nabil G Seidah, Paul Cohen, and Annik Prat. 2000. 'N-arginine dibasic convertase (nardilysin) isoforms are soluble dibasic-specific metalloendopeptidases that localize in the cytoplasm and at the cell surface', *Biochem J*, 349: 587-97.

Hua, Shasha, and Kai Jiang. 2020. 'Expression and Purification of Microtubule-Associated Proteins from HEK293T Cells for In Vitro Reconstitution', *Methods Mol Biol*, 2101: 19-26.

Huang, Shu-Ching, Ramasamy Jagadeeswaran, Eva S Liu, and Edward J Benz, Jr. 2004. 'Protein 4.1R, a microtubule-associated protein involved in microtubule aster assembly in mammalian mitotic extract', *J Biol Chem*, 279: 34595-602.

Hwang, Michael J, Kelly G Bryant, Jae H Seo, Qin Liu, Peter A Humphrey, Mary Ann C Melnick, Dario C Altieri, and Marie E Robert. 2019. 'Syntaphilin Is a Novel Biphasic Biomarker of Aggressive Prostate Cancer and a Metastasis Predictor', *Am J Pathol*, 189: 1180-89.

Irobi, J, E Nelis, J Meuleman, K Venken, P De Jonghe, C Van Broeckhoven, and V Timmerman. 2001. 'Exclusion of 5 functional candidate genes for distal hereditary motor neuropathy type II (distal HMN II) linked to 12q24.3', *Ann Hum Genet*, 65: 517-29.

Jalava, Niina S, Francisco R Lopez-Picon, Tiina-Kaisa Kukko-Lukjanov, and Irma E Holopainen. 2007. 'Changes in microtubule-associated protein-2 (MAP2) expression during development and after status epilepticus in the immature rat hippocampus', *Int J Dev Neurosci*, 25: 121-31.

Jeong, Jae-Yeon, Hyung-Soon Yim, Ji-Young Ryu, Hyun Sook Lee, Jung-Hyun Lee, Dong-Seung Seen, and Sung Gyun Kang. 2012. 'One-step sequence- and ligation-independent

cloning as a rapid and versatile cloning method for functional genomics studies', *Appl Environ Microbiol*, 78: 5440-3.

Jin, Yi, Yoshiki Murakumo, Kaoru Ueno, Mizuo Hashimoto, Tsuyoshi Watanabe, Yoshie Shimoyama, Masatoshi Ichihara, and Masahide Takahashi. 2004. 'Identification of a mouse cytoskeleton-associated protein, CKAP2, with microtubule-stabilizing properties', *Cancer Sci*, 95: 815-21.

Joachim, C. L., J. H. Morris, K. S. Kosik, and D. J. Selkoe. 1987. 'Tau antisera recognize neurofibrillary tangles in a range of neurodegenerative disorders', *Ann Neurol*, 22: 514-20.

Jorgensen, Louise H, Mai-Britt Mosbech, Nils J Faergeman, Jesper Graakjaer, Soren V Jacobsen, and Henrik D Schroder. 2014. 'Duplication in the microtubule-actin cross-linking factor 1 gene causes a novel neuromuscular condition', *Sci Rep*, 4: 5180.

Ka, Minhan, and Woo-Yang Kim. 2016. 'Microtubule-Actin Crosslinking Factor 1 Is Required for Dendritic Arborization and Axon Outgrowth in the Developing Brain', *Mol Neurobiol*, 53: 6018-32.

Kadletz, Lorenz, Dietmar Thurnher, Robert Wiebringhaus, Boban M Erovic, Ulana Kotowski, Sven Schneider, Rainer Schmid, Lukas Kenner, and Gregor Heiduschka. 2017. 'Role of cancer stem-cell marker doublecortin-like kinase 1 in head and neck squamous cell carcinoma', *Oral Oncol*, 67: 109-18.

Kang, Jian-Sheng, Jin-Hua Tian, Ping-Yue Pan, Philip Zald, Cuiling Li, Chuxia Deng, and Zu-Hang Sheng. 2008. 'Docking of axonal mitochondria by syntaphilin controls their mobility and affects short-term facilitation', *Cell*, 132: 137-48.

Karpova, Nina, Yves Bobinnec, Sylvaine Fouix, Philippe Huitorel, and Alain Debec. 2006. 'Jupiter, a new Drosophila protein associated with microtubules', *Cell Motil Cytoskeleton*, 63: 301-12.

Keller, T C, 3rd, and L I Rebhun. 1982. 'Strongylocentrotus purpuratus spindle tubulin. I. Characteristics of its polymerization and depolymerization in vitro', *J Cell Biol*, 93: 788-96.

Kellogg, Elizabeth H, Nisreen M A Hejab, Simon Poepsel, Kenneth H Downing, Frank DiMaio, and Eva Nogales. 2018. 'Near-atomic model of microtubule-tau interactions', *Science*, 360: 1242-46.

Kielar, Michel, Francoise Phan Dinh Tuy, Sara Bizzotto, Cecile Lebrand, Camino de Juan Romero, Karine Poirier, Renske Oegema, Grazia Maria Mancini, Nadia Bahi-Buisson, Robert Olaso, Anne-Gaelle Le Moing, Katia Boutourlinsky, Dominique Boucher, Wassila Carpentier, Patrick Berquin, Jean-Francois Deleuze, Richard Belvindrah, Victor Borrell, Egbert Welker, Jamel Chelly, Alexandre Croquelois, and Fiona Francis. 2014. 'Mutations in Eml1 lead to ectopic progenitors and neuronal heterotopia in mouse and human', *Nat Neurosci*, 17: 923-33.

Kindler, S., B. Schulz, M. Goedert, and C. C. Garner. 1990. 'Molecular structure of microtubule-associated protein 2b and 2c from rat brain', *J Biol Chem*, 265: 19679-84.

Kitada, T, S Asakawa, N Hattori, H Matsumine, Y Yamamura, S Minoshima, M Yokochi, Y Mizuno, and N Shimizu. 1998. 'Mutations in the parkin gene cause autosomal recessive juvenile parkinsonism', *Nature*, 392: 605-8.

Kokkonen, Nina, Sanna-Kaisa Herukka, Laura Huilaja, Merja Kokki, Anne M Koivisto, Paivi Hartikainen, Anne M Remes, and Kaisa Tasanen. 2017. 'Increased Levels of the Bullous Pemphigoid BP180 Autoantibody Are Associated with More Severe Dementia in Alzheimer's Disease', *J Invest Dermatol*, 137: 71-76.

Kumarapeli, Asangi R K, and Xuejun Wang. 2004. 'Genetic modification of the heart: chaperones and the cytoskeleton', *J Mol Cell Cardiol*, 37: 1097-109.

Laffitte, E, P R Burkhard, L Fontao, F Jaunin, J-H Saurat, M Chofflon, and L Borradori. 2005. 'Bullous pemphigoid antigen 1 isoforms: potential new target autoantigens in multiple sclerosis?', *Br J Dermatol*, 152: 537-40.

Lake, Nicole J, Rachael L Taylor, Hugh Trahair, K N Harikrishnan, Joanne E Curran, Marcio Almeida, Hemant Kulkarni, Nigora Mukhamedova, Anh Hoang, Hann Low, Andrew J Murphy, Matthew P Johnson, Thomas D Dyer, Michael C Mahaney, Harald H H Goring, Eric K Moses, Dmitri Sviridov, John Blangero, Jeremy B M Jowett, and Kiymet Bozaoglu. 2017. 'TRAK2, a novel regulator of ABCA1 expression, cholesterol efflux and HDL biogenesis', *Eur Heart J*, 38: 3579-87.

Langer, R, K Specht, K Becker, P Ewald, M Sarbia, R Busch, M Feith, H J Stein, J R Siewert, and H Hofler. 2004. '[Prediction of response to neoadjuvant chemotherapy in Barrett's carcinoma by quantitative gene expression analysis]', *Verh Dtsch Ges Pathol*, 88: 207-13.

Lansky, Zdenek, Marcus Braun, Annemarie Ludecke, Michael Schlierf, Pieter Rein Ten Wolde, Marcel E Janson, and Stefan Diez. 2015. 'Diffusible crosslinkers generate directed forces in microtubule networks', *Cell*, 160: 1159-68.

Leermakers, P A, A M W J Schols, A E M Kneppers, M C J M Kelders, C C de Theije, M Lainscak, and H R Gosker. 2018. 'Molecular signalling towards mitochondrial breakdown is enhanced in skeletal muscle of patients with chronic obstructive pulmonary disease (COPD)', *Sci Rep*, 8: 15007.

Letournel, F, A Bocquet, F Dubas, A Barthelaix, and J Eyer. 2003. 'Stable tubule only polypeptides (STOP) proteins co-aggregate with spheroid neurofilaments in amyotrophic lateral sclerosis', *J Neuropathol Exp Neurol*, 62: 1211-9.

Leung, C L, D Sun, M Zheng, D R Knowles, and R K Liem. 1999. 'Microtubule actin cross-linking factor (MACF): a hybrid of dystonin and dystrophin that can interact with the actin and microtubule cytoskeletons', *J Cell Biol*, 147: 1275-86.

Lewis, Sally A, Ivan E Ivanov, Gwo-Hwa Lee, and Nicolas J Cowan. 1989. 'Organization of microtubules in dendrites and axons is determined by a short hydrophobic zipper in microtubule-associated proteins MAP2 and tau', *Nature*, 342: 498-505.

Li, Dengwen, Xiaodong Sun, Linlin Zhang, Bing Yan, Songbo Xie, Ruming Liu, Min Liu, and Jun Zhou. 2013. 'Histone deacetylase 6 and cytoplasmic linker protein 170 function together to regulate the motility of pancreatic cancer cells', *Protein Cell*.

Li, Zheng, Yongqiang Wang, Linbo Wu, Yalu Dong, Jing Zhang, Fan Chen, Wei Xie, Jianguo Huang, and Ning Lu. 2019. 'Apurinic endonuclease 1 promotes the cisplatin resistance of lung cancer cells by inducing Parkinmediated mitophagy', *Oncol Rep*, 42: 2245-54.

Lin, Eva, Li Li, Yinghui Guan, Robert Soriano, Celina Sanchez Rivers, Sankar Mohan, Ajay Pandita, Jerry Tang, and Zora Modrusan. 2009. 'Exon array profiling detects EML4-ALK fusion in breast, colorectal, and non-small cell lung cancers', *Mol Cancer Res*, 7: 1466-76.

Lin, Xiao-Dan, Yu-Peng Wu, Shao-Hao Chen, Xiong-Lin Sun, Zhi-Bin Ke, Dong-Ning Chen, Xiao-Dong Li, Yun-Zhi Lin, Yong Wei, Qing-Shui Zheng, Ning Xu, and Xue-Yi Xue. 2020. 'Identification of a five-mRNA signature as a novel potential prognostic biomarker in pediatric Wilms tumor', *Mol Genet Genomic Med*, 8: e1032.

Lin, Zhewang, Ivana Gasic, Viswanathan Chandrasekaran, Niklas Peters, Sichen Shao, Timothy J Mitchison, and Ramanujan S Hegde. 2020. 'TTC5 mediates autoregulation of tubulin via mRNA degradation', *Science*, 367: 100-04.

Lipka, Joanna, Lukas C Kapitein, Jacek Jaworski, and Casper C Hoogenraad. 2016. 'Microtubule-binding protein doublecortin-like kinase 1 (DCLK1) guides kinesin-3-mediated cargo transport to dendrites', *EMBO J*, 35: 302-18.

Liu, Leyuan, Amy Vo, Guoqin Liu, and Wallace L McKeehan. 2005. 'Distinct structural domains within C19ORF5 support association with stabilized microtubules and mitochondrial aggregation and genome destruction', *Cancer Res*, 65: 4191-201.

Liu, W, H Xiao, S Wu, H Liu, and B Luo. 2018. 'MAP9 single nucleotide polymorphism rs1058992 is a risk of EBV-associated gastric carcinoma in Chinese population', *Acta Virol*, 62: 435-40.

Liu, Xin, Qingqing Zhou, Zhenyu Ji, Guo Fu, Yi Li, Xiaobei Zhang, Xiaofang Shi, Ting Wang, and Qiaozhen Kang. 2014. 'Protein 4.1R attenuates autoreactivity in experimental autoimmune encephalomyelitis by suppressing CD4(+) T cell activation', *Cell Immunol*, 292: 19-24.

Liu, Xinkui, Jiarui Wu, Dan Zhang, Zhitong Bing, Jinhui Tian, Mengwei Ni, Xiaomeng Zhang, Ziqi Meng, and Shuyu Liu. 2018. 'Identification of Potential Key Genes Associated With the Pathogenesis and Prognosis of Gastric Cancer Based on Integrated Bioinformatics Analysis', *Front Genet*, 9: 265.

Liu, Yu-Hong, Julia Y S Tsang, Yun-Bi Ni, Thazin Hlaing, Siu-Ki Chan, Kui-Fat Chan, Chun-Wai Ko, S Shafaq Mujtaba, and Gary M Tse. 2016. 'Doublecortin-like kinase 1 expression associates with breast cancer with neuroendocrine differentiation', *Oncotarget*, 7: 1464-76.

Louis, Simon N S, Laurie T C Chow, Naghmeh Varghayee, Linda A Rezmann, Albert G Frauman, and William J Louis. 2011. 'The Expression of MTUS1/ATIP and Its Major Isoforms, ATIP1 and ATIP3, in Human Prostate Cancer', *Cancers (Basel)*, 3: 3824-37.

Ludin, B, K Ashbridge, U Funfschilling, and A Matus. 1996. 'Functional analysis of the MAP2 repeat domain', *J Cell Sci*, 109 (Pt 1): 91-9.

Ma, Li, Jiaxin Song, Xueying Sun, Wenyong Ding, Kaiyang Fan, Minghua Qi, Yuefei Xu, and Wenli Zhang. 2019. 'Role of microtubule-associated protein 6 glycosylated with Gal-(beta-1,3)-GalNAc in Parkinson's disease', *Aging (Albany NY)*, 11: 4597-610.

Magiera, Maria M., and Carsten Janke. 2013. 'Investigating tubulin posttranslational modifications with specific antibodies.' in John J. Correia and Leslie Wilson (eds.), *Methods Cell Biol* (Academic Press: Burlington).

Mahad, Don J, Iryna Ziabreva, Graham Campbell, Nichola Lax, Katherine White, Peter S Hanson, Hans Lassmann, and Douglass M Turnbull. 2009. 'Mitochondrial changes within axons in multiple sclerosis', *Brain*, 132: 1161-74.

Maiato, Helder, Paula Sampaio, and Claudio E Sunkel. 2004. 'Microtubule-associated proteins and their essential roles during mitosis', *Int Rev Cytol*, 241: 53-153.

Manabe, Ri ichiroh, Leanna Whitmore, Jonathan M. Weiss, and Alan Rick Horwitz. 2002. 'Identification of a Novel Microtubule-Associated Protein that Regulates Microtubule Organization and Cytokinesis by Using a GFP-Screening Strategy', *Curr Biol*, 12: 1946-51.

Mandelkow, Eckhard, and Eva-Maria Mandelkow. 1995. 'Microtubules and microtubule-associated proteins', *Curr Opin Cell Biol*, 7: 72-81.

Manka, Szymon W, and Carolyn A Moores. 2018. 'Microtubule structure by cryo-EM: snapshots of dynamic instability', *Essays Biochem*, 62: 737-51.

Masson, D, and T E Kreis. 1993. 'Identification and molecular characterization of E-MAP-115, a novel microtubule-associated protein predominantly expressed in epithelial cells', *J Cell Biol*, 123: 357-71.

Matsumoto, S., A. Hirano, and S. Goto. 1990. 'Spinal cord neurofibrillary tangles of Guamanian amyotrophic lateral sclerosis and parkinsonism-dementia complex: an immunohistochemical study', *Neurology*, 40: 975-9.

Matus, Andrew. 1988. 'Microtubule-associated proteins: their potential role in determining neuronal morphology', *Annu Rev Neurosci*, 11: 29-44.

McNally, Francis J, and Antonina Roll-Mecak. 2018. 'Microtubule-severing enzymes: From cellular functions to molecular mechanism', *J Cell Biol*, 217: 4057-69.

Mendes Maia, Teresa, Delphine Gogendeau, Carole Pennetier, Carsten Janke, and Renata Basto. 2014. 'Bug22 influences cilium morphology and the post-translational modification of ciliary microtubules', *Biol Open*, 3: 138-51.

Meng, Qing-bin, Jian-chun Yu, Wei-ming Kang, Zhi-qiang Ma, Wei-xun Zhou, Ji Li, Li Zhou, Zhan-jiang Cao, and Shu-bo Tian. 2013. '[Expression of doublecortin-like kinase 1 in human gastric cancer and its correlation with prognosis]', *Zhongguo Yi Xue Ke Xue Yuan Xue Bao*, 35: 639-44.

Metzger, Thomas, Vincent Gache, Mu Xu, Bruno Cadot, Eric S. Folker, Brian E. Richardson, Edgar R. Gomes, and Mary K. Baylies. 2012. 'MAP and kinesin-dependent nuclear positioning is required for skeletal muscle function', *Nature*, 484: 120-4.

Molina, Angie, Lauriane Velot, Lydia Ghouinem, Mohamed Abdelkarim, Benjamin Pierre Bouchet, Anny-Claude Luissint, Imene Bouhlel, Marina Morel, Elene Sapharikas, Anne Di Tommaso, Stephane Honore, Diane Braguer, Nadege Gruel, Anne Vincent-Salomon, Olivier Delattre, Brigitte Sigal-Zafrani, Fabrice Andre, Benoit Terris, Anna Akhmanova, Melanie Di Benedetto, Clara Nahmias, and Sylvie Rodrigues-Ferreira. 2013. 'ATIP3, a novel prognostic marker of breast cancer patient survival, limits cancer cell migration and slows metastatic progression by regulating microtubule dynamics', *Cancer Res*, 73: 2905-15.

Mollinari, Cristiana, Jean-Philippe Kleman, Wei Jiang, Guy Schoehn, Tony Hunter, and Robert L. Margolis. 2002. 'PRC1 is a microtubule binding and bundling protein essential to maintain the mitotic spindle midzone', *J Cell Biol*, 157: 1175-86.

Monroy, Brigette Y, Danielle L Sawyer, Bryce E Ackermann, Melissa M Borden, Tracy C Tan, and Kassandra M Ori-McKenney. 2018. 'Competition between microtubule-associated proteins directs motor transport', *Nat Commun*, 9: 1487.

Monroy, Brigette Y, Tracy C Tan, Janah May Oclaman, Jisoo S Han, Sergi Simo, Shinsuke Niwa, Dan W Nowakowski, Richard J McKenney, and Kassandra M Ori-McKenney. 2020. 'A Combinatorial MAP Code Dictates Polarized Microtubule Transport', *Dev Cell*.

Murayama, S, H Mori, Y Ihara, and M Tomonaga. 1990. 'Immunocytochemical and ultrastructural studies of Pick's disease', *Ann Neurol*, 27: 394-405.

Murphy, D B, and G G Borisy. 1975. 'Association of high-molecular-weight proteins with microtubules and their role in microtubule assembly in vitro', *Proc Natl Acad Sci U S A*, 72: 2696-700.

Murphy, M, A Hinman, and A J Levine. 1996. 'Wild-type p53 negatively regulates the expression of a microtubule-associated protein', *Genes Dev*, 10: 2971-80.

Nagao, Yuhei, Naoya Mimura, June Takeda, Kenichi Yoshida, Yusuke Shiozawa, Motohiko Oshima, Kazumasa Aoyama, Atsunori Saraya, Shuhei Koide, Ola Rizq, Yoshinori Hasegawa, Yuichi Shiraishi, Kenichi Chiba, Hiroko Tanaka, Dai Nishijima, Yusuke Isshiki, Kensuke Kayamori, Chika Kawajiri-Manako, Nagisa Oshima-Hasegawa, Shokichi Tsukamoto, Shio Mitsukawa, Yusuke Takeda, Chikako Ohwada, Masahiro Takeuchi, Tohru Iseki, Sonoko Misawa, Satoru Miyano, Osamu Ohara, Koutaro Yokote, Emiko Sakaida, Satoshi Kuwabara, Masashi Sanada, Atsushi Iwama, Seishi Ogawa, and Chiaki Nakaseko. 2019. 'Genetic and transcriptional landscape of plasma cells in POEMS syndrome', *Leukemia*, 33: 1723-35.

Navarro-Barriuso, Juan, Maria Jose Mansilla, Bibiana Quirant-Sanchez, Alicia Ardiaca-Martinez, Aina Teniente-Serra, Silvia Presas-Rodriguez, Anja Ten Brinke, Cristina Ramo-Tello, and Eva M Martinez-Caceres. 2019. 'MAP7 and MUCL1 Are Biomarkers

of Vitamin D3-Induced Tolerogenic Dendritic Cells in Multiple Sclerosis Patients', *Front Immunol*, 10: 1251.

Neve, R L, P Harris, K S Kosik, D M Kurnit, and T A Donlon. 1986. 'Identification of cDNA clones for the human microtubule-associated protein tau and chromosomal localization of the genes for tau and microtubule-associated protein 2', *Brain Res*, 387: 271-80.

Niida, Yo, and Akihiro Yachie. 2011. 'MAP7D2 is a brain expressing X-linked maternal imprinted gene in humans', *Nature Precedings*: 10.1038/npre.2011.6684.1.

Ohno, Mikiko, Yoshinori Hiraoka, Tatsuhiko Matsuoka, Hidekazu Tomimoto, Keizo Takao, Tsuyoshi Miyakawa, Naoko Oshima, Hiroshi Kiyonari, Takeshi Kimura, Toru Kita, and Eiichiro Nishi. 2009. 'Nardilysin regulates axonal maturation and myelination in the central and peripheral nervous system', *Nat Neurosci*, 12: 1506-13.

Oliveto, Stefania, Roberta Alfieri, Annarita Miluzio, Alessandra Scagliola, Raissa S Secli, Pierluigi Gasparini, Stefano Grosso, Luciano Cascione, Luciano Mutti, and Stefano Biffo. 2018. 'A Polysome-Based microRNA Screen Identifies miR-24-3p as a Novel Promigratory miRNA in Mesothelioma', *Cancer Res*, 78: 5741-53.

Olmsted, J. B. 1986. 'Microtubule-associated proteins', *Annu Rev Cell Biol*, 2: 421-57.

Oltra, Silvestre, Francisco Martinez, Carmen Orellana, Elena Grau, Jose M Fernandez, Adela Canete, and Victoria Castel. 2005. 'The doublecortin gene, a new molecular marker to detect minimal residual disease in neuroblastoma', *Diagn Mol Pathol*, 14: 53-7.

Orban-Nemeth, Zsuzsanna, Hannes Simader, Sylvia Badurek, Alzbeta Trancikova, and Friedrich Propst. 2005. 'Microtubule-associated protein 1S, a short and ubiquitously expressed member of the microtubule-associated protein 1 family', *J Biol Chem*, 280: 2257-65.

Orlacchio, Antonio, Paolo Calabresi, Adriana Rum, Anna Tarzia, Anna Maria Salvati, Toshitaka Kawarai, Alessandro Stefani, Antonio Pisani, Giorgio Bernardi, Paolo Cianciulli, and Patrizia Caprari. 2007. 'Neuroacanthocytosis associated with a defect of the 4.1R membrane protein', *BMC Neurol*, 7: 4.

Pellman, D., M. Bagget, Y. H. Tu, G. R. Fink, and H. Tu. 1995. 'Two microtubule-associated proteins required for anaphase spindle movement in Saccharomyces cerevisiae', *J Cell Biol*, 130: 1373-85.

Pereira, Ana L, Antonio J Pereira, Ana R R Maia, Ksenija Drabek, C Laura Sayas, Polla J Hergert, Mariana Lince-Faria, Irina Matos, Cristina Duque, Tatiana Stepanova, Conly L Rieder, William C Earnshaw, Niels Galjart, and Helder Maiato. 2006. 'Mammalian CLASP1 and CLASP2 cooperate to ensure mitotic fidelity by regulating spindle and kinetochore function', *Mol Biol Cell*, 17: 4526-42.

Perez, Yonatan, Reut Bar-Yaacov, Rotem Kadir, Ohad Wormser, Ilan Shelef, Ohad S Birk, Hagit Flusser, and Ramon Y Birnbaum. 2019. 'Mutations in the microtubule-associated protein MAP11 (C7orf43) cause microcephaly in humans and zebrafish', *Brain*, 142: 574-85.

Petratos, Steven, Ezgi Ozturk, Michael F Azari, Rachel Kenny, Jae Young Lee, Kylie A Magee, Alan R Harvey, Courtney McDonald, Kasra Taghian, Leon Moussa, Pei Mun Aui, Christopher Siatskas, Sara Litwak, Michael G Fehlings, Stephen M Strittmatter, and Claude C A Bernard. 2012. 'Limiting multiple sclerosis related axonopathy by blocking Nogo receptor and CRMP-2 phosphorylation', *Brain*, 135: 1794-818.

Ray, Monika, Jianhua Ruan, and Weixiong Zhang. 2008. 'Variations in the transcriptome of Alzheimer's disease reveal molecular networks involved in cardiovascular diseases', *Genome Biol*, 9: R148.

Ren, Yong, Jinghui Zhao, and Jian Feng. 2003. 'Parkin binds to alpha/beta tubulin and increases their ubiquitination and degradation', *J Neurosci*, 23: 3316-24.

Richards, Mark W, Laura O'Regan, Daniel Roth, Jessica M Montgomery, Anne Straube, Andrew M Fry, and Richard Bayliss. 2015. 'Microtubule association of EML proteins and the EML4-ALK variant 3 oncoprotein require an N-terminal trimerization domain', *Biochem J*, 467: 529-36.

Rickard, J E, and T E Kreis. 1990. 'Identification of a novel nucleotide-sensitive microtubule-binding protein in HeLa cells', *J Cell Biol*, 110: 1623-33.

Roberts, Anthony J., Takahide Kon, Peter J. Knight, Kazuo Sutoh, and Stan A. Burgess. 2013. 'Functions and mechanics of dynein motor proteins', *Nat Rev Mol Cell Biol*, 14: 713-26.

Rodrigues-Ferreira, Sylvie, Anne Di Tommaso, Ariane Dimitrov, Sylvie Cazaubon, Nadege Gruel, Helene Colasson, Andre Nicolas, Nathalie Chaverot, Vincent Molinie, Fabien Reyal, Brigitte Sigal-Zafrani, Benoit Terris, Olivier Delattre, Francois Radvanyi, Franck Perez, Anne Vincent-Salomon, and Clara Nahmias. 2009. '8p22 MTUS1 gene product ATIP3 is a novel anti-mitotic protein underexpressed in invasive breast carcinoma of poor prognosis', *PLoS ONE*, 4: e7239.

Roger, Benoit, Jawdat Al-Bassam, Leif Dehmelt, Ronald A Milligan, and Shelley Halpain. 2004. 'MAP2c, but not tau, binds and bundles F-actin via its microtubule binding domain', *Curr Biol*, 14: 363-71.

Roll-Mecak, Antonina, and Ronald D. Vale. 2008. 'Structural basis of microtubule severing by the hereditary spastic paraplegia protein spastin', *Nature*, 451: 363-7.

Rosoklija, Gorazd, John G Keilp, Glen Toomayan, Branislav Mancevski, Vanram Haroutunian, Dongmei Liu, Dolores Malespina, Arthur P Hays, Saud Sadiq, Norman Latov, and Andrew J Dwork. 2005. 'Altered subicular MAP2 immunoreactivity in schizophrenia', *Prilozi*, 26: 13-34.

Rouquier, Sylvie, Marie-Jeanne Pillaire, Christophe Cazaux, and Dominique Giorgi. 2014. 'Expression of the microtubule-associated protein MAP9/ASAP and its partners AURKA and PLK1 in colorectal and breast cancers', *Dis Markers*, 2014: 798170.

Saffin, Jean-Michel, Magali Venoux, Claude Prigent, Julien Espeut, Francis Poulat, Dominique Giorgi, Ariane Abrieu, and Sylvie Rouquier. 2005. 'ASAP, a human microtubule-associated protein required for bipolar spindle assembly and cytokinesis', *Proc Natl Acad Sci U S A*, 102: 11302-7.

Sagie, Shira, Tally Lerman-Sagie, Snezana Maljevic, Keren Yosovich, Katja Detert, Seo-Kyung Chung, Mark I Rees, Holger Lerche, and Dorit Lev. 2018. 'Expanding the phenotype of TRAK1 mutations: hyperekplexia and refractory status epilepticus', *Brain*, 141: e55.

Sanchez-Soriano, Natalia, Mark Travis, Federico Dajas-Bailador, Catarina Goncalves-Pimentel, Alan J Whitmarsh, and Andreas Prokop. 2009. 'Mouse ACF7 and drosophila short stop modulate filopodia formation and microtubule organisation during neuronal growth', *J Cell Sci*, 122: 2534-42.

Sandoval, I V, and J S Vandekerckhove. 1981. 'A comparative study of the in vitro polymerization of tubulin in the presence of the microtubule-associated proteins MAP2 and tau', *J Biol Chem*, 256: 8795-800.

Sawamura, D, K Nomura, Y Sugita, M G Mattei, M L Chu, R Knowlton, and J Uitto. 1990. 'Bullous pemphigoid antigen (BPAG1): cDNA cloning and mapping of the gene to the short arm of human chromosome 6', *Genomics*, 8: 722-6.

Schiewek, Johanna, Udo Schumacher, Tobias Lange, Simon A Joosse, Harriet Wikman, Klaus Pantel, Marina Mikhaylova, Matthias Kneussel, Stefan Linder, Barbara Schmalfeldt, Leticia Oliveira-Ferrer, and Sabine Windhorst. 2018. 'Clinical relevance of cytoskeleton associated proteins for ovarian cancer', *J Cancer Res Clin Oncol*, 144: 2195-205.

Schneider, Caroline A, Wayne S Rasband, and Kevin W Eliceiri. 2012. 'NIH Image to ImageJ: 25 years of image analysis', *Nat Methods*, 9: 671-5.

Shimizu, Hiromitsu, Yoshimi Iwayama, Kazuo Yamada, Tomoko Toyota, Yoshio Minabe, Kauhiko Nakamura, Mizuho Nakajima, Eiji Hattori, Norio Mori, Noriko Osumi, and Takeo Yoshikawa. 2006. 'Genetic and expression analyses of the STOP (MAP6) gene in schizophrenia', *Schizophr Res*, 84: 244-52.

Shinkai-Ouchi, Fumiko, Yoshio Yamakawa, Hideyuki Hara, Minoru Tobiume, Masahiro Nishijima, Kentaro Hanada, and Ken'ichi Hagiwara. 2010. 'Identification and structural analysis of C-terminally truncated collapsin response mediator protein-2 in a murine model of prion diseases', *Proteome Sci*, 8: 53.

Siahaan, Valerie, Jochen Krattenmacher, Anthony A Hyman, Stefan Diez, Amayra Hernandez-Vega, Zdenek Lansky, and Marcus Braun. 2019. 'Kinetically distinct phases of tau on microtubules regulate kinesin motors and severing enzymes', *Nat Cell Biol*, 21: 1086-92.

Sim, Sung Hoon, Chang-Dae Bae, Youngmi Kwon, Hai-Li Hwang, Shiv Poojan, Hye-In Hong, Kyungtae Kim, Seo-Hee Kang, Han-Seong Kim, Tae-Hyun Um, In Hae Park, Keun Seok Lee, So-Youn Jung, Seeyoun Lee, Han-Sung Kang, Eun Sook Lee, Mi-Kyung Kim, Kyeong-Man Hong, and Jungsil Ro. 2017. 'CKAP2 (cytoskeleton-associated protein2) is a new prognostic marker in HER2-negative luminal type breast cancer', *PLoS ONE*, 12: e0182107.

Song, Kun, Wei Hu, Fei Yue, Jing Zou, Wenjiao Li, Qi Chen, Qizhi Yao, Weijia Sun, and Leyuan Liu. 2015. 'Transforming Growth Factor TGFbeta Increases Levels of Microtubule-Associated Protein MAP1S and Autophagy Flux in Pancreatic Ductal Adenocarcinomas', *PLoS ONE*, 10: e0143150.

Sood, R, P I Bader, M C Speer, Y H Edwards, E M Eddings, R T Blair, P Hu, M U Faruque, C M Robbins, H Zhang, J Leuders, K Morrison, D Thompson, P L Schwartzberg, P S Meltzer, and J M Trent. 2004. 'Cloning and characterization of an inversion breakpoint at 6q23.3 suggests a role for Map7 in sacral dysgenesis', *Cytogenet Genome Res*, 106: 61-7.

Soppina, Virupakshi, Stephen R Norris, Aslan S Dizaji, Matt Kortus, Sarah Veatch, Michelle Peckham, and Kristen J Verhey. 2014. 'Dimerization of mammalian kinesin-3 motors results in superprocessive motion', *Proc Natl Acad Sci U S A*, 111: 5562-7.

Souphron, Judith, Satish Bodakuntla, A. S. Jijumon, Goran Lakisic, Alexis M. Gautreau, Carsten Janke, and Maria M. Magiera. 2019. 'Purification of tubulin with controlled post-translational modifications by polymerization–depolymerization cycles', *Nat Protoc*, 14: 1634–60.

Spector, I, N R Shochet, Y Kashman, and A Groweiss. 1983. 'Latrunculins: novel marine toxins that disrupt microfilament organization in cultured cells', *Science*, 219: 493-5.

Sun, D, C L Leung, and R K Liem. 2001. 'Characterization of the microtubule binding domain of microtubule actin crosslinking factor (MACF): identification of a novel group of microtubule associated proteins', *J Cell Sci*, 114: 161-72.

Sung, Hsin-Ho, Ivo A Telley, Piyi Papadaki, Anne Ephrussi, Thomas Surrey, and Pernille Rorth. 2008. 'Drosophila ensconsin promotes productive recruitment of Kinesin-1 to microtubules', *Dev Cell*, 15: 866-76.

Suprenant, K A, K Dean, J McKee, and S Hake. 1993. 'EMAP, an echinoderm microtubule-associated protein found in microtubule-ribosome complexes', *J Cell Sci*, 104: 445-50.

Tala, Songbo Xie, Xiaodong Sun, Xiaoou Sun, Jie Ran, Linlin Zhang, Dengwen Li, Min Liu, Gang Bao, and Jun Zhou. 2014. 'Microtubule-associated protein Mdp3 promotes breast cancer growth and metastasis', *Theranostics*, 4: 1052-61.

Tan, Minghui, Caihui Cha, Yongheng Ye, Jifeng Zhang, Sumei Li, Fengming Wu, Sitang Gong, and Guoqing Guo. 2015. 'CRMP4 and CRMP2 Interact to Coordinate Cytoskeleton

Dynamics, Regulating Growth Cone Development and Axon Elongation', *Neural Plast*, 2015: 947423.

Tao, Hiroyuki, Toshiki Tanaka, and Kazunori Okabe. 2017. 'Doublecortin and CaM kinase-like-1 expression in pathological stage I non-small cell lung cancer', *J Cancer Res Clin Oncol*, 143: 1449-59.

Tegha-Dunghu, Justus, Beate Neumann, Simone Reber, Roland Krause, Holger Erfle, Thomas Walter, Michael Held, Phill Rogers, Kerstin Hupfeld, Thomas Ruppert, Jan Ellenberg, and Oliver J. Gruss. 2008. 'EML3 is a nuclear microtubule-binding protein required for the correct alignment of chromosomes in metaphase', *J Cell Sci*, 121: 1718-26.

Togashi, Kentaro, Masaya Hasegawa, Jun Nagai, Aine Tonouchi, Daiki Masukawa, Kenneth Hensley, Yoshio Goshima, and Toshio Ohshima. 2019. 'Genetic suppression of collapsin response mediator protein 2 phosphorylation improves outcome in methyl-4-phenyl-1,2,3,6-tetrahydropyridine-induced Parkinson's model mice', *Genes Cells*, 24: 31-40.

Toyoshima, Manabu, Xuguang Jiang, Tadayuki Ogawa, Tetsuo Ohnishi, Shogo Yoshihara, Shabeesh Balan, Takeo Yoshikawa, and Nobutaka Hirokawa. 2019. 'Enhanced carbonyl stress induces irreversible multimerization of CRMP2 in schizophrenia pathogenesis', *Life Sci Alliance*, 2.

Tymanskyj, Stephen R, Benjamin Yang, Aditi Falnikar, Angelo C Lepore, and Le Ma. 2017. 'MAP7 Regulates Axon Collateral Branch Development in Dorsal Root Ganglion Neurons', *J Neurosci*, 37: 1648-61.

Tyrrell, Daniel J, Muriel G Blin, Jianrui Song, Sherri C Wood, Min Zhang, Daniel A Beard, and Daniel R Goldstein. 2020. 'Age-Associated Mitochondrial Dysfunction Accelerates Atherogenesis', *Circ Res*, 126: 298-314.

Uzquiano, Ana, Carmen Cifuentes-Diaz, Ammar Jabali, Delfina M Romero, Anne Houllier, Florent Dingli, Camille Maillard, Anne Boland, Jean-Francois Deleuze, Damarys Loew, Grazia M S Mancini, Nadia Bahi-Buisson, Julia Ladewig, and Fiona Francis. 2019. 'Mutations in the Heterotopia Gene Eml1/EML1 Severely Disrupt the Formation of Primary Cilia', *Cell Rep*, 28: 1596-611 e10.

Vallee, R B, and G S Bloom. 1983. 'Isolation of sea urchin egg microtubules with taxol and identification of mitotic spindle microtubule-associated proteins with monoclonal antibodies', *Proc Natl Acad Sci U S A*, 80: 6259-63.

Veigel, Claudia, and Christoph F Schmidt. 2011. 'Moving into the cell: single-molecule studies of molecular motors in complex environments', *Nat Rev Mol Cell Biol*, 12: 163-76.

Velazquez-Bernardino, Prisiliana, Francisco Garcia-Sierra, Oscar Hernandez-Hernandez, Mario Bermudez de Leon, Genevieve Gourdon, Mario Gomes-Pereira, and Bulmaro Cisneros. 2012. 'Myotonic dystrophy type 1-associated CTG repeats disturb the expression and subcellular distribution of microtubule-associated proteins MAP1A, MAP2, and MAP6/STOP in PC12 cells', *Mol Biol Rep*, 39: 415-24.

Villanueva-Paz, Marina, Suleva Povea-Cabello, Irene Villalon-Garcia, Monica Alvarez-Cordoba, Juan M Suarez-Rivero, Marta Talaveron-Rey, Sandra Jackson, Rafael Falcon-Moya, Antonio Rodriguez-Moreno, and Jose A Sanchez-Alcazar. 2020. 'Parkin-mediated mitophagy and autophagy flux disruption in cellular models of MERRF syndrome', *Biochim Biophys Acta Mol Basis Dis*, 1866: 165726.

Vourc'h, Patrick, Elisabeth Petit, Jean Pierre Muh, Christian Andres, Thierry Bienvenu, Cherif Beldjord, Jamel Chelly, and Catherine Barthelemy. 2002. 'Exclusion of the coding sequence of the doublecortin gene as a susceptibility locus in autistic disorder', *Am J Med Genet*, 108: 164-7.

Wang, Kuanyu, Ruoyu Huang, Guanzhang Li, Fan Zeng, Zheng Zhao, Yanwei Liu, Huimin Hu, and Tao Jiang. 2018. 'CKAP2 expression is associated with glioma tumor growth and acts as a prognostic factor in highgrade glioma', *Oncol Rep*, 40: 2036-46.

Wang, Xin, Nuomin Li, Nian Xiong, Qi You, Jie Li, Jinlong Yu, Hong Qing, Tao Wang, Heather J Cordell, Ole Isacson, Jeffery M Vance, Eden R Martin, Ying Zhao, Bruce M Cohen, Edgar A Buttner, and Zhicheng Lin. 2017. 'Genetic Variants of Microtubule Actin Cross-linking Factor 1 (MACF1) Confer Risk for Parkinson's Disease', *Mol Neurobiol*, 54: 2878-88.

Wang, Yunfeng, Songyan Zhang, Shuwei Dang, Xuan Fang, and Ming Liu. 2019. 'Overexpression of microRNA-216a inhibits autophagy by targeting regulated MAP1S in colorectal cancer', *Onco Targets Ther*, 12: 4621-29.

Watanabe, T K, F Shimizu, M Nagata, A Kawai, T Fujiwara, Y Nakamura, E Takahashi, and Y Hirai. 1996. 'Cloning, expression, and mapping of CKAPI, which encodes a putative cytoskeleton-associated protein containing a CAP-GLY domain', *Cytogenet Cell Genet*, 72: 208-11.

Webb, B C, and L Wilson. 1980. 'Cold-stable microtubules from brain', *Biochemistry*, 19: 1993-2001.

Wei, Hongen, Shibang Sun, Yonghong Li, and Shunying Yu. 2016. 'Reduced plasma levels of microtubule-associated STOP/MAP6 protein in autistic patients', *Psychiatry Res*, 245: 116-18.

Wei, Z, G Yang, R Xu, C Zhu, F He, Q Dou, and J Tang. 2016. 'Correlation between protein 4.1R and the progression of heart failure in vivo', *Genet Mol Res*, 15.

Weingarten, M. D., A. H. Lockwood, S. Y. Hwo, and M. W. Kirschner. 1975. 'A protein factor essential for microtubule assembly', *Proc Natl Acad Sci U S A*, 72: 1858-62.

Wiegering, Antonia, Ulrich Ruther, and Christoph Gerhardt. 2018. 'The ciliary protein Rpgrip1l in development and disease', *Dev Biol*, 442: 60-68.

Willis, T A, C L Wood, J Hudson, T Polvikoski, R Barresi, H Lochmuller, K Bushby, and V Straub. 2016. 'Muscle hypertrophy as the presenting sign in a patient with a complete FHL1 deletion', *Clin Genet*, 90: 166-70.

Wong, Elaine Y M, Jenny Y M Tse, Kwok-Ming Yao, Vincent C H Lui, Po-Chor Tam, and William S B Yeung. 2004. 'Identification and characterization of human VCY2-interacting protein: VCY2IP-1, a microtubule-associated protein-like protein', *Biol Reprod*, 70: 775-84.

Wu, Xiaoyang, Atsuko Kodama, and Elaine Fuchs. 2008. 'ACF7 regulates cytoskeletal-focal adhesion dynamics and migration and has ATPase activity', *Cell*, 135: 137-48.

Wu, Xiaoyang, Qing-Tao Shen, Daniel S Oristian, Catherine P Lu, Qinsi Zheng, Hong-Wei Wang, and Elaine Fuchs. 2011. 'Skin stem cells orchestrate directional migration by regulating microtubule-ACF7 connections through GSK3beta', *Cell*, 144: 341-52.

Wu, Xin, Yuanyuan Ruan, Hua Jiang, and Congjian Xu. 2017. 'MicroRNA-424 inhibits cell migration, invasion, and epithelial mesenchymal transition by downregulating doublecortin-like kinase 1 in ovarian clear cell carcinoma', *Int J Biochem Cell Biol*, 85: 66-74.

Xia, Xiaochun, Chao He, Anqing Wu, Jundong Zhou, and Jinchang Wu. 2018. 'Microtubule-Associated Protein 4 Is a Prognostic Factor and Promotes Tumor Progression in Lung Adenocarcinoma', *Dis Markers*, 2018: 8956072.

Xie, Rui, Susan Nguyen, Kerstin McKeehan, Fen Wang, Wallace L McKeehan, and Leyuan Liu. 2011. 'Microtubule-associated protein 1S (MAP1S) bridges autophagic components with microtubules and mitochondria to affect autophagosomal biogenesis and degradation', *J Biol Chem*, 286: 10367-77.

Xu, Guibin, Fei Yue, Hai Huang, Yongzhong He, Xun Li, Haibo Zhao, Zhengming Su, Xianhan Jiang, Wenjiao Li, Jing Zou, Qi Chen, and Leyuan Liu. 2016. 'Defects in MAP1S-mediated autophagy turnover of fibronectin cause renal fibrosis', *Aging (Albany NY)*, 8: 977-85.

Yadav, Saroj, Paul J Verma, and Dulal Panda. 2014. 'C-terminal region of MAP7 domain containing protein 3 (MAP7D3) promotes microtubule polymerization by binding at the C-terminal tail of tubulin', *PLoS ONE*, 9: e99539.

Yamada, Nobuhisa, Kohichiroh Yasui, Osamu Dohi, Yasuyuki Gen, Akira Tomie, Tomoko Kitaichi, Naoto Iwai, Hironori Mitsuyoshi, Yoshio Sumida, Michihisa Moriguchi, Kanji Yamaguchi, Taichiro Nishikawa, Atsushi Umemura, Yuji Naito, Shinji Tanaka, Shigeki Arii, and Yoshito Itoh. 2016. 'Genome-wide DNA methylation analysis in hepatocellular carcinoma', *Oncol Rep*, 35: 2228-36.

Yan, Jie, Xiao-Bo Sun, Hong-Quan Wang, Hong Zhao, Xiao-Yan Zhao, Yu-Xia Xu, Jing-Chun Guo, and Cui-Qing Zhu. 2010. 'Chronic restraint stress alters the expression and distribution of phosphorylated tau and MAP2 in cortex and hippocampus of rat brain', *Brain Res*, 1347: 132-41.

Yang, Y, J Dowling, Q C Yu, P Kouklis, D W Cleveland, and E Fuchs. 1996. 'An essential cytoskeletal linker protein connecting actin microfilaments to intermediate filaments', *Cell*, 86: 655-65.

Yang, Yang, Chen Xu, Xingyun Liu, Chao Xu, Yuanyuan Zhang, Li Shen, Mauno Vihinen, and Bairong Shen. 2018. 'NDDVD: an integrated and manually curated Neurodegenerative Diseases Variation Database', *Database (Oxford)*, 2018.

Yano, Tomoki, Takayuki Torisawa, Kazuhiro Oiwa, and Sachiko Tsukita. 2018. 'AMPK-dependent phosphorylation of cingulin reversibly regulates its binding to actin filaments and microtubules', *Sci Rep*, 8: 15550.

Yue, Fei, Wenjiao Li, Jing Zou, Xianhan Jiang, Guibin Xu, Hai Huang, and Leyuan Liu. 2017. 'Spermidine Prolongs Lifespan and Prevents Liver Fibrosis and Hepatocellular Carcinoma by Activating MAP1S-Mediated Autophagy', *Cancer Res*, 77: 2938-51.

Zhang, Bin, Xiaoting Shi, Guifang Xu, Wei Kang, Weijie Zhang, Shu Zhang, Yu Cao, Liping Qian, Ping Zhan, Hongli Yan, Ka Fai To, Lei Wang, and Xiaoping Zou. 2017. 'Elevated PRC1 in gastric carcinoma exerts oncogenic function and is targeted by piperlongumine in a p53-dependent manner', *J Cell Mol Med*, 21: 1329-41.

Zhang, Jin, and Xiao-Ping Dong. 2012. 'Dysfunction of microtubule-associated proteins of MAP2/tau family in Prion disease', *Prion*, 6: 334-8.

Zhang, Li, Xudong Liu, Lina Song, Hui Zhai, and Chaohua Chang. 2020. 'MAP7 promotes migration and invasion and progression of human cervical cancer through modulating the autophagy', *Cancer Cell Int*, 20: 17.

Zhang, Rui, Johanna Roostalu, Thomas Surrey, and Eva Nogales. 2017. 'Structural insight into TPX2-stimulated microtubule assembly', *Elife*, 6.

Zhang, Xiaolan, Chun Lin, Junwei Song, Han Chen, Xuhong Chen, Liangliang Ren, Zhongqiu Zhou, Jinyuan Pan, Zhenjun Yang, Wenhao Bao, Xueping Ke, Jianan Yang, Yingying Liang, Hongbiao Huang, Daolin Tang, Lili Jiang, and Jinbao Liu. 2019. 'Parkin facilitates proteasome inhibitor-induced apoptosis via suppression of NF-kappaB activity in hepatocellular carcinoma', *Cell Death Dis*, 10: 719.

Zhao, Ting, Jie Wu, Xiaohui Liu, Lei Zhang, Gang Chen, and Haojie Lu. 2018. 'Diagnosis of thymic epithelial tumor subtypes by a quantitative proteomic approach', *Analyst*, 143: 2491-500.

Zhu, Yuanfei, Bogale Aredo, Bo Chen, Cynthia X Zhao, Yu-Guang He, and Rafael L Ufret-Vincenty. 2019. 'Mice With a Combined Deficiency of Superoxide Dismutase 1 (Sod1),

DJ-1 (Park7), and Parkin (Prkn) Develop Spontaneous Retinal Degeneration With Aging', *Invest Ophthalmol Vis Sci*, 60: 3740-51.

3.1.1. Additional results (not included in the manuscript):

3.1.1.1. Analysis of CLIP-170 behaviour on MTs: CLIP-170 co-condensates with tubulin as periodic droplets on MT lattice and can nucleate new MTs from it

The Cytoplasmic Linker Protein of 170 kDa, or CLIP-170, was discovered in HeLa cells in 1990 (Rickard and Kreis 1990), with a patchy localization, often correlates with linear arrays of MTs. Subsequent immunostaining analyses of endogenous CLIP-170 in cells revealed its localisation at the MT plus ends, which made it the first member of +TIP family of proteins (Perez et al. 1999). It has then been demonstrated that CLIP-170 does not track MT ends by itself (Dixit et al. 2009), but requires EB1 for the plus-end tracking activity. Without EB1, purified CLIP-170 decorated the entire MT lattice in *in vitro* experiments (Bieling et al. 2008a; Chen, Wang, and Slep 2019). Overexpression studies in cells showed that full-length CLIP-170 could form protein patches or droplets inside cells that also contained soluble tubulin. Biochemical characterization of CLIP-170 further revealed that its C-terminal region is required for the formation of those patches (Pierre, Pepperkok, and Kreis 1994). However, the molecular mechanism and function of these protein droplets remain elusive, due to a low technical and conceptual knowledge about phase separation in biology at that time. Phase separation is the formation of distinct and segregated phases of matter from a homogenous mixture. The most common example is the phase-separated oil-water, from its two-liquid mixture. Recent studies show that TPX2, another MAP, also forms phase-separated condensates together with tubulin (King and Petry 2020).

I applied my cell-free TIRF reconstitution assay to CLIP-170 to investigate its behaviour on dynamic MTs. I found that the full-length CLIP-170 decorates the MT lattice as periodic droplets (Fig. 10A-E). To confirm that this phenomenon is not due to the abnormal combination of protein components due to mixing of cell cytoplasm with the buffer, I tested the effect of CLIP-170 concentration on droplet formation. This was achieved by diluting the CLIP-170-containing lysate with a lysate from untransfected (control) cells of the same total protein concentration, 8 µg/µl. This allowed to only modulate the amount of CLIP-170 in the extracts, while the concentration of all other protein components remains unchanged. These dilution experiments showed that the droplet-forming property of CLIP-170 can be observed in a range of concentrations, confirming that it is an intrinsic property of CLIP-170, and not caused by

other protein components in the lysate (Fig. 10F). Interestingly, the CLIP-170 droplets appear to contain soluble tubulin, as demonstrated by the use of fluorescently labelled tubulin in the experiments (Fig. 11).

Owing that CLIP-170 can accumulate soluble tubulin, I was curious to test its ability to nucleate new MTs. For this, I performed a set of sequential experiments using lysates from cells transfected with CLIP-170 and from untransfected (control) cells (Fig. 12A). First, I washed the TIRF chamber having preformed CLIP-170 droplets with warm BRB80 buffer, subsequently added lysates from the untransfected cells, which has soluble free tubulin, but lacks overexpressed CLIP-170. Strikingly, I observed that new MTs nucleates from CLIP-170-tubulin co-condensates (Fig. 12B&C). The possible explanation for this nucleation event is that CLIP-170 accumulates soluble tubulin locally, thereby attaining the critical concentration of tubulin required for MT nucleation.

I also observed that CLIP-170 decorates both GMPCPP MT seeds and elongating MTs, and allows MT elongation from the seeds. The tubulin staining showed that CLIP-170 droplet formation is more prominent towards the minus end of the MTs (closer to the GMPCPP seed) than at the growing MT end (Fig. 11B). Lastly, the MTs newly nucleating from the CLIP-170-tubulin droplets show a preferred orientation towards the plus-ends of the MTs they polymerise from, which is quantified in Fig. 12D.

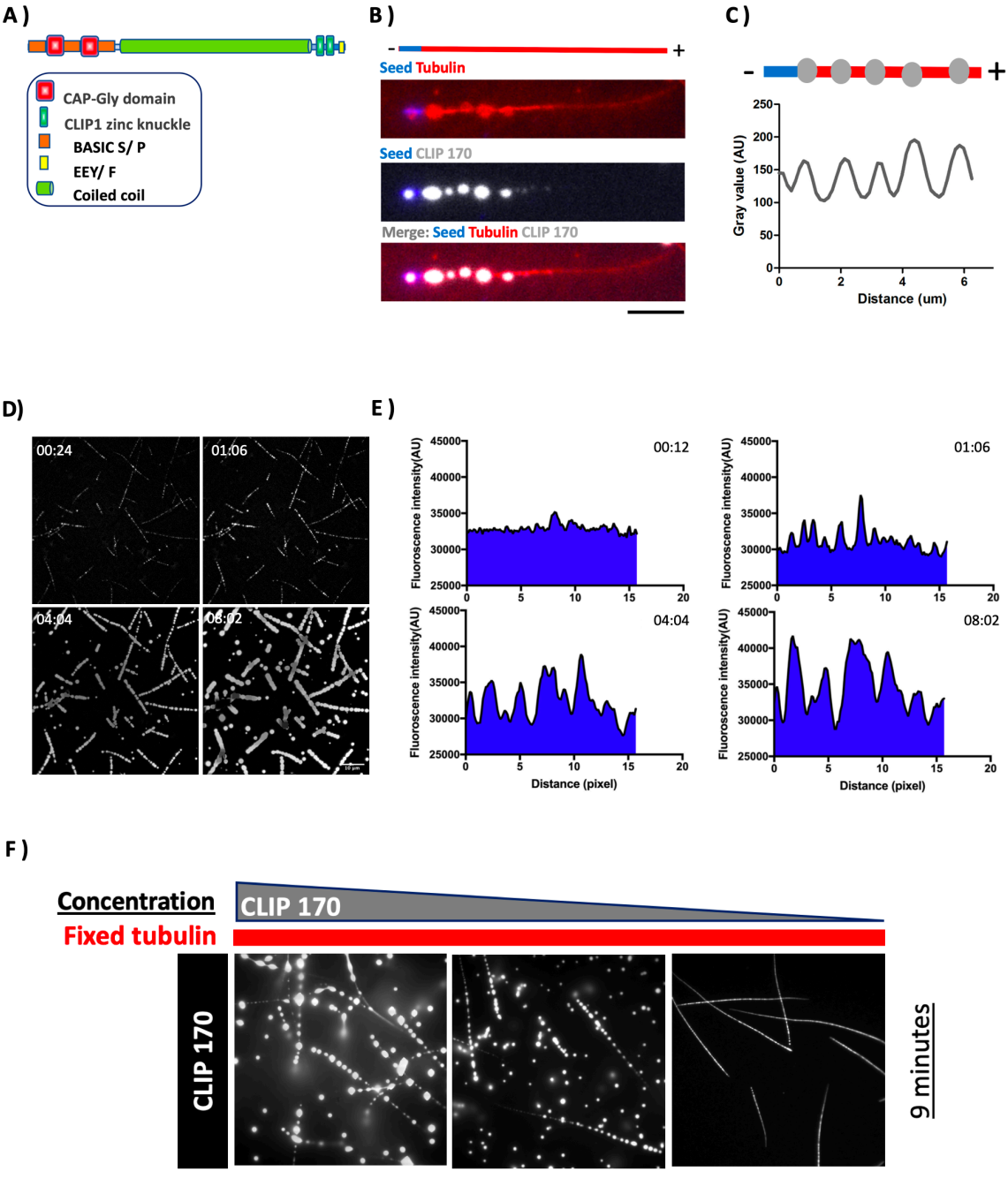

Figure 10: CLIP-170 decorates the MT lattice as periodic droplets. A) Domain organization of full-length CLIP-170 used in this study. **B)** TIRF assay showing CLIP-170 localization on the MT lattice (both on the GMPCPP seed and elongated MT region) along with the tubulin staining. **C)** Lattice intensity profile of CLIP-170 signal on MT showing its periodic distribution. **D)** Time montage of CLIP-170 droplet formation on MT lattice **E)** Fluorescence intensity profile of CLIP-170 over time, starting from a uniform to a strongly periodic distribution (1 pixel=0.133 µm). **F)** TIRF-M images showing MT decoration of CLIP-170 for different CLIP-170 concentrations, after 9 min acquisition.

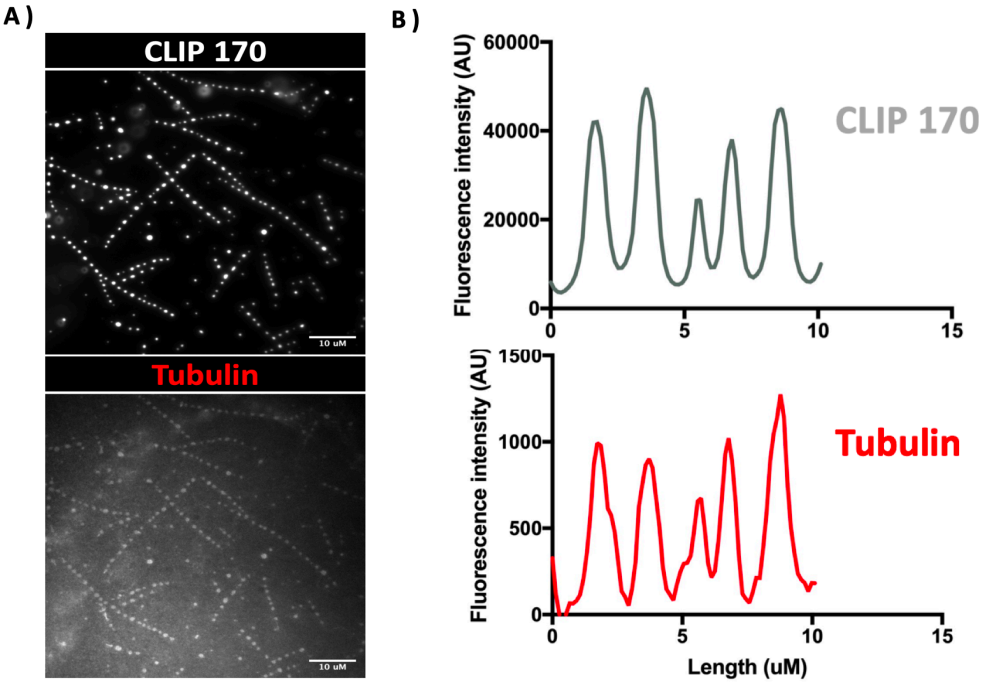

Figure 11: Periodic droplets of CLIP-170 contain soluble tubulin. A) TIRF reconstitution assays with mCherry-tagged alpha-tubulin and GFP-tagged CLIP-170 show that the droplets contain soluble tubulin. **B)** Fluorescence intensity profiles of CLIP-170 and tubulin show co-alignment of tubulin and CLIP-170 signals on the MT lattice.

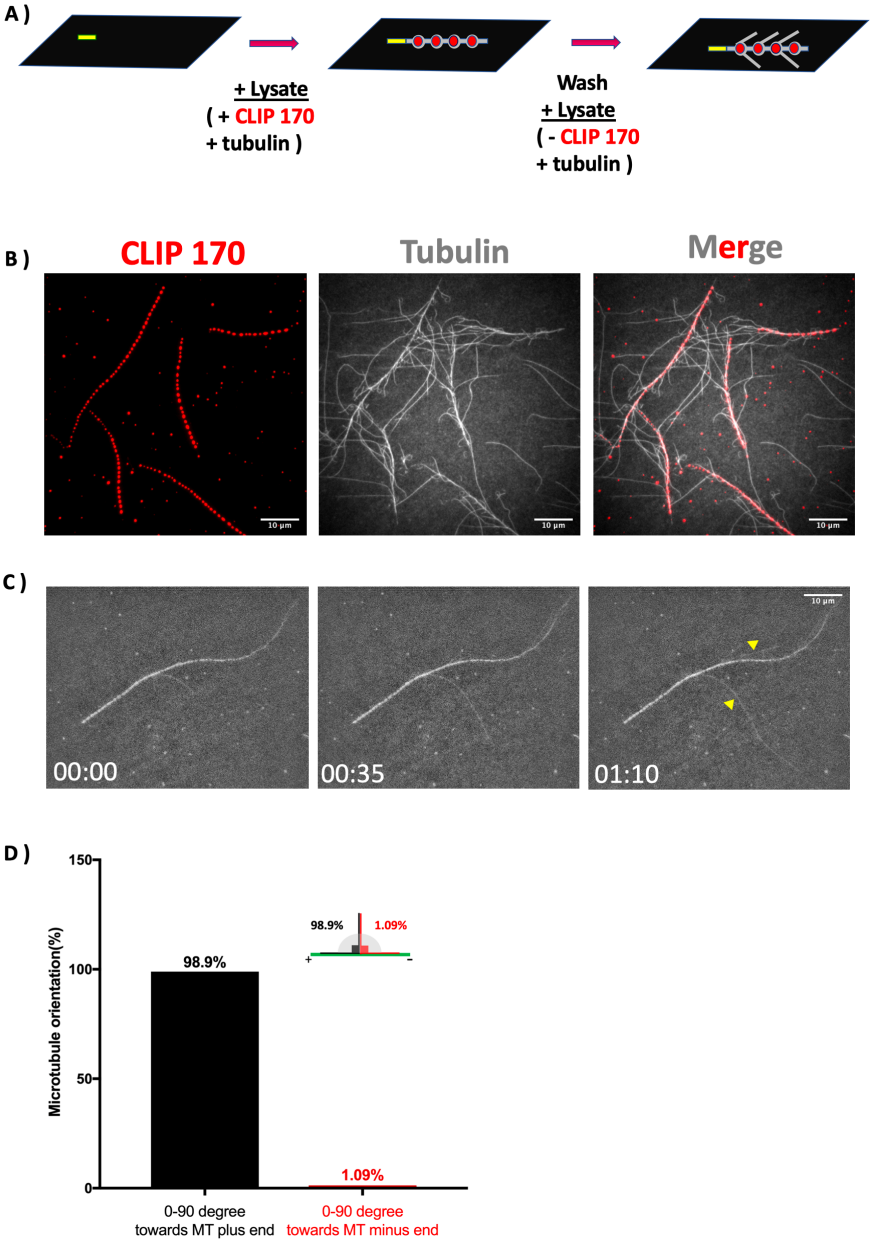

Figure 12: Microtubule nucleation from CLIP-170-tubulin co-condensates. A) Schematic diagram of the experimental steps used to test MT nucleation from CLIP-170 droplets. First, a lysate containing overexpressed CLIP-170 (and endogenous tubulin) was flushed into a TIRF chamber having immobilized GMPCPP seeds, which lead to MT growth and CLIP-170 droplet formation. Second, the excess of the lysate was washed out from the chamber, and lysate from untransfected cells (no CLIP-170, endogenous tubulin) was flushed in. This led to MT polymerization from the CLIP-170-tubulin co-condensates. **B)** TIRF assays showing MT nucleation from existing droplets. **C)** Time montage of MT nucleation events (yellow arrows) from MT lattice decorated with CLIP-170 droplets. **D)** Quantification of the orientation of newly nucleated MTs in comparison to the orientation of the parent MTs from step 1.

Results: chapter 2

3.2. Purification of tubulin with controlled posttranslational modifications by polymerization-depolymerization cycles from mammalian cell lines.

Context, results and author contributions:

A key question in cell biology is how MTs are able to perform diverse functions inside cells. The tubulin code hypothesis proposes that MT heterogeneity can be achieved either by the expression of different tubulin genes, or by several tubulin PTMs. Accumulating studies show that tubulin PTMs can alter the dynamic properties of MTs, and also steer them to interact with different MAPs (Gadadhar et al. 2017; Janke and Magiera 2020).

One of the technical limitations to explore the molecular function of tubulin PTMs is the common use of porcine or bovine brain tubulin in biochemical experiments (Lee 1982; Miller et al. 2010; Souphron et al. 2019). Strikingly, brain tubulin is highly posttranslationally modified, and thus does not allow to study the role of the PTMs on MT properties and functions in detail. Brain has been historically used as a source of purified tubulin because of high tubulin content, also a large amount of starting material is crucial for a good yield of tubulin in the end. Therefore, it is important to have an alternative method for purifying assembly-competent tubulin with controlled tubulin PTMs.

I participated in the development of a tubulin purification method from mammalian cells that uses cycles of polymerization-depolymerization. Other tubulin purification techniques described recently, such as the TOG column-based method, focus on purification of the total tubulin pool, which can lead to the purification of polymerization incompetent tubulin. Our method allows to purify tubulin from limited sources such as adherent- or suspension-grown cell lines or single mouse brains. The obtained tubulin is compatible with *in vitro* reconstitution and TIRF microscopy-based experiments. These experiments allow to study the impact of tubulin PTMs on the dynamic properties of MTs, and also to study their role in MAP-MT interactions. Furthermore, tubulin prepared with our method has been used for solid-state NMR spectroscopy (Luo et al. 2020); mass spectrometry, crystallographic studies and electron microscopy (unpublished work with collaborators). This protocol has been published (Souphron et al. 2019) and I am one of the first authors of this publication (attached below). In connection to this method, a second manuscript has recently been published as a video protocol in JoVE (Journal of Visualized Experiments), which is added in the **annex 6.3.**

Author contributions

My contributions:

I contributed in the improvement of the protocol for purifying pure and assembly-competent tubulin from large quantities of cells grown in suspension. I also participated in the generation of stable cell lines for purifying custom-modified tubulin. I provided all the Coomassie-stained SDS-PAGE gel figures, and also contributed in the refinement of the text and figures.

Contribution of co-authors:

J. Souphron and M.M. Magiera established the spinner cultures for various cell lines (with the help of G. Lakisic and A.M. Gautreau) and adapted the tubulin purification protocol to spinner-grown cells. S. Bodakuntla and M.M. Magiera established the tubulin prep from adherent cells. M.M. Magiera established the tubulin prep protocol from single mouse brains. She performed the western blot for testing different tubulin PTMs. M.M. Magiera and C. Janke supervised the development of this method. C. Janke and M.M. Magiera wrote the manuscript. All the authors contributed to corrections of the text and figures.

The published protocol for the purification of tubulin with controlled PTMs is attached here:

1) Souphron, Bodakuntala, Jijumon et al. 2019, Nature Protocols

Purification of tubulin with controlled posttranslational modifications by polymerization-depolymerization cycles

Judith Souphron, Satish Bodakuntla, Jijumon A.S., Goran Lakisic, Alexis Gautreau, Carsten Janke, Maria Magiera

Purification of tubulin with controlled posttranslational modifications by polymerization-depolymerization cycles

Judith Souphron[1,2#], Satish Bodakuntla[1,2#], Jijumon A.S.[1,2#], Goran Lakisic[3,4], Alexis Gautreau[3], Carsten Janke[1,2]*, Maria M. Magiera[1,2]*

[1]Institut Curie, PSL Research University, CNRS UMR3348, F-91405 Orsay, France

[2]Université Paris Sud, Université Paris-Saclay, CNRS UMR3348, F-91405 Orsay, France

[3]Ecole Polytechnique, CNRS UMR7654, Universite Paris-Saclay, F-91120 Palaiseau, France.

[4]present address: Institut MICALIS, AgroParisTech, Université Paris Saclay, INRA, F-78350 Jouy-en-Josas, France

[#]equal contribution

*corresponding authors:

Carsten Janke, Institut Curie, PSL Research University, CNRS UMR3348, Centre Universitaire, Bâtiment 110, F-91405 Orsay, France

Telephone: +33 1 69863127; Fax: +33 1 69863017; Email: Carsten.Janke@curie.fr

Maria M. Magiera, Institut Curie, PSL Research University, CNRS UMR3348, Centre Universitaire, Bâtiment 110, F-91405 Orsay, France

Telephone: +33 1 69863088; Fax: +33 1 69863017; Email: Maria.Magiera@curie.fr

KEYWORDS Microtubule, tubulin, polymerization, tubulin code, posttranslational modifications, tubulin isotypes, spinner culture, in vitro reconstitution, tubulin purification

EDITORIAL SUMMARY A protocol for purifying tubulin with controlled posttranslational modifications using cycles of polymerisation and depolymerisation. Tubulin can be obtained from cultured cells or single mouse brains and used for *in vitro* reconstitution assays.

TWEET A new protocol for purifying tubulin with controlled posttranslational modifications for *in vitro* reconstitution experiments.

COVER TEASER Purifying tubulin with controlled PTMs

Up to three primary research articles where the protocol has been used and/or developed:

1. Barisic, M. *et al.* Microtubule detyrosination guides chromosomes during mitosis. *Science* **348**, 799-803 (2015).
2. Nirschl, J. J., Magiera, M. M., Lazarus, J. E., Janke, C. & Holzbaur, E. L. F. alpha-Tubulin Tyrosination and CLIP-170 Phosphorylation Regulate the Initiation of Dynein-Driven Transport in Neurons. *Cell Rep* **14**, 2637-2652 (2016)
3. Guedes-Dias P, Nirschl JJ, Abreu N, Tokito MK, Janke C, Magiera MM, Holzbaur ELF (2019) Kinesin-3 Responds to Local Microtubule Dynamics to Target Synaptic Cargo Delivery to the Presynapse. *Curr Biol* **29:** 268-282 e268

Abstract

In vitro reconstitutions of microtubule assemblies have provided essential mechanistic insights into the molecular bases of microtubule dynamics and their interactions with associated proteins. An emerging regulatory mechanism of microtubule functions is the tubulin code, which suggests that tubulin isotypes and posttranslational modifications play important roles in controlling microtubule functions. To investigate the mechanism of the tubulin code, it is essential to analyse different tubulin variants *in vitro*. This has so far been difficult, as most reconstitution experiments used heavily posttranslationally modified tubulin purified from brain tissue. Therefore, we developed a protocol that allows purifying tubulin with controlled posttranslational modifications from limited sources using cycles of polymerisation and depolymerisation. While alternative protocols using affinity purification of tubulin yield very pure tubulin as well, our protocol has the unique advantage to select for fully functional tubulin, as non-polymerizable tubulin is excluded in the successive polymerisation cycles. It thus provides a novel routine procedure to obtain tubulin with controlled posttranslational modifications for *in vitro* reconstitution experiments. We describe specific procedures for tubulin purification from adherent cells, cells grown in suspension cultures, or from single mouse brains. The protocol can be combined with drug treatment, transfection of cells prior to tubulin purification, or enzymatic treatment during the purification process. The amplification of cells and their growth in spinner bottles takes approximately 13 days; the tubulin purification itself 6-7 hours. The tubulin can be used in TIRF-microscopy-based experiments or pelleting assays to investigate the intrinsic properties of microtubules and their interactions with associated proteins.

INTRODUCTION

Microtubules are essential components of the mammalian cytoskeleton, and are important in almost all key biological processes, such as cell division, cell motility, or cell differentiation (neurons, cilia and flagella, platelets etc.). Owing this importance, one of the key concerns of cell biology has been to mechanistically understand how these highly conserved cytoskeletal elements adapt to such a huge variety of biological functions. *In vitro* experiments aiming at reconstructing microtubule assemblies and functions from purified tubulin and other cytoskeletal components have been instrumental in understanding the biochemical,

biophysical and structural properties of microtubules. Tubulin was discovered as the protein building block of microtubules in 1967[1], and soon after, it was shown that tubulin can assemble into microtubules in solution[2]. This led to a plethora of studies on the assembly properties and mechanisms of microtubules[3,4], on how this assembly was regulated by tubulin drugs[5] and by microtubule-associated proteins (MAPs)[6]. *In vitro* studies with tubulin have also allowed to propose the mechanism of microtubule dynamic behaviour, such as treadmilling[7] and dynamic instability[8].

The development of novel light microscopy techniques[9] and the growing availability of molecular biology tools for cloning and purifying recombinant proteins led to more and more complex *in vitro* reconstitutions of microtubule assemblies[10]. This resulted in a large number of amazing discoveries based on *in vitro* reconstitutions of microtubule assemblies, such as the self-organisation of microtubules and motor proteins[11], the reconstitution of mitotic spindle functions in minimal systems[12,13], the analysis of cargo transport with isolated components[14], or the self-repair of microtubules[15] to give a few examples.

The reliability of these experiments strongly depends on the biochemical quality of the protein components used for such reconstitution, in particular on high-quality and high-purity tubulin. For the past 50 years, virtually all *in vitro* reconstitutions were performed with tubulin purified from brain tissue. Brain tubulin can be obtained in large quantities from cow, pig or sheep brain by cycles of warm polymerization and cold depolymerization[16]. This method is highly efficient because of the large abundance of tubulin in brain tissue, and the capacity of tubulin to spontaneously polymerize at high protein concentrations. By cycling several times between polymerized microtubules (warm) and depolymerized soluble tubulin (cold), the method yields highly pure and assembly-competent tubulin, while microtubule aggregates or assembly-incompetent soluble tubulin will be eliminated in the consecutive cycles. The only "contamination" of such-purified tubulin are microtubule-associated proteins (MAPs), which can be removed either by chromatography[16], or by the polymerization of tubulin in a high-molarity buffer that disrupt the binding of MAPs to the microtubules[17].

The ease of purification of large quantities (gram amounts) of brain tubulin was highly convenient, as none of the alternative methods to purify tubulin from other sources could reach the quality, quantity and ease of the brain tubulin preparations. Therefore, brain tubulin is still today the most-used component for *in vitro* reconstitutions as well as structural studies. This massive use of brain tubulin, however, masks the fact that tubulin is heterogenous in different organisms, cells, and even within single cells (e.g. between cytoplasmic and ciliary

microtubules[18]). Both, α- and β-tubulin are expressed from a variety of genes, giving rise to tubulin isotypes, which are further subjected to a large variety of posttranslational modifications (PTMs). Both, specific isotypes and PTMs mark functionally specialized microtubule populations, and might confer specific properties and functions to these microtubules. This concept, known as the 'tubulin code'[19], is so far little explored, and one of the greatest stumbling stones was the impossibility to purify tubulin with controlled isotypes and PTMs that could replace the brain tubulin – a heterogenous mixture of isotypes particularly enriched in PTMs – in *in vitro* assays. While a variety of alternative methods have recently emerged, we argue that it will be essential to purify tubulin with controlled PTMs using an approach that is highly similar to the established purification of brain tubulin, the gold standard in the field.

The method we describe here allows to purify tubulin from large and medium scale cultures of mammalian cells by cycles of polymerization and depolymerization. The quality of such-purified tubulin is equivalent to brain tubulin, as demonstrated in meticulous *in vitro* reconstitutions[20-22]. The tubulin prepared from Hela S3 cells has been shown to be virtually free of tubulin PTMs, and such nonmodified tubulin can be selectively modified with single PTMs[20]. This is a huge advantage over brain tubulin, which contains an uncontrollable mixture of PTMs. Our efforts to downscale the purification procedure has also allowed us to set up a small-scale purification of tubulin from single mouse brains (~400 mg vs. ~500 g of a cow brain), which has become a complementary tool to study the functions of tubulin from an emerging plethora of mouse models with altered tubulin PTMs, isotypes, or with mutations in tubulin genes.

OVERVIEW OF THE PROCEDURE

Our protocol is composed of three main parts. The first part describes the amplification of sources from which tubulin will be purified (**step 1**): cell lines cultured either in spinner bottles (**step 1.A**) or adherently on plastic dishes (**step 1.B**). It is possible to transfect adherently growing cells with expression plasmids, or treat them with drugs (**Box 1**). We further describe how tubulin can be purified from a single mouse brain (**step 1.C**).

The second section of the protocol describes the lysis procedures (step 2): the particularities of lysis of HEK-293 cells (**step 2.A**), Hela S3, Hela and U-2 OS cells (**step 2.B**), or brain tissue (**step 2.C**).

The third part describes the tubulin purification process itself (see Fig. 1). First, cells or tissue is lysed and the lysate is cleared (**steps 3**, then **4.A** for cell extracts, or **4.B** for brain extracts). Next, the first polymerisation is performed in low-molarity buffer (**steps 7-11**), followed by the first depolymerisation step (**steps 12-17**). Optionally, tubulin can then be enzymatically treated at this point (**step 18**). Tubulin is then subjected to the second polymerisation (**steps 19-23**), this time in high-molarity buffer to avoid the binding of MAPs to the polymerised microtubules, and MAP-free microtubules are subsequently depolymerised (**steps 24-30)**. A third cycle of polymerisation (**steps 31-35**) and depolymerisation (**steps 36-41**) in low-molarity buffer can be performed.

We then describe qualitative and quantitative analysis of the purified tubulin (**step 42, Box 2**). We propose quantification by protein band intensity measurements on Coomassie-stained gels, and qualitative analyses using immunoblot with antibodies detecting specific tubulin PTMs.

DEVELOPMENT OF THE APPROACH

When setting up this protocol, one major bottleneck was to polymerise tubulin directly from cell extracts. The most important parameter for this to work is the tubulin concentration in the initial extract. Tubulin is, with ~25% of the total soluble protein, a major component of brain extracts, while it constitutes only ~3% in extracts of cell lines[23]. To avoid that tubulin does not polymerize due to the lower concentration in cell extracts, we modified the first polymerization step, which in our protocol is performed at low PIPES molarity. This allows MAPs present in the cell extract to help the first round of microtubule polymerization. The molarity of PIPES is strongly increased in the second round of polymerisation, in which the concentration of tubulin can be adjusted to allow efficient polymerisation at high-molarity conditions.

The first key step of the protocol is the cell lysis, which should assure that most of the cellular microtubules depolymerise into soluble tubulin. To ensure this, the procedure is carried out at 4°C, which promotes microtubule depolymerisation. Secondly, we found that different cell types and tissues require different lysis techniques. While HEK-293 cells can be disrupted by repetitive pipetting through a narrow pipette tip, Hela S3 cells and other tested cell types need a more severe disruption procedure. Large amounts grown in spinner cultures are thus lysed

using a French press, or an equivalent cell disrupting apparatus, and small amounts by gentle sonication. Brain tissue, in contrast, is best lysed using an Ultra-Turrax® homogeniser.

An unexpected problem was the difficulty to completely clarify the first extract from lysed cells by ultracentrifugation. We encountered substantial problems with a floating layer that easily contaminates the clear supernatant, but cannot be avoided by longer centrifugation times. We thus chose to carefully remove the clear supernatant between this floating layer and the pellet, even if there is some loss of cell extract at this step. We introduced an additional low-speed centrifugation step to further clarify the first supernatant. This problem varies between different cell types, and can lead to complete failure of the purification procedure if too much floating material is included in the first polymerization step. Careful handling is therefore of key importance at this first step.

COMPARISON WITH OTHER METHODS

Compared to its blueprint, the tubulin purification from brain tissue, our method is technically more demanding for two reasons: first, the growth of larger amounts of cells needs to be established before the method can be started, and second, the lysis step of the cells and first clarification of this lysate is more meticulous than it is for brain tissue (see 'Development of the Approach'). Strikingly, a method similar to the here-described has been first used in 1979 to isolate MAPs specific to Hela microtubules[24], but to our knowledge has never been used to produce tubulin for *in vitro* reconstitution approaches. There were also several other successful attempts to purify assembly-competent tubulin from different sources in the 1970ies (reviewed in Farrell, 1982[25]), but none of them has been followed up, perhaps due to difficulties in reproducing the cumbersome biochemical procedures.

Alternative methods to purify tubulin without the need of polymerization-depolymerization cycles have also been described. For instance, isotype-specific antibodies were used in immuno-affinity purifications to partially separate tubulin into isotype-enriched fractions[26]. Many alternative protocols are based on pre-absorption of tubulin from cell extracts onto chromatography columns[27,28]. All of these methods require chromatography equipment and specific expertise, which might be the reason they have not been broadly used.

Finally, there were two recent developments that have considerably advanced the purification of tubulin from sources other than brain tissue: the introduction of the TOG-column and purification of recombinant tubulin from insect cells. The TOG column is an affinity matrix

based on a domain of the TOG-protein Stu2p from budding yeast. This column uses the affinity of tubulin dimers to the TOG-domain to selectively bind tubulin from cell extracts, and has been shown to produce highly pure fractions of tubulin from many different tissues or cell sources[29]. The method has so far allowed to purify tubulin from a range of organisms, such as yeast or *Caenorhabditis elegans*, and study the structure[30,31] and dynamics[32-34] of those evolutionarily divergent tubulins, or their impact on the behaviour of motor proteins[35].

One of the most significant recent advances was the development of a method to generate recombinant tubulin. This method is based on a bi-cistronic expression of an α- and a β-tubulin gene in insect cells using the baculo-virus system. Both genes carry a small epitope tag, which allows for a two-step affinity purification of dimers exclusively composed of the recombinant α- and β-tubulin[36]. This method now allows to systematically study the role of different tubulin isotypes[31,37,38] and tubulin mutations[39] *in vitro*, however, it is a cumbersome and time-consuming method to establish and thus only dedicated labs might decide to commit to it.

ADVANTAGES, LIMITATIONS AND APPLICATIONS

The great advantage of the here-described method is the possibility to rapidly produce milligram-amounts of pure, assembly-competent tubulin from cell lines. When using spinner bottles with Hela S3 cells, the method can be run in the background, and requires only a couple of hours per week for cell harvesting and re-inoculation of new spinners, and one day per week if tubulin purification is carried out immediately (alternatively, cells can be stored in lysis buffer at -80°C, and a larger-scale purification can be performed after collecting several rounds of spinner cultures). This tubulin can, in a simple and straight-forward step, be converted to detyrosinated tubulin, thus providing already two pure PTM versions[20].

In combination with the overexpression of specific tubulin-modifying enzymes, our approach can easily be extended to other tubulin PTMs. Finally, our protocol allows fast and efficient purification of tubulin from single mouse brains, which in the light of a growing number of transgenic mouse models with altered tubulin PTMs, isotypes, or with tubulin mutations, provides great opportunities to study the impact of these alterations directly *in vitro*.

A limitation of our system is its restriction to the native tubulin isotype composition of the cell line used for the tubulin purification. However, all cell lines analysed so far express rather 'generic' α- and β-tubulin isotypes, i.e. isotypes with the high sequence homologies, which

makes such tubulin more homogenous than brain tubulin that is composed of a significant amount of the rather divergent β3-tubulin (TUBB3) isotype[40]. A second limitation of the here-described method is that specific tubulin isotypes, or tubulins carrying particular PTMs, might polymerise less efficiently, or depolymerise less in case they strongly stabilise microtubules. They could therefore be lost, or disproportionally reduced during the purification. One striking example is polyaminated tubulin, which is completely excluded in the brain tubulin purification procedure[41]. However, we have shown that the currently most-studied tubulin modifications, such as acetylation, detyrosination, glutamylation and glycylation, are preserved throughout our protocol (see "Anticipated Results"). Thus, while for quantitative studies of tubulin modifications or isotype composition the TOG-column should be the method of choice[29], our protocol is appropriate for meticulous *in vitro* reconstructions in which the high purity and assembly competence of tubulin are key[20-22].

Our method could fully replace the standard brain tubulin preparation, allowing to use tubulin free of PTMs and assembled from less divergent tubulin isotypes on a daily basis. A typical 4-l spinner culture of Hela S3 cells yields ~15 g of cells, which in our hands gives rise to ~2 mg of tubulin (corresponding to a yield of ~135 µg/g). This is lower than the yield from adherent cells, which is rather ~200 µg/g, however, growing cells on plastic dishes is more time-consuming, and especially harvesting them from the dishes is more cumbersome. We found that ten 15-cm dishes are the maximum number of dishes that can be handled, which gives rise to ~1.2 g of cells, yielding ~250 µg of pure tubulin. The lower yield of cells in suspension culture could be related to a less complex microtubule cytoskeleton in these spherical cells, however this is not a major concern, as spinner cultures are effortlessly grown in large quantities. Overall, cycling of tubulin is bound to engender some loss, which is why it is not surprising that Widlund et al.[29] report three times higher tubulin yields (~460 µg/g) from human cells using the TOG-column.

Finally, our protocol yields ~1 mg/g of tubulin from mouse brains, which is higher as compared to the standard yield from pig brain that in our hands is rather ~400 µg/g. This is most likely related to the longer post-mortem delay of the pig brains as compared to the instantly available mouse brains. Tubulin purified from single mouse brains can be used to directly test the *in vitro* behaviour of microtubules from a growing number of mouse models with altered tubulin isotype composition[42-44], or tubulin PTMs[45,46].

EXPERIMENTAL DESIGN

Upscaling the tubulin production in spinner cultures. While our method also works for relatively small amounts of adherently growing cells, spinner cultures to grow cells in suspension are primordial in order to obtain milligram-amounts of tubulin. The setup we propose here allows growing 4×1 l of suspension cultures in parallel, which yields ~15 ml of cell pellet every 7 days, allowing for the purification of ~2 mg of tubulin. We can also purify tubulin from two spinner bottles, but not less, as at lower amounts the procedure becomes unreliable. Hela S3 cells (ATCC® CCL-2.2™) which have been optimised for growth in suspension, do not agglutinate and can thus be grown, harvested and in parallel be re-diluted for several weeks or months, without preparing new adherent pre-cultures. Other cells, such as HEK-293, have the tendency to form cell aggregates during growth in suspension, which makes it necessary to inoculate them each time from an adhered pre-culture, which is more time-consuming and work-intense. The advantage of HEK-293 cells is the ease of generating stable, inducible cell lines with the Flp-In™ T-REx™ 293 cell line (Thermo Fisher # R78007).

Using a variety of cell and tissue sources to generate custom-modified tubulin. Smaller amounts of tubulin can also be purified from adherently growing cells. The advantage of this approach is that it allows to use any cell line, treat the cells prior to tubulin isolation, e.g. by transfecting expression vectors to express tubulin-modifying enzymes, tubulin isotypes, or to treat cells with drugs, all of which would be difficult to impossible in cells growing in suspension culture. Another advantage is that specific equipment, such as spinner bottles, is not needed. The drawback is that only small amounts of tubulin can be produced (~250 µg for ten 15-cm dishes), and that the method is less easily reproducible, as small variations in cell numbers, or delays during the cell harvest can have a strong impact on the efficiency of tubulin polymerization, and thus on the yield. So far, we successfully prepared tubulin from Hela, U-2 OS, and HEK-293 cell lines. Having downscaled the protocol to very small volumes, it now obviously allows isolating tubulin from very small amounts of brain tissue, i.e. from single brains of transgenic mice.

MATERIALS

BIOLOGICAL MATERIALS:

- **Hela S3 cells** (ATCC® CCL-2.2™) ▲ **CRITICAL**: Hela S3 cells have been specifically selected to be able to grow both as adherent and in suspension cultures. ▲ **CRITICAL**: A minimum of one vial of each cell line is necessary to start this protocol. **! CAUTION** The cell lines used should be regularly checked to ensure that they are authentic and are not contaminated with mycoplasma.
- **Flp-In™ T-REx™ 293 cells** (Thermo Fisher # R78007)
- **U-2 OS cells** (ATCC® HTB-96™)
- **Hela cells** (ATCC® CCL-2™)
- **HEK-293 cells** (ATCC® CRL-1573™)
- **Mouse brain tissue** Mice used here were C57b/6N background, however any mouse strain can be used to purify tubulin from brain. *Atat1*$^{-/-}$ mice lack tubulin acetylation and have been described before[47]. *Ttll1*$^{-/-}$ mice, lacking one of the major brain tubulin polyglutamylases, have been described before[45] **! CAUTION** Any experiments involving mice must conform to relevant Institutional and National regulations. Animal care and use for this study were performed in accordance with the recommendations of the European Community (2010/63/UE). Experimental procedures were specifically approved by the ethics committee of the Institut Curie CEEA-IC #118 (authorization no. 04395.03 given by National Authority) in compliance with the international guidelines.

REAGENTS:

- **PBS** (Life Technologies #14190169)
- **DMEM medium** (Life Technologies #41965062)
- **Fetal bovine serum** (FBS; Sigma #F7524)
- **L-Glutamine** (Life Technologies #25030123)
- **Penicillin-Streptomycin** (Life Technologies #15140130)
- **Trichostatin A** (TSA; Sigma #T8552)
- **jetPEI®** (Polyplus #101)
- **Carboxypeptidase A** (CPA, Sigma C9268, 1.7 U/µl)
- **EDTA** (Euromedex #EU0007-C)

- **Trypsin** (Life Technologies #15090046)
- **PIPES** (Sigma #P6757) ▲ **CRITICAL** We recommend using PIPES from this source because of the reproducible quality standard. We once experienced problems with PIPES from other suppliers
- **EGTA** (Sigma #E3889)
- **1 M $MgCl_2$** (Sigma #M1028)
- **Phenylmethanesulfonyl fluoride** (PMSF; Sigma #P7626) **! CAUTION** PMSF powder is hazardous. Use skin and eye protection when preparing PMSF solutions.
- **Isopropanol** (VWR #20842.298)
- **Aprotinin** (Sigma #A1153)
- **Leupeptin** (Sigma #L2884)
- **4-(2-aminoethyl)-benzenesulfonyl fluoride** (Sigma #A8456)
- **Triton® X-100** (Sigma #T9284,)
- **2-mercaptoethanol** (Sigma #M3148) **! CAUTION** 2-mercaptoethanol is toxic, manipulate it under a fume hood
- **GTP** (Sigma #G8877) ▲ **CRITICAL** We recommend using PIPES from this source because of the reproducible quality standard.
- **Glycerol** (VWR Chemicals #24388.295)
- **KOH** (Sigma #P1767) **! CAUTION** KOH is corrosive and causes burns; use eye and skin protection.
- **Dimethyl sulfoxide** (DMSO; Sigma #D8418) **! CAUTION** DMSO can enhance cell and skin permeability of other compounds. Avoid contact and use skin and eye protection.
- **DTT**, DL-Dithiothreitol (Sigma #D9779)
- **SDS**, Sodium dodecyl sulphate (VWR #442444H)
- **SDS,** Sodium dodecyl sulphate (Sigma #L5750) ▲ **CRITICAL** Only this particular SDS reference allows to separate α- and β-tubulin bands.
- **Tris** (Trizma® base, Sigma #T1503)
- **HCl** Hydrochloric acid (VWR #20252.290) **! CAUTION** HCl is corrosive and causes burns; use eye and skin protection and work in a chemical fume hood
- **Bromophenol blue** (Sigma #1.08122)
- **BSA**, Bovine serum albumin (Sigma #A7906)

- **Liquid nitrogen ! CAUTION** liquid nitrogen causes burns; use eye and skin protection
- **Ethanol** absolute (Fisher Chemical #E/0650DF/15)
- **40% Acrylamide** (Bio-Rad #161-0140)
- **Bis N,N'-Methylene-Bis-Acrylamide** (Bio-Rad #161-0201)
- **TEMED, N, N, N′, N′-Tetramethylethylenediamine** (Sigma #9281) **! CAUTION** TEMED is corrosive, toxic and causes burns; use eye and skin protection.
- **APS, Ammonium persulfate** (Sigma #A3678)
- **Glycine** (Sigma #G8898)

Antibodies

- **Anti-α-tubulin antibody 12G10** (used at 1/500 (vol/vol), Developed by J. Frankel and M. Nelson, obtained from the Developmental Studies Hybridoma Bank, developed under the auspices of the NICHD, and maintained by the University of Iowa)
- **Anti-detyrosinated tubulin antibody** (used at 1/1,000 (vol/vol); Merck #AB3201)
- **Anti-tyrosinated tubulin antibody YL1/2** (used at 1/1,000 (vol/vol); Abcam #ab6160)
- **Anti-glutamylated tubulin antibody GT335** (used at 1/20,000 (vol/vol); AdipoGen #AG-20B-0020)
- **Anti-acetylated tubulin antibody 6-11B-1** (used at 1/2,000 (vol/vol); Sigma #T6793)
- **Anti-polyglutamylated tubulin antibody polyE** (used at 1/20,000 (vol/vol); AdipoGen # AG-25B-0030)
- **Anti-Mouse HRP-conjugated antibody** (used at 1/10,000 (vol/vol); Bethyl #A90-516P)
- **Anti-Rabbit HRP-conjugated antibody** (used at 1/10,000 (vol/vol); Bethyl #A120-201P)

EQUIPMENT:

- **1.5- and 2-ml tubes** (Eppendorf® #0030125150 and #0030120094, respectively) ▲ **CRITICAL** do not replace original Eppendorf references due to possible differences in material
- **14-ml round-bottom tubes** (Falcon #352017)
- **15-ml screw-cap tubes** (Falcon #352095)
- **50-ml screw-cap tubes** (Falcon #352070)
- **Ultracentrifuge tubes** appropriate for the rotor used: Beckman #357448 (for TLA-55); #349622 (for TLA-100.3) and #355631 (for 70.1 Ti)
- **5-ml, 10-ml, 25-ml sterile pipettes** (Corning #4487, #4488 and #4489, respectively)
- **Parafilm** (Parafilm® M, Bemis North America, USA)
- **5-ml, 10-ml, 20-ml syringes** without needles (Terumo #SS+05ES1, #SS+10ES1 and #SS20ES1, respectively)
- **Micropestles** (an alternative method for brain lysis, Eppendorf #0030 120.973)
- **Needles 18G × 1 ½"** (1.2 × 38 mm; Terumo #18G)
- **Needles 20G × 1 ½"** (0.9 × 38 mm; Terumo #20G)
- **Needles 21G × 4 ¾"** (0.8 × 120 mm, B. Braun #466 5643)
- **15-cm-diameter sterile culture dishes** (Corning #430599)
- **Micro-pipettes** p2.5, p10, p20, p100, p200 and p1000 and corresponding tips
- **Pipette-boy (**Drummond Pipette-Aid® XP)
- **Balance** (0.1 – 10 g; Sartorius, CPA64S)
- **pH-meter (**Sartorius, Docu-pHmeter)
- **Vortex mixer** (Scientific Industries, Inc. #SI-0236)
- **Tabletop centrifuge** for 1.5 ml tubes: Eppendorf 5417R (or equivalent)
- **Laboratory centrifuge** for 50-ml tubes: Sigma 4-16 K (or equivalent)
- **Cell culture hood**
- **Cell culture incubator** set at 37°C, 5% CO_2
- **Inverted microscope** (with fluorescence if cell transfection is to be verified)
- **Biological stirrer** Techne MCS-104L installed in the cell culture incubator (for spinner cultures)
- **1-l cell culture vessels**, Techne F7610 (for spinner cultures)
- **Beckman Avanti J-26 XP** centrifuge (for collecting spinner cultures)

- **JLA-8.1000 rotor** (for collecting spinner cultures)
- **Beckman 1-l polypropylene bottles** (for collecting spinner cultures; Beckman #355676)
- **Sonicator** (Branson Sonifier 450)
- **Blender** IKA Ultra-Turrax® (for lysing brain tissue)
- **French pressure cell press** (Thermo electron corporation #FA-078A, with a #FA-032 cell; for lysing big amounts of cells)
- **Ultracentrifuges**: Beckman Optima L80-XP (or equivalent), Beckman Optima MAX-XP (or equivalent)
- **Rotors**: Beckman 70.1 Ti; TLA-100.3; and TLA-55 (Beckman #34218, #349481 and #366725)
- **Water bath** equipped with floaters or tube holders
- **Heating block** (Stuart #SBH130D)
- **SDS-PAGE** electrophoresis equipment (Bio-Rad #1658001FC)

REAGENT SETUP:

Ethanol 70% (vol/vol) Mix 700 ml of absolute ethanol and 300 ml of water. Store at room temperature (20°C) and use as long as it is not contaminated.

Cell culture medium: 1 l DMEM medium supplemented with 10% (vol/vol; 100 ml) FBS, 200 mM (10 ml) L-Glutamine, and 1× Penicillin-Streptomycin (10 ml). Store at 4°C and use as long as it is not contaminated.

Trichostatin A 10 mM Dissolve 1 mg of TSA in 330.7 µl of DMSO. Store at -20°C for up to 3 years. **! CAUTION** DMSO can enhance cell and skin permeability of other compounds. Avoid contact and use skin and eye protection.

EDTA, 0.5 M pH 8 Dissolve 36.5 g of EDTA in water to a final volume of 250 ml, adjust to pH 8.0 with KOH (otherwise EDTA will not dissolve), filter-sterilize or autoclave and store at room temperature indefinitely.

PBS-EDTA, 5 mM Add 5 ml of 0.5 M EDTA to 500 ml of PBS. Filter-sterilize and store at 4°C for up to 3 years (before each use, visually verify that the solution is not contaminated).

PBS-EDTA-TSA, 5 µM Add 25 µl of 10 mM TSA to 50 ml of PBS-EDTA. This solution is used to detach the cells treated with TSA. It should be prepared freshly prior to use.

KOH, 10 M Dissolve 140 g of KOH in water to a final volume of 250 ml. Store at room temperature indefinitely.

K-PIPES, 0.5 M pH 6.8 Mix 75.5 g of PIPES with water, followed by adding KOH (otherwise PIPES will not dissolve). Adjust to pH 6.8 with KOH; final volume: 500 ml. Filter-sterilize or autoclave and store at 4°C for several months.

K-PIPES, 1 M pH 6.8 Mix 15.1 g of PIPES with water, followed by adding KOH (otherwise PIPES will not dissolve). Adjust to pH 6.8 with KOH; final volume: 50 ml. Filter-sterilize or autoclave and store at 4°C for several months.

K-EGTA, 0.5 M, pH 7.7 Dissolve 47.5 g of EGTA in water, adjust to pH 7.7 with KOH; final volume: 250 ml. Filter-sterilize and store at room temperature indefinitely.

▲ **CRITICAL** None of the buffers used for the tubulin prep should contain sodium salts, always use potassium!

BRB80 Mix 20 ml of 0.5 M PIPES, 40 µl of 0.5 M K-EGTA and 20 µl of 1 M $MgCl_2$; the final composition is: 80 mM K-PIPES pH 6.8; 1 mM K-EGTA; 1 mM $MgCl_2$. Filter-sterilize and store at 4°C for several months.

PMSF, 0.1 M Dissolve 435 mg of PMSF in a final volume of 25 ml of isopropanol. Store at -20°C for several months.

Protease inhibitors mix (200× concentrated) Dissolve 10 mg of aprotinin, 10 mg of leupeptin and 10 mg of 4-(2-aminoethyl)-benzenesulfonyl fluoride in 2.5 ml of water, aliquot and store at -20°C for several months.

Triton X-100, 10% (vol/vol) Mix 5 ml of Triton X-100 with 45 ml of water. Filter-sterilize and store at room temperature indefinitely.

Lysis Buffer Mix 20 ml of BRB80 with 1.5 µl of 2-mercaptoethanol, 200 µl of 0.1 M PMSF, 100 µl of the protease inhibitors mix (200× concentrated) and, (optional, for HEK-293 cells only) 400 µl of 10% (vol/vol) Triton® X-100. The final concentrations are: 1 mM 2-mercaptoethanol, 1 mM PMSF, 1× protease inhibitors mix, (optional, for HEK-293 cells only) 0.2% Triton® X-100 (vol/vol). Lysis buffer should be prepared freshly prior to use. **!**

CAUTION 2-mercaptoethanol is toxic, add it under a fume hood

GTP, 0.2 M Dissolve 1 g of GTP in 9.5 ml water, adjust to pH 7.5 with KOH. Aliquot and store at -20°C for up to 6 months. Avoid repetitive freezing and thawing.

Tris-HCl, 1 M Dissolve 60.56 g of Tris in 500 ml of water. Adjust the pH to 6.8 with HCl; filter-sterilize or autoclave the solution and store it at room temperature indefinitely.

Laemmli sample buffer, 5× For 40 ml, heat 16 ml of 1 M Tris-HCl pH 6.8, add 4 g of SDS (from VWR) and mix gently. Add 2.6 g DTT and 20 ml (or 24 g) of 100% glycerol. Add ~2.5 mg of Bromophenol blue to obtain the right colour intensity. Final concentrations: 450 mM DTT, 10% (wt/vol) SDS, 400 µM tris-HCl pH 6.8, 50% (vol/vol) glycerol, ~0.006% (wt/vol) bromophenol blue. Aliquot by desired volumes and store indefinitely at -20°C.

Acrylamide-Bis-acrylamide "TUB" mix Dissolve 2.7 g (0.54%, wt/vol) of Bis-acrylamide powder in 500 ml of 40% Acrylamide solution. Stir overnight at 4°C, then store at 4°C for up to 6 months.

SDS "TUB" 20% (wt/vol) For 500 ml, dissolve 100 g of SDS (Sigma #L5750) 500 ml of water. Filter sterilize and store at room temperature indefinitely. Heat to 40-50°C if precipitate forms.

Resolving gel "TUB" buffer, 4× For 200 ml, dissolve 36.3 g of Tris in 150 ml of water. Adjust the pH to 9.0 with HCl. Add 4 ml of 20% SDS "TUB" (Sigma #L5750) stock solution, and make up the volume to 200 ml with water. Final concentrations: 1.5 M Tris pH 9.0, 0.4% (vol/vol) SDS (Sigma #L5750). Filter sterilize and store at room temperature indefinitely.

Stack gel "TUB" buffer, 4× For 100 ml, dissolve 6 g of Tris in 80 ml of water. Adjust the pH to 6.8 with HCl. Add 2 ml of 20% SDS (Sigma #L5750) stock and make up the volume to

100 ml with water. Final concentrations: 0.5 M Tris pH 6.8, 0.4% (vol/vol) SDS (Sigma #L5750). Filter-sterilize and store at room temperature indefinitely.

SDS-PAGE "TUB", 10% wt/vol For 10 ml of resolving gel, mix 5 ml of water, 2.5 ml of acrylamide-bis-acrylamide "TUB" mix, 2.5 ml of resolving gel "TUB" buffer, 80 µl of 10% (wt/vol) APS and 10 µl TEMED and pour the gel into an appropriate gel stand. Add no more than 300 µl of water on top of the gel and let polymerize undisturbed. For 3 ml of the stack gel, mix 1.93 ml of water with 320 µl of acrylamide-bis-acrylamide "TUB" mix, 750 µl stack "TUB" buffer, 18.5 µl of 10% (wt/vol) APS and 7.4 µl of TEMED. Remove the water from the polymerised resolving gel, add the stack gel mix, insert the appropriate comb avoiding air bubbles, and let polymerize undisturbed. Keep at room temperature and use the same day.

SDS-PAGE "TUB" Running buffer 1× For 1 L, dissolve 28.75 g of glycine, 6 g of Tris in 900 ml of water. Add 5.75 ml of 20% SDS "TUB" (Sigma #L5750), and make up the volume to 1 L with water. Store at room temperature for up to 6 months.

EQUIPMENT SETUP:

Biological stirrer It should be set inside the cell culture incubator. The rotation speed should be 25 rpm for Hela S3 and HEK-293 cells, it should be empirically determined for other cell types.

Blender Set at power 6 or 7. This should be sufficient to lyse the brain tissue by blending 2-3 times for 10-15 s.

Sonicator We use the probe of 6.5 mm diameter (Branson #101-148-070), set at "Output control" 1, "Duty cycle" 10% and time depending on the cell type used.

French press We use the French press at medium ratio, and the gauge pressure of 1,000 psi (which corresponds to 3,000 psi inside the disruption chamber).

Ultracentrifuges If two ultracentrifuges are available, one should be set at 4°C, the other at 30°C. If only one is available, set it first to 4°C and change the temperature to 30°C during Steps 7, 19 and 31 and change it back to 4°C during Steps 12, 24 and 36. It is important to pre-cool or pre-heat the centrifuge before the run, as this will allow the centrifuge start faster for the actual run.

Ultracentrifuge rotors If two rotors are available, one should be stored at 4°C, the other at 30°C. If only one is available, pre-cool it first to 4°C and then heat it to 30°C during the polymerisation step. In order to efficiently change the rotor temperature, you can put it in a watertight plastic bag (to avoid wetting), and put either on ice or in the water bath. The temperature of the rotor should always match the temperature of the sample and of the centrifugation step, on one hand to keep the sample in optimal conditions (for example to not depolymerise microtubules by putting a warm sample into a cold rotor), and on the other hand to allow for a faster starting of the centrifuge.

Water bath Should be set to 30°C.

Spinner bottle cleaning It is important to keep the spinner vessels clean and dry. We recommend the following procedure:

1. Once the cells are collected from the spinner bottles, immediately fill them with tap water, to avoid that remaining cells dry and get stuck to the glass.
2. As soon as possible, remove the glass ball and wash it. Rinse spinner bottles thoroughly with water, using a bottle brush if necessary.

   ▲ **CRITICAL STEP** Avoid using detergent, as trace amounts of not-rinsed detergent could hamper the cell growth during the next culture cycle.

3. Re-assemble the spinner with the glass ball, add app. 200 ml (or enough to cover the glass ball) of deionised water and autoclave them.
4. Once autoclaved, under a sterile hood remove water from the spinners. Remove the lateral caps completely and open the top cap by tilting it over the edge of the opening. Leave in this position in the open hood for a few hours (or overnight) to dry completely. **▲ CRITICAL STEP** Failure to dry the spinners completely before storing them can result in the rusting of the metal screw that holds the glass ball.
5. Once completely dry, close all the caps, remove from under the hood and store in a secure place.

PROCEDURE:

Sources of tubulin

▲ **CRITICAL** Throughout this section, the days are numbered relative to the day of cell lysis and tubulin purification (day 0).

1. Grow cells that will be used as sources for isolating tubulin. For growing cells in spinners (such as Hela S3 and HEK-293), follow Option A (Fig. 2). For growing adherent cells (such as HEK-293, Hela and U-2 OS), follow Option B. When using mouse brain as a source, follow Option C.

A. Cells grown in spinners ● **TIMING** ~10-13 days depending on the number of spinners

(i) ***Amplifying the cells (Steps i-iii):*** Revive the desired cell type in its preferred medium. Amplify cells to obtain app. 6×10^7 cells (day -13).

(ii) Plate those cells on a minimum of six 15-cm-diameter dishes at ~10^7 cells per dish. Cells from six 80-90% confluent 15-cm plates will be needed to inoculate 2 l of suspension culture (two spinners), which is the minimum of cells for a successful purification. Prepare enough cells to inoculate the desired number of spinners (day -10).

(iii) Add 1 l of pre-warmed complete medium to each spinner bottle and incubate on the stirrer table in the cell culture incubator at 20-25 rpm. This step allows for the medium to equilibrate temperature and pH (day -8).

▲ **CRITICAL STEP** To minimize the number of operations, and the risk of contaminations, add all supplements for 1 l of complete medium into one of the two 500-ml DMEM bottles, and add this together with the non-supplemented 500 ml DMEM directly into the spinner bottle.

▲ **CRITICAL STEP** In order to avoid bacterial or fungal contaminations, thoroughly clean the media bottles and spinner bottles with 70% ethanol before transferring them into the cell culture hood.

▲ **CRITICAL STEP** Stir only spinner bottles filled with medium. Stirring empty bottles can result in damage. Slightly open the lateral valves of the spinner bottles to allow the incubator atmosphere to enter the bottle.

(iv) ***Inoculating the spinners (Steps iv-xiii):*** Remove culture medium from 15-cm plates from Step ii with cells at 80-90% confluence (day -7, Fig. 2a).

(v) Rinse the cells very gently with 5 ml PBS (pre-heated to 37°C)

▲ **CRITICAL STEP** pipette PBS to the border of the dish, check by eye that cells do not detach.

(vi) Remove all PBS by slightly inclining the culture dish, and removing PBS from the border of the dish.

(vii) Add 2 ml of Trypsin per 15-cm dish, spread it carefully to the entire surface by slightly inclining and turning the dish. Incubate for 3 min at 37°C (for Hela S3 cells), or at room temperature (for HEK-293 cells).

(viii) Add 3 ml of warm, complete medium to the plate to arrest trypsin activity, and detach cells by pipetting the liquid harshly onto the surface of the dish. Observe the detachment of the cell layer by eye. Detach cells from 3 dishes at a time, transfer them to a 15-ml conical-bottom tube, and incubate in the cell culture incubator while detaching the next lot.

(ix) Pellet cells at 250×g, room temperature, for 5 min.

(x) Re-suspend cells obtained from 3 dishes in 5 ml of fresh complete medium, and mix them well by pipetting up and down thoroughly to separate the cells, but avoid air bubbles.

▲ **CRITICAL STEP** Thorough dissociation of cells at this point is crucial for the optimal growth of cells in suspension. It is particularly important for HEK-293 cells, which tend to form aggregates. Failure to sufficiently dissociate the cells before inoculation can result in larger cell aggregates with cell death inside the aggregates, and consequently lead to lower tubulin yields.

(xi) Add 5 ml of cell suspension to each spinner bottles containing 1 l of pre-equilibrated medium under the cell culture hood (Fig. 2a), and return them to the stirrer table in the cell culture incubator.

▲ **CRITICAL STEP** Keep the lateral valves of the spinner bottles slightly open.

(xii) Let cells grow for 1 week, control occasionally for infections or sedimentation due to cell aggregation (Fig. 2b,c).

? TROUBLESHOOTING

(xiii) ***(Optional)*** Treat cells. If stable inducible cell lines are used, or the cells were to be treated with drugs, this should be done 48-24 h before harvesting (to be optimized for each experiment) (day -2).

(xiv) ***Harvesting the cells (Steps xiv-xx):*** Verify a slightly orange colour of the culture medium in the spinner bottles. Check the absence of bacterial contamination of each

spinner at this point by transferring 0.5 ml of each spinner bottle to one well of a 24-well dish, and observing the samples with an inverted microscope.

(xv) Transfer the cell suspension into 1-l centrifuge bottles. This step can be carried out in the non-sterile conditions, unless you wish to re-inoculate the spinners straight away (applies only for Hela S3 cells, see the Optional step (**xvi**)).

(xvi) **(*Optional*)** To re-inoculate Hela S3 cells for a new culture, leave approximately 100 ml of cell suspension in each spinner bottle, and add 1 l of fresh, complete medium. Return the spinners to the stirrer table in the incubator. Do not forget to keep the lateral valves of the spinner bottles slightly open.

(xvii) Pellet cells at 250×g, 15 min, room temperature.

(xviii) Re-suspend cells from one centrifuge bottle in 10 ml of ice-cold PBS, then transfer them to the next bottle etc., thus collecting the cells from all the centrifuge bottles and transferring them to a 50-ml screw-cap tube on ice. Repeat the rinsing of the bottles with 10 ml of PBS once or twice, if there are still cells left in the bottles. Pool all the cells in one or two 50 ml tube, fill them to 50 ml with ice-cold PBS if necessary.

(xix) Pellet cells at 250×g, 15 min, at 4°C. Remove the supernatant.

▲ **CRITICAL STEP** During the washing step cell lysis should not occur, but microtubules can already start depolymerising inside the cells. This is why we wash and pellet the cells at 4°C.

(xx) Determine the volume of the cell pellet (this should be around 3 ml for a 1-L spinner bottle) and add the same volume of the lysis buffer on cells. Re-suspend the cells in the lysis buffer.

▲ **CRITICAL STEP** In order to maintain the critical concentration of tubulin in the extract, the volume of the lysis buffer should not exceed the volume of the cell pellet.

▲ **CRITICAL STEP** The rest of the protocol refers to a hypothetical cell pellet of 10 ml (+ 10 ml lysis buffer) but a minimum of 6 ml pellet (2 spinner bottles) is sufficient for a successful purification. Please adjust all measures to the real volume of your cells in each experiment.

■ **PAUSE POINT** Once re-suspended in the lysis buffer, cells can be snap-frozen in liquid nitrogen, and stored at -80°C for up to two months.

(xxi) Clean the spinner bottles after use (see Equipment Setup).

B. Adherent cells ● **TIMING** ~5 days

▲ **CRITICAL** Avoid using Hela S3 cells for adherent cell cultures, as their real advantage is to be grown in suspension culture.

(i) ***Amplifying the cells (Steps i-ii):*** Revive the desired cell type in its preferred medium. Amplify cells to obtain ~10^8 cells (day -5).

(ii) Plate all cells on a minimum of ten 15-cm-diameter dishes at ~10^7 cells per dish. Cells from minimum ten 80-90% confluent 15-cm plates will be needed to successfully purify tubulin. (day -3)

(iii) (***Optional***) Transfect the cells with plasmid DNA using the JetPEI® reagent or treat with drugs (see Box 1).

(iv) ***Harvesting the cells (Steps iv-xi):*** Remove the medium from the dishes (done by person 1). Remove the medium by sets of three dishes, incline them slightly to facilitate soaking all the medium off.

▲ **CRITICAL STEP** A rapid cell harvest is very important for the success of the tubulin purification, and should not take more than 15 min for ten 15-cm dishes. For optimal results, at least the first time this experiment is carried out, three people should participate in this step. Later, one experienced person can handle the rapid detachment of cells.

(v) Rinse the cell monolayer very gently with 7 ml of PBS-EDTA, then aspirate by inclining the dishes.

(vi) Add 5 ml of PBS-EDTA (if cells were treated with TSA (Step 1(B)iii, Box 1), they should be detached with PBS-EDTA supplemented with 5 µM TSA [PBS-EDTA-TSA]), and incubate cells for up to 5 min at room temperature

▲ **CRITICAL STEP** We do not detach cells with trypsin to avoid excessive cell lysis during this step.

(vii) Detach cells from the dishes using a cell lifter (done by person 2). Detach the cells by gently shovelling them towards one place on the dish. Detachment of the cell monolayer is visible with naked eye.

? TROUBLESHOOTING

(viii) Collect the detached cells in a 50-ml screw-cap tube (done by person 3).

(ix) Rinse each plate with 2 ml of PBS-EDTA (or PBS-EDTA-TSA for cells treated with TSA), to collect the remaining cells.

(x) Pellet the harvested cells at 250×g, 10 min, at 4°C. Remove the supernatant.

(xi) Determine the volume of the cell pellet, which for ten dishes should be around 1-1.5 ml. Add the same volume of the lysis buffer on cells. Re-suspend the cells in the lysis buffer.

▲ **CRITICAL STEP** In order to maintain the critical concentration of tubulin in the extract, the volume of the lysis buffer should not exceed the volume of the cell pellet.

▲ **CRITICAL STEP** The rest of the protocol refers to a hypothetical cell pellet of 10 ml (+ 10 ml lysis buffer) but a minimum of ~1 ml pellet (from 10 15-cm dishes) is sufficient for a successful purification. Please adjust all measures to the real volume of your cells in each experiment.

■ **PAUSE POINT** Once re-suspended in the lysis buffer, cells can be snap-frozen in liquid nitrogen, and stored at -80°C for up to two months.

C. Mouse brain ● **TIMING** ~15 min

(i) Sacrifice the animal by cervical elongation, open the skull with scissors and extract the brain. Wash the brain briefly in the lysis buffer to remove excess blood.

! CAUTION Animal experimentation is subjected to specific legislation in each country, please ensure that you have all necessary permits to work with mice

■ **PAUSE POINT** It is possible to snap-freeze brains in liquid nitrogen and store them at -80°C before proceeding to the lysis. Frozen mouse brains can be stored at -80°C for up to 3 years.

(ii) Add 500 µl of the lysis buffer per adult mouse brain in a round-bottom tube.

▲ **CRITICAL STEP** Round-bottom tubes are essential for a correct homogenisation of the brain tissue as the probe is too large to reach the tissue in a conical-bottom tube.

▲ **CRITICAL STEP** The rest of the protocol refers to a hypothetical tissue volume of 10 ml (+ 10 ml lysis buffer), but a minimum of 1 mouse brain is sufficient for a successful purification. Please adjust all measures to the real volume of your cells in each experiment.

Cell and tissue lysis

2. Lyse the harvested cells or tissue. For lysis of HEK-293 cells follow Option A (Fig. 2). For lysis of Hela S3, Hela and U-2 OS cells, follow Option B. For lysis of brain tissue, follow Option C.

A. Lysis of HEK-293 cells ● **TIMING** ~30 min

(i) Lyse HEK-293 cells by repetitive pipetting up and down through a p1000 tip. Depending on the initial volume of cells, either a 5- or 10-ml pipette with a p1000 tip stuck on the end (Fig. 3b), or directly a p1000 micropipette should be used. The pipetting should be done on ice, for 1 min every 5 min, for 10 min (3 times).

(ii) Continue pipetting the solution using a p200 tip stuck on the p1000 tip (Fig. 3b) on ice, for 1 min every 5 min for 20 min.

(iii) Take an aliquot of 1/100th volume of the lysis mix (L) for analyses (200 µl for 20 ml of L). Add the same volume of Laemmli buffer 2× and boil for 5 min.

■ **PAUSE POINT** The L sample can be stored at -20°C for up to 1 year. Once all samples are collected, the quality of the purification is determined in Step 42 (see Box 2).

B. Lysis of Hela S3, Hela and U-2 OS cells ● **TIMING** ~30 min

(i) Lyse Hela S3 cells (from spinner culture) using a French press (set at medium ratio, gauge pressure at 1,000 psi), or an equivalent cell lysis equipment. For adherently grown cells (Hela, U-2 OS), sonicate cells gently, using the 6.5-mm diameter probe, set at "Output control" 1, "Duty cycle" 10% and for around 45 pulses. Sonicate the cells in a 14-ml round-bottom tube, which has been cut in height to accommodate the probe.

▲ **CRITICAL STEP** The sonication should be gentle, to avoid damaging the tubulin, but sufficient to lyse the cells. Check the lysis of the cells every 15 pulses (Fig. 3c).

(ii) Pipette cells through a p200 tip stuck on the p1000 tip (Fig. 3b) on ice, for 1 min every 5 min for 10 min.

(iii) Take an aliquot of 1/100th volume of the lysis mix (L) for analyses (200 µl for 20 ml of L). Add the same volume of Laemmli buffer 2× and boil for 5 min.

■ **PAUSE POINT** The L sample can be stored at -20°C for up to 1 year. Once all samples are collected, the quality of the purification is determined in Step 42 (see Box 2).

C. Lysis of brain tissue ● **TIMING** ~30 min

(i) Homogenize the brains with an Ultra-Turrax blender equipped with a small, ∅~5-mm probe. The mix should have the colour and consistency of a strawberry

milkshake. Alternatively, homogenize brain tissue using a potter homogenizer or a microtube potter, followed by thorough tissue dissociation using rapid pipetting up-and-down in a 1-ml syringe with a 18G needle.

(ii) Take an aliquot of 1/100th volume of the lysis mix (L) for analyses (200 µl for 20 ml of L). Add the same volume of Laemmli buffer 2× and boil for 5 min.

■ **PAUSE POINT** The L sample can be stored at -20°C for up to 1 year. Once all samples are collected, the quality of the purification is determined in Step 42 (see Box 2).

Lysate clarification ● **TIMING** 40 - 50 min

3. Clear lysate by centrifugation at 150,000×g, 4°C, 30 min. Choose adequate tubes and rotors: Beckman #357448 for volumes up to 1.5 ml (rotor TLA-55), Beckman #349622 for volumes up to 3.0 ml (rotor TLA-100.3) or Beckman #355631 for volumes up to 30 ml (rotor 70.1 Ti). Beckman #355631 tubes can be centrifuged half-filled, however, for volumes below 10 ml, we recommend using several Beckman #349622 tubes.

4. Remove the supernatant SN1 by following Option A for cell extracts and Option B for brain extracts.

A. Cell extracts: ● **TIMING** ~20 min

(i) ~~I~~Remove the supernatant gently and without perturbing the floating layer, using a syringe with a needle. For volumes below 4 ml use a 20G needle on a 5-ml syringe, for higher volumes use the long, 21G needle on a syringe of appropriate volume.

▲ **CRITICAL STEP** To avoid stirring the solution, remove the supernatant directly when taking tubes out of the centrifuge (instead of carrying them to the bench or placing them in an ice box).

(ii) Enter the needle into the supernatant and slowly soak off the liquid by gently moving the needle tip down toward the pellet. As soon as you observe soaking of the floating layer into the syringe, stop. It is important to remove all supernatant at once; going back and forth with the needle leads to rapid contamination of the clear supernatant.

(iii) Record the volume of SN1. For a 10-ml cell pellet, SN1 should be ~12 ml.

▲ **CRITICAL STEP** Removing clear supernatant is straightforward for brain lysates, from which solid pellets are obtained. It is more difficult for cell extracts,

which yield very unsteady pellets, and a floating instable layer of material on the top of the supernatant. This material should not be transferred to the next step, as it tends to interfere with the efficiency of tubulin polymerisation.

(iv) ***(Optional)*** If despite your efforts, the supernatant is cloudy, transfer it to a 15- or 50-ml tube and centrifuge at 5,000×g, 4°C for 10 min (Fig. 3d).

B. Brain extracts: ● **TIMING** ~10 min

(i) Place the tubes on ice. Remove the supernatant (SN1) with a micropipette of the right volume.

(ii) ***(Optional)*** If the supernatant is cloudy, transfer it to a 15- or 50-ml tube and centrifuge at 5,000×g, 4°C for 10 min (Fig. 3d).

5. Take an aliquot of 1/100th volume of the SN1for analyses (120 µl for 12 ml of SN1). Add the same volume of Laemmli buffer 2× and boil for 5 min.

■ **PAUSE POINT** The SN1 sample can be stored at -20°C for up to 1 year. Once all samples are collected, the quality of the purification is determined in Step 42 (see Box 2).

■ ~~**PAUSE POINT**~~

▲ **CRITICAL STEP** Do not freeze the clarified lysates. Proceed at least until step 10.

6. Resuspend the pellet P1 in BRB80 (use the same volume as SN1), and keep an aliquot of 1/100th of its volume (~200 µl for ~20 ml of P1) for analyses. Add the same volume of Laemmli buffer 2× and boil for 5 min. Discard the remaining P1.

■ **PAUSE POINT** The P1 sample can be stored at -20°C for up to 1 year. Once all samples are collected, the quality of the purification is determined in Step 42 (see Box 2).

First polymerisation in low-molarity buffer ● **TIMING** ~1 h

7. Prepare the polymerization mix in a screw-cap tube of appropriate volume at room temperature:

- 1 volume SN1 (12 ml)
- 1/200th volume 0.2-M GTP (60 µl), final concentration 1 mM
- 0.5 volume glycerol (6 ml), pre-heated to 30°C (glycerol volume is not considered in calculations, as it is used as a crowding agent).

8. Mix well, avoiding air bubbles, and transfer to one or several room temperature ultracentrifuge tubes of the appropriate volume. Equilibrate the weight of tubes in the process (in pairs).

▲ **CRITICAL STEP** Proceeding to the polymerisation step directly in centrifuge tubes equilibrated for centrifugation avoids the risk of depolymerising microtubules when pipetting the solution after polymerisation.

9. Cover the tubes with parafilm and transfer them to a 30°C water bath. Let polymerise for 20 min.

▲ **CRITICAL STEP** In our hands, the efficiency of polymerisation is equivalent at 30°C and 37°C, which is why we opted for 30°C. We restricted the polymerisation time to 20 min (max. 30 min), as longer incubation did not increase yields.

10. Spin down polymerised microtubules at 150,000×g, at 30°C, for 30 min. The pellet P2 (Fig. 3d) contains polymerised microtubules with associated MAPs, as well as other precipitated proteins. The supernatant SN2 contains non-polymerised tubulin and other soluble proteins which do not bind microtubules.

■ **PAUSE POINT** The microtubule pellet can be snap-frozen in liquid nitrogen and stored at -80°C for up to 1 year.

? **TROUBLESHOOTING**

11. Take an aliquot of 1/200th of the SN2 for analyses (90 µl for 18 ml of SN2). Add 90 µl of Laemmli buffer 2× and boil for 5 min. The remaining SN2 can be discarded.

■ **PAUSE POINT** The SN2 sample can be stored at -20°C for up to 1 year. Once all samples are collected, the quality of the purification is determined in Step 42 (see Box 2).

First depolymerisation ● **TIMING** ~1 h

12. Transfer the tube with the microtubule pellet P2 on ice, and add 1/60th (= 200 µl, for tubulin from cells) or 1/20th (= 600 µl, for tubulin from brains) volume of SN1 (=12 ml) of ice-cold BRB80, leave on ice for 5 min.

13. Pipette vigorously up and down with a p1000 micropipette to resuspend and depolymerise microtubules. Avoid air bubbles. (Fig. 3d)

14. Continue pipetting up and down with a p200 micropipette until the suspension is homogenous. Leave on ice for 20-30 min, pipet up and down every 5 min.
▲ **CRITICAL STEP** The high efficiency of this step is fundamental for the overall yield of the tubulin purification. Give it time and patience it needs.

15. Transfer the tubulin-MAP solution to a cold 1.5-ml Beckman #357448 tube. Spin down insoluble components at 150,000×g, 4°C for 20 min. The supernatant SN3 (~200 µl) contains the depolymerised tubulin, MAPs and potentially other soluble proteins. The pellet (P3) contains non-depolymerised microtubules, MAPs, and precipitated proteins.

16. Transfer SN3 to a new 1.5-ml conical tube on ice. Take an aliquot of 1-4 µl of the SN3 for analyses. Add 9 volumes of Laemmli buffer 2× and boil for 5 min.
■ **PAUSE POINT** The SN3 sample can be stored at -20°C for up to 1 year. Once all samples are collected, the quality of the purification is determined in Step 42 (see Box 2).
■ ~~**PAUSE POINT**~~
▲ **CRITICAL STEP** Do not freeze the SN3. Proceed at least until step 22.

17. Resuspend the pellet P3 in BRB80 (use the same volume as SN3), and keep an aliquot of 1-4 µl for analyses. Add 9 volumes of Laemmli buffer 2× and boil for 5 min. The rest of P3 can be discarded.
■ **PAUSE POINT** The P3 sample can be stored at -20°C for up to 1 year. Once all samples are collected, the quality of the purification is determined in Step 42 (see Box 2).

(Optional) Enzymatic treatment of the tubulin ● **TIMING** 10 min - 1 h

18. Incubate SN3 (200 µl) with 1/500th (vol/vol; 0.4 µl ≈ 0.7 U) of Carboxypeptidase A (CPA) for 5 min at 30°C in order to obtain entirely detyrosinated tubulin.
■ ~~**PAUSE POINT**~~
▲ **CRITICAL STEP** Do not freeze the SN3. Proceed at least until step 22.

Second polymerisation in high-molarity buffer ● **TIMING** ~1 h

19. Prepare the high-molarity polymerization mix in a 1.5-ml Beckman #357448 tube at room temperature:

- 1 volume SN3 (200 µl)
- 1 volume 1 M PIPES (200 µl), (pre-heated to 30°C), final concentration 0.5 M
- 1/100th volume 0.2 M GTP (2 µl), final concentration 1 mM
- 1 volume glycerol (200 µl), pre-heated to 30°C (glycerol volume is not considered in calculations, as it is used as a crowding agent)

20. Mix well, avoiding air bubbles, and transfer to one or several room-temperature 1.5-ml Beckman #357448 ultracentrifuge tubes. Pipette precise volumes for rotor equilibration.

▲ **CRITICAL STEP** Proceeding to the polymerisation step directly in centrifuge tubes of equilibrated weight avoids the risk of depolymerising microtubules when pipetting the solution after polymerisation.

21. Polymerize for 20 min in a 30°C water bath.

▲ **CRITICAL STEP** In our hands, the efficiency of polymerisation is equivalent at 30°C and 37°C, which is why we opted for 30°C. We restricted the polymerisation time to 20 min (max. 30 min), as longer incubation did not increase yields.

22. Sediment polymerised microtubules at 150,000×g, 30°C for 30 min. The pellet P4 contains polymerised microtubules. The supernatant SN4 contains the MAPs, and small amounts of non-polymerised tubulin and other soluble proteins (Fig. 3d).

■ **PAUSE POINT** The microtubule pellet can be snap-frozen in liquid nitrogen and stored at -80°C for up to 1 year.

▲ **CRITICAL STEP** Remove the supernatant very carefully, in order to eliminate a maximum of MAPs from the microtubule pellet. Note that with each polymerisation cycle the amount of non-polymerising tubulin, as well as non-depolymerisable microtubules decreases.

■ **PAUSE POINT** For further use of MAPs, SN4 can be snap-frozen in liquid nitrogen and stored at -80°C for up to 3 years. As MAPs are in the polymerisation buffer containing high PIPES and glycerol, a buffer exchange is required before further use.

? **TROUBLESHOOTING**

23. Take an aliquot of 1-4 µl of the SN4 for analyses. Add 9 volumes of Laemmli buffer 2× and boil for 5 min.

■ **PAUSE POINT** The SN4 sample can be stored at -20°C for up to 1 year. Once all samples are collected, the quality of the purification is determined in Step 42 (see Box 2).

Second de-polymerisation ● **TIMING** ~50 min

24. Transfer the tube with the microtubule pellet P4 on ice, and add 1/100th (= 120 µl, for tubulin from cells) or 1/40th (= 300 µl, for tubulin from brains) of the volume of SN1 (= 12 ml) of ice-cold BRB80 on the microtubule pellet P4, leave on ice for 5 min.

25. To resuspend and depolymerise microtubules, pipette up and down with a p200 micropipette. Avoid air bubbles.

26. Continue until the suspension is homogenous. Leave on ice for 20 min, pipet up and down every 5 min.

27. Transfer the tubulin solution to a cold 1.5-ml Beckman #357448 tube. Spin down insoluble components at 150,000×g, 4°C for 20 min.

28. The supernatant SN5 contains almost exclusively depolymerised tubulin. The pellet P5 (Fig. 3d) contains non-depolymerised microtubules. Transfer SN5 to a new 1.5-ml conical tube on ice.

29. Take an aliquot of 1-4 µl of the SN5 for analyses. Add 9 volumes of Laemmli buffer 2× and boil for 5 min.

■ **PAUSE POINT** The SN5 sample can be stored at -20°C for up to 1 year. Once all samples are collected, the quality of the purification is determined in Step 42 (see Box 2).

■ ~~**PAUSE POINT**~~

▲ **CRITICAL STEP** Do not freeze the SN5. Proceed at least until step 34.

30. Resuspend the pellet P5 in BRB80 (use the same volume as SN5), and keep an aliquot of 1-4 µl for analyses. Add 9 volumes of Laemmli buffer 2× and boil for 5 min. The rest of P5 can be discarded.

■ **PAUSE POINT** The P5 sample can be stored at -20°C for up to 1 year. Once all samples are collected, the quality of the purification is determined in Step 42 (see Box 2).

Third polymerisation in low-molarity buffer and warm spin ● **TIMING** ~1 h

▲ **CRITICAL** The third polymerisation-depolymerisation cycle (Steps 31-43) can also be performed directly before the use of the tubulin for the actual in vitro experiments.

31. Prepare the polymerization mix in a 1.5-ml Beckman #357448 tube at room temperature:

- 1 volume SN5 (120 µl)
- 1/200th volume 0.2 M GTP (0.6 µl), final concentration 1 mM
- 0.5 volume glycerol (60 µl), pre-heated to 30°C

32. Mix well, avoiding air bubbles, and transfer to one or several room-temperature 1.5-ml Beckman #357448 ultracentrifuge tubes. Pipette precise volumes for rotor equilibration.

▲ **CRITICAL STEP** Proceeding to the polymerisation step directly in centrifuge tubes of equilibrated weight avoids the risk of depolymerising microtubules when pipetting the solution after polymerisation.

33. Polymerize for 20 min in a 30°C water bath.

▲ **CRITICAL STEP** In our hands, the efficiency of polymerisation is equivalent at 30°C and 37°C, which is why we opted for 30°C. We restricted the polymerisation time to 20 min (max. 30 min), as longer incubation did not increase yields.

34. Sediment polymerised microtubules at 150,000×g, 30°C for 30 min. The pellet P6 contains polymerised microtubules. The supernatant SN6 contains small amounts of non-polymerised tubulin.

■ **PAUSE POINT** The microtubule pellet can be snap-frozen in liquid nitrogen and stored at -80°C for up to 1 year.

35. Take an aliquot of 1-4 µl of the SN6 for analyses. Add 9 volumes of Laemmli buffer 2× and boil for 5 min. The rest of SN6 can be discarded.

■ **PAUSE POINT** The SN6 sample can be stored at -20°C for up to 1 year. Once all samples are collected, the quality of the purification is determined in Step 42 (see Box 2).

Third depolymerisation ● **TIMING** ~50 min

36. Transfer the tube with the microtubule pellet P6 on ice, and add 1/100th (= 120 µl, for tubulin from cells) or 1/40th (= 300 µl, for tubulin from brains) of the volume of SN1 (= 12 ml) of ice-cold BRB80 on the microtubule pellet P6, leave on ice for 5 min.

37. Pipette vigorously up and down with a p200 micropipette to resuspend and depolymerise microtubules. Avoid air bubbles.

38. Continue pipetting up and down with a p20 pipette until the suspension is homogenous. Leave on ice for 20-30 min, pipet up and down every 5 min.

39. Transfer the tubulin solution to a cold 1.5-ml Beckman #357448 tube. Spin down insoluble components at 150,000×g, 4°C for 20 min. The supernatant SN7 contains pure, depolymerised tubulin. The pellet P7 contains non-depolymerised microtubules. Transfer SN7 to a new 1.5-ml conical tube on ice.

40. Take an aliquot of 1-4 µl of the SN7 for analyses. Add 9 volumes of Laemmli buffer 2× and boil for 5 min.

■ **PAUSE POINT** The SN7 sample can be stored at -20°C for up to 1 year. Once all samples are collected, the quality of the purification is determined in Step 42 (see Box 2).

41. Resuspend the pellet P7 in BRB80 (use the same volume as SN7), and keep an aliquot of 1-4 µl for analyses. Add 9 volumes of Laemmli buffer 2× and boil for 5 min. The rest of P7 can be discarded.

■ **PAUSE POINT** The P7 sample can be stored at -20°C for up to 1 year. Once all samples are collected, the quality of the purification is determined in Step 42 (see Box 2).

42. Quantify protein content of SN7 (see Box 2 for more details). ● **TIMING** 10 min – 3 h

43. Aliquot SN7 into small volumes to avoid future thaw-freeze cycles, snap-freeze in liquid nitrogen and store at -80°C. ● **TIMING** 10 – 30 min

■ **PAUSE POINT** Purified tubulin samples can be stored at -80°C until needed. We have not observed any decrease in polymerisation-activity after storing for up to 5 years.

Box 1: Transfection and drug treatment of adherently growing cells. TIMING: 1-4h

Transfection with plasmid DNA using the JetPEI® reagent

(*note that Hela S3 cells are very difficult to transfect using the here-described protocol*)

1. Seed cells the day before the transfection, so that they are at ~75% confluence.
2. Mix the JetPEI® reagent gently by inverting the tube. For each 15-cm dish, dilute 50 µl of jet PEI® in 450 µl of plain DMEM medium (without any supplement). Prepare the total volume needed depending on the number of dishes (500 µl of JetPEI® in 4.5 ml of DMEM if 10 dishes are used).
3. Mix well, spin shortly to collect the whole volume at the bottom of the tube, and leave under the hood for 5 min.
4. Dilute 25 µg of plasmid DNA in 500 µl of plain DMEM per one dish. Prepare the total volume needed for all dishes (250 µg of DNA in 5 ml of DMEM for 10 dishes).
5. Add the diluted jetPEI® into the diluted DNA and vortex vigorously for 15 s. Leave under the hood for 15-30 min before transfection, without exceeding 30 min.

▲ **CRITICAL STEP** Always add the diluted jetPEI® into diluted DNA, and not the other way around. Strictly observe vortexing time. This is essential to form transfection-efficient DNA-jetPEI® complexes.

6. During the 15-min waiting time, replace the complete medium of the cells with the fresh, pre-heated medium.
7. Gently tap the DNA-jetPEI® mix from step 5 and add 1 ml of it dropwise onto each dish. Mix by swirling gently and return to the incubator.

Drug treatment

1. Prepare the drug at the right dilution. For trichostatin A (TSA), an inhibitor of the tubulin deacetylase HDAC6[48,49], add 1.2 µl of 10 mM TSA to 12 ml of fresh medium, per dish (final concentration of 1 µM). Prepare enough TSA depending on the number of dishes (12 µl of 10 mM TSA in 120 ml of medium if 10 dishes are used).
2. Leave the drug on the cells for the desired time, depending on the drug. For trichostatin A (TSA), cells are exposed to the drug for 4 h in the cell culture incubator prior to cell harvest.

Box 2: Analysis of the obtained tubulin. TIMING: 10 min – 3 h

The enrichment of tubulin can be followed throughout the purification procedure using a Coomassie-stained SDS-PAGE gel (Step 2). We also suggest quantifying obtained tubulin on an SDS-PAGE gel (Step 3), because in our hands, spectrometry methods do not give a good reading of the tubulin concentration. The tubulin sample can be further analysed for the presence of expected tubulin isotypes or PTMs by immunoblotting (Step 4). We recommend using the custom-made "TUB" gels, which allow the separation of α- and β-tubulins[50] (see Reagent Setup section).

Procedure:

1. **Analysis sample preparation**

   The volume of the sample collected from each step of the main procedure, but especially from the latest steps, where the volume of the sample can be very limited, depends on the extent of analysis needed (see Table below). If only purification success (Step 2) and quantification (Step 3) are envisaged, a 1-µl sample from each of these steps is sufficient. In case immunoblot analysis (Step 4) is necessary, it is useful to collect up to 4 µl of the solution, giving the possibility to run several SDS-PAGE gels. Add the same volume of 2x Laemmli sample buffer to each sample and boil the sample for 5 min.

   ■ **PAUSE POINT** The samples can be stored at -20°C for up to 3 years

Fraction		**Sample**				**Loading**	
Fraction name	**Total fraction volume**	**Amount (part) collected**	**Volume collected**	**Volume of 2x Laemmli sample buffer added**	**Further dilution in 2x Laemmli sample buffer**	**Volume of the fraction to be loaded (1/2,400th of the total fraction volume)**	**Volume of the sample to load on the gel**
L, P1	20 ml	1/100th	200 µl	200 µl	-	8.33 µl	16.67 µl
SN1	12 ml	1/100th	120 µl	120 µl	-	5 µl	10 µl
SN2	18 ml	1/200th	90 µl	90 µl	-	7,5 µl	15 µl
P2, SN3, P3	200 µl	1/200th or 1/50th	1 or 4 µl	9 or 36 µl	10x	0.083 µl	8.3 µl
SN4	600 µl	1/600th or 1/150th	1 or 4 µl	9 or 36 µl	10x	0.25 µl	25 µl
SN6	180 µl	1/180th or	1 or 4 µl	9 or 36 µl	10x	0.075 µl	7.5 µl

		1/45th					
P4, SN5, P5, P6, SN7, P7	120 µl	1/120th or 1/30th	1 or 4 µl	9 or 36 µl	10x	0.05 µl	5 µl

2. Tubulin purification quality test

To verify the success and purity of the tubulin purified using this protocol, we use Coomassie-stained SDS-PAGE gels allowing to separate α- and β-tubulins and which have been described previousely[50] (see Reagent Setup section). Load an equal fraction of each sample from the purification steps (see Table above) to assess the enrichment of tubulin (Fig. 4a).

3. Quantification of the tubulin

We quantify the tubulin using standardised BSA samples. Load two quantities of the tubulin sample (for example 0.05 µl and 0.1 µl of the SN7) on an SDS-PAGE gel next to a range of different, known quantities of BSA protein (0.5 µg – 1 µg – 2 µg - 3 µg). After staining the gel with Coomassie brilliant blue and scanning it, deduce the concentrations of α- and β-tubulins in your sample using the linear regression of the BSA-band intensities. If using the "TUB" SDS-PAGE gels, note that α- and β-tubulins will have to be quantified separately.

▲ **CRITICAL STEP** Make sure the scanner is set to a linear range, and do not manipulate the contrast setting to allow a correct determination of relative intensities of the analysed bands.

4. Analysis of obtained tubulin by immunoblot (Fig. 4b-d)

In order to confirm the presence of desired tubulin PTMs, we recommend immunoblot analysis. Based on the quantification of the purified tubulin, load between 0.1 – 0.2 µg of tubulin on a "TUB" SDS-PAGE gel (allowing to separate α- and β-tubulins[50], see Reagent Setup section). As the antibodies towards tubulin PTMs are very specific and give strong signals already at low tubulin concentrations, it is crucial to load a small amount of the tubulin sample. We also avoid incubating the membranes with the antibodies for more than 2 h at room temperature. Always check the equal loading of your samples by performing an immunoblot with a PTM-independent anti-α-tubulin antibody (12G10) and include a positive control, for example brain tubulin.

? **TROUBLESHOOTING**

TIMING

Step 1, preparing tubulin source

Option A, cells grown in spinners: 10-13 days

Steps 1A(i-iii), cell amplification (on plates): 3-6 days

Steps 1A(iv-xi), inoculation of spinners: ~2 h

Step 1A(xii) cell growth in spinners: 7 days

Step 1A(xiii) (optional) cell treatment: ~20 min

Steps 1A(xiv-xx), harvesting cells: ~90 min

Option B, adherent cells: 5-6 days

Steps 1B(i-ii), cell amplification: 5-6 days

Step 1B(iii) Box 1, treatment of cells: 1-4 h

Steps 1B(iv-xi), harvesting cells: ~1 h

Option C, mouse brain: 15 min (not considering the time necessary to breed the donor mouse)

Step 2, lysis

Option A, HEK-293 cells: ~30 min

Option B, Hela S3 cells: ~30 min

Option C, mouse brain: ~30 min

Step 3-6, lysate clarification: 40-50 min

Option A, ell extracts: ~50 min

Option B, brain extracts ~40 min

Steps 7-11, first polymerisation and warm spin: ~1 h

Steps 12-17, first de-polymerisation and cold spin: ~1 h

Step 18, (*optional*) enzymatic treatment: 10 min – 1 h

Steps 19-23, second polymerisation and warm spin: ~1 h

Steps 24-30, second de-polymerisation and cold spin: ~50 min

Steps 31-35, third polymerisation and warm spin: ~1 h

Steps 36-41, third de-polymerisation and cold spin: ~50 min

Step 42, Box 2, quantification of obtained tubulin: 10 min – 3 h

Step 43, aliquoting and snap freezing: 10-30 min

TROUBLESHOOTING

Troubleshooting guidance can be found in **Table 1.**

Table 1. Troubleshooting Table

step	problem	Possible reason	Possible solution
1A(xii)	Large cell aggregates (Fig. 2b,c)	Too low rotation speed in spinner cultures	Increase the speed of rod rotation
	Lack of cell growth	Closed lateral spinner flask caps	Open the lateral caps slightly (half a turn) to allow air exchange
	Bacterial or fungal contamination	Contamination carried inside the cell culture hood via media or spinner bottles	Clean all bottles with 70% ethanol before transferring them under the hood
		Manipulation (transfer between the bottle and the spinner flasks) of large quantities of media	Manipulate media with more care; avoid spilling the medium
1B(vi)	Lysis of cells during detachment from plastic dishes	Too brutal treatment of cells	Collect the cells by gently lifting/shovelling them to one side of the dish
		Too slow detachment of cells	Prepare all the necessary material in forehand and ask two colleagues for help with this part of the procedure
10	Large pellet after 1st polymerisation, but devoid of tubulin	Insufficient clearing of the lysate in step 4B(iii)	Collect only clear supernatant in step 4. Further clarify the supernatant by centrifugation in step 4B(iii).
	No microtubule pellet after 1st polymerisation	Insufficient tubulin concentration due to incomplete lysis in step 2	Verify the lysis of the cells and extend incubation time at 4°C prior to clarification in step 2
		Incorrect cell treatment prior to lysis in step 1B(vi)	Speed up cell collection procedure and avoid breaking the cells before the lysis step 1B(vi)
		Insufficient tubulin concentration in the cell extract	Lysis buffer volume should not exceed the volume of the cell pellet in steps 1A(xx); 1B(x)
		Hydrolysed GTP	Use a fresh aliquot of GTP
		Reaction carried out at wrong temperature	Check the temperature of the water-bath with a thermometer
22	No microtubule pellet after 2nd polymerisation	Insufficient tubulin concentration after 1st depolymerisation	Depolymerise tubulin in lower volume in step 12
		Incomplete tubulin de-polymerisation in steps 12-14	Repeat the depolymerisation procedure in steps 12-15 on the pellet P3 from step 15
Box 2 Step 4	Lack of expected modification on purified tubulin	Failed transfection of cells or drug treatment	Use freshly thawed cells, check the quality of plasmid DNA, adapt drug treatment protocol
		Overloading of the SDS-PAGE	Dilute the sample to load 0.2-

		gel with the sample	0.5 µg of tubulin

ANTICIPATED RESULTS

The key application of the here-described tubulin purification protocol are advanced *in vitro* reconstitutions of microtubule assemblies using tubulin purified from cell lines or mouse brains with controlled tubulin PTMs. The rationale of our approach was to adapt the method considered the gold standard for tubulin purification; the repeated polymerisation and depolymerisation of brain tubulin, to purify tubulin from other sources. Using our protocol, we obtain reproducible high-quality, highly pure tubulin (Fig. 4a). Due to the relatively small sample sizes (as compared to the previously used brain-tubulin purification), our protocol shows some variations in yield, but never in quality.

If initially posttranslationally modified, the tubulin purified by our protocol maintains all of the commonly studied PTMs (Fig. 4b-d), and can therefore be used to compare differentially modified microtubules side-by-side[20,21]. However, it should be kept in mind, and eventually tested, that the repeated polymerisation and depolymerisation cycles could bias the composition of the final tubulin. For quantitative analyses of the tubulin composition in cells and tissues, the method by Widlund et al.[29] should be used.

The quantities of tubulin obtained by our protocol are sufficient for a wide range of applications. Using a set of four spinner bottles that are maintained continuously, which is possible with Hela S3 cells that can be constantly diluted without adherent pre-cultures, a laboratory can produce ~2 mg of tubulin per week with a work input of about one day for the tubulin purification. This work load could be even further reduced by collecting cells at -80°C and for a larger-scale tubulin purification. For most TIRF-microscopy based assays, only µg-amounts of tubulin are needed, thus, the PTM-free Hela S3 tubulin produced by this protocol could fully replace brain tubulin for an entire research team. Even classic microtubule co-sedimentation assays, though more tubulin-consuming, require ~100 µg of pure tubulin for one dilution series[51,52], and can thus easily be performed with tubulin purified with our protocol.

The yield of tubulin from single mouse brains is also sufficient to perform virtually all known *in vitro* approaches, given that the mouse strain is easy to breed and sufficient numbers of brains can be obtained. The great advantage of purifying tubulin from a single mouse brain is that biological replicates can be introduced in the *in-vitro* approach; as multiple tubulin samples from individual mouse brains can be used side-by-side.

The most work-intense approach is the purification of tubulin from adherently growing cells. The great advantage of this approach is that it allows to generate virtually any type of posttranslationally modified tubulin, given the availability of a wide range of modifying enzymes[53-60]. We recommend to use this method after only an assay has duly be established using brain tubulin or non-modified tubulin from cells grown in spinner cultures, which are easier to produce.

Our protocol thus could allow research teams that perform *in vitro* reconstitution assays to fully replace brain tubulin by Hela S3 tubulin, a tubulin free of PTMs and exotic tubulin isotypes, on a daily basis. By expanding the protocol to the purification of tubulin modified with a variety of PTMs, their role can now be directly studied *in vitro*, which was so far virtually impossible. The proof of principle has been provided by the direct comparison of fully tyrosinated and fully detyrosinated Hela S3 tubulin in single-molecule motility assays and force measurements for the kinetochore kinesin CENP-E[20], binding assays of neuronal kinesin motors[22], or in transport assays with purified neuronal transport vesicles[21]. These examples demonstrate that PTM-free tubulin obtained by our protocol could be a valid replacement of the so-far used brain tubulin in all currently used *in vitro* reconstitution assays.

ACKNOWLEDGEMENTS

We thank all members of the Janke lab for help during the establishment of the protocol. We would like to thank the animal facility of the Institut Curie for help with mouse breeding and care. This work has received support under the program “Investissements d’Avenir” launched by the French Government and implemented by ANR with the references ANR-10-LBX-0038, ANR-10-IDEX-0001-02 PSL. The work of CJ was supported by the Institut Curie, the French National Research Agency (ANR) award ANR-12-BSV2-0007, the Institut National du Cancer (INCA) grants 2013-1-PL BIO-02-ICR-1 and 2014-PL BIO-11-ICR-1, the Fondation pour la Recherche Medicale (FRM) grant DEQ20170336756, and the CEFIPRA research project 5703-1. MMM is supported by the EMBO short-term fellowship ASTF 148-2015 and by the Fondation Vaincre Alzheimer grant FR-16055p. JS was supported by the FRM fellowship SPF20120523942, and the EMBO ALTF 638-2010 and EMBO ASTF 445-2012. SB was supported by the FRM grant FDT201805005465. JAS was supported by the European Union’s Horizon 2020 research and innovation programme under the Marie Skłodowska-Curie grant agreement No 675737. The antibody 12G10, developed by J. Frankel and M. Nelson, was obtained from the Developmental Studies Hybridoma Bank developed under the auspices of the NICHD and maintained by the University of Iowa.

AUTHOR CONTRIBUTION

J.S. and M.M.M. established, with the help of G.L. and A.G., the spinner cultures for various cell lines and adapted the tubulin purification protocol to spinner-grown cells. S.B. and M.M.M. established the tubulin prep from adherent cells. S.B., M.M.M. and J.A.S. contributed to improving the protocol of the tubulin prep from large cell quantities. M.M.M. established the tubulin prep protocol from single mouse brains. M.M.M. and C.J. supervised the development of this method and wrote the manuscript. All the authors contributed to corrections of the text and figures.

COMPETING FINANCIAL INTEREST STATEMENT

The authors declare that they have no competing financial interests.

DATA AVAILABILITY STATEMENT

The data that support the findings of this study are available from the corresponding author upon reasonable request.

Figure 1: Flow scheme of the tubulin purification protocol.

Different steps of the tubulin purification are schematically depicted. After the lysis and lysate clarification (Steps 2-4), the first polymerisation is carried out in low-molarity conditions (low-molarity pol; polymerisation 1, Steps 7-10). Microtubules are then pelleted, depolymerised, and soluble tubulin is clarified (depolymerisation 1, Steps 12-15). Soluble tubulin is then subjected to a high-molarity polymerisation, excluding the MAPs (polymerisation and depolymerisation 2, Steps 19-28). After polymerisation 2 it is possible to purify microtubule-associated proteins (MAPs). Tubulin can be further subjected to a third, low-molarity polymerisation followed by depolymerisation (polymerisation and depolymerisation 3, Steps 31-39), in order to completely remove the high-molarity buffer from polymerisation 2. The temperature of the step is indicated by the background colour. The nature of the discarded fraction is indicated as well as the possible pause points (optional freezing steps) and additional treatment. Approximative timing of the procedure is also given.

Figure 2: Growing Hela S3 and HEK-293 cells in spinner cultures for tubulin purification.

a. Overview of the spinner culture (step 1A): Cells are first grown on 15-cm plates to 80-90% confluence. They are then detached, thoroughly dissociated and inoculated in spinner bottles. The bottles are then incubated for 7 days in a cell culture incubator equipped with a rotating table. Optionally, cells can be treated one or two days before being harvested and proceeded for the tubulin purification (see Fig. 3). **b.** Close-up view of the spinners with medium only, just after inoculation (Step 1A(xi)), and after 7 days of culture of Hela S3 and HEK-293 cells (Step 1A(xii)). Note the homogeneous aspect of Hela S3 culture after 7 days, in contrast to the aggregates formed by HEK-293 cells. These cell aggregates are visible to naked eye. **c.** Representative images of Hela S3 and HEK-293 cells grown on plastic dishes (Step 1A(iv)), after spinner inoculation (Step 1A(xi)) and after 7 days in the spinners (Step 1A(xii)). Note that HEK-293 form cell aggregates up to several hundred µm in diameter. Scale bar: 50 µm.

Figure 3: Tubulin purification from cells cultured in spinner bottles.

a. Harvesting the cells (Steps 1A(xiv-xx)): Cells grown for 7 days in spinners are transferred to 1-l bottles and pelleted. Cells are re-suspended in PBS and transferred to a 50-ml conical tube and pelleted again. The pellet volume is recorded and cells are re-suspended in the same

volume of lysis buffer. **b.** The set-up used to lyse the cells: while Hela S3 cells are broken using a French press, HEK-293 cells are lysed by repeated passages through a p1000 tip tightly fitted on a 5-ml pipette (step 2A(i)). Both HEK-239 and Hela S3 cell lysates are then repeatedly passed through a p200 tip fitted on a p1000 tip on a p1000 pipette (steps 2A(ii) and 2B(ii)). **c.** Representative images of Hela S3 and HEK-293 cells before and after lysis (steps 2A and 2B). Note the presence of cell debris (purple crosses) in the lysates. Scale bar 50 μm. **d.** Images of the purification process (steps 3-28): After ultracentrifugation, cleared cell lysates contains a white floating layer (→). If this material is transferred together with the supernatant, making it turbid (*), it can be efficiently clarified in a step of low-speed centrifugation. The first-polymerisation microtubule pellet has a white and uneven appearance (#). Following the first depolymerisation and cold centrifugation, a pellet is well visible ($). The second polymerisation gives a clear and transparent pellet (€). The second depolymerisation produces a very small, hardly visible microtubule pellet (>>).

Figure 4: Analyses of purified tubulin obtained from cell lines and mice brains.

a. Coomassie-stained acrylamide gel with samples of different steps throughout the tubulin purification procedure. Note the enrichment of α- and β-tubulin throughout the procedure until its pure fraction (P4), and the tubulin-free fraction containing only MAPs (SN4). Tubulin from P4 can be further submitted to depolymerisation – polymerisation cycles (not shown). **b.** Generation of totally tyrosinated and totally detyrosinated Hela S3 tubulin. Immunoblot analysis of purified pig brain, untreated Hela S3 tubulin, and Hela S3 tubulin treated with carboxypeptidase A (+CPA). While brain tubulin is a mixture of tyrosinated and detyrosinated tubulin, untreated Hela S3 tubulin is entirely tyrosinated. This tyrosinated tubulin is fully converted to detyrosinated tubulin by using CPA. **c.** Different patterns of tubulin polyglutamylation following overexpression of TTLL5 or TTLL7. Immunoblot analysis of tubulin purified from HEK-293 cells overexpressing polyglutamylases TTLL5 or TTLL7. Note that while HEK-293 cells have very low levels of tubulin polyglutamylation, TTLL5 overexpression leads to polyglutamylation of both α- and β-tubulin, while TTLL7 modifies only β-tubulin. **d.** Modification levels of tubulin purified from brains of wild-type, *atat1*$^{-/-}$ *and ttll1*$^{-/-}$ mice. Knockout of aTAT1, the tubulin acetyltransferase[59,60], leads to the loss of acetylation of lysine K40 of α-tubulin. TTLL1, main brain glutamylase[53], leads to a reduction of tubulin polyglutamylation. Note that a special acrylamide gels have been used,

which allow to separate α- and β-tubulin bands that usually co-migrate slightly above 50 kDa[50]. In **b**, **c** and **d** equal levels of total tubulin were verified with 12G10, an anti-α-tubulin antibody. Experimental procedures involving animals were specifically approved by the ethics committee of the Institut Curie CEEA-IC #118 (authorization no. 04395.03 given by National Authority) in compliance with the international guidelines.

REFERENCES

1 Borisy, G. G. & Taylor, E. W. The mechanism of action of colchicine. Binding of colchincine-3H to cellular protein. *J Cell Biol* **34**, 525-533 (1967).

2 Weisenberg, R. C. Microtubule formation in vitro in solutions containing low calcium concentrations. *Science* **177**, 1104-1105 (1972).

3 Borisy, G. G. & Olmsted, J. B. Nucleated assembly of microtubules in porcine brain extracts. *Science* **177**, 1196-1197 (1972).

4 Kirschner, M. W. & Williams, R. C. The mechanism of microtubule assembly in vitro. *J Supramol Struct* **2**, 412-428 (1974).

5 Margolis, R. L. & Wilson, L. Addition of colchicine-tubulin complex to microtubule ends: the mechanism of substoichiometric colchicine poisoning. *Proc Natl Acad Sci U S A* **74**, 3466-3470 (1977).

6 Murphy, D. B. & Borisy, G. G. Association of high-molecular-weight proteins with microtubules and their role in microtubule assembly in vitro. *Proc Natl Acad Sci U S A* **72**, 2696-2700 (1975).

7 Margolis, R. L. & Wilson, L. Opposite end assembly and disassembly of microtubules at steady state in vitro. *Cell* **13**, 1-8 (1978).

8 Mitchison, T. & Kirschner, M. Dynamic instability of microtubule growth. *Nature* **312**, 237-242 (1984).

9 Axelrod, D. Cell-substrate contacts illuminated by total internal reflection fluorescence. *J Cell Biol* **89**, 141-145 (1981).

10 Dogterom, M. & Surrey, T. Microtubule organization in vitro. *Curr Opin Cell Biol* **25**, 23-29 (2013).

11 Nedelec, F. J., Surrey, T., Maggs, A. C. & Leibler, S. Self-organization of microtubules and motors. *Nature* **389**, 305-308 (1997).

12 Bieling, P., Telley, I. A. & Surrey, T. A minimal midzone protein module controls formation and length of antiparallel microtubule overlaps. *Cell* **142**, 420-432 (2010).

13 Roostalu, J. *et al.* Directional switching of the kinesin Cin8 through motor coupling. *Science* **332**, 94-99 (2011).

14 Hendricks, A. G., Goldman, Y. E. & Holzbaur, E. L. F. Reconstituting the motility of isolated intracellular cargoes. *Methods Enzymol* **540**, 249-262 (2014).

15 Schaedel, L. *et al.* Microtubules self-repair in response to mechanical stress. *Nat Mater* **14**, 1156-1163 (2015).

16 Vallee, R. B. Reversible assembly purification of microtubules without assembly-promoting agents and further purification of tubulin, microtubule-associated proteins, and MAP fragments. *Methods Enzymol* **134**, 89-104 (1986).

17 Castoldi, M. & Popov, A. V. Purification of brain tubulin through two cycles of polymerization-depolymerization in a high-molarity buffer. *Protein Expr Purif* **32**, 83-88 (2003).

18 Wloga, D., Joachimiak, E., Louka, P. & Gaertig, J. Posttranslational Modifications of Tubulin and Cilia. *Cold Spring Harb Perspect Biol* **9** (2017).

19 Janke, C. The tubulin code: Molecular components, readout mechanisms, and functions. *J Cell Biol* **206**, 461-472 (2014).

20 Barisic, M. *et al.* Microtubule detyrosination guides chromosomes during mitosis. *Science* **348**, 799-803 (2015).

21 Nirschl, J. J., Magiera, M. M., Lazarus, J. E., Janke, C. & Holzbaur, E. L. F. alpha-Tubulin Tyrosination and CLIP-170 Phosphorylation Regulate the Initiation of Dynein-Driven Transport in Neurons. *Cell Rep* **14**, 2637-2652 (2016).

22 Guedes-Dias, P. *et al.* Kinesin-3 Responds to Local Microtubule Dynamics to Target Synaptic Cargo Delivery to the Presynapse. *Curr Biol* **29**, 268-282 e268 (2019).
23 Hiller, G. & Weber, K. Radioimmunoassay for tubulin: a quantitative comparison of the tubulin content of different established tissue culture cells and tissues. *Cell* **14**, 795-804 (1978).
24 Bulinski, J. C. & Borisy, G. G. Self-assembly of microtubules in extracts of cultured HeLa cells and the identification of HeLa microtubule-associated proteins. *Proc Natl Acad Sci U S A* **76**, 293-297 (1979).
25 Farrell, K. W. Isolation of tubulin from nonneural sources. *Methods Enzymol* **85 Pt B**, 385-393 (1982).
26 Banerjee, A., Roach, M. C., Trcka, P. & Ludueña, R. F. Preparation of a monoclonal antibody specific for the class IV isotype of beta-tubulin. Purification and assembly of alpha beta II, alpha beta III, and alpha beta IV tubulin dimers from bovine brain. *J Biol Chem* **267**, 5625-5630 (1992).
27 Newton, C. N. *et al.* Intrinsically slow dynamic instability of HeLa cell microtubules in vitro. *J Biol Chem* **277**, 42456-42462 (2002).
28 Lacroix, B. & Janke, C. Generation of differentially polyglutamylated microtubules. *Methods Mol Biol* **777**, 57-69 (2011).
29 Widlund, P. O. *et al.* One-step purification of assembly-competent tubulin from diverse eukaryotic sources. *Mol Biol Cell* **23**, 4393-4401 (2012).
30 Howes, S. C. *et al.* Structural differences between yeast and mammalian microtubules revealed by cryo-EM. *J Cell Biol* **216**, 2669-2677 (2017).
31 Pamula, M. C., Ti, S.-C. & Kapoor, T. M. The structured core of human beta tubulin confers isotype-specific polymerization properties. *J Cell Biol* **213**, 425-433 (2016).
32 Vemu, A., Atherton, J., Spector, J. O., Moores, C. A. & Roll-Mecak, A. Tubulin isoform composition tunes microtubule dynamics. *Mol Biol Cell* **28**, 3564-3572 (2017).
33 von Loeffelholz, O. *et al.* Nucleotide- and Mal3-dependent changes in fission yeast microtubules suggest a structural plasticity view of dynamics. *Nat Commun* **8**, 2110 (2017).
34 Chaaban, S. *et al.* The Structure and Dynamics of C. elegans Tubulin Reveals the Mechanistic Basis of Microtubule Growth. *Dev Cell* **47**, 191-204 e198 (2018).
35 Alper, J. D., Decker, F., Agana, B. & Howard, J. The motility of axonemal dynein is regulated by the tubulin code. *Biophys J* **107**, 2872-2880 (2014).
36 Minoura, I. *et al.* Overexpression, purification, and functional analysis of recombinant human tubulin dimer. *FEBS Lett* **587**, 3450-3455 (2013).
37 Vemu, A. *et al.* Structure and Dynamics of Single-isoform Recombinant Neuronal Human Tubulin. *J Biol Chem* **291**, 12907-12915 (2016).
38 Ti, S.-C., Alushin, G. M. & Kapoor, T. M. Human beta-Tubulin Isotypes Can Regulate Microtubule Protofilament Number and Stability. *Dev Cell* **47**, 175-190 e175 (2018).
39 Uchimura, S. *et al.* A flipped ion pair at the dynein-microtubule interface is critical for dynein motility and ATPase activation. *J Cell Biol* **208**, 211-222 (2015).
40 Denoulet, P., Eddé, B. & Gros, F. Differential expression of several neurospecific beta-tubulin mRNAs in the mouse brain during development. *Gene* **50**, 289-297 (1986).
41 Song, Y. *et al.* Transglutaminase and polyamination of tubulin: posttranslational modification for stabilizing axonal microtubules. *Neuron* **78**, 109-123 (2013).
42 Belvindrah, R. *et al.* Mutation of the alpha-tubulin Tuba1a leads to straighter microtubules and perturbs neuronal migration. *J Cell Biol* **216**, 2443-2461 (2017).

43 Breuss, M. *et al.* Mutations in the murine homologue of TUBB5 cause microcephaly by perturbing cell cycle progression and inducing p53 associated apoptosis. *Development* (2016).

44 Latremoliere, A. *et al.* Neuronal-Specific TUBB3 Is Not Required for Normal Neuronal Function but Is Essential for Timely Axon Regeneration. *Cell Rep* **24**, 1865-1879 e1869 (2018).

45 Magiera, M. M. *et al.* Excessive tubulin polyglutamylation causes neurodegeneration and perturbs neuronal transport. *EMBO J* **37**, e100440 (2018).

46 Morley, S. J. *et al.* Acetylated tubulin is essential for touch sensation in mice. *Elife* **5** (2016).

47 Kalebic, N. *et al.* Tubulin acetyltransferase alphaTAT1 destabilizes microtubules independently of its acetylation activity. *Mol Cell Biol* **33**, 1114-1123 (2013).

48 Hubbert, C. *et al.* HDAC6 is a microtubule-associated deacetylase. *Nature* **417**, 455-458 (2002).

49 Matsuyama, A. *et al.* In vivo destabilization of dynamic microtubules by HDAC6-mediated deacetylation. *Embo J* **21**, 6820-6831 (2002).

50 Magiera, M. M. & Janke, C. in *Methods Cell Biol* Vol. 115 *Microtubules, in vitro* (eds John J. Correia & Leslie Wilson) 247-267 (Academic Press, 2013).

51 Maurer, S. P., Bieling, P., Cope, J., Hoenger, A. & Surrey, T. GTP{gamma}S microtubules mimic the growing microtubule end structure recognized by end-binding proteins (EBs). *Proc Natl Acad Sci U S A* **108**, 3988-3993 (2011).

52 Sandblad, L. *et al.* The Schizosaccharomyces pombe EB1 homolog Mal3p binds and stabilizes the microtubule lattice seam. *Cell* **127**, 1415-1424 (2006).

53 Janke, C. *et al.* Tubulin polyglutamylase enzymes are members of the TTL domain protein family. *Science* **308**, 1758-1762 (2005).

54 van Dijk, J. *et al.* A targeted multienzyme mechanism for selective microtubule polyglutamylation. *Mol Cell* **26**, 437-448 (2007).

55 Rogowski, K. *et al.* Evolutionary divergence of enzymatic mechanisms for posttranslational polyglycylation. *Cell* **137**, 1076-1087 (2009).

56 Rogowski, K. *et al.* A family of protein-deglutamylating enzymes associated with neurodegeneration. *Cell* **143**, 564-578 (2010).

57 Aillaud, C. *et al.* Vasohibins/SVBP are tubulin carboxypeptidases (TCPs) that regulate neuron differentiation. *Science* **358**, 1448-1453 (2017).

58 Nieuwenhuis, J. *et al.* Vasohibins encode tubulin detyrosinating activity. *Science* **358**, 1453-1456 (2017).

59 Akella, J. S. *et al.* MEC-17 is an alpha-tubulin acetyltransferase. *Nature* **467**, 218-222 (2010).

60 Shida, T., Cueva, J. G., Xu, Z., Goodman, M. B. & Nachury, M. V. The major alpha-tubulin K40 acetyltransferase alphaTAT1 promotes rapid ciliogenesis and efficient mechanosensation. *Proc Natl Acad Sci U S A* **107**, 21517-21522 (2010).

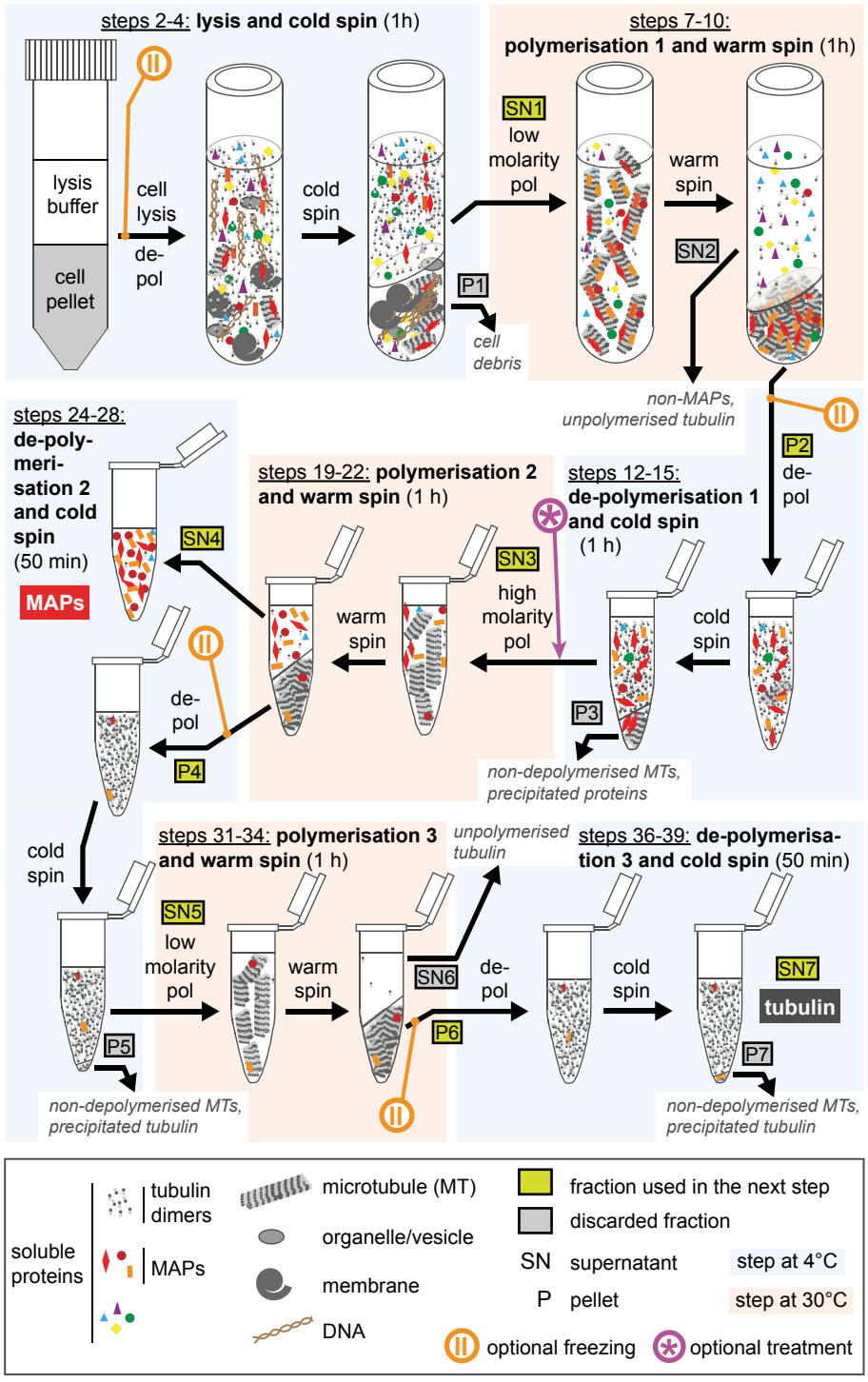
steps 2-4: lysis and cold spin (1h)
lysis buffer
cell pellet
cell lysis
de-pol
cold spin
P1
cell debris
steps 7-10: polymerisation 1 and warm spin (1h)
SN1
low molarity pol
warm spin
SN2
non-MAPs, unpolymerised tubulin
steps 24-28: de-poly-meri-sation 2 and cold spin (50 min)
MAPs
SN4
de-pol
P4
steps 19-22: polymerisation 2 and warm spin (1 h)
warm spin
SN3
high molarity pol
steps 12-15: de-polymerisation 1 and cold spin (1 h)
cold spin
P2
de-pol
P3
non-depolymerised MTs, precipitated proteins
cold spin
steps 31-34: polymerisation 3 and warm spin (1 h)
SN5
low molarity pol
warm spin
SN6
unpolymerised tubulin
de-pol
P6
steps 36-39: de-polymerisa-tion 3 and cold spin (50 min)
cold spin
SN7
tubulin
P7
P5
non-depolymerised MTs, precipitated tubulin
non-depolymerised MTs, precipitated tubulin
soluble proteins
tubulin dimers
MAPs
microtubule (MT)
organelle/vesicle
membrane
DNA
fraction used in the next step
discarded fraction
SN supernatant
P pellet
step at 4°C
step at 30°C
optional freezing
optional treatment

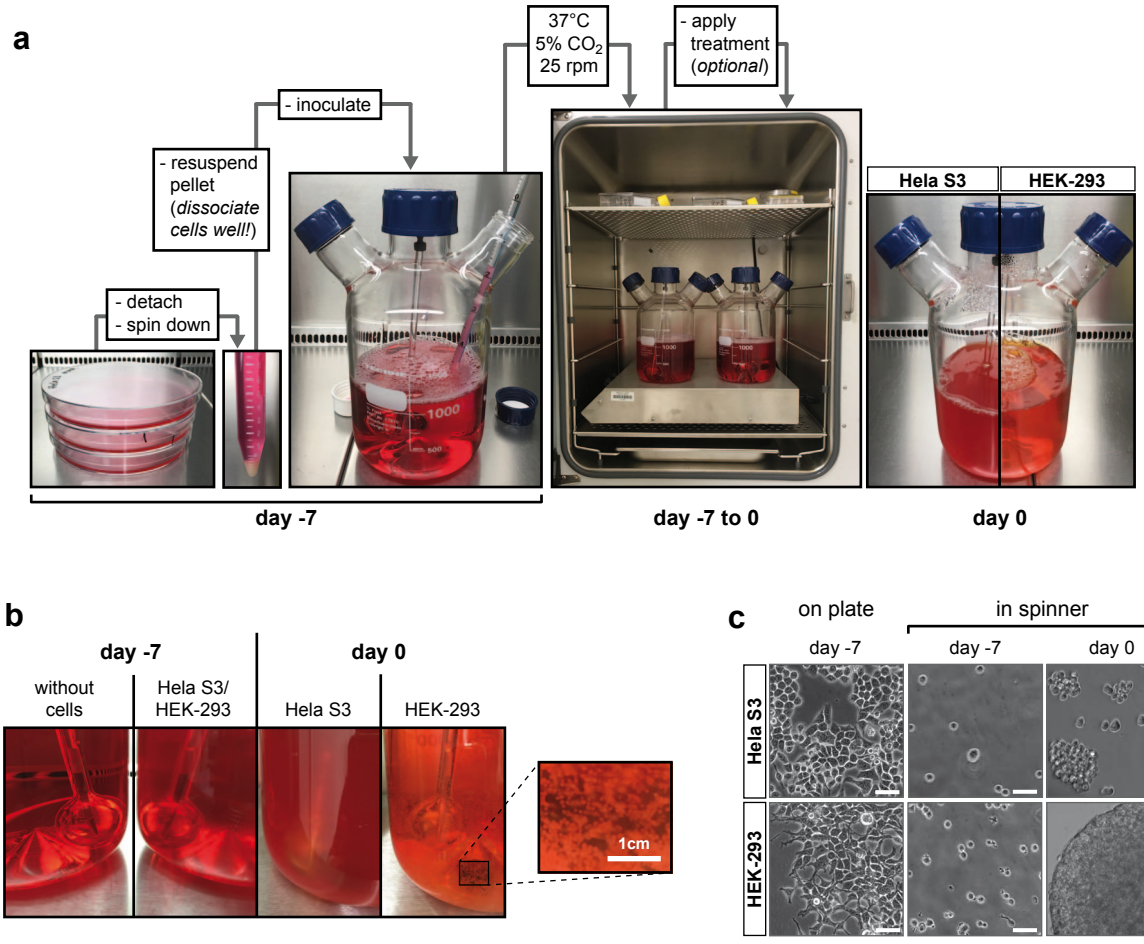
a
37°C
5% CO2
25 rpm
- apply
treatment
(optional)
- inoculate
- resuspend
pellet
(dissociate
cells well!)
- detach
- spin down
Hela S3
HEK-293
day -7
day -7 to 0
day 0
b
day -7
day 0
without
cells
Hela S3/
HEK-293
Hela S3
HEK-293
1cm
c
on plate
in spinner
day -7
day -7
day 0
Hela S3
HEK-293

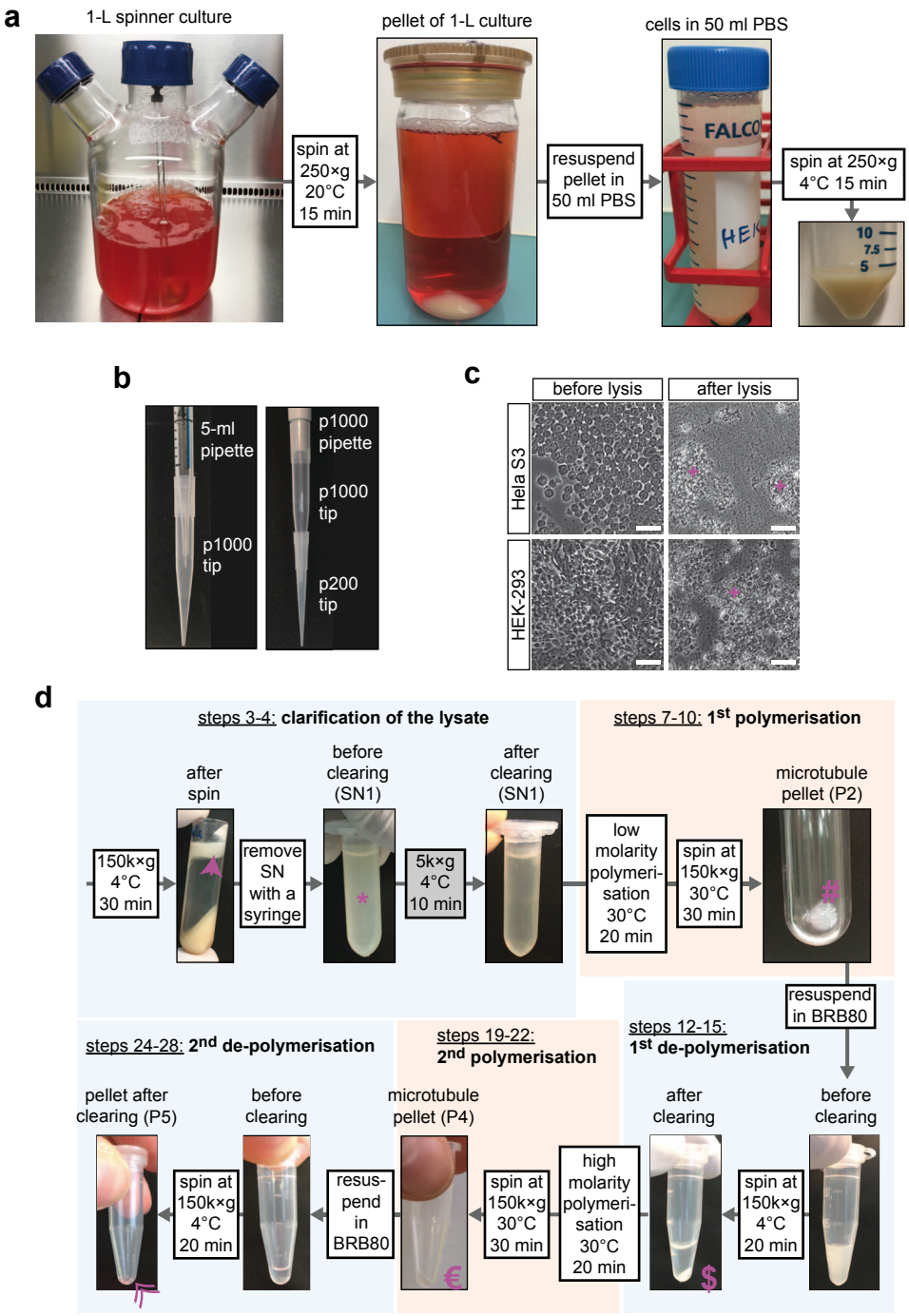
a
1-L spinner culture
spin at 250×g 20°C 15 min
pellet of 1-L culture
resuspend pellet in 50 ml PBS
cells in 50 ml PBS
spin at 250×g 4°C 15 min
b
5-ml pipette
p1000 tip
p1000 pipette
p1000 tip
p200 tip
c
before lysis
after lysis
Hela S3
HEK-293
d
steps 3-4: clarification of the lysate
150k×g 4°C 30 min
after spin
remove SN with a syringe
before clearing (SN1)
5k×g 4°C 10 min
after clearing (SN1)
steps 7-10: 1st polymerisation
low molarity polymeri-sation 30°C 20 min
spin at 150k×g 30°C 30 min
microtubule pellet (P2)
resuspend in BRB80
steps 12-15: 1st de-polymerisation
spin at 150k×g 4°C 20 min
before clearing
after clearing
high molarity polymeri-sation 30°C 20 min
steps 19-22: 2nd polymerisation
spin at 150k×g 30°C 30 min
microtubule pellet (P4)
resus-pend in BRB80
steps 24-28: 2nd de-polymerisation
spin at 150k×g 4°C 20 min
before clearing
pellet after clearing (P5)

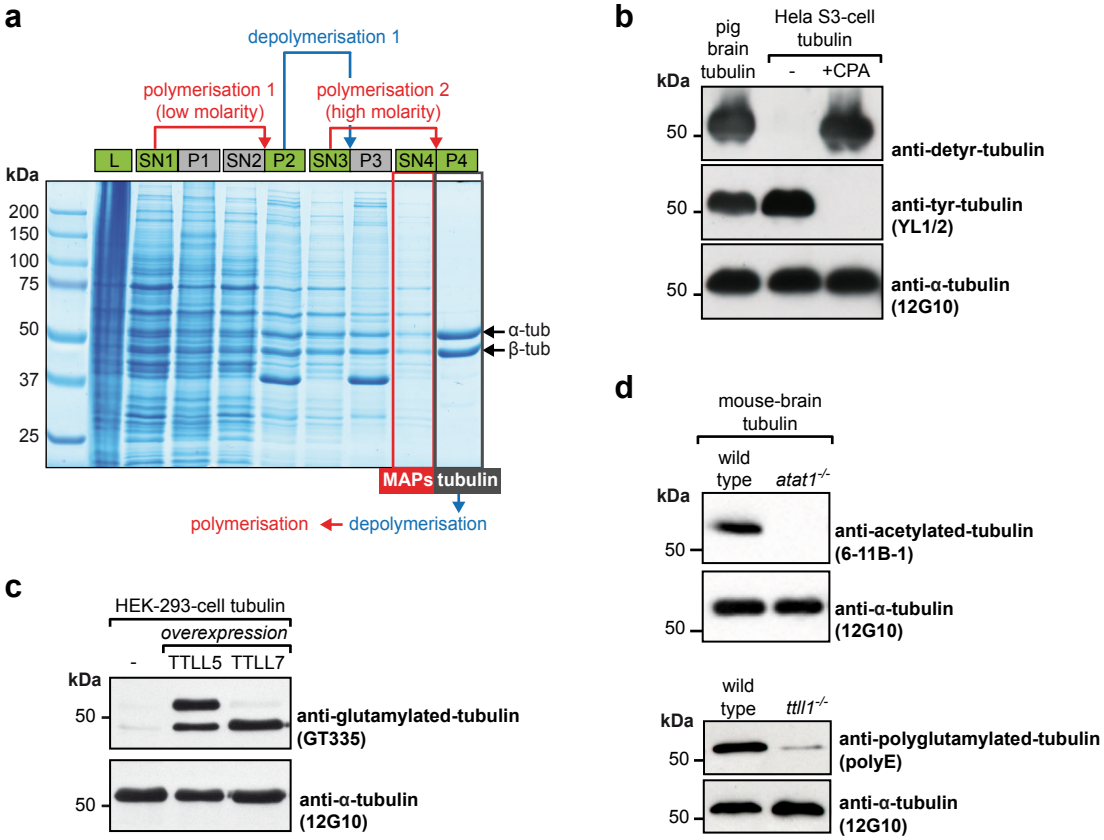
a
depolymerisation 1
polymerisation 1
(low molarity)
polymerisation 2
(high molarity)
L
SN1
P1
SN2
P2
SN3
P3
SN4
P4
kDa
200
150
100
75
50
37
25
α-tub
β-tub
MAPs
tubulin
polymerisation
depolymerisation
b
pig
brain
tubulin
Hela S3-cell
tubulin
-
+CPA
kDa
50
anti-detyr-tubulin
50
anti-tyr-tubulin
(YL1/2)
50
anti-α-tubulin
(12G10)
c
HEK-293-cell tubulin
overexpression
-
TTLL5
TTLL7
kDa
50
anti-glutamylated-tubulin
(GT335)
50
anti-α-tubulin
(12G10)
d
mouse-brain
tubulin
wild
type
atat1-/-
kDa
50
anti-acetylated-tubulin
(6-11B-1)
50
anti-α-tubulin
(12G10)
wild
type
ttll1-/-
kDa
50
anti-polyglutamylated-tubulin
(polyE)
50
anti-α-tubulin
(12G10)

3.2.1. Additional results

3.2.1.1. In vitro folding of recombinant tubulin using the TRiC chaperone.

Current advances, such as the purification of tubulin from cell lines, already allow to purify tubulin without PTMs (Souphron et al. 2019), however, this tubulin is still a mixture of different isotypes. Strikingly, the first method to produce 'real' recombinant tubulin from insect cells is a cumbersome procedure with low yield that requires a high level of experience from the experimenter, and therefore this is not broadly usable (Minoura et al. 2013b). We thus decided to tackle the expression of tubulin in bacteria with the aid of tubulin-folding chaperones.

In order to accomplish the molecular functions inside a cell, proteins need to fold correctly. It has been shown that most proteins require an additional folding machinery, involving chaperones for their functional and structural activity. Furthermore, cytoskeletal proteins like tubulin carry additional complexity in their structure because of their intrinsic property to integrate into dynamic polymers. However, there are two groups of chaperonins: group I (in prokaryotic cells), and group II (in Archaea and Eukarya) (Lopez, Dalton, and Frydman 2015). Strikingly, TRiC (Tailless complex polypeptide 1 ring complex), also known as CCT (Chaperonin-containing tailless complex polypeptide 1) is a group II eukaryotic molecular chaperone which is required for the folding of proteins such as tubulin, actin, CDH1 and CDC20 (Lewis, Tian, and Cowan 1997; Yaffe et al. 1992; Camasses et al. 2003; Vinh and Drubin 1994; Lopez, Dalton, and Frydman 2015; Balchin et al. 2018).

TRiC/CCT is a ~900-kDa ATP-driven protein complex consisting of eight paralogous subunits (CCT1-8), each having a specific role in the substrate recognition, assembly, folding and allosteric cooperativity (Jin et al. 2019; Dunn, Melville, and Frydman 2001). Previous biochemical and genetic data shows that TRiC is required for the folding of tubulin (Yaffe et al. 1992; Dunn, Melville, and Frydman 2001). Given that direct homologs of TRiC/CCT do not exist in prokaryotes, it is likely that the failure to produce functional tubulin from bacteria is due to a lack of this type of chaperone. In contrast to prokaryotes, archaea have a similar, although not homologue chaperon, the thermosome. The thermosome assembles, similar to TRiC, a two-ring structure with eight subunits, arranged together to form a cylindrical structure with a large cavity inside (Klumpp and Baumeister 1998).

We thus wanted to explore to which extent the TRiC chaperone is essential for tubulin folding by using hydrogen/deuterium exchange mass spectrometry (HDX-MS) on tubulin encaged by an active chaperon. With this method we wanted to determine which parts of the tubulin molecule are essentially dependent on TRiC-mediated folding. We set the strategy to use the eukaryotic hetero-oligomeric chaperonin TRiC from pig testis to test the folding of human tubulin *in vitro*.

Together with a postdoc in the lab, I contributed to the purification of TRiC from pig testes (as described in (Ferreyra and Frydman 2000; Villebeck et al. 2007)). Our protocol resulted in a purified TRiC complex being eluted around the fraction 95, as visualized on a Coomasie-stained protein gel (Fig. 13A) and by immunoblot detecting the CCT3 subunit of the complex (Fig. 13B). This project is progressing in a collaborator's lab, in which purified TRiC is used to monitor the folding brain, HeLa, and bacterially produced (recombinant and unfolded) tubulin.

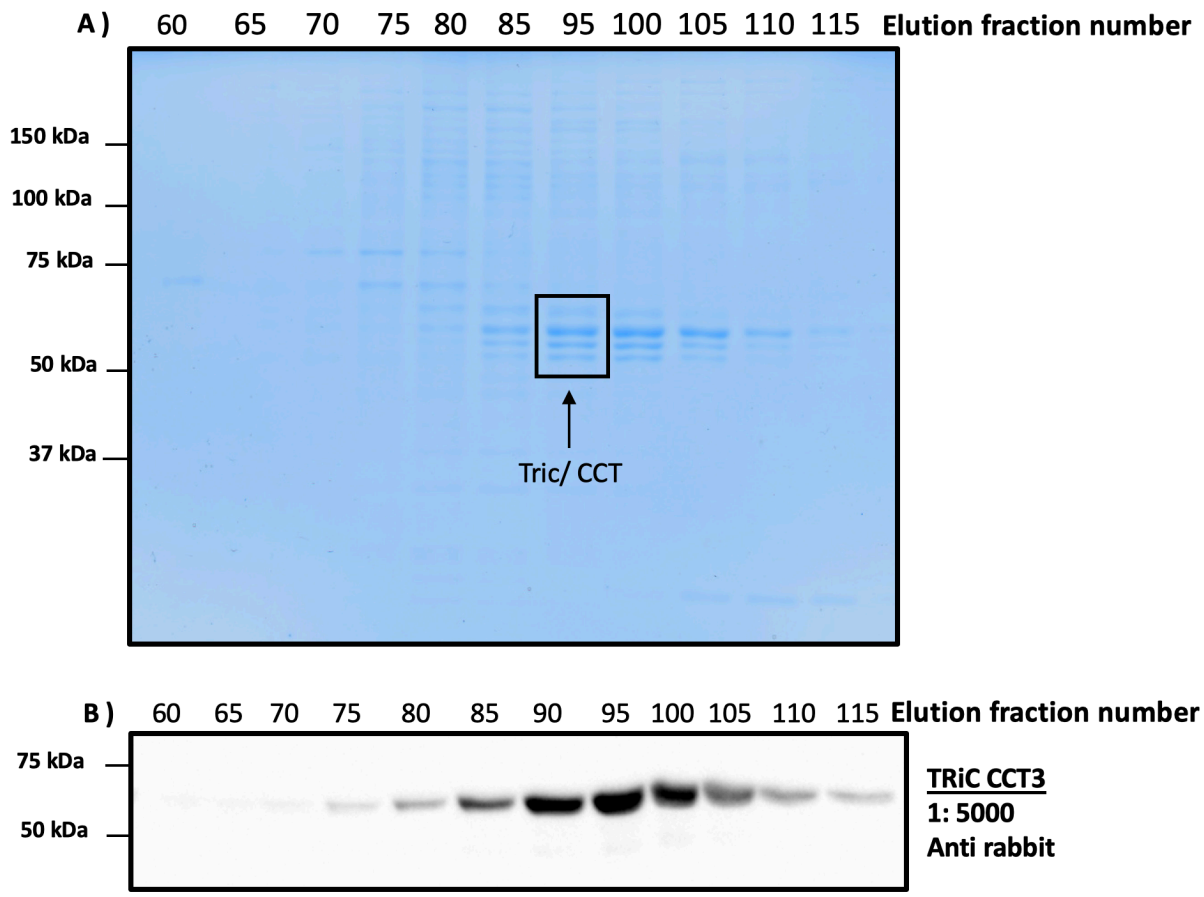

Figure 13: Purification of the TRiC from pig testicles. A) Coomassie-stained SDS-PAGE gel of elution fractions of TRiC. **B)** Immunoblot of elution fractions of TRiC using an antibody against the TRiC CCT3 subunit.

3. 2.1. 2. Studying the role of tubulin PTMs in MAP-MT interactions

Growing evidence points towards the role of tubulin PTMs in different cellular processes and diseases involving MTs(Gadadhar et al. 2017; Magiera, Singh, et al. 2018; Janke and Magiera 2020). In addition, several studies showed that the key molecular players in the regulation of MT properties are MAPs, and the regulatory role of tubulin PTMs in MAP-MT interaction at the molecular level is poorly studied. Furthermore, in the tubulin code hypothesis (detailed in the introduction), MAPs are considered as the reader molecules of tubulin PTMs. Thus, purifying MAPs and testing their affinity towards differentially modified MTs could potentially help to find MAPs which are sensitive to various tubulin PTMs. To address this question, I initially aimed at using MT co-sedimentation assays to detect the influence of tubulin PTMs in the direct binding of MAPs to MTs using purified protein components in vitro (see Fig. 14 for detailed steps). Using these experiments, I expected to observe differences in the binding of selected MAPs to MTs assembled from tubulin with controlled PTMs.

3.2.1.2a. Studying the role of tubulin PTMs in MAP-MT interactions by co-sedimentation assays using purified proteins

Based on preliminary studies in the lab, I aimed to investigate the binding of two purified MAPs, against differentially modified MTs. One is a truncated version of MACF1 and second is the tau protein. I compared the binding of MACF1 to MTs assembled from pig brain tubulin, which carry a variety of PTMs, and also to non-modified MTs assembled from HeLa-cell tubulin. I further compared the MAPs against MTs assembled from tubulin glutamylated by TTLL7 in HEK cells, and also against MTs with the non-glutamylated tubulin from HEK wildtype cells. Finally, I compared against detyrosinated MTs (assembled from CPA-treated HeLa-cell tubulin) and also against tyrosinated (untreated/ HeLa) MTs (Fig. 15). In addition, Tau 3R binding was tested with non-modified (tyrosinated) and detyrosinated MTs (Fig. 16A, B).

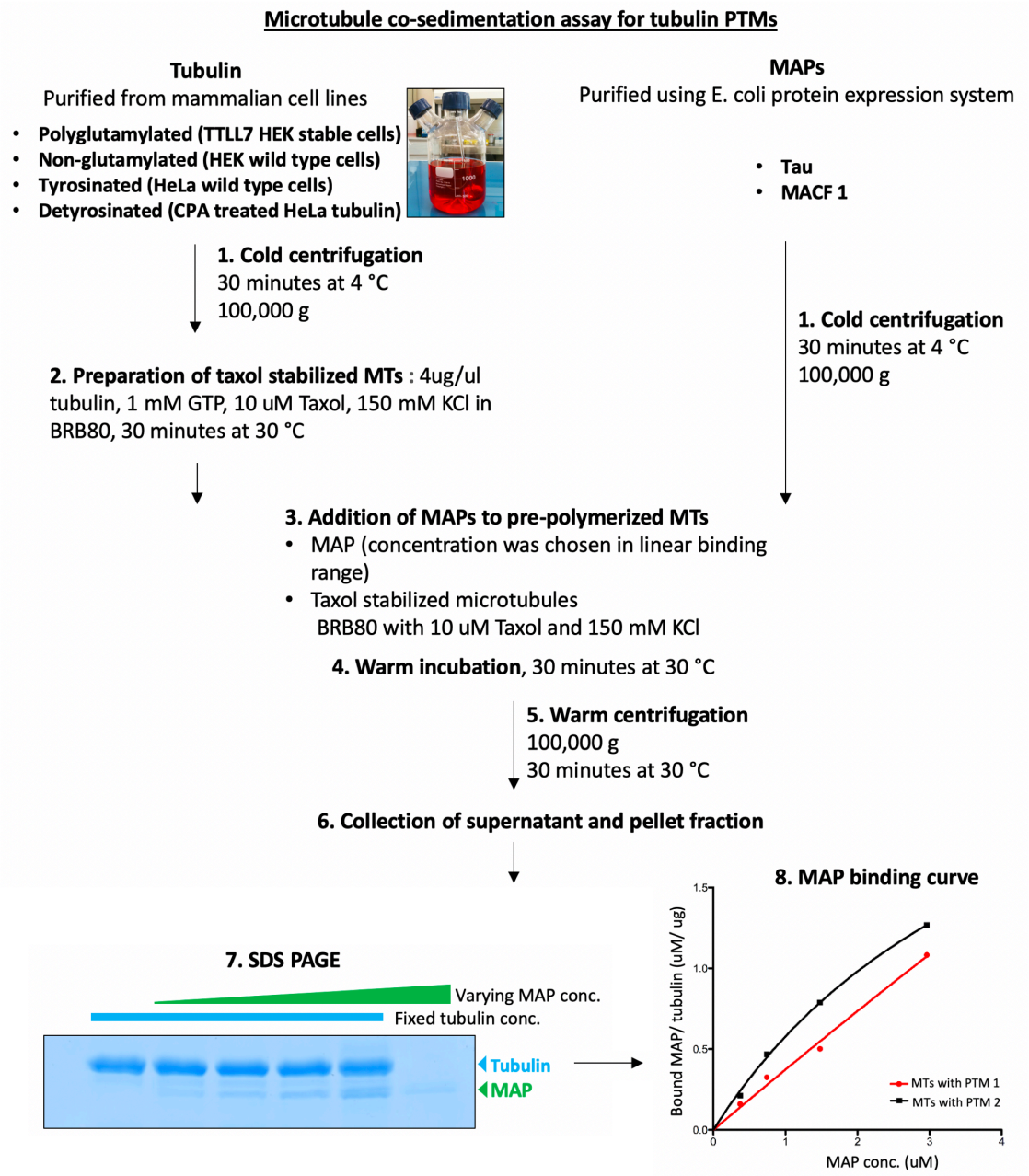

Figure 14: Schematic diagram of different steps of MAP-MT co-sedimentation assays to study the impact of tubulin PTMs on MAP-MT interactions. Tubulin with controlled PTMs was purified according to (Souphron et al. 2019). MAPs were purified from E. coli. as described in (Dutta et al. 2019). Both tubulin and MAP were centrifuged (step 1) to remove precipitated proteins. Subsequently, taxol-stabilized MTs were prepared (step 2) and incubated with different concentrations of the MAP (step 3-4), followed by high-speed centrifugation (step 5). The supernatant and pellet were separately collected and ran on an SDS-PAGE (step 7). Band intensities were measured as described in https://openwetware.org/wiki/Protein_Quantification_Using_ImageJ and plotted binding curve using Prism-GraphPad software (step 8). Ratios between tubulin and MAP band were calculated and plotted.

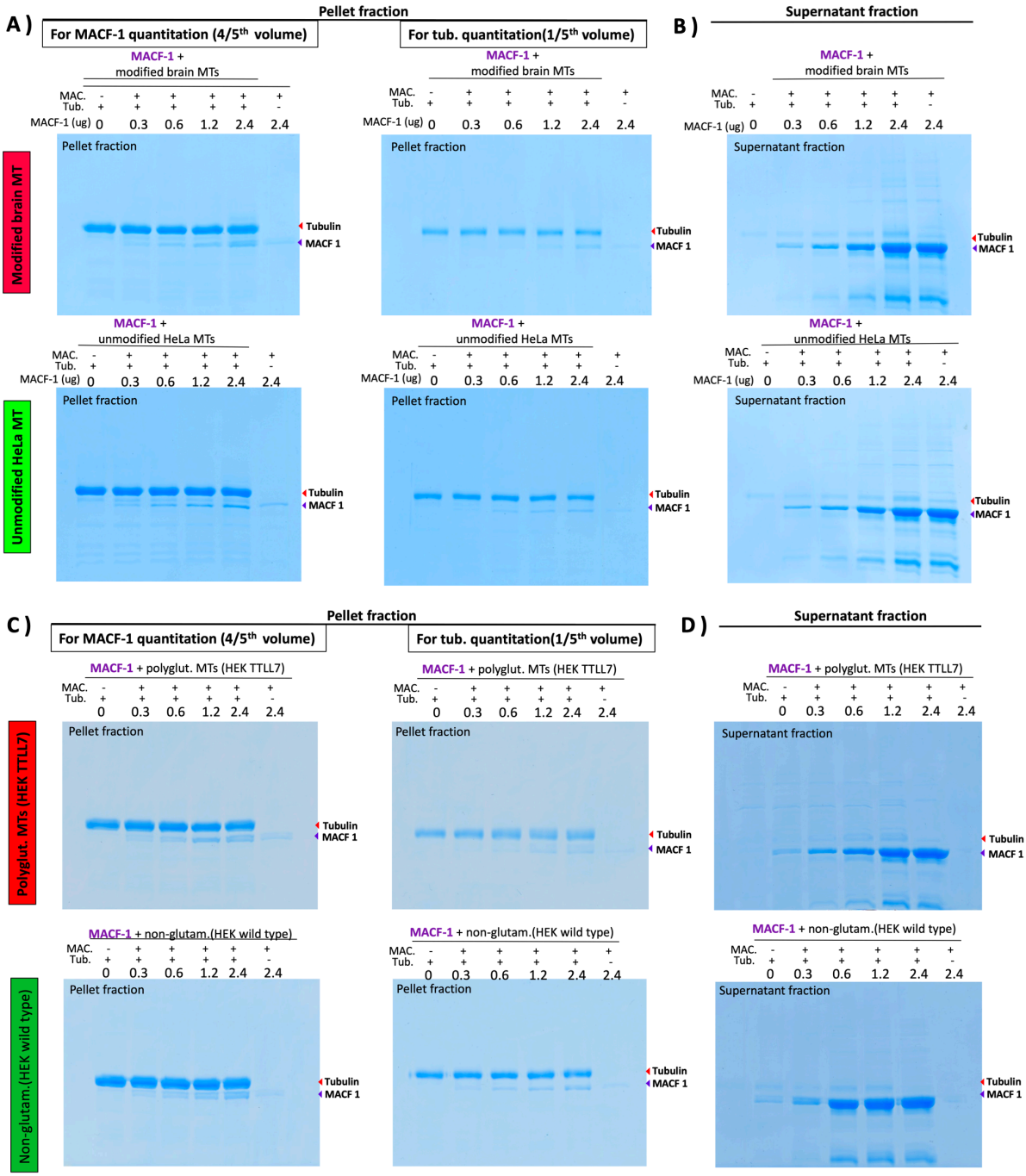

Figure 15: MT co-sedimentation assay of MACF1 with differentially modified MTs. **A-D)** Coomassie staining of 10% SDS PAGE gels showing the supernatant and pellet fractions of MACF1-MT co-sedimentation assays. The affinities of MACF1 towards taxol-stabilized modified (brain tubulin), non-modified, glutamylated, and non-glutamylated MTs were tested. Tubulin concentration was kept constant at 4 µg/µl, while MACF1 concentration was varied. The total reaction volume was 18 µl. 1/5th of the sample was used to quantify tubulin, the rest was used to quantify MACF1. Unbound MACF1 in the supernatant fraction is shown in (**B**) and (**D**).

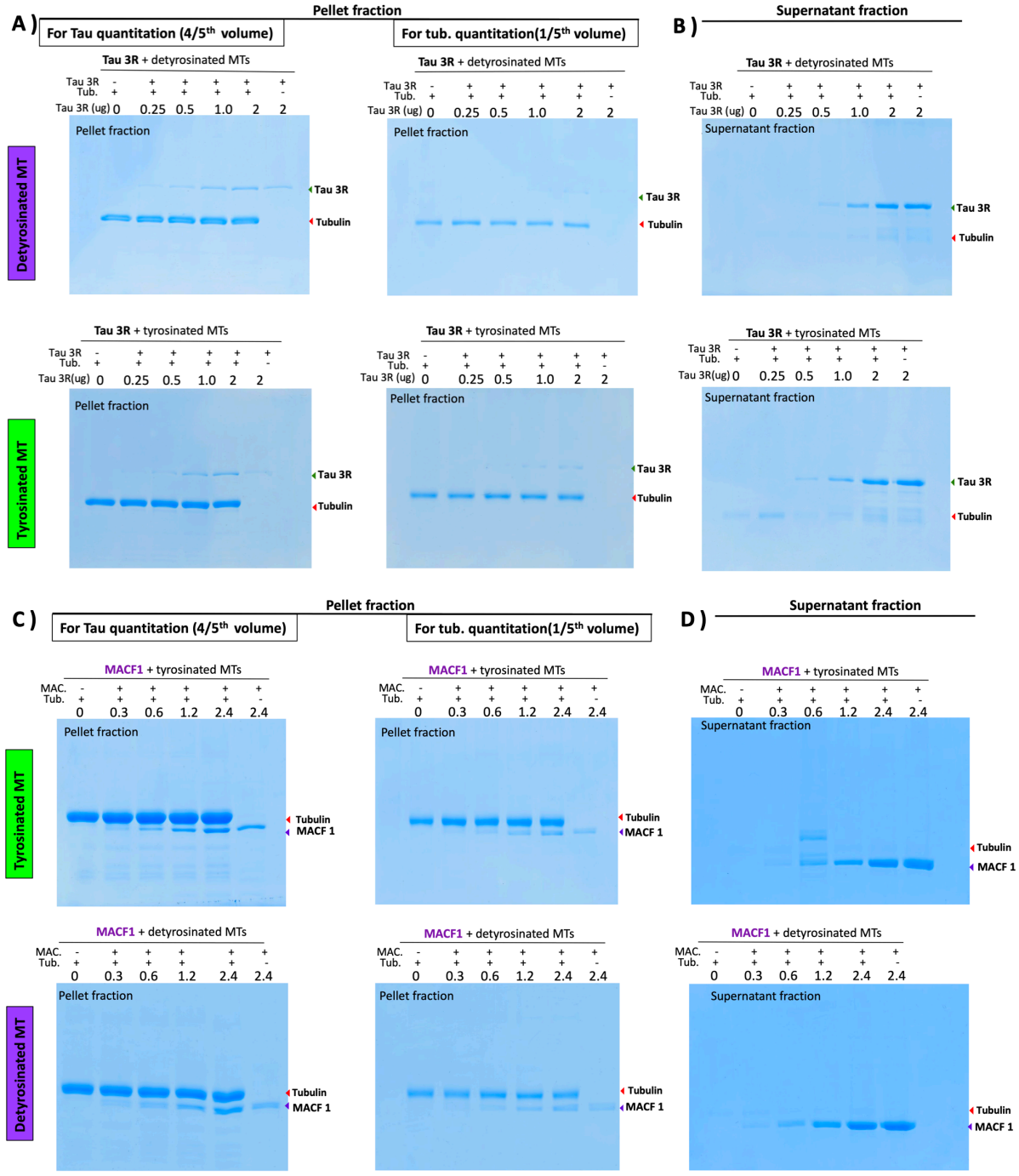

Figure 16: MT co-sedimentation assay of Tau 3R and MACF1 against tyrosinated, detyrosinated MTs. A-D) Coomassie staining of 10% SDS-PAGE gel showing the supernatant and pellet fractions of MT co-sedimentation assay with Tau and MACF1. The affinity of MACF1 against taxol-stabilized tyrosinated and detyrosinated MTs was tested using MT co-pelleting assay. Tubulin concentrations were kept constant at 4 µg/µl, while MAP concentration was varied. The total reaction volume was 18 µl. 1/4th volume of total reaction was loaded in one gel for the measuring tubulin and rest of the volume in another gel for measuring the bound MAP. Unbound MAP in the supernatant fraction is shown in (**B, D**). Preliminary results didn't show any strong difference in the binding affinity of MACF1 against different tubulin kinds.

The preliminary results from the MAP-MT co-sedimentation assays with MTs with different PTMs did not reveal any striking difference in the MAP binding preference. This suggests that for the performed combinations of MAPs at the micromolar range of MAP concentrations, tubulin PTMs might not have strong effects at equilibrium binding conditions. Further experiments need to be done with more MAPs and tubulin-PTM combinations, and using dynamic MT binding assays.

However purifying MAPs is a time-consuming process, and since there are not many prior data available about the sensitivity of MAPs towards tubulin PTMs, a wide screening strategy is required. Thus, I shifted my methodology from co-sedimentation to *in vitro* reconstitution and TIRF microscopy assays with cell lysates, described in detail in the next chapter 3.2.1.3b.

3.2.1.2b. Establishing the tricolour TIRF microscopy assay for studying the impact of tubulin PTMs on MAP-MT interaction

To study the role of tubulin PTMs on the dynamic MT binding of MAPs, I established an *in vitro* reconstitution and TIRF microscopy setup in our lab, including the surface treatment protocols for glass coverslips and slides (Bieling et al. 2010). This new approach has multiple advantages over the co-sedimentation experiments, such as the possibility to work at low MAP concentrations (down to single molecules) and the use of lower quantities of material for tests, which are required for the subsequent statistical analysis. Furthermore, there are more than 100 MAPs reported, and so far, there is not much evidence about which of them might be sensitive to specific PTMs. Therefore, developing a tool for a rapid, systematic probing of these proteins against a diverse range of tubulin PTMs was of high demand and importance in the field.

To perform such a screening, I used a method based on a cell-free system (see Jijumon et al. manuscript in the chapter 1 for the experimental details), in which lysates of cells overexpressing GFP-MAPs are used as a source of MAPs, while the MTs are pre-polymerized from purified tubulin with custom PTMs, stabilized with taxol and immobilized in the TIRF chamber. After the addition of the lysate, the dynamics of the MAP-MT interaction is observed in real time by TIRF time-lapse imaging. Strikingly, all the analysed MAPs were soluble and functional in the lysates, which is another advantage of this approach over the purification method. I further established a tricolour-TIRF assay specifically for studying the role of tubulin PTMs in MAP-MT interactions in a competitive manner. In this assay the MTs are first

separately assembled from two different kinds of modified tubulin, distinguished by two different fluorophores (10-15% labelled tubulin). MTs are immobilized in the microscopy chamber (see the following methodology section of tricolour TIRF microscopy). To achieve better temporal resolution, TIRF chambers were prepared by attaching a coverslip on a glass slide perpendicularly (Fig. 17A) instead of a parallel arrangement. This setup allows to flush the lysate into the chamber installed directly on the microscope stage, and thus to record the MAP binding from the very beginning. In the previous configuration, where the coverslips are aligned parallelly, addition of the sample needed to be carried out on the bench, before mounting on the microscope, which prevented the detection of subtle differences in binding preferences in the initial time points of the assay.

For a preliminary screening, I tested the binding of around 25 MAPs against modified (brain) and unmodified (HeLa) MTs with highly diluted MAP lysates. Among these, I found that Tau protein showed a higher binding affinity to modified brain MTs, and this preference was maintained for both 3R and 4R isoforms of Tau. (Fig. 17B is the TIRF-M assay shown for Tau 4R, $n \geq 10$ independent TIRF assays from more than 4 independent lysate preparations). Similar to Tau 4R, Tau 3R construct also showed a higher binding affinity to modified MTs (data not shown).

In order to estimate the unknown concentration of Tau in the lysates which show the preferential binding, I performed immunoblot with GFP antibody against known dilution series of purified GFP-tagged protein with known concentration (here I used purified MACF1-GFP from *E. coli*). For this, first I quantified the concentration of purified MACF1-GFP protein using BSA dilution series on a Coomassie-stained SDS-PAGE gel (Fig. 17D) (https://openwetware.org/wiki/Protein_Quantification_Using_ImageJ). Then using quantified MACF1-GFP as standard, I performed an immunoblot of tau in lysates (Fig. 17E). The quantifications show that the binding preference of Tau towards modified brain MTs is most pronounced at concentration of 90-100 nM Tau protein in lysates.

Finally, to exclude a potential impact of the fluorophores used for tubulin labelling, I repeated the assays with swapped MT colour labels as an additional control experiment. For obtaining further physical parameters (K_{off}/ dissociation constant or K_{on}/ association constant) involving MAP-MT interactions, other microscopy techniques such as FRAP (Fluorescence Recovery After Photobleaching) and FLIP (Fluorescence Loss In Photobleaching) can be used.

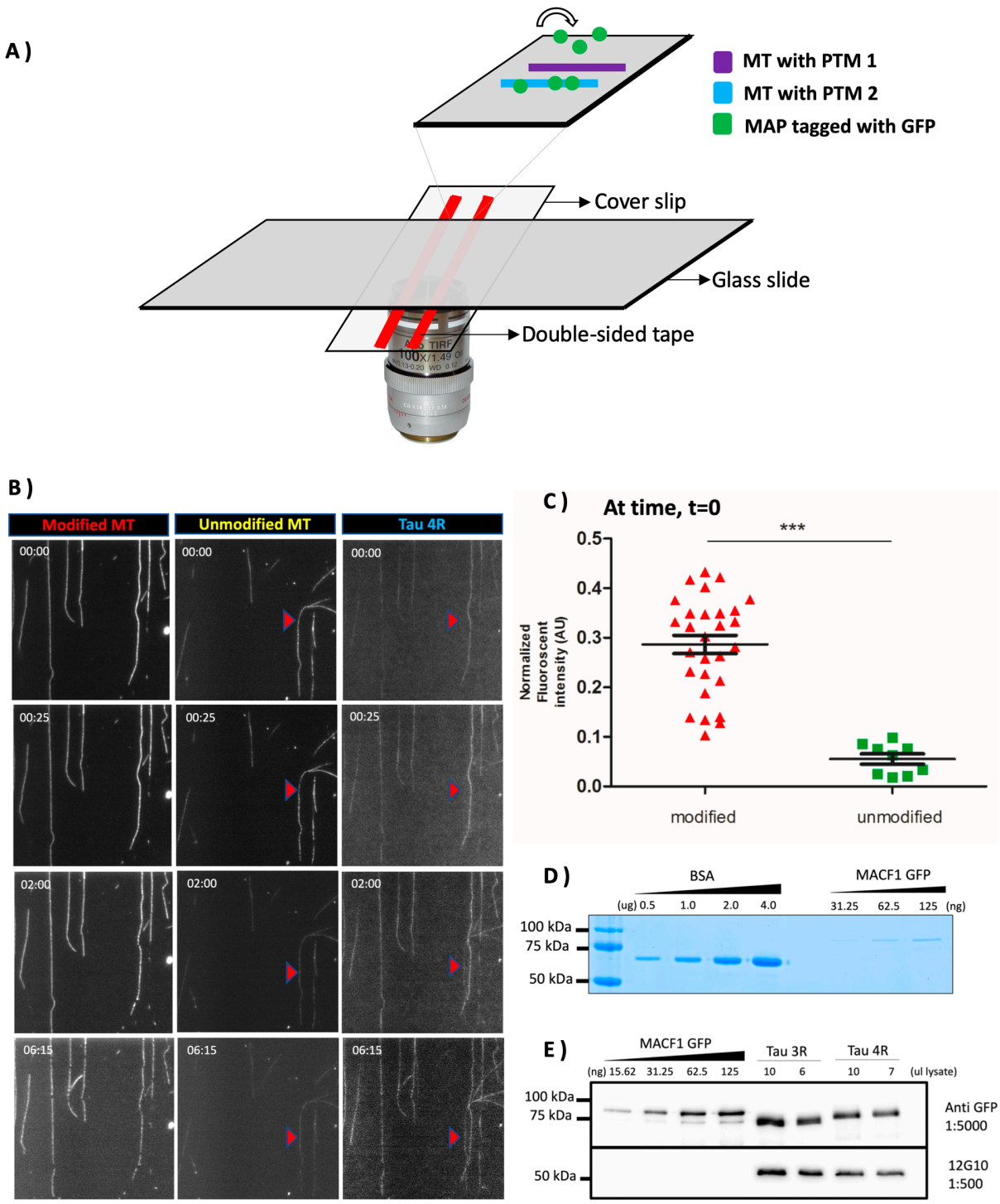

Figure 17: Tau protein shows a binding preference for modified microtubules.
A) Experimental setup established for testing the role of different tubulin PTMs in MAP-MT interactions by tricolour-TIRF microscopy. A TIRF chamber was assembled by sandwiching a glass slide and coverslip in a perpendicular fashion (cross-design of the TIRF chamber helps to flush in the sample, without changing the focus or position of the MT field). In the chamber, pre-polymerized taxol-stabilized MTs with specific PTMs, each labelled with a different fluorophore, were immobilized side by side, and MAPs were flushed-in. Subsequently, the preference of MT binding was visualized by TIRF microscopy in real-time. **B)** Time montage of a TIRF assays showing Tau protein preferentially binding modified (brain) MTs over non-

modified (HeLa) MTs; n>10 independent TIRF assays from more than 4 independent lysate preparations. **C)** Quantification of fluorescence intensity of Tau protein on modified MTs vs. non-modified MTs (normalized to MT length). **D)** Coomassie-stained SDS-PAGE gel for determining the concentration of purified GFP-tagged MACF1 (any purified GFP-tagged protein or GFP alone can be used), using standard BSA dilution series. **E)** A western blot was performed using the known concentration of the GFP-tagged protein as standard.

Protocol to study the role of tubulin PTMs in MAP-MT interactions using MT reconstitution and TIRF microscopy

Step 01: surface preparation: treatment of glass slides and coverslips.

Materials required:

- 100% acetone
- 100% ethanol
- Milli-Q water
- Coverslips (24×60 mm), thickness no. 1.5 (VWR).
- Glass slide (76×26 mm) (Thermo scientific superfrost)
- Glass bottles
- Water bath sonicator

Methodology:

Glass slides and coverslips were treated separately as follows:

1) A clean 500-ml bottle was filled with 100% acetone (1/3rd volume of the bottle) and the slides/coverslips added one by one (made sure that they are not stuck together). In case of the glass slides, each one was wiped with kimtech paper before putting into the acetone.

Notes: Since the MTs will be attached and imaged on the side of the coverslips, their cleaning is more important than that of the glass slides. The number of glass slides or coverslips taken for the treatment depends on the size of the bottle which the water bath sonicator can accommodate at a time.

2) The materials were sonicated in a water bath for 15 min, 27°C or room temperature (medium mode, Diagenode bioruptor standard sonicator).

3) The acetone was discarded; the coverslips and slides were subsequently rinsed with water (adequate amount to immerse the coverslips/glass slides).

4) The bottle was refilled with fresh Milli-Q water and sonicated in a water bath for 15 min, 27°C (medium mode, Diagenode bioruptor standard sonicator).

5) The water was replaced by 100% ethanol and sonicated in a water bath for 15 min, 27°C (medium mode, Diagenode bioruptor standard sonicator).

6) The ethanol was discarded and the glass coverslips and slides were stored in fresh 100% ethanol.

The treated slides and coverslips can be stored at room temperature for 3-5 weeks.

Step 02: preparation of chambers.

Materials required:

- 70% ethanol
- Tesa double-sided sticky tape (15 mm width)
- Scissor
- Forceps
- Gas burner (any flame source)
- Treated glass slides and coverslips from the previous step.

Methodology:

- The workbench/ surface was cleaned thoroughly with 70% ethanol (should be dust-free).
- Glass slides were dried using the flame.
- The Tesa tape was cut in thin strips of around 25 mm in length (slightly longer than the coverslips with dimensions 24×60 mm, the extra length is required to ensure the lanes for flushing and adsorbing the protein samples). Five long strips of Tesa tape were pasted to produce 4 lanes/chambers on a single glass slide with the help of forceps.
- The cover of the double-sided tape was peeled off carefully and a dried clean coverslip was placed on top, gently tapped in place with the forceps.
- The prepared chambers have a volume range of 10-15 µl, and can be stored at room temperature for 2-3 weeks, covered to ensure no accumulation of dust.

Step 03: Preparation of fluorescence-labelled MTs:

Materials required:

- Water bath (37°C)
- Ultracentrifuge (Beckman)
- Beckman rotor TLA55
- Labelled brain tubulin (Cytoskeleton)
- Unlabelled tubulin (with known modifications)
- $MgCl_2$ (1 M stock solution, working conc.: 1-10 mM)
- GTP (0.2 M stock solution, working conc.: 1-2 mM)
- Taxol (stock solution: 1 mg/ml (1.17 mM), working conc.: 20 µM; optional range: 5-40 µM; Paclitaxel= 853.9 g/mol)
- BRB80 buffer

Methodology:

The reaction volume can range between 15–60 µl, with a total tubulin concentration of 15-20 µM. For the final TIRF experiments, the assembled MTs need to be diluted 100-500× to get sparsely distributed MTs in the TIRF chamber.

Following is the composition of the reaction mixture:

Component	Concentration (stock)	Concentration (working)
$MgCl_2$	100 mM (Sigma)	2 mM
Taxol	200 µM	10-20 µM
GTP	50 mM	2 mM
Unlabelled tubulin	variable	variable*
Labelled tubulin	variable	variable* (10-15% of total tubulin)
BRB80	1×	1×

*Total tubulin concentration should be around 15-20 µM.

Detailed steps:

1) Labelled tubulin (Cytoskeleton or homemade) and unlabelled tubulin (with different PTMs) were thawed on ice.

2) Unlabelled tubulin, labelled tubulin and $MgCl_2$ were added to the BRB80 buffer on ice.

3) The above mix was centrifuged at 50,000 g for 25 min in TLA55 rotor at 4°C in a Beckman Coulter optima MAX-XP benchtop ultracentrifuge. Subsequently the supernatant was collected and 2 mM GTP was added, followed by a short incubation on ice for 5 min.

4) Afterwards, the tube was wrapped with an aluminium foil and placed in the water bath at 37°C for 30 min.

5) After 30 min incubation, 20 µM taxol was added and the mix was kept at 37°C for another 90 minutes.

6) The mix was further centrifuged at 50,000 g for 10 min in TLA55 rotor at 37°C.

7) The supernatant was removed, and the pellet was resuspended in warm BRB80 containing 20 µM taxol. These taxol-stabilized MTs can be stored in a 37°C incubator for 12-24 h.

Step 04: Microscopy sample preparation and TIRF imaging

Materials required:

- BRB80 buffer
- Glass chambers (a sandwich of coverslips and glass slides attached with a double-sided sticky tape assembled as described before).
- Thermal block/ incubator (37°C)
- Filter paper (small pieces for absorbing the flushed liquids from the one end).
- ß-Casein (Stock solution: 30 mg/ml, working: 50 µg/ml) Sigma
- Dead kinesin (working conc.: 500 nM- 1 µM)
- Taxol (stock: 1 mg/ml (1.17 mM), working conc.: 20 µM)
- Homemade box for retaining the chamber moisturized (using 200 µl tip box, drenched tissue paper and filter paper).
- Trolox mixture (Oxygen scavenging system)
- PCD (Protocatechuate 3,4-Dioxygenase)- Sigma P8279
- PCA (3,4-Dihydroxybenzoic acid)- Sigma 08992
- Trolox (6-Hydroxy-2,5,7,8-tetramethylchromane-2-carboxylic acid)- Sigma

The following solutions need to be prepared freshly before the assay:

1) Solution 1: ß-Casein (Stock solution: 30 mg/ml, working conc.: 50 µg/ml) – 0.41 µl in 250 µl BRB80.
2) Solution 2: Taxol (stock solution: 1 mg/ml (1.17 mM), working conc.: 20 µM) - 4.27 µl in 245 µl BRB80.
3) Solution 3: ß-Casein (0.41 µl) + Taxol (4.27 µl) in 245 µl BRB80
4) Trolox mixture

Trolox mixture composition:

Components	Stock concentration (10X)
PCD	10 µM
PCA	100 mM
trolox	100 mM
BRB80	1×

Working concentration: 1-2X.

Methodology:

1. Flush in solution 1 (ß-Casein) and incubate for 5 min.

2. Flush in 500 nM dead kinesin and incubate for 5 min.

3. Wash the chamber with solution 2 (BRB80 + taxol).

4. Flush in MTs and incubate for 5 min (the right dilution for sparsely distributed MTs, and for similar number of MTs for both PTMs need to be tested beforehand).

5. Wash twice/ thrice with solution 3 (BRB80+Taxol+ ß-Casein).

6. Flush in 1× Trolox mixture (Oxygen scavengers).

7. Flush in lysates containing MAPs/ purified MAPs, and image using TIRF microscopy.

Note: Since the MAP binding events are quick, and don't require longer acquisition time, use of oxygen scavengers is not always necessary.

3.2.1.3. Impact of tubulin patient mutations on the stability and dynamic properties of MTs.

MTs are dynamic, polar biopolymers that grow and shrink (mostly) from their plus ends in a process called dynamic instability. In in vitro, polymerization and depolymerization events are temperature sensitive. MTs depolymerize at cold, and tubulin dimers polymerize into filaments at physiological warm temperature. The cold sensitivity of complex molecules is extremely rare in nature. Even though temperature sensitivity of MTs is widely known, the molecular reasons behind this process are poorly studied. To investigate this, I established a setup for testing the temperature sensitivity of MTs using lysates from cells overexpressing different tubulin isotypes. This project was developed in collaboration with Cherry biotech company, which provided the hardware, i.e. the manifold compatible with MT *in vitro* reconstitution and the associated apparatus for rapid control of the temperature in the setup (https://www.cherrybiotech.com/heater-cooler-for-microscopy). In the classical reconstitution assays, we use TIRF chambers, which are generally a sandwich of a glass slide and a coverslip separated by double-sided sticky tape, and the assays are performed at ambient temperature.

In this project, we have developed a temperature-controllable manifold (Fig. 18), in which we can rapidly change the assay temperature from 5 to 45°C in 4-8 seconds. A similar chip was developed and was used for yeast and HeLa cell studies. However, specifically for this project, the apparatus was tuned for the first time to be applied for in vitro MT reconstitution experiments and TIRF microscopy (Fig. 18A-C). Using this setup, we are currently studying the dynamic properties of MTs assembled from α-tubulin (TUBA1A) bearing a range of mutations associated with lissencephaly, a neurodevelopmental disorder, and tested the sensitivity of MT assembly to different temperatures. According to molecular simulations carried out earlier in the lab, these mutations could reduce the intra-dimer angle between the α- and β-tubulin. Thus, this aberration could affect the incorporation of tubulin dimer into the MT lattice, and therefore the MT dynamic instability. To test this prediction, I used the lysates of cells overexpressing wild type and mutant tubulins with classical TIRF chambers first, and then with Cherry temperature manifold. The preliminary results show that tubulin mutants associated with lissencephaly are able to polymerize at lower temperature compared to the wild type tubulin (Fig. 18D), suggesting that the dimer curvature influences cold-sensitivity of MTs.

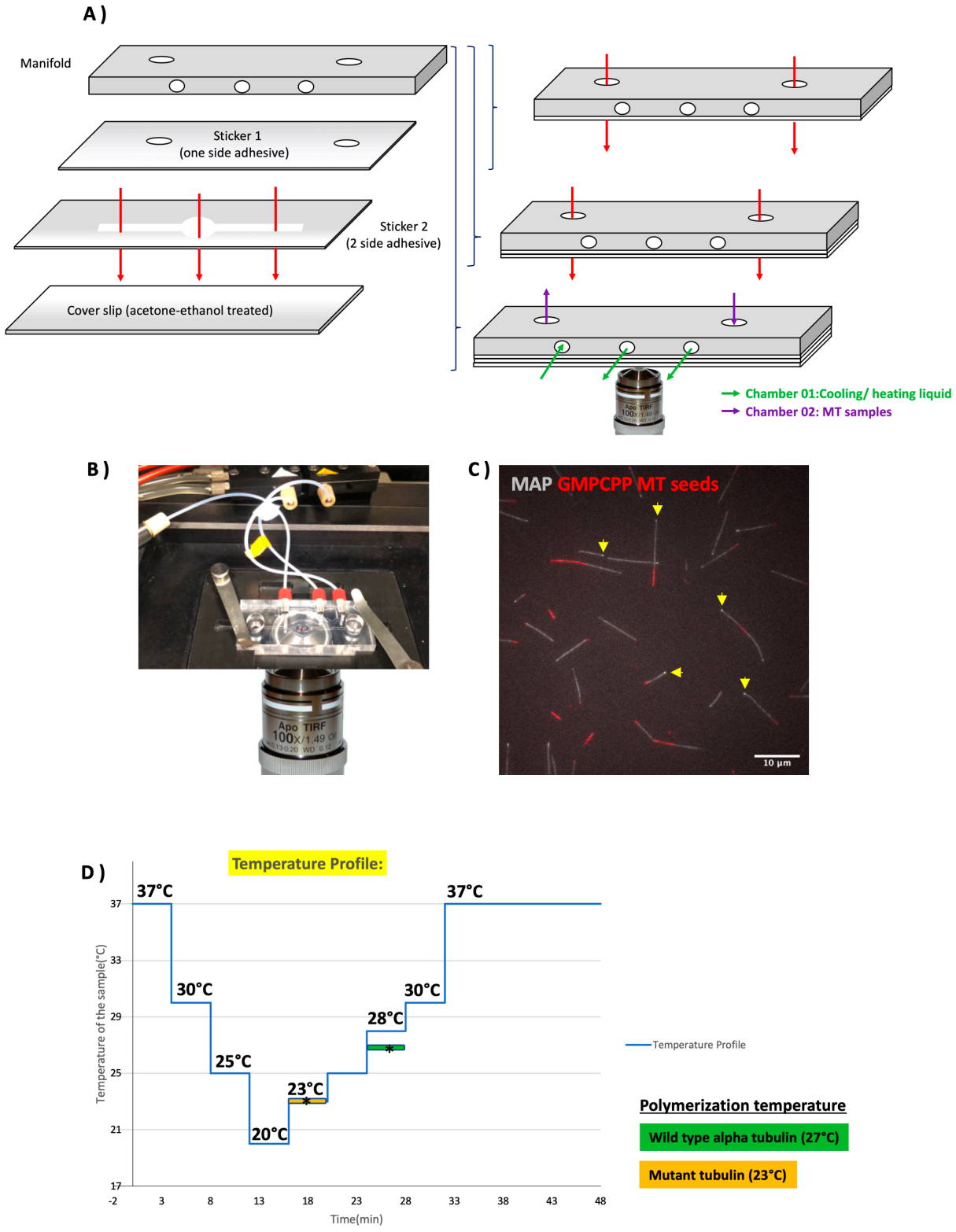

Figure 18: Mutations in tubulin lead to altered temperature sensitivity of MTs.
A) Schematic diagram of the 4-layer-manifold used for MT reconstitution and TIRF-M. The manifold has two chambers, one for flushing in samples (purple arrows) and the second one for flowing the heating/ cooling liquid (green arrows). **B)** Picture showing the mounted manifold on a TIRF 100× oil objective, connected with all the tubes for temperature control. **C)** Reconstituted MTs decorated by a MAP and visualized by TIRF microscopy. GMPCPP pre-

polymerized MT seeds are shown in red and the MAP decorating the growing MTs are shown in grey. In this example the MAP is GFP tagged EB3 (grey), and the yellow arrows show the EB3 comets at the growing tips of the MTs (scale bar: 10 µm). **D)** Temperature profile showing different temperatures applied during the assay. Polymerization temperatures for the wildtype tubulin is shown in green and mutant tubulin is shown in yellow.

4. Discussion

The major goal of my PhD work was to develop an ex-vivo assay that allows to study the binding behaviour of a large number of MAPs to dynamic MTs, and to determine their impact on the MT network at individual MT resolution. In order to accomplish this, the project has three different focus points: the first one was the development and validation of a novel method based on cell lysates to study the binding behaviour of ~50 mammalian MAPs on growing MTs. The second focus was to explore a variety of diverse applications that could be performed using this cell-lysate-based approach, such as cryo-electron microscopy. The third focus was to further expand the ex-vivo approach to study the role of tubulin PTMs in MAP-MT interactions.

4.1. The potential of lysate-based ex-vivo approaches compared to in-vitro reconstitution assays with purified proteins and cell-based studies

In-vitro reconstitution approaches using purified proteins, as well as various studies in cells contributed to our current understanding of MAP-MT interactions. However, both methods have their own advantages and limitations. Major limitations of in-vitro reconstitution approaches in the study of MAPs are work-intense and complex purification steps, including sometimes long buffer optimization processes and sensitive assay conditions. This slowed down the advancement of MAP research in vitro and had limited the in-depth characterization to only a few MAPs on single MTs.

In the case of cell-based studies, the major challenges concerning the investigation of MAP-MT interactions are the difficulty in visualizing and tracking individual MTs, overexpression artefacts, cell lethality and stress associated with MAP overexpression, rapid MT bundling mediated by many MAPs and difficulties to overexpress multiple MAPs in parallel. To date, more than 100 proteins from mammals are considered as MAPs, or suspected to behave like MAPs, however, only a few are well characterized.

To overcome these limitations, I aimed to develop an approach that uses the advantages of the in vitro system, and combines it with the advantages of cellular studies. However, the attempts to create an approach that lies in between in vitro and cell-based studies is not new in the MT field. Xenopus egg extracts (Belmont et al. 1990), mammalian cell lysates (Saredi, Howard, and

Compton 1997), drosophila embryo extracts (Telley et al. 2013), or yeast cell lysates (Bergman et al. 2018) were previously used to explore various biological process involving MTs at a higher resolution, and with some of the cellular complexity. The manipulation of clear extracts allows to bypass the complexity of the intracellular space in cells, which comes from cell organelles, membranes and packed cytoskeletal filaments in a confined cytoplasmic space. Experiments using Xenopus egg extracts have contributed greatly to our understanding of the structure and mechanism of the mitotic spindle, and also in the comprehension of other subcellular structures (reviewed in (Jevtic et al. 2016)). The use of extracts prepared from single drosophila embryos is another example in which an ex vivo approach was taken to study the mitotic machinery (Telley et al. 2013).

First studies using mammalian cell extracts allowed visualizing proteins decorating MT-based structures such as MT aster formations, using a fluorescence microscopy. These experiments helped in the discovery and characterisation of MAPs such as NuMa (Nuclear protein that associates with the Mitotic Apparatus), ch-TOGp and protein 4.1R in MT-aster formation, and later allowed to conduct more refined and detailed experiments to study the importance of those MAPs in cell division (Gaglio, Saredi, and Compton 1995; Dionne, Sanchez, and Compton 2000; Huang et al. 2004). These early studies also opened the possibility to visualize multi-protein complexes based on stable MT structures.

A recent study allowed to follow dynamic MTs using yeast lysates (Bergman et al. 2018). Genetic manipulation in yeast is cheap and easy, thus lysates from a genetically tractable yeast is an advantage. However, drawing conclusions about the behaviour of mammalian proteins in a yeast system is far-fetched. Another example using mammalian lysates was the use of very diluted Cos7 lysates as a source of kinesin motor proteins for single molecule studies (Soppina et al. 2014).

4.2. Specifics and applications of the ex-vivo pipeline

I developed an ex-vivo pipeline to study a large number of MAPs under comparable conditions. This pipeline is based on mammalian cell lysates, that are used as a source of MAP of interest, tubulin and GTP. I showed that this approach can be used for both, TIRF-based MT-reconstitution assays and cryo-EM studies. Using this approach, I studied more than 50 structural MAPs at individual MT resolution. Most of the MAPs were soluble and functional

in the same buffer (BRB80), with which the cell extracts were diluted upon lysis (the ratio of cell pellet volume to BRB80 buffer volume was 1:1). Standard MT-reconstitution assays of dynamic MTs with MAPs requires multiple components such as purified tubulin (both unlabelled and labelled tubulin for visualization), GTP (for MT polymerization), methyl cellulose (to reduce wiggling of growing MTs), 2-mercaptoethanol or DTT (as reducing agents), components of oxygen scavengers (to minimize photobleaching), and the purified MAP of interest. Among these, protein components need to be particularly in high and reproducible quality. By contrast, in the case of my ex-vivo approach, I provide only immobilized GMPCPP-MT seeds (as a MT nucleation template) and the cell lysate with an overexpressed MAP in the TIRF flow chamber. In this setup, the overexpressed MAP, soluble tubulin (endogenous) and GTP (endogenous) were provided from the cell lysate.

My PhD project has shown that the ex-vivo method allows to study a large number of MT-related proteins, including structural MAPs, severing proteins, and MT tip-binding proteins, in a reasonably short amount of time once the method is set up in a lab. Moreover, apart from TIRF-based MT reconstitution assays, we also successfully used the ex-vivo approach to study the ultrastructure of MAP-MT interactions using cryo-electron microscopy. Interestingly, a similar protocol for performing ultra-structural studies of non-MT structures using HEK cell lysates has been reported recently, which led to the observation of proteasome structures in two different biological states (Verbeke et al. 2018).

In summary, the ex vivo approach is likely to have precedence of being a simple and fast method for the characterization of mammalian MAPs on a medium-throughput scale, which can be used for TIRF reconstitution and cryo-EM studies. Using TIRF microscopy and cryo-EM, I employed the approach in diverse applications such as in the identification of new MAPs, in the investigation of MAP behaviour on individual and dynamic MTs, in unravelling the architecture of MAP-MT interaction using cryo-EM, in the evaluation of the role of MAPs in actin-MT crosstalk, in the functional analysis of MAPs and tubulins carrying patient-derived mutations, and in the investigation of role of tubulin PTMs in MAP-MT interactions. Using this technique, one could potentially characterize any protein associated with MTs, without the need for any protein purification. This could accelerate the advancement of MT research field to a great extent.

4.3. What I learned from this study, how this brings new knowledge in the field

To validate the ex-vivo approach and to exclude the possibility that some of the novel MAP functions might arise as an artefact of the approach, first I performed a control experiment, in which I followed the behaviour of two well-characterized non-structural MAPs: EB3 (End-Binding protein 3) and the MT-severing enzyme Spastin (Akhmanova and Steinmetz 2008; Roll-Mecak and Vale 2008). I successfully observed the MT end tracking by EB3 comets, as well as MT severing by Spastin using lysates, suggesting this approach is validated with two previously well-characterized MAPs and thus can be used for studying other MAPs.
In my medium-scale screen of ~50 MAPs, all TIRF assays were performed under similar assay and imaging conditions, and at a fixed total protein concentration of 8 µg/µl (because novel properties of all the MAPs were observed at this lysate concentration). In the lysate experiments, the majority of the MAPs promoted MT elongation and decorated the MT lattice. However, some of the tested proteins prevented MT elongation, some showed novel MT phenotypes, some bind to actin filaments instead of MTs, and several of them didn't bind to MTs despite being predicted to be MAPs. During the acquisition time in the TIRF-M time lapse assay, I used the MT-bound GFP-tagged MAPs as a proxy to visualize MTs, and confirmed the presence of MTs by tubulin-antibody staining at the end of the experiment. This assured that filaments decorated by MAPs were indeed MTs. In addition, some of the MAPs showing unique properties were further characterised with dilution experiments, which helps to check the role of MAP concentrations in the generation of the different MT phenotypes I have observed. These dilution experiments were conducted by mixing untransfected cell lysate with the lysate containing the MAP of interest in order to keep equivalent total extract concentration, at the same time lowering the MAP concentration.

In lysates (cytoplasm-BRB80 buffer mix), almost all MAP candidates I expressed were soluble. This validates the approach as a rapid, medium-throughput method to identify new proteins binding to dynamic MTs, to compare different MAPs under comparable conditions, and to rapidly discover novel properties of MAPs, and their concentration-dependency. My TIRF reconstitution assays showed that a several new proteins, or previously unknown isoforms of known MAPs, decorated MTs - an observation that was not reported before. Out of ≈10 new MAP candidates, Crmp2a decorated elongating MTs in the lysate assays. Besides, new isoforms or uncharacterised orthologs of already reported MAPs such as DCX and GLFND

also decorated polymerizing MTs, and are thus confirmed as bona-fide MAPs. By contrast, our preliminary attempts to purify Crmp2a to further confirm their direct MT binding were unsuccessful due to solubility issues. This indicates that the straight-forward characterisation of a large number of MAPs I was able to perform during my thesis essentially relied on the ex-vivo approach, and would have been impossible with purified proteins. This confirms the unique usefulness of my approach.

Below I will discuss selected MAPs that showed novel, and particularly intriguing properties on dynamic MTs.

4.3.1. Discovery of previously unknown properties of MAPs

MACF1 induce hook formation at the growing plus end

Using the ex-vivo approach, I found that MACF1, a truncated construct containing the MT-binding domain, not only decorates the MT surface, but also induces hook formations at the growing MT end, thereby preventing further MT elongation. Along with single coiled hooks, I also observed MTs with double-coiled hooked ends and MT splaying phenotypes. Experiments with the actin-depolymerizing drug latrunculin A showed that the formation of these hooks is independent of the presence of actin filaments. As our attempts to purify the MACF1 construct were successful, TIRF in vitro reconstitution experiments with purified MACF1 and purified HeLa tubulin showed the formation of MT rings instead of hooks. However, the addition of purified MACF1 in untransfected lysate leads to the formation of MT hooks similar to those observed with MACF1 lysates. This suggests that other components from the lysates might also influence the hook formations. Dilution experiments of MACF1 lysates with untransfected lysates indicated that the hook formation is a concentration-dependent process and does occur less frequently at lower MACF1 concentrations. A similar MT hook or curved protofilament formation was recently reported with axonemal tubulin from *Chlamydomonas reinhardtii* (Orbach and Howard 2019), and with Kinesin-5 in vitro (Chen and Hancock 2015; Chen et al. 2019). This demonstrates the ability of MTs to form diverse structures and assemble in different shapes, which could be induced by intrinsic tubulin properties or by proteins that associate with the MTs. My finding shows that MACF1 is a MAP which could alter their mechanical properties in order to induce the MT hook or ring formations. Further ultrastructural

reconstruction of the MACF1-bound MTs need to be conducted for the full understanding of the MT-hook architecture and to identify possible interacting partners if there is any.

CSAP forces MTs to form coiled filaments

Similar to the hook phenotype induced by MACF1, I found that CSAP can force MT to form coiled structures with a helix width of ~700 nm. These structures were not fully visible in the TIRF-M mode, therefore I used an off-TIRF mode to achieve higher penetration depth. Similar to MACF1, I didn't observe any influence of actin in these MT coil formations. I also observed spontaneous formation of MT coils independent of the MT seeds, suggesting that similar to other MAPs, CSAP itself can template MT polymerisation. I further used tubulin staining to confirm the colocalization of CSAP with coiled MT structures. CSAP is not the only MAP able to induce the formation of MT coils. A recent study showed that MAP6/STOP could also induce MT coils, which surprisingly had a similar helix width of ~700 nm. Ultra-structural studies show that MAP6 is a MT-Inner Protein (MIP) (Cuveillier et al. 2020). Because of coil phenotype and similar width of the helix, it would be interesting to see the ultra-structure of CSAP bound MT coils to confirm it as a MAP or a MIP.

MAP2 induces protofilament peeling

MAP2 exists in a range of different isoforms that are generated by alternative splicing of a single MAP2 gene (Ludin et al. 1996; Murphy and Borisy 1975b). MAP2C and MAP2D are two isoforms of lower molecular weight, however, both isoforms contain the entire MT-binding domain of the MAP2 family, and can therefore be used to study the binding behaviour of MAP2 proteins. Both, MAP2C and MAP2D decorate the entire MT lattice in our experiments, similar to what has been demonstrated before (Saoudi et al. 1995). Despite the fact that MAP2 is a well-known protein that has been studied for many decades, I found a novel activity of MAP2 that had so far not been reported: it can induce the peeling and curling of protofilaments from the polymerizing MT. This peeling can happen either at the side of an existing MT lattice, or at the plus-ends of growing MT. Most strikingly, MAP2 forms spherical patches inside the curled, pealed-off protofilaments alongside the MT lattice. Latrunculin-A experiments showed that this patch formation is an actin-independent process.

Moreover, I observed that MAP2D shows a greater number of protofilament peeling events in comparison to the MAP2C isoform. This is intriguing as the sole difference between MAP2C

and MAP2D is the number of MT-binding repeats. This is very similar to the protein Tau, which exists in a 3-repeat and a 4-repeat form (Goedert et al. 1989). Strikingly, the 4-repeat versions of Tau are known to bind stronger to MTs than the 3-repeat forms (Lu and Kosik 2001). This suggests that the difference in protofilament pealing seem for MAP2D (4 repeats) vs. MAP2C (3 repeats) might also be related to how strong these MAPs bind to MTs. This hypothesis is further supported by my observation that lowering MAP2 concentrations in lysates resulted in decreased patch formation (not shown).

It has been reported that MAP2 binds along individual protofilaments by bridging tubulin interfaces (Al-Bassam et al. 2002). One of the speculations which could explain this peeling phenotype would be a higher affinity of MAP2 to individual protofilaments rather than MT surfaces. However, cryo-EM studies of MAP2-decorated MTs in lysates would be the ultimate experiment to explain the molecular architecture underlying this unique phenotype.

Different MT binding behaviours within the echinoderm MT-associated protein family (EML1-4)

The family of EMAPs or EMLs contains six members in mammals. Using the ex-vivo lysate approach, I tested four members of this family, EML1, EML2, EML3 and EML4, for their binding behaviour on growing MTs. EML5 and EML6 are very large proteins (~2,000 amino acids) and show very low expression levels in cells, which is why I could not include them in my studies.

Except EML2, all three other members of the EML family promoted MT elongation and decorated the MTs, however in a surprisingly different manner. EML1 showed increasingly stronger signals toward the growing plus ends of the MTs as compared to the rest of the MT lattice. This behaviour was concentration-dependent, and was not observed at high levels of EML1 in the extracts. EML1 intensities form a gradient with a steady decrease of intensity starting from the plus tips of MTs, which is different from +TIPs like EB3 that form short comets with peak intensities at the growing plus tip, and a sharp decrease of intensity toward the MT lattice. There are previous studies showing that absence of EML1 leads to slow MT plus end growth (Bizzotto et al. 2017). However, further studies need to be conducted at molecular level for a better understanding of the progressive plus-end enrichment of EML1.
In the case of EML2, I found no MT growth in the lysate assay, which was subsequently confirmed by tubulin immunostaining. This observation agrees with a previous study that

describes EML2 as a MT depolymerizer (Eichenmuller et al. 2002). Interestingly, similar to the lack of new MT formation, I also didn't observe any actin filament formations, suggesting the formation of MT and actin filaments is mutually linked in the extracts, which is very evident for EML2 experiments which abolish MT polymerizations.

EML3 again behaved different from the other family members. I found a slow decoration of EML3 on the MT lattice, seemingly after MTs were already fully polymerised. This suggests that EML3 might have a higher affinity to polymerized MTs, but difficulties to initiate MT polymerisation.

EML4 decorates MT lattice without any specific localization pattern. Interestingly, dilution experiments with EML4 show that by lowering the concentration, EML4 forms island-like patches on MTs, similar to the neuronal MAP Tau (Siahaan et al. 2019; Abdel Karim et al. 2019), which was reported recently. This could signify that different MAPs are able to form such islands, and thus broaden the importance of this phenomenon. Moreover, it confirms that the ex-vivo approach also allows visualisation of island formation on MTs.

MAP7 generates the formation of MT asters

MAP7 family forms four different gene products in mammals: MAP7, MAP7D1, MAP7D2 and MAP7D3 (Bulinski and Bossler 1994; Metzger et al. 2012; Yadav, Verma, and Panda 2014). In my assay, I found that MAP7 had the unique property of inducing MT aster formation, with multiple MTs polymerizing from a common centre, and orienting to entire 360 degrees. The formation of asters was observed both from the end of GMPCPP MT seeds as well as from spontaneous nucleation events without seeds. There are several reports of MT aster formations involving kinesin motors (Juniper et al. 2018; Norris et al. 2018; Nédélec and Surrey 2001). Given that MAP7 is known to interact with kinesins, and promote their MT interactions (Hooikaas et al. 2019), it is possible that the aster-forming ability of MAP7 in cell lysates is mediated by the motor-recruitment property of MAP7. Other in vitro reconstitution studies with purified MAP7 protein and purified tubulin did not show any aster formations (Hooikaas et al. 2019; Monroy et al. 2018), which supports the hypothesis that MAP7 requires additional components such as kinesin motors from the cell lysates to form MT asters. My observation showed that presence of latrunculin A in the lysate experiments did not prevent any aster formations by MAP7, suggesting that it is an actin-independent process.

In contrast to MAP7, all other proteins from the MAP7 family did not induce aster formation, but were binding MTs. Moreover, MAP7D1 and MAPD2 showed a weak decoration on MTs in the TIRF assays, suggesting that they might have lower binding affinities for MTs. MAP7D3 showed no MT binding in my assay conditions due to unknown reasons.

4.3.2. Ultra-structural studies with cell lysates

One of the extended applications of the ex-vivo approach is the possibility of performing cryo-electron microscopy (cryo-EM) of MAP-MT assemblies without any purification process. To demonstrate the feasibility of this, I choose EML1, EML4 and MACF1 for cryo-EM studies. To perform the cryo-EM under optimal conditions, I first performed a TIRF reconstitution assay with appropriate lysate dilutions to make sure the samples are of good quality and the time we gave is enough to polymerise the MTs on EM grids. After obtaining the EM images, we performed a 3D-reconstruction only for EML1. The 3D-reconstructed image of full-length EML1 bound to MT with a resolution of ~3.7 Å shows that EML1 decorates MTs along the protofilaments. This binding pattern of EML1 could possibly block motor proteins (such as kinesin-1) that walk on single protofilaments, which was shown for MAPs such as Tau and MAP4 (Shibata et al. 2012; Schneider et al. 2015; Shigematsu et al. 2018; Monroy et al. 2018). A recent study had already reported the use of HEK lysates for cryo-EM followed by structural reconstruction, but in this case for non-MT structures, which further supports the practicality of the lysate approach for ultra-structural studies (Verbeke et al. 2018). However, the feasibility of cryo-EM studies for all remaining MAPs using lysates is uncertain, as a high MT decoration might be needed for sufficient resolution in the reconstruction of the structures. It is thus possible that our approach can be used only for MAPs with strong binding affinities. A comparative study with a weak-binding MAP from lysates and also with its purified form might help to explore the limitations of this approach further.

4.3.3. Determining the competition between different MAPs

Another powerful application of the lysate approach is the possibility to mix multiple lysates containing different MAPs at different dilutions and see their effect on MTs in real-time without having any buffer compatibility issues. To test this, I performed competition experiments with a wildtype and a mutant version of EML1. EML1 is a neuronal MAP conserved across many species. A single point mutation, threonine 243 to alanine in human EML1 was linked to the brain disorders such as ribbon-like heterotopia (Kielar et al. 2014). This is a neuronal migration

disorder which causes a misdistribution of white and grey matter, and leads to an abnormal shape of the brain and the skull. At the cellular level, it has been reported that the mitotic spindle length and cell body shape are perturbed in the absence of EML1, which could lead to aberrations in neuronal migration mediated by radial glial cells during development (Bizzotto et al. 2017; Cocas and Pleasure 2014). However, so far there are no studies at the molecular level directly comparing how wildtype and mutant EML1 behave on dynamic MTs.

To tackle this, I performed individual binding and competition experiments using the ex-vivo approach with EML1 versions tagged with two different fluorophores. I prepared the lysates separately, performed a TIRF assay with single lysates and by mixing two lysates to compare their MT binding in real-time. In order to exclude a potential bias introduced by the epitope tags, experiments were repeated with swapped fluorescent tags.

My competition experiments clearly showed that mutant EML1 has a weaker binding affinity than wild type EML1, as it was systematically outcompeted from MTs, while in the absence of wild type EML1, it was able to bind. In the individual TIRF experiments (with either wild type or mutant EML1 alone at a time), I found that mutant EML1 promotes less MT elongation comparing the wildtype, further suggesting a reduced ability of this EML1 mutants to bind and promote MT growth. A changed MT interaction in neurons could be the molecular reason for the observed brain disorders.

Current studies with purified MAPs have also performed competition experiments in vitro, pointing at the importance of this type of experiments in the understanding of MT regulation by a manifold of MAPs (Monroy et al. 2018; Monroy et al. 2020). The advantage of our lysate-based approach is that we can combine many more different MAPs as there are no technical restrictions, for example different buffer conditions, that might be difficult to solve for purified proteins.

It has been reported that MAPs are involved in several human diseases (see the Annex 6.2 showing different MAPs used in this study and their links to diseases). Several of them are caused by mutations in MAPs, and strikingly almost all MAPs have multiple substrates other than MTs. Therefore, my lysate approach is certainly a promising tool to quickly test the effect of these MAP mutations on MT-related properties and functions, and thereby helps to consider MAPs and MTs as potential therapeutic targets.

4.3.4. Actin and MT co-reconstitution experiments: to study the role of MAPs in actin-MT crosstalk

In the TIRF assays with lysates, I split all MAP experiments into two sets: one without actin (by using the actin monomer sequestering drug latrunculin A) and one with actin (without the drug). Interestingly, in the experiments without latrunculin A, I observed the formation of actin filament along with MTs. This suggested that the actin network forming in the lysates could affect the MT-MAP assemblies. This was particularly prominent for GLFND1 and Syntaphilin A, where the MAPs appeared to co-align actin with MTs. Strikingly, however, experiments in the presence of the actin polymerisation inhibitor showed that the observed MT phenotypes induced by the MAPs were unaffected by the presence of filamentous actin.

Based on the actin and MT staining in the TIRF assays, I could classify the ~50 MAP candidates into three categories: one group of MAPs which promotes actin-MT coalignments; a second group of MAPs which inhibits the alignment; and a third group showed a mixed phenotypes. The roles of MAPs in actin-MT crosstalk is an emerging topic and has several cellular evidences showing their involvement in actin-MT coalignment in different physiological context (Dogterom and Koenderink 2019; Roeles and Tsiavaliaris 2019; Muller et al. 2019; Kita et al. 2019; Colin et al. 2018; Szikora et al. 2017b; Ketschek et al. 2016b; Farina et al. 2019; Peris et al. 2018; Elie et al. 2015; Doki et al. 2020), thus it requires more attention and need to be further studied.

Moreover, previous studies have shown that BRB80 buffer is compatible for both actin and MT in vitro reconstitution (Elie et al. 2015), proposing the possibility to use my approach to extend towards studying actin-related proteins as well. It will be also possible to keep actin at the same time preventing MT formation by the addition of MT-inhibiting drugs such as nocodazole. This could allow to screen for actin-binding proteins among the MAPs. In the light of emerging roles of the actin-MT crosstalk in many cellular processes, my approach provides an easy tool to test proteins which are difficult to purify, but need to be confirmed as MAPs or as actin-binding proteins. For instance, one of my MAPs of interest: cingulin has been reported as a MAP and also as an actin binder (D'Atri and Citi 2001a; Jones et al. 2019). In my experiments, I observed that cingulin promotes the formation of actin filaments and strongly decorates them, instead of MTs. Even in the presence of an actin-depolymerizing drug cytochalasin-D and latrunculin A, cingulin did not decorate MTs. One possible explanation for this is that the binding of cingulin

to both MT and actin is regulated by AMPK-mediated phosphorylation {Jones, 2019 #6747. Further studies need to be performed to test this mechanism in the ex-vivo approach.

4.4. Outlook: further improvements of the method, future applications

The here-established purification-free method is appropriate to address many important biological questions. Most importantly, it can be used for studying larger numbers of MAPs in parallel than previously possible, and to study MT-actin interactions at the same time. However, the ex-vivo approach also has some limitations. One is the lack of precision about the protein concentration (MAPs and tubulin) in lysates, which could vary from one lysate preparation to the other. Here I addressed this mainly by estimating total protein concentration by standard BCA protein assays. Given that tubulin concentrations are strictly controlled in cells (Ben-Ze'ev, Farmer, and Penman 1979) (Cleveland 1989) (Yen, Machlin, and Cleveland 1988), and ~3% of total protein content in cultured cells is tubulin (Hiller and Weber 1978), we assume that by controlling total protein concentrations, we assure that the tubulin concentrations are similar throughout all experiments. I further quantified MAP concentrations by immunoblots calibrated with purified GFP protein.

These two quantifications could overcome this particular limitation of the lysate approach to a great extent. However, in particular the quantification of the immunoblot is meticulous and work-intense. For instance, finding a linear detection range of protein concentration for each MAP can be a time-consuming step, and might become limiting if many MAPs need to be tested. Thus, new sensitive and fast methods such as fluorimetry-based assays for the GFP quantifications need to be implemented for high-throughput experiments.

Another potential limitation of this approach is that the MT phenotypes observed for MAPs might be induced by additional other, unknown proteins from the lysate. The hook formation induced by MACF1 is an example for this, as it could not be reproduced with purified MACF1 alone. At the same time, this limitation can be considered as an advantage, by acting as a first step in the identification of novel MT activities, and the potential identification of proteins or multi-protein assemblies involved in these processes.
There are a number of technical factors such as the total number of cells taken, transfection efficiency, lysis efficiency and final buffer volume used for the collection of lysates that need to be strictly controlled in order to assure the reproducibility of the assays.

I chose to use the fluorescently-tagged MAPs as a proxy to visualize MTs in my assay, which precluded the need of any additional MT staining that could have interfered with MT assembly and/or MAP binding. To determine the identity of MTs, MTs were immuno stained at the end of each experiment. However, if required, direct visualization of MTs in real-time along with MAP signals is also possible by either using a cell lines expressing fluorescently labelled tubulin (e.g. HeLa EGFP-α-tubulin that I successfully tested) for the lysate preparations, or by mixing fluorescently-labelled, purified tubulin into the lysate in a controlled manner. For the former possibility, I observed an altered MT behaviour with the addition of labelled brain tubulin in lysates.

Since I aimed to develop a rapid and simple method to test a large number of MAPs, I used a rather simple standard method to treat the glass surfaces of the TIRF chambers. But for those who study a small number of proteins or are interested in weak binding MAPs or single-molecule studies, extensive glass surface cleaning and hydrophobicity treatments (Bieling et al. 2010) are highly recommended for obtaining better signal-to-noise ratios.

Furthermore, the proteins binding to endogenous MAPs decorating MTs, and not directly binding to MTs can also be visualized as MT decorators in the lysate approach, and could thus be misinterpreted as MAPs (similar to cell studies). Consequently, MT reconstitution or any in-vitro interaction assay with purified proteins will be inevitable to univocally define a novel protein as a bona fide MAP. However, given that most of the MAPs I investigated were highly overexpressed, it rather unlikely that a potential adapter protein could be present in equimolar concentrations in the cells.

Future applications

In my project I used the purification-free pipeline for studying more than 50 MAPs and presumed MAPs. I showed that my extract-based ex-vivo approach can be used for many applications such as for the identification of new MAPs or novel properties of known MAPs. I also demonstrated that this approach can be used for cryo-EM structural studies, to study actin-MT crosstalk, to study tubulin PTMs and for MAP competition experiments. Apart from all this, my purification-free pipeline could also help to address new questions related to MTs. This includes testing of drugs affecting MT dynamics, experiments with micropatterns to see how

MTs are affected by different MAPs or drugs in confined space at single-MT resolution. By preparing extracts from synchronised cells during division, it would be possible to assess the behaviour of MAPs in different stages of cell division.

Even though I excluded the possibility of having MT-organizing centres (MTOCs), γ-tubulin ring complexes (γ-TuRCs) and other endogenous MT nucleating sources in the cell lysates by the high-speed centrifugation step in the lysate preparation, I observed several spontaneous MT nucleation events for many MAP lysates, along with the GMPCPP-seed-mediated nucleation events. This suggests more than MT stabilizers (either stabilizing short MTs or preventing MT depolymerization), many of the MAPs could act as either MT nucleators or elongators (similar to formins in actin cytoskeleton) - a clue that needs to be further explored in future experiments.

In literature, MAPs have been often classified into neuronal MAPs and cell-division MAPs, a classification based on their abundance and localization. In the here-presented approach I used one single cell line to express all MAPs, irrespective of their known or unknown functions in different cell types. The rationale was to obtain high expression levels (by using HEK cells) and a rapid, simple-to-expand method. Given my observation that other endogenous proteins might participate in the assembly of MT arrays in this assay, it would now be interesting to also consider the natural microenvironment of a given MAP. For instance, a neuronal MAP could be expressed in cultured neurons for lysate preparation. This is technically more challenging because only small amounts of primary cells can be cultured, and because the transfection of the expression plasmids is not straight forward. We have already prepared the ground for this additional step by cloning all MAPs analysed in this study into lentivirus-based expression vectors, which would allow us to transduce any primary cell line efficiently with all MAPs of our study.

4.5. Emerging properties of structural MAPs

The term “structural MAP” is used for MT interactors that are considered to bind and thereby stabilize MTs. This general classification is mainly based on early studies in cells in which MAPs were overexpressed, and also from biochemical experiments for a few MAPs. With the advancement of microscopy-based techniques such as TIRF-based vitro reconstitution assays, we now know MAPs can perform functions other than just stabilizing MTs. For instance, MAPs such as SSNA1 and TPX2 are reported to involve in the MT branching, in which SSNA1-

mediated MT branching is also implicated in neuronal development (Basnet et al. 2018; Alfaro-Aco, Thawani, and Petry 2017). The neuronal MAP Tau and TPX2 can form phase-separated condensates that accumulates soluble tubulin to induce MT polymerisation (Hernandez-Vega et al. 2017) (King and Petry 2020). Moreover, Tau can bind the MT lattice as small stable patches called as Tau islands. This property of Tau is highly dependent on concentrations, and affects several MT functions, in particular the progressive movements of kinesin motors (Siahaan et al. 2019; Tan et al. 2019).

In cell-based studies, there are some reports indicating MAPs could alter the MT structures and thereby influence cell morphology. For instance, SSNA1 self-assembles into fibrils are proposed to guide MT protofilaments to form branched MTs, and strikingly SSNA1 highly concentrated at the branching sites of neuronal axons (Tymanskyj et al. 2017; Basnet et al. 2018), suggesting that it can influence the axon branching by inducing MT branching. In dorsal root ganglion (DRG) neurons, MAP7 has been shown to modulates axon collateral branch development (Tymanskyj et al. 2017). CLIP-170 was implicated in the regulation of neuronal polarity by altering MT-, and thus growth-cone dynamics (Neukirchen and Bradke 2011). Thus, it is highly tempting to speculate that similar to SSNA1, the observation I made for MAP7 (MT aster formations) and CLIP-170 (MT branching events from CLIP-170-tubulin droplets) might influence neuronal morphology through MT branching and nucleation. However, immunostaining of these MAPs in axon branching sites, or an ultrastructural study to better localise CLIP-170 and MAP7 in neurons is needed to obtain more insights.

In summary, the use of the term “structural MAPs” might not be appropriate in light of emerging roles of MAPs, and they refute the simplistic idea that MAPs simply stabilise MTs. My work opens a new field of MAP research, however many of my findings require more detailed follow-up studies to better understand the novel diversity of functions of the heterogenous group MAPs. To discover novel properties of MAPs at a higher resolution in a cellular context, the advancement of new and sensitive techniques is required. The progress in current developments of super-resolution and expansion microscopy is promising in this respect. In addition, the cytosol-based approaches such as the use of cell lysates, Xenopus egg extract and drosophila embryo extract also gives high hopes for the understanding of multi-protein based sub-cellular structures comprising MTs and MAPs at high resolution.

4.6. The need of purification procedures for tubulin with controlled PTMs

The early research on MTs was driven mainly by in vitro studies using purified tubulin mostly from bovine or porcine brains, and have been extensively used to determine the structure, polarity and dynamic properties of MTs (Johnson and Borisy 1975; Weisenberg 1972b; Weisenberg, Borisy, and Taylor 1968). After 1970s, with the fast development of light microscopy, more sensitive assays emerged. This advanced our understanding of MT properties such as dynamic instability, their possible mechanisms, and their different functions (Mitchison and Kirschner 1984a; Borisy and Olmsted 1972; Kirschner and Williams 1974; Bieling, Telley, and Surrey 2010; Dogterom and Surrey 2013). Many of the in-vitro experiments performed so far used tubulin from brain. Although tubulin purification from brain tissue has the advantage of obtaining large quantities of assembly-competent tubulin, one of the major drawbacks was that brain tubulin is highly heterogeneous due to its composition of different tubulin isotypes and the enrichment of tubulin PTMs. This heterogeneity limited our understanding of the molecular functions of tubulin PTMs and isotypes. Therefore, the development of methods for the purification of homogenous and assembly-competent tubulin was crucial to study the molecular mechanism of tubulin code, particularly to study their role in dynamic properties of MTs and their role in MAP-MT interactions.

In recent times, new strategies were developed for purifying tubulin to address different biological questions. For instance, tubulin purification with affinity chromatography was made possible by immobilising the MT-binding TOG (tumour-overexpressed gene) domain of the yeast protein Stu2p. This TOG column helped to isolate whole tubulin pools from a wide variety of cells or tissues (Widlund et al. 2012b). While still purifying mixtures of tubulin, this novel method allowed to broaden the sources used for tubulin purification. Recombinant tubulin, by contrast, cannot be purified from bacteria. An elaborate method to purify recombinant tubulin was developed using the baculo-virus based expression system (Minoura et al. 2013b). However, this method is complex and very cumbersome, and might thus be restricted to laboratories that have a great expertise in protein purification. It has so far been used to study the impact of specific tubulin isotypes and tubulin mutations in vitro (Uchimura et al. 2015; Pamula, Ti, and Kapoor 2016; Vemu et al. 2016; Ti, Alushin, and Kapoor 2018).

We developed a method to purify assembly-competent tubulin with controlled tubulin PTMs that is based on the classical polymerization-depolymerization cycles. Our method allows to purify tubulin from limited tubulin sources such as adherent-or-suspension cell culture (having specific overexpressed tubulin isotypes or PTM enzymes), or from single mouse brain lacking different tubulin modifying enzymes (and thus, specific PTMs). Owing that this method is very similar to the classical protocol for the large-scale purification from brain, tubulin purified with our method has comparable quality and polymerization competency as tubulin from large-scale brain tubulin preparations. Thus, the purified tubulin from our method is appropriate for in vitro reconstitution and TIRF-M based experiments, that can help us to understand the molecular functions of tubulin PTMs in the dynamic properties of MTs and MAP-MT interactions. In addition, these tubulins can be used to study motility of motor proteins (Even et al. 2019) (Barisic et al. 2015), to test the specificity of chemical sensors against specific tubulin modifications (Kesarwani et al. 2020), in solid-state NMR spectroscopy (Luo et al. 2020), MT-MAP co-sedimentation assays, mass spectrometry, electron microscopy and crystallographic studies.

Although this purification method could help to address many questions regarding the tubulin PTMs, the repeated cycles of warm polymerization and cold depolymerization could influence the composition of the final tubulin, and still would not be completely homogenous, because of different tubulin isotypes and their polymerization competency. Thus, for any quantitative analyses of the composition of tubulin in samples, the method by (Widlund et al. 2012b) would be recommended.

4.7. Tubulin PTMs could regulate MAP-MT interactions

Tubulin undergoes a wide range of PTMs, and are one of the factors that affect the MT properties, and this could regulate its function with the interaction of different MT interacting proteins or MAPs. However, a few molecular studies that have been done so far mostly investigated the role of detyrosination, and more rarely polyglutamylation. For instance, it has been shown that CAP-Gly domain-containing proteins were localized to the plus ends of tyrosinated MTs, but lose this localisation when MTs are detyrosinated (Peris et al. 2006; Bieling et al. 2008b; Weisbrich et al. 2007). The dynactin subunit 1, a CAP-Gly protein that forms a complex of dynein, dynactin and bicaudal D homologue 2 (BICD2), is also sensitive to MT tyrosination, which was reported to have a role in the landing of this complex on MTs

in vitro (McKenney et al. 2016). Another study showed that the MT-depolymerising motors KIF2A and mitotic centromere-associated kinesin (MCAK) are sensitive to tubulin tyrosination, and do less efficiently depolymerise detyrosinated MTs. This suggested a mechanism explaining why detyrosinated MTs are more stable in cells (Peris et al. 2009).A study using using chimeric yeast tubulins to imitate tubulin PTMs and isotypes show that kinesin-2 has increased motility and processivity on detyrosinated MTs, which was not true for kinesin-1 (Sirajuddin, Rice, and Vale 2014b). Similarly, centromere-associated protein E (CENP-E), a kinesin-7 motor associated with kinetochores, shows higher processivity on detyrosinated MTs (Barisic et al. 2015; Souphron et al. 2019).

Yeast tubulin chimeras were also used to study the role of polyglutamylation by controlling the number of glutamate residues incorporated into the C-terminal tubulin tails. While kinesin-2 motility was induced by addition of chains of three or ten glutamate residues, kinesin-1 was uniquely activated by side chains of ten glutamate residues. By contrast, neither the depolymerizing activity of kinesin-13, nor the motility of dynein were affected by glutamate side chains of any length (Sirajuddin, Rice, and Vale 2014b). This suggests a selective regulation of motor protein behaviour by specific polyglutamylation patterns on MTs. Strikingly, another study showed that MT-severing protein spastin is regulated by polyglutamylation in a biphasic manner. That is, initially added polyglutamylation could activate spastin severing (Lacroix et al. 2010), but very high levels of polyglutamylation could inhibit its severing activity (Valenstein and Roll-Mecak 2016). A similar idea had been proposed earlier for other MAPs for glutamylation using blot-overlay assays (Boucher et al. 1994; Bonnet et al. 2001; Larcher et al. 1996; Bonnet et al. 2002), but so-far not been confirmed under more native experimental conditions.

It thus appears that the regulatory role of tubulin PTMs in MAP-MT interactions at the molecular level was so far only explored for a few MAPs. The major reasons could be the lack of appropriate tools, such as purified tubulin with controlled PTMs. Our successful effort to overcome this (Souphron et al. 2019) also allowed me to initiate experiments to test the role of tubulin PTMs in MAP-MT interactions.

For this, I first performed MT-MAP co-sedimentation assays with purified MAPs, and MTs polymerized from tubulin modified with different PTMs. I conducted assays for Tau and MACF1 against tyrosinated, detyrosinated, glutamylated and non-glutamylated MTs. However, the preliminary results from these co-sedimentation assays did not show any striking

difference in the MAP binding preference to a MT kind with a particular tubulin PTM. This suggests that for the tested MAP-MT combinations, the tubulin PTMs I tested might not have a strong effect at a micromolar range of MAP concentrations used in these experiments. Detecting and quantifying MAPs at nanomolar or picomolar concentration, which correspond more to their physiological concentrations is not possible in these co-sedimentation assays. In addition, the lack of data about which MAPs could be sensitive to tubulin PTMs, combined with the difficulty in purifying large numbers of different MAPs strongly directed the choice to switch my strategy from co-sedimentation assays to in-vitro MT reconstitution and TIRF-M assays using cell lysates. Owing to the fact that these assays require less material (tubulin and MAPs) comparing most biochemical experiments, it also provides the advantage of having the capacity to perform repeated experiments for statistical analyses. Thus, I established a method in the lab based on MT reconstitution and TIRF-M to study the tubulin PTMs using cleared cell lysates.

In these assays, I used purified MTs with controlled PTMs and used cleared lysates as source of soluble MAPs. In the tricolour TIRF microscopy assay, two kinds of MTs having different PTMs, labelled with distinct fluorophores were immobilized in a TIRF chamber. Subsequently, the binding of MAP in the third colour was imaged in real-time to see their binding affinity for different PTMs. As an initial screening, I performed the tricolour TIRF microscopy for around 25 MAPs. From these experiments, tau showed a higher binding affinity to modified brain MTs comparing the unmodified MTs from HeLa cells. My estimation of a ~100 nM concentration of tau protein in these assays shows that the binding preferences become visible at rather low MAP concentrations, as expected.

However, future assays need to be designed carefully with the appropriate controls. For example, I found some MAPs were sensitive to fluorophores used for the MT labelling rather than the tubulin PTMs. To reveal such artefacts, switching the fluorophores of the MTs is required to confirm the influence of tubulin PTMs in the MAP-MT interaction.

Tubulin PTMs could regulate the binding parameters of MAPs, thus could control MT functions. In contrast, upon binding, MAPs might also control the PTMs on the MT lattice. To date, there is no evidence directly supporting this; however, a recent observation showed that axonal transport of ATAT1-enriched vesicles using MT as motor path could drive the acetylation of α-tubulin in axons (Even et al. 2019). Using the lysate approach, we could also

perform experiments to test the role of MAP binding in regulating the tubulin PTMs. For instance, decorating unmodified MTs with a particular MAP from lysates, followed by immunostaining of the MT with antibodies against specific tubulin PTMs, which might explain the role of MAPs in controlling tubulin PTMs.

Methods for purifying tubulin with controlled PTMs (Souphron et al. 2019; Widlund et al. 2012b; Minoura et al. 2013b), and lysate approaches for obtaining soluble MAPs are available now. This enables us now to test the sensitivity of any MAPs against different tubulin PTMs or vice versa. Furthermore, to measure the physical parameters such as association (K_{on}) or dissociation (K_{off}) constant of MAP binding on differentially modified MTs, techniques such as FRAP (Fluorescence Recovery After Photobleaching) and FLIP (Fluorescence Loss In Photobleaching) can be used.

5. Conclusion

The main goal of my PhD project was to established a cell-lysate based method to study a broad spectrum of MT interacting proteins using MT reconstitution and TIRF microscopy. This medium-throughput approach aims to understand the mechanistic role of MAPs on dynamic MTs at an individual MT resolution. The MAP candidates used in this study are involved in different cellular processes such as cell division, cell shape, neuronal differentiation and ciliary beating, and are also linked to several human diseases. Secondly, it was necessary to develop novel tubulin purifications approaches to obtain tubulin with better defined composition in terms of tubulin PTMs and isotypes. A part of my thesis project was to elaborate such a method in collaboration with other lab members.

In combination, the novel ex-vivo approach I developed, together with the availability of different tubulin samples now allows to systematically test the impact of the tubulin code on MT-MAP interactions, MT dynamics and structure in vitro.

The major outcomes and findings from my PhD projects are:

- I successfully established and developed a purification-free method to study a large number of MAPs (>50) using MT reconstitution and TIRF microscopy.

- I identified novel properties of MAPs on dynamic MTs, including MACF1 (hooked MT ends), CSAP (helicoid MTs), MAP7 (MT asters), MAP2 (protofilament peeling), MAP8 and Tau (MT fragmentation), and EML1 (higher binding affinity to the growing MT ends).

- I showed the formation of CLIP-170 co-condensates with tubulin as periodic droplets on MT lattice, and I demonstrated that they can nucleate new MTs from it.

- In collaboration, I performed cryo-EM studies of EML1 in lysates, which showed that EML1 binds along MT protofilaments.

- I set up MAP competition experiments (by mixing lysates containing MAPs tagged with different coloured fluorophores). These experiments revealed that the disease-related mutant EML1^{T243A} binds less to, and promotes less MT growth than wildtype EML1.

- I performed TIRF reconstitution assays with and without actin inhibitor drug (Latrunculin A), which showed that out of the ~50 MAP candidates, some MAPs (e.g. GLFND1) induce the actin-MT co-alignment, some prevents the co-alignment (e.g. MAP10), while other MAPs showed a mixed phenotype (Eg: EML3).

- I participated in the establishment of purification methods to obtain tubulin with controlled PTMs by polymerization–depolymerization cycles.

- I set up a tricolour TIRF assay to measure the impact of tubulin PTMs on the binding of MAPs. I showed that Tau has a higher binding affinity to taxol-stabilized PTM-rich brain MTs as compared to unmodified HeLa MTs.

- I participated in establishing an in vitro setup to study the role of tubulin carrying patient mutations. This setup allows us to determine the impact of temperature on MT assembly and stability. Our Preliminary studies show that lissencephaly-derived mutations in α-tubulin (TUBA1A) could affect the dynamics as well as the cold-sensitivity of MTs.

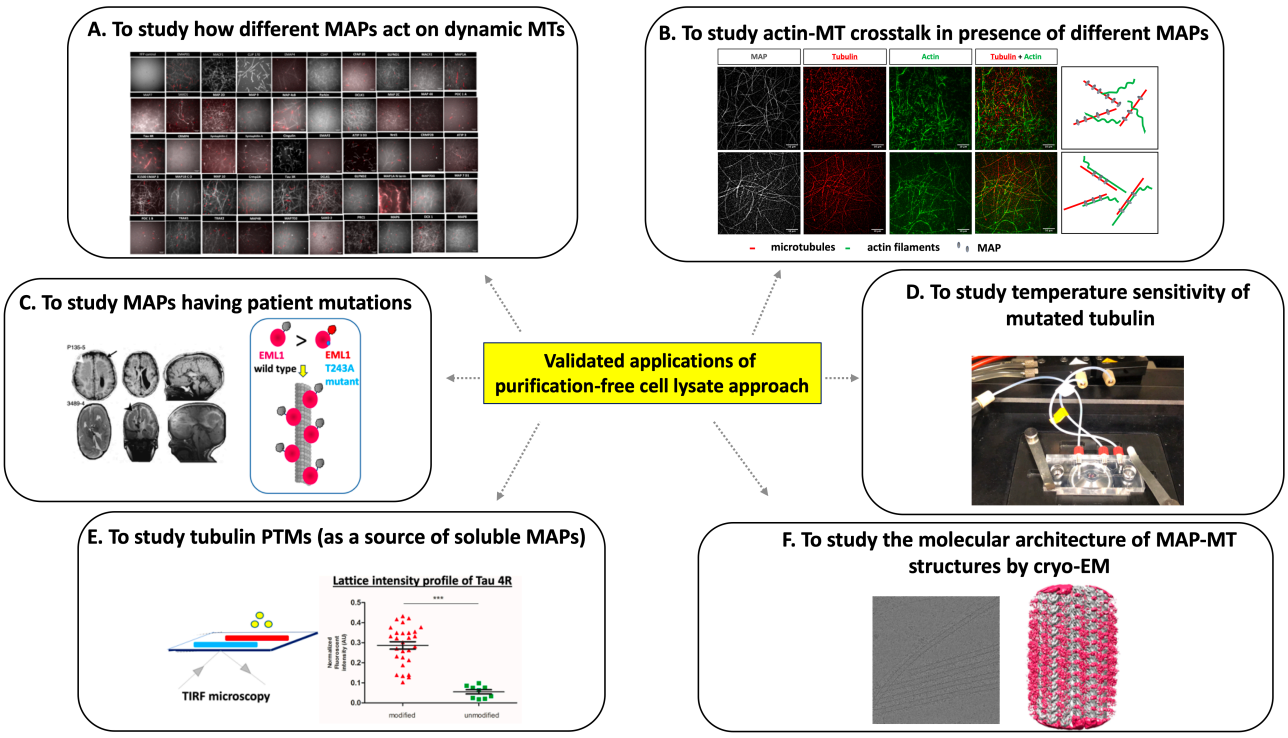

Figure 19: Different validated applications of purification-free cell lysate approach.
Based on TIRF microscopy and MT reconstitution assays, there are different validated applications of lysate approach (**A-E**). In addition, the lysate approach can also be used for ultra-structural studies for understanding MAP-MT binding architecture by cryo-electron microscopy (**F**). Application **A, B, C** and **F** are shown in the Jijumon et al. manuscript (result section, chapter 1). Application **D** and **E** are shown in the additional result sections of chapter 2.

Fig. 19 shows different validated applications of the cell-free ex vivo approach. The major advantage of the lysate approach is that all tested MAP candidates were soluble in the cell lysates, which provides the ability to test any protein of interest as a bona fide MAP, and also to study the binding behaviour of MAPs on dynamic MTs at individual MT resolution (Fig. 19A). In addition, the lysate approach can also be used for in vitro reconstitution of actin filaments and for the screening of actin-binding proteins. For example, cingulin (a previously reported actin nucleator (D'Atri and Citi 2001b)), decorated newly nucleated actin filaments by consuming soluble endogenous G-actin from cell lysates. Since it is possible to reconstitute both actin and MTs from lysates, it is also possible to test the influence of different MAPs and actin-binding proteins in the actin-MT crosstalk (Fig. 19B). A wide range of MAP and MT related diseases are due to the mutations in specific MAPs and tubulin isotypes. Using the lysate approach and TIRF reconstitution assays, I tested mutated EML1 for its binding affinity to MTs, and the impact of mutated TUBA1A on the dynamic properties of MTs at different temperatures (Fig. 19C, D). This demonstrates that lysate-based ex-vivo approach is a powerful

tool to study a large number of mutations linked to MT cytoskeleton and its associated proteins. Strikingly, we also succeed in successfully using the lysate approach for performing cryo-electron microscopy, which could detail the molecular architecture of MAP-MT interactions at high molecular resolution (Fig. 19F).

Another important application of the lysate approach is to study the role of tubulin PTMs in MAP-MT interactions (Fig. 19E). Coupling lysate approach with the purified custom-modified MTs (Souphron et al. 2019), one could screen the binding sensitivity of almost any bona fide MAPs against different tubulin PTMs. The future possibilities of the lysate approach in studying tubulin PTMs are immense. For example, to test the influence of tubulin PTMs in the novel MT phenotypes generated by different MAPs, one could either co-transfect the MAP of interest and the tubulin-modifying enzyme in the same cells and can perform the TIRF dynamic assays with the lysates, or can transfect one of these proteins to a stable cell line having the constitutive expression of the other. A similar strategy can be followed for testing the effect of PTMs in the dynamic properties of MTs; instead of a MAP, here it would be a tubulin-modifying enzyme. Another experiment one could perform to study tubulin PTMs is to test the competitive affinity of different tubulin-modifying enzymes against an unmodified MT substrate. For instance, a polyglutamylase labelled in one colour can be allowed to compete against a polyglycylase labelled in the second colour, for a common unmodified MT substrate which can be labelled in a third colour. Here, the use of the lysate approach would provide the advantage of having both enzymes soluble, and functional in the same buffer. Furthermore, in contrast to the idea of tubulin PTMs attracts MAPs, it is also possible to test the role of MAP bound MTs in attracting tubulin modifiers from the cell lysates. For example, after decorating an unmodified MT with different MAPs, immunostaining of specific tubulin PTMs might help to understand the converse role of MAPs in regulating tubulin PTMs.

In summary, the cell-free lysate approach is likely to set a precedence of being a simple and fast method for the characterization of MAPs in a medium-throughput scale, and for studying tubulin PTMs. It can be used for both TIRF reconstitution and cryo-EM studies. Using this technique, we could potentially characterize any proteins associated with MTs, independent of its source, and without the need for any customized purification procedures. The impressive solubility of a wide range of different proteins in our approach opened it to broad applications such as the identification of new MAPs and new properties of MAPs, to study the actin-MT crosstalk, in MAP competition experiments, and to study the tubulin code. In total, the cell-free

pipeline developed during my PhD project opens many possibilities to advance our understanding of the MT cytoskeleton, its associated proteins, and the role of tubulin PTMs in MAP-MT interactions, which are collectively involved in several cellular processes and human diseases.

6. Annexes

Annex 6.1. Microtubule-Associated Proteins: structuring the cytoskeleton (published article).

Annex 6.2. Short descriptions of MAP candidates used in this study

Annex 6.2.1. Proteins used in this study which are already reported as MAPs with in vitro confirmations.

Annex 6.2.2. Proteins used in this study which are already reported as MAPs, but without in vitro confirmations.

Annex 6.2.3. Proteins used in this study which are not reported as MAPs before.

Annex 6.3. Purification of tubulin with controlled posttranslational modifications and isotypes from limited sources by polymerization-depolymerization cycles (published article).

Annex 6.1. Microtubule-Associated Proteins: Structuring the Cytoskeleton (published article)

Here, I added a published review (where I am a co-author) about structural MAPs. Understanding the binding behaviour of a large number of structural MAPs on dynamic MTs is the central focus of my PhD project.

Microtubule-associated proteins: structuring the cytoskeleton

Satish Bodakuntla, A.S. .Jijumon, Cristopher Villablanca, Christian Gonzalez-Billault, Carsten Janke

Microtubule-associated proteins: structuring the cytoskeleton

Satish Bodakuntla[1,2], Jijumon A.S.[1,2], Cristopher Villablanca[3,4], Christian Gonzalez-Billault[3,4,*], Carsten Janke[1,2,*]

[1]Institut Curie, PSL Research University, CNRS UMR3348, F-91405 Orsay, France

[2]Université Paris Sud, Université Paris-Saclay, CNRS UMR3348, F-91405 Orsay, France

[3]Center for Geroscience, Brain Health and Metabolism (GERO), Santiago, Chile

[4]Department of Biology, Faculty of Sciences, University of Chile, Santiago, Chile

*Correspondence: chrgonza@uchile.cl (C. Gonzalez-Billault); Carsten.Janke@curie.fr (C.Janke)

Christian Gonzalez-Billault, Department of Biology, Faculty of Sciences, Universidad de Chile, Las Palmeras 3425, 7800024 Santiago, Chile

Telephone: +56 22 9787442

Carsten Janke, Institut Curie, Centre Universitaire, Bâtiment 110, F-91405 Orsay Cedex, France

Telephone: +33 1 69863127

Abstract:

Microtubule-associated proteins (MAPs) were initially discovered as proteins that bind and stabilise microtubules. Today, an ever-growing number of MAPs reveals a more complex picture of these proteins as organisers of the microtubule cytoskeleton with a large variety of functions. MAPs enable microtubules to participate in a plethora of cellular processes such as the assembly of mitotic and meiotic spindles, neuronal development, or the formation of the ciliary axoneme. While some subgroups of MAPs have been exhaustively characterised, a strikingly large number of MAPs remains barely characterized, other than their interactions with microtubules. Here, we provide a comprehensive view on the currently known MAPs in mammals. We discuss their molecular mechanisms and functions, as well as their physiological role and links to pathologies.

Defining Structural MAPs.

Microtubules are a major component of the eukaryotic cytoskeleton that are uniformly assembled from conserved α/β-tubulin heterodimers. Microtubules play important roles in virtually every cellular process, such as cell division, cell motility, intracellular organization and trafficking of organelles. To fulfil these divergent functions, microtubules assemble into distinct arrays that are characterized by a defined architecture and dynamics. Formation of these assemblies requires specialized proteins that interact with microtubules – the microtubule-associated proteins (MAPs). Based on their mode of action, MAPs can be classified into **(a)** motile MAPs or motor proteins that generate forces and movement [1, 2], **(b)** enzymes that break or depolymerize microtubules [3], **(c)** microtubule nucleators [4], **(d)** end-binding proteins that specifically associate with plus- or minus-ends of microtubules [5], and **(e)** the so-called structural MAPs. While the first four categories (a-d) of MAPs are clearly defined by their functions, the latter category (e) is a rather vaguely defined, heterogenous group of proteins that bind, and thus stabilize microtubules, but no systematic view on their functions has so far emerged. Here, we discuss the current understanding of the mechanisms and functions of those structural MAPs. Our review focusses on mammalian MAPs, and we refrain from discussing the extensively-studied posttranslational regulation of MAPs, which has been reviewed in detail elsewhere [6, 7].

Discovery of microtubule-associated proteins

Early efforts to purify tubulin from brain extracts using cycles of assembly-disassembly led to the identification of the first MAPs, MAP1 and MAP2, as higher-molecular components of microtubule assemblies [8, 9]. At the same time, a different biochemical purification procedure led to the discovery of tau, another protein factor essential for microtubule assembly [10-12]. In contrast to MAP1 and MAP2, tau protein was of lower molecular weight, strikingly correlated with the impact of those proteins on microtubule assemblies: while MAP2 formed long projections at the microtubule surface that increased the distance between single microtubules, microtubules decorated with the smaller tau protein were packed much denser [13]. It thus appeared that MAPs have the ability to control the structure of microtubule assemblies, hence referred to as ‘structural MAPs’.

The development of a method to purify tubulin from HeLa cells was instrumental in the discovery of two novel, non-neuronal, MAPs of 210 kDa and 125 kDa [14]. The 210-kDa MAP was considered a bona fide MAP based on its similarity to previously characterized

MAPs [15], and was named MAP4 [16]. The 125-kDa protein corresponded to the later-described MAP7 [17, 18].

All MAPs had to this point been identified by their capacity to promote the assembly of tubulin into microtubules. However, a considerable share of microtubules never disassembles when tubulin is purified from brain tissue. A closer biochemical characterization of these cold-stable microtubules led to the discovery of the protein STOP (stable tubule only peptide) as a factor that confers cold-stability to microtubules [19, 20]. As purified STOP protein behaves like a MAP [21], it was later named MAP6.

Apart from those initially characterized major MAPs, several minor proteins were detected in fractions of polymerized tubulin, which all could potentially be MAPs as well [22, 23]. Monoclonal antibody technologies bolstered the purification of some of these potential MAPs, for instance MAP3 [24] and MAP5 [25]. Strikingly, another protein, MAP1C, turned out to be the retrograde motor protein, cytoplasmic dynein [26, 27].

By the end of the 1980s, advances in molecular cloning clarified the identity of many of the MAPs that were so far only biochemically characterized. MAP1 and MAP5 were found to be encoded by distinct genes, but as they are highly similar proteins, were renamed MAP1A and MAP1B [28]. In contrast, different isoforms of MAP2, referred to as MAP2A, 2B and 2C, originate from alternative splicing of the same transcript [29, 30]. Surprisingly, MAP3 and MAP4, thought to be two distinct proteins based on immunological assays, appeared to be identical gene products, and are now referred to as MAP4 [31]. The cloning of tau protein revealed that a single gene gives rise to six distinct splice isoforms [32, 33]. The differential splicing of tau protein received a particularly broad attention, given that tau is the main component of paired helical filaments (PHFs) – one of the pathological hallmarks of Alzheimer's disease [34].

In the 1990s, annotated genome and cDNA sequences allowed the bioinformatic identification of novel MAPs, such as the entire family of mammalian MAPs, the EMAP-like (EML) proteins. EMAPs had initially been discovered as main components of the microtubule cytoskeleton in sea urchin eggs [35, 36], and the human homologs of these proteins were found based on sequence similarities [37, 38]. The fact that the EMAP family has six members in mammals strongly suggests important functions, however so far, little is known.

Another technological advance - cDNA libraries - allowed the setup of screens to identify novel MAPs based on their localization to microtubules in cells. This allowed for the identification of epithelial MAP of 115 kDa (E-MAP-115, later named MAP7) [17], GLFND

[39], and MTR120 (MAP10) [40]. Even screens designed for other purposes could reveal the association of novel proteins with microtubules. For instance, MAP8 was initially discovered as an interaction partner of a protein related to male infertility [41]. Because of its homology to MAP1A/B proteins, MAP8 was also referred to as MAP1S [42]. MAP9, also known as ASAP (Aster-associated protein) was discovered in a screen for proteins involved in intracellular trafficking [43]. Using genome-wide linkage analysis and whole-exome sequencing, mutations of the gene C7orf43 were linked to cases of human microcephaly. C7orf43 encodes a protein that binds microtubules in cells, and was hence named MAP11 [44]. Figure 1 summarizes the timeline of MAPs discovery (Fig. 1).

Finally, advances in proteomics now allow for a more complete identification of proteins that co-purify with microtubules, for instance from *Xenopus laevis* egg extracts [45]. However, thorough biochemical characterization of newly identified proteins remains an essential prerequisite before validating them as bona fide MAPs (Box 1).

The role of MAPs in structuring the microtubule cytoskeleton

Since their discovery in the early 1970s, it was clear that MAPs can promote microtubule polymerization, stabilisation and bundling *in vitro* [10, 46, 47]. When overexpressed in mammalian cells, all MAPs decorated the microtubule cytoskeleton, however only some of them, such as tau, induced microtubule bundling [48, 49]. There have been different hypotheses on how MAPs directly participate in microtubule bundling. MAPs could create a direct physical connection between neighbouring microtubules [50], or alternatively, the stabilisation of microtubules alone could be sufficient to induce bundling [51]. Early studies with the microtubule-stabilising drugs Taxol, or the nonhydrolyzable analogue of GTP, GMPCPP, had already suggested that suppression of microtubule dynamics might be sufficient for the formation of microtubule bundles (discussed in [51]). Indeed, the same appears to be true for MAPs: expression of a minimal microtubule-binding domain of tau, for instance, was sufficient to induce microtubule bundling *in vitro* [52]. A mechanism by which a minimal MAP domain could promote microtubule bundling was recently proposed based on structural data: upon binding, the positively charged amino-acid patches typically present in MAPs would neutralize the high negative charge of carboxy-terminal tails of tubulins, thus reducing electrostatic repulsion between microtubules, thus allowing spontaneous bundling [53]. A strong argument in favour of this hypothesis is that removal of the negatively charged tubulin tails by subtilisin alone induces microtubule bundling [54].

It thus appears that regions of MAPs that do not directly interact with microtubules do not participate in the microtubule bundling. On the contrary, they might even prevent it by pushing microtubules apart from each other. For example, overexpressed full-length MAP4, which has a long projection domain (Fig. 2), binds microtubules without inducing their bundling [48, 55], while the MAP4 microtubule-binding domain alone does induce bundling [56]. This essentially leads back to some of the initial observations *in vitro* [13] and *in vivo* [57, 58], which showed that microtubule spacing is regulated by the size of the projection domains of different MAPs, and therefore, longer projection domains would prevent bundling by keeping microtubules apart (Fig. 3A). In this light, the fact that several MAPs express isoforms with projection domains of variable length [30, 33, 59] suggests a regulatory mechanism for microtubule network organization. At the same time, the extended projection domains could also serve as interaction platforms for other proteins, discussed below.

Notwithstanding the mechanisms involved, presence of MAPs reduces microtubule depolymerization frequency as apparent from longer microtubule life times in the presence of depolymerizing drugs [49, 60], or from accumulation of posttranslational modifications on MAP-stabilized microtubules [61]. However, how this stabilization is achieved on the molecular level has for a long time remained difficult to decipher due to the absence of structural data, which is mainly attributed to the disordered structure of many MAPs.

Most MAPs do not adapt a defined structure in solution and were thus generally considered to be disordered proteins. Recently, advances in cryo-electron microscopy have allowed to directly visualize how MAPs bind to microtubules [62]. The protein tau forms an extended structure that binds the microtubule surface along a protofilament, thereby spanning both intra-and inter-dimer tubulin interfaces and interacting with three tubulin monomers [63]. Strikingly, tau was found adjacent to the unstructured C-terminal tails of tubulin, thus underpinning the potential importance of these tails [64] and their posttranslational modifications [65] in controlling the tau-microtubule interactions.

It is highly likely that high-resolution structures of other MAPs will follow soon [66], allowing us to understand their functions from a novel, structural perspective. Similarities of the microtubule-binding domains of several MAPs, such as tau, MAP2 and MAP4 will certainly reflect the way these MAPs bind to microtubules.

A large number of MAPs can potentially coexist on a microtubule and a number of different MAP binding sites exist on the microtubule surface. For example, doublecortin (DCX), a MAP particularly abundant in neurons during development, binds microtubules on a different

site than tau. The DCX binding site is found between adjacent protofilaments, thus allowing this MAP to connect four tubulin molecules, which both strengthens and determines the inter-protofilament and tubulin-dimer interactions. As a result, DCX forces microtubules into a 13-protofilament configuration (Fig. 3E) [67].

In the light of the emerging structural biology of MAPs, it is important to remember that MAPs are not merely a 'glue' that sticks to the microtubule surface thereby preventing depolymerization, but rather dynamically bind and unbind microtubules as recently shown for tau [68]. Current work even suggests that tau protein does not stabilize microtubules, but rather allows some of them to remain labile in axons [69, 70]. This echoes earlier observations for MAP1B, which suggested that this protein actually regulates the dynamic fraction of microtubules [71, 72].

MAPs as crosslinkers of different cytoskeletal components

Apart from the 25-nm microtubules, eukaryotic cells contain two other principal cytoskeletal fibre networks: 4-nm actin filaments, and ~10-nm intermediate filaments. The interaction of these different cytoskeletal elements is essential for a range of cellular functions, such as directional cell migration [73], or neuronal pathfinding [74]. Today we know a number of MAPs able to connect microtubules to actin and/or intermediate filaments, which are therefore referred to as cytoskeletal crosslinkers (Fig. 3D).

Two major cytoskeletal crosslinkers are the microtubule-actin crosslinking factors 1 and 2 (MACF1, MACF2). MACF1 was initially discovered as actin crosslinking factor 7 (ACF7) [75], and MACF2 as bullous pemphagoid antigen 1 (BPAG1) [76], or dystonin (DST) [77]. Both proteins are bona fide crosslinkers of the microtubule and actin cytoskeletons [78, 79], but they also interact with intermediate filaments [80, 81]. The striking feature of MACF proteins is their large size (MACF1 ~600 kDa, MACF2 ~900 kDa), and both proteins contain amino-terminal actin- and carboxy-terminal microtubule-binding domains, separated by very long spectrin repeat domains that provide physical spacers between the actin and microtubule networks. The dominant localization cue for MACF proteins appears to be the microtubule network [79], which is why these proteins could primarily be considered as MAPs [82]. Dystrophin, another protein consisting extended spectrin repeats, had initially been described as an actin-binding proteins [83], and only the recent discovery that it can bind microtubules in the muscle cells now qualifies dystrophin as cytoskeletal crosslinker [84].

To be able to study the actin-microtubule crosslinking mechanism of MACF1 *in vitro*, a short version of the protein, called TipAct, was prepared by excluding its long central spectrin domain (Fig. 2), thus encompassing only the amino-terminal actin- and the carboxy-terminal microtubule-binding domains. TipAct tracks microtubule plus-ends in an EB-protein-dependent manner, and links them to actin filaments, thus guiding microtubule growth along actin bundles [85].

With their ability to bind three cytoskeletal elements, MACF proteins can participate in a large variety of cellular functions. MACF1 plays a key role in cell migration, thus controlling wound healing [86, 87], neuronal migration during brain development [88, 89], as well as dendritic arborisation and axon outgrowth [90, 91]. MACF2 is essential for the correct alignment of microtubules and intermediate neurofilaments in large-calibre sensory neurons, which in MACF2-knockout mice are hugely disorganized. This cytoskeletal disorganisation is accompanied by organelle accumulations that reveal defects in axonal transport [80, 92]. Moreover, mutations in MACF2 lead to *dystonia musculorum* in mice [77] and humans [93]. Alternative splicing of MACF1 and MACF2 can generate variants of the proteins with different domain composition, which can alter their molecular roles in connecting the different cytoskeletal networks. Strikingly, different splice isoforms give rise to distinct biological roles of the proteins, and are also linked to specific pathologies (reviewed in ref. [94-96])

The clear distinction of actin-, intermediate-filament- and microtubule-binding motifs of MACFs makes these proteins prime example of cytoskeletal linkers. Nevertheless, other MAPs have also been implicated in the binding of multiple cytoskeletal components, though their most-studied function relates to their microtubule binding. All members of the MAP1 family, MAP1A, MAP1B and MAP1S, have been shown to interact with actin as well as with microtubules [42, 97-99], with the actin- and microtubule-binding sites clearly separated within the primary sequence of these proteins. It is thus conceivable that these MAPs can serve as cytoskeletal linker proteins and this notion is supported by the observation that MAP1B-deficient neurons display decreased activity of the actin regulators Rac1 and Cdc42 [100].

Finally, a number of reports suggest that other MAPs also interact with different cytoskeletal networks, however the physiological relevance of these mostly biochemically determined interactions still needs to be elucidated (Box 2).

Physiological functions of MAPs

MAPs help cells in organising the microtubule cytoskeleton (Fig. 3). However, how MAP-induced changes in the cytoskeleton alter the physiological processes is just beginning to be understood. One of the key reasons for this lack of insight is that exogenous expression of MAPs, which was for decades the only way of introducing them into mammalian cells, leads to a variety of artefacts that are most frequently related to an overstabilisation of microtubules. Given that the regulation of microtubule dynamics by stabilisation or destabilisation with MAPs is a highly concentration-dependent biophysical process, any kind of non-physiological expression level can henceforth be artificial. It will thus be key to use gene-targeting approaches to directly label endogenous MAPs to observe their functions at physiological levels.

Still, several insights into cellular functions of MAPs have been gained by overexpression approaches, especially for tau, which is particularly well-explored due to its key role in neurodegenerative disorders (for a detailed review, see [101]). Tau was implicated in intracellular traffic control, as its overexpression [102] and hyperphosphorylation impede transport of synaptic vesicles and organelles *in vivo* [103, 104]. Strikingly, reduction of tau levels could rescue axonal transport defects observed in mouse models for Alzheimer's disease [105]. It will be important to understand if these effects are due to changes in the structural organisation of the microtubule cytoskeleton, i.e. an alteration in the spacing of axonal microtubules [57, 106], or due to a direct regulation of the transport processes by tau protein, as suggested by *in vitro* reconstitutions of transport in the presence of tau [107, 108].

In a similar manner, other MAPs such as MAP1B [109], MAP2, MAP4 [110, 111], MAP6 [112] and MAP7 [113-116] were shown to influence intracellular transport but perhaps not with the same selectivity (Fig. 3F). Indeed, MAP2, a neuronal MAP that is excluded from axons in differentiated neurons, controls cargo sorting at pre-axonal filtering zone by distinguishing KIF1- from KIF5-dependent cargoes [117]. MAP4 showed a specific inhibition of dynein-driven movements in *Xenopus laevis* melanocytes, whereas it activated kinesin-2-driven transport in these cells [111].

MAPs can also regulate microtubule dynamics by controlling the activity of microtubule-severing enzymes. For instance, MAP4 from *Xenopus laevis* can inhibit katanin-mediated microtubule severing *in vitro* [118], and tau, MAP2 and MAP4 can protect microtubules against severing by overexpressed katanin in mammalian cells (Fig. 3C) [119].

On the mechanistic side, MAPs might physically impede motors or severing enzymes to interact with microtubules in regions densely decorated with MAPs. The recently discovered tau islands that stall kinesin motility provide a first model for a mechanism that could potentially shield microtubule stretches in cells [120, 121]. However, there are multiple other mechanisms by which MAPs could influence the function of the microtubule cytoskeleton. Members of the MAP7 family for example directly regulate the motor activity of kinesin-1 [115, 122].

MAPs can also control each other. A number of MAPs interact with microtubules at similar sites, and could thus compete for microtubule binding. This has been so far demonstrated for MAP7, which is able to displace tau protein from microtubules *in vitro* [113]. The competition between tau and MAP7 might play an important role in the determination of neuronal connectivity, as both MAPs are distinctly involved in formation of axonal branches [123, 124]. These exciting discoveries provide first glimpses at the potentially large variety of regulatory roles of MAPs.

In general, MAPs interact with a plethora of proteins and might thus link the microtubule cytoskeleton to many other cellular functions, such as signal transduction pathways and synaptic functions [125]. For instance, MAP1A/B that interact with postsynaptic density proteins and several ligand-gated ion channels or transmembrane receptors [99, 126], thus controlling synaptic functions. MAP2 associates with a number of protein kinases such as cAMP-dependent protein kinase (PKA) and its regulatory subunit [127], or the tyrosine protein kinases Src and Fyn [128, 129], thus sorting these signalling proteins into the somato-dendritic compartment of neurons [127, 130]. The close link between neuronal, and in particular synaptic signal-transduction machineries and MAPs opens the exciting possibility that neuronal activity could be directly propagated to the microtubule cytoskeleton, and thus regulate its function. Indeed, recent work shows that MACF1 associates with acetylcholine receptors (AChRs) at the neuromuscular synapses and controls the efficiency of signal transmission in mice [131].

MAPs can further interact with membranes, but so far only a few examples are known. The protein tau localizes to the inner side of the plasma membrane [132], which might either titrate this MAP away from the microtubules, or connect microtubules to the plasma membrane (Fig. 3B). MACF1 also associates with the membrane of Golgi vesicles, thus mediating their transport from the trans-Golgi network to the cell periphery [133]. Moreover, the finding that MAP1B regulates the degradation of Rab35 [134] suggests a role in

membrane trafficking in neurons. It is highly likely that other MAPs also interact with cellular membranes, potentially playing a key role in intracellular integration. Last but not least, MAPs can facilitate viral infections by serving as adapters between the viral particles and the microtubule tracks, on which the virus is transported into the cell nucleus [135].

The multiple interactions of MAPs with functionally important cellular machineries clearly point towards their essential roles in coordinating cytoskeletal functions with a variety of physiological processes. The large size of many MAPs predestines them to be scaffold proteins for entire machineries working on the microtubules, such as transport and signalling complexes. Strikingly, these complexes might even contain tubulin-modifying enzymes [72], thus allowing MAPs to directly regulate the tracks to which they bind.

Implications of MAPs in pathologies

Given the large number of functions performed by MAPs, it is not surprising that they are also involved in various pathological conditions (reviewed in [136]). Transgenic mice for mutant/missing MAPs have underpinned their importance in maintaining structure and functions of the mammalian brain. For example, mice lacking tau display age-onset neurodegeneration [137]. MAP2- or MAP1B-knockout mice show neurodevelopmental defects [100, 130, 138-140], and mice with disrupted MAP1A gene display Purkinje-cell degeneration [141]. The MAP6-knockout mouse is recognised as a model of schizophrenia [142, 143]. Strikingly, in all these cases, it is not the pathological accumulation of the MAPs, but their deficiency that leads to the pathology. This underpins their importance in cellular homeostasis, and points toward the possibility that changes in the balance of MAP-microtubule interactions are sufficient to induce pathological events that lead to neuronal disorders.

This perspective opens up novel prospects for alternative molecular pathways in MAP-related disorders. For example, Alzheimer's and Parkinson's disease, as well as frontotemporal dementia and other tauopathies are characterized by the prevalent pathological hallmark of aggregated tau protein [34, 144, 145], and research has focussed on tau aggregation as the key event in their pathogenesis. However, it is likely that the initial events are rather early perturbations of the physiological functions of MAPs. Moreover, these initial events could be also regulated by the tubulin posttranslational modifications, proposed to control MAP-microtubule interactions. For example, recent findings demonstrating that abnormally increased microtubule polyglutamylation leads to neurodegeneration in a variety of neuronal

cell types in mouse, as well as in a newly discovered human disorder strongly underpin this notion [146, 147].

Concluding remarks and future directions: the emerging roles of MAPs

In this review, we have discussed how 'structural MAPs' fulfil different functions on the microtubule cytoskeleton, beyond their common characteristics – the binding to microtubules. MAPs can regulate microtubule dynamics and organization of microtubules, but also interactions of microtubules with other functionally important proteins such as molecular motors or regulators of microtubule stability. MAPs further link microtubules to other cytoskeletal elements, non-cytoskeletal proteins and protein complexes, or membrane compartments in cells.

Little is known so far about the regulation of local MAP concentrations in cells, which will be one of the crucial questions to answer if the patterning of the microtubule cytoskeleton with MAPs is to be understood. MAPs could recognize specific microtubule configurations, such as parallel or anti-parallel arrays (Fig. 3G). This is well-studied for the proteins TRIM46, a MAP that assembles plus-end-out microtubule arrays in the axon initial segment [148], and PRC1, which accumulates specifically at antiparallel overlapping microtubules at the mitotic spindle midzone [149, 150]. Another potential regulatory mechanism for MAP localisation could be the tubulin code, i.e. specific tubulin isotypes or posttranslational modifications of microtubules [151], which could attract MAPs to distinct microtubule arrays in cells. In addition, MAPs themselves are posttranslationally modified [6], and might be able to control the posttranslational modifications of the microtubules they bind to [72]. A complex regulatory network coupling the tubulin code to a hypothetical MAP code could thus create a broad variety of microtubule identities that coordinate cytoskeletal functions in cells. Indeed, different MAPs show distinct subcellular localisations in neurons, which correlates with their specific contributions to a variety of neuronal functions [136].

Finally, the concentration of MAPs can be drastically increased by phase transitions. In this process, a protein separates from the surrounding cytosol into a liquid phase droplet of which it is the sole constituent [152]. Droplets of the protein tau could serve as microtubule nucleation centres due to the extraordinarily high concentration of the MAP, which could enrich tubulin above the critical concentration needed for its polymerization [153]. It is tempting to imagine that reversible phase separation takes place on the microtubules, with the

more tempting possibility that local concentrations needed to initiate phase transition of MAPs are induced by locally enriched tubulin modifications (Fig. 4).

Another emerging concept is that MAPs can impact the molecular structure of microtubules. It has already been shown that DCX can determine the precise number of protofilaments (Fig. 3E) [67], which might explain why in cells microtubules have a much more controlled protofilament number than *in-vitro* assembled microtubules [154]. Moreover, recent findings suggest that MAPs can generate a whole range of 'unusual' microtubule structures. For example, the protein SSNA1 (a.k.a. NA14), which stabilises single-protofilament protrusions, can generate microtubule branches [155]. Mechanisms of protofilament stabilisation might also allow for the maintenance of damaged microtubules until they are repaired by re-incorporation of tubulin dimers (Fig. 4) [156]. Such mechanisms could be rather common in cells, and many MAPs might have such activities depending on their local concentrations [157]. The control of microtubule damage and repair has recently gained an even greater dimension with the discovery that motor proteins damage the microtubule tracks they walk on [158, 159]. Lattice maintenance might thus be one of the previously neglected cellular functions of MAPs. Moreover, MAPs that bind to the luminal side of microtubules, the so-called microtubule-inner proteins (MIPs), have only recently come into focus [160], and provide novel options for the regulation of microtubule dynamics and structure [161]. Last, but certainly not least, there is an emerging family of proteins that bind to tubulin dimers, called tubulin-associated proteins (TAPs) [162]. While some TAPs might just be MAPs able to interact with soluble tubulin dimers, others could bind exclusively to unpolymerized tubulin dimers, and have a strong impact on microtubule homeostasis in cells, as it was demonstrated for the tubulin-sequestering protein stathmin [163].

In the light of those emerging mechanisms it appears that the name 'structural MAPs', which had been coined for a vaguely defined family of proteins whose only common characteristics is that they bind to microtubules, has gained a greater mechanistic dimension: many of the here-discussed MAPs, and others yet to be identified, might turn out to be the key determinants of cytoskeletal architecture.

Outstanding questions

- Does the abundance of MAPs in a cell really reflect their biological importance? What are the functions of less abundant MAPs?
- What could be a novel definition of a MAP, and which experiments/approaches could be used to validate a protein as bona fide MAP?
- How do different MAPs function in a single cell? Do they all have distinct or redundant functions, or do they compete with each other?
- How are local MAP concentrations controlled in cells, and how does this contribute to the patterning of the microtubule cytoskeleton?
- How does the tubulin code, i.e. tubulin isotypes and their posttranslational modifications, control MAP binding to functionally specific microtubules? To what extent do MAPs influence the tubulin code?

Acknowledgement

This work was supported by the ANR-10-IDEX-0001-02 and the LabEx CelTisPhyBio ANR-11-LBX-0038. CJ is supported by the Institut Curie, the French National Research Agency (ANR) award ANR-17-CE13-0021, the Institut National du Cancer (INCA) grant 2014-PL BIO-11-ICR-1, and the Fondation pour la Recherche Medicale (FRM) grant DEQ20170336756. SB was supported by the FRM grant FDT201805005465. JAS was supported by the European Union's Horizon 2020 research and innovation programme under the Marie Skłodowska-Curie grant agreement No 675737, and the FRM grant FDT201904008210. SB, CV, CG-B and CJ are supported by the ECOS-CONICYT grant C14B01. CG-B is supported by Fondecyt 1180419 and Fondap 15150012 grants from CONICYT. We are grateful to M Genova, MM Magiera, S Gadadhar (Institut Curie, Orsay, France) for critical reading and instructive discussions of our manuscript.

Figures and Boxes

Box 1: Redefining MAPs

Over the years, proteins were discovered to interact with microtubules by various assays. However, there are a number of difficulties in designing functional experiments to test newly identified proteins for validating their potential role as MAPs. An important question is thus how to define novel proteins as bona-fide MAPs. The early definition of a MAP was that *"it copolymerizes with tubulin through repeated cycles of microtubule assembly in vitro; it is not associated with any brain subcellular fraction other than microtubules; in double-label immunofluorescence experiments antibodies against this protein stain the same fibrous elements in cultured cells as are stained by anti-tubulin; and this fibrous staining pattern is dispersed when cytoplasmic microtubules are disrupted by colchicine."* [24]. While this definition is somewhat still valid, it might need some refinement to consider potential artefacts, for instance that overexpression of some proteins can force them into non-physiological microtubule decoration or that overexpression of these MAPs could favour low-affinity interactions. Therefore, thorough biochemical characterization of newly identified proteins is still an essential prerequisite before considering them MAPs.

Box 2: Potentially more cytoskeletal crosslinker MAPs?

Several MAPs including MAP2 [164], MAP4 [165], or tau protein [166] have been demonstrated to bind actin. However, the actin-binding domains of MAP2, MAP4 and tau protein have been mapped to the very microtubule binding regions of these proteins [165, 166]. In the case of MAP2 for instance, actin binding is only possible in the absence of tubulin [164], which appears to preclude this MAP from acting as a cytoskeletal crosslinker. Thus, under physiological conditions, an association of those MAPs with the actin cytoskeleton might only happen in cellular compartments with low microtubule content, such as filopodia or leading edges of migrating cells. Strikingly, a recent reconstruction of microtubule and actin networks *in vitro* has clearly shown that tau protein can connect these two networks with its microtubule-binding repeats. It appears that tau binds to microtubules with at least one of its microtubule-binding repeat, and connects to actin with another of these repeats [167]. Considering that several MAPs, such as MAP2 and MAP4, have similar microtubule-binding repeats, this study provides a new model how MAPs could link microtubule and actin networks only with their microtubule-binding domains.

A number of MAPs can also interact with intermediate filaments. MAP2 can localize to vimentin in cells, which suggested that it could coordinate intermediate filaments and microtubule networks [168, 169]. The protein tau has equally been reported to bind vimentin intermediate filaments [170], however, no further functional studies on the role of MAPs in intermediate filament organization and crosstalk with microtubules have been performed. Finally, MAP4 was demonstrated to interact with septins [171], another filamentous network important for a range of cellular functions [172].

Thus, many MAPs have been shown to bind to different cytoskeleton networks, and were thus suggested to act as cytoskeletal crosslinkers. The physiological relevance of these findings, however, remains to be explored.

Figure 1: Timeline of the discovery of mammalian MAPs, and their dependency on the development and availability of experimental approaches. The timeline starts with the first ultrastructural description of microtubules [173], and the identification of their protein building block tubulin [174].

Figure 2: Schematic representation of MAPs scaled to their relative sizes. The approximate localisation of different cytoskeleton-interacting domains is shown (no precise domain boundaries are given due to different representations in the literature). Domain information were obtained from the following references: MACF1, MACF2 [95, 175], MAP1A, MAP1B, MAP8/MAP1S [6, 136], MAP2, MAP4, Tau, MAP6 [136], MAP7, MAP7D1, MAP7D2, MAP7D3 [115], MAP9 [136], MAP10 [40], EML1, EML2, EML3, EML4, EML5, EML6 [176, 177], DCX [6]. The longest annotated human isoforms of each MAP are depicted: MACF1 (XM_006710540), MACF2 (XM_005249315), MAP1A (XM_017022189), MAP1B (NM_005909), MAP8/MAP1S (NM_018174), MAP2 (NM_002374), MAP4 (NM_002375), Tau (NM_005910), MAP6 (NM_033063), MAP7 (NM_001198609), MAP7D1 (BC106053), MAP7D2 (BC136379), MAP7D3 (XM_024452448), MAP9 (AY690636), MAP10 (AB037804), MAP11 (NM_018275), EML1 (NM_004434), EML2 (NM_012155),EML3 (NM_153265), EML4 (NM_019063), EML5 (NM_183387), EML6 (NM_001039753) and DCX (NM_000555).

Figure 3: Schematic representation of the different ways MAPs can bind to microtubules, and how these modes of binding influences microtubule structure, behaviour, and functions: (A) binding and spacing microtubules with long MAP projection domains, (B) connecting microtubules to membranes, (C) protecting microtubules from severing enzymes, and thus, from disassembly, (D) crosslinking different cytoskeletal elements, (E) controlling the protofilament numbers of microtubules, (F) affecting the binding and motility of motor proteins by either forming a complex with the motor, or by occupying the motor path at the microtubule surface, (G) promoting microtubule bundling, by neutralising acidic tubulin carboxy-terminal tails.

Figure 4: Schematic representation of some emerging mechanisms of MAPs. Depending on their concentration at the microtubules surface, MAPs can form condensates (islands) or undergo phase transition to form liquid droplets. Some MAPs can bind incomplete microtubules, or single protofilaments, thus stabilising such structures, and eventually allowing microtubule repair, or branching. Posttranslational modifications of tubulin could regulate the binding parameters of MAP, thus controlling MAP functions. Vice versa, MAPs might be implicated in controlling microtubule modifications.

References:

1. Hirokawa, N. et al. (2009) Kinesin superfamily motor proteins and intracellular transport. Nat Rev Mol Cell Biol 10 (10), 682-96.
2. Bhabha, G. et al. (2016) How Dynein Moves Along Microtubules. Trends Biochem Sci 41 (1), 94-105.
3. McNally, F.J. and Roll-Mecak, A. (2018) Microtubule-severing enzymes: From cellular functions to molecular mechanism. J Cell Biol 217 (12), 4057-4069.
4. Roostalu, J. and Surrey, T. (2017) Microtubule nucleation: beyond the template. Nat Rev Mol Cell Biol 18 (11), 702-710.
5. Akhmanova, A. and Steinmetz, M.O. (2015) Control of microtubule organization and dynamics: two ends in the limelight. Nat Rev Mol Cell Biol 16 (12), 711-26.
6. Ramkumar, A. et al. (2018) ReMAPping the microtubule landscape: How phosphorylation dictates the activities of microtubule-associated proteins. Dev Dyn 247 (1), 138-155.
7. Frost, B. et al. (2015) Connecting the dots between tau dysfunction and neurodegeneration. Trends Cell Biol 25 (1), 46-53.
8. Sloboda, R.D. et al. (1975) Cyclic AMP-dependent endogenous phosphorylation of a microtubule-associated protein. Proc Natl Acad Sci U S A 72 (1), 177-81.
9. Borisy, G.G. et al. (1974) Microtubule assembly in vitro. Fed Proc 33 (2), 167-74.
10. Weingarten, M.D. et al. (1975) A protein factor essential for microtubule assembly. Proc Natl Acad Sci U S A 72 (5), 1858-1862.
11. Cleveland, D.W. et al. (1977) Purification of tau, a microtubule-associated protein that induces assembly of microtubules from purified tubulin. J Mol Biol 116 (2), 207-225.
12. Cleveland, D.W. et al. (1977) Physical and chemical properties of purified tau factor and the role of tau in microtubule assembly. J Mol Biol 116 (2), 227-247.
13. Herzog, W. and Weber, K. (1978) Fractionation of brain microtubule-associated proteins. Isolation of two different proteins which stimulate tubulin polymerization in vitro. Eur J Biochem 92 (1), 1-8.
14. Bulinski, J.C. and Borisy, G.G. (1979) Self-assembly of microtubules in extracts of cultured HeLa cells and the identification of HeLa microtubule-associated proteins. Proc Natl Acad Sci U S A 76 (1), 293-7.
15. Bulinski, J.C. and Borisy, G.G. (1980) Microtubule-associated proteins from cultured HeLa cells. Analysis of molecular properties and effects on microtubule polymerization. J Biol Chem 255 (23), 11570-6.
16. Parysek, L.M. et al. (1984) MAP 4: occurrence in mouse tissues. J Cell Biol 99 (4 Pt 1), 1309-15.
17. Masson, D. and Kreis, T.E. (1993) Identification and molecular characterization of E-MAP-115, a novel microtubule-associated protein predominantly expressed in epithelial cells. J Cell Biol 123 (2), 357-71.
18. Faire, K. et al. (1999) E-MAP-115 (ensconsin) associates dynamically with microtubules in vivo and is not a physiological modulator of microtubule dynamics. J Cell Sci 112 (Pt 23), 4243-55.
19. Webb, B.C. and Wilson, L. (1980) Cold-stable microtubules from brain. Biochemistry 19 (9), 1993-2001.

20. Job, D. et al. (1982) Recycling of cold-stable microtubules: evidence that cold stability is due to substoichiometric polymer blocks. Biochemistry 21 (3), 509-15.

21. Margolis, R.L. et al. (1986) Purification and assay of a 145-kDa protein (STOP145) with microtubule- stabilizing and motility behavior. Proc Natl Acad Sci U S A 83 (3), 639-43.

22. Black, M.M. and Kurdyla, J.T. (1983) Microtubule-associated proteins of neurons. J Cell Biol 97 (4), 1020-8.

23. Murphy, D.B. et al. (1977) Identity and polymerization-stimulatory activity of the nontubulin proteins associated with microtubules. Biochemistry 16 (12), 2598-605.

24. Huber, G. et al. (1985) MAP3: characterization of a novel microtubule-associated protein. J Cell Biol 100 (2), 496-507.

25. Riederer, B. et al. (1986) MAP5: a novel brain microtubule-associated protein under strong developmental regulation. J Neurocytol 15 (6), 763-75.

26. Paschal, B.M. and Vallee, R.B. (1987) Retrograde transport by the microtubule-associated protein MAP 1C. Nature 330 (6144), 181-3.

27. Paschal, B.M. et al. (1987) MAP 1C is a microtubule-activated ATPase which translocates microtubules in vitro and has dynein-like properties. J Cell Biol 105 (3), 1273-82.

28. Garner, C.C. et al. (1990) Molecular cloning of microtubule-associated protein 1 (MAP1A) and microtubule-associated protein 5 (MAP1B): identification of distinct genes and their differential expression in developing brain. J Neurochem 55 (1), 146-54.

29. Papandrikopoulou, A. et al. (1989) Embryonic MAP2 lacks the cross-linking sidearm sequences and dendritic targeting signal of adult MAP2. Nature 340 (6235), 650-2.

30. Kindler, S. et al. (1990) Molecular structure of microtubule-associated protein 2b and 2c from rat brain. J Biol Chem 265 (32), 19679-84.

31. Kobayashi, N. et al. (2000) Molecular characterization reveals identity of microtubule-associated proteins MAP3 and MAP4. Biochem Biophys Res Commun 268 (2), 306-9.

32. Goedert, M. et al. (1989) Multiple isoforms of human microtubule-associated protein tau: sequences and localization in neurofibrillary tangles of Alzheimer's disease. Neuron 3 (4), 519-526.

33. Himmler, A. (1989) Structure of the bovine tau gene: alternatively spliced transcripts generate a protein family. Mol Cell Biol 9 (4), 1389-96.

34. Goedert, M. et al. (1988) Cloning and sequencing of the cDNA encoding a core protein of the paired helical filament of Alzheimer disease: identification as the microtubule-associated protein tau. Proc Natl Acad Sci U S A 85 (11), 4051-5.

35. Vallee, R.B. and Bloom, G.S. (1983) Isolation of sea urchin egg microtubules with taxol and identification of mitotic spindle microtubule-associated proteins with monoclonal antibodies. Proc Natl Acad Sci U S A 80 (20), 6259-63.

36. Keller, T.C., 3rd and Rebhun, L.I. (1982) Strongylocentrotus purpuratus spindle tubulin. I. Characteristics of its polymerization and depolymerization in vitro. J Cell Biol 93 (3), 788-96.

37. Lepley, D.M. et al. (1999) Sequence and expression patterns of a human EMAP-related protein-2 (HuEMAP-2). Gene 237 (2), 343-9.

38. Eudy, J.D. et al. (1997) Isolation of a novel human homologue of the gene coding for echinoderm microtubule-associated protein (EMAP) from the Usher syndrome type 1a locus at 14q32. Genomics 43 (1), 104-6.

39. Manabe, R.i. et al. (2002) Identification of a Novel Microtubule-Associated Protein that Regulates Microtubule Organization and Cytokinesis by Using a GFP-Screening Strategy. Curr Biol 12 (22), 1946-1951.

40. Fong, K.-W. et al. (2013) MTR120/KIAA1383, a novel microtubule-associated protein, promotes microtubule stability and ensures cytokinesis. J Cell Sci 126 (Pt 3), 825-37.

41. Wong, E.Y.M. et al. (2004) Identification and characterization of human VCY2-interacting protein: VCY2IP-1, a microtubule-associated protein-like protein. Biol Reprod 70 (3), 775-84.

42. Orban-Nemeth, Z. et al. (2005) Microtubule-associated protein 1S, a short and ubiquitously expressed member of the microtubule-associated protein 1 family. J Biol Chem 280 (3), 2257-65.

43. Saffin, J.-M. et al. (2005) ASAP, a human microtubule-associated protein required for bipolar spindle assembly and cytokinesis. Proc Natl Acad Sci U S A 102 (32), 11302-7.

44. Perez, Y. et al. (2019) Mutations in the microtubule-associated protein MAP11 (C7orf43) cause microcephaly in humans and zebrafish. Brain 142 (3), 574-585.

45. Gache, V. et al. (2010) Xenopus meiotic microtubule-associated interactome. PLoS One 5 (2), e9248.

46. Murphy, D.B. and Borisy, G.G. (1975) Association of high-molecular-weight proteins with microtubules and their role in microtubule assembly in vitro. Proc Natl Acad Sci U S A 72 (7), 2696-700.

47. Sloboda, R.D. et al. (1976) Microtubule-associated proteins and the stimulation of tubulin assembly in vitro. Biochemistry 15 (20), 4497-505.

48. Barlow, S. et al. (1994) Stable expression of heterologous microtubule-associated proteins (MAPs) in Chinese hamster ovary cells: evidence for differing roles of MAPs in microtubule organization. J Cell Biol 126 (4), 1017-29.

49. Kanai, Y. et al. (1989) Expression of multiple tau isoforms and microtubule bundle formation in fibroblasts transfected with a single tau cDNA. J Cell Biol 109 (3), 1173-84.

50. Lewis, S.A. et al. (1989) Organization of microtubules in dendrites and axons is determined by a short hydrophobic zipper in microtubule-associated proteins MAP2 and tau. Nature 342 (6249), 498-505.

51. Chapin, S.J. et al. (1991) Microtubule bundling in cells. Nature 349 (6304), 24.

52. Scott, C.W. et al. (1992) Tau protein induces bundling of microtubules in vitro: comparison of different tau isoforms and a tau protein fragment. J Neurosci Res 33 (1), 19-29.

53. Wang, Q. et al. (2014) Structural basis for the extended CAP-Gly domains of p150(glued) binding to microtubules and the implication for tubulin dynamics. Proc Natl Acad Sci U S A 111 (31), 11347-52.

54. Sackett, D.L. et al. (1985) Tubulin subunit carboxyl termini determine polymerization efficiency. J Biol Chem 260 (1), 43-5.

55. Nguyen, H.L. et al. (1997) Overexpression of full- or partial-length MAP4 stabilizes microtubules and alters cell growth. J Cell Sci 110 (Pt 2), 281-94.

56. Iida, J. et al. (2002) The projection domain of MAP4 suppresses the microtubule-bundling activity of the microtubule-binding domain. J Mol Biol 320 (1), 97-106.

57. Chen, J. et al. (1992) Projection domains of MAP2 and tau determine spacings between microtubules in dendrites and axons. Nature 360 (6405), 674-7.

58. Harada, A. et al. (1994) Altered microtubule organization in small-calibre axons of mice lacking tau protein. Nature 369 (6480), 488-91.

59. Georgieff, I.S. et al. (1993) Expression of high molecular weight tau in the central and peripheral nervous systems. J Cell Sci 105 (Pt 3), 729-37.

60. Kanai, Y. et al. (1992) Microtubule bundling by tau proteins in vivo: analysis of functional domains. Embo J 11 (11), 3953-61.

61. Takemura, R. et al. (1992) Increased microtubule stability and alpha tubulin acetylation in cells transfected with microtubule-associated proteins MAP1B, MAP2 or tau. J Cell Sci 103 (Pt 4), 953-64.

62. Nogales, E. (2016) The development of cryo-EM into a mainstream structural biology technique. Nat Methods 13 (1), 24-7.

63. Kellogg, E.H. et al. (2018) Near-atomic model of microtubule-tau interactions. Science 360 (6394), 1242-1246.

64. Serrano, L. et al. (1985) Localization of the tubulin binding site for tau protein. Eur J Biochem 153 (3), 595-600.

65. Boucher, D. et al. (1994) Polyglutamylation of tubulin as a progressive regulator of in vitro interactions between the microtubule-associated protein Tau and tubulin. Biochemistry 33 (41), 12471-12477.

66. Shigematsu, H. et al. (2018) Structural insight into microtubule stabilization and kinesin inhibition by Tau family MAPs. J Cell Biol 217 (12), 4155-4163.

67. Fourniol, F.J. et al. (2010) Template-free 13-protofilament microtubule-MAP assembly visualized at 8 A resolution. J Cell Biol 191 (3), 463-70.

68. Janning, D. et al. (2014) Single-molecule tracking of tau reveals fast kiss-and-hop interaction with microtubules in living neurons. Mol Biol Cell 25 (22), 3541-51.

69. Qiang, L. et al. (2018) Tau Does Not Stabilize Axonal Microtubules but Rather Enables Them to Have Long Labile Domains. Curr Biol 28 (13), 2181-2189 e4.

70. Baas, P.W. and Qiang, L. (2019) Tau: It's Not What You Think. Trends Cell Biol 29 (6), 452-461.

71. Gonzalez-Billault, C. et al. (2001) Evidence for the role of MAP1B in axon formation. Mol Biol Cell 12 (7), 2087-98.

72. Utreras, E. et al. (2008) Microtubule-associated protein 1B interaction with tubulin tyrosine ligase contributes to the control of microtubule tyrosination. Dev Neurosci 30 (1-3), 200-10.

73. Palazzo, A.F. and Gundersen, G.G. (2002) Microtubule-actin cross-talk at focal adhesions. Sci STKE 2002 (139), pe31.

74. Vitriol, E.A. and Zheng, J.Q. (2012) Growth cone travel in space and time: the cellular ensemble of cytoskeleton, adhesion, and membrane. Neuron 73 (6), 1068-81.

75. Bernier, G. et al. (1996) Cloning and characterization of mouse ACF7, a novel member of the dystonin subfamily of actin binding proteins. Genomics 38 (1), 19-29.

76. Sawamura, D. et al. (1990) Bullous pemphigoid antigen (BPAG1): cDNA cloning and mapping of the gene to the short arm of human chromosome 6. Genomics 8 (4), 722-6.

77. Bernier, G. et al. (1995) Dystonin expression in the developing nervous system predominates in the neurons that degenerate in dystonia musculorum mutant mice. Mol Cell Neurosci 6 (6), 509-20.

78. Leung, C.L. et al. (1999) Microtubule actin cross-linking factor (MACF): a hybrid of dystonin and dystrophin that can interact with the actin and microtubule cytoskeletons. J Cell Biol 147 (6), 1275-86.

79. Karakesisoglou, I. et al. (2000) An epidermal plakin that integrates actin and microtubule networks at cellular junctions. J Cell Biol 149 (1), 195-208.

80. Yang, Y. et al. (1996) An essential cytoskeletal linker protein connecting actin microfilaments to intermediate filaments. Cell 86 (4), 655-65.

81. Leung, C.L. et al. (1999) The intermediate filament protein peripherin is the specific interaction partner of mouse BPAG1-n (dystonin) in neurons. J Cell Biol 144 (3), 435-46.

82. Sun, D. et al. (2001) Characterization of the microtubule binding domain of microtubule actin crosslinking factor (MACF): identification of a novel group of microtubule associated proteins. J Cell Sci 114 (Pt 1), 161-172.

83. Levine, B.A. et al. (1990) The interaction of actin with dystrophin. FEBS Lett 263 (1), 159-62.

84. Prins, K.W. et al. (2009) Dystrophin is a microtubule-associated protein. J Cell Biol 186 (3), 363-9.

85. Preciado Lopez, M. et al. (2014) Actin-microtubule coordination at growing microtubule ends. Nat Commun 5, 4778.

86. Wu, X. et al. (2008) ACF7 regulates cytoskeletal-focal adhesion dynamics and migration and has ATPase activity. Cell 135 (1), 137-48.

87. Wu, X. et al. (2011) Skin stem cells orchestrate directional migration by regulating microtubule-ACF7 connections through GSK3beta. Cell 144 (3), 341-52.

88. Goryunov, D. et al. (2010) Nervous-tissue-specific elimination of microtubule-actin crosslinking factor 1a results in multiple developmental defects in the mouse brain. Mol Cell Neurosci 44 (1), 1-14.

89. Ka, M. et al. (2014) MACF1 regulates the migration of pyramidal neurons via microtubule dynamics and GSK-3 signaling. Dev Biol 395 (1), 4-18.

90. Sanchez-Soriano, N. et al. (2009) Mouse ACF7 and drosophila short stop modulate filopodia formation and microtubule organisation during neuronal growth. J Cell Sci 122 (Pt 14), 2534-42.

91. Ka, M. and Kim, W.-Y. (2016) Microtubule-Actin Crosslinking Factor 1 Is Required for Dendritic Arborization and Axon Outgrowth in the Developing Brain. Mol Neurobiol 53 (9), 6018-6032.

92. Dalpe, G. et al. (1998) Dystonin is essential for maintaining neuronal cytoskeleton organization. Mol Cell Neurosci 10 (5-6), 243-57.

93. Kunzli, K. et al. (2016) One gene but different proteins and diseases: the complexity of dystonin and bullous pemphigoid antigen 1. Exp Dermatol 25 (1), 10-6.

94. Jefferson, J.J. et al. (2004) Plakins: goliaths that link cell junctions and the cytoskeleton. Nat Rev Mol Cell Biol 5 (7), 542-53.

95. Zhang, J. et al. (2017) Spectraplakin family proteins - cytoskeletal crosslinkers with versatile roles. J Cell Sci 130 (15), 2447-2457.

96. Houseweart, M.K. and Cleveland, D.W. (1999) Cytoskeletal linkers: new MAPs for old destinations. Curr Biol 9 (22), R864-866.

97. Pedrotti, B. et al. (1994) Microtubule associated protein MAP1A is an actin-binding and crosslinking protein. Cell Motil Cytoskeleton 29 (2), 110-6.

98. Tögel, M. et al. (1998) Novel features of the light chain of microtubule-associated protein MAP1B: microtubule stabilization, self interaction, actin filament binding, and regulation by the heavy chain. J Cell Biol 143 (3), 695-707.

99. Halpain, S. and Dehmelt, L. (2006) The MAP1 family of microtubule-associated proteins. Genome Biol 7 (6), 224.

100. Montenegro-Venegas, C. et al. (2010) MAP1B regulates axonal development by modulating Rho-GTPase Rac1 activity. Mol Biol Cell 21 (20), 3518-28.

101. Wang, Y. and Mandelkow, E. (2016) Tau in physiology and pathology. Nat Rev Neurosci 17 (1), 22-35.

102. Ishihara, T. et al. (1999) Age-dependent emergence and progression of a tauopathy in transgenic mice overexpressing the shortest human tau isoform. Neuron 24 (3), 751-62.

103. Mandelkow, E.-M. et al. (2003) Clogging of axons by tau, inhibition of axonal traffic and starvation of synapses. Neurobiol Aging 24 (8), 1079-85.

104. Ebneth, A. et al. (1998) Overexpression of tau protein inhibits kinesin-dependent trafficking of vesicles, mitochondria, and endoplasmic reticulum: implications for Alzheimer's disease. J Cell Biol 143 (3), 777-94.

105. Vossel, K.A. et al. (2010) Tau reduction prevents Abeta-induced defects in axonal transport. Science 330 (6001), 198.

106. Shahpasand, K. et al. (2012) Regulation of mitochondrial transport and inter-microtubule spacing by tau phosphorylation at the sites hyperphosphorylated in Alzheimer's disease. J Neurosci 32 (7), 2430-41.

107. Vershinin, M. et al. (2007) Multiple-motor based transport and its regulation by Tau. Proc Natl Acad Sci U S A 104 (1), 87-92.

108. Dixit, R. et al. (2008) Differential regulation of dynein and kinesin motor proteins by tau. Science 319 (5866), 1086-9.

109. Jimenez-Mateos, E.-M. et al. (2006) Role of MAP1B in axonal retrograde transport of mitochondria. Biochem J 397 (1), 53-9.

110. Mandelkow, E.-M. et al. (2004) MARK/PAR1 kinase is a regulator of microtubule-dependent transport in axons. J Cell Biol 167 (1), 99-110.

111. Semenova, I. et al. (2014) Regulation of microtubule-based transport by MAP4. Mol Biol Cell 25 (20), 3119-32.

112. Daoust, A. et al. (2014) Neuronal transport defects of the MAP6 KO mouse - a model of schizophrenia - and alleviation by Epothilone D treatment, as observed using MEMRI. Neuroimage 96, 133-42.

113. Monroy, B.Y. et al. (2018) Competition between microtubule-associated proteins directs motor transport. Nat Commun 9 (1), 1487.

114. Tymanskyj, S.R. et al. (2018) MAP7 regulates axon morphogenesis by recruiting kinesin-1 to microtubules and modulating organelle transport. Elife 7.

115. Hooikaas, P.J. et al. (2019) MAP7 family proteins regulate kinesin-1 recruitment and activation. J Cell Biol 218 (4), 1298-1318.

116. Metivier, M. et al. (2018) Mechanisms of Kinesin-1 activation by Ensconsin/MAP7 in vivo. bioRxiv, 325035.

117. Gumy, L.F. et al. (2017) MAP2 Defines a Pre-axonal Filtering Zone to Regulate KIF1- versus KIF5-Dependent Cargo Transport in Sensory Neurons. Neuron 94 (2), 347-362 e7.

118. McNally, K.P. et al. (2002) Katanin-mediated microtubule severing can be regulated by multiple mechanisms. Cell Motil Cytoskeleton 53 (4), 337-49.

119. Qiang, L. et al. (2006) Tau protects microtubules in the axon from severing by katanin. J Neurosci 26 (12), 3120-9.

120. Siahaan, V. et al. (2018) Kinetically distinct phases of tau on microtubules regulate kinesin motors and severing enzymes. bioRxiv, 424374.

121. Tan, R. et al. (2018) Microtubules Gate Tau Condensation to Spatially Regulate Microtubule Functions. bioRxiv, 423376.

122. Barlan, K. et al. (2013) The microtubule-binding protein ensconsin is an essential cofactor of kinesin-1. Curr Biol 23 (4), 317-22.

123. Yu, W. et al. (2008) The Microtubule-severing Proteins Spastin and Katanin Participate Differently in the Formation of Axonal Branches. Mol Biol Cell 19 (4), 1485-98.

124. Tymanskyj, S.R. et al. (2017) MAP7 Regulates Axon Collateral Branch Development in Dorsal Root Ganglion Neurons. J Neurosci 37 (6), 1648-1661.

125. Dehmelt, L. and Halpain, S. (2005) The MAP2/Tau family of microtubule-associated proteins. Genome Biol 6 (1), 204.

126. Villarroel-Campos, D. and Gonzalez-Billault, C. (2014) The MAP1B case: an old MAP that is new again. Dev Neurobiol 74 (10), 953-71.

127. Obar, R.A. et al. (1989) The RII subunit of cAMP-dependent protein kinase binds to a common amino-terminal domain in microtubule-associated proteins 2A, 2B, and 2C. Neuron 3 (5), 639-45.

128. Lim, R.W. and Halpain, S. (2000) Regulated association of microtubule-associated protein 2 (MAP2) with Src and Grb2: evidence for MAP2 as a scaffolding protein. J Biol Chem 275 (27), 20578-87.

129. Zamora-Leon, S.P. et al. (2001) Binding of Fyn to MAP-2c through an SH3 binding domain. Regulation of the interaction by ERK2. J Biol Chem 276 (43), 39950-8.

130. Harada, A. et al. (2002) MAP2 is required for dendrite elongation, PKA anchoring in dendrites, and proper PKA signal transduction. J Cell Biol 158 (3), 541-9.

131. Oury, J. et al. (2019) MACF1 links Rapsyn to microtubule- and actin-binding proteins to maintain neuromuscular synapses. J Cell Biol 218 (5), 1686-1705.

132. Brandt, R. et al. (1995) Interaction of tau with the neural plasma membrane mediated by tau's amino-terminal projection domain. J Cell Biol 131 (5), 1327-1340.

133. Kakinuma, T. et al. (2004) Interaction between p230 and MACF1 is associated with transport of a glycosyl phosphatidyl inositol-anchored protein from the Golgi to the cell periphery. Exp Cell Res 298 (2), 388-98.

134. Villarroel-Campos, D. et al. (2016) Rab35 Functions in Axon Elongation Are Regulated by P53-Related Protein Kinase in a Mechanism That Involves Rab35 Protein Degradation and the Microtubule-Associated Protein 1B. J Neurosci 36 (27), 7298-313.

135. Fernandez, J. et al. (2015) Microtubule-associated proteins 1 (MAP1) promote human immunodeficiency virus type I (HIV-1) intracytoplasmic routing to the nucleus. J Biol Chem 290 (8), 4631-46.

136. Tortosa, E. et al. (2016) Microtubule Organization and Microtubule-Associated Proteins (MAPs). In Dendrites: Development and Disease (Emoto, K. et al. eds), pp. 31-75, Springer Japan.

137. Lei, P. et al. (2012) Tau deficiency induces parkinsonism with dementia by impairing APP-mediated iron export. Nat Med 18 (2), 291-5.

138. Meixner, A. et al. (2000) MAP1B is required for axon guidance and Is involved in the development of the central and peripheral nervous system [In Process Citation]. J Cell Biol 151 (6), 1169-1178.

139. Bouquet, C. et al. (2004) Microtubule-associated protein 1B controls directionality of growth cone migration and axonal branching in regeneration of adult dorsal root ganglia neurons. J Neurosci 24 (32), 7204-13.

140. Bodaleo, F.J. et al. (2016) Microtubule-associated protein 1B (MAP1B)-deficient neurons show structural presynaptic deficiencies in vitro and altered presynaptic physiology. Sci Rep 6, 30069.

141. Liu, Y. et al. (2015) Mutations in the Microtubule-Associated Protein 1A (Map1a) Gene Cause Purkinje Cell Degeneration. J Neurosci 35 (11), 4587-98.

142. Andrieux, A. et al. (2002) The suppression of brain cold-stable microtubules in mice induces synaptic defects associated with neuroleptic-sensitive behavioral disorders. Genes Dev 16 (18), 2350-2364.

143. Powell, K.J. et al. (2007) Cognitive impairments in the STOP null mouse model of schizophrenia. Behav Neurosci 121 (5), 826-35.

144. Goedert, M. and Jakes, R. (2005) Mutations causing neurodegenerative tauopathies. Biochim Biophys Acta 1739 (2-3), 240-50.

145. Kovacs, G.G. (2017) Tauopathies. Handb Clin Neurol 145, 355-368.

146. Magiera, M.M. et al. (2018) Excessive tubulin polyglutamylation causes neurodegeneration and perturbs neuronal transport. EMBO J 37 (23), e100440.

147. Shashi, V. et al. (2018) Loss of tubulin deglutamylase CCP1 causes infantile-onset neurodegeneration. EMBO J 37 (23), e100540.

148. van Beuningen, S.F.B. et al. (2015) TRIM46 Controls Neuronal Polarity and Axon Specification by Driving the Formation of Parallel Microtubule Arrays. Neuron 88 (6), 1208-26.

149. Bieling, P. et al. (2010) A minimal midzone protein module controls formation and length of antiparallel microtubule overlaps. Cell 142 (3), 420-32.

150. Subramanian, R. et al. (2010) Insights into antiparallel microtubule crosslinking by PRC1, a conserved nonmotor microtubule binding protein. Cell 142 (3), 433-43.

151. Janke, C. (2014) The tubulin code: Molecular components, readout mechanisms, and functions. J Cell Biol 206 (4), 461-472.

152. Zwicker, D. et al. (2014) Centrosomes are autocatalytic droplets of pericentriolar material organized by centrioles. Proc Natl Acad Sci U S A 111 (26), E2636-45.

153. Hernandez-Vega, A. et al. (2017) Local Nucleation of Microtubule Bundles through Tubulin Concentration into a Condensed Tau Phase. Cell Rep 20 (10), 2304-2312.

154. Chretien, D. et al. (1992) Lattice defects in microtubules: protofilament numbers vary within individual microtubules. J Cell Biol 117 (5), 1031-40.

155. Basnet, N. et al. (2018) Direct induction of microtubule branching by microtubule nucleation factor SSNA1. Nat Cell Biol 20 (10), 1172-1180.

156. Aumeier, C. et al. (2016) Self-repair promotes microtubule rescue. Nat Cell Biol 18 (10), 1054-64.

157. Aher, A. et al. (2018) CLASP Suppresses Microtubule Catastrophes through a Single TOG Domain. Dev Cell 46 (1), 40-58 e8.

158. Dumont, E.L.P. et al. (2015) Molecular wear of microtubules propelled by surface-adhered kinesins. Nat Nanotechnol 10 (2), 166-9.

159. Triclin, S. et al. (2018) Self-repair protects microtubules from their destruction by molecular motors. bioRxiv, 499020.

160. Ichikawa, M. and Bui, K.H. (2018) Microtubule Inner Proteins: A Meshwork of Luminal Proteins Stabilizing the Doublet Microtubule. Bioessays 40 (3).

161. Schmidt-Cernohorska, M. et al. (2019) Flagellar microtubule doublet assembly in vitro reveals a regulatory role of tubulin C-terminal tails. Science 363 (6424), 285-288.

162. Yu, N. et al. (2016) Isolation of Functional Tubulin Dimers and of Tubulin-Associated Proteins from Mammalian Cells. Curr Biol 26 (13), 1728-36.

163. Jourdain, L. et al. (1997) Stathmin: a tubulin-sequestering protein which forms a ternary T2S complex with two tubulin molecules. Biochemistry 36 (36), 10817-21.

164. Sattilaro, R.F. (1986) Interaction of microtubule-associated protein 2 with actin filaments. Biochemistry 25 (8), 2003-9.

165. Matsushima, K. et al. (2012) Microtubule-associated protein 4 binds to actin filaments and modulates their properties. J Biochem 151 (1), 99-108.

166. Correas, I. et al. (1990) The tubulin-binding sequence of brain microtubule-associated proteins, tau and MAP-2, is also involved in actin binding. Biochem J 269 (1), 61-4.

167. Elie, A. et al. (2015) Tau co-organizes dynamic microtubule and actin networks. Sci Rep 5, 9964.

168. Bloom, G.S. and Vallee, R.B. (1983) Association of microtubule-associated protein 2 (MAP 2) with microtubules and intermediate filaments in cultured brain cells. J Cell Biol 96 (6), 1523-31.

169. Vallee, R.B. et al. (1984) Microtubule-associated proteins: subunits of the cytomatrix. J Cell Biol 99 (1 Pt 2), 38s-44s.

170. Capote, C. and Maccioni, R.B. (1998) The association of tau-like proteins with vimentin filaments in cultured cells. Exp Cell Res 239 (2), 202-13.

171. Kremer, B.E. et al. (2005) Mammalian septins regulate microtubule stability through interaction with the microtubule-binding protein MAP4. Mol Biol Cell 16 (10), 4648-59.

172. Mostowy, S. and Cossart, P. (2012) Septins: the fourth component of the cytoskeleton. Nat Rev Mol Cell Biol 13 (3), 183-94.

173. Pease, D.C. (1963) The Ultrastructure of Flagellar Fibrils. J Cell Biol 18, 313-26.

174. Borisy, G.G. and Taylor, E.W. (1967) The mechanism of action of colchicine. Binding of colchincine-3H to cellular protein. J Cell Biol 34 (2), 525-33.

175. Liem, R.K.H. (2016) Cytoskeletal Integrators: The Spectrin Superfamily. Cold Spring Harb Perspect Biol 8 (10), 8:a018259.

176. Fry, A.M. et al. (2016) EML proteins in microtubule regulation and human disease. Biochem Soc Trans 44 (5), 1281-1288.

177. Richards, M.W. et al. (2015) Microtubule association of EML proteins and the EML4-ALK variant 3 oncoprotein require an N-terminal trimerization domain. Biochem J 467 (3), 529-36.

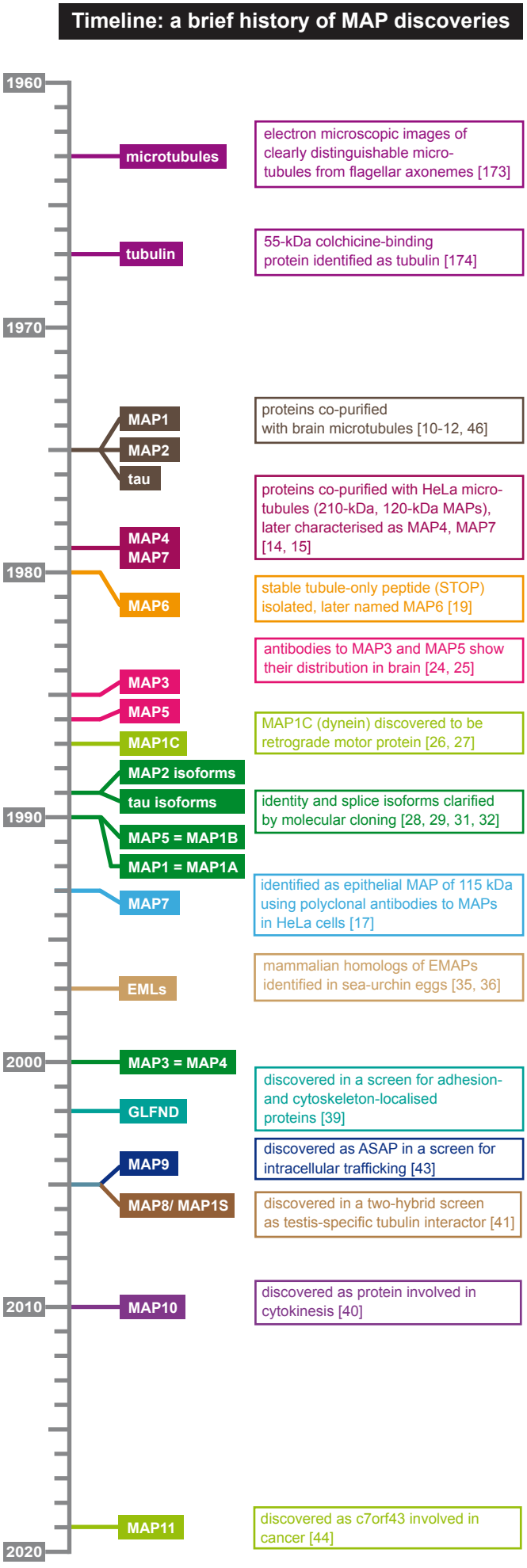
Timeline: a brief history of MAP discoveries
1960
microtubules
electron microscopic images of clearly distinguishable micro-tubules from flagellar axonemes [173]
tubulin
55-kDa colchicine-binding protein identified as tubulin [174]
1970
MAP1
MAP2
tau
proteins co-purified with brain microtubules [10-12, 46]
MAP4
MAP7
proteins co-purified with HeLa micro-tubules (210-kDa, 120-kDa MAPs), later characterised as MAP4, MAP7 [14, 15]
1980
MAP6
stable tubule-only peptide (STOP) isolated, later named MAP6 [19]
antibodies to MAP3 and MAP5 show their distribution in brain [24, 25]
MAP3
MAP5
MAP1C
MAP1C (dynein) discovered to be retrograde motor protein [26, 27]
MAP2 isoforms
tau isoforms
identity and splice isoforms clarified by molecular cloning [28, 29, 31, 32]
1990
MAP5 = MAP1B
MAP1 = MAP1A
MAP7
identified as epithelial MAP of 115 kDa using polyclonal antibodies to MAPs in HeLa cells [17]
EMLs
mammalian homologs of EMAPs identified in sea-urchin eggs [35, 36]
2000
MAP3 = MAP4
GLFND
discovered in a screen for adhesion- and cytoskeleton-localised proteins [39]
MAP9
discovered as ASAP in a screen for intracellular trafficking [43]
MAP8/ MAP1S
discovered in a two-hybrid screen as testis-specific tubulin interactor [41]
2010
MAP10
discovered as protein involved in cytokinesis [40]
MAP11
discovered as c7orf43 involved in cancer [44]
2020


Relative size and domain organisation of MAPs
MACF1
609 kDa
MACF2
884 kDa
MAP1A
331 kDa
proteolysis into HC and LC
MAP1B
271 kDa
proteolysis into HC and LC
MAP8/MAP1S
112 kDa
proteolysis into HC and LC
MAP2
199 kDa
MAP4
121 kDa
Tau
44 kDa
MAP6
86 kDa
MAP7
87 kDa
MAP7D1
93 kDa
MAP7D2
82 kDa
MAP7D3
98 kDa
MAP9
74 kDa
MAP10
100 kDa
MAP11
62 kDa
approximate domain distribution
microtubule binding
actin interactions
intermediate-filament interactions
EML1
90 kDa
EML2
71 kDa
EML3
95 kDa
EML4
109 kDa
EML5
220 kDa
EML6
218 kDa
DCX
49 kDa

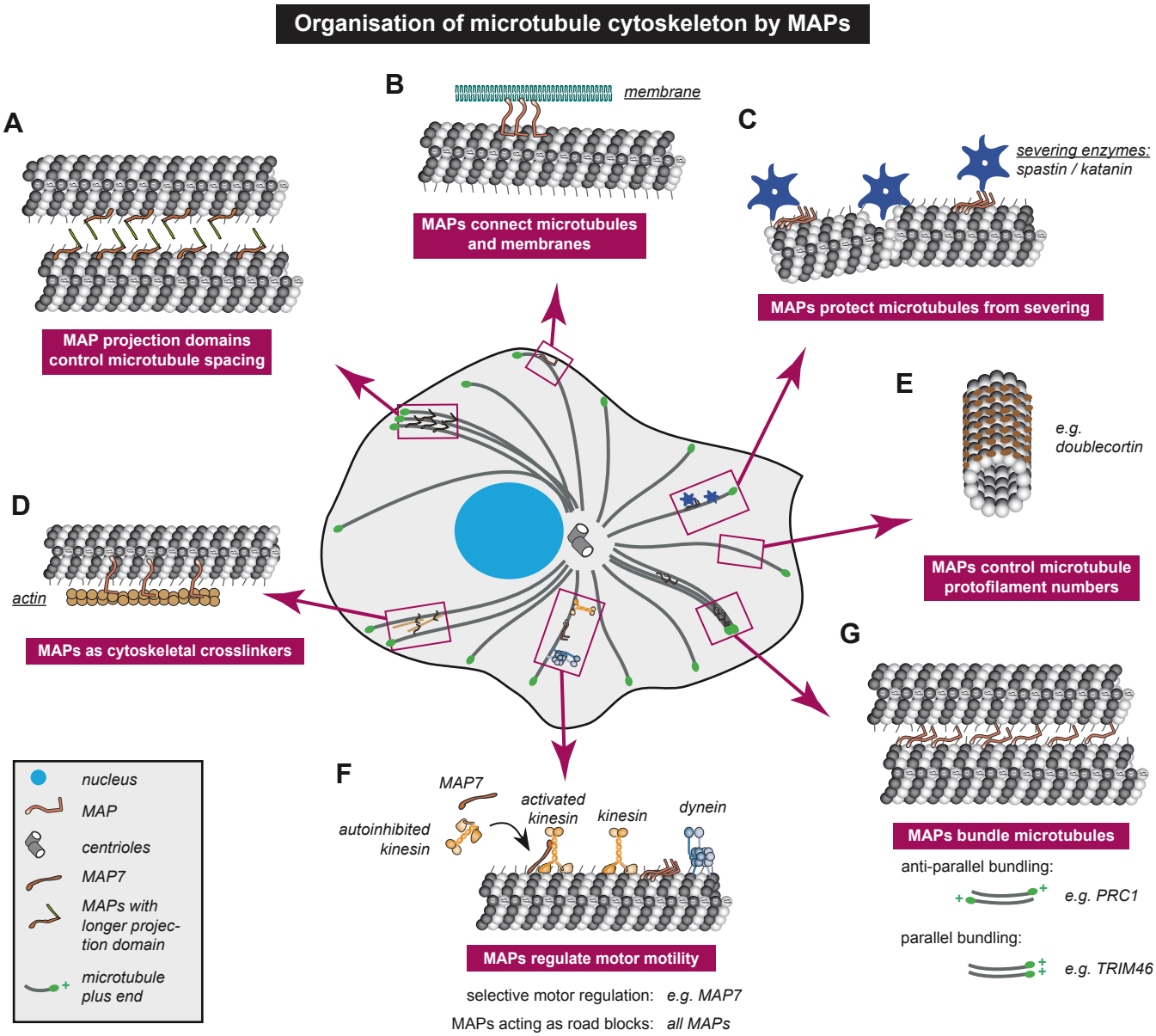
Organisation of microtubule cytoskeleton by MAPs
A
MAP projection domains control microtubule spacing
B
membrane
MAPs connect microtubules and membranes
C
severing enzymes: spastin / katanin
MAPs protect microtubules from severing
D
actin
MAPs as cytoskeletal crosslinkers
E
e.g. doublecortin
MAPs control microtubule protofilament numbers
F
MAP7
activated kinesin
kinesin
dynein
autoinhibited kinesin
MAPs regulate motor motility
selective motor regulation: e.g. MAP7
MAPs acting as road blocks: all MAPs
G
MAPs bundle microtubules
anti-parallel bundling:
e.g. PRC1
parallel bundling:
e.g. TRIM46
nucleus
MAP
centrioles
MAP7
MAPs with longer projec-tion domain
microtubule plus end

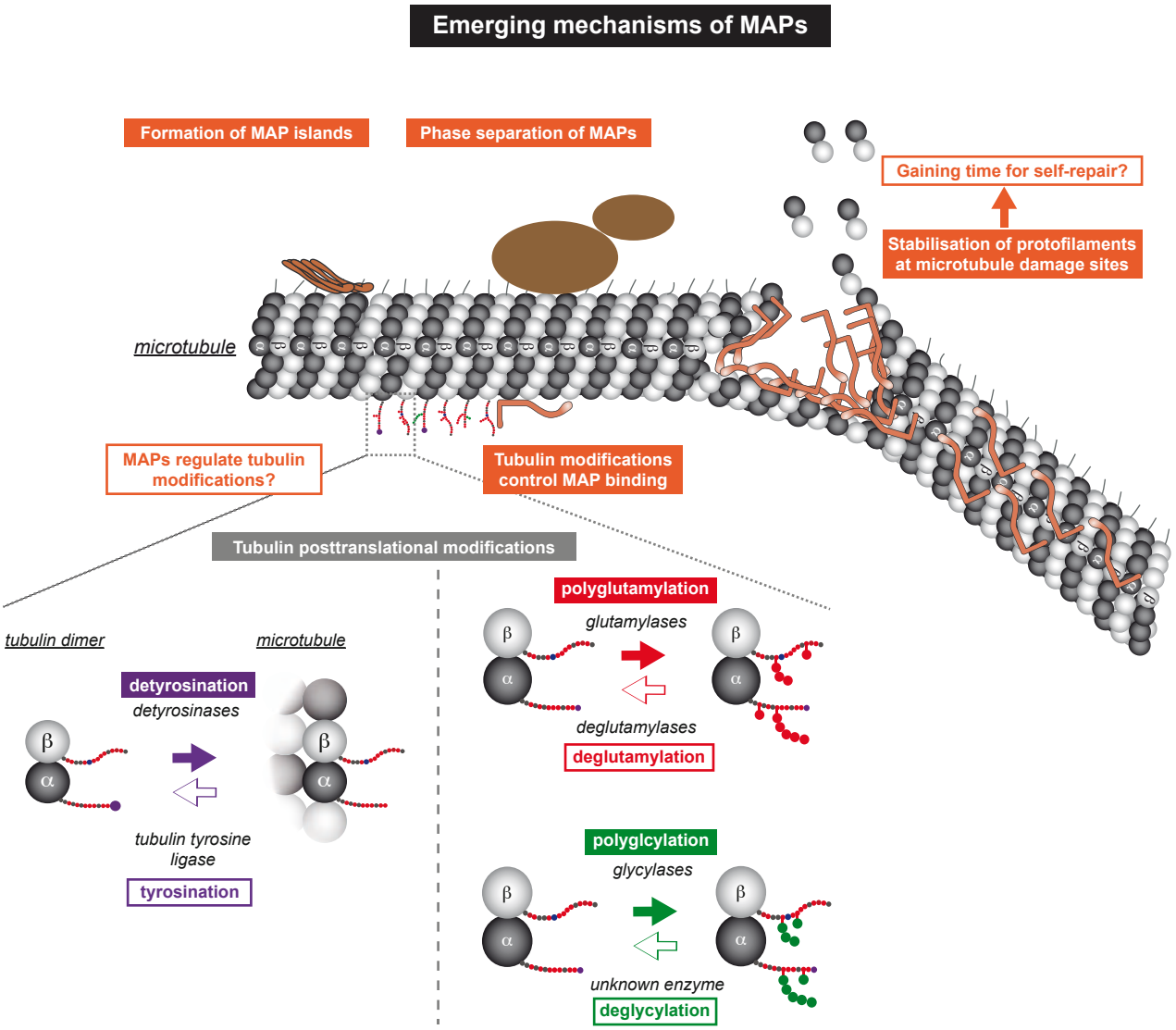
Emerging mechanisms of MAPs
Formation of MAP islands
Phase separation of MAPs
Gaining time for self-repair?
Stabilisation of protofilaments at microtubule damage sites
microtubule
MAPs regulate tubulin modifications?
Tubulin modifications control MAP binding
Tubulin posttranslational modifications
tubulin dimer
microtubule
detyrosination
detyrosinases
tubulin tyrosine ligase
tyrosination
polyglutamylation
glutamylases
deglutamylases
deglutamylation
polyglcylation
glycylases
unknown enzyme
deglycylation

Annex 6.2. Short chapters about MAP candidates used in this study

All the MAP candidates studied in this project are further classified into following three groups:

a) Proteins already reported as MAPs with in vitro confirmations.

b) Proteins already reported as MAPs without in vitro confirmations.

c) Proteins not reported as MAPs before.

The following are the short descriptions of each MAP used in this project, covering its alternative names, background information, known relation to MTs, physiological functions, interacting partners other than MTs, and direct or indirect links to diseases. In the section "MAPs and their disease links", only the name of the disease is mentioned along with corresponding references. A detailed explanation of the role of MAPs in those diseases is out of the scope of my thesis and thus not given.

The first section is about **proteins already reported as MAPs with in vitro confirmations**. Here I included proteins that are reported as MAPs before, and shown to interact with MTs using in vitro approaches, specifically with an in-vitro MT reconstitution and TIRF microscopy setup (individual MT resolution). This chapter includes MAPs such as Tau, MAP7, PRC1, DCX, DCLK1, PRC1 and MAP6.

The second section is about **proteins already reported as MAPs without in vitro confirmations**. Here I include proteins which are reported as MAPs but not having any in vitro evidence about its direct binding ability on dynamic MTs. Most of this evidence came from MAP-MT co-localization experiments from cellular studies or from biochemical assays using pre-polymerized, stabilised MTs. The MAPs included in this chapter are CSAP, ATIP3, CFAP20, EF-1alpha, GLFND1, GLFND2, Protein 4.1R, MAP9, MAP10, MAP11, Parkin, Syntaphilin, MAP2, MAP4, TRAK1, TRAK2 and members of EML1 group of MAPs.

The third section is about **proteins not reported as MAPs before**. The proteins included in this section are SAXO1, SAXO2, Jpl1, CRMP2A, CRMP4, Nardilysin, POC1 and POC2. There are studies showing indirect evidence that these proteins either colocalize with MT-based

structures, or the isoforms of some of these proteins are already reported as MAPs. The details showing indirect evidence are shown in Table 1 of the MAP manuscript in the result section.

6.2.1 Proteins already reported as MAPs with in vitro confirmations

Tau/ MAP T

Alternative names:

Tau is also known as MAPT.

Tau and MTs

Tau is one of the most studied structural MAPs, and its affinity for MTs was confirmed by numerous studies *in vitro* and *in vivo*. Tau stabilizes MTs (Bre and Karsenti 1990), regulates the number of MT protofilaments (Choi et al. 2009), enhances the MT stiffness thereby altering mechanical properties of the MTs (Samsonov et al. 2004) and also acts as a spacer protein between neighbouring MTs (Chen et al. 1992). Recent studies show that tau has an inhibitory role on kinesin-3 (Monroy et al. 2018) and can form islands on the microtubule surface at low concentrations, which are dissembled by kinesin-8 (Siahaan et al. 2019; Tan et al. 2019). Tau can also regulate MT PTMs by acting as an inhibitor of the deacetylase HDAC6 (Perez et al. 2009).

Background and physiological functions

Tau was described early as a protein that decreases the concentration at which tubulin polymerizes (Weingarten et al. 1975a). Homologues of tau are found in many species such as *Caenorhabditis elegans*, Drosophila, goldfish, bullfrog, rodents, bovines, goats, monkeys, and humans (Buee et al. 2000). Tau has six alternatively spliced isoforms, which are differentially expressed during development. 16 exons are present in the primary tau transcript, among which only three exons (2, 3 and 10) are translated to the final protein. Splicing of exon 10 changes the number of MT-binding repeats, and thus the affinity of tau to MTs (Goedert et al. 1989). Tau is organised into three main domains: acidic N-terminus, followed by a basic proline-rich region, a projection domain (it projects away from the MT surface in its bound form, and may thus also interact with other proteins simultaneously) and a C-terminus containing the MT-binding domain (MTBD). The MTBD interacts with MTs through multiple imperfect binding repeats (R1, R2, R3, and R4), with R2 being alternatively spliced in different isoforms (Hirokawa, Shiomura, and Okabe 1988; Buee et al. 2000). Moreover, tau undergoes many post translational modifications such as phosphorylation, ubiquitinylation, glycosylation, glycation, oxidation, deamidation and truncation (reviewed in (Avila et al. 2004)).

Links to diseases:

Tau is mostly studied in relation to tauopathies, such as Alzheimer's disease (Goedert et al. 1988), Pick's disease (Murayama et al. 1990), and parkinsonism-dementia of Guam (Arif et al. 2014). In healthy neurons, tau is mainly present in the axons with a strong enrichment at the distal region relative to the proximal region (Binder, Frankfurter, and Rebhun 1985) (Kempf et al. 1996). Under pathological conditions, tau is relocalized in the dendrites and in the dendritic spines, where it suppresses synaptic responses (Kremer et al. 2011). In pathological conditions, abnormally phosphorylated tau dissociates from MTs and forms insoluble tau aggregates called paired helical filaments (PHFs) which directly affect normal MT functions. PHFs further form neurofibrillary tangles (NFTs), and lead to neuronal degeneration (Lim et al. 2014). Several models aim at explaining the possible reasons for tau misdistribution and the after-effects causing tauopathies (Hall and Yao 2005; Orr, Sullivan, and Frost 2017). However, more studies need to be conducted for a better understanding of how tau changes from normal to pathological forms.

Other interacting partners:

Other than MTs, tau interacts with a wide number of other cellular components such as spectrin (Carlier et al. 1984), actin (Griffith and Pollard 1982), PP1 and PP2A (Sontag et al. 1999), presenilin 1 (Takashima et al. 1998), kinases like CDK5 (Sobue et al. 2000), α-synuclein (Jensen et al. 1999), phospholipase C (Hwang et al. 1996), the Fyn tyrosine kinase (Klein et al. 2002), apolipoprotein E (Strittmatter et al. 1994), calmodulin (Baudier et al. 1987) and CAPON (Hashimoto et al. 2019). Tau can also bind to chaperones: Hsp90, Hsp70 (Dou et al. 2003), and Pin-1 (Lu et al. 1999).

MACFs: MACF1 and MACF2

Alternative names:

MACF1 (Microtubule-actin cross-linking factor-1) is also known as ACF7 (Actin Crosslinking Factor 7), ABP620 (620 kDa Actin-binding Protein), Trabeculin-alpha, macrophin-1 and Kakapo (in Drosophila).

MACF2 (Microtubule-actin cross-linking factor-2) is also known as BPAG1 (Bullous pemphigoid antigen 1), Dystonin, Dystonia musculorum protein, and Hemidesmosomal plaque protein.

Background:

MACFs (MT-actin cross-linking factors) are gigantic MAPs comprising two members: MACF1 (~600 kDa) and MACF2 (~900 kDa). MACF1 was first reported as actin crosslinking factor 7 (ACF7) and MACF2 as bullous pemphagoid antigen 1 (BPAG1) or dystonin (DST) (Bernier et al. 1996; Sawamura et al. 1990a). MACF1 and MACF2 belong to the spectraplakin family of proteins, which are known for their cytoskeleton cross-linking properties (Zhang, Yue, and Wu 2017). Both proteins crosslink MTs and filamentous actin (Leung et al. 1999; Karakesisoglou, Yang, and Fuchs 2000a), but can also interact with intermediate filaments (Yang et al. 1996; Leung, Sun, and Liem 1999b). Both MACFs contain an N-terminal calponin homology (CH) domain to bind filamentous (F)-actin, followed by a plakin domain for association with intermediate filaments, a C-terminal EF-hand and a GAS2-related protein domain (GAR) for MT binding. The N-terminal actin- and the C-terminal MT-binding domains are separated by a very long spectrin repeat domain, thought to provide a physical spacer between actin and MT filaments (Karakesisoglou, Yang, and Fuchs 2000a).

MACFs and MTs:

In comparison to MACF2, MACF1 is studied more in relation to MTs. Cellular studies show that the MT-binding domain of MACF1 stabilizes MTs (Leung, Sun, and Liem 1999a). The difficulty of cloning and expression of these large proteins is the primary reason hindering their *in-vitro* characterization. However, truncated constructs of MACFs containing only the actin- or MT- binding domains were cloned. A bonsai version of MACF1 is the TipAct construct, which contains only the MT-binding (Tip) and the actin-binding (Act) regions, and is devoid of the linker spectrin repeats. *In vitro* studies with purified TipAct show that it can end-track MT plus ends in an EB3-dependent manner, and can also guide MT growth along with F-actin bundles (Preciado Lopez et al. 2014). Similarly, a truncated MACF2/ BPAG1 construct containing the MT binding region can bind and stabilize MTs in cells, and also in vitro using purified proteins (Yang et al. 1999). MACF1 also carries a SxIP motif, which is recognized and bound by EB proteins with their EBH domains. For this reason, MACF1 is widely considered as a +TIP protein (Akhmanova and Steinmetz 2010). However, further studies are required to confirm that the full-length MACF1 is indeed behaving as a +Tip protein.

Physiological functions:

MACFs participate in a wide range of cellular functions. MACF1/ ACF7 is involved in cell migration (Wu, Kodama, and Fuchs 2008), wound healing (Wu et al. 2011), brain development (Goryunov et al. 2010), axon outgrowth, dendritic arborization (Sanchez-Soriano et al. 2009; Ka and Kim 2016) and lung and muscle development (Bernier et al. 2000). MACF1 is also involved in the Wnt signalling pathway by forming complex that comprises Axin, GSK3β, β-catenin and APC, and its association is regulated by the presence or absence of wnt (Chen et al. 2006). MACF2 is involved in inner-ear development (Leonova and Lomax 2002), structural modulation of the Golgi apparatus, vesicular transport and cell migration in C2.7 myoblasts (Poliakova et al. 2014), as well as herpes simplex virus-1 infection (McElwee et al. 2013).

Links to diseases:

MACF1

Lissencephaly (Dobyns et al. 2018), Parkinson's Disease (Wang et al. 2017), spectraplakinopathy type 1 (Jorgensen et al. 2014) and glioblastoma (Afghani et al. 2017).

MACF2

Multiple sclerosis (Laffitte et al. 2005), Alzheimer's disease (Kokkonen et al. 2017). In addition, mutations in MACF2/ dystonin lead to dystonia (Bernier et al. 1995; Brown et al. 1995).

Chemical drugs

Temozolomide (TMZ) is reported to have an effect in the MACF1 expression levels in glioma cells (Xie et al. 2017).

CLIP-170

Alternative names:

CLIP-170 (Cytoplasmic Linker Protein of 170 kDa) is also known as Restin, Tip1 and Bik1p (budding yeast).

Background

CLIP-170 was first reported in 1990 in HeLa cells (Rickard and Kreis 1990). Later CLIP-170 was found to localize at the growing ends of MTs *in vivo* and became the first identified MT

plus-end tracking protein (Perez et al. 1999). The domain organization of CLIP-170 mainly comprises three central regions: the N-terminus containing two CAP-Gly domains (cytoskeleton-associated protein glycine-rich regions that bind to the plus end of the MTs and generally include one or more glycine-rich repeats), separated by serine-rich regions. The C-terminus has an ETF motif that can autoinhibit the CAP-Gly domains, and two zinc-knuckles (Mishima et al. 2007a). Both are separated by a coiled-coiled region that is involved in the homodimerization of the protein, and is important for the binding of the MT pause factor CLASP (CLIP-associated protein) (Akhmanova et al. 2001). When CLIP-170 is not in its autoinhibited state, the N-terminal CAP-Gly domain binds to the C-terminal EEY motifs found both in EB1 and the acidic tail of α-tubulin (Mishima et al. 2007b; Bieling et al. 2008a).

CLIP-170 and MTs

Overexpression in cells show that full-length CLIP-170 forms cytosolic patches or clumps containing soluble tubulin. The C-terminal region of CLIP-170 is responsible for this patch formation (Pierre, Pepperkok, and Kreis 1994). Antibody staining of endogenous CLIP-170 reveals its localization at the growing MT ends, making it known as the first +TIP member protein (Perez et al. 1999). It has been demonstrated that CLIP-170 requires EB1 for the end tracking property, and CLIP-170 doesn't end track by itself (Bieling et al. 2008c; Dixit et al. 2009). In the absence of EB1, purified CLIP-170 decorates the entire MT lattice *in vitro* (Chen, Wang, and Slep 2019). CLIP-170 is also involved in the repair and rescue of MT lattice defects (de Forges et al. 2016). In neurons, both *Drosophila* CLIP-190 and mammalian CLIP-170 are not prominent as plus end tracker (Beaven et al. 2015).

Physiological functions:

CLIP-170 is involved in the attachment of endocytic vesicles to MTs, and recruits the dynein/dynactin complex to MT plus-ends by interacting with dynactin $p150^{Glued}$ component (Pierre et al. 1992; Lansbergen et al. 2004; Watson and Stephens 2006). In addition, CLIP-170 is involved in neuronal polarization by regulating MT- and growth-cone dynamics (Neukirchen and Bradke 2011). It also plays a role in MTOC (Microtubule-Organizing Centre) repositioning during T-cell activation (Lim et al. 2018). CLIP-170 has also been shown to regulate the receptor tyrosine kinase recycling during cell migration (Zaoui et al. 2019), tethering and stabilizing the kinetochore-MT plus-end attachment by dynein (Amin, Kobayashi, and Tanaka 2015), thus playing a role in chromosome alignment (Amin et al. 2014). It was further

implicated in phagocytosis (Lewkowicz et al. 2008), spermatogenesis (Akhmanova et al. 2005), tumour angiogenesis (Sun et al. 2013), and also acts as an autoantigen (Griffith et al. 2002). CLIP-170 forms complex with the formin Dia1 and can accelerate actin polymerization from MT plus ends (Henty-Ridilla et al. 2016). Also, CLIP-170 undergoes phosphorylation by FRAP (FKBP12-rapamycin-associated Protein) which positively regulates the MT binding ability of CLIP-170, and AMPK (AMP-activated protein kinase) phosphorylates CLIP-170 which alters MT dynamics and directional cell migration (Choi et al. 2002; Nakano et al. 2010). Phosphorylation of the MT plus end protein CLIP-170 by AMPK is required for MT dynamics and the regulation of directional cell migration (Choi et al. 2002; Nakano et al. 2010).

Links to diseases:

CLIP-170 is linked to Hodgkin's disease (Bilbe et al. 1992), CDKL5 deficiency disorder (Barbiero et al. 2020), Anaplastic large cell lymphoma (ALCL) (Delabie et al. 1992), pancreatic cancer (Li et al. 2013), and distal hereditary motor neuropathy type II (distal HMN II) (Irobi et al. 2001).

MAP7

MAP7, MAP7D1, MAP7D2, MAP7D3

Alternative names:

MAP7: EMAP115 (Epithelial microtubule-associated protein of 115 kDa), E-MAP-115, Mtap7 and Ensconsin (Drosophila).

MAP7D 1: MAP7 domain-containing protein 1, KIAA1187, PARCC1 (Proline/arginine-rich coiled-coil domain-containing protein 1), RPRC1 (Arginine/proline-rich coiled-coil domain-containing protein 1).

MAP7D2: MAP7 domain-containing protein 2.

MAP7D3: MAP7 domain-containing protein 3, Mdp3 (MAP7 domain-containing 3).

Background

MAP7 was discovered as EMAP115 (Epithelial microtubule-associated protein of 115 kDa) in HeLa cells in 1993. It is prominently expressed in epithelial cells (Masson and Kreis 1993). Later, a GFP-fused version with the N-terminal MT-binding region of ensconsin (GFP-EMTB)

was used as a fluorescent probe to label MTs in living cells, because it didn't affect the intrinsic MT network organization and MT dynamics (Bulinski et al. 1999).

In mammals there are 4 MAP7 isoforms encoded by 4 different genes: MAP7, MAP7D1, MAP7D2 and MAP7D3 (Bulinski and Bossler 1994; Metzger et al. 2012; Yadav, Verma, and Panda 2014). MAP7, MAP7D1 and MAP7D2 are highly expressed in the brain (Koizumi et al. 2017b; Tymanskyj et al. 2017). Immunostaining of endogenous MAP7 isoforms show that MAP7 and MAP7D3, are expressed in HeLa cells, but not MAP7D2 (Hooikaas et al. 2019).

Domain organization of the four MAP7 member proteins:

All MAP7 family members have a similar domain organization. They all contain an N-terminal MT-binding domain and a C-terminal kinesin-1-binding domain. Both of these domains are predicted as helical and connected via a linker region (Sun et al. 2011; Metzger et al. 2012; Monroy et al. 2018). In case of MAP7 and MAP7D3, it has been shown that there are additional regions which have MT-binding affinity (Yadav, Verma, and Panda 2014), suggesting the presence of those additional MT-interacting sites could lead to stronger MT binding.

MAP 7 family and MTs

All four members of the MAP7 family can bind MTs in cells (Hooikaas et al. 2019; Pan et al. 2019). Moreover, in *in vitro* studies this affinity was confirmed for purified MAP7 (Bulinski and Bossler 1994; Hooikaas et al. 2019) and MAP7D3 (Hooikaas et al. 2019). One peculiarity of all members of the MAP7 family is that all contain a kinesin-1-binding domain (Hooikaas et al. 2019). Recent studies show that MAP7 can recruit kinesin-1 motors onto MT lattice (Sung et al. 2008), and kinesin-1 could co-transport MAP7 proteins along MTs (Pan et al. 2019).

In cortical neurons, MAP7D1 is phosphorylated by another MAP - the Doublecortin-like kinase 1 (DCLK1), and phosphorylated MAP7D1 promotes elongation of the axon (Koizumi et al. 2017b). In hippocampal neuron cultures, MAP7D2 localizes to the proximal region of the axon through its N-terminal MT-binding domain (Pan et al. 2019). Biochemical characterization of MAP7D3 shows that its C-terminal region promotes MT assembly by interacting with the tubulin C-terminal tails (Yadav, Verma, and Panda 2014), and Mdp3/ MAP7D3 contributes to MT polymerization and stability (Sun et al. 2011). Interestingly, in addition to tubulin and MTs, MAP7D3 can also interact with HDAC6 (histone deacetylase 6), a tubulin deacetylase with its

amino end (Tala, Sun, et al. 2014). The MAP7D1 and MAP7D2 isoforms are relatively less explored members in the MAP 7 family. Also, *in vitro* studies show that MAP7 can displace tau from MT lattice (Monroy et al. 2018).

Physiological functions:

MAP7 is involved in the nuclear positioning in fruit fly muscles and in cultured myotubes. In contrast, MAP7D1, MAP7D2 and MAP7D3 don't affect nuclear positioning in muscle cells (Metzger et al. 2012). In dorsal root ganglion (DRG) neurons, MAP7 regulates axonal branching, suggesting a role in neural circuit formations and functions (Tymanskyj et al. 2017). Also, it has been shown that MAP7 is involved in oocyte cell polarity establishment (Choi et al. 2008), regulation of mitotic spindle length in neural stem cells (Gallaud et al. 2014) and transport of organelles in cultured S2 cells (Barlan, Lu, and Gelfand 2013). MAP7 family proteins are generally considered neuronal MAPs. In comparison to MAP7, there are fewer studies about the other isoforms.

Links to diseases:

MAP7 is linked to human cervical cancer (Zhang et al. 2020), multiple sclerosis (Navarro-Barriuso et al. 2019), thymic epithelial tumour (Zhao et al. 2018), myeloid leukaemia (Fu et al. 2016), hepatocellular carcinoma (Geng et al. 2011), stage II colon cancer (Blum et al. 2008), Barrett's carcinoma (Langer et al. 2004) and sacral dysgenesis (Sood et al. 2004).

For MAP7D1, there are no reports so far linking it to any disease.
MAP7D2 is associated with gastric cancer (Liu, Wu, et al. 2018).
MAP7D3 is related to paediatric Wilms tumour (Lin et al. 2020), muscle hypertrophy (Willis et al. 2016) and breast cancer (Tala, Xie, et al. 2014).

MAP1

Background

The MAP1 family comprises MAP1A, MAP1B and MAP1S/ MAP8, three proteins encoded by different genes. MAP1A and MAP 1B proteins form multiprotein complexes made up of one heavy chain (HC) and two light chains (LC). MAP1A and MAP1B are expressed as one protein that is then proteolyzed into HC and LC. The LC stays associated with the HC. But there is also an LC3, which is expressed apart, but can associate with both, MAP1A and

MAP1B HC. MAP1A and MAP1B proteins can bind both actin and MTs (Halpain and Dehmelt 2006). MAP1C was initially considered to be a member of the MAP1 family but was later characterized as a cytoplasmic dynein (Vallee et al. 1988).

MAP1A

Alternative names:

MAP1A: Proliferation-related protein p80 and MTAP1A.

MAP 1A and MTs

Cellular studies show that a MAP1A-LC3 complex promotes stable MT growth by suppressing MT dynamics (Faller and Brown 2009). Also, cells with overexpressed MAP1A cDNA have a higher proportion of detyrosinated and acetylated MTs, which are tubulin PTMs that mark long-lived MTs in cells (Vaillant et al. 1998).
Early in vitro studies using purified native MAP1A from bovine brain show that it promotes the formation of straight MTs (Pedrotti and Islam 1994; Pedrotti et al. 1996).

Physiological functions:

MAP1A is highly expressed in neurons, and its expression is increased with development (Schoenfeld et al. 1989). MAP1A is associated with dendritic growth, length, and branching.

Links to diseases:

MAP1A is associated with autism (Satterstrom et al. 2019), Alzheimer's disease (Cui et al. 2019), obesity (Dhana et al. 2018), aging (Ma et al. 2014), Parkinson's disease (Wettergren et al. 2012), breast cancer (Knutson et al. 2012), amyotrophic lateral sclerosis (Farah et al. 2003), hearing loss (Ikeda et al. 2002) and AIDS (Fernandez et al. 2015). MAP1A-PSD95 interaction is linked to synaptic function in neuronal cells and hearing loss (Ikeda et al. 2002).

Other interacting partners:

Other MAP1A interacting partners are actin, postsynaptic components such as PSD93/PSD95, and NMDA receptors, which it anchors to the cytoskeleton (Pedrotti, Colombo, and Islam 1994b; Reese et al. 2007).

MAP1B/ MAP5

Alternative names:

MAP1B: MAP5, MAP1.2, MAP1(X).

MAP 1B and MTs

Early cellular studies show that MAP1B is a weak MT stabilizer compared to other MAPs (Takemura et al. 1992). MAP1B associates with tyrosinated and more dynamic MTs (Tymanskyj, Scales, and Gordon-Weeks 2012; Utreras et al. 2008). *In vitro* studies confirmed that a truncated construct of purified MAP1B decorates MTs (Bondallaz et al. 2006).

Physiological functions:

Similar to MAP1A, MAP1B is developmentally regulated, it is highly expressed in the nervous system in early embryonic stages and downregulated in later developmental stages. Studies using cultured neurons show that MAP1B is involved in axon outgrowth, axon elongation, dendritic spine formation, and synaptic maturation processes (Tortosa et al. 2011; Villarroel-Campos and Gonzalez-Billault 2014).

Links to diseases:

MAP1B has been linked to Parkinson's disease (Jensen et al. 2000), Alzheimer's disease (Hasegawa, Arai, and Ihara 1990), fragile X syndrome (Brown et al. 2001), giant axonal neuropathy (Allen et al. 2005), spinocerebellar ataxia type 1 (Opal et al. 2003) and CFEOM (congenital fibrosis of the extraocular muscles type 1) (Alexander et al. 2014).

Other interacting partners:

Other interacting partners of MAP1B are actin, TTL (tubulin-tyrosine ligase), EB1/ EB3, LIS1, KIF21A, dystonin-α2. MAP1B can crosslink both actin and MTs (Cheng et al. 2014; Villarroel-Campos and Gonzalez-Billault 2014). In addition, MAP1B can interact with a wide range of receptors including mGluR receptors, GABAc receptor, glycine receptor α1 subunit, NMDA receptor subunit NR3A, serotonin receptors, and receptor regulating proteins: GRIP1(glutamate receptor-interacting protein) and stargazin. Also, it can interact with cellular channels: Ca(V)2.2 and Nav1.6 (Villarroel-Campos and Gonzalez-Billault 2014).

MAP1S/ MAP8

Alternative names:
MAP1S: MAP8, MAP-1S, BPY2IP1 (Basic Protein on Y chromosome 2 Interacting Protein 1), VCY2IP-1 (Variable Charge Y chromosome 2 Interacting Protein 1) and C19ORF5.

MAP1S and MTs

In vitro studies using purified proteins have shown that MAP1S light chain can bind, bundle and stabilize MTs (Orban-Nemeth et al. 2005; Liu et al. 2005).

Physiological functions:

Among all three members of the MAP1 family, MAP1S is the smallest. It is expressed in various tissues, most evidently in neurons, but at low levels compared to other MAPs such as tau and MAP2 (Orban-Nemeth et al. 2005). MAP1S light chain can bind to both MTs and actin filaments, suggesting it may crosslink these two cytoskeletal elements (Ding, Valle, et al. 2006). In addition, recent studies show that MAP1S can link autophagosomes and mitochondria to MTs (Xie et al. 2011) and is linked to aggregation of mitochondria and genome destruction (Liu et al. 2005). Also, high levels of MAP1S cause MT stabilization, thereby disrupting the axonal transport and eventually leading to the death of neurons (Ding, Allen, et al. 2006).

Links to diseases:

MAP1S is linked to colorectal cancer (Wang, Zhang, et al. 2019), liver fibrosis and hepatocellular carcinoma (Yue et al. 2017), Crohn's disease (Bai et al. 2017), renal fibrosis (Xu et al. 2016), and adenocarcinomas (Song et al. 2015).

Other interacting partners:

MAP1S interacts with actin (Ding, Valle, et al. 2006), NR3 (receptor subunit of NMD) and nemitin (neuronal enriched MAP-interacting protein) (Wang et al. 2012).

MAP2

MAP2C, MAP 2D

Alternative names:
MAP2: not available.

Background:

Early studies show that MAP2 is the most expressed MAP in the brain (Matus 1988). It is expressed in neurons, glial cells such as astrocytes and oligodendrocytes (Papasozomenos and Binder 1986; Vouyiouklis and Brophy 1995). MAP2 has multiple isoforms, all transcribed from a single gene by alternative splicing. MAP2 isoforms are classified into two groups: high molecular weight MAP2 (HMWMAP2) and low molecular weight MAP2 (LMWMAP2). HMWMAP2 comprise MAP2A and MAP2B, while LMWMAP2 comprise MAP2C and MAP2D. LMWMAP2 are expressed in all types of brain cells; in contrast HMWMAP2 are specifically localized in neuronal dendrites and cell bodies (Binder et al. 1984; Burgoyne and Cumming 1984). MAP2 also binds to actin and neurofilaments (Pedrotti, Colombo, and Islam 1994a).

MAP2 and MTs

In cells, MAP2 bundles MTs and projection domains of MAP2 have been suggested to control MT spacing (Chen et al. 1992). MAP2 is also reported to affect MT-based transport and to participate in the association of rough ER membranes to MTs (Farah et al. 2005). Also, it has been shown that MAP2 interacts with CRMP5 (Brot et al. 2010), a protein of the CRMP family, which has been reported to include some structural MAPs, but there is no confirmation that CRMP5 particularly can act as such. Studies in cells show that both low molecular weight MAP2C and MAP2D bind and stabilize MTs (Ferhat et al. 1996; Ludin et al. 1996).

Comparative studies of MAP-2a and MAP-2b cDNA in COS-7 cells show that cells transfected with MAP2a cDNA can induce stable and rapid MT bundling even in the presence of nocodazole (Kalcheva et al. 1998). In cultured Sf9 cells, MAP2b regulates the MT protrusion formations (Belanger et al. 2002).

Early *in vitro* experiments with purified MAP2 shown that localizes to MTs in a periodic manner, as seen in electron micrographs of MAP2-decorated MTs (Kim, Binder, and Rosenbaum 1979). Furthermore, purified MAP2C reduces the MT dynamic instability *in vitro* (Gamblin et al. 1996).

Physiological functions:

MAP2 is expressed in the neurons (Matus 1988), astrocytes and oligodendrocytes (Papasozomenos and Binder 1986; Vouyiouklis and Brophy 1995). MAP2 can also bind to actin and neurofilaments (Pedrotti, Colombo, and Islam 1994a), and is considered as a structural protein crucial for neurite outgrowth, MT architecture in dendrites and in neuronal plasticity processes (Fanara et al. 2010; Harada et al. 2002).

Links to diseases:

MAP2 is linked to epilepsy (Jalava et al. 2007), schizophrenia (Rosoklija et al. 2005), Alzheimer's disease (Moolman et al. 2004), myotonic dystrophy (Velazquez-Bernardino et al. 2012), spinal cord injury (Gonzalez et al. 2009) and prion diseases (Zhang and Dong 2012).

Other interacting partners:

MAP2 can bind to actin and neurofilaments (Pedrotti, Colombo, and Islam 1994a). In addition, MAP2 also interacts with many other cellular components such as calcium channels (Davare et al. 1999), MARTA (MAP2 RNA transacting proteins) (Rehbein et al. 2000), L1CAM (neural cell adhesion molecule L1) (Poplawski et al. 2012), CRMP5 (Brot et al. 2010) and very-KIND (Huang, Furuya, and Furuichi 2007).

MAP6

Alternative names:

MAP6 is also named as STOP (stable tubule-only peptides), and Mtap6.

MAP6 and MTs

Purified MAP6 binds MTs *in vitro* (Baratier et al. 2006). In neurons, MAP6 is preferentially associated with the stable region of axonal MTs, suggesting that MAP6 has a strong preference for stable MTs (Slaughter and Black 2003). It has for a long time not been understood how MAP6 achieves MT stabilisation. A recent study shows that MAP6 is localised in the MT lumen, and therefore a MIP. MAP6 can induce the formation of MT coils *in vitro* (Cuveillier et al. 2020).

In mice lacking MAP6, loss of MT was observed upon cold or nocodazole treatment (Andrieux et al. 2002). Cell studies described that MAP6 is more enriched on tyrosinated-poor-MTs than tyrosinated-rich-MTs (Slaughter and Black 2003).

Physiological functions:

MAP6 is only reported in vertebrates and is known to be expressed in the brain, heart, kidney, muscles, testis, and lung tissues (Aguezzoul, Andrieux, and Denarier 2003). MAP6 has three splice isoforms: two neuronal ones - MAP6-E and MAP6-N, and one in fibroblasts - MAP6-F (Aguezzoul, Andrieux, and Denarier 2003; Bosc, Andrieux, and Job 2003). MAP6-E is the more abundant isoform in the embryonic mouse brain compared to MAP6-N, but both persist in the adult brain (Bosc et al. 1996). MAP6 is important for dendritic arborization and neurite formation (Guillaud et al. 1998). MAP6 knockout mice have aberrated synaptic plasticity and a reduced number of synaptic vesicles (Andrieux et al. 2002). Manganese-enhanced magnetic resonance imaging (MEMRI) studies of MAP6 KO mouse showed defects in axonal transport and synaptic transmissions (Daoust et al. 2014).

Links to diseases:

MAP6 is linked to Parkinson's disease (Ma et al. 2019), autism (Wei, Sun, et al. 2016), oral leukoplakia (Abe et al. 2016), schizophrenia (Shimizu et al. 2006) and amyotrophic lateral sclerosis (Letournel et al. 2003).

Other interacting partners:

MAP6 can also interact with actin and is regulated by calmodulin kinase II-mediated phosphorylation (Baratier et al. 2006).

DCX and DCLK1:

Alternative names:

Doublecortin or DCX is also known as Doublin, Lissencephalin-X, Lis-X, Neuronal migration protein doublecortin.

Doublecortin like kinase-1or DCLK1 is also known as Doublecortin domain-containing protein 3A, Doublecortin-like, and CAM kinase-like 1, (Dcamkl1) or KIAA0369.

Background:

DCX was first reported in 1998 in a genetic screen of patients having subcortical band heterotopia, also known as doublecortex syndrome, which is a neuronal migration disorder (des Portes, Pinard, et al. 1998; Gleeson et al. 1998).
DCLK1 or Doublecortin-like kinase-1 is a MAP having a serine/threonine kinase domain at its C-terminus. DCLK1 is a paralog of DCX with an additional kinase activity. This protein is a biomarker of many cancer types, because of which it is widely studied (Westphalen, Quante, and Wang 2017).

DCX, DCLK1, and MTs:

DCX binds the growing MT ends by interacting with MT polymerization intermediates, thus stabilizing the 13 protofilament tips and acting as a template for 13 protofilament MTs, similar to the γTuRC (Bechstedt and Brouhard 2012). DCX-MT interaction is regulated by DCX phosphorylation by Cdk5, Protein Kinase A (PKA), and the MARK/PAR-1 family of kinases (Tanaka et al. 2004; Schaar, Kinoshita, and McConnell 2004). Along with MTs, DCX also interacts with actin filaments, and promotes cross-linking and bundling of MTs and actin filaments *in vitro* (Tsukada et al. 2005). DCX has two tubulin-binding domains named N-terminal Doublecortin domain (N-DC) and C-terminal Doublecortin domain (C-DC) (Taylor et al. 2000).

Both DCX and DCLK1 were found to bind MTs in cells, and they also interact with MTs as purified proteins *in vitro* (Taylor et al. 2000; Monroy et al. 2020). Moreover, both have been reported to interact with the motor domain of kinesin-3, promoting cargo transport in dendrites (Liu et al. 2012), while having an inhibitory effect on kinesin-1in landing and progressing on MT surface in vitro (Monroy et al. 2020). Besides, studies in neurons show that DCLK1 phosphorylates MAP7D1 on Ser 315, which could promote elongation of axons in cortical neurons (Koizumi et al. 2017a).

Physiological functions:

DCX is essential for neuronal migration, and DCX depletion by RNAi in cultured neurons leads to a reduction in axon length, dendrite arborization and collateral branching (Deuel et al. 2006; Tint et al. 2009). DCX is expressed in differentiating and migrating neurons and is developmentally regulated (Francis et al. 1999). Both *in vitro* and *in vivo* studies show that

DCX binds to lissencephaly gene product-LIS 1, indicating that crosstalk of LIS1 and DCX could be important for the development of cerebral cortex (Caspi et al. 2000).

DCLK1 is linked to neuronal migration, neurogenesis, tumorigenesis and the regulation of the activity of multiple pathways, such as the Wnt/β-catenin signalling pathway and KRAS signalling (Wang, Li, et al. 2019; Qu et al. 2019).

Links to diseases:

DCX is related to disease such as epilepsy (D'Alessio et al. 2010), neuroblastoma (Oltra et al. 2005), autism (Vourc'h et al. 2002), double-cortex syndrome (Aigner et al. 2000), and subcortical laminar heterotopia (SCLH) (des Portes, Francis, et al. 1998).

DCLK1 is linked to non-small cell lung cancer (NSCLC) (Tao, Tanaka, and Okabe 2017), head and neck squamous cell carcinoma (HNSCC) (Kadletz et al. 2017), ovarian clear cell carcinoma (OCCC) (Wu et al. 2017), breast cancer (Liu et al. 2016), gastric cancer (Meng et al. 2013), pancreatic cancer (Yan et al. 2020) and colorectal cancer (Makino et al. 2020).

MAP 9/ Microtubule-associated protein 9

Alternative names:

MAP9 is also known as ASAP or ASter-Associated Protein.

MAP9 and MTs

In cells, MAP9 localizes to interphase, mitotic-spindle- and midbody-MTs in cytokinesis. MAP9 overexpression leads to MT bundling in interphase cells and formation of abnormal mitotic spindles (Saffin et al. 2005). It is also reported that MAP9 binds MTs via its C-terminal domain *in vitro* (Saffin et al. 2005).

Physiological functions:

MAP9/ ASAP is involved in the mitotic spindle assembly, mitotic progression, and cytokinesis (Saffin et al. 2005). MAP9 is a crucial factor in the early stages of zebrafish development (Fontenille et al. 2014). In addition, MAP9 is regulated by mitotic kinases Aurora A- and PLK1-mediated phosphorylation (Eot-Houllier et al. 2010; Venoux et al. 2008). Along with MTs, MAP9 also interacts with and stabilizes tumour-suppressor protein p53 in response to DNA damage (Basbous et al. 2012).

Links to diseases:

MAP9 is linked to colorectal and breast cancers (Rouquier et al. 2014), gastric carcinoma (Liu, Xiao, et al. 2018), ovarian cancer (Schiewek et al. 2018) and hepatocellular carcinoma (Yamada et al. 2016).

PRC1/ Protein regulator of cytokinesis 1

Alternative names:

No other names.

Background and physiological functions:

PRC1 was first reported in 1998, associated with mitotic spindle and involved in cytokinesis. Later studies show that PRC1 is a MAP (Mollinari et al. 2002a). Ase1p is the budding yeast ortholog of PRC1 (Loiodice et al. 2005), and MAP65, a 65-kDa protein in plants (Chang-Jie and Sonobe 1993). All three proteins are characterized and are known for their intrinsic MT-bundling property (Walczak and Shaw 2010). Full-length PRC1 has three major domains: a N-terminal domain responsible for the homodimerization, a central domain in which the MT binding regions are situated, and a C-terminal domain, which is hypothesized to have a regulatory function in MT interaction (Walczak and Shaw 2010).

PRC1 is a substrate of cyclin-dependent kinase CDK1 (Jiang et al. 1998). PRC1 is inhibited until anaphase by CDK1 phosphorylation, which averts its dimerization. Upon dephosphorylation, PRC1 forms dimers, which specifically recognize and bind antiparallel MTs, thereby promoting their crosslinking and sliding. This process also requires other cellular proteins including kinesin-4. The PRC1-mediated regulation of the mitotic spindle midzone is crucial in cell division and for proper cytokinesis (Zhu et al. 2006; Fededa and Gerlich 2012).

PRC1 and MTs

PRC1 binds and bundles MTs both in vitro and in vivo (Mollinari et al. 2002a). PRC1 binds selectively to antiparallel MTs in the mitotic spindle and maintains mitotic spindle midzone organization by recruiting kinesin-4 motors (Mollinari et al. 2002a; Bieling, Telley, and Surrey 2010).

Links to diseases:

PRC1 is linked to gastric carcinoma (Zhang et al. 2017), breast carcinoma (Brynychova et al. 2016)and hepatocellular carcinoma (Chen, Rajasekaran, et al. 2016). Moreover, in gastric cancer, PRC1 is a downstream target of piperlongumine (Zhang et al. 2017).

6.2.2. Proteins already reported as MAPs without in vitro confirmations

CSAP

Alternative names:

C1orf96 (chromosome 1 open reading frame 96), or Centriole, Cilia and Spindle-Associated Protein (CSAP) or CCSAP

Background:

The Cilia and Spindle-Associated Protein (CSAP) was first reported as a MAP in 2012, which colocalizes with polyglutamylated tubulin on centrioles, mitotic spindles and cilia in cultured human cells (Backer et al. 2012). CSAP was then extensively studied in relation to tubulin posttranslational polyglutamylation, and it was shown that the polyglutamylating enzyme TTLL5 forms a complex with CSAP. This can induce recruitment of TTLL5 to MTs, thus amplifying the activity of the enzyme (Bompard et al. 2018).

CSAP and MTs:

Studies in cells and in vitro reconstructions with the purified protein show that CSAP decorates MTs (Bompard et al. 2018). In cultured cells, loss of CSAP leads to instability of spindle MTs, resulting in mislocalization of NuMA (Nuclear protein that associates with the Mitotic Apparatus), and perturbed MT dynamics (Ohta et al. 2015).

Physiological functions:

Compared to other MAPs, little is known about the physiological functions of CSAP. However, there are studies showing that CSAP is involved in the proper beating of cilia, development of the brain, and left-right symmetry establishment in zebrafish (Backer et al. 2012).

Links to diseases:

Loss of CSAP leads to critical issues in the development of the brain and during mitosis progression (Ohta et al. 2015). Direct evidence that shows how binding of CSAP on MTs contributes to this is lacking, but there are accumulating studies indicating that CSAP regulates tubulin glutamylation via TTLLs, which is linked to diseases such as retinal degeneration, neurodegeneration and male infertility (Bompard et al. 2018), suggesting CSAP could have some indirect links to these diseases.

EMAPs/ EMLs

Alternative names:

EMAPs (Echinoderm Microtubule-Associated Protein) are also called as EMLs or ELPs (both for EMAP-Like proteins).

EML1: EMAP1, ELP79, EMAPL1, EMAP, EMAPL, HuEMAP, HuEMAP-1

EML2: EMAP2, ELP70 (Human EMAP-like Protein-70), EMAPL2, HuEMAP-2

EML3: EMAP3, ELP95, FLJ35827,

EML4: EMAP4, ROPP120, C2orf2, EMAPL4, ELP120

EML5: EMAP5

EML6: EMAP6, EML5L, FLJ42562

Background:

EMAPs are a family of MT-associated proteins discovered in echinoderms. The first reported EMAP is the 77-kDa EMAP1 identified in unfertilized sea urchin eggs (Suprenant et al. 1993). Other EMAP orthologues were found later in sand dollar, starfish, worms, flies and vertebrates, and given the name EMLs or ELPs (both for EMAP like proteins). Currently, the mammalian EMAP family has six members: EMAP1-6, which often referred to as cell-division MAPs (Fry et al. 2016).

Domain organization in EMAP1-6:

All EMLs (EML1-6) carry at least one TAPE (tandem atypical β-propellers in EMLs) domain. TAPE domains are structured domains containing multiple WD (tryptophan–aspartate) repeats that form a pair of β-propellers, which acts as a single globular tubulin-binding unit. Towards the start of the TAPE domain, there is a highly conserved HELP (hydrophobic EMAP-like protein) motif containing key residues at the interface connecting two β-propellers (Bayliss et al. 2016). TAPE domains alone don't localize to MTs, though they bind to tubulin dimers. In addition to the TAPE domain, EML1, 2, 3, and 4 contain an NTD or N-terminal domain comprising a coiled-coil region. Crystallographic studies showed that the coiled-coil region forms a homotrimer, and is thus known as trimerization domain or TD (Richards et al. 2015). EML1-4 bind MTs through the NTD, and require TD and a basic region located in between TD and beginning of the TAPE domain. In the case of EML5 and EML6, they contain only three repeats of TAPE domains and lack the NTD. The MT binding ability of EML5 and EML6 is still unclear and need to be tested. EML1- 4 can assemble into trimeric complexes (Adib et al. 2019; Richards et al. 2014). Besides, the 77-kDa EMAP1 has epitopes similar to the brain MAPs Tau and MAP2 (Li, Callaghan, and Suprenant 1998)

EMLs and MTs

EML1

The first study demonstrating that EML1 binds MTs *in vitro* used EML1 purified from unfertilized sea urchin eggs (Suprenant et al. 1993). The binding ratio of EMAP1 to tubulin dimers is 1 to 3. Unlike tau, MAP4 and MAP2, EMAP1 binds to subtilisin-treated MTs, which lack the unstructured C-terminal tubulin tails (Hamill et al. 1998). Also, sea urchin EMAP1 lowers the MT rescue frequency without changing the frequency of catastrophe events, suggesting that EMAP1 promotes MT dynamics (Suprenant et al. 1993; Hamill et al. 1998).

Recent studies with purified mouse EML1 show that it can bind directly to MTs *in vitro*, and. EML1 highly localizes to the MT networks in both interphase and mitosis in neuronal progenitor cells (Kielar et al. 2014). The crystal structure of the EML1 TAPE domain has been solved with 2.6-Å resolution (Carstens et al. 2014), but the EML1-MT binding architecture remains unknown.

EML2/ ELP70

In vitro studies show that the 70-kDa EML2/ ELP70 has a MT-destabilizing property. It can alter MT dynamics by lowering seeded nucleation, reducing polymerization rate, and promoting catastrophes. Also, indirect immunofluorescence studies in HeLa cells show that it localizes to the mitotic apparatus (Eichenmuller et al. 2002), suggesting that EML2 is regulated to bind to MTs at least in some stages of cell division, although it behaves as a MT depolymerizer *in vitro*. However, further studies need to be conducted to understand its regulatory mechanisms.

EML3

Immunofluorescence studies showed that EML3 decorates spindle MTs in all mitotic stages (Tegha-Dunghu et al. 2008). In cells, EML3 can modulate mitotic spindle assembly and kinetochore-MT connection by recruiting augmin/ γ-TuRC to spindle MTs. This is regulated by the Thr-881 phosphorylation of EML3 by CDK1. EML3 also controls small MT aster formation through augmin and γ-TuRC (Luo et al. 2019). There is no study so far showing if purified EML3 binds MTs *in vitro*.

EML4

Co-sedimentation assays have showed that purified full-length EML4 binds to MTs *in vitro*. Moreover, cryo-EM studies reveal that the NTD of EML4 interacts with the C-terminal tails of tubulin, whereby the affinity of EML4 is regulated by NEK6- and NEK7-mediated phosphorylation (Adib et al. 2019). In cells, EML4-decorated MTs were resistant to nocodazole-induced depolymerization, suggesting that EML4 stabilizes MTs. This was confirmed by the observation that loss of EML4 reduces interphase MT stability (Houtman et al. 2007; Adib et al. 2019).

EML5 and EML6

So far, there is no direct evidence showing that EML5 and EML6 could directly bind to MTs. Also, based on previous studies, the conserved MT-binding NTD region of other EML proteins is not found in these two EMLs (Fry et al. 2016).

Physiological functions:

EML1

In mice, loss of EML1 in developing cerebral cortex altered the shape of neuronal progenitor cells and spindle length (Bizzotto et al. 2017). EML1 highly localizes with the MT network in both interphase and mitosis in neuronal progenitor cells, and its absence alters spindle length and orientation (Kielar et al. 2014). In eggs of the echinoderm sea urchin, EMAP1 is abundant and controls MT assembly – an observation also confirmed in studies using purified EMAP1 *in vitro* (Suprenant et al. 1993; Hamill et al. 1998).

EML2

EML2/ ELP70 is reported as a MT destabilizer and localized to the mitotic apparatus in HeLa cells (Eichenmuller et al. 2002). One study shows that purified rat EMAP is having 94% DNA sequence identity and 95% similarity with human EMAP2, can bind to δ-glutamate receptors, and is highly expressed in the brainstem and postsynaptic density (PSD) (Ly et al. 2002).

EML3

EML3 decorates the mitotic spindle at all stages of mitosis, and in interphase EML3 decorates cytoplasmic MTs, but does also accumulates inside the nucleus. EML3 is essential for the correct chromosome alignment in metaphase (Tegha-Dunghu et al. 2008), suggesting it is an important mitotic MT-binding protein, or in other words, a cell division MAP.

EML4

In mouse, EML4 is temporally regulated, it is highly expressed in embryos at embryonal day 11, and declines to lower levels in adults. In brain, EML4 expression is spatially limited to the hippocampus, cerebellum and the olfactory bulb. *In cellulo*, EML4 decorates MTs in both dividing and non-dividing cells (Houtman et al. 2007). EML4 also takes part in the loading of NUDC (nuclear distribution gene C) protein onto the spindle MTs which is a critical factor for mitotic progression (Chen et al. 2015).

EML5 and EML6

There are not many studies conducted on EML5 and 6. However, it has been reported that EML5 is expressed in the cerebellum, hippocampus and the olfactory bulb in rat brain (O'Connor et al. 2004). Also, EML5 plays a role in muscle differentiation and growth (Szuhai et al. 2014). However, the molecular functions of both of these EMLs are still unknown.

Links to diseases:

EML fusion proteins:

EMLs also make fusions with other proteins. So far, around four such fusions with cancer-related kinases have been reported: 1) EML1-ABL1 (EML1 to Abelson 1); 2) Two variants (variant 1 and variant 3b) of EML4-ALK (EML4 to anaplastic lymphoma kinase (ALK)) (Fry et al. 2016); 3) a double ALK fusion variant EML6-ALK FBXO11 (F-box only protein 11)-ALK (Lin, Ren, and Liang 2018); and 4) EML4-NTRK3 (neurotrophic receptor tyrosine kinase 3 or also known as NT-3 growth factor receptor or TrkC) (Church et al. 2018). EML1-ABL1 is a constitutively phosphorylated tyrosine kinase, associated with T-cell acute lymphoblastic leukaemia (De Keersmaecker et al. 2005). EML4-ALK are constitutive tyrosine kinases in which ALK belongs to the insulin-receptor tyrosine kinase superfamily. EML4-ALK oncoproteins are inked to colorectal, breast and non-small cell lung cancers (NSCLC) (Lin et al. 2009). For more details about EML4-ALK fusion proteins, see review by Bayliss 2016, (Bayliss et al. 2016). The EML6-ALK FBXO11-ALK fusion protein was recently reported in relation to lung adenocarcinoma (Lin, Ren, and Liang 2018). The molecular mechanism of this MAP-kinase fusions needs to be explored. However, ABL and ALK form fusions with other non-MAP proteins as well (Ducray et al. 2019; Fujisawa et al. 2008). In literature, so far there are more studies about EML-fusion oncoproteins than EMLs functions as MAPs.

EML1

The first report of a disease linked to EML1 is the Usher syndrome type 1a in which patients have sight and hearing disabilities (Eudy et al. 1997). Later on, point mutations in the TAPE domain of EML1 were implicated in neuronal migration disorders causing neuronal heterotopia in both mice and humans (Kielar et al. 2014). Also, EML1 can interact with a primary-cilium

protein called RPGRIP1L and mutations in RPGRIP1L is related to in Joubert and Meckel ciliopathy syndromes (Wiegering, Ruther, and Gerhardt 2018; Delous et al. 2007).

Recent publications show that mutations in EML1 lead to heterotopia, a neuronal migration disorder in both humans and rodents (Kielar et al. 2014), and disrupt primary cilia formation in apical radial glial cells in the brain (Uzquiano et al. 2019). Besides, EML1 interacts with RPGRIP1L, which is known to localize at the base of primary cilia (Wiegering, Ruther, and Gerhardt 2018). The molecular role of EML1- RPGRIP1L interaction is not clear yet. Other recent studies show that EML1 having heterotopia gene mutations affects the formation of primary cilia (Uzquiano et al. 2019). In the case of EML1 fusion proteins, the N-terminal EML1 sequences fused to the C-terminal ABL polypeptide leads to the formation of a 190-kDa EML1-ABL1 oncoprotein. This EML1-ABL1 acts as a dysregulated tyrosine kinase that activates cell survival signalling and proliferation pathways in T-cell acute lymphoblastic leukaemia (De Keersmaecker et al. 2005).

EML2/ ELP70, and EML3

There are no studies to date that showing a direct connection of EML2 and 3 to any diseases.

EML4

More than EML4 alone, there are many studies discussing EML4-ALK fusion proteins and their role in cancers. EML4–ALK fusion protein is associated with colorectal, breast and non-small cell lung cancer (NSCLC) (Lin et al. 2009). Besides, some mutations in EML4 are related to POEMS syndrome, a rare blood disorder that mainly damages nerves (Nagao et al. 2019).

There are 15 variants of EML4-ALK fusion oncoproteins in lung cancers, and they could potentially activate multiple oncogenic signalling pathways through ALK binding partners such as JAK/STAT, PI3K/Akt, and MEK/ERK /RAS/RAF. It is shown that many kinases, including the oncogenic ALK, depend on chaperones like HSP90 for stability. Thus, HSP90 inhibitors are also used as potential drugs against EML4-ALK oncoproteins (Sabir et al. 2017). For further details about EML-ALK fusions and ALK proteins, see reviews (Sabir et al. 2017; Katayama, Lovly, and Shaw 2015; Hallberg and Palmer 2016).

EML5

EML5 expression level is high in both glial cells and neurons of the anterior temporal neocortex of patients having intractable epilepsy (Sun et al. 2015). Also, EML5 is related to hyperglycaemic memory in the diabetic mouse model (Friedrichs et al. 2017).

EML6

EML6-ALK FBXO11-ALK fusion protein is reported in relation to lung adenocarcinoma (Lin, Ren, and Liang 2018). Also, EML6 is overexpressed in human prostate cancer tissues and cells (Zhao et al. 2019).

Chemical drugs:

EML1-ABL1 is a therapeutic target of imatinib in acute T-cell lymphoblastic leukaemia (De Keersmaecker et al. 2005).

EML4-ALK is a therapeutic target of crizotinib, ceritinib and alectinib, which are FDA-approved drugs for metastatic non-small-cell lung carcinoma (NSCLC) (Herden and Waller 2018; Holla et al. 2017).

EML6-ALK FBXO11-ALK double fusion variant in lung adenocarcinoma responds to Crizotinib (Lin, Ren, and Liang 2018).

MAP3/ MAP4

Alternative names:

MAP4 was initially known as MAP3.

MAP4 and MTs

Full-length MAP4 promotes polymerization of MTs *in vitro,* and co-localizes with the MT network *in vivo*, with preference to tyrosinated MTs (Chapin and Bulinski 1994; Huber, Alaimo-Beuret, and Matus 1985). Structural studies show that MAP4 changes its conformation upon binding to MTs and promotes their stability (Xiao, Wang, et al. 2012). Full-length MAP4

also interacts with part of the dynein-dynactin complex and inhibits MT sliding (Samora et al. 2011). Overexpression studies in non-neuronal cells show that MAP4 inhibits kinesin-driven MT gliding, thereby affecting organelle motility and trafficking.
MAP4 also regulates the functions of other MAPs such as MCAK/XKCM1 (Holmfeldt, Brattsand, and Gullberg 2002), stathmin (Holmfeldt, Brattsand, and Gullberg 2002) and katanin (inhibition) (McNally, Buster, and McNally 2002). In the context of transport, MAP4 negatively regulates dynein-dependent motility and positively regulates kinesin-2-based motility (Semenova et al. 2014). *In vitro* studies using purified MAP4 show that it alters the surface properties of MTs, thereby affecting kinesin-driven motility (Tokuraku et al. 2007).

A short isoform of MAP4 can induce MT assembly, but is unable to bundle MTs. Instead, it's proposed to space adjacent MTs at a constant distance (Matsushima et al. 2005).

Physiological functions:

MAP4 is a ubiquitous MAP, predominantly expressed in the brain, and present in both glial cells and neurons in the adult central nervous system (Bernhardt, Huber, and Matus 1985). MAP4 is abundant in neurofilament-rich axons, suggesting it could crosslink MT and neurofilaments (Huber, Alaimo-Beuret, and Matus 1985). In primary cultured neurons, MAP4 is localized in patches and at branching points (Tokuraku et al. 2010). The full-length MAP4 isoform contains a MT binding region rich in proline and basic residues. In epithelial cells, MAP4 is associated with spindle orientation (Samora et al. 2011).

MAP4 is regulated with different kinases: protein kinase C (PKC) (Mori et al. 1991), mitogen activated protein kinase (MAPK) (Hoshi et al. 1992) and MAP/MT-affinity regulating kinase (MARK) (Illenberger et al. 1996). In addition, full length MAP4 also interacts with $p150^{Glued}$ and thus with the dynein-dynactin complex to inhibit MT sliding (Samora et al. 2011).

Links to diseases:

MAP4 is associated to Alzheimer's disease (Ray, Ruan, and Zhang 2008), chronic stress, cardiac hypertrophy (Kumarapeli and Wang 2004), breast cancer (Bash-Babula et al. 2002) and ovarian cancer (Yang et al. 2018).

ATIP3 (Angiotensin II type 2 (AT (2)) receptor-interacting protein 3)

Alternative names:

Microtubule-associated Tumour Suppressor 1 gene (MTUS1), Mitochondrial Tumour Suppressor gene, Angiotensin II type 2 (AT (2)) receptor-interacting protein (ATIP) and AT2 receptor-binding protein.

Background:

ATIP was first reported in 2011(Molina et al. 2011), ATIP has five splice isoforms: ATIP1, ATIP2, ATIP3a, ATIP3b, and ATIP4. Based on tissue specificity and utilization of 5′ exon, ATIP is classified in to three groups: ATIP1, ATIP3 (comprising ATIP2, ATIP3a, ATIP3b) and ATIP4 (Di Benedetto, Bieche, et al. 2006; Bozgeyik, Yumrutas, and Bozgeyik 2017). ATIPs carry distinctive motifs at their N-termini, which determine their localization; ATIP1 localizes to the cytosol, ATIP3 to the nucleus, and ATIP4 to the plasma membrane. Among all isoforms, ATIP3 is the most characterized MAP in relation to MTs. ATIP3 has three functional domains: D1, D2, and D3 (from N- to C-terminus). ATIP3 D3 alone forms protein patches inside the cell containing soluble tubulin. On the other hand, the MT binding region D2 is sufficient to show the full-length ATIP3 properties such as MT stabilization, and effects on cell motility and proliferation (Molina et al. 2013). Among all MAPs in my study, based on existing reports, ATIP is the most-studied MAP in association with different types of cancers.

ATIP3 and MTs

Cellular studies show that ATIP3 decorates and stabilizes MTs, and also can regulate their dynamics (Molina et al. 2013). There are no MT binding studies so far with purified ATIP3 *in vitro*.

Physiological functions:

ATIP3 is a tumour suppressor gene, its expression slows metastatic progression and controls cancer cell migration (Molina et al. 2013) ATIP is also involved in mouse development (Bundschu and Schuh 2014), DNA repair (Min et al. 2012), inflammation (Fujita et al. 2009); vascular remodelling, cell proliferation, differentiation and senescence (Min et al. 2012) (Bozgeyik, Yumrutas, and Bozgeyik 2017). For further details about the role of ATIP3 in health and disease, see review (Bozgeyik, Yumrutas, and Bozgeyik 2017).

Links to diseases:

In breast cancer patients, ATIP3 is a prognostic marker (Rodrigues-Ferreira et al. 2009; Molina et al. 2013). ATIP3 is related to hepatocellular carcinoma (Di Benedetto, Pineau, et al. 2006), prostate cancer (Louis et al. 2011), gastric (Li et al. 2014), bladder (Xiao, Chen, et al. 2012), oral (Ding et al. 2012), lung (Gu et al. 2017) and colon cancer (Zuern et al. 2010).

CFAP20 (Cilia Flagella Associated Protein 20)

Alternative names:

CFAP20 or Cilia Flagella Associated Protein 20 is also known as the Basal body up-regulated gene 22 (BUG22) and Flagella Associated Protein 20 (FAP 20).

Background

CFAP20 is mostly known as Bug22 (Basal body up-regulated gene 22) was first reported in 1996 as a 22-kDa mouse protein (Rijkers and Ruther 1996). Later CFAP20 was characterized and shown to have functions associated with MT-based ciliary and flagellar structures (Yanagisawa et al. 2014; Mendes Maia et al. 2014). Other proteins associated to cilia and flagella structures with similar nomenclature are CFAP69, CFAP70, CFAP221, CFAP43, CFAP44, CFAP65, CFAP46 and CFAP300 (OMIM database), these proteins are poorly studied in terms of their MT binding capabilities.

CFAP20 and MTs

CFAP20 is an inner-junction protein of the MT doublets in cilia and flagella (Owa et al. 2019). In drosophila, CFAP20 influences the morphology and the post-translational modifications of ciliary MTs, for instance, polyglycylation and polyglutamylation on the axonemal MTs (Mendes Maia et al. 2014). There are no studies so far using purified CFAP20 to confirm its binding to MTs *in vitro*.

Physiological functions:

CFAP20 is mostly studied in association with ciliary and flagellar structures. In *Chlamydomonas*, CFAP20 takes part in the stability and asymmetric waveform of flagella (Yanagisawa et al. 2014). Also, the removal of human CFAP20 in RPE1 cells leads to the formation of longer primary cilia (Mendes Maia et al. 2014). In motile cilia, CFAP20 interacts

with PACRG, which has a crucial role in the regulation of dynein-driven MT sliding (Dymek et al. 2019).

Links to diseases:

There are no reports so far directly linking CFAP20 to any disease.

Cingulin

Alternative names:

Cingulin is also abbreviated as CGN.

Background:

Cingulin (from the latin word *cingere* meaning "to form a belt around") was first reported in 1988, discovered as a tight junction protein co-purified with myosin II from intestinal epithelial cells, and found to localize as a circumferential belt in these cells (Citi et al. 1988b; Citi et al. 1989). Cingulin is a heat-stable acidic protein with an elongated structure, structurally similar to a kinesin motor, that exists as a homodimer (Citi et al. 1988a). Each monomeric unit of cingulin comprises 3 major parts: a head, a tail and a rod connecting them. It has a large globular head at the amino terminus, a small globular tail region at carboxyl-terminal, and a coiled-coil rod domain connecting head and tail, which is homologous to nonmuscle myosins. The amino-terminus of Cingulin interacts with actin, Zonula Occludens (ZO)-1, 2, 3; myosin, afadin, JAM-A, while the carboxy-terminus interacts only with myosin and ZO-3 (Cordenonsi et al. 1999), (González-Mariscal et al., 2012, DOI: 10.5772/35166). Another tight junction protein closer to cingulin is the paracingulin, also known as Cingulin-like protein-1 or JACOP (Junction-Associated-Coiled-Coil Protein) (Citi, Pulimeno, and Paschoud 2012).

Cingulin and MTs:

Cingulin is mostly characterized as a F-actin-interacting protein. However, it has been shown that purified cingulin interacts also with MTs *in vitro* (D'Atri and Citi 2001b; Yano et al. 2018). Studies in epithelial cells show that AMPK-phosphorylated Cingulin can reversibly bind to MTs and actin filaments (Yano et al. 2013; Yano et al. 2018).

Physiological functions:

Cingulin is a tight junction protein mostly reported in epithelial cells. Cingulin takes part in a range of cellular functions, including in Rho signalling (Aijaz et al. 2005), lumen formation in polarized epithelial cells (Mangan et al. 2016) and epithelial junction assembly (Guillemot et al. 2014).

Links to diseases:

Cingulin is linked to mesothelioma (Oliveto et al. 2018), ulcerative colitis (Soroosh et al. 2019) and pulmonary edema(Tian et al. 2016).

EF-1alpha (Elongation factor 1 alpha)

Alternative names:

EF-1alpha (Elongation factor 1 alpha) is also known as Elongation factor Tu, EF-Tu.

EF-1 alpha and MTs:

EF-1 alpha was found associated with the spindle MTs in sea urchin eggs, and can bind, stabilize and bundle MTs in a calmodulin/ calcium-dependent manner (Ohta et al. 1990; Sasikumar, Perez, and Kinzy 2012; Moore, Durso, and Cyr 1998). EF-1 alpha was first reported in 1994 as a severing MAP *in vitro* and EF-1 alpha microinjected into fibroblasts induced rapid MT severing (Shiina et al. 1994). There are no follow up studies thereafter about EF-1 alpha mediated MT severing, and the molecular mechanism of EF-1 alpha-MT interactions remains unclear.

Physiological functions:

In protein translation system, EF-1 alpha is responsible for the selection and transfer of aminoacyl-tRNA to the ribosome (Andersen and Nyborg 2001). Along with this it has a multitude of other functions, such as in the oxidative stress response pathway, in proteolysis, in apoptosis and in viral propagation (Sasikumar, Perez, and Kinzy 2012). In vitro studies show EF-1 alpha interacts with Parkinson's disease-related kinase LRRK2 (leucine-rich repeat kinase 2), impairs its activity and leads to MT bundling (Gillardon 2009). Along with MTs, EF-1 alpha also interacts with filamentous actin by bundling it and inhibiting its polymerization from growing ends (Murray et al. 1996). EF-1 alpha was found associated with the mitotic spindle

(Ohta et al. 1990) and undergoes phosphorylation by a number of serine/ threonine protein kinases (Sasikumar, Perez, and Kinzy 2012).

Links to diseases:

Opitz syndrome (Aranda-Orgilles et al. 2008), erythroleukemia (Kato 1999).

GLFND

Alternative names:

Fibronectin type III and SPRY domain-containing protein; MID1-related protein 1.

Background:

GLFND is one of the least studied MAPs in our list. GLFND was first reported in 2002, and it was discovered using a GFP cDNA library screening strategy. In this method, the total RNA was isolated from a human fibrosarcoma cell line (HT1080). The cDNAs were then prepared with the SuperScript Plasmid System (Invitrogen), and were cloned in pCIneohEGFP (a GFP expression plasmid), subsequently transfected in REF52 cells in 96-well plates and checked the MT binding (Manabe et al. 2002b). GLFND is homologous to MID1/Fxy1 (an E3 ubiquitin-protein ligase Midline-1) in humans, which is already reported as a MAP associated with Opitz syndrome (Quaderi et al. 1997). There are not many studies on GLFND, however predictions are pointing towards multiple potential phosphorylation sites in GLFND for kinases such as MT affinity-regulating kinase MARK (KXGS) and MAP kinase (PXSP), suggesting that its interactions to the MTs could be regulated by phosphorylation (Manabe et al. 2002a).

GLFND and MTs

In cells, GLFND localizes to acetylated MTs and protects them against nocodazole-mediated MT depolymerization (Manabe et al. 2002a).
There are no *in vitro* studies so far with purified GLFND showing its binding to MTs.

Physiological functions:

Studies in cells show that GLFND is involved in cell division. In the beginning of mitosis, GLFND dissociates from the MTs and then re-associates during cytokinesis. In CHO cells, overexpression of GLFND leads to the inhibition of cell division and cytokinesis (Manabe et al. 2002a).

Relation with diseases

There is no evidence linking GLFND to any disease.

Protein 4.1 R

Alternative names:

Protein 4.1, P4.1, band 4.1, 4.1R, EPB 4.1.

Background:

Protein 4.1R was first reported in 1971, as a structural component of human erythrocytes or red blood cells (RBCs) (Fairbanks, Steck, and Wallach 1971; Leto and Marchesi 1984). Protein 4.1R provides structural stability and elasticity of RBC's by forming a junctional complex with actin and spectrins (Baines, Lu, and Bennett 2014). The three other homologues of 4.1R are 4.1G, 4.1N, and 4.1B, and are also present in non-erythroid cell types (Parra et al. 2000). Along with MTs, Protein 4.1 R also interacts with actin filaments. The 4.1R protein consists of an N-terminal extension domain, a 16kDa signature domain, present in all members of Protein 4.1 family, a membrane-binding domain (MBD1), a spectrin/actin-binding domain (SAB) and a C-terminal domain (CTD) (Huang et al. 2004). Protein 4.1R is a member of FERM (Protein 4.1R, ezrin, radixin, and moesin) superfamily of proteins. For more information about Protein 4.1 family of proteins, see reviews (Baines, Lu, and Bennett 2014; Bosanquet et al. 2014).

Protein 4.1R and MTs

Cell studies have shown that protein 4.1R is localized to interphase MTs in human T cells. Purified 4.1R also binds *MTs in vitro* (Perez-Ferreiro, Luque, and Correas 2001). Using mammalian mitotic extracts, it has been shown that Protein 4.1R could also aid assembly of MT asters (Huang et al. 2004).

Physiological functions:

Protein 4.1R is involved in many cellular functions such as association of the centrosome with the nucleus, localization of nuclear envelope proteins, transcriptional signalling (Meyer et al. 2011), organization of peripheral myelinated axons (Cifuentes-Diaz et al. 2011) and control of ion channels (Baines et al. 2009). It has been shown that Protein 4.1R localizes to mammalian centrosomes and could be an integral part of them (Krauss et al. 1997). Moreover, Protein 4.1R takes part in the formation of spindle poles and mitotic spindles by interacting with mitotic MTs, suggests its importance in cell division (Huang et al. 2004).

Links to diseases:

Protein 4.1R is linked to heart failure (Wei, Yang, et al. 2016), encephalomyelitis (Liu et al. 2014), myeloid malignancies (Alanio-Brechot et al. 2008) and neuroacanthocytosis (Orlacchio et al. 2007).

MAP 10/ Microtubule-associated protein 10

Alternative names:

MAP10 is also known as MTR120 (Microtubule regulator of 120-kDa) and KIAA1383.

MAP10 and MTs

In interphase cells, MAP10 localizes to acetylated/ stable MTs, and also to the mitotic spindle. Overexpression of MAP10 results in bundling of MTs and increased MT acetylation (Fong et al. 2013).
In vitro studies using purified MAP10 show that it can decorate and bundle preassembled MTs (Fong et al. 2013).

Physiological functions:

MAP10 is a cell division-related MAP first reported in 2012. There are not many studies on MAP10. Cell studies show that MAP10 is essential for cytokinesis: Depletion of MAP10 by RNAi show aberrations in cytokinesis and leads to polyploidy (Fong et al. 2013).

Links to diseases:

No reports.

MAP 11/ Microtubule-associated protein 11

Alternative names:

MAP11 is also known as C7orf43 and TRAPPC14.

MAP11 and MTs:

Cell studies showed that MAP11 binds to the mitotic spindle MTs, specifically binding α-tubulin in mitosis (Perez et al. 2019a).

There are no in vitro studies so far using purified MAP11 showing it can bind MTs.

Physiological functions:

MAP11 was first reported in 2019 (Perez et al. 2019a), and considering its role in cell division and spindle dynamics, it is called a cell-division MAP. Given that MAP11 was very recently discovered, there are only few studies about it. RT-PCR studies show that MAP11 is present at a high level in all tissues examined in brain, testis and blood (Perez et al. 2019a). MAP11 also has a regulatory role in abscission at the midbody during cytokinesis (Perez et al. 2019a).

Links to diseases:

Mutations in MAP11 leads to microcephaly in both humans and zebrafish (Perez et al. 2019b) and MAP 11 is also linked to hepatocellular carcinoma (Amisaki et al. 2019).

Other interacting partners:

Other than MTs, MAP11 can also bind to Rabin8, TRAPPC (transport particle protein complex) proteins, FBF1 (Fas-binding factor 1) and CEP83 (centrosomal protein 83) (Cuenca et al. 2019).

Parkin

Alternative names:

No other names.

Parkin and MTs:

Co-precipitation studies with Parkin-bound MTs show that Parkin interacts with tubulin heterodimers and MTs with three independent domains (Yang et al. 2005). Cell studies support

the observation that Parkin binds to α/β-tubulin and show that it can ubiquitinylate them and thus destine for degradation (Ren, Zhao, and Feng 2003a).

However, cellular studies in COS1 and PC12 cells, which shows that Parkin localizes to actin filaments, but not to MTs (Huynh et al. 2000). Considering previous evidences, this study is confusing about the MT binding ability of Parkin (Huynh et al. 2000), and further experiments need to be carried down to clarify this. A co-sedimentation assay with purified Parkin, purified MTs and actin is an experiment which could shed light on this.

Physiological functions:

Parkin is an E3 ubiquitin ligase. The ubiquitination process requires three enzymes: E1 (binds to inactive Ubiquitin (Ub)), E2 (transfers ubiquitin to E3), and E3 (conjugating Ub to target protein) (Feng 2006; Pickart and Eddins 2004). The primary function of Parkin is to ligate ubiquitin (Ub) to lysine residues of target substrates.

In simple words, Parkinson's disease (PD) is a movement disorder caused by the death of neurons (dopamine-producing) in the mid-brain. Studies indicate that mitophagy (removal of damaged mitochondria by autophagy) may play an important role in PD pathology. It has been shown that Parkin (E3 ubiquitin ligase) and PINK1 (a protein kinase) are two key molecular players in this, which controls mitochondrial quality and selective mitophagy (Narendra, Walker, and Youle 2012). Under normal conditions, ligase activity of parkin E3 is blocked, and under pathogenic conditions, Parkin ubiquitinates various outer membrane proteins in mitochondria and leads to mitophagy. Aberrations in this quality control mechanism contribute to one of the common causes of PD (Seirafi, Kozlov, and Gehring 2015; Dawson and Dawson 2010). Recent studies suggest a new role of Parkin as a MAP which can strongly bind MTs (Yang et al. 2005).

Other interacting partners:

Co-immunoprecipitation experiments show that Parkin is also able to interact with LRRK2 (Leucine-rich repeat kinase 2), a well-characterized protein linked to familial Parkinson's disease (Islam and Moore 2017; Smith et al. 2005). Parkin also binds with wide range of cellular components such as alpha-synuclein (Choi et al. 2001; Kawahara et al. 2008), CASK (Fallon et al. 2002), CUL1 (Staropoli et al. 2003), CHIP (Imai et al. 2002), programmed cell death-2 isoform 1 (PDCD2-1) (Fukae et al. 2009a), p38 subunit of the aminoacyl-tRNA synthetase

complex (Corti et al. 2003), Programmed cell death-2 isoform1 (Fukae et al. 2009b), SEPT5_v2 (Choi et al. 2003), synphilin-1 (Chung et al. 2001) and synaptotagmin XI (Huynh et al. 2003).

Links to diseases:

Parkin is linked to Parkinson's disease (Kitada et al. 1998), MERRF syndrome (Villanueva-Paz et al. 2020), atherogenesis (Tyrrell et al. 2020), Juvenile Huntington's disease (Aladdin et al. 2019), lung cancer (Li, Wang, et al. 2019), hepatocellular carcinoma (Zhang et al. 2019), retinal degeneration (Zhu et al. 2019) and chronic obstructive pulmonary disease (COPD) (Leermakers et al. 2018).

Syntaphilin (SNPH)

Alternative names:

Also abbreviated as SNPH.

Background and physiological functions:

Syntaphilin/SNPH was first reported in 2000, in relation to the assembly of the SNARE complex in cytosis (Lao et al. 2000). In 2008 it was reported that syntaphilin docks mitochondria on MTs, and thus is one of the major regulators of mitochondrial motility on MTs in the axon (Kang et al. 2008). Upon sensing a signal (i.e. elevated calcium levels at synapses) SNPH puts a brake on mitochondria motility by inhibiting kinesin, in what is called the engine-switch and brake model. SNPH inhibits kinesin-1 motility by inhibiting its ATPase activity (Chen and Sheng 2013). In neurons lacking syntaphilin, mitochondria are more mobile in the axons (Chen and Sheng 2013). Syntaphilin undergoes phosphorylation by cAMP-dependent protein kinase which regulates its interaction with Syntaxin-1 in vesicle exocytosis (Boczan, Leenders, and Sheng 2004). Besides, studies show that dynein light chain LC8 modulates SNPH- mitochondria docking on axonal MTs (Chen, Gerwin, and Sheng 2009). Similar to the SNPH–KIF5 system, the Miro–Trak–kinesin complex is another example for MT-based transport regulatory mechanism (Macaskill et al. 2009).

Domain organization of SNPH:
SNPH has three major domains: a C-terminal mitochondria-binding domain (MitoBD), an N-terminal MT-binding domain (MTB), and a central axon-targeting domain (ATD) (Kang et al. 2008; Chen, Gerwin, and Sheng 2009).

Syntaphilin and MTs:

In cells, syntaphilin co-localizes with MTs (Chen, Gerwin, and Sheng 2009) and docks mitochondria on MTs (Kang et al. 2008). So far, there is no evidence about purified syntaphilin binding MTs *in vitro*.

Links to diseases:

Syntaphilin is linked to prostate cancer (Hwang et al. 2019) and multiple sclerosis (Mahad et al. 2009).

Chemical drugs

Rotenone could affect the expression level of syntaphilin in rat brains (Chaves et al. 2013).

TRAK 1 and TRAK 2

Alternative names:

TRAK1(Trafficking kinesin-binding protein 1) is known as Milton in drosophila.

Background and physiological functions:

TRAK1 and TRAK2 belong to the TRAK family of adapter proteins which link mitochondria to motor proteins. TRAK was first reported in 2002 in *Drosophila,* then named Milton (Stowers et al. 2002). TRAK proteins are important for the control of mitochondrial mobility in axons and dendrites. TRAK1 binds to both Kinesin-1 and dynein/dynactin motors, but TRAK2 exclusively binds to the dynein/dynactin complex. Recent studies with primary neuronal cultures show that TRAK1 is enriched in the axons of hippocampal and cortical neurons, while TRAK2 is localized mainly in dendrites of hippocampal neurons, and equally distributed between dendrites and axons of cortical neurons (van Spronsen et al. 2013) (Loss and Stephenson 2015). To the current knowledge, TRAK acts as a mediator protein which binds to motor proteins (kinesin and dynein) on the one hand, and Miro (Mitochondrial Rho GTPase) on the other hand, and Miro binds to the outer mitochondrial membrane (Oeding et al. 2018; Schwarz 2013).

TRAK and MTs

The Miro–TRAK–kinesin complex is one of the MT-based transport regulatory mechanisms (Macaskill et al. 2009). TRAK1 and TRAK2 are both motor adaptor proteins. Purified TRAK1

diffuses on MTs in vitro (Henrichs et al. 2020). There is no evidence showing that purified TRAK2 alone binds MTs in vitro.

Links to diseases:

TRAK1 is linked to encephalopathy (Barel et al. 2017) and hyperekplexia (Sagie et al. 2018). TRAK2 is linked to atherosclerosis (Lake et al. 2017).

6.2.3. Proteins not reported as MAPs before

CRMPs (Collapsin response mediator proteins):

Alternative names:

CRMPs (Collapsin response mediator proteins) are also called as TUC, TOAD-64 and Ulip.

CRMP-1: Dihydropyrimidinase-related protein 1(DRP-1), DPYSL1, Unc-33-like phosphoprotein 3 (ULIP-3)
CRMP-2: Dihydropyrimidinase-related protein 2 (DPYSL2), CRMP-62,
CRMP-3: Ulip4, Dihydropyrimidinase-related protein 4 (Dpysl4).
CRMP-4: Ulip (Unc-33 like phosphoprotein), TUC4, DRP-3, Ulip1, Dpysl3
CRMP-5: Dihydropyrimidinase-related protein 5, DPYSL5, ULIP6

Background

CRMPs (Collapsin response mediator proteins) family of proteins comprises 5 cytosolic phosphoproteins: CRMP1, CRMP2, CRMP3, CRMP4 and CRMP5. CRMP2 was the first discovered member of the CRMP family, reported in 1995 (Goshima et al. 1995). CRMP2 was initially named CRMP-62 because of its molecular mass of 62 kDa, but was later referred to as CRMP2. Among all CRMPs, CRMP2 is the most studied member. In 1996, CRMP1 and CRMP4 were discovered in foetal brain, and CRMP5 was reported later in 2000 (Charrier et al. 2003). CRMP2 has two splice variants: CRMP2A and CRMP2B. In mouse, CRMP2A (75 kDa) and CRMP2B (64 kDa) have differential expression pattern in distinct neurons (Bretin et al. 2005).

CRMPs and MTs

In cellular studies, it has been shown that CRMP1 and CRMP2 localize to mitotic MTs by binding directly to the MT through a conserved C-terminal region. Also, they can stabilize MTs, and this process is regulated by phosphorylation (Lin et al. 2011).

CRMP2 induces tubulin polymerization through its globular domain *in vitro* (Niwa et al. 2017). Two splice isoforms of CRMP2: CRMP2A and CRMP2B have antagonistic roles in MT organization (Quinn et al. 2003; Yuasa-Kawada et al. 2003). The longer CRMP2A isoform induces oriented MT patterns in cultured axons and fibroblasts. On the contrary, the shorter CRMP2B isoform induces the disoriented MT patterns (Yuasa-Kawada et al. 2003).

Full-length CRMP3 inhibits MT polymerization and leads to shorter MTs *in vitro* (Aylsworth et al. 2009). CRMP4 promotes MT assembly *in vitro*. Mouse CRMP4 is important for maintaining axon outgrowth and the size of the growth cone (Khazaei et al. 2014). CRMP5 promotes MT polymerization and interacts with tubulin through its C-terminal region (Brot et al. 2010). It has been shown that CRMP5 can interact with spastin *in vivo* and *in vitro* (Ji et al. 2018).

Physiological functions:

CRMPs are downregulated in the adult brain. They have multiple cellular and molecular functions in cell migration, differentiation and apoptosis (Charrier et al. 2003). CRMPs were originally discovered as mediators of collapsin-1/Sema3A signalling. Collapsin acts as an inhibitory protein for axonal guidance and causes the collapse of growth cone lamellipodium because of the redistribution of actin filaments (Fan et al. 1993). Mouse studies showed that CRMP3 has histone-H4 deacetylase (HDAC) activity (Hou et al. 2013). Overexpression studies of CRMP2B in chicken retinae show that the protein promotes axon branching and suppresses axon elongation of ganglion cells. In contrary to the co-expression of CRMP2B and CRMP2A, CRMP2A suppresses axon branching and promotes axon elongation of ganglion cells (Yuasa-Kawada et al. 2003). In addition, in cell studies it has been shown that Prolyl isomerase Pin1 interacts with CRMP2A and promotes axon outgrowth (Balastik et al. 2015).

Links to diseases

The CRMP family of proteins has been reported in association with different diseases. For example, it has been shown that the expression pattern of CRMPs is altered in some neurodegenerative disorders (Charrier et al. 2003).

CRMP1/ DRP-1/ DPYSL1/ ULIP-3 is linked to medulloblastoma (Li et al. 2015), Huntington's disease (HD) (Stroedicke et al. 2015), prostate cancer (Cai et al. 2017) and schizophrenia (Bader et al. 2012).

CRMP2/ DPYSL2/ CRMP-62 is involved in prion diseases in murine models (Shinkai-Ouchi et al. 2010), in schizophrenia (Toyoshima et al. 2019) (Arai and Itokawa 2010), in Alzheimer's disease (Gu, Hamajima, and Ihara 2000), in Parkinson's disease (Togashi et al. 2019) and in multiple sclerosis (Petratos et al. 2012). The hyperphosphorylation of CRMP2 is a characteristic of AD (Williamson et al. 2011).
In the case of the CRMP2A and CRMP2B isoforms, there is no evidence revealing their direct relation with any disease.

CRMP3/ Ulip4/ Dpysl4 is found in patients having small-cell lung cancers with paraneoplastic neurologic syndrome (Honnorat et al. 1999).

CRMP4/ Ulip/ TUC4/ DRP-3/Ulip1/ Dpysl3 is associated to colorectal cancer (Chen, Cai, et al. 2016)and prostate cancer (Gao et al. 2010).

CRMP5/ DPYSL5/ ULIP6 is linked to lung cancer and thymoma-related autoimmunity (Yu et al. 2001), neuropathy (Dubey et al. 2018), vitritis, retinitis and optic disc edema(Cohen et al. 2020) and parkinsonism (Tada et al. 2016).

Other major interacting partners:

CRMP1interacts with actin and WAVE1. WAVE1 is a protein complex that acts as Arp2/3 activator (Sweeney et al. 2015; Abushouk et al. 2018). CRMP2 directly binds to kinesin light chain 1 (KLC1) via its C-terminal domain, and can modulate the transport of tubulin dimer by linking it to Kinesin-1 (Kimura et al. 2005).

CRMP4 bundles actin filaments *in vitro*, and also regulates the actin cytoskeleton in neuronal growth cones (Khazaei et al. 2014). CRMP5 associates with spastin both *in vitro* and *in vivo*. The C-terminal fragment of CRMP5 can interact with the N-terminal fragment of spastin (Ji et al. 2018). Also, CRMP5 was shown to interact with MAP2 (Brot et al. 2010).

Chemical drugs

An antiepileptic drug lacosamide (LCM; SPM927, Vimpat®) targets CRMP2 (Wilson and Khanna 2015).

Nardilysin/ Nrd1

Alternative names:

Nardilysin (N-arginine dibasic convertase), NRD convertase, NRD1, NRDc, NdK and Nrd1.

Background

Nardilysin (N-arginine dibasic convertase) is a zinc metallo endopeptidase, first reported in 1985 with a different name (Gomez et al. 1985). Nardilysin cleaves substrates that have arginine residues in dibasic pairs (Gluschankof et al. 1987). The electron microscopy of the sperm cells showed that Nardilysin is accumulated in two MT-based structures: the sperm manchette and the axoneme of sperm flagella (Chesneau et al. 1996; Segretain et al. 2016).Overexpression of Nardilysin in cultured cells shows a localized in the cytoplasm and at the cell surface (Hospital et al. 2000).

Nardilysin and MTs:

The only reports so far linking Nardilysin and MTs are ultrastructural studies carried out in 1996 (Chesneau et al. 1996) and 2016 (Segretain et al. 2016). In these studies, the authors observed immuno-gold-labelled Nardylisin accumulated at MT-based structures: manchette and axoneme. Besides that, there are no further studies in this context, and thus there is no complementary evidence confirming that Nardilysin could be a MAP. The spermatid manchette is a specialized MT-based structure that circumferences the sperm nucleus, which is seen in early spermatids, but disappears when sperm matures (Wolosewick and Bryan 1977). The manchette is associated with the positioning and shaping of the sperm head, as well as intracellular trafficking involving cytoplasmic dynein. Axonemes are also MT-based structures that assemble the core machinery of the sperm flagellum (Wolosewick and Bryan 1977).

Other physiological functions:

Nardylisin has also been explored in contexts different than its role in spermatogenesis.
In mouse, Nardilysin has a function in controlling body temperature homeostasis (Hiraoka et al. 2014). In Alzheimer's disease mouse model (intercrossed AD mouse model with transgenic mice expressing NRDc), overexpressed Nardilysin enhances α-secretase activity, and thereby prevents the formation of amyloid plaques (Ohno et al. 2014). It can further regulate maturation and myelination of axons in the central and peripheral nervous systems. Nrd1-knockout mouse brains are smaller, contain less myelinated fibres, and show smaller axon diameters (Ohno et al. 2009).

Links to diseases

Mouse studies further show that Nardilysin is involved in the regulation of gastric tumorigenesis, metaplasia, inflammation in murine stomach (Kimura et al. 2017), steatohepatitis, liver fibrogenesis (Ishizu-Higashi et al. 2014) and pancreatic β-cell function (Nishi et al. 2016).
Nardilysin is associated with many diseases such as Alzheimer's disease, schizophrenia, cancer, Down's syndrome, as well as with conditions like alcohol abuse, mood disorders and heroin addiction. However, these studies are not related to the MT-associated functions of Nardilysin. For a detailed review of its role in brain diseases, see Bernstein 2013 (Bernstein et al. 2013).

Chemical drugs

There are no drugs available so far that target Nardilysin.

Jupiter1 (Jpl1)

Alternative names:

No other names.

Background:

Jupiter has first been reported as a MAP in *Drosophila* in 2006, identified through a protein trap method, in which random proteins are tagged with GFP and their localization was observed. There are no reports about Jupiter as a MAP in other species so far. In *Drosophila,* Jupiter is a positive-charge-rich protein, which might explain its affinity to MTs (Karpova et al. 2006).

Jupiter and MTs

Drosophila Jupiter is characterized as a MAP. Cell studies show that Jupiter binds MTs in both interphase and mitosis. And there are also studies of purified Jupiter (drosophila) binding MTs *in vitro* (Karpova et al. 2006).

Physiological functions:

Drosophila Jupiter localizes to MTs throughout the cell cycle in all stages of development, especially in the young embryo, adult ovary, larval nervous system, and photoreceptor precursors in the eye. Moreover, it has been proposed that Drosophila Jupiter can be used as a live probe for following MT dynamics in living cells, and they don't alter the MT properties nor the effect of anti-mitotic drugs such as taxol and colchicine on MTs (Karpova et al. 2006).

Links to diseases:

No reports.

SAXO1/ Stabilizer of Axonemal Microtubules 1

Alternative names:

SAXO1 or Stabilizer of axonemal microtubules 1, is also known as FAM154A.

Background and physiological functions:

SAXO was first reported in 2012 as a member of the MAP6-related family of proteins (Dacheux et al. 2012). SAXO is conserved from protozoans to mammals. In mammals, two genes are encoding SAXO: SAXO 1 (FAM154A) and SAXO 2 (FAM154B).
SAXO proteins are similar to MAP6, by having similar Mn protein modules and a cysteine-rich domain at the N-terminus. *In vitro* and *in vivo* studies show that the Mn module is necessary for the MT localization of SAXO and for ensuring MT stability in the presence of nocodazole. In addition, Mn modules help SAXO1 localize to cilia *in vivo* (Dacheux et al. 2015). There are only few studies about SAXO1 protein in relation with MTs, and there are no studies about SAXO2 so far.

SAXO and MTs:

Cell studies show that SAXO1 decorates MTs. Human SAXO1 localizes specifically to the primary cilium, basal body, and centriole MTs. In *Trypanosoma brucei*, SAXO1 stabilizes MTs

upon nocodazole- or cold-induced MT depolymerization. hSAXO1 also influences axoneme length (Dacheux et al. 2012; Dacheux et al. 2015).

Links to diseases:

There is no evidence linking SAXO to any diseases so far.

Annex 6.3. Purification of tubulin with controlled posttranslational modifications and isotypes from limited sources by polymerization-depolymerization cycles (published article).

In connection to the protocol for the purification of tubulin with controlled PTMs (chapter 2), here I added another published protocol on which I am a co-author.

Purification of tubulin with controlled posttranslational modifications and isotypes from limited sources by polymerization-depolymerization cycles

Satish Bodakuntla[1,2#], Jijumon A.S.[1,2#], Carsten Janke[1,2], Maria M. Magiera[1,2*]

[1]Institut Curie, PSL Research University, CNRS UMR3348, F-91405 Orsay, France

[2]Université Paris Sud, Université Paris-Saclay, CNRS UMR3348, F-91405 Orsay, France

[#]equal contribution, *corresponding author:

Maria M. Magiera, Institut Curie, Centre Universitaire, Bâtiment 110, F-91401 Orsay, France

Telephone: +33 1 69863088; Fax: +33 1 69863017; Email: Maria.Magiera@curie.fr

Email of other authors: Satish.Bodakuntla@curie.fr, Jijumon.sn@curie.fr, Carsten.Janke@curie.fr

KEYWORDS:

Microtubules, in vitro reconstitution, tubulin, tubulin purification, polymerization, microtubule dynamics, tubulin code, tubulin isotypes, suspension culture, tubulin posttranslational modifications

SUMMARY:

This protocol describes the purification of tubulin from small/medium-scale sources such as cultured cells or single mouse brains, using cycles of polymerization and depolymerization. It allows to purify tubulin enriched in specific isotypes, or tubulin with specific posttranslational modifications to be used for *in-vitro* reconstitution assays to study microtubule dynamics and interactions.

ABSTRACT:

One important aspect of microtubule cytoskeleton studies is the investigation of the behavior of microtubules by *in vitro* reconstitution experiments. They allow to analyze microtubule intrinsic properties, such as dynamics, but also their interactions with microtubule-associated proteins (MAPs). The “tubulin code” is an emerging concept which points to the use of different tubulin isotypes and various posttranslational modifications (PTMs) as regulators of microtubule properties and functions. To explore the molecular mechanisms of the tubulin code, it is crucial to perform *in vitro* reconstitution experiments using purified tubulin with specific isotypes and PTMs. Up until now, this was technically challenging as brain tubulin, which is widely used in *in vitro* experiments, bears many PTMs and has a defined isotype composition. For this reason, we developed the here-described protocol. Our protocol allows purifying tubulin from different sources, and therefore with different isotype compositions and controlled PTMs, using the classical approach of polymerization and depolymerization cycles. Compared to existing methods based on affinity purification, our approach allows to obtain pure, polymerization-competent tubulin, as tubulin resistant to polymerization or depolymerization is discarded during the successive purification steps.

We describe the purification of tubulin from cell lines, grown either in suspension or as adherent cultures, or from single mouse brains. The method first details the generation of cell mass in both suspension and adherent settings, the lysis step, followed by the successive stages of tubulin purification by polymerization-depolymerization cycles. Our method allows to generate tubulin which can be used in experiments addressing the impact of the tubulin code on the intrinsic properties of microtubules and microtubule interactions with associated proteins.

INTRODUCTION:

Microtubules play critical roles in many cellular processes. They give cells their shape, build meiotic and mitotic spindles for chromosome segregation, and serve as tracks for intracellular transport. To fulfil these diverse functions, microtubules form a wide variety of different organizations. One of the intriguing questions in the field is to understand the molecular mechanisms that allow the structurally and evolutionarily conserved microtubules to adapt to this plethora of different organizations and functions. One potential mechanism is the diversification of microtubules which is defined by the concept known as the 'tubulin code'[1-3]. The tubulin code includes two principal components: differential incorporation of α- and β-tubulin gene products (tubulin isotypes) into the microtubules, and tubulin posttranslational modifications (PTMs).

Since the 1970s, *in vitro* reconstitution experiments combined with evolving light microscopy techniques have paved the way to important discoveries about the assembly properties of microtubules: dynamic instability[4] and treadmilling[5], and their other mechanisms and functions[6-15]. Almost all the *in vitro* experiments performed so far have been based on tubulin purified from brain tissue using repeated cycles of polymerization and depolymerization[16,17]. While purification from the brain tissue has a huge advantage to produce high-quality tubulin in large quantities (usually gram amounts), one of its important drawbacks is that it overshadows the effect of tubulin heterogeneity: tubulin purified from brain tissue is a mixture of different tubulin isotypes, and is enriched with many tubulin PTMs. This heterogeneity made it impossible to delineate the role of a particular tubulin PTM or isotype in the control of microtubule properties and functions. Thus, producing assembly-competent tubulin with controlled tubulin PTMs and homogenous isotype composition is essential to address the molecular mechanisms of the tubulin code.

Recently, an approach to purify tubulin by affinity chromatography using the microtubule-binding TOG (tumor overexpressed gene) domain of yeast Stu2p has been developed[18]. In this method, tubulin contained in crude lysates of cells or tissue is passed through the column where it binds to matrix-immobilized TOG domain, which allows the analysis of the whole tubulin pool of a given, even very small sample. A long-awaited approach to purify recombinant tubulin has also been described in recent years. It is based on the baculovirus system, in which a bi-cistronic vector containing an α- and a β-tubulin gene is expressed in insect cells[19]. This method is very cumbersome and time-consuming, and therefore mostly used for studying the impact of tubulin mutations[20] and tubulin isotypes[21-23] *in vitro*.

In the current protocol we describe a method which uses the well-established and widely-used polymerization-depolymerization approach as a blueprint to generate tubulin with different modification levels either from cell lines or from mouse brain tissue[24]. In this procedure, tubulin is cycled between the soluble (tubulin dimer, at 4°C) and polymerized form (microtubule, at 30°C and in the presence of GTP). Each form is separated through successive steps of centrifugation: tubulin dimers will remain in the supernatant after a cold (4°C) spin, while microtubules will be pelleted at 30°C. Furthermore, one polymerization step is carried out at high PIPES concentration, which allows to remove microtubule-associated proteins from the microtubules, and thus, from the finally purified tubulin. Tubulin purified from HeLa S3 cells grown as suspension or adherent cultures is virtually free of any tubulin PTM and has been used in recent *in vitro* reconstitution experiments[25-28]. We have further adapted our method to purify tubulin from single mouse brains which can be used for a large number of mouse models with changes in tubulin isotypes and PTMs available today.

In our protocol, we first describe the generation of the source material (cell mass or brain tissue), its lysis (Figure 1A), followed by the successive steps of tubulin polymerization and depolymerization to purify the tubulin (Figure 1B). We further detail the process to assess the purity (Figure 2A, B) and quantity (Figure 3A, B) of the purified tubulin. Our method can be adapted to produce tubulin enriched with a selected PTM by overexpressing a modifying enzyme in cells prior to tubulin purification (Figure 4B). Alternatively, tubulin-modifying enzymes can be added to tubulin during the purification process. Finally, we can purify tubulin lacking specific isotypes or PTMs from brains of mice deficient for the corresponding tubulin-modifying enzymes (Figure 4B)[29].

The method we describe here has two main advantages: (i) it allows to produce sufficiently large amounts of tubulin in a relatively short time, and (ii) it generates high-quality, pure tubulin, with either specific tubulin isotype composition or PTMs. In the associated video of this manuscript, we highlight some of the critical steps involved in this procedure.

PROTOCOL:

1. Preparation of reagents for the tubulin purification

NOTE: All the buffers used for tubulin purification should contain potassium salts and NOT sodium salts[30].

1.1. Prepare 1 L of DMEM complete medium, with 10% FBS (100 mL), 200 mM L-Glutamine (10 mL of 2 M stock), and 1× Penicillin-Streptomycin (10 mL of 100× stock). Store at 4°C.

1.2. Prepare 10 M KOH by dissolving 140 g of KOH in water, adjust the final volume to 250 mL and store at room temperature.

1.3. Prepare 0.5 M EDTA pH 8 by dissolving 36.5 g of EDTA in water, adjust the pH to 8.0 using KOH (otherwise EDTA will not dissolve) and the final volume to 250 mL, filter-sterilize and store at room temperature.

1.4. Prepare 5 mM PBS-EDTA by adding 5 mL of 0.5 M EDTA to 500 mL of PBS, filter-sterilize and store at room temperature.

1.5. Prepare 0.5 M K-PIPES pH 6.8, by dissolving 75.5 g of PIPES in water, adjust to pH 6.8 with KOH (otherwise PIPES will not dissolve) and the final volume to 500 mL, filter-sterilize and store at 4°C.

1.6. Prepare 1 M K-PIPES pH 6.8 by dissolving 15.1 g of PIPES in water, adjust to pH 6.8 with KOH and the final volume to 50 mL, filter-sterilize and store at 4°C.

1.7. Prepare 0.5 M K-EGTA pH 7.7 by dissolving 47.5 g of EGTA in water, adjust to pH 7.7 with KOH and the final volume to 250 mL, filter-sterilize and store at room temperature.

1.8. Prepare BRB80 (80 mM K-PIPES pH 6.8; 1 mM K-EGTA; 1 mM $MgCl_2$) solution by mixing 3.2 mL of 0.5 M PIPES, 40 µL of 0.5 M K-EGTA and 20 µL of 1 M $MgCl_2$ and adjust the final volume to 20 mL. Store at 4°C.

1.9. Prepare 0.1 M Phenylmethanesulfonyl fluoride (PMSF) by dissolving 435 mg of PMSF in isopropanol to a final volume of 25 mL and store at -20°C.

1.10. Prepare protease inhibitors mix (200×) by dissolving 10 mg of aprotinin, 10 mg of leupeptin and 10 mg of 4-(2-aminoethyl)-benzenesulfonyl fluoride in water to a final volume of 2.5 mL, make aliquots of 100 µl and store at -20°C.

1.11. Prepare 10% Triton X-100 by mixing 5 mL of Triton X-100 in 45 mL of water, filter-sterilize and store at room temperature.

1.12. Prepare Lysis buffer (BRB80 supplemented with 1 mM 2-mercaptoethanol, 1 mM PMSF, 1×protease inhibitors mix and, optionally for HEK-293 cells, 0.2% Triton X-100) on the day of tubulin purification by mixing 20 mL of BRB80 with 1.5 µL of 2-mercaptoethanol,

200 µL of 0.1 M PMSF, 100 µL of the protease inhibitors mix and, optionally for HEK-293 cells, 400 µL of 10% Triton X-100.

NOTE: 2-mercaptoethanol is toxic and should be used in the fume-hood.

1.13. Prepare 0.2 M GTP by dissolving 1 g of GTP in 9.5 mL of water, adjust the pH to 7.5 using KOH, make aliquots of 20 µl and store at -20°C. Avoid repeated freeze-thaw cycles.

1.14. Prepare 1 M Tris-HCl by dissolving 60.56 g of Tris in water, adjust to pH 6.8 with HCl, complete to a final volume of 500 mL, filter-sterilize and store at room temperature.

1.15. Prepare 5× Laemmli sample buffer (450 mM DTT, 10% SDS, 400 µM Tris-HCl pH 6.8, 50% glycerol, ~0.006% bromophenol blue), by adding 4 g of SDS to 16 mL of preheated 1 M Tris-HCl pH 6.8 and mix the solution gently. Add 2.6 g of DTT and 20 mL of 100% glycerol to the mix and stir until solution becomes homogenous. Add the desired amount of bromophenol blue (usually 2.5 mg) to reach the required color intensity. Make 5-ml aliquots and store at -20°C. Prepare the 2× working solution of Laemmli sample buffer by diluting the 5× stock in distilled water.

2. Amplification and harvesting the sources of tubulin

NOTE: In this protocol, three sources of tubulin were used: (i) cells (HeLa S3 and HEK-293) grown as suspension cultures (ii) cells grown as adherent cultures (HEK-293, Hela and U-2 OS) and (iii) mouse brain tissue. This protocol considers the day of tubulin purification as 'day 0' and accordingly, other steps have been described relative to day 0.

2.1. Amplification of cells

2.1.1. Cells grown as suspension cultures

NOTE: To successfully purify tubulin from suspension cultures, we recommend to use at least 2 L of suspension culture.

2.1.1.1. For 2 L of suspension culture, revive and grow the preferred cell type to obtain 6×10^7 cells 10 days before the preparation day. On day -10, plate cells on six 15-cm-diameter dishes at 10^7 cells per plate.

2.1.1.2. On day -8, preheat the required amount of DMEM complete medium to 37°C. Add 1 L of pre-heated medium to each spinner bottle under a laminar flow cabinet. Place the spinners on a stirrer table set at 20-25 rpm inside the cell culture incubator, open slightly the lateral spinner caps to allow the medium to equilibrate to the incubator's atmosphere.

NOTE: To avoid any contaminations, thoroughly clean the outer surface of media and spinner bottles using 70% ethanol.

2.1.1.3. On day -7, trypsinize and collect the cells grown to 80-90% confluence (approximately 1.8×10^8 cells). Collect cells from 3 dishes at a time, spin down (200×g, 5 min, room temperature) and re-suspend all cells in 10 mL of DMEM medium.

NOTE: Thorough dissociation of the cells at this point is very important, otherwise they tend to form larger aggregates in the spinner bottles, which affects the cell survival and results in low tubulin yield.

2.1.1.4. Add 5 mL of the cell suspension to each spinner bottle containing 1 L of DMEM medium, return the spinners to the stirrer table in the cell culture incubator and allow cells to grow for one week.

2.1.2. Cells grown as adherent cultures

NOTE: To successfully purify tubulin from adherent cells, we recommend to use a minimum of 10 dishes of 80-90% confluent cells.

2.1.2.1. Revive and amplify the desired cell type to obtain 1×10^8 cells three days before the day of the tubulin preparation.

2.1.2.2. On day -3, plate these cells on ten 15-cm dishes at 1×10^7cells per dish and allow them to grow 80-90% confluent.

2.1.2.3. On day -1, if required, transfect cells with a plasmid to express a tubulin-modifying enzyme, or a particular tubulin isotype.

2.2. Harvesting the cells/brain tissue

2.2.1. Cells grown as suspension cultures

2.2.1.1. Transfer the cell suspension from spinners into 1-L centrifuge bottles (**see Table of Materials**) and pellet cells at 250×g, 15 min, room temperature. For immediately starting another culture of HeLa S3 cells in the spinner bottles, leave 100 mL of cell suspension in the spinners and add 1 L of complete, pre-heated DMEM medium to the spinner bottle.

NOTE: Carefully check for bacterial contamination before proceeding for tubulin purification.

2.2.1.2. Resuspend pelleted cells from each centrifuge bottle in 10 mL of ice-cold PBS and transfer all the cells into a 50-mL screw-cap tubes. During re-suspension, keep the cells on ice. Pellet the cells at 250×g, 15 min, 4°C.

NOTE: Follow recommendations for spinner bottle cleaning and storage (see **Table of materials**).

2.2.1.3. Discard the supernatant and determine the volume of the cell pellet. From 2 L of suspension culture (two spinner bottles), expect a cell pellet of 5-6 mL.

NOTE: In the protocol below, the cell-pellet volume is assumed to be 10 mL. Adjust for each experiment to the real volume of the pellet.

2.2.1.4. Add 1 volume (10 mL) of lysis buffer and re-suspend the cell pellet.

NOTE: The ratio of cell pellet volume to the lysis buffer is very important for a successful tubulin purification. Adding more lysis buffer decreases tubulin concentration, which then fails to reach the critical concentration needed for polymerization, thus greatly reducing the tubulin yield.

NOTE: Cells resuspended in lysis buffer can be snap-frozen in liquid nitrogen and stored at -80°C for two months.

2.2.2. Cells grown as adherent cultures

NOTE: Cells from adherent cultures must be harvested very quickly for the successful tubulin purification (approximately 15 mins for harvesting ten 15-cm dishes). It is recommended that three people participate in this step.

2.2.2.1. Remove the medium from 15-cm dishes by inclining the dishes and then gently wash the cells with 7 mL of room-temperature PBS-EDTA (person 1). It is crucial not to leave the cells without medium or buffer. Therefore, work only with three 15-cm dishes at a time.

2.2.2.2. Add 5 mL of PBS-EDTA to the cells and incubate them for 5 min at room temperature.

2.2.2.3. Use a cell lifter to gently detach the cells by shoveling them to one edge of the dish (person 2) and collect all the cells in to 50-mL screw-cap tube (person 3). Rinse each plate with an additional 2 mL of PBS-EDTA to collect any remaining cells from the dishes. During this step, keep the 50-mL screw-cap tube containing cell suspension on ice.

2.2.2.4. Pellet the cells at 250×g, 10 min, 4°C. Discard the supernatant and determine the volume of the cell pellet. Expect a volume of ~1 mL from ten 15-cm dishes.

NOTE: In the protocol below, the cell-pellet volume is assumed to be 10 mL. Adjust for each experiment to the real volume of the pellet.

2.2.2.5. Resuspend the cells in 1 volume (10 mL) of lysis buffer.

NOTE: Cells resuspended in lysis buffer can be stored at -80°C for up to two months.

2.2.3. Brain tissue

NOTE: Animal care and use for this study were performed in accordance with the recommendations of the European Community (2010/63/UE). Experimental procedures were specifically approved by the ethics committee of the Institut Curie CEEA-IC #118 (authorization no. 04395.03 given by National Authority) in compliance with the international guidelines.

Mice of any age, sex or genetic background can be used. The choice of the transgenic mouse strain will depend on the scientific question to be addressed. In this manuscript, we show the example of tubulin purified from the *ttll1*$^{-/-}$ mouse, lacking a major brain glutamylating enzyme, the tubulin tyrosine ligase-like 1 (TTLL1) protein [31].

2.2.3.1. Sacrifice the mouse by cervical dislocation, quickly decapitate and collect the brain into a round-bottom tube. If there is excess blood on the brain, quickly wash with lysis buffer. Collect the brain as soon as the mouse is sacrificed, as a post-mortem delay can affect the success of tubulin purification. Use round-bottom tubes to accommodate the width of the probe used for homogenization.

NOTE: Collected brains from the mouse can be snap-frozen in liquid nitrogen and stored at -80°C for up to 3 years.

2.2.3.2. Add 500 µL of lysis buffer to a single brain extracted from an adult mouse. For the rest of the protocol, the volume of lysis buffer added is assumed to be 10 mL. Adjust for each experiment to the number of brains used.

3. Lysis of cells or brain tissue

3.1. Cells grown as suspension cultures

3.1.1. For HEK-293, lyse the cells on ice by repetitive pipetting up and down using pipettes with different widths. First, attach a p1000 tip to a 10-mL pipette and pipette the cell suspension up and down every 5 min, for 10 min (three cycles of pipetting). Second, attach a p200 tip to a p1000 tip and further pipette every 5 min, for 20 min (five cycles of pipetting).

3.1.2. For HeLa S3, lyse the cells using a French press (see **Table of Materials** for settings).

3.1.3. Take 1/100th volume of the lysis mix (L) (200 µL for 20 mL of L) and add the same volume of 2× Laemmli buffer, boil for 5 min and store at -20°C for further analysis.

3.2. Cells grown as adherent cultures

3.2.1. Transfer the cells into a 14-mL round-bottom tube that has been cut in height to accommodate the sonicator probe (see **Table of Materials** for settings). Sonicate the cells for about 45 pulses and ensure the cell lysis by sampling a drop of the lysis mix under a microscope.

NOTE: Number of pulses could vary according to the cell type used for the tubulin purification. Sonicating cells too much could cause tubulin to precipitate and will negatively affect the purification yield.

3.2.2. Pipette the cells up and down on ice every 5 min for 20 min (five cycles of pipetting), using a p200 tip.

3.2.3. Take 1/100th volume of lysis mix (L) (200 µL for 20 mL of L) and add the same volume of 2× Laemmli buffer, boil for 5 min and store at -20°C for further analysis.

3.3. Brain tissue

3.3.1. Lyse the brain tissue using a tissue blender (see **Table of Materials** for settings). Alternatively, lyse the tissue using a microtube pestle or an equivalent equipment and pipette up and down on ice with a 1-mL syringe with an 18G needle.

3.3.2. Take 1/100th volume of lysis mix (L) (200 µL for 20 mL of L) and add the same volume of 2× Laemmli buffer, boil for 5 min and store at -20°C for further analysis.

4. Purification of tubulin

4.1. Lysate clarification

4.1.1. Clear the lysate (separating pellet and soluble fraction of the lysis mix) by centrifugation at 150,000×g, 4°C, 30 min. See **Table of Materials** for details about ultracentrifuge rotors and tubes. For cell extracts, a white floating layer is often formed after centrifugation. Do not transfer this floating layer along with the supernatant, as it interferes with tubulin polymerization. Use a syringe of appropriate volume attached to a long 20G or 21G needle to gently remove the supernatant without disturbing the floating layer. If the supernatant is still cloudy, centrifuge at 5,000×g, 4°C for 10 min.

4.1.2. Transfer the supernatant (SN1) to ultracentrifuge tubes and note its volume. For a 10-mL cell pellet, expect a volume of ~12 mL for SN1.

4.1.3. Take 1/100th volume of SN1 (120 µL for 12 mL of SN1) and add the same volume of 2× Laemmli buffer, boil for 5 min and store at -20°C for further analysis.

4.1.4. Resuspend the pellet (P1) in BRB80 (see **Table of Materials**) using the same volume as SN1. Take 1/100th volume of P1 (200 µL for 20 mL of P1) and add the same volume of 2× Laemmli buffer, boil for 5 min and store at -20°C for further analysis.

4.2. First polymerization in the low-molarity buffer

4.2.1. Prepare the polymerization mix by combining 1 volume of SN1 (12 mL), 1/200th volume of 0.2-M GTP (60 µL; final concentration 1 mM), 0.5 volume of pre-heated glycerol (6 mL) in a screw-cap tube of the appropriate volume.

NOTE: Glycerol is used as a crowding agent in polymerization steps throughout the protocol and thus is not considered in calculations of other components' concentrations.

4.2.2. Pipette the mix up and down gently avoiding the formation of air bubbles and transfer it to the appropriate ultracentrifuge tubes.

NOTE: While transferring the mix to the tubes, adjust the weight of the tubes (in pairs). This allows to directly proceed to the sedimentation of microtubules after the polymerization step. Do this for all polymerization steps throughout the protocol.

4.2.3. Cover the tubes with parafilm, transfer to a water bath set at 30°C, and incubate for 20 min.

4.2.4. Centrifuge the tubes at 150,000×g, 30°C for 30 min. Remove the supernatant (SN2) and keep the pellet of polymerized microtubules (P2).

NOTE: Microtubule pellet can be snap-frozen and stored at -80°C for up to 1 year.

4.2.5. Take 1/200th volume of SN2 (90 µL for 18 mL SN2) and add the same volume of 2× Laemmli buffer, boil for 5 min and store at -20°C for further analysis.

4.3. First depolymerization

4.3.1. Depolymerize microtubules by adding ice-cold BRB80 to the pellet P2 and leave on ice for 5 min: for tubulin from cells, add 1/60th (200 µL), and for tubulin from brains, add 1/20th (600 µL) of the volume of the SN1.

NOTE: The volume of ice-cold BRB80 added to the pellet during depolymerization steps is always relative to the volume of SN1.

4.3.2. Resuspend the microtubule pellet gently, avoiding air bubbles, until the solution is completely homogeneous. Use a p1000 tip for a couple of times followed by a p200 tip every 5 min, for 20 min (five cycles of pipetting). This is a crucial step for the success of the tubulin purification.

4.3.3. Transfer the solution to appropriate ultracentrifuge tubes and spin down at 150,000×g, 4°C for 20 min. Transfer the SN3 to new 1.5-mL ultracentrifuge tube. The pellet formed after this centrifugation step (P3) contains precipitated proteins (microtubule-associated proteins or MAPs) and non-depolymerized microtubules. The supernatant (SN3) contains soluble components: depolymerized tubulin dimers and MAPs, which detached from the depolymerized microtubules.

4.3.4. Take 1-4 µL of SN3 and add the 9 volumes of 2× Laemmli buffer, boil for 5 min and store at -20°C for further analyses.

4.3.5. Resuspend the pellet P3 in BRB80 (in the same volume of SN3), take 1-4 µL and add the 9 volumes of 2× Laemmli buffer, boil for 5 min and store at -20°C.

4.4. Second polymerization (in high-molarity buffer)

4.4.1. Prepare the polymerization mix by combining 1 volume of SN3 (200 µl), 1 volume of pre-heated 1 M PIPES (200 µl; final concentration 0.5 M), 1/100th volume of 0.2-M GTP (2 µL;

final concentration 1 mM), 1 volume of pre-heated glycerol (200 µL) in a tube of the appropriate volume.

4.4.2. Pipette the mix up and down, avoiding the formation of air bubbles and transfer it to appropriate ultracentrifuge tubes.

4.4.3. Cover the tubes with parafilm, transfer them to a water bath set at 30°C and incubate for 20 min.

4.4.4. Centrifuge the tubes at 150,000×g, 30°C for 30 min. Remove the supernatant (SN4) and keep the pellet of polymerized microtubules (P4). The pellet P4 contains the polymerized microtubules and the supernatant SN4 contains unpolymerized tubulin, MAPs and other soluble proteins.

NOTE: The microtubule pellet after the second polymerization step can be snap-frozen and stored at -80°C for up to 1 year.

4.4.5. Take 1-4 µL and add 9 volumes of 2× Laemmli buffer, boil for 5 min and store at -20°C for further analyses.

4.5. Second depolymerization

4.5.1. Depolymerize microtubules by adding ice-cold BRB80 to the pellet P4 and leave on ice for 5 min: for tubulin from cells, add 1/100th (120 µL), and for tubulin from brains, add 1/40th (300 µL) of the volume of the SN1.

4.5.2. Pipette up and down with a p200 tip every 5 min, for 20 min (five cycles of pipetting).

4.5.3. Transfer the solution to a 1.5-mL ultracentrifuge tube and spin down at 150,000×g, 4°C for 20 min. Transfer the SN5 to a new 1.5-mL ultracentrifuge tube. The pellet formed after this centrifugation step (P5) contains non-depolymerized microtubules. The supernatant (SN5) contains the soluble tubulin.

4.5.4. Take 1-4 µL and add the 9 volumes of 2× Laemmli buffer, boil for 5 min and store at -20°C for further analyses.

4.5.5. Resuspend the pellet P5 in BRB80 (same volume of SN5), take 1-4 µL and add the 9 volumes of 2× Laemmli buffer, boil for 5 min and store at -20°C for further analyses.

4.6. Third polymerization (in low-molarity buffer)

4.6.1. Prepare the polymerization mix (1 volume of SN5 (120 µL), 1/200th volume of 0.2-M GTP (0.6 µL; final concentration is 1 mM), 0.5 volume of pre-heated glycerol (60 µL) in a tube of the appropriate volume.

4.6.2. Pipette the mix up and down gently avoiding formation of air bubbles and transfer it to the appropriate ultracentrifuge tubes.

4.6.3. Cover the tubes with parafilm, transfer them to a water bath set at 30°C and incubate for 20 min.

4.6.4. Centrifuge the tubes at 150,000×g, 30°C for 30 min. The pellet (P6) contains polymerized microtubules and supernatant SN6 contains small amounts of non-polymerized tubulin.

NOTE: Microtubule pellets can be snap-frozen and stored at -80°C for up to 1 year.

4.6.5. Take 1-4 µL and add 9 volumes of 2× Laemmli buffer, boil for 5 min and store at -20°C for further analyses.

4.7. Third depolymerization

4.7.1. Depolymerize microtubules by adding ice-cold BRB80 to the pellet P6 and leave on ice for 5 min: for tubulin from cells, add 1/100th (120 µL), and for tubulin from brains, add 1/40th (300 µL) of the volume of the SN1.

4.7.2. Pipette up and down with a p200 tip every 5 min, for 20 min (five cycles of pipetting).

4.7.3. Transfer the solution to the appropriate ultracentrifuge tubes and spin down at 150,000×g, 4°C for 20 min. Transfer the SN7 to a new 1.5-mL ultracentrifuge tube. The pellet (P7) contains small amounts of non-depolymerized microtubules. The supernatant (SN7) contains exclusively depolymerized microtubules (soluble tubulin).

4.7.4. Take 1-4 µL and add the 9 volumes of 2× Laemmli buffer, boil for 5 min and store at -20°C for further analyses.

4.7.5. Resuspend the pellet P7 in BRB80 (same volume of SN7), take 1-4 µL and add the 9 volumes of 2× Laemmli buffer, boil for 5 min and store at -20°C for further analyses.

4.7.6. Quantify the amount of tubulin (see the **representative results** section) and aliquot SN7 into small volumes, snap-freeze and store at -80°C.

REPRESENTATIVE RESULTS:

The main goal of this method is to produce high-quality, assembly-competent tubulin in quantities sufficient to perform repeated *in vitro* experiments with purified components. Microtubules assembled from this tubulin can be used in reconstitution assays taking advantage of total internal reflection fluorescence (TIRF) microscopy technique with either dynamic or stable microtubules, in experiments testing microtubule dynamics, interactions with MAPs or molecular motors, and force generation by the motors[25]. They can also be used in microtubule-MAP co-pelleting assays and solid-state NMR spectroscopy[28].

The enrichment and purity of tubulin throughout the purification process can be monitored by using a Coomassie-stained SDS-PAGE gel, preferably the 'TUB' SDS-PAGE gels, that allow for the separation of α- and β-tubulins, which co-migrate as a single band in classical gels [32].

Lysates collected at different steps (except for the very last depolymerization, see protocol) are loaded onto the gel at comparable amounts for assessing the success of the tubulin purification (Figure 2A)[24]. The final tubulin sample, which is very precious, is only loaded on the gel allowing to determine tubulin concentration (see next paragraph). It is normal to lose some tubulin in the process of repeated cycles of polymerization and depolymerization. A lower-than-expected yield of the final purified tubulin can be due to either (i) incomplete depolymerization of microtubules, visualized by the presence of an important amount of tubulin in fractions P3, P5 and P7, or (ii) an inefficient tubulin polymerization into microtubules, in which case a lower amount of tubulin is present in fractions P2, P4 and P6 and higher in fractions SN2, SN4 and SN6 (Figure 2B). If the tubulin is lost during polymerization steps (lower amounts of P2 and P4), (i) ensure sufficient tubulin concentration during polymerization, (ii) use a fresh aliquot of GTP and/or (iii) reconfirm the temperature of the polymerization reaction. If the tubulin is lost during depolymerization steps (lower amounts of SN3 and SN5), increase the time as well as pipetting of the mix on ice.

For the quantification of purified tubulin, run the samples along with the known quantities of BSA (0.5 µg – 1 µg – 2 µg – 4 µg) (Figure 3A) on SDS-PAGE. Gels are stained with Coomassie brilliant blue, scanned, and the intensities of BSA and tubulin bands are measured by quantitative densitometry (Figure 3B) as described at https://openwetware.org/wiki/Protein_Quantification_Using_ImageJ. Please note that the same analysis can be done in Fiji, an upgraded version of ImageJ[33]. Values from the BSA bands were used to calculate the linear regression equation, which then allowed to calculate the amount of protein in the tubulin bands. Only tubulin band intensities within the range of the BSA curve are used to determine tubulin concentration. Based on the calculated tubulin concentration, aliquots of desired volumes of tubulin are prepared, snap-frozen in liquid nitrogen, and stored at -80°C. We usually obtain about ~2 mg of tubulin from four spinner bottles of HeLa S3 suspension cultures (~15 g of cells), ~250 µg of tubulin from ten 15-cm diameter dishes (~1.2 g of cells) and ~1 mg of tubulin from 1 g of mouse brain tissue.
To confirm the enrichment of a particular tubulin isotype or modification, ~0.1 µg of the purified tubulin can be immunoblotted using respective antibodies[34,35]. The control tubulin to use will vary depending on the tubulin of interest. For tubulin modified *in vitro* with a modifying enzyme, the control tubulin will be the non-treated tubulin. For tubulin modified *in cellulo* by overexpression of a modifying enzyme, the control is tubulin purified from cells that do not express the enzyme (Figure 4A). Control tubulin for tubulin purified from knockout-mouse brains will be tubulin from wild type mice (Figure 4B). In all immuno blot analyses, an equal load of tubulin is verified by using a PTM-independent anti-α-tubulin antibody (12G10).

FIGURE LEGENDS:

Figure 1: Tubulin purification from different sources using polymerization-depolymerization cycles. (A) Different sources of tubulin are lysed using specific strategies. HeLa S3 cells cultured in suspension are lysed using a French press, while HEK-293 cells are lysed by repetitive pipetting. Adherently grown cells were lysed using short pulses of sonication, and mouse brain tissue using a tissue homogenizer. **(B)** Schematic representation of the successive steps of the tubulin purification protocol using cycles of cold-

depolymerization and warm-polymerization. After lysis and lysate clarification, microtubules are polymerized and pelleted. Microtubules are then depolymerized and subsequently allowed to polymerize in a high-molarity buffer, preventing MAP co-sedimentation with the microtubules. MAP-free microtubules are then depolymerized, and can be further subjected to a third cycle of polymerization-depolymerization to remove trace amounts of the high-molarity buffer.

Figure 2: Evaluating the success of the tubulin purification. Samples collected at different steps of the tubulin purification protocol were run on a 'TUB' SDS-PAGE gel (see the methods for details) and stained with Coomassie brilliant blue. **(A)** In a successful tubulin purification, α- and β-tubulins are progressively enriched throughout the process. After the second polymerization, the microtubule pellet (P4) is virtually free of contamination from other proteins or MAPs. Note that it is normal to lose some tubulin during the procedure. **(B)** In an unsuccessful tubulin purification, the final tubulin yield is low, and tubulin remains either in the pellet after depolymerization, or in the supernatant after polymerization (red boxes). In the example shown here, tubulin did not polymerize efficiently in both polymerization steps.

Figure 3: Quantification of the purified tubulin using Coomassie-stained SDS-PAGE gels and densitometry. (A) Coomassie-stained SDS-PAGE gel with known quantities of BSA (0.5, 1, 2 and 4 µg, gray gradient line) and different volumes (0.5 and 1 µl, light and dark colors, respectively) of purified tubulin. In the example shown, tyrosinated tubulin (Hela S3 tubulin, light and dark orange) and detyrosinated tubulin (Hela S3 tubulin treated with carboxypeptidase A, light and dark blue) were loaded on the gel. **(B)** BSA bands from (A) were quantified using ImageJ and plotted against the amount of protein loaded (gray to black points). Those points were used to calculate the linear regression line (the gray gradient line) and equation, which then allowed to calculate the amount of protein in the tubulin samples (light and dark orange and blue points) loaded on the gel. This then allowed to calculate the concentration of the tubulin samples. Note that the points that lie beyond the BSA standard curve should not be used to determine concentration (dark orange and blue points).

Figure 4: Immunoblot analysis of purified tubulin with different PTMs. (A) Tubulins purified from HEK-293 cells: wild type, or cells overexpressing TTLL5 or TTLL7 were analyzed for the specific enrichment of polyglutamylation using the GT335 antibody. While TTLL5 overexpression increases polyglutamylation on α- and β-tubulin, TTLL7 overexpression specifically enriches β-tubulin glutamylation. **(B)** Tubulin purified from brain tissues of wild type and *ttll1*$^{-/-}$ mice were analyzed for patterns of glutamylation. Note the strong reduction of polyglutamylation of tubulin from *ttll1*$^{-/-}$ mice, which lack the major brain glutamylase TTLL1[36]. 'TUB' gels were used to separate α- and β-tubulin. An equal amount of tubulin load was confirmed by 12G10, an anti-α-tubulin antibody.

DISCUSSION:

Our method described here provides a platform to rapidly generate high-quality, assembly-competent tubulin in medium-large quantities from cell lines and single mouse brains. It is based on the gold-standard protocol of tubulin purification from bovine brains used in the

field for many years[16,17]. One particular advantage of our approach is the use of suspension cultures of HeLa S3 cells, which, once established, allows to produce large amounts of cells while requiring little hands-on time. This makes our protocol relatively easy to perform in any cell biology lab, whereas other tubulin purification methods[18,19,32,37] require specific equipment and expertise, thus mostly used by laboratories with a strong background in protein purification. When producing smaller quantities of tubulin from adherent cell lines, a variety of cell lines can be used. We have successfully purified tubulin from Hela, U-2 OS, and HEK-293 cells. If a larger-scale purification is needed, harvested cells or brains can be snap-frozen in lysis buffer and stored at -80°C, and multiple cell pellets or brains can be pooled together to purify larger amounts of tubulin.

Tubulin purified from cell lines is virtually free of tubulin PTMs. This tyr-tubulin can readily be converted to detyrosinated (detyr-) tubulin in a single straightforward step[25]. To produce tubulin with other PTMs, specific tubulin-modifying enzymes can be overexpressed in cells prior to tubulin purification. Furthermore, using cell lines from human origin as the source of material allows to avoid potential cross-species issues when studying interactions between microtubules and human MAPs. Further, tubulin from untransformed (such as HEK293) or transformed (such as Hela) cells can inform about the effect of microtubule-directed drugs, for example Taxanes, on normal- vs. tumor-cell microtubules.

Finally, our protocol provides the possibility to purify tubulin from single mouse brains. As an increasing number of mouse models of tubulin mutations and modifications are being generated, this now allows to directly analyze the properties and interactions of microtubules with altered tubulin isotype composition[38-40] or tubulin PTMs[31,41].

Our approach is based on cycles of polymerization and depolymerization. Thus, specific tubulin isotypes or tubulin with particular PTMs that affect the assembly and disassembly properties of microtubules could result in the disproportionate loss or reduction of such tubulin forms during the purification process. Nevertheless, we have shown that major tubulin PTMs such as acetylation, detyrosination, glutamylation and glycylation are retained on the microtubules throughout the tubulin purification process[24]. However, it should be kept in mind that for quantitative analyses of the tubulin composition in cells or tissues, the TOG-column-based tubulin purification approach is more appropriate as it should allow an unbiased, polymerization-independent tubulin purification[18]. Despite its limitation, our protocol offers a great advantage to generate large amounts of high-quality tubulin that can be used in meticulous *in vitro* reconstitution experiments. In particular, it allows to fully replace the use of the PTM-rich brain tubulin in the day-to-day experiments.

DISCLOSURES:

The authors have nothing to disclose.

ACKNOWLEDGMENTS:

This work was supported by the ANR-10-IDEX-0001-02, the LabEx Cell'n'Scale ANR-11-LBX-0038 and the Institut de convergence Q-life ANR-17-CONV-0005. CJ is supported by the Institut Curie, the French National Research Agency (ANR) awards ANR-12-BSV2-0007 and ANR-17-CE13-0021, the Institut National du Cancer (INCA) grant 2014-PL BIO-11-ICR-1, and the Fondation pour la Recherche Medicale (FRM) grant DEQ20170336756. MMM is supported by the Fondation Vaincre Alzheimer grant FR-16055p, and by the France Alzheimer grant AAP SM 2019 n°2023. JAS was supported by the European Union's Horizon 2020 research and innovation program under the Marie Skłodowska-Curie grant agreement No 675737, and the FRM grant FDT201904008210. SB was supported by the FRM grant FDT201805005465.

We thank all members of the Janke lab, in particular J. Souphron, as well as G. Lakisic (Institut MICALIS, AgroParisTech) and A. Gautreau (Ecole Polytechnique) for help during the establishment of the protocol. We would like to thank the animal facility of the Institut Curie for help with mouse breeding and care.

The antibody 12G10, developed by J. Frankel and M. Nelson, was obtained from the Developmental Studies Hybridoma Bank developed under the auspices of the NICHD and maintained by the University of Iowa.

REFERENCES:

1 Verhey, K. J. & Gaertig, J. The Tubulin Code. *Cell Cycle.* **6** (17), 2152-2160, (2007).
2 Janke, C. The tubulin code: Molecular components, readout mechanisms, and functions. *Journal of Cell Biology.* **206** (4), 461-472, (2014).
3 Janke, C. & Magiera, M. M. The tubulin code and its role in controlling microtubule properties and functions. *Nature Reviews: Molecular Cell Biology.* **21** (6), 307-326, (2020).
4 Mitchison, T. & Kirschner, M. Dynamic instability of microtubule growth. *Nature.* **312** (5991), 237-242, (1984).
5 Margolis, R. L. & Wilson, L. Opposite end assembly and disassembly of microtubules at steady state in vitro. *Cell.* **13** (1), 1-8, (1978).
6 Borisy, G. G. & Olmsted, J. B. Nucleated assembly of microtubules in porcine brain extracts. *Science.* **177** (55), 1196-1197, (1972).
7 Kirschner, M. W. & Williams, R. C. The mechanism of microtubule assembly in vitro. *Journal of Supramolecular Structure.* **2** (2-4), 412-428, (1974).
8 Baas, P. W. & Lin, S. Hooks and comets: The story of microtubule polarity orientation in the neuron. *Developmental Neurobiology.* **71** (6), 403-418, (2011).
9 Stepanova, T. *et al.* Visualization of microtubule growth in cultured neurons via the use of EB3-GFP (end-binding protein 3-green fluorescent protein). *Journal of Neuroscience.* **23** (7), 2655-2664, (2003).
10 Nedelec, F. J., Surrey, T., Maggs, A. C. & Leibler, S. Self-organization of microtubules and motors. *Nature.* **389** (6648), 305-308, (1997).
11 Bieling, P., Telley, I. A. & Surrey, T. A minimal midzone protein module controls formation and length of antiparallel microtubule overlaps. *Cell.* **142** (3), 420-432, (2010).
12 Roostalu, J. *et al.* Directional switching of the kinesin Cin8 through motor coupling. *Science.* **332** (6025), 94-99, (2011).
13 Schaedel, L. *et al.* Microtubules self-repair in response to mechanical stress. *Nature Materials.* **14** (11), 1156-1163, (2015).
14 Hendricks, A. G., Goldman, Y. E. & Holzbaur, E. L. F. Reconstituting the motility of isolated intracellular cargoes. *Methods in Enzymology.* **540** 249-262, (2014).
15 Dogterom, M. & Surrey, T. Microtubule organization in vitro. *Current Opinion in Cell Biology.* **25** (1), 23-29, (2013).
16 Vallee, R. B. Reversible assembly purification of microtubules without assembly-promoting agents and further purification of tubulin, microtubule-associated proteins, and MAP fragments. *Methods in Enzymology.* **134** 89-104, (1986).
17 Castoldi, M. & Popov, A. V. Purification of brain tubulin through two cycles of polymerization-depolymerization in a high-molarity buffer. *Protein Expression and Purification.* **32** (1), 83-88, (2003).
18 Widlund, P. O. *et al.* One-step purification of assembly-competent tubulin from diverse eukaryotic sources. *Molecular Biology of the Cell.* **23** (22), 4393-4401, (2012).
19 Minoura, I. *et al.* Overexpression, purification, and functional analysis of recombinant human tubulin dimer. *FEBS Letters.* **587** (21), 3450-3455, (2013).
20 Uchimura, S. *et al.* A flipped ion pair at the dynein-microtubule interface is critical for dynein motility and ATPase activation. *Journal of Cell Biology.* **208** (2), 211-222, (2015).
21 Pamula, M. C., Ti, S.-C. & Kapoor, T. M. The structured core of human beta tubulin confers isotype-specific polymerization properties. *Journal of Cell Biology.* **213** (4), 425-433, (2016).
22 Vemu, A. *et al.* Structure and Dynamics of Single-isoform Recombinant Neuronal Human Tubulin. *Journal of Biological Chemistry.* **291** (25), 12907-12915, (2016).

23 Ti, S.-C., Alushin, G. M. & Kapoor, T. M. Human beta-Tubulin Isotypes Can Regulate Microtubule Protofilament Number and Stability. *Developmental Cell.* **47** (2), 175-190 e175, (2018).
24 Souphron, J. *et al.* Purification of tubulin with controlled post-translational modifications by polymerization–depolymerization cycles. *Nature Protocols.* **14** 1634–1660, (2019).
25 Barisic, M. *et al.* Microtubule detyrosination guides chromosomes during mitosis. *Science.* **348** (6236), 799-803, (2015).
26 Nirschl, J. J., Magiera, M. M., Lazarus, J. E., Janke, C. & Holzbaur, E. L. F. alpha-Tubulin Tyrosination and CLIP-170 Phosphorylation Regulate the Initiation of Dynein-Driven Transport in Neurons. *Cell Reports.* **14** (11), 2637-2652, (2016).
27 Guedes-Dias, P. *et al.* Kinesin-3 Responds to Local Microtubule Dynamics to Target Synaptic Cargo Delivery to the Presynapse. *Current Biology.* **29** (2), 268-282 e268, (2019).
28 Luo, Y. *et al.* Direct observation of dynamic protein interactions involving human microtubules using solid-state NMR spectroscopy. *Nature Communications.* **11** (1), 18, (2020).
29 Even, A. *et al.* ATAT1-enriched vesicles promote microtubule acetylation via axonal transport. *Science Advances.* **5** (12), eaax2705, (2019).
30 Wolff, J., Sackett, D. L. & Knipling, L. Cation selective promotion of tubulin polymerization by alkali metal chlorides. *Protein Science* **5** (10), 2020-2028, (1996).
31 Magiera, M. M. *et al.* Excessive tubulin polyglutamylation causes neurodegeneration and perturbs neuronal transport. *EMBO Journal.* **37** (23), e100440, (2018).
32 Lacroix, B. & Janke, C. Generation of differentially polyglutamylated microtubules. *Methods in Molecular Biology.* **777** 57-69, (2011).
33 Schneider, C. A., Rasband, W. S. & Eliceiri, K. W. NIH Image to ImageJ: 25 years of image analysis. *Nature Methods.* **9** (7), 671-675, (2012).
34 Magiera, M. M. & Janke, C. in *Methods in Cell Biology* Vol. 115 *Microtubules, in vitro* eds John J. Correia & Leslie Wilson) 247-267 (Academic Press, 2013).
35 Hausrat, T. J., Radwitz, J., Lombino, F. L., Breiden, P. & Kneussel, M. Alpha- and beta-tubulin isotypes are differentially expressed during brain development. *Developmental Neurobiology.* 10.1002/dneu.22745, (2020).
36 Janke, C. *et al.* Tubulin polyglutamylase enzymes are members of the TTL domain protein family. *Science.* **308** (5729), 1758-1762, (2005).
37 Newton, C. N. *et al.* Intrinsically slow dynamic instability of HeLa cell microtubules in vitro. *Journal of Biological Chemistry.* **277** (45), 42456-42462, (2002).
38 Belvindrah, R. *et al.* Mutation of the alpha-tubulin Tuba1a leads to straighter microtubules and perturbs neuronal migration. *Journal of Cell Biology.* **216** (8), 2443-2461, (2017).
39 Breuss, M. *et al.* Mutations in the murine homologue of TUBB5 cause microcephaly by perturbing cell cycle progression and inducing p53 associated apoptosis. *Development.* dev.131516 [pii]
10.1242/dev.131516, (2016).
40 Latremoliere, A. *et al.* Neuronal-Specific TUBB3 Is Not Required for Normal Neuronal Function but Is Essential for Timely Axon Regeneration. *Cell Reports.* **24** (7), 1865-1879 e1869, (2018).
41 Morley, S. J. *et al.* Acetylated tubulin is essential for touch sensation in mice. *Elife.* **5**, (2016).

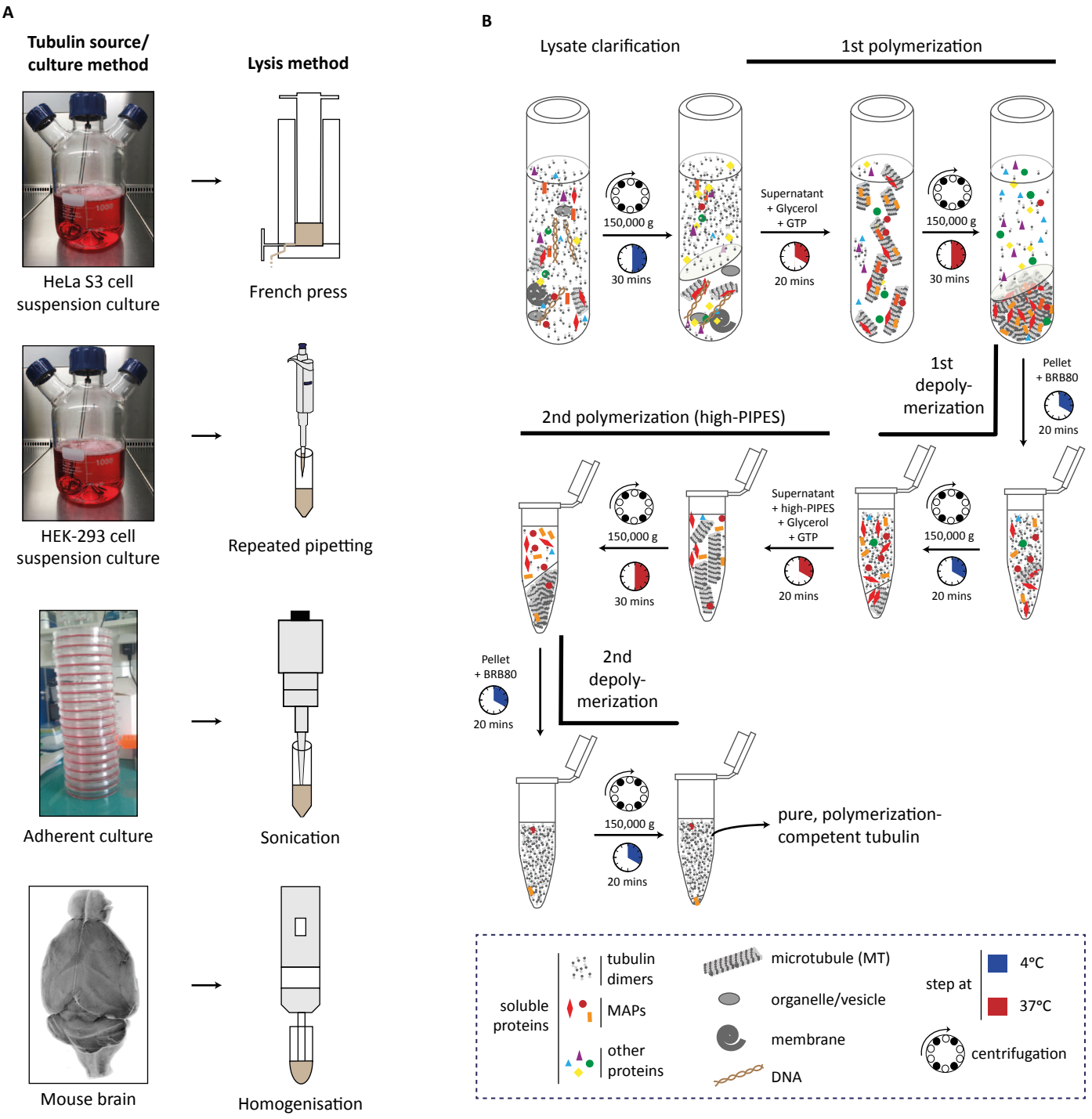
A
Tubulin source/ culture method
Lysis method
HeLa S3 cell suspension culture
French press
HEK-293 cell suspension culture
Repeated pipetting
Adherent culture
Sonication
Mouse brain
Homogenisation
B
Lysate clarification
1st polymerization
150,000 g
30 mins
Supernatant + Glycerol + GTP
20 mins
150,000 g
30 mins
1st depoly-merization
Pellet + BRB80
20 mins
2nd polymerization (high-PIPES)
150,000 g
30 mins
Supernatant + high-PIPES + Glycerol + GTP
20 mins
150,000 g
20 mins
Pellet + BRB80
20 mins
2nd depoly-merization
150,000 g
20 mins
pure, polymerization-competent tubulin
soluble proteins
tubulin dimers
MAPs
other proteins
microtubule (MT)
organelle/vesicle
membrane
DNA
step at
4°C
37°C
centrifugation

Bodakuntla et al., Figure 2

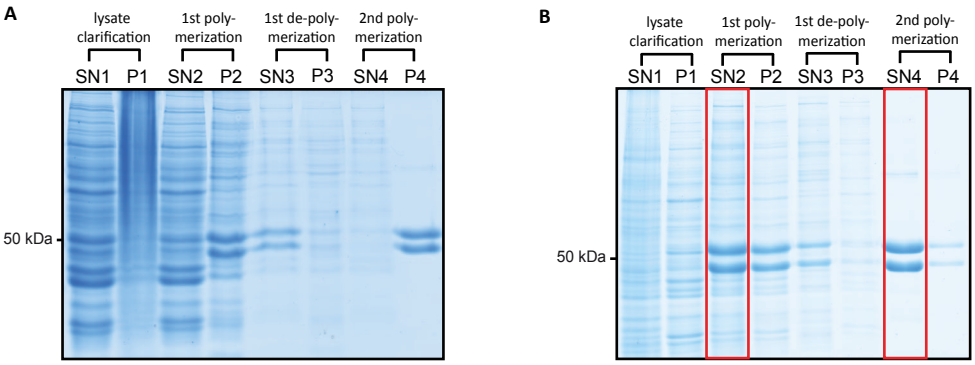

Bodakuntla et al., Figure 3

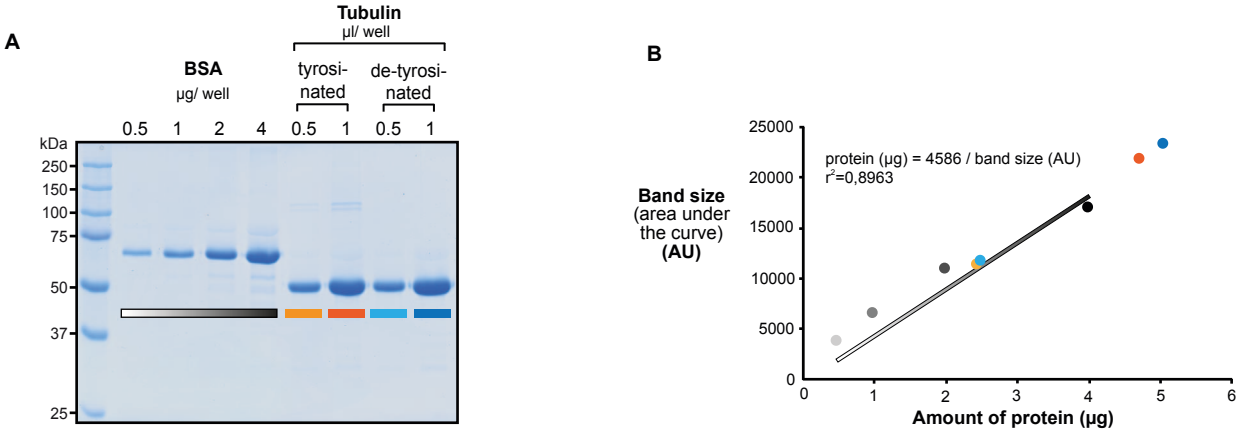

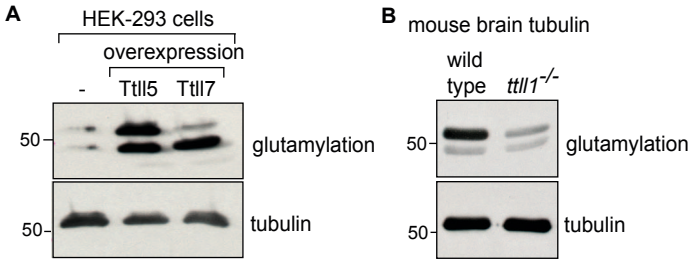
A
HEK-293 cells
overexpression
-
Ttll5
Ttll7
50
glutamylation
50
tubulin
B
mouse brain tubulin
wild type
ttll1-/-
50
glutamylation
50
tubulin

Extended summary in French

Le cytosquelette des microtubules (MTs) est un composant structurel et mécanique clé de toute cellule eucaryote. Les MTs s'assemblent en une grande variété de réseaux et de structures dynamiques qui sont impliqués dans de nombreuses fonctions cellulaires différentes, telles que la division cellulaire, la motilité cellulaire, la forme des cellules et le transport intracellulaire. On sait depuis des décennies que la construction de ces structures nécessite des ensembles distincts de protéines associées aux microtubules (MAPs). Toute protéine capable d'interagir avec les MTs pourrait être techniquement classée comme une MAP, cependant le terme a été adapté pour décrire des protéines non mobiles et non enzymatiques qui se lient au réseau des MTs, et qui sont souvent appelées "MAPs structurelles" (Bodakuntla et al., 2019 ; Mandelkow et Mandelkow, 1995 ; Olmsted, 1986).
Par rapport aux progrès significatifs qui ont été réalisés dans la compréhension de la fonction des moteurs moléculaires basés sur les MTs (Hirokawa et al., 2009 ; Roberts et al., 2013 ; Veigel et Schmidt, 2011), des enzymes de séparation (McNally et Roll-Mecak, 2018), ou des protéines qui régulent les extrémités + ou - des MTs (Akhmanova et Steinmetz, 2015), seuls quelques membres de la famille des MAPs structurales ont été caractérisés de manière approfondie sur le plan biochimique et fonctionnel (Bodakuntla et al., 2019). Ces quelques MAPs sont souvent liées à des pathologies tel que la MAP tau neuronale, qui est le principal composant des filaments hélicoïdaux appariés pathologiques - une caractéristique de la maladie d'Alzheimer et d'autres tauopathies (Goedert et al., 2017). De même, la protéine MAP4, une MAP impliquée dans différentes formes de cancer (Murphy et al., 1996 ; Xia et al., 2018), ou les MAPs importantes pour la division cellulaire telles que PRC1 et les CLASPs (Bieling et al., 2010 ; Forth et al., 2014 ; Lansky et al., 2015 ; Maiato et al., 2004 ; Pereira et al., 2006) ont été étudiées plus en détail.

Des travaux récents démontrent que les fonctions des microtubules telles que nous les connaissons peuvent résulter d'une interaction entre différentes MAPs sur le même microtubule (Monroy et al., 2020). En outre, les progrès réalisés dans la cartographie des mutations ont révélé de nombreux liens inédits entre diverses MAPs et un large spectre de maladies humaines. Il semble donc que l'accent mis actuellement sur certaines MAPs sélectionnées et bien

caractérisées entrave les progrès vers une compréhension holistique de l'architecture et des fonctions des MTs. Cela constitue un obstacle majeur à la compréhension générale de la régulation des MTs dans les cellules, et empêche également d'exploiter les liens nouvellement découverts entre les MAPs et les maladies humaines à des fins thérapeutiques. Cependant, l'étude des MAPs à une plus grande échelle n'a pas été possible jusqu'à présent en raison des limitations expérimentales. Les approches basées sur les cellules, qui pourraient facilement être étendues à l'étude d'un grand nombre de protéines, sont limitées par le fait que la surexpression des MAPs entraîne divers artefacts, tels qu'un regroupement excessif de MT, qui entraîne souvent des perturbations des fonctions cellulaires normales et la mort des cellules. D'autre part, pour déterminer les fonctions moléculaires des nouvelles MAPs, une caractérisation biochimique et biophysique approfondie est nécessaire, qui utilise classiquement des essais de reconstitution in vitro nécessitant la purification de la MAP sous une forme fonctionnelle. Des études récentes ont réussi à purifier et à étudier le rôle de plusieurs MAPs, telles que les MAP7, tau, MAP2, DCX, DCLK1 et MAP9 (Monroy et al., 2020), ou encore le rôle des quatre membres de la famille MAP7 dans le contrôle de la kinésine-1 (Hooikaas et al., 2019). Cependant, étant donné que la purification des protéines est un processus fastidieux dans lequel de nombreuses conditions doivent être testées, et que certaines protéines résistent même entièrement à la purification biochimique, cette approche restera impraticable pour les analyses à moyen ou à grande échelle.

Pour surmonter ces limites, j'ai ici établi une méthode ex-vivo qui permet d'étudier une grande variété de MAPs à une résolution d'un seul microtubule dans des essais en microscopie TIRF sans purification préalable des protéines. Ma méthode est largement applicable, elle nécessite un petit nombre de composants et peut être étendue à pratiquement toutes les MAPs d'intérêts. L'utilisation de cette approche m'a permis de caractériser les interactions de plus de 40 protéines avec les MTs. J'ai ainsi analysé des MAPs bien connues ainsi que des protéines dont on soupçonnait être des MAPs sur la base d'études de colocalisation dans les cellules ou par analyses bio-informatique. Toutes les protéines testées étaient invariablement solubles dans mon approche ex-vivo, ce qui a permis de déterminer sans ambiguïté leurs activités de liaison aux MTs. J'ai découvert ici une variété d'activités frappantes, et jusqu'alors inconnues, des MAPs sur les MTs, ouvrant ainsi un angle de recherche entièrement nouveau sur les structures des MTs. Mon essai me permet en outre de déterminer directement l'implication des MAPs dans le co-alignement de la F-actine et des MTs. Enfin, je démontre que les assemblages MAP-MT peuvent être directement utilisés pour obtenir des structures à haute résolution par cryo-

microscopie électronique, ce qui augmentera considérablement la faisabilité et le rendement des études structurelles du cytosquelette de MT. Ma méthode est donc un outil unique et puissant permettant d'analyser à moyen terme des MAPs nouvelles ou déjà connues, et de découvrir une grande variété de propriétés qui auraient pu être négligées avec d'autres approches.

En outre, il était nécessaire de développer de nouvelles approches de purification de la tubuline afin d'obtenir une tubuline de composition mieux définie en terme de modification post traductionnel et d'isoformes. Une partie de mon projet de thèse consistait à élaborer une telle méthode en collaboration avec d'autres membres du laboratoire. En combinant la nouvelle approche ex-vivo que j'ai développée avec la disponibilité de différents échantillons de tubuline, il est possible maintenant de tester de manière systématique l'impact du code de la tubuline sur les interactions MT-MAP, la dynamique et la structure des MTs in vitro.

Voici en détail les principaux résultats de mon projet de doctorat, qui comprend le développement d'une méthode sans purification, les nouvelles propriétés observées pour différentes MAPs et différentes applications validées de cette approche.

Mise en place d'une méthode ex-vivo pour la caractérisation des MAPs à moyen debit

Vue d'ensemble de la méthode ex-vivo:

Pour pouvoir effectuer des analyses sur n'importe quel candidat MAP dans ma méthode ex-vivo, une condition préalable était d'être totalement indépendant des ressources externes pour les constructions des MAPs. Par conséquent, la première étape de la méthode a consisté à cloner les gènes d'intérêts en utilisant la méthode SLIC, rapide et simple. L'expression des protéines marquées par fluorescence a ensuite été testée dans des cellules U2OS, ce qui a permis de vérifier globalement la localisation intracellulaire des protéines. Pour les analyses ex vivo, les vecteurs d'expression vérifiés ont été transfectés dans des cellules HEK 293, à partir desquelles des lysats cytosoliques solubles contenant les protéines surexprimées et marquées par fluorescence ont été générés. Ces lysats ont été directement introduits dans une chambre de flux contenant des amorces immobilisées de MT GMPCPP (Gell et al., 2010), et la polymérisation des MTs a été enregistrée par microscopie TIRF. Le principal avantage de mon approche ex-vivo est que tous les composants nécessaires à la polymérisation des MTs, comme la tubuline

libre et le GTP, proviennent directement des lysats cellulaires, ce qui rend le test hautement reproductible et indépendant de facteurs supplémentaires, comme la disponibilité de tubuline purifiée qui doit être de qualité reproductible.
Au départ, tous les extraits contenant des MAPs ont été testés dans des conditions d'essai similaires, qui ont pu être affinées par la suite en fonction des observations initiales. J'ai estimé la concentration en protéines de tous les lysats cellulaires à l'aide du dosage des protéines de l'acide bicinchoninique (BCA) (Smith et al., 1985), et j'ai ajusté les concentrations en protéines à une valeur définie pour tous les échantillons. Une première série de tests a été réalisée avec la concentration fixe de lysats, indépendamment des niveaux d'expression des MAPs marquées par la GFP. Pour déterminer plus précisément la dépendance du comportement des MAPs observée par rapport à leur concentration dans les lysats, j'ai estimé la concentration des MAP-GFP dans les extraits par des analyses immuno-blot, et j'ai ensuite effectué des séries de dilutions pour ces MAPs. J'ai ensuite effectué des études ultrastructurales en utilisant la cryo-microscopie électronique, et des expériences de compétition entre les MAPs sur les mêmes MTs. Mon approche ex vivo m'a permis d'étudier systématiquement l'impact de chaque MAP testé sur l'interaction des MTs aux filaments d'actine.

1. Découverte de nouvelles activités des MAPs dans la formation des réseaux de MT

Après la caractérisation systématique de 58 candidats MAP, je souligne dans ce chapitre de nouvelles propriétés de MAPs connues que j'ai découvert grâce à ma méthode ex vivo. Toutes les figures montrant les nouveaux phénotypes de MTs induits par les MAPs sont des images représentatives de plus de trois essais TIRF indépendants provenant d'au moins trois préparations de lysats cellulaires indépendantes.

a) La protéine MACF1 induit la formation de crochets à l'extrémité "+" :

En utilisant l'approche ex-vivo, j'ai découvert que la protéine MACF1, une construction tronquée contenant le domaine de liaison de la MT, peut non seulement décorer la surface du MT, mais induit également des formations de crochets à l'extrémité du MT en croissance, empêchant ainsi un allongement supplémentaire du MT. En plus des crochets à simple enroulement, j'ai également observé des MTs à double enroulement aux extrémités crochues et des phénotypes d'évasement de MT. Des expériences avec la latrunculine A, une drogue qui dépolymérise l'actine, ont montré que la formation de ces crochets est indépendante de la

présence de filaments d'actine. Comme mes tentatives de purification de la construction MACF1 ont été couronnées de succès, les expériences de reconstitution in vitro TIRF avec la protéine MACF1 purifiée et de la tubuline HeLa purifiée ont montré la formation d'anneaux MT au lieu de crochets. Cependant, l'ajout de MACF1 purifiée dans un lysat non transfécté entraîne la formation d'anneaux MT similaires à ceux observés avec les lysats MACF1. Cela suggère que d'autres composants provenant des lysats pourraient également influencer la formation des crochets. Les expériences de dilution des lysats MACF1 avec des lysats non transfectés ont indiqué que la formation de crochets est un processus dépendant de la concentration et se produit moins fréquemment à des concentrations plus faibles de MACF1. Une formation similaire de crochets du MT ou de protofilaments courbés ont récemment été signalé avec la tubuline axonémique de *Chlamydomonas reinhardtii* (Orbach et Howard 2019), et avec la Kinesin-5 in vitro (Chen et Hancock 2015 ; Chen et al. 2019). Cela démontre la capacité des MTs à former diverses structures et à s'assembler sous différentes formes, ce qui pourrait être induit par les propriétés intrinsèques de la tubuline ou par les protéines qui s'associent aux MTs. Ma découverte montre que la protéine MACF1 est une MAP qui pourrait modifier les propriétés mécaniques afin d'induire la formation de crochets ou d'anneaux des MTs. Une reconstruction ultrastructurale plus poussée des MTs liées à MACF1 doit être menée pour comprendre pleinement l'architecture du crochet des MTs et pour identifier le cas échéant les éventuels partenaires qui interagissent.

b) Le CSAP oblige les MTs à former des filaments enroulés:

Comme pour le phénotype du crochet induit par la protéine MACF1, j'ai découvert que la protéine CSAP peut forcer les MTs à former des structures enroulées avec une largeur d'hélice de ~700 nm. Ces structures n'étaient pas entièrement visibles en mode TIRF-M, j'ai donc utilisé un mode off-TIRF pour obtenir une plus grande profondeur de pénétration. Comme pour la protéine MACF1, je n'ai observé aucune influence de l'actine dans ces formations de MTs. Enroulés. J'ai également observé la formation spontanée de MT enroulés indépendamment des amorces de MTs, ce qui suggère que, comme pour les autres MAPs, la protéine CSAP elle-même peut servir de modèle à la polymérisation du MT. J'ai en outre utilisé la coloration de la tubuline pour confirmer la colocalisation de la protéine CSAP avec les structures de MT enroulées. La protéine CSAP n'est pas la seule MAP capable d'induire la formation de MT enroulé. Une étude récente a montré que la MAP6/ STOP pouvait également induire des MTs enroulés, qui ont étonnement une largeur d'hélice similaire de ~700 nm. Des études ultra-

structurelles montrent que la MAP6 est une protéine MT-Inner (MIP) (Cuveillier et al. 2020). En raison du phénotype des enroulements et de la largeur similaire de l'hélice, il serait intéressant de voir l'ultrastructure des MTs enourlées liées à la protéine CSAP pour confirmer qu'il s'agit d'une MAP ou d'une MIP.

c) La protéine MAP2 induit un pelage des protofilaments:

La protéine MAP2 existe sous différentes isoformes qui sont générées par l'épissage alternatif d'un seul gène MAP2 (Ludin et al. 1996 ; Murphy et Borisy 1975b). MAP2C et MAP2D sont deux isoformes de poids moléculaire inférieur, cependant, les deux isoformes contiennent l'ensemble du domaine de liaison MT de la famille MAP2, et peuvent donc être utilisées pour étudier le comportement de liaison des protéines MAP2. Ces deux protéines, MAP2C et MAP2D décorent l'ensemble du réseau MT dans mes expériences, comme cela a été démontré auparavant (Saoudi et al. 1995). Malgré le fait que MAP2 soit une protéine bien connue qui a été étudiée pendant de nombreuses décennies, j'ai trouvé une nouvelle activité de MAP2 qui n'avait pas encore été signalée jusqu'à présent : elle peut induire le pelage et le frisage des protofilaments du MT en cours de polymérisation. Ce pelage peut se produire soit sur le côté d'un réseau de MT existant, soit aux extrémités positives du MT en croissance. Le plus frappant est que la protéine MAP2 forme des plaques sphériques à l'intérieur des protofilaments pelés et enroulés, le long du réseau de MT. Les expériences avec la latrunculine A ont montré que cette formation de plaques est un processus indépendant de l'actine.

De plus, j'ai observé que la MAP2D présente un plus grand nombre d'événements de pelage des protofilaments par rapport à l'isoforme MAP2C. Ceci est intriguant car la seule différence entre MAP2C et MAP2D est le nombre de répétitions de liaison au MT. Ceci est très similaire à la protéine Tau, qui existe sous une forme à 3 répétitions et une forme à 4 répétitions (Goedert et al. 1989). Il est frappant de constater que les versions à 4 répétitions de Tau sont connues pour se lier plus fortement aux MTs que les formes à 3 répétitions (Lu et Kosik 2001). Cela suggère que la différence dans le pelage des protofilaments pour MAP2D (4 répétitions) vs MAP2C (3 répétitions) semble être également liée à la force avec laquelle ces MAPs se lient aux MTs. Cette hypothèse est en outre soutenue par mon observation selon laquelle la réduction des concentrations de MAP2 dans les lysats a entraîné une diminution de la formation de patchs (non montré).

Il a été rapporté que les protéines MAP2 se lient le long des protofilaments individuels en pontant les interfaces de la tubuline (Al-Bassam et al. 2002). Une des spéculations qui pourrait expliquer ce phénotype de pelage serait une affinité plus élevée des MAP2 pour les protofilaments individuels plutôt que pour les surfaces de MT. Cependant, des études par cryo-EM sur les MTs décorées de MAP2 dans des lysats seraient l'expérience ultime pour expliquer l'architecture moléculaire sous-jacente à ce phénotype unique.

d) Différents comportements de liaison au MT au sein de la famille des protéines associées au MT des échinodermes (EML1-4):

La famille des EMAP ou EML comprend six membres chez les mammifères. En utilisant l'approche ex-vivo des lysats, j'ai testé quatre membres de cette famille, EML1, EML2, EML3 et EML4, pour leur comportement de liaison sur les MTs en croissance. EML5 et EML6 sont de très grandes protéines (~2 000 acides aminés) et présentent des niveaux d'expression très faibles dans les cellules, c'est pourquoi je n'ai pas pu les inclure dans mes études.

À l'exception d'EML2, les trois autres membres de la famille EML ont favorisé l'élongation des MTs et ont décoré les MTs, mais d'une manière étonnamment différente. La protéine EML1 a montré des signaux de plus en plus forts vers les extrémités positives des MTs par rapport au reste du réseau des MTs. Ce comportement dépendait de la concentration et n'a pas été observé à des niveaux élevés d'EML1 dans les extraits. Les intensités d'EML1 forment un gradient avec une diminution constante de l'intensité à partir des extrémités plus des MTs, ce qui est diffèrent des +TIPs comme EB3 qui forment de courtes comètes avec des pics d'intensité à l'extrémité croissant « + », et une forte diminution de l'intensité vers le réseau des MTs. Des études antérieures ont montré que l'absence d'EML1 entraîne une croissance lente de l'extrémité plus des MTs (Bizzotto et al. 2017). Cependant, des études supplémentaires doivent être menées au niveau moléculaire pour mieux comprendre l'enrichissement progressif de la partie supérieure de la protéines EML1.

Dans le cas de la protéine EML2, je n'ai trouvé aucune croissance de MT dans le dosage des lysats, ce qui a été confirmé en suite par l'immunocoloration des tubulines. Cette observation concorde avec une étude précédente qui décrit EML2 comme un dépolymérisateur de MT (Eichenmuller et al. 2002). Il est intéressant de noter que, comme pour l'absence de nouvelle formation de MT, je n'ai pas non plus observé de formation de filaments d'actine, ce qui suggère

que la formation de MTs et de filaments d'actine est mutuellement liée dans les extraits, ce qui est très évident pour les expériences avec EML2 qui abolissent les polymérisations de MT.

La protéine EML3 s'est comportée différemment des autres membres de la famille. J'ai trouvé une lente décoration d'EML3 sur le réseau de MT, apparemment après que les MTs aient déjà été complètement polymérisés. Cela suggère que EML3 pourrait avoir une plus grande affinité avec les MTs polymérisés, mais avec des difficultés à initier la polymérisation des MTs.

La protéine EML4 décore le réseau de MT sans aucun motif de localisation spécifique. Il est intéressant de noter que les expériences de dilution de la protéine EML4 montrent qu'en diminuant la concentration, EML4 forme des plaques en forme d'îlots sur les MTs, similaires à la MAP Tau neuronale (Siahaan et al. 2019 ; Abdel Karim et al. 2019), qui a été signalée récemment. Cela pourrait signifier que différentes MAPs sont capables de former de tels îlots, et donc élargir l'importance de ce phénomène. En outre, cela confirme que l'approche ex-vivo permet également de visualiser la formation d'îlots sur les MTs.

e) La protéine MAP7 génère la formation d'asters de MT:

La famille MAP7 forme quatre produits géniques différents chez les mammifères : MAP7, MAP7D1, MAP7D2 et MAP7D3 (Bulinski et Bossler 1994 ; Metzger et al. 2012 ; Yadav, Verma, et Panda 2014). Dans mon essai, j'ai trouvé que la protéine MAP7 avait la propriété unique d'induire la formation d'asters de MT, avec de multiples MTs polymérisant à partir d'un centre commun, et s'orientant à 360 degrés. La formation d'asters a été observée à la fois à partir de la fin des amorces de MT GMPCPP ainsi que d'événements de nucléation spontanée sans amorces. Plusieurs rapports font état de formations d'asters de MT impliquant des moteurs à kinésine (Juniper et al. 2018 ; Norris et al. 2018 ; Nédélec et Surrey 2001). Étant donné que la protéine MAP7 est connue pour interagir avec les kinésines et favoriser leurs interactions avec le MT (Hooikaas et al. 2019), il est possible que la capacité de formation d'asters de MAP7 dans les lysats cellulaires soit médiée par la propriété de recrutement moteur de MAP7. D'autres études de reconstitution in vitro avec la protéine MAP7 purifiée et la tubuline purifiée n'ont pas montré de formation d'asters (Hooikaas et al. 2019 ; Monroy et al. 2018), ce qui soutient l'hypothèse que MAP7 a besoin de composants supplémentaires tels que les moteurs à kinésine des lysats cellulaires pour former des asters de MT. Mon observation a montré que la présence

de latrunculine A dans les expériences sur les lysats n'a pas empêché la formation d'asters par MAP7, ce qui suggère qu'il s'agit d'un processus indépendant de l'actine.

Contrairement à MAP7, toutes les autres protéines de la famille MAP7 n'ont pas induit la formation d'asters, mais se sont liées aux MTs. De plus, MAP7D1 et MAPD2 ont montré une faible décoration sur les MTs dans les essais TIRF, ce qui suggère qu'elles pourraient avoir des affinités de liaison plus faibles pour les MTs. MAP7D3 n'a montré aucune liaison des MTs dans mes conditions d'essai pour des raisons inconnues.

2. Études ultra-structurelles avec des lysats cellulaires

Une des applications étendue de l'approche ex-vivo est la possibilité de réaliser la cryo-microscopie électronique (cryo-EM) des assemblages MAP-MT sans aucun procédé de purification. Pour en démontrer la faisabilité, j'ai choisi EML1, EML4 et MACF1 pour les études de cryo-EM. Pour réaliser la cryo-EM dans des conditions optimales, j'ai d'abord effectué un essai de reconstitution TIRF avec des dilutions de lysats appropriés pour m'assurer que les échantillons sont de bonnes qualités et que le temps que nous avons donné est suffisant pour polymériser les MTs sur les grilles EM. Après avoir obtenu les images EM, nous avons effectué une reconstitution 3D uniquement pour EML1. L'image reconstruite en 3D d'EML1 complet lié à la MT avec une résolution d'environ 3,7 Å montre que EML1 décore les MTs le long des protofilaments. Ce schéma de liaison d'EML1 pourrait éventuellement bloquer les protéines motrices (telles que la kinésine 1) qui marchent sur des protofilaments uniques, ce qui a été montré pour les MAPs telles que Tau et MAP4 (Shibata et al. 2012 ; Schneider et al. 2015 ; Shigematsu et al. 2018 ; Monroy et al. 2018).
Une étude récente avait déjà signalé l'utilisation de lysats HEK pour la cryo-EM suivie d'une reconstruction structurelle, mais dans ce cas pour des structures non-MT, ce qui confirme encore la praticabilité de l'approche par lysats pour les études ultra-structurelles (Verbeke et al. 2018). Cependant, la faisabilité des études cryo-EM pour toutes les MAPs restantes utilisant des lysats est incertaine, car une décoration par MT élevée pourrait être nécessaire pour une résolution suffisante dans la reconstitution des structures. Il est donc possible que mon approche ne puisse pas être utilisée que pour les MAPs ayant de fortes affinités de liaison. Une étude comparative avec une MAP à faible affinité de liaison provenant de lysats et avec sa forme purifiée pourrait aider à explorer davantage les limites de cette approche.

Résumé des principaux résultats et conclusions de mes projets de doctorat:

- J'ai réussi à établir et à développer une méthode sans purification de protéine pour étudier un grand nombre de MAP (>50) par reconstitution des MTs et la microscopie TIRF.

- J'ai identifié de nouvelles propriétés des MAPs sur les MTs dynamiques, y compris MACF1 (extrémités de MT crochus), CSAP (MT hélicoïdale), MAP7 (asters de MT), MAP2 (pelage de protofilaments), MAP8 et Tau (fragmentation de MT), et EML1 (affinité de liaison plus élevée avec les extrémités de MT en croissance).

- J'ai montré la formation de co-condensats CLIP-170 avec la tubuline sous forme de gouttelettes périodiques sur le réseau de MT, et j'ai démontré qu'ils peuvent nucléer de nouveaux MTs.

- En collaboration, j'ai effectué des études cryo-EM sur EML1 dans des lysats, qui ont montré qu'EML1 se lie le long des protofilaments de MT.

- J'ai mis en place des expériences de compétition de MAP (en mélangeant des lysats contenant des MAPs marqués avec des fluorophores de différentes couleurs). Ces expériences ont révélé que le mutant EML1T243A lié à la maladie se lie moins et défavorise la croissance de MT comparé à EML1 de type sauvage.

- J'ai effectué des essais de reconstitution TIRF avec et sans drogue inhibitrice de l'actine (Latrunculine A), qui ont montré que sur les ~50 MAPs candidats, certaines MAP (par exemple GLFND1) induisent le co-alignement actine-MT, certaines empêchent le co-alignement (par exemple MAP10), tandis que d'autres MAPs présentent un phénotype mixte (par exemple : EML3).

- J'ai participé à la mise en place de méthodes de purification pour obtenir de la tubuline avec des PTMs contrôlées par des cycles de polymérisation-dépolymérisation.

- J'ai mis en place un test TIRF tricolore pour mesurer l'impact des PTMs de la tubuline sur la liaison des MAPs. J'ai montré que la protéine Tau a une plus grande affinité de liaison avec les MTs cérébrales riches en PTMs stabilisés par le taxol que les MTs HeLa non modifiés.

- J'ai participé à la mise en place d'un dispositif in vitro pour étudier le rôle de la tubuline porteuse de mutations chez des patients. Ce dispositif nous permet de déterminer l'impact de la température sur l'assemblage et la stabilité des MTs. Mes études préliminaires montrent que les mutations de la tubuline (TUBA1A) dérivées de la lissencephalie pourraient affecter la dynamique ainsi que la sensibilité au froid des MTs.

Au total, l'approche des lysats cellulaires est susceptible d'établir une priorité en tant que méthode simple et rapide pour la caractérisation des MAPs à une échelle de débit moyen, et pour l'étude des PTMs de la tubuline. Elle peut être utilisée à la fois pour la reconstitution TIRF et pour les études de cryo-EM. En utilisant cette technique, je pourrais potentiellement caractériser toute protéines associées aux MTs, indépendamment de sa source, et sans avoir besoin de procédures de purification personnalisées.

L'impressionnante solubilité d'une large gamme de protéines différentes dans mon approche a ouvert de larges applications telles que l'identification de nouvelles MAPs et de nouvelles propriétés des MAPs, l'étude de l'interaction actine-MT, dans les expériences de compétition de MAPs, et l'étude du code de la tubuline. Au total, la méthode sans cellule développée au cours de mon projet de doctorat ouvre de nombreuses possibilités pour faire progresser ma compréhension du cytosquelette de MT, de ses protéines associées et du rôle des PTMs de la tubuline dans les interactions MAP-MT, qui sont collectivement impliquées dans plusieurs processus cellulaires et maladies humaines.

7. Bibliography

Abdel Karim, N., O. Gaber, I. Eldessouki, E. M. Bahassi, and J. Morris. 2019. 'Exosomes as a Surrogate Marker for Autophagy in Peripheral Blood, Correlative Data from Phase I Study of Chloroquine in Combination with Carboplatin/Gemcitabine in Advanced Solid Tumors', *Asian Pac J Cancer Prev*, 20: 3789-96.

Abdrabou, A., D. Brandwein, and Z. Wang. 2020. 'Differential Subcellular Distribution and Translocation of Seven 14-3-3 Isoforms in Response to EGF and During the Cell Cycle', *Int J Mol Sci*, 21.

Abe, M., S. Yamashita, Y. Mori, T. Abe, H. Saijo, K. Hoshi, T. Ushijima, and T. Takato. 2016. 'High-risk oral leukoplakia is associated with aberrant promoter methylation of multiple genes', *BMC Cancer*, 16: 350.

Abushouk, A. I., A. Negida, R. A. Elshenawy, H. Zein, A. M. Hammad, A. Menshawy, and W. M. Y. Mohamed. 2018. 'C-Abl Inhibition; A Novel Therapeutic Target for Parkinson's Disease', *CNS Neurol Disord Drug Targets*, 17: 14-21.

Adamopoulos, A., L. Landskron, T. Heidebrecht, F. Tsakou, O. B. Bleijerveld, M. Altelaar, J. Nieuwenhuis, P. H. N. Celie, T. R. Brummelkamp, and A. Perrakis. 2019. 'Crystal structure of the tubulin tyrosine carboxypeptidase complex VASH1-SVBP', *Nat Struct Mol Biol*, 26: 567-70.

Adib, R., J. M. Montgomery, J. Atherton, L. O'Regan, M. W. Richards, K. R. Straatman, D. Roth, A. Straube, R. Bayliss, C. A. Moores, and A. M. Fry. 2019. 'Mitotic phosphorylation by NEK6 and NEK7 reduces the microtubule affinity of EML4 to promote chromosome congression', *Sci Signal*, 12.

Afghani, N., T. Mehta, J. Wang, N. Tang, O. Skalli, and Q. A. Quick. 2017. 'Microtubule actin cross-linking factor 1, a novel target in glioblastoma', *Int J Oncol*, 50: 310-16.

Aguezzoul, M., A. Andrieux, and E. Denarier. 2003. 'Overlap of promoter and coding sequences in the mouse STOP gene (Mtap6)', *Genomics*, 81: 623-7.

Aher, A., M. Kok, A. Sharma, A. Rai, N. Olieric, R. Rodriguez-Garcia, E. A. Katrukha, T. Weinert, V. Olieric, L. C. Kapitein, M. O. Steinmetz, M. Dogterom, and A. Akhmanova. 2018. 'CLASP Suppresses Microtubule Catastrophes through a Single TOG Domain', *Dev Cell*, 46: 40-58 e8.

Aher, A., D. Rai, L. Schaedel, J. Gaillard, K. John, Q. Liu, M. Altelaar, L. Blanchoin, M. Thery, and A. Akhmanova. 2020. 'CLASP Mediates Microtubule Repair by Restricting Lattice Damage and Regulating Tubulin Incorporation', *Curr Biol*, 30: 2175-83 e6.

Aigner, L., D. Fluegel, J. Dietrich, S. Ploetz, and J. Winkler. 2000. 'Isolated lissencephaly sequence and double-cortex syndrome in a German family with a novel doublecortin mutation', *Neuropediatrics*, 31: 195-8.

Aijaz, S., F. D'Atri, S. Citi, M. S. Balda, and K. Matter. 2005. 'Binding of GEF-H1 to the tight junction-associated adaptor cingulin results in inhibition of Rho signaling and G1/S phase transition', *Dev Cell*, 8: 777-86.

Aillaud, C., C. Bosc, L. Peris, A. Bosson, P. Heemeryck, J. Van Dijk, J. Le Friec, B. Boulan, F. Vossier, L. E. Sanman, S. Syed, N. Amara, Y. Coute, L. Lafanechere, E. Denarier, C. Delphin, L. Pelletier, S. Humbert, M. Bogyo, A. Andrieux, K. Rogowski, and M. J. Moutin. 2017. 'Vasohibins/SVBP are tubulin carboxypeptidases (TCPs) that regulate neuron differentiation', *Science*, 358: 1448-53.

Aillaud, C., C. Bosc, Y. Saoudi, E. Denarier, L. Peris, L. Sago, N. Taulet, A. Cieren, O. Tort, M. M. Magiera, C. Janke, V. Redeker, A. Andrieux, and M. J. Moutin. 2016. 'Evidence for new C-terminally truncated variants of alpha- and beta-tubulins', *Mol Biol Cell*, 27: 640-53.

Akella, J. S., D. Wloga, J. Kim, N. G. Starostina, S. Lyons-Abbott, N. S. Morrissette, S. T. Dougan, E. T. Kipreos, and J. Gaertig. 2010. 'MEC-17 is an alpha-tubulin acetyltransferase', *Nature*, 467: 218-22.

Akhmanova, A., and C. C. Hoogenraad. 2015. 'Microtubule minus-end-targeting proteins', *Curr Biol*, 25: R162-71.

Akhmanova, A., C. C. Hoogenraad, K. Drabek, T. Stepanova, B. Dortland, T. Verkerk, W. Vermeulen, B. M. Burgering, C. I. De Zeeuw, F. Grosveld, and N. Galjart. 2001. 'Clasps are CLIP-115 and -170 associating proteins involved in the regional regulation of microtubule dynamics in motile fibroblasts', *Cell*, 104: 923-35.

Akhmanova, A., A. L. Mausset-Bonnefont, W. van Cappellen, N. Keijzer, C. C. Hoogenraad, T. Stepanova, K. Drabek, J. van der Wees, M. Mommaas, J. Onderwater, H. van der Meulen, M. E. Tanenbaum, R. H. Medema, J. Hoogerbrugge, J. Vreeburg, E. J. Uringa, J. A. Grootegoed, F. Grosveld, and N. Galjart. 2005. 'The microtubule plus-end-tracking protein CLIP-170 associates with the spermatid manchette and is essential for spermatogenesis', *Genes Dev*, 19: 2501-15.

Akhmanova, A., and M. O. Steinmetz. 2008. 'Tracking the ends: a dynamic protein network controls the fate of microtubule tips', *Nat Rev Mol Cell Biol*, 9: 309-22.

———. 2010. 'Microtubule +TIPs at a glance', *J Cell Sci*, 123: 3415-9.

———. 2015. 'Control of microtubule organization and dynamics: two ends in the limelight', *Nat Rev Mol Cell Biol*, 16: 711-26.

———. 2019. 'Microtubule minus-end regulation at a glance', *J Cell Sci*, 132.

Al-Bassam, J., R. S. Ozer, D. Safer, S. Halpain, and R. A. Milligan. 2002. 'MAP2 and tau bind longitudinally along the outer ridges of microtubule protofilaments', *J Cell Biol*, 157: 1187-96.

Aladdin, A., R. Kiraly, P. Boto, Z. Regdon, and K. Tar. 2019. 'Juvenile Huntington's Disease Skin Fibroblasts Respond with Elevated Parkin Level and Increased Proteasome Activity as a Potential Mechanism to Counterbalance the Pathological Consequences of Mutant Huntingtin Protein', *Int J Mol Sci*, 20.

Alanio-Brechot, C., P. O. Schischmanoff, M. Feneant-Thibault, T. Cynober, G. Tchernia, J. Delaunay, and L. Garcon. 2008. 'Association between myeloid malignancies and acquired deficit in protein 4.1R: a retrospective analysis of six patients', *Am J Hematol*, 83: 275-8.

Alexander, J. E., D. F. Hunt, M. K. Lee, J. Shabanowitz, H. Michel, S. C. Berlin, T. L. MacDonald, R. J. Sundberg, L. I. Rebhun, and A. Frankfurter. 1991. 'Characterization of posttranslational modifications in neuron-specific class III beta-tubulin by mass spectrometry', *Proc Natl Acad Sci U S A*, 88: 4685-9.

Alexander, R. E., R. Montironi, A. Lopez-Beltran, S. R. Williamson, M. Wang, K. M. Post, J. D. Sen, A. K. Arnold, S. Zhang, X. Wang, M. O. Koch, N. M. Hahn, T. A. Masterson, G. T. MacLennan, D. D. Davidson, E. Comperat, and L. Cheng. 2014. 'EGFR alterations and EML4-ALK rearrangement in primary adenocarcinoma of the urinary bladder', *Mod Pathol*, 27: 107-12.

Alfaro-Aco, R., A. Thawani, and S. Petry. 2017. 'Structural analysis of the role of TPX2 in branching microtubule nucleation', *J Cell Biol*, 216: 983-97.

Allen, E., J. Ding, W. Wang, S. Pramanik, J. Chou, V. Yau, and Y. Yang. 2005. 'Gigaxonin-controlled degradation of MAP1B light chain is critical to neuronal survival', *Nature*, 438: 224-8.

Amin, M. A., G. Itoh, K. Iemura, M. Ikeda, and K. Tanaka. 2014. 'CLIP-170 recruits PLK1 to kinetochores during early mitosis for chromosome alignment', *J Cell Sci*, 127: 2818-24.

Amin, M. A., K. Kobayashi, and K. Tanaka. 2015. 'CLIP-170 tethers kinetochores to microtubule plus ends against poleward force by dynein for stable kinetochore-microtubule attachment', *FEBS Lett*, 589: 2739-46.

Amisaki, M., H. Tsuchiya, T. Sakabe, Y. Fujiwara, and G. Shiota. 2019. 'Identification of genes involved in the regulation of TERT in hepatocellular carcinoma', *Cancer Sci*, 110: 550-60.

Andersen, G. R., and J. Nyborg. 2001. 'Structural studies of eukaryotic elongation factors', *Cold Spring Harb Symp Quant Biol*, 66: 425-37.

Andrieux, A., P. A. Salin, M. Vernet, P. Kujala, J. Baratier, S. Gory-Faure, C. Bosc, H. Pointu, D. Proietto, A. Schweitzer, E. Denarier, J. Klumperman, and D. Job. 2002. 'The suppression of brain cold-stable microtubules in mice induces synaptic defects associated with neuroleptic-sensitive behavioral disorders', *Genes Dev*, 16: 2350-64.

Arai, M., and M. Itokawa. 2010. 'A hard road in psychiatric genetics: schizophrenia and DPYSL2', *J Hum Genet*, 55: 397-9.

Aranda-Orgilles, B., A. Trockenbacher, J. Winter, J. Aigner, A. Kohler, E. Jastrzebska, J. Stahl, E. C. Muller, A. Otto, E. E. Wanker, R. Schneider, and S. Schweiger. 2008. 'The Opitz syndrome gene product MID1 assembles a microtubule-associated ribonucleoprotein complex', *Hum Genet*, 123: 163-76.

Arce, C. A., H. S. Barra, J. A. Rodriguez, and R. Caputto. 1975. 'Tentative identification of the amino acid that binds tyrosine as a single unit into a soluble brain protein', *FEBS Lett*, 50: 5-7.

Arif, M., S. F. Kazim, I. Grundke-Iqbal, R. M. Garruto, and K. Iqbal. 2014. 'Tau pathology involves protein phosphatase 2A in parkinsonism-dementia of Guam', *Proc Natl Acad Sci U S A*, 111: 1144-9.

Audebert, S., E. Desbruyeres, C. Gruszczynski, A. Koulakoff, F. Gros, P. Denoulet, and B. Edde. 1993. 'Reversible polyglutamylation of alpha- and beta-tubulin and microtubule dynamics in mouse brain neurons', *Mol Biol Cell*, 4: 615-26.

Audebert, S., A. Koulakoff, Y. Berwald-Netter, F. Gros, P. Denoulet, and B. Edde. 1994. 'Developmental regulation of polyglutamylated alpha- and beta-tubulin in mouse brain neurons', *J Cell Sci*, 107 (Pt 8): 2313-22.

Aumeier, C., L. Schaedel, J. Gaillard, K. John, L. Blanchoin, and M. Thery. 2016. 'Self-repair promotes microtubule rescue', *Nat Cell Biol*, 18: 1054-64.

Avila, J., J. J. Lucas, M. Perez, and F. Hernandez. 2004. 'Role of tau protein in both physiological and pathological conditions', *Physiol Rev*, 84: 361-84.

Aylsworth, A., S. X. Jiang, A. Desbois, and S. T. Hou. 2009. 'Characterization of the role of full-length CRMP3 and its calpain-cleaved product in inhibiting microtubule polymerization and neurite outgrowth', *Exp Cell Res*, 315: 2856-68.

Backer, C. B., J. H. Gutzman, C. G. Pearson, and I. M. Cheeseman. 2012. 'CSAP localizes to polyglutamylated microtubules and promotes proper cilia function and zebrafish development', *Mol Biol Cell*, 23: 2122-30.

Bader, V., L. Tomppo, S. V. Trossbach, N. J. Bradshaw, I. Prikulis, S. R. Leliveld, C. Y. Lin, K. Ishizuka, A. Sawa, A. Ramos, I. Rosa, A. Garcia, J. R. Requena, M. Hipolito, N. Rai, E. Nwulia, U. Henning, S. Ferrea, C. Luckhaus, J. Ekelund, J. Veijola, M. R. Jarvelin, W. Hennah, and C. Korth. 2012. 'Proteomic, genomic and translational approaches identify CRMP1 for a role in schizophrenia and its underlying traits', *Hum Mol Genet*, 21: 4406-18.

Bai, W., J. Bai, Y. Li, D. Tian, and R. Shi. 2017. 'Microtubule-associated protein 1S-related autophagy inhibits apoptosis of intestinal epithelial cells via Wnt/beta-catenin signaling in Crohn's disease', *Biochem Biophys Res Commun*, 485: 635-42.

Baines, A. J., P. M. Bennett, E. W. Carter, and C. Terracciano. 2009. 'Protein 4.1 and the control of ion channels', *Blood Cells Mol Dis*, 42: 211-5.

Baines, A. J., H. C. Lu, and P. M. Bennett. 2014. 'The Protein 4.1 family: hub proteins in animals for organizing membrane proteins', *Biochim Biophys Acta*, 1838: 605-19.

Balastik, M., X. Z. Zhou, M. Alberich-Jorda, R. Weissova, J. Ziak, M. F. Pazyra-Murphy, K. E. Cosker, O. Machonova, I. Kozmikova, C. H. Chen, L. Pastorino, J. M. Asara, A. Cole, C. Sutherland, R. A. Segal, and K. P. Lu. 2015. 'Prolyl Isomerase Pin1 Regulates Axon Guidance by Stabilizing CRMP2A Selectively in Distal Axons', *Cell Rep*, 13: 812-28.

Balchand, S. K., B. J. Mann, J. Titus, J. L. Ross, and P. Wadsworth. 2015. 'TPX2 Inhibits Eg5 by Interactions with Both Motor and Microtubule', *J Biol Chem*, 290: 17367-79.

Balchin, D., G. Milicic, M. Strauss, M. Hayer-Hartl, and F. U. Hartl. 2018. 'Pathway of Actin Folding Directed by the Eukaryotic Chaperonin TRiC', *Cell*, 174: 1507-21 e16.

Baratier, J., L. Peris, J. Brocard, S. Gory-Faure, F. Dufour, C. Bosc, A. Fourest-Lieuvin, L. Blanchoin, P. Salin, D. Job, and A. Andrieux. 2006. 'Phosphorylation of microtubule-associated protein STOP by calmodulin kinase II', *J Biol Chem*, 281: 19561-9.

Barbiero, I., D. Peroni, P. Siniscalchi, L. Rusconi, M. Tramarin, R. De Rosa, P. Motta, M. Bianchi, and C. Kilstrup-Nielsen. 2020. 'Pregnenolone and pregnenolone-methyl-ether rescue neuronal defects caused by dysfunctional CLIP170 in a neuronal model of CDKL5 Deficiency Disorder', *Neuropharmacology*, 164: 107897.

Barel, O., M. C. V. Malicdan, B. Ben-Zeev, J. Kandel, H. Pri-Chen, J. Stephen, I. G. Castro, J. Metz, O. Atawa, S. Moshkovitz, E. Ganelin, I. Barshack, S. Polak-Charcon, D. Nass, D. Marek-Yagel, N. Amariglio, N. Shalva, T. Vilboux, C. Ferreira, B. Pode-Shakked, G. Heimer, C. Hoffmann, T. Yardeni, A. Nissenkorn, C. Avivi, E. Eyal, N. Kol, E. Glick Saar, D. C. Wallace, W. A. Gahl, G. Rechavi, M. Schrader, D. M. Eckmann, and Y. Anikster. 2017. 'Deleterious variants in TRAK1 disrupt mitochondrial movement and cause fatal encephalopathy', *Brain*, 140: 568-81.

Barisic, M., R. Silva e Sousa, S. K. Tripathy, M. M. Magiera, A. V. Zaytsev, A. L. Pereira, C. Janke, E. L. Grishchuk, and H. Maiato. 2015. 'Mitosis. Microtubule detyrosination guides chromosomes during mitosis', *Science*, 348: 799-803.

Barlan, K., W. Lu, and V. I. Gelfand. 2013. 'The microtubule-binding protein ensconsin is an essential cofactor of kinesin-1', *Curr Biol*, 23: 317-22.

Barlow, S., M. L. Gonzalez-Garay, R. R. West, J. B. Olmsted, and F. Cabral. 1994. 'Stable expression of heterologous microtubule-associated proteins (MAPs) in Chinese hamster ovary cells: evidence for differing roles of MAPs in microtubule organization', *J Cell Biol*, 126: 1017-29.

Basbous, J., D. Knani, N. Bonneaud, D. Giorgi, J. M. Brondello, and S. Rouquier. 2012. 'Induction of ASAP (MAP9) contributes to p53 stabilization in response to DNA damage', *Cell Cycle*, 11: 2380-90.

Bash-Babula, J., D. Toppmeyer, M. Labassi, J. Reidy, M. Orlick, R. Senzon, E. Alli, T. Kearney, D. August, W. Shih, J. M. Yang, and W. N. Hait. 2002. 'A Phase I/pilot study of sequential doxorubicin/vinorelbine: effects on p53 and microtubule-associated protein 4', *Clin Cancer Res*, 8: 1057-64.

Basnet, N., H. Nedozralova, A. H. Crevenna, S. Bodakuntla, T. Schlichthaerle, M. Taschner, G. Cardone, C. Janke, R. Jungmann, M. M. Magiera, C. Biertumpfel, and N. Mizuno. 2018. 'Direct induction of microtubule branching by microtubule nucleation factor SSNA1', *Nat Cell Biol*, 20: 1172-80.

Baudier, J., D. Mochly-Rosen, A. Newton, S. H. Lee, D. E. Koshland, Jr., and R. D. Cole. 1987. 'Comparison of S100b protein with calmodulin: interactions with melittin and

microtubule-associated tau proteins and inhibition of phosphorylation of tau proteins by protein kinase C', *Biochemistry*, 26: 2886-93.

Bayliss, R., J. Choi, D. A. Fennell, A. M. Fry, and M. W. Richards. 2016. 'Molecular mechanisms that underpin EML4-ALK driven cancers and their response to targeted drugs', *Cell Mol Life Sci*, 73: 1209-24.

Beaven, R., N. S. Dzhindzhev, Y. Qu, I. Hahn, F. Dajas-Bailador, H. Ohkura, and A. Prokop. 2015. 'Drosophila CLIP-190 and mammalian CLIP-170 display reduced microtubule plus end association in the nervous system', *Mol Biol Cell*, 26: 1491-508.

Bechstedt, S., and G. J. Brouhard. 2012. 'Doublecortin recognizes the 13-protofilament microtubule cooperatively and tracks microtubule ends', *Dev Cell*, 23: 181-92.

Belanger, D., C. A. Farah, M. D. Nguyen, M. Lauzon, S. Cornibert, and N. Leclerc. 2002. 'The projection domain of MAP2b regulates microtubule protrusion and process formation in Sf9 cells', *J Cell Sci*, 115: 1523-39.

Belmont, L. D., A. A. Hyman, K. E. Sawin, and T. J. Mitchison. 1990. 'Real-time visualization of cell cycle-dependent changes in microtubule dynamics in cytoplasmic extracts', *Cell*, 62: 579-89.

Belvindrah, R., K. Natarajan, P. Shabajee, E. Bruel-Jungerman, J. Bernard, M. Goutierre, I. Moutkine, X. H. Jaglin, M. Savariradjane, T. Irinopoulou, J. C. Poncer, C. Janke, and F. Francis. 2017. 'Mutation of the alpha-tubulin Tuba1a leads to straighter microtubules and perturbs neuronal migration', *J Cell Biol*, 216: 2443-61.

Ben-Ze'ev, A., S. R. Farmer, and S. Penman. 1979. 'Mechanisms of regulating tubulin synthesis in cultured mammalian cells', *Cell*, 17: 319-25.

Berezniuk, I., H. T. Vu, P. J. Lyons, J. J. Sironi, H. Xiao, B. Burd, M. Setou, R. H. Angeletti, K. Ikegami, and L. D. Fricker. 2012. 'Cytosolic carboxypeptidase 1 is involved in processing alpha- and beta-tubulin', *J Biol Chem*, 287: 6503-17.

Bergman, Z. J., J. Wong, D. G. Drubin, and G. Barnes. 2018. 'Microtubule dynamics regulation reconstituted in budding yeast lysates', *J Cell Sci*, 132.

Bernhardt, R., G. Huber, and A. Matus. 1985. 'Differences in the developmental patterns of three microtubule-associated proteins in the rat cerebellum', *J Neurosci*, 5: 977-91.

Bernier, G., A. Brown, G. Dalpe, Y. De Repentigny, M. Mathieu, and R. Kothary. 1995. 'Dystonin expression in the developing nervous system predominates in the neurons that degenerate in dystonia musculorum mutant mice', *Mol Cell Neurosci*, 6: 509-20.

Bernier, G., M. Mathieu, Y. De Repentigny, S. M. Vidal, and R. Kothary. 1996. 'Cloning and characterization of mouse ACF7, a novel member of the dystonin subfamily of actin binding proteins', *Genomics*, 38: 19-29.

Bernier, G., M. Pool, M. Kilcup, J. Alfoldi, Y. De Repentigny, and R. Kothary. 2000. 'Acf7 (MACF) is an actin and microtubule linker protein whose expression predominates in neural, muscle, and lung development', *Dev Dyn*, 219: 216-25.

Bernstein, H. G., R. Stricker, H. Dobrowolny, J. Steiner, B. Bogerts, K. Trubner, and G. Reiser. 2013. 'Nardilysin in human brain diseases: both friend and foe', *Amino Acids*, 45: 269-78.

Bieling, P., S. Kandels-Lewis, I. A. Telley, J. van Dijk, C. Janke, and T. Surrey. 2008a. 'CLIP-170 tracks growing microtubule ends by dynamically recognizing composite EB1/tubulin-binding sites', *J Cell Biol*, 183: 1223-33.

———. 2008b. 'CLIP-170 tracks growing microtubule ends by dynamically recognizing composite EB1/tubulin-binding sites', *J Cell Biol*, 183: 1223-33.

———. 2008c. 'CLIP-170 tracks growing microtubule ends by dynamically recognizing composite EB1/tubulin-binding sites', *J Cell Biol*, 183: 1223-33.

Bieling, P., I. A. Telley, C. Hentrich, J. Piehler, and T. Surrey. 2010. 'Fluorescence microscopy assays on chemically functionalized surfaces for quantitative imaging of microtubule, motor, and +TIP dynamics', *Methods Cell Biol*, 95: 555-80.

Bieling, P., I. A. Telley, and T. Surrey. 2010. 'A minimal midzone protein module controls formation and length of antiparallel microtubule overlaps', *Cell*, 142: 420-32.

Bilbe, G., J. Delabie, J. Bruggen, H. Richener, F. A. Asselbergs, N. Cerletti, C. Sorg, K. Odink, L. Tarcsay, W. Wiesendanger, and et al. 1992. 'Restin: a novel intermediate filament-associated protein highly expressed in the Reed-Sternberg cells of Hodgkin's disease', *EMBO J*, 11: 2103-13.

Binder, L. I., A. Frankfurter, H. Kim, A. Caceres, M. R. Payne, and L. I. Rebhun. 1984. 'Heterogeneity of microtubule-associated protein 2 during rat brain development', *Proc Natl Acad Sci U S A*, 81: 5613-7.

Binder, L. I., A. Frankfurter, and L. I. Rebhun. 1985. 'The distribution of tau in the mammalian central nervous system', *J Cell Biol*, 101: 1371-8.

Bizzotto, S., A. Uzquiano, F. Dingli, D. Ershov, A. Houllier, G. Arras, M. Richards, D. Loew, N. Minc, A. Croquelois, A. Houdusse, and F. Francis. 2017. 'Eml1 loss impairs apical progenitor spindle length and soma shape in the developing cerebral cortex', *Sci Rep*, 7: 17308.

Blum, C., A. Graham, M. Yousefzadeh, J. Shrout, K. Benjamin, M. Krishna, R. Hoda, R. Hoda, D. J. Cole, E. Garrett-Mayer, C. Reed, M. Wallace, and M. Mitas. 2008. 'The expression ratio of Map7/B2M is prognostic for survival in patients with stage II colon cancer', *Int J Oncol*, 33: 579-84.

Boczan, J., A. G. Leenders, and Z. H. Sheng. 2004. 'Phosphorylation of syntaphilin by cAMP-dependent protein kinase modulates its interaction with syntaxin-1 and annuls its inhibitory effect on vesicle exocytosis', *J Biol Chem*, 279: 18911-9.

Bodakuntla, S., A. S. Jijumon, C. Villablanca, C. Gonzalez-Billault, and C. Janke. 2019. 'Microtubule-Associated Proteins: Structuring the Cytoskeleton', *Trends Cell Biol*, 29: 804-19.

Bodakuntla, S., A. Schnitzler, C. Villablanca, C. Gonzalez-Billault, I. Bieche, C. Janke, and M. M. Magiera. 2020. 'Tubulin polyglutamylation is a general traffic-control mechanism in hippocampal neurons', *J Cell Sci*, 133.

Bompard, G., J. van Dijk, J. Cau, Y. Lannay, G. Marcellin, A. Lawera, S. van der Laan, and K. Rogowski. 2018. 'CSAP Acts as a Regulator of TTLL-Mediated Microtubule Glutamylation', *Cell Rep*, 25: 2866-77 e5.

Bondallaz, P., A. Barbier, S. Soehrman, G. Grenningloh, and B. M. Riederer. 2006. 'The control of microtubule stability in vitro and in transfected cells by MAP1B and SCG10', *Cell Motil Cytoskeleton*, 63: 681-95.

Bonnet, C., D. Boucher, S. Lazereg, B. Pedrotti, K. Islam, P. Denoulet, and J. C. Larcher. 2001. 'Differential binding regulation of microtubule-associated proteins MAP1A, MAP1B, and MAP2 by tubulin polyglutamylation', *J Biol Chem*, 276: 12839-48.

Bonnet, C., E. Denarier, C. Bosc, S. Lazereg, P. Denoulet, and J. C. Larcher. 2002. 'Interaction of STOP with neuronal tubulin is independent of polyglutamylation', *Biochem Biophys Res Commun*, 297: 787-93.

Borisy, G. G., J. M. Marcum, J. B. Olmsted, D. B. Murphy, and K. A. Johnson. 1975. 'Purification of tubulin and associated high molecular weight proteins from porcine brain and characterization of microtubule assembly in vitro', *Ann N Y Acad Sci*, 253: 107-32.

Borisy, G. G., and J. B. Olmsted. 1972. 'Nucleated assembly of microtubules in porcine brain extracts', *Science*, 177: 1196-7.

Borisy, G. G., and E. W. Taylor. 1967. 'The mechanism of action of colchicine. Binding of colchincine-3H to cellular protein', *J Cell Biol*, 34: 525-33.

Bosanquet, D. C., L. Ye, K. G. Harding, and W. G. Jiang. 2014. 'FERM family proteins and their importance in cellular movements and wound healing (review)', *Int J Mol Med*, 34: 3-12.

Bosc, C., A. Andrieux, and D. Job. 2003. 'STOP proteins', *Biochemistry*, 42: 12125-32.

Bosc, C., J. D. Cronk, F. Pirollet, D. M. Watterson, J. Haiech, D. Job, and R. L. Margolis. 1996. 'Cloning, expression, and properties of the microtubule-stabilizing protein STOP', *Proc Natl Acad Sci U S A*, 93: 2125-30.

Bosch Grau, M., G. Gonzalez Curto, C. Rocha, M. M. Magiera, P. Marques Sousa, T. Giordano, N. Spassky, and C. Janke. 2013. 'Tubulin glycylases and glutamylases have distinct functions in stabilization and motility of ependymal cilia', *J Cell Biol*, 202: 441-51.

Boucher, D., J. C. Larcher, F. Gros, and P. Denoulet. 1994. 'Polyglutamylation of tubulin as a progressive regulator of in vitro interactions between the microtubule-associated protein Tau and tubulin', *Biochemistry*, 33: 12471-7.

Bowne-Anderson, H., A. Hibbel, and J. Howard. 2015. 'Regulation of Microtubule Growth and Catastrophe: Unifying Theory and Experiment', *Trends Cell Biol*, 25: 769-79.

Bozgeyik, I., O. Yumrutas, and E. Bozgeyik. 2017. 'MTUS1, a gene encoding angiotensin-II type 2 (AT2) receptor-interacting proteins, in health and disease, with special emphasis on its role in carcinogenesis', *Gene*, 626: 54-63.

Bre, M. H., and E. Karsenti. 1990. 'Effects of brain microtubule-associated proteins on microtubule dynamics and the nucleating activity of centrosomes', *Cell Motil Cytoskeleton*, 15: 88-98.

Bre, M. H., V. Redeker, M. Quibell, J. Darmanaden-Delorme, C. Bressac, J. Cosson, P. Huitorel, J. M. Schmitter, J. Rossler, T. Johnson, A. Adoutte, and N. Levilliers. 1996. 'Axonemal tubulin polyglycylation probed with two monoclonal antibodies: widespread evolutionary distribution, appearance during spermatozoan maturation and possible function in motility', *J Cell Sci*, 109 (Pt 4): 727-38.

Bressac, C., M. H. Bre, J. Darmanaden-Delorme, M. Laurent, N. Levilliers, and A. Fleury. 1995. 'A massive new posttranslational modification occurs on axonemal tubulin at the final step of spermatogenesis in Drosophila', *Eur J Cell Biol*, 67: 346-55.

Bretin, S., S. Reibel, E. Charrier, M. Maus-Moatti, N. Auvergnon, A. Thevenoux, J. Glowinski, V. Rogemond, J. Premont, J. Honnorat, and C. Gauchy. 2005. 'Differential expression of CRMP1, CRMP2A, CRMP2B, and CRMP5 in axons or dendrites of distinct neurons in the mouse brain', *J Comp Neurol*, 486: 1-17.

Brickley, K., and F. A. Stephenson. 2011. 'Trafficking kinesin protein (TRAK)-mediated transport of mitochondria in axons of hippocampal neurons', *J Biol Chem*, 286: 18079-92.

Brot, S., V. Rogemond, V. Perrot, N. Chounlamountri, C. Auger, J. Honnorat, and M. Moradi-Ameli. 2010. 'CRMP5 interacts with tubulin to inhibit neurite outgrowth, thereby modulating the function of CRMP2', *J Neurosci*, 30: 10639-54.

Brown, A., G. Bernier, M. Mathieu, J. Rossant, and R. Kothary. 1995. 'The mouse dystonia musculorum gene is a neural isoform of bullous pemphigoid antigen 1', *Nat Genet*, 10: 301-6.

Brown, J. R., C. L. Schwartz, J. M. Heumann, S. C. Dawson, and A. Hoenger. 2016. 'A detailed look at the cytoskeletal architecture of the Giardia lamblia ventral disc', *J Struct Biol*, 194: 38-48.

Brown, V., P. Jin, S. Ceman, J. C. Darnell, W. T. O'Donnell, S. A. Tenenbaum, X. Jin, Y. Feng, K. D. Wilkinson, J. D. Keene, R. B. Darnell, and S. T. Warren. 2001. 'Microarray

identification of FMRP-associated brain mRNAs and altered mRNA translational profiles in fragile X syndrome', *Cell*, 107: 477-87.

Brynychova, V., M. Ehrlichova, V. Hlavac, V. Nemcova-Furstova, V. Pecha, J. Leva, M. Trnkova, M. Mrhalova, R. Kodet, D. Vrana, J. Kovar, R. Vaclavikova, I. Gut, and P. Soucek. 2016. 'Genetic and functional analyses do not explain the association of high PRC1 expression with poor survival of breast carcinoma patients', *Biomed Pharmacother*, 83: 857-64.

Buee, L., T. Bussiere, V. Buee-Scherrer, A. Delacourte, and P. R. Hof. 2000. 'Tau protein isoforms, phosphorylation and role in neurodegenerative disorders', *Brain Res Brain Res Rev*, 33: 95-130.

Bulinski, J. C., and G. G. Borisy. 1979. 'Self-assembly of microtubules in extracts of cultured HeLa cells and the identification of HeLa microtubule-associated proteins', *Proc Natl Acad Sci U S A*, 76: 293-7.

Bulinski, J. C., and A. Bossler. 1994. 'Purification and characterization of ensconsin, a novel microtubule stabilizing protein', *J Cell Sci*, 107 (Pt 10): 2839-49.

Bulinski, J. C., D. Gruber, K. Faire, P. Prasad, and W. Chang. 1999. 'GFP chimeras of E-MAP-115 (ensconsin) domains mimic behavior of the endogenous protein in vitro and in vivo', *Cell Struct Funct*, 24: 313-20.

Bundschu, K., and K. Schuh. 2014. 'Cardiovascular ATIP (Angiotensin receptor type 2 interacting protein) expression in mouse development', *Dev Dyn*, 243: 699-711.

Burgoyne, R. D., and R. Cumming. 1984. 'Ontogeny of microtubule-associated protein 2 in rat cerebellum: differential expression of the doublet polypeptides', *Neuroscience*, 11: 156-67.

Burkhardt, J. K. 1998. 'The role of microtubule-based motor proteins in maintaining the structure and function of the Golgi complex', *Biochim Biophys Acta*, 1404: 113-26.

Cai, G., D. Wu, Z. Wang, Z. Xu, K. B. Wong, C. F. Ng, F. L. Chan, and S. Yu. 2017. 'Collapsin response mediator protein-1 (CRMP1) acts as an invasion and metastasis suppressor of prostate cancer via its suppression of epithelial-mesenchymal transition and remodeling of actin cytoskeleton organization', *Oncogene*, 36: 546-58.

Camasses, A., A. Bogdanova, A. Shevchenko, and W. Zachariae. 2003. 'The CCT chaperonin promotes activation of the anaphase-promoting complex through the generation of functional Cdc20', *Mol Cell*, 12: 87-100.

Carlier, M. F., C. Simon, R. Cassoly, and L. A. Pradel. 1984. 'Interaction between microtubule-associated protein tau and spectrin', *Biochimie*, 66: 305-11.

Caron, J. M. 1997. 'Posttranslational modification of tubulin by palmitoylation: I. In vivo and cell-free studies', *Mol Biol Cell*, 8: 621-36.

Caron, J. M., L. R. Vega, J. Fleming, R. Bishop, and F. Solomon. 2001. 'Single site alpha-tubulin mutation affects astral microtubules and nuclear positioning during anaphase in Saccharomyces cerevisiae: possible role for palmitoylation of alpha-tubulin', *Mol Biol Cell*, 12: 2672-87.

Carstens, P. D., A. R. Sharifi, T. S. Brand, and L. C. Hoffman. 2014. 'The growth response of ostrich (Struthio camelus var. domesticus) chicks fed on diets with three different dietary protein and amino acid concentrations', *Br Poult Sci*, 55: 510-7.

Caspi, M., R. Atlas, A. Kantor, T. Sapir, and O. Reiner. 2000. 'Interaction between LIS1 and doublecortin, two lissencephaly gene products', *Hum Mol Genet*, 9: 2205-13.

Caudron, F., E. Denarier, J. C. Thibout-Quintana, J. Brocard, A. Andrieux, and A. Fourest-Lieuvin. 2010. 'Mutation of Ser172 in yeast beta tubulin induces defects in microtubule dynamics and cell division', *PLoS One*, 5: e13553.

Chakraborti, S., K. Natarajan, J. Curiel, C. Janke, and J. Liu. 2016. 'The emerging role of the tubulin code: From the tubulin molecule to neuronal function and disease', *Cytoskeleton (Hoboken)*, 73: 521-50.

Chang-Jie, J., and S. Sonobe. 1993. 'Identification and preliminary characterization of a 65 kDa higher-plant microtubule-associated protein', *J Cell Sci*, 105 (Pt 4): 891-901.

Chapin, S. J., and J. C. Bulinski. 1994. 'Cellular microtubules heterogeneous in their content of microtubule-associated protein 4 (MAP4)', *Cell Motil Cytoskeleton*, 27: 133-49.

Charrier, E., S. Reibel, V. Rogemond, M. Aguera, N. Thomasset, and J. Honnorat. 2003. 'Collapsin response mediator proteins (CRMPs): involvement in nervous system development and adult neurodegenerative disorders', *Mol Neurobiol*, 28: 51-64.

Chaudhary, A. R., F. Berger, C. L. Berger, and A. G. Hendricks. 2018. 'Tau directs intracellular trafficking by regulating the forces exerted by kinesin and dynein teams', *Traffic*, 19: 111-21.

Chaves, R. S., T. Q. Melo, A. M. D'Unhao, K. L. Farizatto, and M. F. Ferrari. 2013. 'Dynein c1h1, dynactin and syntaphilin expression in brain areas related to neurodegenerative diseases following exposure to rotenone', *Acta Neurobiol Exp (Wars)*, 73: 541-56.

Chen, D., S. Ito, H. Yuan, T. Hyodo, K. Kadomatsu, M. Hamaguchi, and T. Senga. 2015. 'EML4 promotes the loading of NUDC to the spindle for mitotic progression', *Cell Cycle*, 14: 1529-39.

Chen, G. Y., J. M. Cleary, A. B. Asenjo, Y. Chen, J. A. Mascaro, D. F. J. Arginteanu, H. Sosa, and W. O. Hancock. 2019. 'Kinesin-5 Promotes Microtubule Nucleation and Assembly by Stabilizing a Lattice-Competent Conformation of Tubulin', *Curr Biol*, 29: 2259-69 e4.

Chen, H. J., C. M. Lin, C. S. Lin, R. Perez-Olle, C. L. Leung, and R. K. Liem. 2006. 'The role of microtubule actin cross-linking factor 1 (MACF1) in the Wnt signaling pathway', *Genes Dev*, 20: 1933-45.

Chen, J., Y. Kanai, N. J. Cowan, and N. Hirokawa. 1992. 'Projection domains of MAP2 and tau determine spacings between microtubules in dendrites and axons', *Nature*, 360: 674-7.

Chen, J., M. Rajasekaran, H. Xia, X. Zhang, S. N. Kong, K. Sekar, V. P. Seshachalam, A. Deivasigamani, B. K. Goh, L. L. Ooi, W. Hong, and K. M. Hui. 2016. 'The microtubule-associated protein PRC1 promotes early recurrence of hepatocellular carcinoma in association with the Wnt/beta-catenin signalling pathway', *Gut*, 65: 1522-34.

Chen, S. L., S. R. Cai, X. H. Zhang, W. F. Li, E. T. Zhai, J. J. Peng, H. Wu, C. Q. Chen, J. P. Ma, Z. Wang, and Y. L. He. 2016. 'Targeting CRMP-4 by lentivirus-mediated RNA interference inhibits SW480 cell proliferation and colorectal cancer growth', *Exp Ther Med*, 12: 2003-08.

Chen, X. J., H. Xu, H. M. Cooper, and Y. Liu. 2014. 'Cytoplasmic dynein: a key player in neurodegenerative and neurodevelopmental diseases', *Sci China Life Sci*, 57: 372-7.

Chen, Y., and W. O. Hancock. 2015. 'Kinesin-5 is a microtubule polymerase', *Nat Commun*, 6: 8160.

Chen, Y. M., C. Gerwin, and Z. H. Sheng. 2009. 'Dynein light chain LC8 regulates syntaphilin-mediated mitochondrial docking in axons', *J Neurosci*, 29: 9429-38.

Chen, Y., and Z. H. Sheng. 2013. 'Kinesin-1-syntaphilin coupling mediates activity-dependent regulation of axonal mitochondrial transport', *J Cell Biol*, 202: 351-64.

Chen, Y., P. Wang, and K. C. Slep. 2019. 'Mapping multivalency in the CLIP-170-EB1 microtubule plus-end complex', *J Biol Chem*, 294: 918-31.

Cheng, L., J. Desai, C. J. Miranda, J. S. Duncan, W. Qiu, A. A. Nugent, A. L. Kolpak, C. C. Wu, E. Drokhlyansky, M. M. Delisle, W. M. Chan, Y. Wei, F. Propst, S. L. Reck-Peterson, B. Fritzsch, and E. C. Engle. 2014. 'Human CFEOM1 mutations attenuate KIF21A autoinhibition and cause oculomotor axon stalling', *Neuron*, 82: 334-49.

Chesneau, V., A. Prat, D. Segretain, V. Hospital, A. Dupaix, T. Foulon, B. Jegou, and P. Cohen. 1996. 'NRD convertase: a putative processing endoprotease associated with the axoneme and the manchette in late spermatids', *J Cell Sci*, 109 (Pt 11): 2737-45.

Choi, J. H., P. G. Bertram, R. Drenan, J. Carvalho, H. H. Zhou, and X. F. Zheng. 2002. 'The FKBP12-rapamycin-associated protein (FRAP) is a CLIP-170 kinase', *EMBO Rep*, 3: 988-94.

Choi, J. M., M. S. Woo, H. I. Ma, S. Y. Kang, Y. H. Sung, S. W. Yong, S. J. Chung, J. S. Kim, H. W. Shin, C. H. Lyoo, P. H. Lee, J. S. Baik, S. J. Kim, M. Y. Park, Y. H. Sohn, J. H. Kim, J. W. Kim, M. S. Lee, M. C. Lee, D. H. Kim, and Y. J. Kim. 2008. 'Analysis of PARK genes in a Korean cohort of early-onset Parkinson disease', *Neurogenetics*, 9: 263-9.

Choi, M. C., U. Raviv, H. P. Miller, M. R. Gaylord, E. Kiris, D. Ventimiglia, D. J. Needleman, M. W. Kim, L. Wilson, S. C. Feinstein, and C. R. Safinya. 2009. 'Human microtubule-associated-protein tau regulates the number of protofilaments in microtubules: a synchrotron x-ray scattering study', *Biophys J*, 97: 519-27.

Choi, P., N. Golts, H. Snyder, M. Chong, L. Petrucelli, J. Hardy, D. Sparkman, E. Cochran, J. M. Lee, and B. Wolozin. 2001. 'Co-association of parkin and alpha-synuclein', *Neuroreport*, 12: 2839-43.

Choi, P., H. Snyder, L. Petrucelli, C. Theisler, M. Chong, Y. Zhang, K. Lim, K. K. Chung, K. Kehoe, L. D'Adamio, J. M. Lee, E. Cochran, R. Bowser, T. M. Dawson, and B. Wolozin. 2003. 'SEPT5_v2 is a parkin-binding protein', *Brain Res Mol Brain Res*, 117: 179-89.

Chretien, D., F. Metoz, F. Verde, E. Karsenti, and R. H. Wade. 1992. 'Lattice defects in microtubules: protofilament numbers vary within individual microtubules', *J Cell Biol*, 117: 1031-40.

Chu, C. W., F. Hou, J. Zhang, L. Phu, A. V. Loktev, D. S. Kirkpatrick, P. K. Jackson, Y. Zhao, and H. Zou. 2011. 'A novel acetylation of beta-tubulin by San modulates microtubule polymerization via down-regulating tubulin incorporation', *Mol Biol Cell*, 22: 448-56.

Chung, K. K., Y. Zhang, K. L. Lim, Y. Tanaka, H. Huang, J. Gao, C. A. Ross, V. L. Dawson, and T. M. Dawson. 2001. 'Parkin ubiquitinates the alpha-synuclein-interacting protein, synphilin-1: implications for Lewy-body formation in Parkinson disease', *Nat Med*, 7: 1144-50.

Church, A. J., M. L. Calicchio, V. Nardi, A. Skalova, A. Pinto, D. A. Dillon, C. R. Gomez-Fernandez, N. Manoj, J. D. Haimes, J. A. Stahl, F. S. Dela Cruz, S. Tannenbaum-Dvir, J. L. Glade-Bender, A. L. Kung, S. G. DuBois, H. P. Kozakewich, K. A. Janeway, A. R. Perez-Atayde, and M. H. Harris. 2018. 'Recurrent EML4-NTRK3 fusions in infantile fibrosarcoma and congenital mesoblastic nephroma suggest a revised testing strategy', *Mod Pathol*, 31: 463-73.

Cifuentes-Diaz, C., F. Chareyre, M. Garcia, J. Devaux, M. Carnaud, G. Levasseur, M. Niwa-Kawakita, S. Harroch, J. A. Girault, M. Giovannini, and L. Goutebroze. 2011. 'Protein 4.1B contributes to the organization of peripheral myelinated axons', *PLoS One*, 6: e25043.

Citi, S., P. Pulimeno, and S. Paschoud. 2012. 'Cingulin, paracingulin, and PLEKHA7: signaling and cytoskeletal adaptors at the apical junctional complex', *Ann N Y Acad Sci*, 1257: 125-32.

Citi, S., H. Sabanay, R. Jakes, B. Geiger, and J. Kendrick-Jones. 1988a. 'Cingulin, a new peripheral component of tight junctions', *Nature*, 333: 272-6.

———. 1988b. 'Cingulin, a new peripheral component of tight junctions', *Nature*, 333: 272-6.

Citi, S., H. Sabanay, J. Kendrick-Jones, and B. Geiger. 1989. 'Cingulin: characterization and localization', *J Cell Sci*, 93 (Pt 1): 107-22.

Cleveland, D. W. 1989. 'Autoregulated control of tubulin synthesis in animal cells', *Curr Opin Cell Biol*, 1: 10-4.

Cleveland, D. W., M. W. Kirschner, and N. J. Cowan. 1978. 'Isolation of separate mRNAs for alpha- and beta-tubulin and characterization of the corresponding in vitro translation products', *Cell*, 15: 1021-31.

Cleveland, D. W., M. A. Lopata, R. J. MacDonald, N. J. Cowan, W. J. Rutter, and M. W. Kirschner. 1980. 'Number and evolutionary conservation of alpha- and beta-tubulin and cytoplasmic beta- and gamma-actin genes using specific cloned cDNA probes', *Cell*, 20: 95-105.

Cocas, L., and S. J. Pleasure. 2014. 'Wrong place, wrong time: ectopic progenitors cause cortical heterotopias', *Nat Neurosci*, 17: 894-5.

Cohen, D. A., M. T. Bhatti, J. S. Pulido, V. A. Lennon, D. Dubey, E. P. Flanagan, S. J. Pittock, C. J. Klein, and J. J. Chen. 2020. 'Collapsin Response-Mediator Protein 5-Associated Retinitis, Vitritis, and Optic Disc Edema', *Ophthalmology*, 127: 221-29.

Colin, A., P. Singaravelu, M. Thery, L. Blanchoin, and Z. Gueroui. 2018. 'Actin-Network Architecture Regulates Microtubule Dynamics', *Curr Biol*, 28: 2647-56 e4.

Cordenonsi, M., F. D'Atri, E. Hammar, D. A. Parry, J. Kendrick-Jones, D. Shore, and S. Citi. 1999. 'Cingulin contains globular and coiled-coil domains and interacts with ZO-1, ZO-2, ZO-3, and myosin', *J Cell Biol*, 147: 1569-82.

Correas, I., R. Padilla, and J. Avila. 1990. 'The tubulin-binding sequence of brain microtubule-associated proteins, tau and MAP-2, is also involved in actin binding', *Biochem J*, 269: 61-4.

Corti, O., C. Hampe, H. Koutnikova, F. Darios, S. Jacquier, A. Prigent, J. C. Robinson, L. Pradier, M. Ruberg, M. Mirande, E. Hirsch, T. Rooney, A. Fournier, and A. Brice. 2003. 'The p38 subunit of the aminoacyl-tRNA synthetase complex is a Parkin substrate: linking protein biosynthesis and neurodegeneration', *Hum Mol Genet*, 12: 1427-37.

Cuenca, A., C. Insinna, H. Zhao, P. John, M. A. Weiss, Q. Lu, V. Walia, S. Specht, S. Manivannan, J. Stauffer, A. A. Peden, and C. J. Westlake. 2019. 'The C7orf43/TRAPPC14 component links the TRAPPII complex to Rabin8 for preciliary vesicle tethering at the mother centriole during ciliogenesis', *J Biol Chem*, 294: 15418-34.

Cui, J., J. Reed, G. Crynen, G. Ait-Ghezala, F. Crawford, Y. Shen, and R. Li. 2019. 'Proteomic Identification of Pathways Responsible for the Estradiol Therapeutic Window in AD Animal Models', *Front Cell Neurosci*, 13: 437.

Cuveillier, C., J. Delaroche, M. Seggio, S. Gory-Faure, C. Bosc, E. Denarier, M. Bacia, G. Schoehn, H. Mohrbach, I. Kulic, A. Andrieux, I. Arnal, and C. Delphin. 2020. 'MAP6 is an intraluminal protein that induces neuronal microtubules to coil', *Sci Adv*, 6: eaaz4344.

D'Alessio, L., H. Konopka, E. M. Lopez, E. Seoane, D. Consalvo, S. Oddo, S. Kochen, and J. J. Lopez-Costa. 2010. 'Doublecortin (DCX) immunoreactivity in hippocampus of chronic refractory temporal lobe epilepsy patients with hippocampal sclerosis', *Seizure*, 19: 567-72.

D'Atri, F., and S. Citi. 2001a. 'Cingulin interacts with F-actin in vitro', *FEBS Lett*, 507: 21-4.

———. 2001b. 'Cingulin interacts with F-actin in vitro', *FEBS Lett*, 507: 21-4.

Dacheux, D., N. Landrein, M. Thonnus, G. Gilbert, A. Sahin, H. Wodrich, D. R. Robinson, and M. Bonhivers. 2012. 'A MAP6-related protein is present in protozoa and is involved in flagellum motility', *PLoS One*, 7: e31344.

Dacheux, D., B. Roger, C. Bosc, N. Landrein, E. Roche, L. Chansel, T. Trian, A. Andrieux, A. Papaxanthos-Roche, R. Marthan, D. R. Robinson, and M. Bonhivers. 2015. 'Human

FAM154A (SAXO1) is a microtubule-stabilizing protein specific to cilia and related structures', *J Cell Sci*, 128: 1294-307.

Daoust, A., S. Bohic, Y. Saoudi, C. Debacker, S. Gory-Faure, A. Andrieux, E. L. Barbier, and J. C. Deloulme. 2014. 'Neuronal transport defects of the MAP6 KO mouse - a model of schizophrenia - and alleviation by Epothilone D treatment, as observed using MEMRI', *Neuroimage*, 96: 133-42.

Davare, M. A., F. Dong, C. S. Rubin, and J. W. Hell. 1999. 'The A-kinase anchor protein MAP2B and cAMP-dependent protein kinase are associated with class C L-type calcium channels in neurons', *J Biol Chem*, 274: 30280-7.

Dawson, T. M., and V. L. Dawson. 2010. 'The role of parkin in familial and sporadic Parkinson's disease', *Mov Disord*, 25 Suppl 1: S32-9.

de Forges, H., A. Pilon, I. Cantaloube, A. Pallandre, A. M. Haghiri-Gosnet, F. Perez, and C. Pous. 2016. 'Localized Mechanical Stress Promotes Microtubule Rescue', *Curr Biol*, 26: 3399-406.

De Keersmaecker, K., C. Graux, M. D. Odero, N. Mentens, R. Somers, J. Maertens, I. Wlodarska, P. Vandenberghe, A. Hagemeijer, P. Marynen, and J. Cools. 2005. 'Fusion of EML1 to ABL1 in T-cell acute lymphoblastic leukemia with cryptic t(9;14)(q34;q32)', *Blood*, 105: 4849-52.

Delabie, J., R. Shipman, J. Bruggen, B. De Strooper, F. van Leuven, L. Tarcsay, N. Cerletti, K. Odink, V. Diehl, G. Bilbe, and et al. 1992. 'Expression of the novel intermediate filament-associated protein restin in Hodgkin's disease and anaplastic large-cell lymphoma', *Blood*, 80: 2891-6.

Delous, M., L. Baala, R. Salomon, C. Laclef, J. Vierkotten, K. Tory, C. Golzio, T. Lacoste, L. Besse, C. Ozilou, I. Moutkine, N. E. Hellman, I. Anselme, F. Silbermann, C. Vesque, C. Gerhardt, E. Rattenberry, M. T. Wolf, M. C. Gubler, J. Martinovic, F. Encha-Razavi, N. Boddaert, M. Gonzales, M. A. Macher, H. Nivet, G. Champion, J. P. Bertheleme, P. Niaudet, F. McDonald, F. Hildebrandt, C. A. Johnson, M. Vekemans, C. Antignac, U. Ruther, S. Schneider-Maunoury, T. Attie-Bitach, and S. Saunier. 2007. 'The ciliary gene RPGRIP1L is mutated in cerebello-oculo-renal syndrome (Joubert syndrome type B) and Meckel syndrome', *Nat Genet*, 39: 875-81.

des Portes, V., F. Francis, J. M. Pinard, I. Desguerre, M. L. Moutard, I. Snoeck, L. C. Meiners, F. Capron, R. Cusmai, S. Ricci, J. Motte, B. Echenne, G. Ponsot, O. Dulac, J. Chelly, and C. Beldjord. 1998. 'doublecortin is the major gene causing X-linked subcortical laminar heterotopia (SCLH)', *Hum Mol Genet*, 7: 1063-70.

des Portes, V., J. M. Pinard, P. Billuart, M. C. Vinet, A. Koulakoff, A. Carrie, A. Gelot, E. Dupuis, J. Motte, Y. Berwald-Netter, M. Catala, A. Kahn, C. Beldjord, and J. Chelly. 1998. 'A novel CNS gene required for neuronal migration and involved in X-linked subcortical laminar heterotopia and lissencephaly syndrome', *Cell*, 92: 51-61.

Desai, A., and T. J. Mitchison. 1997. 'Microtubule polymerization dynamics', *Annu Rev Cell Dev Biol*, 13: 83-117.

Desai, A., S. Verma, T. J. Mitchison, and C. E. Walczak. 1999. 'Kin I kinesins are microtubule-destabilizing enzymes', *Cell*, 96: 69-78.

Deuel, T. A., J. S. Liu, J. C. Corbo, S. Y. Yoo, L. B. Rorke-Adams, and C. A. Walsh. 2006. 'Genetic interactions between doublecortin and doublecortin-like kinase in neuronal migration and axon outgrowth', *Neuron*, 49: 41-53.

Dhana, K., K. V. E. Braun, J. Nano, T. Voortman, E. W. Demerath, W. Guan, M. Fornage, J. B. J. van Meurs, A. G. Uitterlinden, A. Hofman, O. H. Franco, and A. Dehghan. 2018. 'An Epigenome-Wide Association Study of Obesity-Related Traits', *Am J Epidemiol*, 187: 1662-69.

Di Benedetto, M., I. Bieche, F. Deshayes, S. Vacher, S. Nouet, V. Collura, I. Seitz, S. Louis, P. Pineau, D. Amsellem-Ouazana, P. O. Couraud, A. D. Strosberg, D. Stoppa-Lyonnet, R. Lidereau, and C. Nahmias. 2006. 'Structural organization and expression of human MTUS1, a candidate 8p22 tumor suppressor gene encoding a family of angiotensin II AT2 receptor-interacting proteins, ATIP', *Gene*, 380: 127-36.

Di Benedetto, M., P. Pineau, S. Nouet, S. Berhouet, I. Seitz, S. Louis, A. Dejean, P. O. Couraud, A. D. Strosberg, D. Stoppa-Lyonnet, and C. Nahmias. 2006. 'Mutation analysis of the 8p22 candidate tumor suppressor gene ATIP/MTUS1 in hepatocellular carcinoma', *Mol Cell Endocrinol*, 252: 207-15.

Diamantopoulos, G. S., F. Perez, H. V. Goodson, G. Batelier, R. Melki, T. E. Kreis, and J. E. Rickard. 1999. 'Dynamic localization of CLIP-170 to microtubule plus ends is coupled to microtubule assembly', *J Cell Biol*, 144: 99-112.

Ding, J., E. Allen, W. Wang, A. Valle, C. Wu, T. Nardine, B. Cui, J. Yi, A. Taylor, N. L. Jeon, S. Chu, Y. So, H. Vogel, R. Tolwani, W. Mobley, and Y. Yang. 2006. 'Gene targeting of GAN in mouse causes a toxic accumulation of microtubule-associated protein 8 and impaired retrograde axonal transport', *Hum Mol Genet*, 15: 1451-63.

Ding, J., A. Valle, E. Allen, W. Wang, T. Nardine, Y. Zhang, L. Peng, and Y. Yang. 2006. 'Microtubule-associated protein 8 contains two microtubule binding sites', *Biochem Biophys Res Commun*, 339: 172-9.

Ding, X., N. Zhang, Y. Cai, S. Li, C. Zheng, Y. Jin, T. Yu, A. Wang, and X. Zhou. 2012. 'Down-regulation of tumor suppressor MTUS1/ATIP is associated with enhanced proliferation, poor differentiation and poor prognosis in oral tongue squamous cell carcinoma', *Mol Oncol*, 6: 73-80.

Dionne, M. A., A. Sanchez, and D. A. Compton. 2000. 'ch-TOGp is required for microtubule aster formation in a mammalian mitotic extract', *J Biol Chem*, 275: 12346-52.

Dixit, R., B. Barnett, J. E. Lazarus, M. Tokito, Y. E. Goldman, and E. L. Holzbaur. 2009. 'Microtubule plus-end tracking by CLIP-170 requires EB1', *Proc Natl Acad Sci U S A*, 106: 492-7.

Dixit, R., J. L. Ross, Y. E. Goldman, and E. L. Holzbaur. 2008. 'Differential regulation of dynein and kinesin motor proteins by tau', *Science*, 319: 1086-9.

Dobyns, W. B., K. A. Aldinger, G. E. Ishak, G. M. Mirzaa, A. E. Timms, M. E. Grout, M. H. G. Dremmen, R. Schot, L. Vandervore, M. A. van Slegtenhorst, M. Wilke, E. Kasteleijn, A. S. Lee, B. J. Barry, K. R. Chao, K. Szczaluba, J. Kobori, A. Hanson-Kahn, J. A. Bernstein, L. Carr, F. D'Arco, K. Miyana, T. Okazaki, Y. Saito, M. Sasaki, S. Das, M. M. Wheeler, M. J. Bamshad, D. A. Nickerson, Genomics University of Washington Center for Mendelian, M. I. T. Center for Mendelian Genomics at the Broad Institute of, Harvard, E. C. Engle, F. W. Verheijen, D. Doherty, and G. M. S. Mancini. 2018. 'MACF1 Mutations Encoding Highly Conserved Zinc-Binding Residues of the GAR Domain Cause Defects in Neuronal Migration and Axon Guidance', *Am J Hum Genet*, 103: 1009-21.

Dogterom, M., and G. H. Koenderink. 2019. 'Actin-microtubule crosstalk in cell biology', *Nat Rev Mol Cell Biol*, 20: 38-54.

Dogterom, M., and T. Surrey. 2013. 'Microtubule organization in vitro', *Curr Opin Cell Biol*, 25: 23-9.

Doki, C., K. Nishida, S. Saito, M. Shiga, H. Ogara, A. Kuramoto, M. Kuragano, M. Nozumi, M. Igarashi, H. Nakagawa, S. Kotani, and K. Tokuraku. 2020. 'Microtubule elongation along actin filaments induced by microtubule-associated protein 4 contributes to the formation of cellular protrusions', *J Biochem*.

Dou, F., W. J. Netzer, K. Tanemura, F. Li, F. U. Hartl, A. Takashima, G. K. Gouras, P. Greengard, and H. Xu. 2003. 'Chaperones increase association of tau protein with microtubules', *Proc Natl Acad Sci U S A*, 100: 721-6.

Drechsel, D. N., and M. W. Kirschner. 1994. 'The minimum GTP cap required to stabilize microtubules', *Curr Biol*, 4: 1053-61.

Dubey, D., V. A. Lennon, A. Gadoth, S. J. Pittock, E. P. Flanagan, J. E. Schmeling, A. McKeon, and C. J. Klein. 2018. 'Autoimmune CRMP5 neuropathy phenotype and outcome defined from 105 cases', *Neurology*, 90: e103-e10.

Ducray, S. P., K. Natarajan, G. D. Garland, S. D. Turner, and G. Egger. 2019. 'The Transcriptional Roles of ALK Fusion Proteins in Tumorigenesis', *Cancers (Basel)*, 11.

Dumont, E. L., C. Do, and H. Hess. 2015. 'Molecular wear of microtubules propelled by surface-adhered kinesins', *Nat Nanotechnol*, 10: 166-9.

Dunn, A. Y., M. W. Melville, and J. Frydman. 2001. 'Review: cellular substrates of the eukaryotic chaperonin TRiC/CCT', *J Struct Biol*, 135: 176-84.

Dunn, S., E. E. Morrison, T. B. Liverpool, C. Molina-Paris, R. A. Cross, M. C. Alonso, and M. Peckham. 2008. 'Differential trafficking of Kif5c on tyrosinated and detyrosinated microtubules in live cells', *J Cell Sci*, 121: 1085-95.

Duselder, A., V. Fridman, C. Thiede, A. Wiesbaum, A. Goldstein, D. R. Klopfenstein, O. Zaitseva, M. E. Janson, L. Gheber, and C. F. Schmidt. 2015. 'Deletion of the Tail Domain of the Kinesin-5 Cin8 Affects Its Directionality', *J Biol Chem*, 290: 16841-50.

Dutta, P., A. S. Jijumon, M. Mazumder, D. Dileep, A. K. Mukhopadhyay, S. Gourinath, and S. Maiti. 2019. 'Presence of actin binding motif in VgrG-1 toxin of Vibrio cholerae reveals the molecular mechanism of actin cross-linking', *Int J Biol Macromol*, 133: 775-85.

Dymek, E. E., J. Lin, G. Fu, M. E. Porter, D. Nicastro, and E. F. Smith. 2019. 'PACRG and FAP20 form the inner junction of axonemal doublet microtubules and regulate ciliary motility', *Mol Biol Cell*, 30: 1805-16.

Ebina, H., L. Ji, and M. Sato. 2019. 'CLASP promotes microtubule bundling in metaphase spindle independently of Ase1/PRC1 in fission yeast', *Biol Open*, 8.

Edde, B., J. Rossier, J. P. Le Caer, E. Desbruyeres, F. Gros, and P. Denoulet. 1990. 'Posttranslational glutamylation of alpha-tubulin', *Science*, 247: 83-5.

Eichenmuller, B., P. Everley, J. Palange, D. Lepley, and K. A. Suprenant. 2002. 'The human EMAP-like protein-70 (ELP70) is a microtubule destabilizer that localizes to the mitotic apparatus', *J Biol Chem*, 277: 1301-9.

Elie, A., E. Prezel, C. Guerin, E. Denarier, S. Ramirez-Rios, L. Serre, A. Andrieux, A. Fourest-Lieuvin, L. Blanchoin, and I. Arnal. 2015. 'Tau co-organizes dynamic microtubule and actin networks', *Sci Rep*, 5: 9964.

Endow, S. A., F. J. Kull, and H. Liu. 2010. 'Kinesins at a glance', *J Cell Sci*, 123: 3420-4.

Eot-Houllier, G., M. Venoux, S. Vidal-Eychenie, M. T. Hoang, D. Giorgi, and S. Rouquier. 2010. 'Plk1 regulates both ASAP localization and its role in spindle pole integrity', *J Biol Chem*, 285: 29556-68.

Erck, C., L. Peris, A. Andrieux, C. Meissirel, A. D. Gruber, M. Vernet, A. Schweitzer, Y. Saoudi, H. Pointu, C. Bosc, P. A. Salin, D. Job, and J. Wehland. 2005. 'A vital role of tubulin-tyrosine-ligase for neuronal organization', *Proc Natl Acad Sci U S A*, 102: 7853-8.

Eriksson, J. E., T. Dechat, B. Grin, B. Helfand, M. Mendez, H. M. Pallari, and R. D. Goldman. 2009. 'Introducing intermediate filaments: from discovery to disease', *J Clin Invest*, 119: 1763-71.

Ersfeld, K., J. Wehland, U. Plessmann, H. Dodemont, V. Gerke, and K. Weber. 1993. 'Characterization of the tubulin-tyrosine ligase', *J Cell Biol*, 120: 725-32.

Eschbach, J., and L. Dupuis. 2011. 'Cytoplasmic dynein in neurodegeneration', *Pharmacol Ther*, 130: 348-63.

Eudy, J. D., M. Ma-Edmonds, S. F. Yao, C. B. Talmadge, P. M. Kelley, M. D. Weston, W. J. Kimberling, and J. Sumegi. 1997. 'Isolation of a novel human homologue of the gene coding for echinoderm microtubule-associated protein (EMAP) from the Usher syndrome type 1a locus at 14q32', *Genomics*, 43: 104-6.

Even, A., G. Morelli, L. Broix, C. Scaramuzzino, S. Turchetto, I. Gladwyn-Ng, R. Le Bail, M. Shilian, S. Freeman, M. M. Magiera, A. S. Jijumon, N. Krusy, B. Malgrange, B. Brone, P. Dietrich, I. Dragatsis, C. Janke, F. Saudou, M. Weil, and L. Nguyen. 2019. 'ATAT1-enriched vesicles promote microtubule acetylation via axonal transport', *Sci Adv*, 5: eaax2705.

Fairbanks, G., T. L. Steck, and D. F. Wallach. 1971. 'Electrophoretic analysis of the major polypeptides of the human erythrocyte membrane', *Biochemistry*, 10: 2606-17.

Faller, E. M., and D. L. Brown. 2009. 'Modulation of microtubule dynamics by the microtubule-associated protein 1a', *J Neurosci Res*, 87: 1080-9.

Fallon, L., F. Moreau, B. G. Croft, N. Labib, W. J. Gu, and E. A. Fon. 2002. 'Parkin and CASK/LIN-2 associate via a PDZ-mediated interaction and are co-localized in lipid rafts and postsynaptic densities in brain', *J Biol Chem*, 277: 486-91.

Fan, J., S. G. Mansfield, T. Redmond, P. R. Gordon-Weeks, and J. A. Raper. 1993. 'The organization of F-actin and microtubules in growth cones exposed to a brain-derived collapsing factor', *J Cell Biol*, 121: 867-78.

Fanara, P., K. H. Husted, K. Selle, P. Y. Wong, J. Banerjee, R. Brandt, and M. K. Hellerstein. 2010. 'Changes in microtubule turnover accompany synaptic plasticity and memory formation in response to contextual fear conditioning in mice', *Neuroscience*, 168: 167-78.

Farah, C. A., D. Liazoghli, S. Perreault, M. Desjardins, A. Guimont, A. Anton, M. Lauzon, G. Kreibich, J. Paiement, and N. Leclerc. 2005. 'Interaction of microtubule-associated protein-2 and p63: a new link between microtubules and rough endoplasmic reticulum membranes in neurons', *J Biol Chem*, 280: 9439-49.

Farah, C. A., M. D. Nguyen, J. P. Julien, and N. Leclerc. 2003. 'Altered levels and distribution of microtubule-associated proteins before disease onset in a mouse model of amyotrophic lateral sclerosis', *J Neurochem*, 84: 77-86.

Farina, F., N. Ramkumar, L. Brown, D. Samandar Eweis, J. Anstatt, T. Waring, J. Bithell, G. Scita, M. Thery, L. Blanchoin, T. Zech, and B. Baum. 2019. 'Local actin nucleation tunes centrosomal microtubule nucleation during passage through mitosis', *EMBO J*, 38.

Fassier, C., A. Freal, L. Gasmi, C. Delphin, D. Ten Martin, S. De Gois, M. Tambalo, C. Bosc, P. Mailly, C. Revenu, L. Peris, S. Bolte, S. Schneider-Maunoury, C. Houart, F. Nothias, J. C. Larcher, A. Andrieux, and J. Hazan. 2018. 'Motor axon navigation relies on Fidgetin-like 1-driven microtubule plus end dynamics', *J Cell Biol*, 217: 1719-38.

Fededa, J. P., and D. W. Gerlich. 2012. 'Molecular control of animal cell cytokinesis', *Nat Cell Biol*, 14: 440-7.

Feng, J. 2006. 'Microtubule: a common target for parkin and Parkinson's disease toxins', *Neuroscientist*, 12: 469-76.

Feng, S., Y. Song, M. Shen, S. Xie, W. Li, Y. Lu, Y. Yang, G. Ou, J. Zhou, F. Wang, W. Liu, X. Yan, X. Liang, and T. Zhou. 2017. 'Microtubule-binding protein FOR20 promotes microtubule depolymerization and cell migration', *Cell Discov*, 3: 17032.

Ferhat, L., A. Represa, A. Bernard, Y. Ben-Ari, and M. Khrestchatisky. 1996. 'MAP2d promotes bundling and stabilization of both microtubules and microfilaments', *J Cell Sci*, 109 (Pt 5): 1095-103.

Fernandez, J., D. M. Portilho, A. Danckaert, S. Munier, A. Becker, P. Roux, A. Zambo, S. Shorte, Y. Jacob, P. O. Vidalain, P. Charneau, F. Clavel, and N. J. Arhel. 2015. 'Microtubule-associated proteins 1 (MAP1) promote human immunodeficiency virus type I (HIV-1) intracytoplasmic routing to the nucleus', *J Biol Chem*, 290: 4631-46.

Ferreyra, R. G., and J. Frydman. 2000. 'Purification of the cytosolic chaperonin TRiC from bovine testis', *Methods Mol Biol*, 140: 153-60.

Findeisen, P., S. Muhlhausen, S. Dempewolf, J. Hertzog, A. Zietlow, T. Carlomagno, and M. Kollmar. 2014. 'Six subgroups and extensive recent duplications characterize the evolution of the eukaryotic tubulin protein family', *Genome Biol Evol*, 6: 2274-88.

Fletcher, D. A. 2010. 'On force and function', *Mol Biol Cell*, 21: 3795-6.

Fong, K. W., J. W. Leung, Y. Li, W. Wang, L. Feng, W. Ma, D. Liu, Z. Songyang, and J. Chen. 2013. 'MTR120/KIAA1383, a novel microtubule-associated protein, promotes microtubule stability and ensures cytokinesis', *J Cell Sci*, 126: 825-37.

Fontenille, L., S. Rouquier, G. Lutfalla, and D. Giorgi. 2014. 'Microtubule-associated protein 9 (Map9/Asap) is required for the early steps of zebrafish development', *Cell Cycle*, 13: 1101-14.

Forth, S., K. C. Hsia, Y. Shimamoto, and T. M. Kapoor. 2014. 'Asymmetric friction of nonmotor MAPs can lead to their directional motion in active microtubule networks', *Cell*, 157: 420-32.

Fouquet, J. P., B. Edde, M. L. Kann, A. Wolff, E. Desbruyeres, and P. Denoulet. 1994. 'Differential distribution of glutamylated tubulin during spermatogenesis in mammalian testis', *Cell Motil Cytoskeleton*, 27: 49-58.

Fourniol, F. J., C. V. Sindelar, B. Amigues, D. K. Clare, G. Thomas, M. Perderiset, F. Francis, A. Houdusse, and C. A. Moores. 2010. 'Template-free 13-protofilament microtubule-MAP assembly visualized at 8 A resolution', *J Cell Biol*, 191: 463-70.

Francis, F., A. Koulakoff, D. Boucher, P. Chafey, B. Schaar, M. C. Vinet, G. Friocourt, N. McDonnell, O. Reiner, A. Kahn, S. K. McConnell, Y. Berwald-Netter, P. Denoulet, and J. Chelly. 1999. 'Doublecortin is a developmentally regulated, microtubule-associated protein expressed in migrating and differentiating neurons', *Neuron*, 23: 247-56.

Frickey, T., and A. N. Lupas. 2004. 'Phylogenetic analysis of AAA proteins', *J Struct Biol*, 146: 2-10.

Friedrichs, P., A. Schlotterer, C. Sticht, M. Kolibabka, P. Wohlfart, A. Dietrich, T. Linn, G. Molema, and H. P. Hammes. 2017. 'Hyperglycaemic memory affects the neurovascular unit of the retina in a diabetic mouse model', *Diabetologia*, 60: 1354-58.

Fry, A. M., L. O'Regan, J. Montgomery, R. Adib, and R. Bayliss. 2016. 'EML proteins in microtubule regulation and human disease', *Biochem Soc Trans*, 44: 1281-88.

Fu, C., J. J. Ward, I. Loiodice, G. Velve-Casquillas, F. J. Nedelec, and P. T. Tran. 2009. 'Phospho-regulated interaction between kinesin-6 Klp9p and microtubule bundler Ase1p promotes spindle elongation', *Dev Cell*, 17: 257-67.

Fu, L., H. Fu, L. Zhou, K. Xu, Y. Pang, K. Hu, J. Wang, L. Tian, Y. Liu, J. Wang, H. Jing, W. Huang, X. Ke, and J. Shi. 2016. 'High expression of MAP7 predicts adverse prognosis in young patients with cytogenetically normal acute myeloid leukemia', *Sci Rep*, 6: 34546.

Fujisawa, S., S. Nakamura, K. Naito, M. Kobayashi, and K. Ohnishi. 2008. 'A variant transcript, e1a3, of the minor BCR-ABL fusion gene in acute lymphoblastic leukemia: case report and review of the literature', *Int J Hematol*, 87: 184-88.

Fujita, T., M. Mogi, L. J. Min, J. Iwanami, K. Tsukuda, A. Sakata, H. Okayama, M. Iwai, C. Nahmias, J. Higaki, and M. Horiuchi. 2009. 'Attenuation of cuff-induced neointimal formation by overexpression of angiotensin II type 2 receptor-interacting protein 1', *Hypertension*, 53: 688-93.

Fukae, J., S. Sato, K. Shiba, K. Sato, H. Mori, P. A. Sharp, Y. Mizuno, and N. Hattori. 2009a. 'Programmed cell death-2 isoform1 is ubiquitinated by parkin and increased in the substantia nigra of patients with autosomal recessive Parkinson's disease', *FEBS Lett*, 583: 521-5.

———. 2009b. 'Programmed cell death-2 isoform1 is ubiquitinated by parkin and increased in the substantia nigra of patients with autosomal recessive Parkinson's disease', *FEBS Lett*, 583: 521-5.

Fukushima, N., D. Furuta, Y. Hidaka, R. Moriyama, and T. Tsujiuchi. 2009. 'Post-translational modifications of tubulin in the nervous system', *J Neurochem*, 109: 683-93.

Gadadhar, S., S. Bodakuntla, K. Natarajan, and C. Janke. 2017. 'The tubulin code at a glance', *J Cell Sci*, 130: 1347-53.

Gaglio, T., A. Saredi, and D. A. Compton. 1995. 'NuMA is required for the organization of microtubules into aster-like mitotic arrays', *J Cell Biol*, 131: 693-708.

Gallaud, E., R. Caous, A. Pascal, F. Bazile, J. P. Gagne, S. Huet, G. G. Poirier, D. Chretien, L. Richard-Parpaillon, and R. Giet. 2014. 'Ensconsin/Map7 promotes microtubule growth and centrosome separation in Drosophila neural stem cells', *J Cell Biol*, 204: 1111-21.

Gamblin, T. C., K. Nachmanoff, S. Halpain, and R. C. Williams, Jr. 1996. 'Recombinant microtubule-associated protein 2c reduces the dynamic instability of individual microtubules', *Biochemistry*, 35: 12576-86.

Gao, X., J. Pang, L. Y. Li, W. P. Liu, J. M. Di, Q. P. Sun, Y. Q. Fang, X. P. Liu, X. Y. Pu, D. He, M. T. Li, Z. L. Su, and B. Y. Li. 2010. 'Expression profiling identifies new function of collapsin response mediator protein 4 as a metastasis-suppressor in prostate cancer', *Oncogene*, 29: 4555-66.

Gee, M. A., J. E. Heuser, and R. B. Vallee. 1997. 'An extended microtubule-binding structure within the dynein motor domain', *Nature*, 390: 636-9.

Geng, W., K. T. Ng, C. K. Sun, W. L. Yau, X. B. Liu, Q. Cheng, R. T. Poon, C. M. Lo, K. Man, and S. T. Fan. 2011. 'The role of proline rich tyrosine kinase 2 (Pyk2) on cisplatin resistance in hepatocellular carcinoma', *PLoS One*, 6: e27362.

Gibbons, I. R., and A. J. Rowe. 1965. 'Dynein: A Protein with Adenosine Triphosphatase Activity from Cilia', *Science*, 149: 424-6.

Gillardon, F. 2009. 'Interaction of elongation factor 1-alpha with leucine-rich repeat kinase 2 impairs kinase activity and microtubule bundling in vitro', *Neuroscience*, 163: 533-9.

Gilmore-Hall, S., J. Kuo, J. M. Ward, R. Zahra, R. S. Morrison, G. Perkins, and A. R. La Spada. 2019. 'CCP1 promotes mitochondrial fusion and motility to prevent Purkinje cell neuron loss in pcd mice', *J Cell Biol*, 218: 206-19.

Gittes, F., B. Mickey, J. Nettleton, and J. Howard. 1993a. 'Flexural rigidity of microtubules and actin filaments measured from thermal fluctuations in shape', *J Cell Biol*, 120: 923-34.

———. 1993b. 'Flexural rigidity of microtubules and actin filaments measured from thermal fluctuations in shape', *J Cell Biol*, 120: 923-34.

Gleeson, J. G., K. M. Allen, J. W. Fox, E. D. Lamperti, S. Berkovic, I. Scheffer, E. C. Cooper, W. B. Dobyns, S. R. Minnerath, M. E. Ross, and C. A. Walsh. 1998. 'Doublecortin, a brain-specific gene mutated in human X-linked lissencephaly and double cortex syndrome, encodes a putative signaling protein', *Cell*, 92: 63-72.

Gluschankof, P., S. Gomez, A. Morel, and P. Cohen. 1987. 'Enzymes that process somatostatin precursors. A novel endoprotease that cleaves before the arginine-lysine doublet is involved in somatostatin-28 convertase activity of rat brain cortex', *J Biol Chem*, 262: 9615-20.

Goddard, T. D., C. C. Huang, E. C. Meng, E. F. Pettersen, G. S. Couch, J. H. Morris, and T. E. Ferrin. 2018. 'UCSF ChimeraX: Meeting modern challenges in visualization and analysis', *Protein Sci*, 27: 14-25.

Goedert, M., D. S. Eisenberg, and R. A. Crowther. 2017. 'Propagation of Tau Aggregates and Neurodegeneration', *Annu Rev Neurosci*, 40: 189-210.

Goedert, M., M. G. Spillantini, R. Jakes, D. Rutherford, and R. A. Crowther. 1989. 'Multiple isoforms of human microtubule-associated protein tau: sequences and localization in neurofibrillary tangles of Alzheimer's disease', *Neuron*, 3: 519-26.

Goedert, M., C. M. Wischik, R. A. Crowther, J. E. Walker, and A. Klug. 1988. 'Cloning and sequencing of the cDNA encoding a core protein of the paired helical filament of Alzheimer disease: identification as the microtubule-associated protein tau', *Proc Natl Acad Sci U S A*, 85: 4051-5.

Goldstein, L. S. 1995. 'Structural features involved in force generation in the kinesin superfamily', *Biophys J*, 68: 260S-65S; discussion 65S-66S.

———. 2001. 'Kinesin molecular motors: transport pathways, receptors, and human disease', *Proc Natl Acad Sci U S A*, 98: 6999-7003.

Gomez, S., P. Gluschankof, A. Morel, and P. Cohen. 1985. 'The somatostatin-28 convertase of rat brain cortex is associated with secretory granule membranes', *J Biol Chem*, 260: 10541-5.

Gonzalez, S. L., J. J. Lopez-Costa, F. Labombarda, M. C. Gonzalez Deniselle, R. Guennoun, M. Schumacher, and A. F. De Nicola. 2009. 'Progesterone effects on neuronal ultrastructure and expression of microtubule-associated protein 2 (MAP2) in rats with acute spinal cord injury', *Cell Mol Neurobiol*, 29: 27-39.

Goodson, H. V., and E. M. Jonasson. 2018. 'Microtubules and Microtubule-Associated Proteins', *Cold Spring Harb Perspect Biol*, 10.

Goryunov, D., C. Z. He, C. S. Lin, C. L. Leung, and R. K. Liem. 2010. 'Nervous-tissue-specific elimination of microtubule-actin crosslinking factor 1a results in multiple developmental defects in the mouse brain', *Mol Cell Neurosci*, 44: 1-14.

Goshima, Y., F. Nakamura, P. Strittmatter, and S. M. Strittmatter. 1995. 'Collapsin-induced growth cone collapse mediated by an intracellular protein related to UNC-33', *Nature*, 376: 509-14.

Griffith, K. J., J. P. Ryan, J. L. Senecal, and M. J. Fritzler. 2002. 'The cytoplasmic linker protein CLIP-170 is a human autoantigen', *Clin Exp Immunol*, 127: 533-8.

Griffith, L. M., and T. D. Pollard. 1982. 'The interaction of actin filaments with microtubules and microtubule-associated proteins', *J Biol Chem*, 257: 9143-51.

Grotjahn, D. A., and G. C. Lander. 2019. 'Setting the dynein motor in motion: New insights from electron tomography', *J Biol Chem*, 294: 13202-17.

Gu, Y., N. Hamajima, and Y. Ihara. 2000. 'Neurofibrillary tangle-associated collapsin response mediator protein-2 (CRMP-2) is highly phosphorylated on Thr-509, Ser-518, and Ser-522', *Biochemistry*, 39: 4267-75.

Gu, Y., S. Liu, X. Zhang, G. Chen, H. Liang, M. Yu, Z. Liao, Y. Zhou, C. Y. Zhang, T. Wang, C. Wang, J. Zhang, and X. Chen. 2017. 'Oncogenic miR-19a and miR-19b co-regulate tumor suppressor MTUS1 to promote cell proliferation and migration in lung cancer', *Protein Cell*, 8: 455-66.

Guillaud, L., C. Bosc, A. Fourest-Lieuvin, E. Denarier, F. Pirollet, L. Lafanechere, and D. Job. 1998. 'STOP proteins are responsible for the high degree of microtubule stabilization observed in neuronal cells', *J Cell Biol*, 142: 167-79.

Guillemot, L., D. Guerrera, D. Spadaro, R. Tapia, L. Jond, and S. Citi. 2014. 'MgcRacGAP interacts with cingulin and paracingulin to regulate Rac1 activation and development of the tight junction barrier during epithelial junction assembly', *Mol Biol Cell*, 25: 1995-2005.

Gumy, L. F., E. A. Katrukha, I. Grigoriev, D. Jaarsma, L. C. Kapitein, A. Akhmanova, and C. C. Hoogenraad. 2017. 'MAP2 Defines a Pre-axonal Filtering Zone to Regulate KIF1- versus KIF5-Dependent Cargo Transport in Sensory Neurons', *Neuron*, 94: 347-62 e7.

Gundersen, G. G., M. H. Kalnoski, and J. C. Bulinski. 1984. 'Distinct populations of microtubules: tyrosinated and nontyrosinated alpha tubulin are distributed differently in vivo', *Cell*, 38: 779-89.

Hall, G. F., and J. Yao. 2005. 'Modeling tauopathy: a range of complementary approaches', *Biochim Biophys Acta*, 1739: 224-39.

Hallak, M. E., J. A. Rodriguez, H. S. Barra, and R. Caputto. 1977. 'Release of tyrosine from tyrosinated tubulin. Some common factors that affect this process and the assembly of tubulin', *FEBS Lett*, 73: 147-50.

Hallberg, B., and R. H. Palmer. 2016. 'The role of the ALK receptor in cancer biology', *Ann Oncol*, 27 Suppl 3: iii4-iii15.

Halpain, S., and L. Dehmelt. 2006. 'The MAP1 family of microtubule-associated proteins', *Genome Biol*, 7: 224.

Hamill, D. R., B. Howell, L. Cassimeris, and K. A. Suprenant. 1998. 'Purification of a WD repeat protein, EMAP, that promotes microtubule dynamics through an inhibition of rescue', *J Biol Chem*, 273: 9285-91.

Harada, A., J. Teng, Y. Takei, K. Oguchi, and N. Hirokawa. 2002. 'MAP2 is required for dendrite elongation, PKA anchoring in dendrites, and proper PKA signal transduction', *J Cell Biol*, 158: 541-9.

Hartwell, L. H. 1971. 'Genetic control of the cell division cycle in yeast. IV. Genes controlling bud emergence and cytokinesis', *Exp Cell Res*, 69: 265-76.

Hasegawa, M., T. Arai, and Y. Ihara. 1990. 'Immunochemical evidence that fragments of phosphorylated MAP5 (MAP1B) are bound to neurofibrillary tangles in Alzheimer's disease', *Neuron*, 4: 909-18.

Hashimoto, S., Y. Matsuba, N. Kamano, N. Mihira, N. Sahara, J. Takano, S. I. Muramatsu, T. C. Saido, and T. Saito. 2019. 'Author Correction: Tau binding protein CAPON induces tau aggregation and neurodegeneration', *Nat Commun*, 10: 2964.

Hazan, J., N. Fonknechten, D. Mavel, C. Paternotte, D. Samson, F. Artiguenave, C. S. Davoine, C. Cruaud, A. Durr, P. Wincker, P. Brottier, L. Cattolico, V. Barbe, J. M. Burgunder, J. F. Prud'homme, A. Brice, B. Fontaine, B. Heilig, and J. Weissenbach. 1999. 'Spastin, a new AAA protein, is altered in the most frequent form of autosomal dominant spastic paraplegia', *Nat Genet*, 23: 296-303.

Henrichs, V., L. Grycova, C. Barinka, Z. Nahacka, J. Neuzil, S. Diez, J. Rohlena, M. Braun, and Z. Lansky. 2020. 'Mitochondria-adaptor TRAK1 promotes kinesin-1 driven transport in crowded environments', *Nat Commun*, 11: 3123.

Henty-Ridilla, J. L., A. Rankova, J. A. Eskin, K. Kenny, and B. L. Goode. 2016. 'Accelerated actin filament polymerization from microtubule plus ends', *Science*, 352: 1004-9.

Herden, M., and C. F. Waller. 2018. 'Alectinib', *Recent Results Cancer Res*, 211: 247-56.

Hernandez-Vega, A., M. Braun, L. Scharrel, M. Jahnel, S. Wegmann, B. T. Hyman, S. Alberti, S. Diez, and A. A. Hyman. 2017. 'Local Nucleation of Microtubule Bundles through Tubulin Concentration into a Condensed Tau Phase', *Cell Rep*, 20: 2304-12.

Herrmann, H., and U. Aebi. 2004. 'Intermediate filaments: molecular structure, assembly mechanism, and integration into functionally distinct intracellular Scaffolds', *Annu Rev Biochem*, 73: 749-89.

Hiller, G., and K. Weber. 1978. 'Radioimmunoassay for tubulin: a quantitative comparison of the tubulin content of different established tissue culture cells and tissues', *Cell*, 14: 795-804.

Hino, M., I. Kijima-Suda, Y. Nagai, and H. Hosoya. 2003. 'Glycosylation of the alpha and beta tubulin by sialyloligosaccharides', *Zoolog Sci*, 20: 709-15.

Hiraoka, Y., T. Matsuoka, M. Ohno, K. Nakamura, S. Saijo, S. Matsumura, K. Nishi, J. Sakamoto, P. M. Chen, K. Inoue, T. Fushiki, T. Kita, T. Kimura, and E. Nishi. 2014. 'Critical roles of nardilysin in the maintenance of body temperature homoeostasis', *Nat Commun*, 5: 3224.

Hirokawa, N., Y. Noda, Y. Tanaka, and S. Niwa. 2009. 'Kinesin superfamily motor proteins and intracellular transport', *Nat Rev Mol Cell Biol*, 10: 682-96.

Hirokawa, N., K. K. Pfister, H. Yorifuji, M. C. Wagner, S. T. Brady, and G. S. Bloom. 1989. 'Submolecular domains of bovine brain kinesin identified by electron microscopy and monoclonal antibody decoration', *Cell*, 56: 867-78.

Hirokawa, N., Y. Shiomura, and S. Okabe. 1988. 'Tau proteins: the molecular structure and mode of binding on microtubules', *J Cell Biol*, 107: 1449-59.

Hol, E. M., and Y. Capetanaki. 2017. 'Type III Intermediate Filaments Desmin, Glial Fibrillary Acidic Protein (GFAP), Vimentin, and Peripherin', *Cold Spring Harb Perspect Biol*, 9.

Holla, V. R., Y. Y. Elamin, A. M. Bailey, A. M. Johnson, B. C. Litzenburger, Y. B. Khotskaya, N. S. Sanchez, J. Zeng, M. A. Shufean, K. R. Shaw, J. Mendelsohn, G. B. Mills, F. Meric-Bernstam, and G. R. Simon. 2017. 'ALK: a tyrosine kinase target for cancer therapy', *Cold Spring Harb Mol Case Stud*, 3: a001115.

Holmfeldt, P., G. Brattsand, and M. Gullberg. 2002. 'MAP4 counteracts microtubule catastrophe promotion but not tubulin-sequestering activity in intact cells', *Curr Biol*, 12: 1034-9.

Honnorat, J., T. Byk, I. Kusters, M. Aguera, D. Ricard, V. Rogemond, T. Quach, D. Aunis, A. Sobel, M. G. Mattei, P. Kolattukudy, M. F. Belin, and J. C. Antoine. 1999. 'Ulip/CRMP proteins are recognized by autoantibodies in paraneoplastic neurological syndromes', *Eur J Neurosci*, 11: 4226-32.

Hooikaas, P. J., M. Martin, T. Muhlethaler, G. J. Kuijntjes, C. A. E. Peeters, E. A. Katrukha, L. Ferrari, R. Stucchi, D. G. F. Verhagen, W. E. van Riel, I. Grigoriev, A. F. M. Altelaar, C. C. Hoogenraad, S. G. D. Rudiger, M. O. Steinmetz, L. C. Kapitein, and A. Akhmanova. 2019. 'MAP7 family proteins regulate kinesin-1 recruitment and activation', *J Cell Biol*, 218: 1298-318.

Hook, P., and R. B. Vallee. 2006. 'The dynein family at a glance', *J Cell Sci*, 119: 4369-71.

Hoshi, M., K. Ohta, Y. Gotoh, A. Mori, H. Murofushi, H. Sakai, and E. Nishida. 1992. 'Mitogen-activated-protein-kinase-catalyzed phosphorylation of microtubule-associated proteins, microtubule-associated protein 2 and microtubule-associated protein 4, induces an alteration in their function', *Eur J Biochem*, 203: 43-52.

Hospital, V., V. Chesneau, A. Balogh, C. Joulie, N. G. Seidah, P. Cohen, and A. Prat. 2000. 'N-arginine dibasic convertase (nardilysin) isoforms are soluble dibasic-specific metalloendopeptidases that localize in the cytoplasm and at the cell surface', *Biochem J*, 349: 587-97.

Hou, S. T., S. X. Jiang, A. Aylsworth, M. Cooke, and L. Zhou. 2013. 'Collapsin response mediator protein 3 deacetylates histone H4 to mediate nuclear condensation and neuronal death', *Sci Rep*, 3: 1350.

Hou, Y., and G. B. Witman. 2015. 'Dynein and intraflagellar transport', *Exp Cell Res*, 334: 26-34.

Houtman, S. H., M. Rutteman, C. I. De Zeeuw, and P. J. French. 2007. 'Echinoderm microtubule-associated protein like protein 4, a member of the echinoderm microtubule-associated protein family, stabilizes microtubules', *Neuroscience*, 144: 1373-82.

Hu, K., D. S. Roos, and J. M. Murray. 2002. 'A novel polymer of tubulin forms the conoid of Toxoplasma gondii', *J Cell Biol*, 156: 1039-50.

Huang, J., A. Furuya, and T. Furuichi. 2007. 'Very-KIND, a KIND domain containing RasGEF, controls dendrite growth by linking Ras small GTPases and MAP2', *J Cell Biol*, 179: 539-52.

Huang, K., D. R. Diener, and J. L. Rosenbaum. 2009. 'The ubiquitin conjugation system is involved in the disassembly of cilia and flagella', *J Cell Biol*, 186: 601-13.

Huang, S. C., R. Jagadeeswaran, E. S. Liu, and E. J. Benz, Jr. 2004. 'Protein 4.1R, a microtubule-associated protein involved in microtubule aster assembly in mammalian mitotic extract', *J Biol Chem*, 279: 34595-602.

Huber, G., D. Alaimo-Beuret, and A. Matus. 1985. 'MAP3: characterization of a novel microtubule-associated protein', *J Cell Biol*, 100: 496-507.

Huynh, D. P., D. R. Scoles, T. H. Ho, M. R. Del Bigio, and S. M. Pulst. 2000. 'Parkin is associated with actin filaments in neuronal and nonneural cells', *Ann Neurol*, 48: 737-44.

Huynh, D. P., D. R. Scoles, D. Nguyen, and S. M. Pulst. 2003. 'The autosomal recessive juvenile Parkinson disease gene product, parkin, interacts with and ubiquitinates synaptotagmin XI', *Hum Mol Genet*, 12: 2587-97.

Hwang, M. J., K. G. Bryant, J. H. Seo, Q. Liu, P. A. Humphrey, M. A. C. Melnick, D. C. Altieri, and M. E. Robert. 2019. 'Syntaphilin Is a Novel Biphasic Biomarker of Aggressive Prostate Cancer and a Metastasis Predictor', *Am J Pathol*, 189: 1180-89.

Hwang, S. C., D. Y. Jhon, Y. S. Bae, J. H. Kim, and S. G. Rhee. 1996. 'Activation of phospholipase C-gamma by the concerted action of tau proteins and arachidonic acid', *J Biol Chem*, 271: 18342-9.

Ichikawa, M., and K. H. Bui. 2018. 'Microtubule Inner Proteins: A Meshwork of Luminal Proteins Stabilizing the Doublet Microtubule', *Bioessays*, 40.

Ikeda, A., Q. Y. Zheng, A. R. Zuberi, K. R. Johnson, J. K. Naggert, and P. M. Nishina. 2002. 'Microtubule-associated protein 1A is a modifier of tubby hearing (moth1)', *Nat Genet*, 30: 401-5.

Ikegami, K., R. L. Heier, M. Taruishi, H. Takagi, M. Mukai, S. Shimma, S. Taira, K. Hatanaka, N. Morone, I. Yao, P. K. Campbell, S. Yuasa, C. Janke, G. R. Macgregor, and M. Setou. 2007. 'Loss of alpha-tubulin polyglutamylation in ROSA22 mice is associated with abnormal targeting of KIF1A and modulated synaptic function', *Proc Natl Acad Sci U S A*, 104: 3213-8.

Illenberger, S., G. Drewes, B. Trinczek, J. Biernat, H. E. Meyer, J. B. Olmsted, E. M. Mandelkow, and E. Mandelkow. 1996. 'Phosphorylation of microtubule-associated proteins MAP2 and MAP4 by the protein kinase p110mark. Phosphorylation sites and regulation of microtubule dynamics', *J Biol Chem*, 271: 10834-43.

Imai, Y., M. Soda, S. Hatakeyama, T. Akagi, T. Hashikawa, K. I. Nakayama, and R. Takahashi. 2002. 'CHIP is associated with Parkin, a gene responsible for familial Parkinson's disease, and enhances its ubiquitin ligase activity', *Mol Cell*, 10: 55-67.

Irobi, J., E. Nelis, J. Meuleman, K. Venken, P. De Jonghe, C. Van Broeckhoven, and V. Timmerman. 2001. 'Exclusion of 5 functional candidate genes for distal hereditary motor neuropathy type II (distal HMN II) linked to 12q24.3', *Ann Hum Genet*, 65: 517-29.

Ishizu-Higashi, S., H. Seno, E. Nishi, Y. Matsumoto, K. Ikuta, M. Tsuda, Y. Kimura, Y. Takada, Y. Kimura, Y. Nakanishi, K. Kanda, H. Komekado, and T. Chiba. 2014. 'Deletion of nardilysin prevents the development of steatohepatitis and liver fibrotic changes', *PLoS One*, 9: e98017.

Islam, M. S., and D. J. Moore. 2017. 'Mechanisms of LRRK2-dependent neurodegeneration: role of enzymatic activity and protein aggregation', *Biochem Soc Trans*, 45: 163-72.

Jalava, N. S., F. R. Lopez-Picon, T. K. Kukko-Lukjanov, and I. E. Holopainen. 2007. 'Changes in microtubule-associated protein-2 (MAP2) expression during development and after status epilepticus in the immature rat hippocampus', *Int J Dev Neurosci*, 25: 121-31.

Janke, C. 2014. 'The tubulin code: molecular components, readout mechanisms, and functions', *J Cell Biol*, 206: 461-72.

Janke, C., and M. M. Magiera. 2020. 'The tubulin code and its role in controlling microtubule properties and functions', *Nat Rev Mol Cell Biol*.

Janke, C., K. Rogowski, D. Wloga, C. Regnard, A. V. Kajava, J. M. Strub, N. Temurak, J. van Dijk, D. Boucher, A. van Dorsselaer, S. Suryavanshi, J. Gaertig, and B. Edde. 2005. 'Tubulin polyglutamylase enzymes are members of the TTL domain protein family', *Science*, 308: 1758-62.

Jensen, P. H., H. Hager, M. S. Nielsen, P. Hojrup, J. Gliemann, and R. Jakes. 1999. 'alpha-synuclein binds to Tau and stimulates the protein kinase A-catalyzed tau phosphorylation of serine residues 262 and 356', *J Biol Chem*, 274: 25481-9.

Jensen, P. H., K. Islam, J. Kenney, M. S. Nielsen, J. Power, and W. P. Gai. 2000. 'Microtubule-associated protein 1B is a component of cortical Lewy bodies and binds alpha-synuclein filaments', *J Biol Chem*, 275: 21500-7.

Jevtic, P., A. Milunovic-Jevtic, M. R. Dilsaver, J. C. Gatlin, and D. L. Levy. 2016. 'Use of Xenopus cell-free extracts to study size regulation of subcellular structures', *Int J Dev Biol*, 60: 277-88.

Ji, Z., G. Zhang, L. Chen, J. Li, Y. Yang, C. Cha, J. Zhang, H. Lin, and G. Guo. 2018. 'Spastin Interacts with CRMP5 to Promote Neurite Outgrowth by Controlling the Microtubule Dynamics', *Dev Neurobiol*, 78: 1191-205.

Jiang, W., G. Jimenez, N. J. Wells, T. J. Hope, G. M. Wahl, T. Hunter, and R. Fukunaga. 1998. 'PRC1: a human mitotic spindle-associated CDK substrate protein required for cytokinesis', *Mol Cell*, 2: 877-85.

Jin, M., C. Liu, W. Han, and Y. Cong. 2019. 'TRiC/CCT Chaperonin: Structure and Function', *Subcell Biochem*, 93: 625-54.

Johnson, K. A. 1998. 'The axonemal microtubules of the Chlamydomonas flagellum differ in tubulin isoform content', *J Cell Sci*, 111 (Pt 3): 313-20.

Johnson, K. A., and G. G. Borisy. 1975. 'The equilibrium assembly of microtubules in vitro', *Soc Gen Physiol Ser*, 30: 119-41.

Jones, J. L., D. Peana, A. B. Veteto, M. D. Lambert, Z. Nourian, N. G. Karasseva, M. A. Hill, B. R. Lindman, C. P. Baines, M. Krenz, and T. L. Domeier. 2019. 'TRPV4 increases cardiomyocyte calcium cycling and contractility yet contributes to damage in the aged heart following hypoosmotic stress', *Cardiovasc Res*, 115: 46-56.

Jordan, M. A., and L. Wilson. 2004. 'Microtubules as a target for anticancer drugs', *Nat Rev Cancer*, 4: 253-65.

Jorgensen, L. H., M. B. Mosbech, N. J. Faergeman, J. Graakjaer, S. V. Jacobsen, and H. D. Schroder. 2014. 'Duplication in the microtubule-actin cross-linking factor 1 gene causes a novel neuromuscular condition', *Sci Rep*, 4: 5180.

Juniper, M. P. N., M. Weiss, I. Platzman, J. P. Spatz, and T. Surrey. 2018. 'Spherical network contraction forms microtubule asters in confinement', *Soft Matter*, 14: 901-09.

Ka, M., and W. Y. Kim. 2016. 'Microtubule-Actin Crosslinking Factor 1 Is Required for Dendritic Arborization and Axon Outgrowth in the Developing Brain', *Mol Neurobiol*, 53: 6018-32.

Kadletz, L., D. Thurnher, R. Wiebringhaus, B. M. Erovic, U. Kotowski, S. Schneider, R. Schmid, L. Kenner, and G. Heiduschka. 2017. 'Role of cancer stem-cell marker doublecortin-like kinase 1 in head and neck squamous cell carcinoma', *Oral Oncol*, 67: 109-18.

Kalcheva, N., J. M. Rockwood, Y. Kress, A. Steiner, and B. Shafit-Zagardo. 1998. 'Molecular and functional characteristics of MAP-2a: ability of MAP-2a versus MAP-2b to induce stable microtubules in COS cells', *Cell Motil Cytoskeleton*, 40: 272-85.

Kalebic, N., S. Sorrentino, E. Perlas, G. Bolasco, C. Martinez, and P. A. Heppenstall. 2013. 'alphaTAT1 is the major alpha-tubulin acetyltransferase in mice', *Nat Commun*, 4: 1962.

Kanai, Y., R. Takemura, T. Oshima, H. Mori, Y. Ihara, M. Yanagisawa, T. Masaki, and N. Hirokawa. 1989. 'Expression of multiple tau isoforms and microtubule bundle formation in fibroblasts transfected with a single tau cDNA', *J Cell Biol*, 109: 1173-84.

Kang, J. S., J. H. Tian, P. Y. Pan, P. Zald, C. Li, C. Deng, and Z. H. Sheng. 2008. 'Docking of axonal mitochondria by syntaphilin controls their mobility and affects short-term facilitation', *Cell*, 132: 137-48.

Karakesisoglou, I., Y. Yang, and E. Fuchs. 2000a. 'An epidermal plakin that integrates actin and microtubule networks at cellular junctions', *J Cell Biol*, 149: 195-208.

———. 2000b. 'An epidermal plakin that integrates actin and microtubule networks at cellular junctions', *J Cell Biol*, 149: 195-208.

Kardon, J. R., and R. D. Vale. 2009. 'Regulators of the cytoplasmic dynein motor', *Nat Rev Mol Cell Biol*, 10: 854-65.

Karpova, N., Y. Bobinnec, S. Fouix, P. Huitorel, and A. Debec. 2006. 'Jupiter, a new Drosophila protein associated with microtubules', *Cell Motil Cytoskeleton*, 63: 301-12.

Katayama, R., C. M. Lovly, and A. T. Shaw. 2015. 'Therapeutic targeting of anaplastic lymphoma kinase in lung cancer: a paradigm for precision cancer medicine', *Clin Cancer Res*, 21: 2227-35.

Kato, M. V. 1999. 'The mechanisms of death of an erythroleukemic cell line by p53: involvement of the microtubule and mitochondria', *Leuk Lymphoma*, 33: 181-6.

Kaul, N., V. Soppina, and K. J. Verhey. 2014. 'Effects of alpha-tubulin K40 acetylation and detyrosination on kinesin-1 motility in a purified system', *Biophys J*, 106: 2636-43.

Kawahara, K., M. Hashimoto, P. Bar-On, G. J. Ho, L. Crews, H. Mizuno, E. Rockenstein, S. Z. Imam, and E. Masliah. 2008. 'alpha-Synuclein aggregates interfere with Parkin solubility and distribution: role in the pathogenesis of Parkinson disease', *J Biol Chem*, 283: 6979-87.

Kawauchi, T. 2017. 'Tubulin isotype specificity in neuronal migration: Tuba8 can't fill in for Tuba1a', *J Cell Biol*, 216: 2247-49.

Kellogg, E. H., N. M. A. Hejab, S. Poepsel, K. H. Downing, F. DiMaio, and E. Nogales. 2018. 'Near-atomic model of microtubule-tau interactions', *Science*, 360: 1242-46.

Kempf, M., A. Clement, A. Faissner, G. Lee, and R. Brandt. 1996. 'Tau binds to the distal axon early in development of polarity in a microtubule- and microfilament-dependent manner', *J Neurosci*, 16: 5583-92.

Kesarwani, S., P. Lama, A. Chandra, P. P. Reddy, A. S. Jijumon, S. Bodakuntla, B. M. Rao, C. Janke, R. Das, and M. Sirajuddin. 2020. 'Genetically encoded live-cell sensor for tyrosinated microtubules', *J Cell Biol*, 219.

Ketschek, A., M. Spillane, X. P. Dun, H. Hardy, J. Chilton, and G. Gallo. 2016a. 'Drebrin coordinates the actin and microtubule cytoskeleton during the initiation of axon collateral branches', *Dev Neurobiol*, 76: 1092-110.

———. 2016b. 'Drebrin coordinates the actin and microtubule cytoskeleton during the initiation of axon collateral branches', *Dev Neurobiol*, 76: 1092-110.

Khazaei, M. R., M. P. Girouard, R. Alchini, S. Ong Tone, T. Shimada, S. Bechstedt, M. Cowan, D. Guillet, P. W. Wiseman, G. Brouhard, J. F. Cloutier, and A. E. Fournier. 2014. 'Collapsin response mediator protein 4 regulates growth cone dynamics through the actin and microtubule cytoskeleton', *J Biol Chem*, 289: 30133-43.

Khmelinskii, A., J. Roostalu, H. Roque, C. Antony, and E. Schiebel. 2009. 'Phosphorylation-dependent protein interactions at the spindle midzone mediate cell cycle regulation of spindle elongation', *Dev Cell*, 17: 244-56.

Kielar, M., F. P. Tuy, S. Bizzotto, C. Lebrand, C. de Juan Romero, K. Poirier, R. Oegema, G. M. Mancini, N. Bahi-Buisson, R. Olaso, A. G. Le Moing, K. Boutourlinsky, D. Boucher, W. Carpentier, P. Berquin, J. F. Deleuze, R. Belvindrah, V. Borrell, E. Welker, J. Chelly, A. Croquelois, and F. Francis. 2014. 'Mutations in Eml1 lead to ectopic progenitors and neuronal heterotopia in mouse and human', *Nat Neurosci*, 17: 923-33.

Kim, H., L. I. Binder, and J. L. Rosenbaum. 1979. 'The periodic association of MAP2 with brain microtubules in vitro', *J Cell Biol*, 80: 266-76.

Kimble, M., J. P. Incardona, and E. C. Raff. 1989. 'A variant beta-tubulin isoform of Drosophila melanogaster (beta 3) is expressed primarily in tissues of mesodermal origin in embryos and pupae, and is utilized in populations of transient microtubules', *Dev Biol*, 131: 415-29.

Kimura, T., H. Watanabe, A. Iwamatsu, and K. Kaibuchi. 2005. 'Tubulin and CRMP-2 complex is transported via Kinesin-1', *J Neurochem*, 93: 1371-82.

Kimura, Y., K. Ikuta, T. Kimura, T. Chiba, H. Oshima, M. Oshima, E. Nishi, and H. Seno. 2017. 'Nardilysin regulates inflammation, metaplasia, and tumors in murine stomach', *Sci Rep*, 7: 43052.

Kimura, Y., N. Kurabe, K. Ikegami, K. Tsutsumi, Y. Konishi, O. I. Kaplan, H. Kunitomo, Y. Iino, O. E. Blacque, and M. Setou. 2010. 'Identification of tubulin deglutamylase among Caenorhabditis elegans and mammalian cytosolic carboxypeptidases (CCPs)', *J Biol Chem*, 285: 22936-41.

King, M. R., and S. Petry. 2020. 'Phase separation of TPX2 enhances and spatially coordinates microtubule nucleation', *Nat Commun*, 11: 270.

Kinoshita, M. 2003. 'The septins', *Genome Biol*, 4: 236.

Kirschner, M. W., and R. C. Williams. 1974. 'The mechanism of microtubule assembly in vitro', *J Supramol Struct*, 2: 412-28.

Kita, A. M., Z. T. Swider, I. Erofeev, M. C. Halloran, A. B. Goryachev, and W. M. Bement. 2019. 'Spindle-F-actin interactions in mitotic spindles in an intact vertebrate epithelium', *Mol Biol Cell*, 30: 1645-54.

Kitada, T., S. Asakawa, N. Hattori, H. Matsumine, Y. Yamamura, S. Minoshima, M. Yokochi, Y. Mizuno, and N. Shimizu. 1998. 'Mutations in the parkin gene cause autosomal recessive juvenile parkinsonism', *Nature*, 392: 605-8.

Klein, C., E. M. Kramer, A. M. Cardine, B. Schraven, R. Brandt, and J. Trotter. 2002. 'Process outgrowth of oligodendrocytes is promoted by interaction of fyn kinase with the cytoskeletal protein tau', *J Neurosci*, 22: 698-707.

Klumpp, M., and W. Baumeister. 1998. 'The thermosome: archetype of group II chaperonins', *FEBS Lett*, 430: 73-7.

Klymkowsky, M. W., J. B. Bachant, and A. Domingo. 1989. 'Functions of intermediate filaments', *Cell Motil Cytoskeleton*, 14: 309-31.

Knutson, T. P., A. R. Daniel, D. Fan, K. A. Silverstein, K. R. Covington, S. A. Fuqua, and C. A. Lange. 2012. 'Phosphorylated and sumoylation-deficient progesterone receptors drive proliferative gene signatures during breast cancer progression', *Breast Cancer Res*, 14: R95.

Koizumi, H., H. Fujioka, K. Togashi, J. Thompson, J. R. Yates, 3rd, J. G. Gleeson, and K. Emoto. 2017a. 'DCLK1 phosphorylates the microtubule-associated protein MAP7D1 to promote axon elongation in cortical neurons', *Dev Neurobiol*, 77: 493-510.

———. 2017b. 'DCLK1 phosphorylates the microtubule-associated protein MAP7D1 to promote axon elongation in cortical neurons', *Dev Neurobiol*, 77: 493-510.

Kokkonen, N., S. K. Herukka, L. Huilaja, M. Kokki, A. M. Koivisto, P. Hartikainen, A. M. Remes, and K. Tasanen. 2017. 'Increased Levels of the Bullous Pemphigoid BP180 Autoantibody Are Associated with More Severe Dementia in Alzheimer's Disease', *J Invest Dermatol*, 137: 71-76.

Konishi, Y., and M. Setou. 2009. 'Tubulin tyrosination navigates the kinesin-1 motor domain to axons', *Nat Neurosci*, 12: 559-67.

Konno, A., M. Setou, and K. Ikegami. 2012. 'Ciliary and flagellar structure and function--their regulations by posttranslational modifications of axonemal tubulin', *Int Rev Cell Mol Biol*, 294: 133-70.

Krauss, S. W., J. A. Chasis, C. Rogers, N. Mohandas, G. Krockmalnic, and S. Penman. 1997. 'Structural protein 4.1 is located in mammalian centrosomes', *Proc Natl Acad Sci U S A*, 94: 7297-302.

Kreitzer, G., G. Liao, and G. G. Gundersen. 1999. 'Detyrosination of tubulin regulates the interaction of intermediate filaments with microtubules in vivo via a kinesin-dependent mechanism', *Mol Biol Cell*, 10: 1105-18.

Kremer, A., H. Maurin, D. Demedts, H. Devijver, P. Borghgraef, and F. Van Leuven. 2011. 'Early improved and late defective cognition is reflected by dendritic spines in Tau.P301L mice', *J Neurosci*, 31: 18036-47.

Kumar, N., and M. Flavin. 1981. 'Preferential action of a brain detyrosinolating carboxypeptidase on polymerized tubulin', *J Biol Chem*, 256: 7678-86.

Kumarapeli, A. R., and X. Wang. 2004. 'Genetic modification of the heart: chaperones and the cytoskeleton', *J Mol Cell Cardiol*, 37: 1097-109.

Kuo, Yin-Wei, Olivier Trottier, Mohammed Mahamdeh, and Jonathon Howard. 2019. 'Spastin is a dual-function enzyme that severs microtubules and promotes their regrowth to increase the number and mass of microtubules', *Proceedings of the National Academy of Sciences*, 116: 5533-41.

L'Hernault, S. W., and J. L. Rosenbaum. 1985. 'Chlamydomonas alpha-tubulin is posttranslationally modified by acetylation on the epsilon-amino group of a lysine', *Biochemistry*, 24: 473-8.

Lacroix, B., J. van Dijk, N. D. Gold, J. Guizetti, G. Aldrian-Herrada, K. Rogowski, D. W. Gerlich, and C. Janke. 2010. 'Tubulin polyglutamylation stimulates spastin-mediated microtubule severing', *J Cell Biol*, 189: 945-54.

Laffitte, E., P. R. Burkhard, L. Fontao, F. Jaunin, J. H. Saurat, M. Chofflon, and L. Borradori. 2005. 'Bullous pemphigoid antigen 1 isoforms: potential new target autoantigens in multiple sclerosis?', *Br J Dermatol*, 152: 537-40.

Lake, N. J., R. L. Taylor, H. Trahair, K. N. Harikrishnan, J. E. Curran, M. Almeida, H. Kulkarni, N. Mukhamedova, A. Hoang, H. Low, A. J. Murphy, M. P. Johnson, T. D. Dyer, M. C. Mahaney, H. H. H. Goring, E. K. Moses, D. Sviridov, J. Blangero, J. B. M. Jowett, and K. Bozaoglu. 2017. 'TRAK2, a novel regulator of ABCA1 expression, cholesterol efflux and HDL biogenesis', *Eur Heart J*, 38: 3579-87.

Langer, R., K. Specht, K. Becker, P. Ewald, M. Sarbia, R. Busch, M. Feith, H. J. Stein, J. R. Siewert, and H. Hofler. 2004. '[Prediction of response to neoadjuvant chemotherapy in Barrett's carcinoma by quantitative gene expression analysis]', *Verh Dtsch Ges Pathol*, 88: 207-13.

Lansbergen, G., Y. Komarova, M. Modesti, C. Wyman, C. C. Hoogenraad, H. V. Goodson, R. P. Lemaitre, D. N. Drechsel, E. van Munster, T. W. Gadella, Jr., F. Grosveld, N. Galjart, G. G. Borisy, and A. Akhmanova. 2004. 'Conformational changes in CLIP-170 regulate its binding to microtubules and dynactin localization', *J Cell Biol*, 166: 1003-14.

Lansky, Z., M. Braun, A. Ludecke, M. Schlierf, P. R. ten Wolde, M. E. Janson, and S. Diez. 2015. 'Diffusible crosslinkers generate directed forces in microtubule networks', *Cell*, 160: 1159-68.

Lao, G., V. Scheuss, C. M. Gerwin, Q. Su, S. Mochida, J. Rettig, and Z. H. Sheng. 2000. 'Syntaphilin: a syntaxin-1 clamp that controls SNARE assembly', *Neuron*, 25: 191-201.

Larcher, J. C., D. Boucher, S. Lazereg, F. Gros, and P. Denoulet. 1996. 'Interaction of kinesin motor domains with alpha- and beta-tubulin subunits at a tau-independent binding site. Regulation by polyglutamylation', *J Biol Chem*, 271: 22117-24.

Leandro-Garcia, L. J., S. Leskela, I. Landa, C. Montero-Conde, E. Lopez-Jimenez, R. Leton, A. Cascon, M. Robledo, and C. Rodriguez-Antona. 2010. 'Tumoral and tissue-specific expression of the major human beta-tubulin isotypes', *Cytoskeleton (Hoboken)*, 67: 214-23.

Lee, J. C. 1982. 'Purification and chemical properties of brain tubulin', *Methods Cell Biol*, 24: 9-30.

Leermakers, P. A., Amwj Schols, A. E. M. Kneppers, Mcjm Kelders, C. C. de Theije, M. Lainscak, and H. R. Gosker. 2018. 'Molecular signalling towards mitochondrial breakdown is enhanced in skeletal muscle of patients with chronic obstructive pulmonary disease (COPD)', *Sci Rep*, 8: 15007.

Leonova, E. V., and M. I. Lomax. 2002. 'Expression of the mouse Macf2 gene during inner ear development', *Brain Res Mol Brain Res*, 105: 67-78.

Lessard, D. V., O. J. Zinder, T. Hotta, K. J. Verhey, R. Ohi, and C. L. Berger. 2019. 'Polyglutamylation of tubulin's C-terminal tail controls pausing and motility of kinesin-3 family member KIF1A', *J Biol Chem*, 294: 6353-63.

Leto, T. L., and V. T. Marchesi. 1984. 'A structural model of human erythrocyte protein 4.1', *J Biol Chem*, 259: 4603-8.

Letournel, F., A. Bocquet, F. Dubas, A. Barthelaix, and J. Eyer. 2003. 'Stable tubule only polypeptides (STOP) proteins co-aggregate with spheroid neurofilaments in amyotrophic lateral sclerosis', *J Neuropathol Exp Neurol*, 62: 1211-9.

Leung, C. L., D. Sun, and R. K. Liem. 1999a. 'The intermediate filament protein peripherin is the specific interaction partner of mouse BPAG1-n (dystonin) in neurons', *J Cell Biol*, 144: 435-46.

———. 1999b. 'The intermediate filament protein peripherin is the specific interaction partner of mouse BPAG1-n (dystonin) in neurons', *J Cell Biol*, 144: 435-46.

Leung, C. L., D. Sun, M. Zheng, D. R. Knowles, and R. K. Liem. 1999. 'Microtubule actin cross-linking factor (MACF): a hybrid of dystonin and dystrophin that can interact with the actin and microtubule cytoskeletons', *J Cell Biol*, 147: 1275-86.

Levilliers, N., A. Fleury, and A. M. Hill. 1995. 'Monoclonal and polyclonal antibodies detect a new type of post-translational modification of axonemal tubulin', *J Cell Sci*, 108 (Pt 9): 3013-28.

Lewis, S. A., W. Gu, and N. J. Cowan. 1987. 'Free intermingling of mammalian beta-tubulin isotypes among functionally distinct microtubules', *Cell*, 49: 539-48.

Lewis, S. A., I. E. Ivanov, G. H. Lee, and N. J. Cowan. 1989. 'Organization of microtubules in dendrites and axons is determined by a short hydrophobic zipper in microtubule-associated proteins MAP2 and tau', *Nature*, 342: 498-505.

Lewis, S. A., G. Tian, and N. J. Cowan. 1997. 'The alpha- and beta-tubulin folding pathways', *Trends Cell Biol*, 7: 479-84.

Lewkowicz, E., F. Herit, C. Le Clainche, P. Bourdoncle, F. Perez, and F. Niedergang. 2008. 'The microtubule-binding protein CLIP-170 coordinates mDia1 and actin reorganization during CR3-mediated phagocytosis', *J Cell Biol*, 183: 1287-98.

Li, D., X. Sun, L. Zhang, B. Yan, S. Xie, R. Liu, M. Liu, and J. Zhou. 2013. 'Histone deacetylase 6 and cytoplasmic linker protein 170 function together to regulate the motility of pancreatic cancer cells', *Protein Cell*.

Li, F., Y. Hu, S. Qi, X. Luo, and H. Yu. 2019. 'Structural basis of tubulin detyrosination by vasohibins', *Nat Struct Mol Biol*, 26: 583-91.

Li, K. K., Y. Qi, T. Xia, Y. Yao, L. Zhou, K. M. Lau, and H. K. Ng. 2015. 'CRMP1 Inhibits Proliferation of Medulloblastoma and Is Regulated by HMGA1', *PLoS One*, 10: e0127910.

Li, Q., M. Callaghan, and K. A. Suprenant. 1998. 'The 77-kDa echinoderm microtubule-associated protein (EMAP) shares epitopes with the mammalian brain MAPs, MAP-2 and tau', *Biochem Biophys Res Commun*, 250: 502-5.

Li, X., H. Liu, T. Yu, Z. Dong, L. Tang, and X. Sun. 2014. 'Loss of MTUS1 in gastric cancer promotes tumor growth and metastasis', *Neoplasma*, 61: 128-35.

Li, Z., Y. Wang, L. Wu, Y. Dong, J. Zhang, F. Chen, W. Xie, J. Huang, and N. Lu. 2019. 'Apurinic endonuclease 1 promotes the cisplatin resistance of lung cancer cells by inducing Parkinmediated mitophagy', *Oncol Rep*, 42: 2245-54.

Liao, G., and G. G. Gundersen. 1998. 'Kinesin is a candidate for cross-bridging microtubules and intermediate filaments. Selective binding of kinesin to detyrosinated tubulin and vimentin', *J Biol Chem*, 273: 9797-803.

Liao, S., G. Rajendraprasad, N. Wang, S. Eibes, J. Gao, H. Yu, G. Wu, X. Tu, H. Huang, M. Barisic, and C. Xu. 2019. 'Molecular basis of vasohibins-mediated detyrosination and its impact on spindle function and mitosis', *Cell Res*, 29: 533-47.

Lim, S., M. M. Haque, D. Kim, D. J. Kim, and Y. K. Kim. 2014. 'Cell-based Models To Investigate Tau Aggregation', *Comput Struct Biotechnol J*, 12: 7-13.

Lim, W. M., Y. Ito, K. Sakata-Sogawa, and M. Tokunaga. 2018. 'CLIP-170 is essential for MTOC repositioning during T cell activation by regulating dynein localisation on the cell surface', *Sci Rep*, 8: 17447.

Lin, E., L. Li, Y. Guan, R. Soriano, C. S. Rivers, S. Mohan, A. Pandita, J. Tang, and Z. Modrusan. 2009. 'Exon array profiling detects EML4-ALK fusion in breast, colorectal, and non-small cell lung cancers', *Mol Cancer Res*, 7: 1466-76.

Lin, H., G. Ren, and X. Liang. 2018. 'A Novel EML6-ALK FBXO11-ALK Double Fusion Variant in Lung Adenocarcinoma and Response to Crizotinib', *J Thorac Oncol*, 13: e234-e36.

Lin, P. C., P. M. Chan, C. Hall, and E. Manser. 2011. 'Collapsin response mediator proteins (CRMPs) are a new class of microtubule-associated protein (MAP) that selectively interacts with assembled microtubules via a taxol-sensitive binding interaction', *J Biol Chem*, 286: 41466-78.

Lin, X. D., Y. P. Wu, S. H. Chen, X. L. Sun, Z. B. Ke, D. N. Chen, X. D. Li, Y. Z. Lin, Y. Wei, Q. S. Zheng, N. Xu, and X. Y. Xue. 2020. 'Identification of a five-mRNA signature as a novel potential prognostic biomarker in pediatric Wilms tumor', *Mol Genet Genomic Med*, 8: e1032.

Lipka, J., L. C. Kapitein, J. Jaworski, and C. C. Hoogenraad. 2016. 'Microtubule-binding protein doublecortin-like kinase 1 (DCLK1) guides kinesin-3-mediated cargo transport to dendrites', *EMBO J*, 35: 302-18.

Liu, J. S., C. R. Schubert, X. Fu, F. J. Fourniol, J. K. Jaiswal, A. Houdusse, C. M. Stultz, C. A. Moores, and C. A. Walsh. 2012. 'Molecular basis for specific regulation of neuronal kinesin-3 motors by doublecortin family proteins', *Mol Cell*, 47: 707-21.

Liu, L., A. Vo, G. Liu, and W. L. McKeehan. 2005. 'Distinct structural domains within C19ORF5 support association with stabilized microtubules and mitochondrial aggregation and genome destruction', *Cancer Res*, 65: 4191-201.

Liu, W., H. Xiao, S. Wu, H. Liu, and B. Luo. 2018. 'MAP9 single nucleotide polymorphism rs1058992 is a risk of EBV-associated gastric carcinoma in Chinese population', *Acta Virol*, 62: 435-40.

Liu, X., J. Wu, D. Zhang, Z. Bing, J. Tian, M. Ni, X. Zhang, Z. Meng, and S. Liu. 2018. 'Identification of Potential Key Genes Associated With the Pathogenesis and Prognosis of Gastric Cancer Based on Integrated Bioinformatics Analysis', *Front Genet*, 9: 265.

Liu, X., Q. Zhou, Z. Ji, G. Fu, Y. Li, X. Zhang, X. Shi, T. Wang, and Q. Kang. 2014. 'Protein 4.1R attenuates autoreactivity in experimental autoimmune encephalomyelitis by suppressing CD4(+) T cell activation', *Cell Immunol*, 292: 19-24.

Liu, Y. H., J. Y. Tsang, Y. B. Ni, T. Hlaing, S. K. Chan, K. F. Chan, C. W. Ko, S. S. Mujtaba, and G. M. Tse. 2016. 'Doublecortin-like kinase 1 expression associates with breast cancer with neuroendocrine differentiation', *Oncotarget*, 7: 1464-76.

Loiodice, I., J. Staub, T. G. Setty, N. P. Nguyen, A. Paoletti, and P. T. Tran. 2005. 'Ase1p organizes antiparallel microtubule arrays during interphase and mitosis in fission yeast', *Mol Biol Cell*, 16: 1756-68.

Lopez, T., K. Dalton, and J. Frydman. 2015. 'The Mechanism and Function of Group II Chaperonins', *J Mol Biol*, 427: 2919-30.

Loss, O., and F. A. Stephenson. 2015. 'Localization of the kinesin adaptor proteins trafficking kinesin proteins 1 and 2 in primary cultures of hippocampal pyramidal and cortical neurons', *J Neurosci Res*, 93: 1056-66.

Louis, S. N., L. T. Chow, N. Varghayee, L. A. Rezmann, A. G. Frauman, and W. J. Louis. 2011. 'The Expression of MTUS1/ATIP and Its Major Isoforms, ATIP1 and ATIP3, in Human Prostate Cancer', *Cancers (Basel)*, 3: 3824-37.

Lowe, J., H. Li, K. H. Downing, and E. Nogales. 2001. 'Refined structure of alpha beta-tubulin at 3.5 A resolution', *J Mol Biol*, 313: 1045-57.

Lu, M., and K. S. Kosik. 2001. 'Competition for microtubule-binding with dual expression of tau missense and splice isoforms', *Mol Biol Cell*, 12: 171-84.

Lu, P. J., G. Wulf, X. Z. Zhou, P. Davies, and K. P. Lu. 1999. 'The prolyl isomerase Pin1 restores the function of Alzheimer-associated phosphorylated tau protein', *Nature*, 399: 784-8.

Ludin, B., K. Ashbridge, U. Funfschilling, and A. Matus. 1996. 'Functional analysis of the MAP2 repeat domain', *J Cell Sci*, 109 (Pt 1): 91-9.

Ludueña, Richard F., and Asok Banerjee. 2008a. 'The Isotypes of Tubulin.' in Tito Fojo (ed.), *The Role of Microtubules in Cell Biology, Neurobiology, and Oncology* (Humana Press: Totowa, NJ).

———. 2008b. 'The Tubulin Superfamily.' in Tito Fojo (ed.), *The Role of Microtubules in Cell Biology, Neurobiology, and Oncology* (Humana Press: Totowa, NJ).

Luo, J., B. Yang, G. Xin, M. Sun, B. Zhang, X. Guo, Q. Jiang, and C. Zhang. 2019. 'The microtubule-associated protein EML3 regulates mitotic spindle assembly by recruiting the Augmin complex to spindle microtubules', *J Biol Chem*, 294: 5643-56.

Luo, Y., S. Xiang, P. J. Hooikaas, L. van Bezouwen, A. S. Jijumon, C. Janke, F. Forster, A. Akhmanova, and M. Baldus. 2020. 'Direct observation of dynamic protein interactions involving human microtubules using solid-state NMR spectroscopy', *Nat Commun*, 11: 18.

Ly, C. D., K. W. Roche, H. K. Lee, and R. J. Wenthold. 2002. 'Identification of rat EMAP, a delta-glutamate receptor binding protein', *Biochem Biophys Res Commun*, 291: 85-90.

Ma, L., J. Song, X. Sun, W. Ding, K. Fan, M. Qi, Y. Xu, and W. Zhang. 2019. 'Role of microtubule-associated protein 6 glycosylated with Gal-(beta-1,3)-GalNAc in Parkinson's disease', *Aging (Albany NY)*, 11: 4597-610.

Ma, N., J. Titus, A. Gable, J. L. Ross, and P. Wadsworth. 2011. 'TPX2 regulates the localization and activity of Eg5 in the mammalian mitotic spindle', *J Cell Biol*, 195: 87-98.

Ma, Q. L., X. Zuo, F. Yang, O. J. Ubeda, D. J. Gant, M. Alaverdyan, N. C. Kiosea, S. Nazari, P. P. Chen, F. Nothias, P. Chan, E. Teng, S. A. Frautschy, and G. M. Cole. 2014. 'Loss of MAP function leads to hippocampal synapse loss and deficits in the Morris Water Maze with aging', *J Neurosci*, 34: 7124-36.

Macaskill, A. F., J. E. Rinholm, A. E. Twelvetrees, I. L. Arancibia-Carcamo, J. Muir, A. Fransson, P. Aspenstrom, D. Attwell, and J. T. Kittler. 2009. 'Miro1 is a calcium sensor for glutamate receptor-dependent localization of mitochondria at synapses', *Neuron*, 61: 541-55.

Magiera, M. M., S. Bodakuntla, J. Ziak, S. Lacomme, P. Marques Sousa, S. Leboucher, T. J. Hausrat, C. Bosc, A. Andrieux, M. Kneussel, M. Landry, A. Calas, M. Balastik, and C. Janke. 2018. 'Excessive tubulin polyglutamylation causes neurodegeneration and perturbs neuronal transport', *EMBO J*, 37.

Magiera, M. M., and C. Janke. 2014. 'Post-translational modifications of tubulin', *Curr Biol*, 24: R351-4.

Magiera, M. M., P. Singh, S. Gadadhar, and C. Janke. 2018. 'Tubulin Posttranslational Modifications and Emerging Links to Human Disease', *Cell*, 173: 1323-27.

Mahad, D. J., I. Ziabreva, G. Campbell, N. Lax, K. White, P. S. Hanson, H. Lassmann, and D. M. Turnbull. 2009. 'Mitochondrial changes within axons in multiple sclerosis', *Brain*, 132: 1161-74.

Maiato, H., P. Sampaio, and C. E. Sunkel. 2004. 'Microtubule-associated proteins and their essential roles during mitosis', *Int Rev Cytol*, 241: 53-153.

Makino, S., H. Takahashi, D. Okuzaki, N. Miyoshi, N. Haraguchi, T. Hata, C. Matsuda, H. Yamamoto, T. Mizushima, M. Mori, and Y. Doki. 2020. 'DCLK1 integrates induction of TRIB3, EMT, drug resistance and poor prognosis in colorectal cancer', *Carcinogenesis*.

Manabe, Ri, L. Whitmore, J. M. Weiss, and A. R. Horwitz. 2002a. 'Identification of a novel microtubule-associated protein that regulates microtubule organization and cytokinesis by using a GFP-screening strategy', *Curr Biol*, 12: 1946-51.

———. 2002b. 'Identification of a novel microtubule-associated protein that regulates microtubule organization and cytokinesis by using a GFP-screening strategy', *Curr Biol*, 12: 1946-51.

Mandelkow, E., and E. M. Mandelkow. 2002. 'Kinesin motors and disease', *Trends Cell Biol*, 12: 585-91.

Mangan, A. J., D. V. Sietsema, D. Li, J. K. Moore, S. Citi, and R. Prekeris. 2016. 'Cingulin and actin mediate midbody-dependent apical lumen formation during polarization of epithelial cells', *Nat Commun*, 7: 12426.

Manka, S. W., and C. A. Moores. 2018. 'Microtubule structure by cryo-EM: snapshots of dynamic instability', *Essays Biochem*, 62: 737-51.

Maresca, T. J., H. Niederstrasser, K. Weis, and R. Heald. 2005. 'Xnf7 contributes to spindle integrity through its microtubule-bundling activity', *Curr Biol*, 15: 1755-61.

Maruta, H., K. Greer, and J. L. Rosenbaum. 1986. 'The acetylation of alpha-tubulin and its relationship to the assembly and disassembly of microtubules', *J Cell Biol*, 103: 571-9.

Masson, D., and T. E. Kreis. 1993. 'Identification and molecular characterization of E-MAP-115, a novel microtubule-associated protein predominantly expressed in epithelial cells', *J Cell Biol*, 123: 357-71.

Matsushima, K., M. Aosaki, K. Tokuraku, M. R. Hasan, H. Nakagawa, and S. Kotani. 2005. 'Identification of a neural cell specific variant of microtubule-associated protein 4', *Cell Struct Funct*, 29: 111-24.

Matsushima, K., K. Tokuraku, M. R. Hasan, and S. Kotani. 2012. 'Microtubule-associated protein 4 binds to actin filaments and modulates their properties', *J Biochem*, 151: 99-108.

Matus, A. 1988. 'Microtubule-associated proteins: their potential role in determining neuronal morphology', *Annu Rev Neurosci*, 11: 29-44.

McElwee, M., F. Beilstein, M. Labetoulle, F. J. Rixon, and D. Pasdeloup. 2013. 'Dystonin/BPAG1 promotes plus-end-directed transport of herpes simplex virus 1 capsids on microtubules during entry', *J Virol*, 87: 11008-18.

McKenney, R. J., W. Huynh, R. D. Vale, and M. Sirajuddin. 2016. 'Tyrosination of alpha-tubulin controls the initiation of processive dynein-dynactin motility', *EMBO J*, 35: 1175-85.

McNally, F. J., and R. D. Vale. 1993. 'Identification of katanin, an ATPase that severs and disassembles stable microtubules', *Cell*, 75: 419-29.

McNally, K. P., D. Buster, and F. J. McNally. 2002. 'Katanin-mediated microtubule severing can be regulated by multiple mechanisms', *Cell Motil Cytoskeleton*, 53: 337-49.

McVicker, D. P., L. R. Chrin, and C. L. Berger. 2011. 'The nucleotide-binding state of microtubules modulates kinesin processivity and the ability of Tau to inhibit kinesin-mediated transport', *J Biol Chem*, 286: 42873-80.

Mendes Maia, T., D. Gogendeau, C. Pennetier, C. Janke, and R. Basto. 2014. 'Bug22 influences cilium morphology and the post-translational modification of ciliary microtubules', *Biol Open*, 3: 138-51.

Meng, Q. B., J. C. Yu, W. M. Kang, Z. Q. Ma, W. X. Zhou, J. Li, L. Zhou, Z. J. Cao, and S. B. Tian. 2013. '[Expression of doublecortin-like kinase 1 in human gastric cancer and its correlation with prognosis]', *Zhongguo Yi Xue Ke Xue Yuan Xue Bao*, 35: 639-44.

Metivier, M., B. Y. Monroy, E. Gallaud, R. Caous, A. Pascal, L. Richard-Parpaillon, A. Guichet, K. M. Ori-McKenney, and R. Giet. 2019. 'Dual control of Kinesin-1 recruitment to microtubules by Ensconsin in Drosophila neuroblasts and oocytes', *Development*, 146.

Metzger, T., V. Gache, M. Xu, B. Cadot, E. S. Folker, B. E. Richardson, E. R. Gomes, and M. K. Baylies. 2012. 'MAP and kinesin-dependent nuclear positioning is required for skeletal muscle function', *Nature*, 484: 120-4.

Meyer, A. J., D. K. Almendrala, M. M. Go, and S. W. Krauss. 2011. 'Structural protein 4.1R is integrally involved in nuclear envelope protein localization, centrosome-nucleus association and transcriptional signaling', *J Cell Sci*, 124: 1433-44.

Miller, L. M., H. Xiao, B. Burd, S. B. Horwitz, R. H. Angeletti, and P. Verdier-Pinard. 2010. 'Methods in tubulin proteomics', *Methods Cell Biol*, 95: 105-26.

Min, L. J., M. Mogi, J. Iwanami, F. Jing, K. Tsukuda, K. Ohshima, and M. Horiuchi. 2012. 'Angiotensin II type 2 receptor-interacting protein prevents vascular senescence', *J Am Soc Hypertens*, 6: 179-84.

Minoura, I., Y. Hachikubo, Y. Yamakita, H. Takazaki, R. Ayukawa, S. Uchimura, and E. Muto. 2013a. 'Overexpression, purification, and functional analysis of recombinant human tubulin dimer', *FEBS Lett*, 587: 3450-5.

———. 2013b. 'Overexpression, purification, and functional analysis of recombinant human tubulin dimer', *FEBS Lett*, 587: 3450-5.

Mishima, M., R. Maesaki, M. Kasa, T. Watanabe, M. Fukata, K. Kaibuchi, and T. Hakoshima. 2007a. 'Structural basis for tubulin recognition by cytoplasmic linker protein 170 and its autoinhibition', *Proc Natl Acad Sci U S A*, 104: 10346-51.

———. 2007b. 'Structural basis for tubulin recognition by cytoplasmic linker protein 170 and its autoinhibition', *Proc Natl Acad Sci U S A*, 104: 10346-51.

Mitchison, T., and M. Kirschner. 1984a. 'Dynamic instability of microtubule growth', *Nature*, 312: 237-42.

———. 1984b. 'Dynamic instability of microtubule growth', *Nature*, 312: 237-42.

Mohri, H. 1968. 'Amino-acid composition of "Tubulin" constituting microtubules of sperm flagella', *Nature*, 217: 1053-4.

Molina, A., S. Rodrigues-Ferreira, A. Di Tommaso, and C. Nahmias. 2011. '[ATIP, a novel superfamily of microtubule-associated proteins]', *Med Sci (Paris)*, 27: 244-6.

Molina, A., L. Velot, L. Ghouinem, M. Abdelkarim, B. P. Bouchet, A. C. Luissint, I. Bouhlel, M. Morel, E. Sapharikas, A. Di Tommaso, S. Honore, D. Braguer, N. Gruel, A. Vincent-Salomon, O. Delattre, B. Sigal-Zafrani, F. Andre, B. Terris, A. Akhmanova, M. Di Benedetto, C. Nahmias, and S. Rodrigues-Ferreira. 2013. 'ATIP3, a novel prognostic marker of breast cancer patient survival, limits cancer cell migration and slows metastatic progression by regulating microtubule dynamics', *Cancer Res*, 73: 2905-15.

Mollinari, C., J. P. Kleman, W. Jiang, G. Schoehn, T. Hunter, and R. L. Margolis. 2002a. 'PRC1 is a microtubule binding and bundling protein essential to maintain the mitotic spindle midzone', *J Cell Biol*, 157: 1175-86.

———. 2002b. 'PRC1 is a microtubule binding and bundling protein essential to maintain the mitotic spindle midzone', *J Cell Biol*, 157: 1175-86.

Monroy, B. Y., D. L. Sawyer, B. E. Ackermann, M. M. Borden, T. C. Tan, and K. M. Ori-McKenney. 2018. 'Competition between microtubule-associated proteins directs motor transport', *Nat Commun*, 9: 1487.

Monroy, B. Y., T. C. Tan, J. M. Oclaman, J. S. Han, S. Simo, S. Niwa, D. W. Nowakowski, R. J. McKenney, and K. M. Ori-McKenney. 2020. 'A Combinatorial MAP Code Dictates Polarized Microtubule Transport', *Dev Cell*, 53: 60-72 e4.

Moolman, D. L., O. V. Vitolo, J. P. Vonsattel, and M. L. Shelanski. 2004. 'Dendrite and dendritic spine alterations in Alzheimer models', *J Neurocytol*, 33: 377-87.

Moore, R. C., N. A. Durso, and R. J. Cyr. 1998. 'Elongation factor-1alpha stabilizes microtubules in a calcium/calmodulin-dependent manner', *Cell Motil Cytoskeleton*, 41: 168-80.

Moores, C. A., M. Perderiset, C. Kappeler, S. Kain, D. Drummond, S. J. Perkins, J. Chelly, R. Cross, A. Houdusse, and F. Francis. 2006. 'Distinct roles of doublecortin modulating the microtubule cytoskeleton', *EMBO J*, 25: 4448-57.

Mori, A., H. Aizawa, T. C. Saido, H. Kawasaki, K. Mizuno, H. Murofushi, K. Suzuki, and H. Sakai. 1991. 'Site-specific phosphorylation by protein kinase C inhibits assembly-promoting activity of microtubule-associated protein 4', *Biochemistry*, 30: 9341-6.

Mori, Y., Y. Taniyama, S. Tanaka, H. Fukuchi, and Y. Terada. 2015. 'Microtubule-bundling activity of the centrosomal protein, Cep169, and its binding to microtubules', *Biochem Biophys Res Commun*, 467: 754-9.

Moritz, M., M. B. Braunfeld, V. Guenebaut, J. Heuser, and D. A. Agard. 2000. 'Structure of the gamma-tubulin ring complex: a template for microtubule nucleation', *Nat Cell Biol*, 2: 365-70.

Mostowy, S. 2014. 'Multiple roles of the cytoskeleton in bacterial autophagy', *PLoS Pathog*, 10: e1004409.

Muller, M. T., R. Schempp, A. Lutz, T. Felder, E. Felder, and P. Miklavc. 2019. 'Interaction of microtubules and actin during the post-fusion phase of exocytosis', *Sci Rep*, 9: 11973.

Murayama, S., H. Mori, Y. Ihara, and M. Tomonaga. 1990. 'Immunocytochemical and ultrastructural studies of Pick's disease', *Ann Neurol*, 27: 394-405.

Murphy, D. B., and G. G. Borisy. 1975a. 'Association of high-molecular-weight proteins with microtubules and their role in microtubule assembly in vitro', *Proc Natl Acad Sci U S A*, 72: 2696-700.

———. 1975b. 'Association of high-molecular-weight proteins with microtubules and their role in microtubule assembly in vitro', *Proc Natl Acad Sci U S A*, 72: 2696-700.

Murphy, S. M., and T. Stearns. 1996. 'Cytoskeleton: microtubule nucleation takes shape', *Curr Biol*, 6: 642-4.

Murray, J. W., B. T. Edmonds, G. Liu, and J. Condeelis. 1996. 'Bundling of actin filaments by elongation factor 1 alpha inhibits polymerization at filament ends', *J Cell Biol*, 135: 1309-21.

Nagao, Y., N. Mimura, J. Takeda, K. Yoshida, Y. Shiozawa, M. Oshima, K. Aoyama, A. Saraya, S. Koide, O. Rizq, Y. Hasegawa, Y. Shiraishi, K. Chiba, H. Tanaka, D. Nishijima, Y. Isshiki, K. Kayamori, C. Kawajiri-Manako, N. Oshima-Hasegawa, S. Tsukamoto, S. Mitsukawa, Y. Takeda, C. Ohwada, M. Takeuchi, T. Iseki, S. Misawa, S. Miyano, O. Ohara, K. Yokote, E. Sakaida, S. Kuwabara, M. Sanada, A. Iwama, S. Ogawa, and C. Nakaseko. 2019. 'Genetic and transcriptional landscape of plasma cells in POEMS syndrome', *Leukemia*, 33: 1723-35.

Nakano, A., H. Kato, T. Watanabe, K. D. Min, S. Yamazaki, Y. Asano, O. Seguchi, S. Higo, Y. Shintani, H. Asanuma, M. Asakura, T. Minamino, K. Kaibuchi, N. Mochizuki, M. Kitakaze, and S. Takashima. 2010. 'AMPK controls the speed of microtubule polymerization and directional cell migration through CLIP-170 phosphorylation', *Nat Cell Biol*, 12: 583-90.

Narendra, D., J. E. Walker, and R. Youle. 2012. 'Mitochondrial quality control mediated by PINK1 and Parkin: links to parkinsonism', *Cold Spring Harb Perspect Biol*, 4.

Navarro-Barriuso, J., M. J. Mansilla, B. Quirant-Sanchez, A. Ardiaca-Martinez, A. Teniente-Serra, S. Presas-Rodriguez, A. Ten Brinke, C. Ramo-Tello, and E. M. Martinez-Caceres. 2019. 'MAP7 and MUCL1 Are Biomarkers of Vitamin D3-Induced Tolerogenic Dendritic Cells in Multiple Sclerosis Patients', *Front Immunol*, 10: 1251.

Nédélec, F., and T. Surrey. 2001. 'Dynamics of microtubule aster formation by motor complexes', *Comptes Rendus de l'Académie des Sciences - Series IV - Physics*, 2: 841-47.

Neukirchen, D., and F. Bradke. 2011. 'Cytoplasmic linker proteins regulate neuronal polarization through microtubule and growth cone dynamics', *J Neurosci*, 31: 1528-38.

Nieuwenhuis, J., A. Adamopoulos, O. B. Bleijerveld, A. Mazouzi, E. Stickel, P. Celie, M. Altelaar, P. Knipscheer, A. Perrakis, V. A. Blomen, and T. R. Brummelkamp. 2017. 'Vasohibins encode tubulin detyrosinating activity', *Science*, 358: 1453-56.

Nirschl, J. J., M. M. Magiera, J. E. Lazarus, C. Janke, and E. L. Holzbaur. 2016. 'alpha-Tubulin Tyrosination and CLIP-170 Phosphorylation Regulate the Initiation of Dynein-Driven Transport in Neurons', *Cell Rep*, 14: 2637-52.

Nishi, K., Y. Sato, M. Ohno, Y. Hiraoka, S. Saijo, J. Sakamoto, P. M. Chen, Y. Morita, S. Matsuda, K. Iwasaki, K. Sugizaki, N. Harada, Y. Mukumoto, H. Kiyonari, K. Furuyama, Y. Kawaguchi, S. Uemoto, T. Kita, N. Inagaki, T. Kimura, and E. Nishi. 2016. 'Nardilysin Is Required for Maintaining Pancreatic beta-Cell Function', *Diabetes*, 65: 3015-27.

Niwa, S., F. Nakamura, Y. Tomabechi, M. Aoki, H. Shigematsu, T. Matsumoto, A. Yamagata, S. Fukai, N. Hirokawa, Y. Goshima, M. Shirouzu, and R. Nitta. 2017. 'Structural basis for CRMP2-induced axonal microtubule formation', *Sci Rep*, 7: 10681.

Nogales, E. 2000. 'Structural insights into microtubule function', *Annu Rev Biochem*, 69: 277-302.

Nogales, E., M. Whittaker, R. A. Milligan, and K. H. Downing. 1999. 'High-resolution model of the microtubule', *Cell*, 96: 79-88.

Nogales, E., S. G. Wolf, and K. H. Downing. 1998. 'Structure of the alpha beta tubulin dimer by electron crystallography', *Nature*, 391: 199-203.

Norris, S. R., S. Jung, P. Singh, C. E. Strothman, A. L. Erwin, M. D. Ohi, M. Zanic, and R. Ohi. 2018. 'Microtubule minus-end aster organization is driven by processive HSET-tubulin clusters', *Nat Commun*, 9: 2659.

North, B. J., B. L. Marshall, M. T. Borra, J. M. Denu, and E. Verdin. 2003. 'The human Sir2 ortholog, SIRT2, is an NAD+-dependent tubulin deacetylase', *Mol Cell*, 11: 437-44.

O'Connor, V., S. H. Houtman, C. I. De Zeeuw, T. V. Bliss, and P. J. French. 2004. 'Eml5, a novel WD40 domain protein expressed in rat brain', *Gene*, 336: 127-37.

Oeding, S. J., K. Majstrowicz, X. P. Hu, V. Schwarz, A. Freitag, U. Honnert, P. Nikolaus, and M. Bahler. 2018. 'Identification of Miro1 and Miro2 as mitochondrial receptors for myosin XIX', *J Cell Sci*, 131.

Ohno, M., Y. Hiraoka, S. F. Lichtenthaler, K. Nishi, S. Saijo, T. Matsuoka, H. Tomimoto, W. Araki, R. Takahashi, T. Kita, T. Kimura, and E. Nishi. 2014. 'Nardilysin prevents amyloid plaque formation by enhancing alpha-secretase activity in an Alzheimer's disease mouse model', *Neurobiol Aging*, 35: 213-22.

Ohno, M., Y. Hiraoka, T. Matsuoka, H. Tomimoto, K. Takao, T. Miyakawa, N. Oshima, H. Kiyonari, T. Kimura, T. Kita, and E. Nishi. 2009. 'Nardilysin regulates axonal maturation and myelination in the central and peripheral nervous system', *Nat Neurosci*, 12: 1506-13.

Ohta, K., M. Toriyama, M. Miyazaki, H. Murofushi, S. Hosoda, S. Endo, and H. Sakai. 1990. 'The mitotic apparatus-associated 51-kDa protein from sea urchin eggs is a GTP-binding protein and is immunologically related to yeast polypeptide elongation factor 1 alpha', *J Biol Chem*, 265: 3240-7.

Ohta, S., M. Hamada, N. Sato, and I. Toramoto. 2015. 'Polyglutamylated Tubulin Binding Protein C1orf96/CSAP Is Involved in Microtubule Stabilization in Mitotic Spindles', *PLoS One*, 10: e0142798.

Olenick, M. A., and E. L. F. Holzbaur. 2019. 'Dynein activators and adaptors at a glance', *J Cell Sci*, 132.

Oliveto, S., R. Alfieri, A. Miluzio, A. Scagliola, R. S. Secli, P. Gasparini, S. Grosso, L. Cascione, L. Mutti, and S. Biffo. 2018. 'A Polysome-Based microRNA Screen Identifies miR-24-3p as a Novel Promigratory miRNA in Mesothelioma', *Cancer Res*, 78: 5741-53.

Oltra, S., F. Martinez, C. Orellana, E. Grau, J. M. Fernandez, A. Canete, and V. Castel. 2005. 'The doublecortin gene, a new molecular marker to detect minimal residual disease in neuroblastoma', *Diagn Mol Pathol*, 14: 53-7.

Opal, P., J. J. Garcia, F. Propst, A. Matilla, H. T. Orr, and H. Y. Zoghbi. 2003. 'Mapmodulin/leucine-rich acidic nuclear protein binds the light chain of microtubule-associated protein 1B and modulates neuritogenesis', *J Biol Chem*, 278: 34691-9.

Orbach, R., and J. Howard. 2019. 'The dynamic and structural properties of axonemal tubulins support the high length stability of cilia', *Nat Commun*, 10: 1838.

Orban-Nemeth, Z., H. Simader, S. Badurek, A. Trancikova, and F. Propst. 2005. 'Microtubule-associated protein 1S, a short and ubiquitously expressed member of the microtubule-associated protein 1 family', *J Biol Chem*, 280: 2257-65.

Orlacchio, A., P. Calabresi, A. Rum, A. Tarzia, A. M. Salvati, T. Kawarai, A. Stefani, A. Pisani, G. Bernardi, P. Cianciulli, and P. Caprari. 2007. 'Neuroacanthocytosis associated with a defect of the 4.1R membrane protein', *BMC Neurol*, 7: 4.

Orr, M. E., A. C. Sullivan, and B. Frost. 2017. 'A Brief Overview of Tauopathy: Causes, Consequences, and Therapeutic Strategies', *Trends Pharmacol Sci*, 38: 637-48.

Owa, M., T. Uchihashi, H. A. Yanagisawa, T. Yamano, H. Iguchi, H. Fukuzawa, K. I. Wakabayashi, T. Ando, and M. Kikkawa. 2019. 'Inner lumen proteins stabilize doublet microtubules in cilia and flagella', *Nat Commun*, 10: 1143.

Pamula, M. C., S. C. Ti, and T. M. Kapoor. 2016. 'The structured core of human beta tubulin confers isotype-specific polymerization properties', *J Cell Biol*, 213: 425-33.

Pan, X., Y. Cao, R. Stucchi, P. J. Hooikaas, S. Portegies, L. Will, M. Martin, A. Akhmanova, M. Harterink, and C. C. Hoogenraad. 2019. 'MAP7D2 Localizes to the Proximal Axon and Locally Promotes Kinesin-1-Mediated Cargo Transport into the Axon', *Cell Rep*, 26: 1988-99 e6.

Panse, V. G., U. Hardeland, T. Werner, B. Kuster, and E. Hurt. 2004. 'A proteome-wide approach identifies sumoylated substrate proteins in yeast', *J Biol Chem*, 279: 41346-51.

Papasozomenos, S. C., and L. I. Binder. 1986. 'Microtubule-associated protein 2 (MAP2) is present in astrocytes of the optic nerve but absent from astrocytes of the optic tract', *J Neurosci*, 6: 1748-56.

Park, I. Y., P. Chowdhury, D. N. Tripathi, R. T. Powell, R. Dere, E. A. Terzo, W. K. Rathmell, and C. L. Walker. 2016. 'Methylated alpha-tubulin antibodies recognize a new microtubule modification on mitotic microtubules', *MAbs*, 8: 1590-97.

Parra, M., P. Gascard, L. D. Walensky, J. A. Gimm, S. Blackshaw, N. Chan, Y. Takakuwa, T. Berger, G. Lee, J. A. Chasis, S. H. Snyder, N. Mohandas, and J. G. Conboy. 2000. 'Molecular and functional characterization of protein 4.1B, a novel member of the protein 4.1 family with high level, focal expression in brain', *J Biol Chem*, 275: 3247-55.

Paschal, B. M., H. S. Shpetner, and R. B. Vallee. 1987. 'MAP 1C is a microtubule-activated ATPase which translocates microtubules in vitro and has dynein-like properties', *J Cell Biol*, 105: 1273-82.

Paschal, B. M., and R. B. Vallee. 1987. 'Retrograde transport by the microtubule-associated protein MAP 1C', *Nature*, 330: 181-3.

Pedrotti, B., R. Colombo, and K. Islam. 1994a. 'Interactions of microtubule-associated protein MAP2 with unpolymerized and polymerized tubulin and actin using a 96-well microtiter plate solid-phase immunoassay', *Biochemistry*, 33: 8798-806.

———. 1994b. 'Microtubule associated protein MAP1A is an actin-binding and crosslinking protein', *Cell Motil Cytoskeleton*, 29: 110-6.

Pedrotti, B., M. Francolini, F. Cotelli, and K. Islam. 1996. 'Modulation of microtubule shape in vitro by high molecular weight microtubule associated proteins MAP1A, MAP1B, and MAP2', *FEBS Lett*, 384: 147-50.

Pedrotti, B., and K. Islam. 1994. 'Purified native microtubule associated protein MAP1A: kinetics of microtubule assembly and MAP1A/tubulin stoichiometry', *Biochemistry*, 33: 12463-70.

Pereira, A. L., A. J. Pereira, A. R. Maia, K. Drabek, C. L. Sayas, P. J. Hergert, M. Lince-Faria, I. Matos, C. Duque, T. Stepanova, C. L. Rieder, W. C. Earnshaw, N. Galjart, and H. Maiato. 2006. 'Mammalian CLASP1 and CLASP2 cooperate to ensure mitotic fidelity by regulating spindle and kinetochore function', *Mol Biol Cell*, 17: 4526-42.

Perez, F., G. S. Diamantopoulos, R. Stalder, and T. E. Kreis. 1999. 'CLIP-170 highlights growing microtubule ends in vivo', *Cell*, 96: 517-27.

Perez, M., I. Santa-Maria, E. Gomez de Barreda, X. Zhu, R. Cuadros, J. R. Cabrero, F. Sanchez-Madrid, H. N. Dawson, M. P. Vitek, G. Perry, M. A. Smith, and J. Avila. 2009. 'Tau--an inhibitor of deacetylase HDAC6 function', *J Neurochem*, 109: 1756-66.

Perez, Y., R. Bar-Yaacov, R. Kadir, O. Wormser, I. Shelef, O. S. Birk, H. Flusser, and R. Y. Birnbaum. 2019a. 'Mutations in the microtubule-associated protein MAP11 (C7orf43) cause microcephaly in humans and zebrafish', *Brain*, 142: 574-85.

———. 2019b. 'Mutations in the microtubule-associated protein MAP11 (C7orf43) cause microcephaly in humans and zebrafish', *Brain*, 142: 574-85.

Perez-Ferreiro, C. M., C. M. Luque, and I. Correas. 2001. '4.1R proteins associate with interphase microtubules in human T cells: a 4.1R constitutive region is involved in tubulin binding', *J Biol Chem*, 276: 44785-91.

Peris, L., M. Bisbal, J. Martinez-Hernandez, Y. Saoudi, J. Jonckheere, M. Rolland, M. Sebastien, J. Brocard, E. Denarier, C. Bosc, C. Guerin, S. Gory-Faure, J. C. Deloulme, F. Lante, I. Arnal, A. Buisson, Y. Goldberg, L. Blanchoin, C. Delphin, and A. Andrieux. 2018. 'A key function for microtubule-associated-protein 6 in activity-dependent stabilisation of actin filaments in dendritic spines', *Nat Commun*, 9: 3775.

Peris, L., M. Thery, J. Faure, Y. Saoudi, L. Lafanechere, J. K. Chilton, P. Gordon-Weeks, N. Galjart, M. Bornens, L. Wordeman, J. Wehland, A. Andrieux, and D. Job. 2006. 'Tubulin tyrosination is a major factor affecting the recruitment of CAP-Gly proteins at microtubule plus ends', *J Cell Biol*, 174: 839-49.

Peris, L., M. Wagenbach, L. Lafanechere, J. Brocard, A. T. Moore, F. Kozielski, D. Job, L. Wordeman, and A. Andrieux. 2009. 'Motor-dependent microtubule disassembly driven by tubulin tyrosination', *J Cell Biol*, 185: 1159-66.

Petratos, S., E. Ozturk, M. F. Azari, R. Kenny, J. Y. Lee, K. A. Magee, A. R. Harvey, C. McDonald, K. Taghian, L. Moussa, P. Mun Aui, C. Siatskas, S. Litwak, M. G. Fehlings, S. M. Strittmatter, and C. C. Bernard. 2012. 'Limiting multiple sclerosis related axonopathy by blocking Nogo receptor and CRMP-2 phosphorylation', *Brain*, 135: 1794-818.

Pickart, C. M., and M. J. Eddins. 2004. 'Ubiquitin: structures, functions, mechanisms', *Biochim Biophys Acta*, 1695: 55-72.

Pierre, P., R. Pepperkok, and T. E. Kreis. 1994. 'Molecular characterization of two functional domains of CLIP-170 in vivo', *J Cell Sci*, 107 (Pt 7): 1909-20.

Pierre, P., J. Scheel, J. E. Rickard, and T. E. Kreis. 1992. 'CLIP-170 links endocytic vesicles to microtubules', *Cell*, 70: 887-900.

Piperno, G., M. LeDizet, and X. J. Chang. 1987. 'Microtubules containing acetylated alpha-tubulin in mammalian cells in culture', *J Cell Biol*, 104: 289-302.

Poliakova, K., A. Adebola, C. L. Leung, B. Favre, R. K. Liem, I. Schepens, and L. Borradori. 2014. 'BPAG1a and b associate with EB1 and EB3 and modulate vesicular transport, Golgi apparatus structure, and cell migration in C2.7 myoblasts', *PLoS One*, 9: e107535.

Poplawski, G. H., A. K. Tranziska, I. Leshchyns'ka, I. D. Meier, T. Streichert, V. Sytnyk, and M. Schachner. 2012. 'L1CAM increases MAP2 expression via the MAPK pathway to promote neurite outgrowth', *Mol Cell Neurosci*, 50: 169-78.

Portran, D., L. Schaedel, Z. Xu, M. Thery, and M. V. Nachury. 2017. 'Tubulin acetylation protects long-lived microtubules against mechanical ageing', *Nat Cell Biol*, 19: 391-98.

Preciado Lopez, M., F. Huber, I. Grigoriev, M. O. Steinmetz, A. Akhmanova, G. H. Koenderink, and M. Dogterom. 2014. 'Actin-microtubule coordination at growing microtubule ends', *Nat Commun*, 5: 4778.

Prota, A. E., M. M. Magiera, M. Kuijpers, K. Bargsten, D. Frey, M. Wieser, R. Jaussi, C. C. Hoogenraad, R. A. Kammerer, C. Janke, and M. O. Steinmetz. 2013. 'Structural basis of tubulin tyrosination by tubulin tyrosine ligase', *J Cell Biol*, 200: 259-70.

Qu, D., N. Weygant, J. Yao, P. Chandrakesan, W. L. Berry, R. May, K. Pitts, S. Husain, S. Lightfoot, M. Li, T. C. Wang, G. An, C. Clendenin, B. Z. Stanger, and C. W. Houchen. 2019. 'Overexpression of DCLK1-AL Increases Tumor Cell Invasion, Drug Resistance, and KRAS Activation and Can Be Targeted to Inhibit Tumorigenesis in Pancreatic Cancer', *J Oncol*, 2019: 6402925.

Quaderi, N. A., S. Schweiger, K. Gaudenz, B. Franco, E. I. Rugarli, W. Berger, G. J. Feldman, M. Volta, G. Andolfi, S. Gilgenkrantz, R. W. Marion, R. C. Hennekam, J. M. Opitz, M. Muenke, H. H. Ropers, and A. Ballabio. 1997. 'Opitz G/BBB syndrome, a defect of

midline development, is due to mutations in a new RING finger gene on Xp22', *Nat Genet*, 17: 285-91.

Quinn, C. C., E. Chen, T. G. Kinjo, G. Kelly, A. W. Bell, R. C. Elliott, P. S. McPherson, and S. Hockfield. 2003. 'TUC-4b, a novel TUC family variant, regulates neurite outgrowth and associates with vesicles in the growth cone', *J Neurosci*, 23: 2815-23.

Ramkumar, A., B. Y. Jong, and K. M. Ori-McKenney. 2018. 'ReMAPping the microtubule landscape: How phosphorylation dictates the activities of microtubule-associated proteins', *Dev Dyn*, 247: 138-55.

Ray, M., J. Ruan, and W. Zhang. 2008. 'Variations in the transcriptome of Alzheimer's disease reveal molecular networks involved in cardiovascular diseases', *Genome Biol*, 9: R148.

Raybin, D., and M. Flavin. 1975. 'An enzyme tyrosylating alpha-tubulin and its role in microtubule assembly', *Biochem Biophys Res Commun*, 65: 1088-95.

Reck-Peterson, S. L., W. B. Redwine, R. D. Vale, and A. P. Carter. 2018. 'The cytoplasmic dynein transport machinery and its many cargoes', *Nat Rev Mol Cell Biol*, 19: 382-98.

Redeker, V., N. Levilliers, J. M. Schmitter, J. P. Le Caer, J. Rossier, A. Adoutte, and M. H. Bre. 1994. 'Polyglycylation of tubulin: a posttranslational modification in axonemal microtubules', *Science*, 266: 1688-91.

Reese, M. L., S. Dakoji, D. S. Bredt, and V. Dotsch. 2007. 'The guanylate kinase domain of the MAGUK PSD-95 binds dynamically to a conserved motif in MAP1a', *Nat Struct Mol Biol*, 14: 155-63.

Regnard, C., D. Fesquet, C. Janke, D. Boucher, E. Desbruyeres, A. Koulakoff, C. Insina, P. Travo, and B. Edde. 2003. 'Characterisation of PGs1, a subunit of a protein complex co-purifying with tubulin polyglutamylase', *J Cell Sci*, 116: 4181-90.

Rehbein, M., S. Kindler, S. Horke, and D. Richter. 2000. 'Two trans-acting rat-brain proteins, MARTA1 and MARTA2, interact specifically with the dendritic targeting element in MAP2 mRNAs', *Brain Res Mol Brain Res*, 79: 192-201.

Ren, Y., J. Zhao, and J. Feng. 2003a. 'Parkin binds to alpha/beta tubulin and increases their ubiquitination and degradation', *J Neurosci*, 23: 3316-24.

———. 2003b. 'Parkin binds to alpha/beta tubulin and increases their ubiquitination and degradation', *J Neurosci*, 23: 3316-24.

Richards, M. W., E. W. Law, L. P. Rennalls, S. Busacca, L. O'Regan, A. M. Fry, D. A. Fennell, and R. Bayliss. 2014. 'Crystal structure of EML1 reveals the basis for Hsp90 dependence of oncogenic EML4-ALK by disruption of an atypical beta-propeller domain', *Proc Natl Acad Sci U S A*, 111: 5195-200.

Richards, M. W., L. O'Regan, D. Roth, J. M. Montgomery, A. Straube, A. M. Fry, and R. Bayliss. 2015. 'Microtubule association of EML proteins and the EML4-ALK variant 3 oncoprotein require an N-terminal trimerization domain', *Biochem J*, 467: 529-36.

Rickard, J. E., and T. E. Kreis. 1990. 'Identification of a novel nucleotide-sensitive microtubule-binding protein in HeLa cells', *J Cell Biol*, 110: 1623-33.

Rijkers, T., and U. Ruther. 1996. 'Sequence and expression pattern of an evolutionarily conserved transcript identified by gene trapping', *Biochim Biophys Acta*, 1307: 294-300.

Rodrigues-Ferreira, S., A. Di Tommaso, A. Dimitrov, S. Cazaubon, N. Gruel, H. Colasson, A. Nicolas, N. Chaverot, V. Molinie, F. Reyal, B. Sigal-Zafrani, B. Terris, O. Delattre, F. Radvanyi, F. Perez, A. Vincent-Salomon, and C. Nahmias. 2009. '8p22 MTUS1 gene product ATIP3 is a novel anti-mitotic protein underexpressed in invasive breast carcinoma of poor prognosis', *PLoS One*, 4: e7239.

Roeles, J., and G. Tsiavaliaris. 2019. 'Actin-microtubule interplay coordinates spindle assembly in human oocytes', *Nat Commun*, 10: 4651.

Rogowski, K., F. Juge, J. van Dijk, D. Wloga, J. M. Strub, N. Levilliers, D. Thomas, M. H. Bre, A. Van Dorsselaer, J. Gaertig, and C. Janke. 2009. 'Evolutionary divergence of enzymatic mechanisms for posttranslational polyglycylation', *Cell*, 137: 1076-87.

Rogowski, K., J. van Dijk, M. M. Magiera, C. Bosc, J. C. Deloulme, A. Bosson, L. Peris, N. D. Gold, B. Lacroix, M. Bosch Grau, N. Bec, C. Larroque, S. Desagher, M. Holzer, A. Andrieux, M. J. Moutin, and C. Janke. 2010. 'A family of protein-deglutamylating enzymes associated with neurodegeneration', *Cell*, 143: 564-78.

Roll-Mecak, A., and F. J. McNally. 2010. 'Microtubule-severing enzymes', *Curr Opin Cell Biol*, 22: 96-103.

Roll-Mecak, A., and R. D. Vale. 2008. 'Structural basis of microtubule severing by the hereditary spastic paraplegia protein spastin', *Nature*, 451: 363-7.

Rosas-Acosta, G., W. K. Russell, A. Deyrieux, D. H. Russell, and V. G. Wilson. 2005. 'A universal strategy for proteomic studies of SUMO and other ubiquitin-like modifiers', *Mol Cell Proteomics*, 4: 56-72.

Rosoklija, G., J. G. Keilp, G. Toomayan, B. Mancevski, V. Haroutunian, D. Liu, D. Malespina, A. P. Hays, S. Sadiq, N. Latov, and A. J. Dwork. 2005. 'Altered subicular MAP2 immunoreactivity in schizophrenia', *Prilozi*, 26: 13-34.

Rouquier, S., M. J. Pillaire, C. Cazaux, and D. Giorgi. 2014. 'Expression of the microtubule-associated protein MAP9/ASAP and its partners AURKA and PLK1 in colorectal and breast cancers', *Dis Markers*, 2014: 798170.

Rudiger, M., J. Wehland, and K. Weber. 1994. 'The carboxy-terminal peptide of detyrosinated alpha tubulin provides a minimal system to study the substrate specificity of tubulin-tyrosine ligase', *Eur J Biochem*, 220: 309-20.

Rüdiger, Manfred, Uwe Plessman, Klaus-Dieter Klöppel, Jürgen Wehland, and Klaus Weber. 1992. 'Class II tubulin, the major brain β tubulin isotype is polyglutamylated on glutamic acid residue 435', *FEBS Letters*, 308: 101-05.

Sabir, S. R., S. Yeoh, G. Jackson, and R. Bayliss. 2017. 'EML4-ALK Variants: Biological and Molecular Properties, and the Implications for Patients', *Cancers (Basel)*, 9.

Saffin, J. M., M. Venoux, C. Prigent, J. Espeut, F. Poulat, D. Giorgi, A. Abrieu, and S. Rouquier. 2005. 'ASAP, a human microtubule-associated protein required for bipolar spindle assembly and cytokinesis', *Proc Natl Acad Sci U S A*, 102: 11302-7.

Sagie, S., T. Lerman-Sagie, S. Maljevic, K. Yosovich, K. Detert, S. K. Chung, M. I. Rees, H. Lerche, and D. Lev. 2018. 'Expanding the phenotype of TRAK1 mutations: hyperekplexia and refractory status epilepticus', *Brain*, 141: e55.

Saillour, Y., L. Broix, E. Bruel-Jungerman, N. Lebrun, G. Muraca, J. Rucci, K. Poirier, R. Belvindrah, F. Francis, and J. Chelly. 2014. 'Beta tubulin isoforms are not interchangeable for rescuing impaired radial migration due to Tubb3 knockdown', *Hum Mol Genet*, 23: 1516-26.

Samora, C. P., B. Mogessie, L. Conway, J. L. Ross, A. Straube, and A. D. McAinsh. 2011. 'MAP4 and CLASP1 operate as a safety mechanism to maintain a stable spindle position in mitosis', *Nat Cell Biol*, 13: 1040-50.

Samsonov, A., J. Z. Yu, M. Rasenick, and S. V. Popov. 2004. 'Tau interaction with microtubules in vivo', *J Cell Sci*, 117: 6129-41.

Sanchez-Huertas, C., M. Bonhomme, A. Falco, C. Fagotto-Kaufmann, J. van Haren, F. Jeanneteau, N. Galjart, A. Debant, and J. Boudeau. 2020. 'The +TIP Navigator-1 is an actin-microtubule crosslinker that regulates axonal growth cone motility', *J Cell Biol*, 219.

Sanchez-Soriano, N., M. Travis, F. Dajas-Bailador, C. Goncalves-Pimentel, A. J. Whitmarsh, and A. Prokop. 2009. 'Mouse ACF7 and drosophila short stop modulate filopodia

formation and microtubule organisation during neuronal growth', *J Cell Sci*, 122: 2534-42.

Saoudi, Y., I. Paintrand, L. Multigner, and D. Job. 1995. 'Stabilization and bundling of subtilisin-treated microtubules induced by microtubule associated proteins', *J Cell Sci*, 108 (Pt 1): 357-67.

Saredi, A., L. Howard, and D. A. Compton. 1997. 'Phosphorylation regulates the assembly of NuMA in a mammalian mitotic extract', *J Cell Sci*, 110 (Pt 11): 1287-97.

Sasikumar, A. N., W. B. Perez, and T. G. Kinzy. 2012. 'The many roles of the eukaryotic elongation factor 1 complex', *Wiley Interdiscip Rev RNA*, 3: 543-55.

Satterstrom, F. K., R. K. Walters, T. Singh, E. M. Wigdor, F. Lescai, D. Demontis, J. A. Kosmicki, J. Grove, C. Stevens, J. Bybjerg-Grauholm, M. Baekvad-Hansen, D. S. Palmer, J. B. Maller, Psych-Broad Consortium i, M. Nordentoft, O. Mors, E. B. Robinson, D. M. Hougaard, T. M. Werge, P. Bo Mortensen, B. M. Neale, A. D. Borglum, and M. J. Daly. 2019. 'Autism spectrum disorder and attention deficit hyperactivity disorder have a similar burden of rare protein-truncating variants', *Nat Neurosci*, 22: 1961-65.

Sattilaro, R. F. 1986. 'Interaction of microtubule-associated protein 2 with actin filaments', *Biochemistry*, 25: 2003-9.

Sawamura, D., K. Nomura, Y. Sugita, M. G. Mattei, M. L. Chu, R. Knowlton, and J. Uitto. 1990a. 'Bullous pemphigoid antigen (BPAG1): cDNA cloning and mapping of the gene to the short arm of human chromosome 6', *Genomics*, 8: 722-6.

———. 1990b. 'Bullous pemphigoid antigen (BPAG1): cDNA cloning and mapping of the gene to the short arm of human chromosome 6', *Genomics*, 8: 722-6.

Schaar, B. T., K. Kinoshita, and S. K. McConnell. 2004. 'Doublecortin microtubule affinity is regulated by a balance of kinase and phosphatase activity at the leading edge of migrating neurons', *Neuron*, 41: 203-13.

Schaedel, L., K. John, J. Gaillard, M. V. Nachury, L. Blanchoin, and M. Thery. 2015. 'Microtubules self-repair in response to mechanical stress', *Nat Mater*, 14: 1156-63.

Schiewek, J., U. Schumacher, T. Lange, S. A. Joosse, H. Wikman, K. Pantel, M. Mikhaylova, M. Kneussel, S. Linder, B. Schmalfeldt, L. Oliveira-Ferrer, and S. Windhorst. 2018. 'Clinical relevance of cytoskeleton associated proteins for ovarian cancer', *J Cancer Res Clin Oncol*, 144: 2195-205.

Schmidt-Cernohorska, M., I. Zhernov, E. Steib, M. Le Guennec, R. Achek, S. Borgers, D. Demurtas, L. Mouawad, Z. Lansky, V. Hamel, and P. Guichard. 2019. 'Flagellar microtubule doublet assembly in vitro reveals a regulatory role of tubulin C-terminal tails', *Science*, 363: 285-88.

Schneider, R., T. Korten, W. J. Walter, and S. Diez. 2015. 'Kinesin-1 motors can circumvent permanent roadblocks by side-shifting to neighboring protofilaments', *Biophys J*, 108: 2249-57.

Schoenfeld, T. A., L. McKerracher, R. Obar, and R. B. Vallee. 1989. 'MAP 1A and MAP 1B are structurally related microtubule associated proteins with distinct developmental patterns in the CNS', *J Neurosci*, 9: 1712-30.

Schulze, E., D. J. Asai, J. C. Bulinski, and M. Kirschner. 1987. 'Posttranslational modification and microtubule stability', *J Cell Biol*, 105: 2167-77.

Schwarz, T. L. 2013. 'Mitochondrial trafficking in neurons', *Cold Spring Harb Perspect Biol*, 5.

Scott, C. W., A. B. Klika, M. M. Lo, T. E. Norris, and C. B. Caputo. 1992. 'Tau protein induces bundling of microtubules in vitro: comparison of different tau isoforms and a tau protein fragment', *J Neurosci Res*, 33: 19-29.

Segretain, D., J. Gilleron, J. N. Bacro, M. Di Marco, D. Carette, and G. Pointis. 2016. 'Ultrastructural localization and distribution of Nardilysin in mammalian male germ cells', *Basic Clin Androl*, 26: 5.

Seirafi, M., G. Kozlov, and K. Gehring. 2015. 'Parkin structure and function', *FEBS J*, 282: 2076-88.

Semenova, I., K. Ikeda, K. Resaul, P. Kraikivski, M. Aguiar, S. Gygi, I. Zaliapin, A. Cowan, and V. Rodionov. 2014. 'Regulation of microtubule-based transport by MAP4', *Mol Biol Cell*, 25: 3119-32.

Sgro, F., F. T. Bianchi, M. Falcone, G. Pallavicini, M. Gai, A. M. Chiotto, G. E. Berto, E. Turco, Y. J. Chang, W. B. Huttner, and F. Di Cunto. 2016. 'Tissue-specific control of midbody microtubule stability by Citron kinase through modulation of TUBB3 phosphorylation', *Cell Death Differ*, 23: 801-13.

Sharp, D. J., and J. L. Ross. 2012. 'Microtubule-severing enzymes at the cutting edge', *J Cell Sci*, 125: 2561-9.

Sheffield, P. J., C. J. Oliver, B. E. Kremer, S. Sheng, Z. Shao, and I. G. Macara. 2003. 'Borg/septin interactions and the assembly of mammalian septin heterodimers, trimers, and filaments', *J Biol Chem*, 278: 3483-8.

Shibata, K., M. Miura, Y. Watanabe, K. Saito, A. Nishimura, K. Furuta, and Y. Y. Toyoshima. 2012. 'A single protofilament is sufficient to support unidirectional walking of dynein and kinesin', *PLoS One*, 7: e42990.

Shida, T., J. G. Cueva, Z. Xu, M. B. Goodman, and M. V. Nachury. 2010. 'The major alpha-tubulin K40 acetyltransferase alphaTAT1 promotes rapid ciliogenesis and efficient mechanosensation', *Proc Natl Acad Sci U S A*, 107: 21517-22.

Shigematsu, H., T. Imasaki, C. Doki, T. Sumi, M. Aoki, T. Uchikubo-Kamo, A. Sakamoto, K. Tokuraku, M. Shirouzu, and R. Nitta. 2018. 'Structural insight into microtubule stabilization and kinesin inhibition by Tau family MAPs', *J Cell Biol*, 217: 4155-63.

Shiina, N., Y. Gotoh, N. Kubomura, A. Iwamatsu, and E. Nishida. 1994. 'Microtubule severing by elongation factor 1 alpha', *Science*, 266: 282-5.

Shimizu, H., Y. Iwayama, K. Yamada, T. Toyota, Y. Minabe, K. Nakamura, M. Nakajima, E. Hattori, N. Mori, N. Osumi, and T. Yoshikawa. 2006. 'Genetic and expression analyses of the STOP (MAP6) gene in schizophrenia', *Schizophr Res*, 84: 244-52.

Shin, S. C., S. K. Im, E. H. Jang, K. S. Jin, E. M. Hur, and E. E. Kim. 2019. 'Structural and Molecular Basis for Katanin-Mediated Severing of Glutamylated Microtubules', *Cell Rep*, 26: 1357-67 e5.

Shinkai-Ouchi, F., Y. Yamakawa, H. Hara, M. Tobiume, M. Nishijima, K. Hanada, and K. Hagiwara. 2010. 'Identification and structural analysis of C-terminally truncated collapsin response mediator protein-2 in a murine model of prion diseases', *Proteome Sci*, 8: 53.

Siahaan, V., J. Krattenmacher, A. A. Hyman, S. Diez, A. Hernandez-Vega, Z. Lansky, and M. Braun. 2019. 'Kinetically distinct phases of tau on microtubules regulate kinesin motors and severing enzymes', *Nat Cell Biol*, 21: 1086-92.

Sirajuddin, M., L. M. Rice, and R. D. Vale. 2014a. 'Regulation of microtubule motors by tubulin isotypes and post-translational modifications', *Nat Cell Biol*, 16: 335-44.

———. 2014b. 'Regulation of microtubule motors by tubulin isotypes and post-translational modifications', *Nat Cell Biol*, 16: 335-44.

Slaughter, T., and M. M. Black. 2003. 'STOP (stable-tubule-only-polypeptide) is preferentially associated with the stable domain of axonal microtubules', *J Neurocytol*, 32: 399-413.

Sloboda, R. D., W. L. Dentler, and J. L. Rosenbaum. 1976. 'Microtubule-associated proteins and the stimulation of tubulin assembly in vitro', *Biochemistry*, 15: 4497-505.

Smith, W. W., Z. Pei, H. Jiang, D. J. Moore, Y. Liang, A. B. West, V. L. Dawson, T. M. Dawson, and C. A. Ross. 2005. 'Leucine-rich repeat kinase 2 (LRRK2) interacts with parkin, and mutant LRRK2 induces neuronal degeneration', *Proc Natl Acad Sci U S A*, 102: 18676-81.

Sobue, K., A. Agarwal-Mawal, W. Li, W. Sun, Y. Miura, and H. K. Paudel. 2000. 'Interaction of neuronal Cdc2-like protein kinase with microtubule-associated protein tau', *J Biol Chem*, 275: 16673-80.

Song, K., W. Hu, F. Yue, J. Zou, W. Li, Q. Chen, Q. Yao, W. Sun, and L. Liu. 2015. 'Transforming Growth Factor TGFbeta Increases Levels of Microtubule-Associated Protein MAP1S and Autophagy Flux in Pancreatic Ductal Adenocarcinomas', *PLoS One*, 10: e0143150.

Song, Y., L. L. Kirkpatrick, A. B. Schilling, D. L. Helseth, N. Chabot, J. W. Keillor, G. V. Johnson, and S. T. Brady. 2013. 'Transglutaminase and polyamination of tubulin: posttranslational modification for stabilizing axonal microtubules', *Neuron*, 78: 109-23.

Sontag, E., V. Nunbhakdi-Craig, G. Lee, R. Brandt, C. Kamibayashi, J. Kuret, C. L. White, 3rd, M. C. Mumby, and G. S. Bloom. 1999. 'Molecular interactions among protein phosphatase 2A, tau, and microtubules. Implications for the regulation of tau phosphorylation and the development of tauopathies', *J Biol Chem*, 274: 25490-8.

Sood, R., P. I. Bader, M. C. Speer, Y. H. Edwards, E. M. Eddings, R. T. Blair, P. Hu, M. U. Faruque, C. M. Robbins, H. Zhang, J. Leuders, K. Morrison, D. Thompson, P. L. Schwartzberg, P. S. Meltzer, and J. M. Trent. 2004. 'Cloning and characterization of an inversion breakpoint at 6q23.3 suggests a role for Map7 in sacral dysgenesis', *Cytogenet Genome Res*, 106: 61-7.

Soppina, V., S. R. Norris, A. S. Dizaji, M. Kortus, S. Veatch, M. Peckham, and K. J. Verhey. 2014. 'Dimerization of mammalian kinesin-3 motors results in superprocessive motion', *Proc Natl Acad Sci U S A*, 111: 5562-7.

Soroosh, A., C. R. Rankin, C. Polytarchou, Z. A. Lokhandwala, A. Patel, L. Chang, C. Pothoulakis, D. Iliopoulos, and D. M. Padua. 2019. 'miR-24 Is Elevated in Ulcerative Colitis Patients and Regulates Intestinal Epithelial Barrier Function', *Am J Pathol*, 189: 1763-74.

Souphron, J., S. Bodakuntla, A. S. Jijumon, G. Lakisic, A. M. Gautreau, C. Janke, and M. M. Magiera. 2019. 'Purification of tubulin with controlled post-translational modifications by polymerization-depolymerization cycles', *Nat Protoc*, 14: 1634-60.

Staropoli, J. F., C. McDermott, C. Martinat, B. Schulman, E. Demireva, and A. Abeliovich. 2003. 'Parkin is a component of an SCF-like ubiquitin ligase complex and protects postmitotic neurons from kainate excitotoxicity', *Neuron*, 37: 735-49.

Steinmetz, M. O., and A. E. Prota. 2018. 'Microtubule-Targeting Agents: Strategies To Hijack the Cytoskeleton', *Trends Cell Biol*, 28: 776-92.

Stowers, R. S., L. J. Megeath, J. Gorska-Andrzejak, I. A. Meinertzhagen, and T. L. Schwarz. 2002. 'Axonal transport of mitochondria to synapses depends on milton, a novel Drosophila protein', *Neuron*, 36: 1063-77.

Strassel, C., M. M. Magiera, A. Dupuis, M. Batzenschlager, A. Hovasse, I. Pleines, P. Gueguen, A. Eckly, S. Moog, L. Mallo, Q. Kimmerlin, S. Chappaz, J. M. Strub, N. Kathiresan, H. de la Salle, A. Van Dorsselaer, C. Ferec, J. Y. Py, C. Gachet, C. Schaeffer-Reiss, B. T. Kile, C. Janke, and F. Lanza. 2019. 'An essential role for alpha4A-tubulin in platelet biogenesis', *Life Sci Alliance*, 2.

Straub, F. B., and G. Feuer. 1989. 'Adenosinetriphosphate. The functional group of actin. 1950', *Biochim Biophys Acta*, 1000: 180-95.

Strittmatter, W. J., A. M. Saunders, M. Goedert, K. H. Weisgraber, L. M. Dong, R. Jakes, D. Y. Huang, M. Pericak-Vance, D. Schmechel, and A. D. Roses. 1994. 'Isoform-specific

interactions of apolipoprotein E with microtubule-associated protein tau: implications for Alzheimer disease', *Proc Natl Acad Sci U S A*, 91: 11183-6.

Stroedicke, M., Y. Bounab, N. Strempel, K. Klockmeier, S. Yigit, R. P. Friedrich, G. Chaurasia, S. Li, F. Hesse, S. P. Riechers, J. Russ, C. Nicoletti, A. Boeddrich, T. Wiglenda, C. Haenig, S. Schnoegl, D. Fournier, R. K. Graham, M. R. Hayden, S. Sigrist, G. P. Bates, J. Priller, M. A. Andrade-Navarro, M. E. Futschik, and E. E. Wanker. 2015. 'Systematic interaction network filtering identifies CRMP1 as a novel suppressor of huntingtin misfolding and neurotoxicity', *Genome Res*, 25: 701-13.

Subramanian, R., E. M. Wilson-Kubalek, C. P. Arthur, M. J. Bick, E. A. Campbell, S. A. Darst, R. A. Milligan, and T. M. Kapoor. 2010. 'Insights into antiparallel microtubule crosslinking by PRC1, a conserved nonmotor microtubule binding protein', *Cell*, 142: 433-43.

Sun, J. J., M. Huang, F. Xiao, and Z. Q. Xi. 2015. 'Echinoderm microtubule-associated protein -like protein 5 in anterior temporal neocortex of patients with intractable epilepsy', *Iran J Basic Med Sci*, 18: 1008-13.

Sun, X., F. Li, B. Dong, S. Suo, M. Liu, D. Li, and J. Zhou. 2013. 'Regulation of tumor angiogenesis by the microtubule-binding protein CLIP-170', *Protein Cell*, 4: 266-76.

Sun, X., J. H. Park, J. Gumerson, Z. Wu, A. Swaroop, H. Qian, A. Roll-Mecak, and T. Li. 2016. 'Loss of RPGR glutamylation underlies the pathogenic mechanism of retinal dystrophy caused by TTLL5 mutations', *Proc Natl Acad Sci U S A*, 113: E2925-34.

Sun, X., X. Shi, M. Liu, D. Li, L. Zhang, X. Liu, and J. Zhou. 2011. 'Mdp3 is a novel microtubule-binding protein that regulates microtubule assembly and stability', *Cell Cycle*, 10: 3929-37.

Sung, H. H., I. A. Telley, P. Papadaki, A. Ephrussi, T. Surrey, and P. Rorth. 2008. 'Drosophila ensconsin promotes productive recruitment of Kinesin-1 to microtubules', *Dev Cell*, 15: 866-76.

Suprenant, K. A., K. Dean, J. McKee, and S. Hake. 1993. 'EMAP, an echinoderm microtubule-associated protein found in microtubule-ribosome complexes', *J Cell Sci*, 104: 445-50.

Sweeney, M. O., A. Collins, S. B. Padrick, and B. L. Goode. 2015. 'A novel role for WAVE1 in controlling actin network growth rate and architecture', *Mol Biol Cell*, 26: 495-505.

Szikora, S., I. Foldi, K. Toth, E. Migh, A. Vig, B. Bugyi, J. Maleth, P. Hegyi, P. Kaltenecker, N. Sanchez-Soriano, and J. Mihaly. 2017a. 'The formin DAAM is required for coordination of the actin and microtubule cytoskeleton in axonal growth cones', *J Cell Sci*, 130: 2506-19.

———. 2017b. 'The formin DAAM is required for coordination of the actin and microtubule cytoskeleton in axonal growth cones', *J Cell Sci*, 130: 2506-19.

Szuhai, K., D. de Jong, W. Y. Leung, C. D. Fletcher, and P. C. Hogendoorn. 2014. 'Transactivating mutation of the MYOD1 gene is a frequent event in adult spindle cell rhabdomyosarcoma', *J Pathol*, 232: 300-7.

Tada, S., M. Furuta, K. Fukada, D. Hirozawa, M. Matsui, F. Aoike, T. Okuno, J. Sawada, H. Mochizuki, and T. Hazama. 2016. 'Severe parkinsonism associated with anti-CRMP5 antibody-positive paraneoplastic neurological syndrome and abnormal signal intensity in the bilateral basal ganglia', *J Neurol Neurosurg Psychiatry*, 87: 907-10.

Takashima, A., M. Murayama, O. Murayama, T. Kohno, T. Honda, K. Yasutake, N. Nihonmatsu, M. Mercken, H. Yamaguchi, S. Sugihara, and B. Wolozin. 1998. 'Presenilin 1 associates with glycogen synthase kinase-3beta and its substrate tau', *Proc Natl Acad Sci U S A*, 95: 9637-41.

Takemura, R., S. Okabe, T. Umeyama, Y. Kanai, N. J. Cowan, and N. Hirokawa. 1992. 'Increased microtubule stability and alpha tubulin acetylation in cells transfected with microtubule-associated proteins MAP1B, MAP2 or tau', *J Cell Sci*, 103 (Pt 4): 953-64.

Tala, X. Sun, J. Chen, L. Zhang, N. Liu, J. Zhou, D. Li, and M. Liu. 2014. 'Microtubule stabilization by Mdp3 is partially attributed to its modulation of HDAC6 in addition to its association with tubulin and microtubules', *PLoS One*, 9: e90932.

Tala, S. Xie, X. Sun, X. Sun, J. Ran, L. Zhang, D. Li, M. Liu, G. Bao, and J. Zhou. 2014. 'Microtubule-associated protein Mdp3 promotes breast cancer growth and metastasis', *Theranostics*, 4: 1052-61.

Tan, R., A. J. Lam, T. Tan, J. Han, D. W. Nowakowski, M. Vershinin, S. Simo, K. M. Ori-McKenney, and R. J. McKenney. 2019. 'Microtubules gate tau condensation to spatially regulate microtubule functions', *Nat Cell Biol*, 21: 1078-85.

Tanaka, T., F. F. Serneo, H. C. Tseng, A. B. Kulkarni, L. H. Tsai, and J. G. Gleeson. 2004. 'Cdk5 phosphorylation of doublecortin ser297 regulates its effect on neuronal migration', *Neuron*, 41: 215-27.

Tao, H., T. Tanaka, and K. Okabe. 2017. 'Doublecortin and CaM kinase-like-1 expression in pathological stage I non-small cell lung cancer', *J Cancer Res Clin Oncol*, 143: 1449-59.

Taylor, K. R., A. K. Holzer, J. F. Bazan, C. A. Walsh, and J. G. Gleeson. 2000. 'Patient mutations in doublecortin define a repeated tubulin-binding domain', *J Biol Chem*, 275: 34442-50.

Tegha-Dunghu, J., B. Neumann, S. Reber, R. Krause, H. Erfle, T. Walter, M. Held, P. Rogers, K. Hupfeld, T. Ruppert, J. Ellenberg, and O. J. Gruss. 2008. 'EML3 is a nuclear microtubule-binding protein required for the correct alignment of chromosomes in metaphase', *J Cell Sci*, 121: 1718-26.

Telley, I. A., I. Gaspar, A. Ephrussi, and T. Surrey. 2013. 'A single Drosophila embryo extract for the study of mitosis ex vivo', *Nat Protoc*, 8: 310-24.

Ti, S. C., G. M. Alushin, and T. M. Kapoor. 2018. 'Human beta-Tubulin Isotypes Can Regulate Microtubule Protofilament Number and Stability', *Dev Cell*, 47: 175-90 e5.

Tian, Y., G. Gawlak, X. Tian, A. S. Shah, N. Sarich, S. Citi, and A. A. Birukova. 2016. 'Role of Cingulin in Agonist-induced Vascular Endothelial Permeability', *J Biol Chem*, 291: 23681-92.

Tint, I., D. Jean, P. W. Baas, and M. M. Black. 2009. 'Doublecortin associates with microtubules preferentially in regions of the axon displaying actin-rich protrusive structures', *J Neurosci*, 29: 10995-1010.

Togashi, K., M. Hasegawa, J. Nagai, A. Tonouchi, D. Masukawa, K. Hensley, Y. Goshima, and T. Ohshima. 2019. 'Genetic suppression of collapsin response mediator protein 2 phosphorylation improves outcome in methyl-4-phenyl-1,2,3,6-tetrahydropyridine-induced Parkinson's model mice', *Genes Cells*, 24: 31-40.

Tokuraku, K., T. Q. Noguchi, M. Nishie, K. Matsushima, and S. Kotani. 2007. 'An isoform of microtubule-associated protein 4 inhibits kinesin-driven microtubule gliding', *J Biochem*, 141: 585-91.

Tokuraku, K., S. Okuyama, K. Matsushima, T. Ikezu, and S. Kotani. 2010. 'Distinct neuronal localization of microtubule-associated protein 4 in the mammalian brain', *Neurosci Lett*, 484: 143-7.

Tortosa, E., C. Montenegro-Venegas, M. Benoist, S. Hartel, C. Gonzalez-Billault, J. A. Esteban, and J. Avila. 2011. 'Microtubule-associated protein 1B (MAP1B) is required for dendritic spine development and synaptic maturation', *J Biol Chem*, 286: 40638-48.

Toyoshima, M., X. Jiang, T. Ogawa, T. Ohnishi, S. Yoshihara, S. Balan, T. Yoshikawa, and N. Hirokawa. 2019. 'Enhanced carbonyl stress induces irreversible multimerization of CRMP2 in schizophrenia pathogenesis', *Life Sci Alliance*, 2.

Tsukada, M., A. Prokscha, E. Ungewickell, and G. Eichele. 2005. 'Doublecortin association with actin filaments is regulated by neurabin II', *J Biol Chem*, 280: 11361-8.

Turk, E., A. A. Wills, T. Kwon, J. Sedzinski, J. B. Wallingford, and T. Stearns. 2015. 'Zeta-Tubulin Is a Member of a Conserved Tubulin Module and Is a Component of the Centriolar Basal Foot in Multiciliated Cells', *Curr Biol*, 25: 2177-83.

Tymanskyj, S. R., T. M. Scales, and P. R. Gordon-Weeks. 2012. 'MAP1B enhances microtubule assembly rates and axon extension rates in developing neurons', *Mol Cell Neurosci*, 49: 110-9.

Tymanskyj, S. R., B. Yang, A. Falnikar, A. C. Lepore, and L. Ma. 2017. 'MAP7 Regulates Axon Collateral Branch Development in Dorsal Root Ganglion Neurons', *J Neurosci*, 37: 1648-61.

Tymanskyj, S. R., B. H. Yang, K. J. Verhey, and L. Ma. 2018. 'MAP7 regulates axon morphogenesis by recruiting kinesin-1 to microtubules and modulating organelle transport', *Elife*, 7.

Tyrrell, D. J., M. G. Blin, J. Song, S. C. Wood, M. Zhang, D. A. Beard, and D. R. Goldstein. 2020. 'Age-Associated Mitochondrial Dysfunction Accelerates Atherogenesis', *Circ Res*, 126: 298-314.

Uchimura, S., T. Fujii, H. Takazaki, R. Ayukawa, Y. Nishikawa, I. Minoura, Y. Hachikubo, G. Kurisu, K. Sutoh, T. Kon, K. Namba, and E. Muto. 2015. 'A flipped ion pair at the dynein-microtubule interface is critical for dynein motility and ATPase activation', *J Cell Biol*, 208: 211-22.

Utreras, E., E. M. Jimenez-Mateos, E. Contreras-Vallejos, E. Tortosa, M. Perez, S. Rojas, L. Saragoni, R. B. Maccioni, J. Avila, and C. Gonzalez-Billault. 2008. 'Microtubule-associated protein 1B interaction with tubulin tyrosine ligase contributes to the control of microtubule tyrosination', *Dev Neurosci*, 30: 200-10.

Uzquiano, A., C. Cifuentes-Diaz, A. Jabali, D. M. Romero, A. Houllier, F. Dingli, C. Maillard, A. Boland, J. F. Deleuze, D. Loew, G. M. S. Mancini, N. Bahi-Buisson, J. Ladewig, and F. Francis. 2019. 'Mutations in the Heterotopia Gene Eml1/EML1 Severely Disrupt the Formation of Primary Cilia', *Cell Rep*, 28: 1596-611 e10.

Vaillant, A. R., R. Muller, A. Langkopf, and D. L. Brown. 1998. 'Characterization of the microtubule-binding domain of microtubule-associated protein 1A and its effects on microtubule dynamics', *J Biol Chem*, 273: 13973-81.

Vale, R. D. 1991. 'Severing of stable microtubules by a mitotically activated protein in Xenopus egg extracts', *Cell*, 64: 827-39.

Vale, R. D., T. S. Reese, and M. P. Sheetz. 1985. 'Identification of a novel force-generating protein, kinesin, involved in microtubule-based motility', *Cell*, 42: 39-50.

Valenstein, M. L., and A. Roll-Mecak. 2016. 'Graded Control of Microtubule Severing by Tubulin Glutamylation', *Cell*, 164: 911-21.

Vallee, R. B., R. J. McKenney, and K. M. Ori-McKenney. 2012. 'Multiple modes of cytoplasmic dynein regulation', *Nat Cell Biol*, 14: 224-30.

Vallee, R. B., J. S. Wall, B. M. Paschal, and H. S. Shpetner. 1988. 'Microtubule-associated protein 1C from brain is a two-headed cytosolic dynein', *Nature*, 332: 561-3.

van Beuningen, S. F. B., L. Will, M. Harterink, A. Chazeau, E. Y. van Battum, C. P. Frias, M. A. M. Franker, E. A. Katrukha, R. Stucchi, K. Vocking, A. T. Antunes, L. Slenders, S. Doulkeridou, P. Sillevis Smitt, A. F. M. Altelaar, J. A. Post, A. Akhmanova, R. J. Pasterkamp, L. C. Kapitein, E. de Graaff, and C. C. Hoogenraad. 2015. 'TRIM46 Controls Neuronal Polarity and Axon Specification by Driving the Formation of Parallel Microtubule Arrays', *Neuron*, 88: 1208-26.

van Dijk, J., J. Miro, J. M. Strub, B. Lacroix, A. van Dorsselaer, B. Edde, and C. Janke. 2008a. 'Polyglutamylation is a post-translational modification with a broad range of substrates', *J Biol Chem*, 283: 3915-22.

———. 2008b. 'Polyglutamylation is a post-translational modification with a broad range of substrates', *J Biol Chem*, 283: 3915-22.

van Dijk, J., K. Rogowski, J. Miro, B. Lacroix, B. Edde, and C. Janke. 2007. 'A targeted multienzyme mechanism for selective microtubule polyglutamylation', *Mol Cell*, 26: 437-48.

van Spronsen, M., M. Mikhaylova, J. Lipka, M. A. Schlager, D. J. van den Heuvel, M. Kuijpers, P. S. Wulf, N. Keijzer, J. Demmers, L. C. Kapitein, D. Jaarsma, H. C. Gerritsen, A. Akhmanova, and C. C. Hoogenraad. 2013. 'TRAK/Milton motor-adaptor proteins steer mitochondrial trafficking to axons and dendrites', *Neuron*, 77: 485-502.

Velazquez-Bernardino, P., F. Garcia-Sierra, O. Hernandez-Hernandez, M. Bermudez de Leon, G. Gourdon, M. Gomes-Pereira, and B. Cisneros. 2012. 'Myotonic dystrophy type 1-associated CTG repeats disturb the expression and subcellular distribution of microtubule-associated proteins MAP1A, MAP2, and MAP6/STOP in PC12 cells', *Mol Biol Rep*, 39: 415-24.

Vemu, A., J. Atherton, J. O. Spector, A. Szyk, C. A. Moores, and A. Roll-Mecak. 2016. 'Structure and Dynamics of Single-isoform Recombinant Neuronal Human Tubulin', *J Biol Chem*, 291: 12907-15.

Vemu, A., E. Szczesna, E. A. Zehr, J. O. Spector, N. Grigorieff, A. M. Deaconescu, and A. Roll-Mecak. 2018. 'Severing enzymes amplify microtubule arrays through lattice GTP-tubulin incorporation', *Science*, 361.

Venoux, M., J. Basbous, C. Berthenet, C. Prigent, A. Fernandez, N. J. Lamb, and S. Rouquier. 2008. 'ASAP is a novel substrate of the oncogenic mitotic kinase Aurora-A: phosphorylation on Ser625 is essential to spindle formation and mitosis', *Hum Mol Genet*, 17: 215-24.

Verbeke, E. J., A. L. Mallam, K. Drew, E. M. Marcotte, and D. W. Taylor. 2018. 'Classification of Single Particles from Human Cell Extract Reveals Distinct Structures', *Cell Rep*, 24: 259-68 e3.

Verhey, K. J., and T. A. Rapoport. 2001. 'Kinesin carries the signal', *Trends Biochem Sci*, 26: 545-50.

Vershinin, M., B. C. Carter, D. S. Razafsky, S. J. King, and S. P. Gross. 2007. 'Multiple-motor based transport and its regulation by Tau', *Proc Natl Acad Sci U S A*, 104: 87-92.

Villanueva-Paz, M., S. Povea-Cabello, I. Villalon-Garcia, M. Alvarez-Cordoba, J. M. Suarez-Rivero, M. Talaveron-Rey, S. Jackson, R. Falcon-Moya, A. Rodriguez-Moreno, and J. A. Sanchez-Alcazar. 2020. 'Parkin-mediated mitophagy and autophagy flux disruption in cellular models of MERRF syndrome', *Biochim Biophys Acta Mol Basis Dis*, 1866: 165726.

Villarroel-Campos, D., and C. Gonzalez-Billault. 2014. 'The MAP1B case: an old MAP that is new again', *Dev Neurobiol*, 74: 953-71.

Villebeck, L., M. Persson, S. L. Luan, P. Hammarstrom, M. Lindgren, and B. H. Jonsson. 2007. 'Conformational rearrangements of tail-less complex polypeptide 1 (TCP-1) ring complex (TRiC)-bound actin', *Biochemistry*, 46: 5083-93.

Vinh, D. B., and D. G. Drubin. 1994. 'A yeast TCP-1-like protein is required for actin function in vivo', *Proc Natl Acad Sci U S A*, 91: 9116-20.

Vourc'h, P., E. Petit, J. P. Muh, C. Andres, T. Bienvenu, C. Beldjord, J. Chelly, and C. Barthelemy. 2002. 'Exclusion of the coding sequence of the doublecortin gene as a susceptibility locus in autistic disorder', *Am J Med Genet*, 108: 164-7.

Vouyiouklis, D. A., and P. J. Brophy. 1995. 'Microtubule-associated proteins in developing oligodendrocytes: transient expression of a MAP2c isoform in oligodendrocyte precursors', *J Neurosci Res*, 42: 803-17.

Wacker, S. A., and T. M. Kapoor. 2010. 'Targeting a kinetochore-associated motor protein to kill cancer cells', *Proc Natl Acad Sci U S A*, 107: 5699-700.

Walczak, C. E., and S. L. Shaw. 2010. 'A MAP for bundling microtubules', *Cell*, 142: 364-7.

Walker, R. A., E. T. O'Brien, N. K. Pryer, M. F. Soboeiro, W. A. Voter, H. P. Erickson, and E. D. Salmon. 1988. 'Dynamic instability of individual microtubules analyzed by video light microscopy: rate constants and transition frequencies', *J Cell Biol*, 107: 1437-48.

Wang, D., A. Villasante, S. A. Lewis, and N. J. Cowan. 1986. 'The mammalian beta-tubulin repertoire: hematopoietic expression of a novel, heterologous beta-tubulin isotype', *J Cell Biol*, 103: 1903-10.

Wang, N., C. Bosc, S. Ryul Choi, B. Boulan, L. Peris, N. Olieric, H. Bao, F. Krichen, L. Chen, A. Andrieux, V. Olieric, M. J. Moutin, M. O. Steinmetz, and H. Huang. 2019. 'Structural basis of tubulin detyrosination by the vasohibin-SVBP enzyme complex', *Nat Struct Mol Biol*, 26: 571-82.

Wang, Q., A. H. Crevenna, I. Kunze, and N. Mizuno. 2014. 'Structural basis for the extended CAP-Gly domains of p150(glued) binding to microtubules and the implication for tubulin dynamics', *Proc Natl Acad Sci U S A*, 111: 11347-52.

Wang, W., V. F. Lundin, I. Millan, A. Zeng, X. Chen, J. Yang, E. Allen, N. Chen, G. Bach, A. Hsu, M. T. Maloney, M. Kapur, and Y. Yang. 2012. 'Nemitin, a novel Map8/Map1s interacting protein with Wd40 repeats', *PLoS One*, 7: e33094.

Wang, X., N. Li, N. Xiong, Q. You, J. Li, J. Yu, H. Qing, T. Wang, H. J. Cordell, O. Isacson, J. M. Vance, E. R. Martin, Y. Zhao, B. M. Cohen, E. A. Buttner, and Z. Lin. 2017. 'Genetic Variants of Microtubule Actin Cross-linking Factor 1 (MACF1) Confer Risk for Parkinson's Disease', *Mol Neurobiol*, 54: 2878-88.

Wang, Y. L., Y. Li, Y. G. Ma, and W. Y. Wu. 2019. 'DCLK1 promotes malignant progression of breast cancer by regulating Wnt/beta-Catenin signaling pathway', *Eur Rev Med Pharmacol Sci*, 23: 9489-98.

Wang, Y., S. Zhang, S. Dang, X. Fang, and M. Liu. 2019. 'Overexpression of microRNA-216a inhibits autophagy by targeting regulated MAP1S in colorectal cancer', *Onco Targets Ther*, 12: 4621-29.

Watson, P., and D. J. Stephens. 2006. 'Microtubule plus-end loading of p150(Glued) is mediated by EB1 and CLIP-170 but is not required for intracellular membrane traffic in mammalian cells', *J Cell Sci*, 119: 2758-67.

Wei, H., S. Sun, Y. Li, and S. Yu. 2016. 'Reduced plasma levels of microtubule-associated STOP/MAP6 protein in autistic patients', *Psychiatry Res*, 245: 116-18.

Wei, Z., G. Yang, R. Xu, C. Zhu, F. He, Q. Dou, and J. Tang. 2016. 'Correlation between protein 4.1R and the progression of heart failure in vivo', *Genet Mol Res*, 15.

Weingarten, M. D., A. H. Lockwood, S. Y. Hwo, and M. W. Kirschner. 1975a. 'A protein factor essential for microtubule assembly', *Proc Natl Acad Sci U S A*, 72: 1858-62.

———. 1975b. 'A protein factor essential for microtubule assembly', *Proc Natl Acad Sci U S A*, 72: 1858-62.

Weisbrich, A., S. Honnappa, R. Jaussi, O. Okhrimenko, D. Frey, I. Jelesarov, A. Akhmanova, and M. O. Steinmetz. 2007. 'Structure-function relationship of CAP-Gly domains', *Nat Struct Mol Biol*, 14: 959-67.

Weisenberg, R. C. 1972a. 'Microtubule formation in vitro in solutions containing low calcium concentrations', *Science*, 177: 1104-5.

———. 1972b. 'Microtubule formation in vitro in solutions containing low calcium concentrations', *Science*, 177: 1104-5.

Weisenberg, R. C., G. G. Borisy, and E. W. Taylor. 1968. 'The colchicine-binding protein of mammalian brain and its relation to microtubules', *Biochemistry*, 7: 4466-79.

Westphalen, C. B., M. Quante, and T. C. Wang. 2017. 'Functional implication of Dclk1 and Dclk1-expressing cells in cancer', *Small GTPases*, 8: 164-71.

Wettergren, E. E., F. Gussing, L. Quintino, and C. Lundberg. 2012. 'Novel disease-specific promoters for use in gene therapy for Parkinson's disease', *Neurosci Lett*, 530: 29-34.

Widlund, P. O., M. Podolski, S. Reber, J. Alper, M. Storch, A. A. Hyman, J. Howard, and D. N. Drechsel. 2012a. 'One-step purification of assembly-competent tubulin from diverse eukaryotic sources', *Mol Biol Cell*, 23: 4393-401.

———. 2012b. 'One-step purification of assembly-competent tubulin from diverse eukaryotic sources', *Mol Biol Cell*, 23: 4393-401.

Wiegering, A., U. Ruther, and C. Gerhardt. 2018. 'The ciliary protein Rpgrip1l in development and disease', *Dev Biol*, 442: 60-68.

Williamson, R., L. van Aalten, D. M. Mann, B. Platt, F. Plattner, L. Bedford, J. Mayer, D. Howlett, A. Usardi, C. Sutherland, and A. R. Cole. 2011. 'CRMP2 hyperphosphorylation is characteristic of Alzheimer's disease and not a feature common to other neurodegenerative diseases', *J Alzheimers Dis*, 27: 615-25.

Willis, T. A., C. L. Wood, J. Hudson, T. Polvikoski, R. Barresi, H. Lochmuller, K. Bushby, and V. Straub. 2016. 'Muscle hypertrophy as the presenting sign in a patient with a complete FHL1 deletion', *Clin Genet*, 90: 166-70.

Wilson, S. M., and R. Khanna. 2015. 'Specific binding of lacosamide to collapsin response mediator protein 2 (CRMP2) and direct impairment of its canonical function: implications for the therapeutic potential of lacosamide', *Mol Neurobiol*, 51: 599-609.

Wloga, D., D. M. Webster, K. Rogowski, M. H. Bre, N. Levilliers, M. Jerka-Dziadosz, C. Janke, S. T. Dougan, and J. Gaertig. 2009. 'TTLL3 Is a tubulin glycine ligase that regulates the assembly of cilia', *Dev Cell*, 16: 867-76.

Woehlke, G., and M. Schliwa. 2000. 'Directional motility of kinesin motor proteins', *Biochim Biophys Acta*, 1496: 117-27.

Wolff, A., B. de Nechaud, D. Chillet, H. Mazarguil, E. Desbruyeres, S. Audebert, B. Edde, F. Gros, and P. Denoulet. 1992. 'Distribution of glutamylated alpha and beta-tubulin in mouse tissues using a specific monoclonal antibody, GT335', *Eur J Cell Biol*, 59: 425-32.

Wolff, J. 2009. 'Plasma membrane tubulin', *Biochim Biophys Acta*, 1788: 1415-33.

Wolosewick, J. J., and J. H. Bryan. 1977. 'Ultrastructural characterization of the manchette microtubules in the seminiferous epithelium of the mouse', *Am J Anat*, 150: 301-31.

Wong, C. C., T. Xu, R. Rai, A. O. Bailey, J. R. Yates, 3rd, Y. I. Wolf, H. Zebroski, and A. Kashina. 2007. 'Global analysis of posttranslational protein arginylation', *PLoS Biol*, 5: e258.

Wu, X., A. Kodama, and E. Fuchs. 2008. 'ACF7 regulates cytoskeletal-focal adhesion dynamics and migration and has ATPase activity', *Cell*, 135: 137-48.

Wu, X., Y. Ruan, H. Jiang, and C. Xu. 2017. 'MicroRNA-424 inhibits cell migration, invasion, and epithelial mesenchymal transition by downregulating doublecortin-like kinase 1 in ovarian clear cell carcinoma', *Int J Biochem Cell Biol*, 85: 66-74.

Wu, X., Q. T. Shen, D. S. Oristian, C. P. Lu, Q. Zheng, H. W. Wang, and E. Fuchs. 2011. 'Skin stem cells orchestrate directional migration by regulating microtubule-ACF7 connections through GSK3beta', *Cell*, 144: 341-52.

Xia, X., C. He, A. Wu, J. Zhou, and J. Wu. 2018. 'Microtubule-Associated Protein 4 Is a Prognostic Factor and Promotes Tumor Progression in Lung Adenocarcinoma', *Dis Markers*, 2018: 8956072.

Xiao, H., K. El Bissati, P. Verdier-Pinard, B. Burd, H. Zhang, K. Kim, A. Fiser, R. H. Angeletti, and L. M. Weiss. 2010. 'Post-translational modifications to Toxoplasma gondii alpha- and beta-tubulins include novel C-terminal methylation', *J Proteome Res*, 9: 359-72.

Xiao, H., H. Wang, X. Zhang, Z. Tu, C. Bulinski, M. Khrapunovich-Baine, R. Hogue Angeletti, and S. B. Horwitz. 2012. 'Structural evidence for cooperative microtubule stabilization by Taxol and the endogenous dynamics regulator MAP4', *ACS Chem Biol*, 7: 744-52.

Xiao, J., J. X. Chen, Y. P. Zhu, L. Y. Zhou, Q. A. Shu, and L. W. Chen. 2012. 'Reduced expression of MTUS1 mRNA is correlated with poor prognosis in bladder cancer', *Oncol Lett*, 4: 113-18.

Xie, R., S. Nguyen, K. McKeehan, F. Wang, W. L. McKeehan, and L. Liu. 2011. 'Microtubule-associated protein 1S (MAP1S) bridges autophagic components with microtubules and mitochondria to affect autophagosomal biogenesis and degradation', *J Biol Chem*, 286: 10367-77.

Xie, S. D., Z. Y. Chen, H. Wang, M. Y. He, Y. T. Lu, B. X. Lei, H. Z. Li, Y. W. Liu, and S. T. Qi. 2017. '[MACF1 knockdown in glioblastoma multiforme cells increases temozolomide-induced cytotoxicity]', *Nan Fang Yi Ke Da Xue Xue Bao*, 37: 1183-89.

Xu, G., F. Yue, H. Huang, Y. He, X. Li, H. Zhao, Z. Su, X. Jiang, W. Li, J. Zou, Q. Chen, and L. Liu. 2016. 'Defects in MAP1S-mediated autophagy turnover of fibronectin cause renal fibrosis', *Aging (Albany NY)*, 8: 977-85.

Yadav, S., P. J. Verma, and D. Panda. 2014. 'C-terminal region of MAP7 domain containing protein 3 (MAP7D3) promotes microtubule polymerization by binding at the C-terminal tail of tubulin', *PLoS One*, 9: e99539.

Yaffe, M. B., G. W. Farr, D. Miklos, A. L. Horwich, M. L. Sternlicht, and H. Sternlicht. 1992. 'TCP1 complex is a molecular chaperone in tubulin biogenesis', *Nature*, 358: 245-8.

Yamada, N., K. Yasui, O. Dohi, Y. Gen, A. Tomie, T. Kitaichi, N. Iwai, H. Mitsuyoshi, Y. Sumida, M. Moriguchi, K. Yamaguchi, T. Nishikawa, A. Umemura, Y. Naito, S. Tanaka, S. Arii, and Y. Itoh. 2016. 'Genome-wide DNA methylation analysis in hepatocellular carcinoma', *Oncol Rep*, 35: 2228-36.

Yan, R., J. Li, Y. Zhou, L. Yao, R. Sun, Y. Xu, Y. Ge, and G. An. 2020. 'Inhibition of DCLK1 down-regulates PD-L1 expression through Hippo pathway in human pancreatic cancer', *Life Sci*, 241: 117150.

Yanagisawa, H. A., G. Mathis, T. Oda, M. Hirono, E. A. Richey, H. Ishikawa, W. F. Marshall, M. Kikkawa, and H. Qin. 2014. 'FAP20 is an inner junction protein of doublet microtubules essential for both the planar asymmetrical waveform and stability of flagella in Chlamydomonas', *Mol Biol Cell*, 25: 1472-83.

Yang, F., Q. Jiang, J. Zhao, Y. Ren, M. D. Sutton, and J. Feng. 2005. 'Parkin stabilizes microtubules through strong binding mediated by three independent domains', *J Biol Chem*, 280: 17154-62.

Yang, H., W. Mao, C. Rodriguez-Aguayo, L. S. Mangala, G. Bartholomeusz, L. R. Iles, N. B. Jennings, A. A. Ahmed, A. K. Sood, G. Lopez-Berestein, Z. Lu, and R. C. Bast, Jr. 2018. 'Paclitaxel Sensitivity of Ovarian Cancer Can be Enhanced by Knocking Down Pairs of Kinases that Regulate MAP4 Phosphorylation and Microtubule Stability', *Clin Cancer Res*, 24: 5072-84.

Yang, Y., C. Bauer, G. Strasser, R. Wollman, J. P. Julien, and E. Fuchs. 1999. 'Integrators of the cytoskeleton that stabilize microtubules', *Cell*, 98: 229-38.

Yang, Y., J. Dowling, Q. C. Yu, P. Kouklis, D. W. Cleveland, and E. Fuchs. 1996. 'An essential cytoskeletal linker protein connecting actin microfilaments to intermediate filaments', *Cell*, 86: 655-65.

Yano, T., T. Matsui, A. Tamura, M. Uji, and S. Tsukita. 2013. 'The association of microtubules with tight junctions is promoted by cingulin phosphorylation by AMPK', *J Cell Biol*, 203: 605-14.

Yano, T., T. Torisawa, K. Oiwa, and S. Tsukita. 2018. 'AMPK-dependent phosphorylation of cingulin reversibly regulates its binding to actin filaments and microtubules', *Sci Rep*, 8: 15550.

Yen, T. J., P. S. Machlin, and D. W. Cleveland. 1988. 'Autoregulated instability of beta-tubulin mRNAs by recognition of the nascent amino terminus of beta-tubulin', *Nature*, 334: 580-5.

Yu, N., and N. Galjart. 2020. 'Purification of Mammalian Tubulins and Tubulin-Associated Proteins Using a P2A-Based Expression System', *Methods Mol Biol*, 2101: 1-17.

Yu, Z., T. J. Kryzer, G. E. Griesmann, K. Kim, E. E. Benarroch, and V. A. Lennon. 2001. 'CRMP-5 neuronal autoantibody: marker of lung cancer and thymoma-related autoimmunity', *Ann Neurol*, 49: 146-54.

Yuasa-Kawada, J., R. Suzuki, F. Kano, T. Ohkawara, M. Murata, and M. Noda. 2003. 'Axonal morphogenesis controlled by antagonistic roles of two CRMP subtypes in microtubule organization', *Eur J Neurosci*, 17: 2329-43.

Yue, F., W. Li, J. Zou, X. Jiang, G. Xu, H. Huang, and L. Liu. 2017. 'Spermidine Prolongs Lifespan and Prevents Liver Fibrosis and Hepatocellular Carcinoma by Activating MAP1S-Mediated Autophagy', *Cancer Res*, 77: 2938-51.

Zaoui, K., S. Duhamel, C. A. Parachoniak, and M. Park. 2019. 'CLIP-170 spatially modulates receptor tyrosine kinase recycling to coordinate cell migration', *Traffic*, 20: 187-201.

Zhang, B., X. Shi, G. Xu, W. Kang, W. Zhang, S. Zhang, Y. Cao, L. Qian, P. Zhan, H. Yan, K. F. To, L. Wang, and X. Zou. 2017. 'Elevated PRC1 in gastric carcinoma exerts oncogenic function and is targeted by piperlongumine in a p53-dependent manner', *J Cell Mol Med*, 21: 1329-41.

Zhang, J., and X. P. Dong. 2012. 'Dysfunction of microtubule-associated proteins of MAP2/tau family in Prion disease', *Prion*, 6: 334-8.

Zhang, J., J. Yue, and X. Wu. 2017. 'Spectraplakin family proteins - cytoskeletal crosslinkers with versatile roles', *J Cell Sci*, 130: 2447-57.

Zhang, L., X. Liu, L. Song, H. Zhai, and C. Chang. 2020. 'MAP7 promotes migration and invasion and progression of human cervical cancer through modulating the autophagy', *Cancer Cell Int*, 20: 17.

Zhang, X., C. Lin, J. Song, H. Chen, X. Chen, L. Ren, Z. Zhou, J. Pan, Z. Yang, W. Bao, X. Ke, J. Yang, Y. Liang, H. Huang, D. Tang, L. Jiang, and J. Liu. 2019. 'Parkin facilitates proteasome inhibitor-induced apoptosis via suppression of NF-kappaB activity in hepatocellular carcinoma', *Cell Death Dis*, 10: 719.

Zhao, H., W. Su, C. Zhu, T. Zeng, S. Yang, W. Wu, and D. Wang. 2019. 'Cell fate regulation by reticulon-4 in human prostate cancers', *J Cell Physiol*, 234: 10372-85.

Zhao, T., J. Wu, X. Liu, L. Zhang, G. Chen, and H. Lu. 2018. 'Diagnosis of thymic epithelial tumor subtypes by a quantitative proteomic approach', *Analyst*, 143: 2491-500.

Zhao, W. M., A. Seki, and G. Fang. 2006. 'Cep55, a microtubule-bundling protein, associates with centralspindlin to control the midbody integrity and cell abscission during cytokinesis', *Mol Biol Cell*, 17: 3881-96.

Zheng, J., H. Liu, L. Zhu, Y. Chen, H. Zhao, W. Zhang, F. Li, L. Xie, X. Yan, and X. Zhu. 2019. 'Microtubule-bundling protein Spef1 enables mammalian ciliary central apparatus formation', *J Mol Cell Biol*, 11: 67-77.

Zhu, C., E. Lau, R. Schwarzenbacher, E. Bossy-Wetzel, and W. Jiang. 2006. 'Spatiotemporal control of spindle midzone formation by PRC1 in human cells', *Proc Natl Acad Sci U S A*, 103: 6196-201.

Zhu, Y., B. Aredo, B. Chen, C. X. Zhao, Y. G. He, and R. L. Ufret-Vincenty. 2019. 'Mice With a Combined Deficiency of Superoxide Dismutase 1 (Sod1), DJ-1 (Park7), and Parkin

(Prkn) Develop Spontaneous Retinal Degeneration With Aging', *Invest Ophthalmol Vis Sci*, 60: 3740-51.

Zuern, C., J. Heimrich, R. Kaufmann, K. K. Richter, U. Settmacher, C. Wanner, J. Galle, and S. Seibold. 2010. 'Down-regulation of MTUS1 in human colon tumors', *Oncol Rep*, 23: 183-9.

Zwetsloot, A. J., G. Tut, and A. Straube. 2018. 'Measuring microtubule dynamics', *Essays Biochem*, 62: 725-35.

université PARIS-SACLAY
ÉCOLE DOCTORALE
Structure et dynamique des systèmes vivants (SDSV)

Titre: Caractérisation systématique d'un grand nombre de protéines associées aux microtubules à l'aide d'essais de reconstitution TIRF sans purification de protéines.

Mots clés: cytosquelette des microtubules, microscopie TIRF, Microtubule Associated proteins (MAPs), reconstitution in vitro, dynamique des microtubules

Résumé: Le cytosquelette des microtubules (MTs) est constitué de filaments dynamiques et complexes impliqués dans une multitude de fonctions telles que la division cellulaire, le maintien de forme des cellules, les battements ciliaires ou encore la différenciation neuronale. Une régulation stricte des fonctions des microtubules est donc d'une grande importance pour l'homéostasie cellulaire, et toute perturbation pourrait potentiellement conduire à des maladies comme le cancer, les ciliopathies et la neurodégénérescence.
Dans un contexte cellulaire, les propriétés des microtubules peuvent être contrôlées par l'interaction des microtubules avec une grande variété de protéines associées aux microtubules (MAP). Notre connaissance de ces interacteurs s'est continuellement enrichie au cours des dernières décennies, mais il n'existe à ce jour aucune étude systématique visant à décrire et à classer ces protéines en fonction de leurs mécanismes de liaison et de leurs effets structuraux sur les microtubules.
Dans le présent travail, nous avons mis au point un essai permettant une analyse rapide et systématique de lysats clarifiés de cellules humaines surexprimant les MAPs d'intérêt. Le comportement dynamique des MT en présence d'environ 50 MAP différentes a été imagé à l'aide de la microscopie TIRF. Cela nous permet d'étudier le comportement des MAP dans une situation proche de leur environnement naturel, mais en éliminant la complexité de l'espace intracellulaire, telle que l'encombrement par des organelles et des filaments du cytosquelette à l'intérieur de l'espace intracellulaire confiné. En effet, la plupart des MAPs étaient bien solubles dans notre approche d'extraction, tandis que les approches de purification pour beaucoup d'entre elles ont conduit à la précipitation des protéines.
Notre nouvelle approche nous a permis de définir plusieurs protéines comme de véritables MAP. Nous montrons que des MAPs non caractérisées auparavant ont des effets étonnamment différents sur la polymérisation et la structure des MTs, créant ainsi une variété de réseaux de MT distincts. Notre approche sans cellules nous a en outre permis d'étudier les structures des complexes MAP-MT par cryo-microscopie électronique, d'étudier le dynamique des MTs porteuses de mutations trouvées dans les pathologies humaines, de produire des MAPs pour tester leur sensibilité aux modifications posttraductionnelles de la tubuline, ou d'étudier le rôle des MAPs dans les interactions antre l'actine et les MTs. Notre approche expérimentale permet donc de mieux comprendre comment les MAP et les MT contrôlent ensemble le fonctionnement du cytosquelette.

Title: Systematic characterization of a large number of Microtubule-Associated Proteins using purification-free TIRF-reconstitution assays

Keywords: microtubule cytoskeleton, TIRF microscopy, Microtubule Associated proteins (MAPs), in vitro reconstitution, microtubule dynamics

Abstract: Microtubules (MTs) are dynamic filaments involved in a plethora of functions such as cell division, cell shape, ciliary beating, neuronal differentiation. Strict regulation of microtubule functions is therefore of high importance for the cellular homeostasis, and any perturbations could potentially lead to diseases like cancer, ciliopathies and neurodegeneration. At the protein level, there are accumulating studies showing that MT properties can be controlled via interaction with a large variety of microtubule-associated proteins (MAPs). Our knowledge of MAPs has been enriched over time, but up to this date no systematic studies exist that aim to describe and categorize these proteins according to their binding mechanisms and structural effects on microtubules. In my PhD project, I have developed an assay for rapid and systematic analysis of MAPs using cleared lysates of cultured human cells in which I overexpress the MAPs of interest. The dynamic behaviour of growing MTs in the presence of different MAPs were imaged using TIRF microscopy. This allows me to study the behaviour of around 50 MAP candidates in a situation close to their natural environment, but eliminating complexity coming from different organelles and crammed cytoskeleton filaments inside the confined intracellular space. Indeed, most MAPs were nicely soluble in the extract approach, while purification attempts of several of them led to protein precipitation, thus making reconstitution experiments impossible.

This novel approach allowed me to compare many MAPs under similar experimental conditions, and helps to define several novel proteins as bona-fide MAPs. I show that previously uncharacterized MAPs have strikingly different effects on MT polymerization and MT structure, thus creating a variety of distinct MT arrays. Also, I extended this cell-free pipeline to study MAP-MT structures by cryo-electron microscopy, to study MAPs and microtubules carrying patient mutations, used to produce MAPs to test its sensitivity against tubulin PTMs and to study the role of MAPs in actin-MT crosstalk. In the future, this novel approach will allow for a better mechanistic understanding of how MAPs and MTs together control cytoskeleton functions.

Université Paris-Saclay
Maison du doctorat de l'Université Paris-Saclay
2ème étage aile ouest, Ecole normale supérieure Paris-Saclay
4 avenue des Sciences,
91190 Gif sur Yvette, France